Understanding the Exchange Process of Surface and Sub-surface Hydrological System for Safe and Sustainable Water Security Plan in Shilabati River Basin: Associated Risks and Eco-friendly Remediation

Thesis

Submitted by

Sudipa Halder

(Registration Number: D-7/ISLM/79/18)

For the fulfillment of

Doctor of Philosophy

(Science)

School of Water Resources Engineering

Faculty of Interdisciplinary Studies, Law and Management

Jadavpur University

Kolkata, India

2023

Dedicated to

I dedicate this Ph.D. thesis with heartfelt sincerity to the **people living in the water stress zone of Shilabati River Basin of West Bengal, India**. It is with great humility and a deep sense of purpose that I undertake this endeavor, driven by the noble mission of bringing smiles to the water deprived society. In the face of water scarcity, I witnessed the struggles and hardships endured by the resilient communities residing along the banks of Shilabati River. The unwavering determination to thrive in the midst of such challenging circumstances has been an inspiration to me throughout my research journey. My research endeavors were fueled by the belief that access to clean water is not only a fundamental human right but also a catalyst for progress, well-being, and happiness. It is my sincere hope that the findings and recommendations presented in this thesis will serve as a guiding light for policymakers, stakeholders, and community leaders, inspiring them to take decisive action in alleviating the water stress challenges faced by the people of Shilabati River Basin. May this endeavor actively contribute to the advancement and execution of sustainable eco-friendly solutions, empowering individuals to safeguard a future where an abundance of pure, clean water flows freely throughout their communities. My dedication to the cause extends beyond the pages of this thesis, as I pledge to continue advocating for the rights and actively supporting initiatives that promote water conservation and equitable access.

I would also like to dedicate this doctoral thesis to **my parents, brother and Dr. Kartik Samanta** who have been the unwavering pillars of support throughout my academic journey. Their boundless love, encouragement, and sacrifices have played a pivotal role in shaping the person I am today. Their belief in my abilities and constant motivation have been invaluable in overcoming challenges and pursuing excellence. This achievement would not have been possible without their unconditional love and unwavering support. Thank you, **Ma (Mrs. Namita Halder), Baba (Shri Dukhiram Halder)**, **Bhai (Mr. Snehashis Halder) and Dr. Kartik Samanta** for being my greatest source of inspiration and for instilling in me the values of hard work, perseverance, and determination. I dedicate this thesis to you also with all my love and gratitude.

Index No: D-7/ISLM/79/18

Title

Understanding the Exchange Process of Surface and Sub-surface Hydrological System for Safe and Sustainable Water Security Plan in Shilabati River Basin: Associated Risks and Eco-friendly Remediation

Name, Designation & Institution of the Supervisor(s):

Prof. Pankaj Kumar Roy
Professor and Director
School of Water Resources Engineering
Jadavpur University

Prof. (Dr.) Pankaj Kumar Roy
Director & Professor
School of Water Resources Engineering
Jadavpur University

Malabika Biswas Roy

Dr. Malabika Biswas Roy
Assistant Professor (Stage-III) and Head
Department of Geography
Women's College, Calcutta

Dr. Malabika Biswas Roy
Assistant Professor Stage 3 and Head
Women's' College Calcutta
University of Calcutta

JOURNAL PUBLICATIONS: NATIONAL AND INTERNATIONAL

Halder, S., Roy, M. B. & Roy, P. K. (2023). Understanding the exchange process between ground and surface water using mini drive point piezometer and mathematical models to identify suitable managed aquifer recharge sites. **Environmental Science and Pollution Research**, **Springer (IF-5.80)**

Halder, S., Roy, M. B., Roy, P. K., & Sedighi, M. (2023). Groundwater vulnerability assessment for drinking water suitability using Fuzzy Shannon Entropy model in a semi-arid river basin**. Catena, Elsevier (IF-6.367)** 229, 107206.

Halder, S., Maiti, P., Karmakar, S., Roy, M. B., & Roy, P. K. (2023). Enhanced fluoride removal from groundwater using red and white kaolinite lithomarge to develop a low cost eco-friendly defluoridation unit in rural areas of Shilabati river basin, West Bengal. **Journal of Water Process Engineering**, **Elsevier (IF-7.34)** 53, 103698.

Halder, S., Bhattacharya, S., Roy, M. B., & Roy, P. K. (2023). Application of fuzzy C-means clustering and fuzzy EDAS to assess groundwater irrigation suitability and prioritization for agricultural development in a complex hydrogeological basin. **Environmental Science and Pollution Research**, **Springer (IF-5.80)**, 1-29.

Biswas Roy, M., Nag, **S., Halder, S**., & Kumar Roy, P. (2022). Assessment of wetland potential and bibliometric review: a critical analysis of the Ramsar sites of India. **Bulletin of the National Research Centre, Springer** 46(1), 1-11.

Roy, P. K., Basak, S. K., Mohinuddin, S., Roy, M. B**., Halder, S.,** & Ghosh, T. (2022). Modelling groundwater potential zone using fuzzy logic and geospatial technology of a deltaic island. **Modeling Earth Systems and Environment, Springer** 8(4), 5565-5584 **(IF-3.0).**

Halder, S., Roy, M. B., & Roy, P. K. (2022). Modelling drought vulnerability tracts under changed climate scenario using fuzzy DEMATEL and GIS techniques. **Theoretical and Applied Climatology, Springer (IF-3.410)** 150(1-2), 425-452.

Roy, M. B., Kumar, A., Chatterjee, D., & **Halder, S. (**2022). Comprehensive Assessment of Meta-Analysis and Contingent Valuation Technique for Sustainable Management of Wetland of Middle Ganga Plain. **Quaestiones Geographicae, Sciendo (IF-0.315)** 41(2), 153-165.

Halder, S., Roy, M. B., & Roy, P. K. (2021). Tropical plateau basin prioritisation for sustainable groundwater management using classical algorithms. **Arabian Journal of Geosciences, Springer (IF-1.80)** 14, 1-30.

Halder, S., Roy, M. B., & Roy, P. K. (2021). Modelling soil erosion risk of a tropical plateau basin to identify priority areas for conservation. **Environmental Earth Sciences, Springer (IF-3.119)** 80, 1-24.

Halder, S., Roy, M. B., & Roy, P. K. (2020). Fuzzy logic algorithm based analytic hierarchy process for delineation of groundwater potential zones in complex topography. **Arabian Journal of Geosciences, Springer (IF-1.80)**, 13, 1-22.

Halder, S., Roy, M. B., & Roy, P. K. (2020). Analysis of groundwater level trend and groundwater drought using Standard Groundwater Level Index: a case study of an eastern river basin of West Bengal, India. **SN Applied Sciences, Springer** 2, 1-24 **(IF-2.6)**

Roy et al., 2018 P.K. Roy, **S. Halder**, S. Nag, M.B. Roy, A. Majumder Study of ganga river health condition based on water quality indicators with environmental aspects and adaptation strategies thereof. **Indian Journal of Environmental Protection,** 38 (8) (2018), pp. 659-670

BOOK CHAPTERS: NATIONAL AND INTERNATIONAL

Roy, P. K., Roy, M. B., Chatterjee, **S., Halder**, S., Nag, S., & Majumder, A. (2021). Land reclamation and reuse of waste water on the backdrop of urban sprawl of Kolkata metropolitan: a case study of East Kolkata, Wetland, India. In Modern Cartography Series (Vol. 10, pp. 557-579). Academic Press.

Bhattacharya, **S., Halder,** S., Nag, S., Roy, P. K., & Roy, M. B. (2021). Assessment of drought using multi-parameter indices. Advances in water resources management for sustainable use, 243-255.

Halder, S., Roy, M. B., Bhattacharya, S., Mondal, S., & Roy, P. K. (2021). Soil loss estimation for sustainable watershed conservation in semi-arid Bengal basin. In Advances in Water Resources Management for Sustainable Use (pp. 413-439). Singapore: Springer Singapore.

Roy, M. B., **Halder, S.,** Ghosh, A., Basu, S., & Roy, P. K. (2021). Trend Analysis of Highly Cited Papers on Sustainable Watershed Management: A Bibliometric Review. Advances in Water Resources Management for Sustainable Use, 23-37.

Roy, M. B., Roy, P. K., **Halder, S.,** Banerjee, G., & Mazumdar, A. (2021). Assessment of Stream Flow Impact on Physicochemical Properties of Water and Soil in Forest Hydrology through Statistical Approach. In India: Climate Change Impacts, Mitigation and Adaptation in Developing Countries (pp. 207-225). Cham: Springer International Publishing.

LIST OF PATENTS: **Nil**

AWARDS AND ACHIEVEMENTS

Received the prestigious ***Commonwealth Split-site Ph.D. Scholarship*** funded by **United Kingdom Foreign Commonwealth and Development Office (FCDO), 2021** to study in the **University of Manchester (World QS rank-28)** as ***Post Graduate Research Scholar*** from April, 2022 - March, 2023.

Ranked 2nd in poster presentation in ***International Conference on Sustainable Water Management*** organized by **Department of Water Resources, River Development and Ganga Rejuvenation, Ministry of Jal Shakti, National Hydrology Project (NHP) and Australian Water Partnership**, 2019

Ranked 1st in poster presentation in ***International Conference on Sustainable Water Management*** organized by **Department of Water Resources, River Development and Ganga Rejuvenation, Ministry of Jal Shakti, National Hydrology Project (NHP) and Australian Water Partnership**, 2018

Received the prestigious ***Junior Research Fellowship (JRF)*** scheme of the **University Grants Commission, Government of India** from 2018-2023.

ACADEMIC CONFERENCE

Presented paper in ***Postgraduate Summer Research Showcase*** on "**Groundwater vulnerability assessment for drinking water suitability**" organized by **University of Manchester, United Kingdom**, 2022.

Presented paper in ***Water for All - Emerging Issues & Innovations (AQUA-360)*** on "**Groundwater vulnerability assessment for drinking water suitability using Fuzzy Shannon Entropy model in a semi-arid river basin**" organized by **University of Exeter, United Kingdom**, 2021.

Presented paper in ***International Conference on Sustainable Water Resources Management under Changed Climate*** on "**Soil Loss Estimation for Sustainable Watershed Management: A Case Study of Eastern River Basin of West Bengal, India**" organized by **School of Water Resources Engineering, Jadavpur University**, 2020.

Presented poster in ***2nd International Conference on Sustainable Water Management*** on "**Modelling Drought Vulnerability Tracts under Changed Climate Scenario using FUZZY DEMATEL and GIS techniques**" organized by **National Hydrology Project (NHP) and Australian Water Partnership, Pune**, 2019.

Presented paper in the ***5th International Conference on Water Resources (WRE 2019)*** on "**Fuzzy Logic Base Decision-Making Trial and Evaluation Laboratory Modelling for Prediction of Drought Risk Zone using Remote Sensing Derived Indices**" organized by **WRE, MACAO, China**, 2019.

Presented paper in the ***30th National Conference of Indian Institute of Geomorphologists (IGI)*** on "**Assessment of Land Use and Land Cover Parameters and Delineation of Groundwater Potential Zones Based on Fuzzy AHP and Geospatial Techniques**" organized by **Department of Geography, Jamia Mila Islamia, New Delhi**, 2018.

Presented psoter in the ***1st International Conference on Sustainable Water Management*** on "**Delineation of Groundwater potential zones in complex topography based on Fuzzy Logic Algorithm Based Analytic Hierarchy Process**" organized by **National Hydrology** Project (NHP), Chandigarh,2018.

Presented paper in the ***29th National Conference of Indian Institute of Geomorphologists (IGI***) on "**Interdependence of Geomorphic, Biogenic and Sedimentation Processes in Bakkhali, South 24-Parganas District: A Case Study**" organized by **Department of Geography, University of Calcutta**, 2016.

Participated in ***National Conference on Development and Environment*** organized by **Department of Geography, West Bengal State University**, 2016.

SEMINAR AND WORKSHOP ATTENDED

Participated in a seminar on ***Women in STEM Conference*** organized **by University of Manchester, United Kingdom,** 2022.

Participated in a seminar on ***Issues Related to Water Crisis, Mitigation and Conservation Techniques under Changed Climate Scenario*** organized **by School of Water Resources Engineering, Jadavpur University,** 2020.

Participated in a seminar on ***Local Groundwater Management Issues*** organized by **Tier II Training Programme by Central Ground Water Board, Easter Region, Kolkata,** 2018.

Participated in a seminar on ***Environmental Challenges at Present Issues of Concern*** organized **by Department of Civil Engineering, Calcutta Institute of Engineering and Management,** 2018.

Participated in a seminar ***One Day Workshop on Quantitative and Qualitative Research Methods in Geographical Studies*** organized by **Department of Geography, Vivekananda College, Kolkata, West Bengal India,** 2018.

Participated in a seminar ***One Day Workshop on Water, Sanitation and Hygiene for All-Sustainability Issues under Rural Indian Conditions*** organized by **IIEST Shibpur,** 2018.

STATEMENT OF ORIGINALITY

I **Miss Sudipa Halder**, Index No: **D-7/ISLM/79/18** registered on the date of **04.01.2019 (academic session: 2019-2024)** do hereby declare that this thesis entitled "***Understanding the Exchange Process of Surface and Sub-surface Hydrological System for Safe and Sustainable Water Security Plan in Shilabati River Basin: Associated Risks and Eco-friendly Remediation***" contains literature survey and original research work done by the undersigned candidate as part of the fulfillment of the requirements for the **degree of Doctor of Philosophy in Science.**

All information in this thesis have been obtained and presented in accordance with existing academic rules and ethical conduct. I declare that, as required by these rules and conduct, I have fully cited and referred all materials and results that are not original to this work.

I also declare that I have checked this thesis as per the "Policy on Anti-Plagiarism, Jadavpur University, 2019", and the level of similarity as checked by iThenticate Software is **7%**

Name of the Candidate: **Miss Sudipa Halder**

Signature of the Candidate: Sudipa Halder

Date: 14.08.2023

Location: Kolkata

Certified by Supervisor(s):
(Signature with date & seal)

Malabika Biswas Roy

Prof. (Dr.) Pankaj Kumar Roy
Director & Professor
School of Water Resources Engineering
Jadavpur University

Dr. Malabika Biswas Roy
Assistant Professor (Stage-III) and Head
Department of Geography
Women's College, Calcutta

Prof. Pankaj Kumar Roy
Professor and Director
School of Water Resources Engineering
Jadavpur University

Dr. Malabika Biswas Roy
Assistant Professor Stage 3 and Head
Women's' College Calcutta
University of Calcutta

CERTIFICATE FROM THE SUPERVISOR/S

This is to certify that the thesis entitled "***Understanding the Exchange Process of Surface and Sub-surface Hydrological System for Safe and Sustainable Water Security Plan in Shilabati River Basin: Associated Risks and Eco-friendly Remediation***" submitted by **Miss. Sudipa Halder**, Index No: **D-7/ISLM/79/18,** who got her name registered on **04.01.2019** in the academic session **2019-2024** for the award of the **Doctor of Philosophy** in **Science** from **Jadavpur University**, is absolutely based on her own work under the supervision of **Prof. (Dr.) Pankaj Kumar Roy** and **Dr. Malabika Biswas Roy** and that neither her thesis nor any part of her thesis has been submitted for any degree/diploma or any other academic award anywhere before.

Certified by Supervisor(s):
(Signature with date & seal)

Prof. (Dr.) Pankaj Kumar Roy
Director & Professor
School of Water Resources Engineering
Jadavpur University

Prof. Pankaj Kumar Roy
Professor and Director
School of Water Resources Engineering
Jadavpur University

Malabika Biswas Roy

Dr. Malabika Biswas Roy
Assistant Professor (Stage-III) and Head
Department of Geography
Women's College, Calcutta

Dr. Malabika Biswas Roy
Assistant Professor Stage 3 and Head
Women's' College Calcutta
University of Calcutta

ACKNOWLEDGMENT

I am deeply grateful to the following individuals who have played a significant role in the completion of my doctoral thesis entitled "Understanding the Exchange Process of Surface and Sub-surface Hydrological System for Safe and Sustainable Water Security Plan in Shilabati river basin: Associated Risks and Eco-friendly Remediation". First and foremost, I would like to express my sincere gratitude to my esteemed thesis advisor and supervisor **Prof. Pankaj Kumar Roy**, for his invaluable guidance, unwavering support, and exceptional mentorship throughout this research journey. I am immensely thankful to my co-supervisor **Dr. Malabika Biswas Roy** for encouraging me to do research work for societal benefit. Their expertise, insightful feedback, and constant encouragement and support have been instrumental in shaping the direction and quality of this thesis.

I am also indebted to the members of my thesis research committee members for their valuable input, constructive criticism, and scholarly contributions. Their expertise and insightful suggestions have greatly enriched the content and overall quality of this work.

I would like to express my gratitude to the **Department of Physics, Jadavpur University,** for their technical support and granting me access to the XRD and FESEM facility. Their assistance has been invaluable in my research. Additionally, I am thankful to the **School of Materials Science and Nanotechnology, Jadavpur University**, for their support in conducting the FTIR analysis. I am also grateful to **Prof. Partha Ghosh** for generously allowing me to access the Soil Mechanics Laboratory of the Construction Engineering Department, Jadavpur University. This access has greatly facilitated my research endeavors. Furthermore, I would like to thank the **Danish Hydraulic Institute (DHI)** for providing me with the MIKE FEFLOW student license, which has been instrumental in advancing my research in the course of my study.

I am also immensely grateful to the **University of Manchester** for providing me with the opportunity to pursue a part of my doctoral studies as a **Commonwealth Split-Site Scholar**. The year I spent at the University of Manchester was a transformative experience, and I am indebted to the **Dr. Majid Sedighi** and the water quality, materials and earth and environmental laboratory staffs and technicians for their warm hospitality, intellectual stimulation, and the remarkable research environment they provided.

My sincere thanks go to my friends and fellow researchers, **Mr. Saurabh Kumar Basak**, **Mr. Bishal Ghosh, Mrs. Swetasree Nag, Miss. Shilpa Saha, Miss. Poulami Ray, Mr. Priyabrata Mondal, Mr. Debdas Chowdhury, Mrs. Sritama Chatterjee, Mr. Sayak Karmakar, Mr. Pratik Maiti and Mr. Debanik Ghosh** for their constant research engagement, encouragement, stimulating discussions, and camaraderie throughout this academic journey. Their support, understanding, and motivation have provided me with the strength to overcome challenges and stay focused.

I would like to extend my sincere appreciation to the dedicated team led by **Giyasuddin Sekh**, the drilling and boring contractor, for their unwavering commitment during the field survey and exhausting pumping test, even under challenging conditions such as scorching sunlight. Their contribution has been crucial to the success of my research.

I would like to express my heartfelt gratitude to the **Shantanu da, Raju Bhai** and the **kind villagers** who extended their unwavering support and assistance during the field survey conducted as part of my doctoral research. Their willingness to lend a helping hand, whether it was guiding me through unfamiliar terrain, providing valuable local knowledge, or assisting with logistics, played a vital role in the success of my study. Their hospitality, generosity, and willingness to go above and beyond have left a lasting impression on me.

Last but certainly not least, I would like to express my deepest appreciation to my family and loved ones for their unwavering support, love, and encouragement. Their belief in my abilities and continuous encouragement have been the driving force behind my perseverance and determination to succeed.

To all those who have contributed to my journey, whether mentioned or not, I am truly grateful for your support, encouragement, and belief in my capabilities. Your contributions, both big and small, have shaped the outcome of this thesis and have been instrumental in my personal and academic growth.

Last but surely not the least I am immensely thankful, grateful and indebted to the supreme power, who provided me all the strength to perform all the work I do and guiding me throughout my life till now and in upcoming days.

Thank you all for being a part of this remarkable chapter in my life.

Contents

Journal Publications: National and International....iv
Book Chapters: National and International....v
List of Patents....v
Awards and Achievements....vi
Academic Conference....vii
Seminar and Workshop Attended....viii
Statement of Originality....ix
Certificate from The Supervisor/s....x
Acknowledgment....xi
List of Tables....xxii
List of Figures....xxiv
List of Pictures....xxvii
List of Abreviations....xxix
Abstract....xxxii
Chapter 1 Research Background....1
1.1 Introduction....1
1.1.1 Issues and Challenges of Groundwater Water under Changed Climate Scenario....1
1.1.2 Global fresh water distribution and Appropriation....4
1.1.3 Status of Groundwater in Rural and Urban areas of India....6
1.1.4 Groundwater Vulnerability to pollution....8
1.1.5 Advances in Remote Sensing/Geographical Information System and modelling techniques in Groundwater potential and vulnerability studies....11
1.1.6 General Framework of the Current Research....14
1.1.7 Overall Research Gap....15
1.1.8 Over all Aims and Objectives....15
1.1.9 Novelty of the Current Research....16
1.1.10 Study Expectations....16
1.1.11 Overall Study Limitations....17
1.1.12 Global Importance....17
1.1.13 Comprehensive Thesis structure....18
Chapter 2 General Features of the study area....20

2.1 Locational description of the river basin: Shilabati River 20
2.2 General characteristics of the study area 22
2.2.1 Soil types 22
2.2.2 Geomorphology 23
2.2.3 Land use and Land cover 23
2.2.4 Runoff and Discharge 26
2.2.5 Slope 28
2.2.6 Drainage Density 29
2.2.7 Relative Relief 30
2.2.8 Geology and hydrogeology 31
2.2.9 Climate and Vegetation 32
2.2.10 Groundwater Recharge 33
2.3 Major Hydro-Environmental Problems within the Study Area 34
2.4 Evidences of the research problem from the study area 35
2.5 Index map of the study area 37
Chapter 3 Basin Prioritization for Sustainable Groundwater Management 38
3.1 Introduction 38
3.2 Research Gap and Novelty of Work 40
3.3 Objectives of the Research Work 40
3.4 Area of Investigation 40
3.5 Research Design and Methodology 41
3.5.1 Data source 41
3.5.2 Hypsometric Curve and Integral 42
3.5.3 Principle Component Analysis 43
3.5.4 K- Means Clustering Analysis 45
3.6 Multicriteria Decision Making (MCDM) Technique 45
3.6.1 Entropy Method of weight calculation 45
3.6.2 TOPSIS model 46
3.6.3 VIKOR Model 47
3.6.4 COPRAS 47
3.7 Selection of Best Model through Nonparametric Correlation Test 48
3.1 Results and Discussion 48
3.1.1 Analysis of morphometric parameters 48
3.1.2 Drainage Network 49

3.1.3 Basin Geometry 50
3.1.4 Drainage Texture Analysis 53
3.1.5 Relief Aspects 57
3.1.6 Assessment of Inter-Relationship among Morphometric Parameters using Principal Component analysis 58
3.1.7 Morphometric asymmetry using K-means cluster analysis 60
3.2 Recharge and infiltration capacity prioritization of sub-basins by TOPSIS, COPRAS and VIKOR models 62
3.3 Selection of the best model and validation using yield data 64
3.4 Conclusion and Recommendations 65
3.5 Limitation and Future work 66
Chapter 4 Impact of Climate Change on Hydrometeorological events and hydrogeological system using Fuzzy and statistical techniques 67
4.1 Modelling drought vulnerability tracts of the river basin under climatic scenario 67
4.1.1 Introduction 67
4.1.2 Research Gap and Novelty of Work 68
4.1.3 Objective of the Research Work 69
4.1.4 Area of Investigation 69
4.1.5 Materials and methods 70
4.1.5.1 Data source 70
4.1.5.2 Conditioning factors/ criteria 71
4.1.5.2.1 Normalised Difference Vegetation Index (NDVI) 71
4.1.5.2.2 Vegetation Condition Index (VCI) 71
4.1.5.2.3 Land Surface Temperature (LST) 71
4.1.5.2.4 Temperature Condition Index (TCI) 72
4.1.5.2.5 Vegetation Health Index (VHI) 72
4.1.5.2.6 Normalized Difference Water Index (NDWI) 72
4.1.5.2.7 Soil Moisture Index (SMI) 73
4.1.5.2.8 Soil Adjusted Vegetation Index (SAVI) 73
4.1.5.2.9 Standard Precipitation Index (SPI) 74
4.1.5.2.10 Yield Anomaly Index (YAI) 74
4.1.5.3 Fuzzy DAMETAL 74
4.1.5.4 Model prioritization using Compound factor (CF) 78
4.1.5.5 Estimation of Drought Vulnerability zone 78

4.1.6 Results 79
4.1.6.1 Drought Monitoring through Standard Precipitation Index (SPI) 79
4.1.6.2 Long term drought analysis using LST and NDVI derived indices 83
4.1.6.3 Long term drought and water stress analysis using NDWI 85
4.1.6.4 Drought monitoring through SMI and SAVI 85
4.1.6.5 Identification of Drought risk prone zone using Fuzzy DAMETAL and causal diagram 88
4.1.6.6 Validation of drought prone zone using YAI and prioritization of CD blocks using Composite score method 89
4.1.6.7 Association of drought prone zone and cropping pattern practiced 94
4.1.7 Discussion 95
4.1.8 Conclusion and Recommendation 96
4.1.9 Limitation and Future Work 97
4.2 Analysis of Groundwater Level Trend and Groundwater Drought using Standard Groundwater Level Index 97
4.2.1 Research Gap and Novelty of Work 99
4.2.2 Objectives of the Research Work 99
4.2.3 Area of Investigation 99
4.2.4 Research Design and Methodology 100
4.2.4.1 Date source 100
4.2.4.2 Mann Kendall Test 106
4.2.4.3 Sen's Slope Estimator 107
4.2.4.4 Agglomerated Hierarchical Clustering 107
4.2.4.5 Standard Groundwater Level Index (SGWI) 107
4.2.5 Results and Discussion 108
4.2.5.1 Influence of Climate Variable on Groundwater Level 108
4.2.5.2 Impact of Land Use and Land Cover change (LULC) on Groundwater level 112
4.2.5.3 Spatio- Temporal Distribution of Groundwater Level Since 1996 116
4.2.5.4 Groundwater Level Trend Analysis 120
4.2.5.5 Cluster Analysis of Wells Based on Their Fluctuation Scenario 120
4.2.5.6 Identification of Groundwater Drought Years using Standard Groundwater Level Index 128
4.2.6 Conclusion and Recommendations 128
4.2.7 Limitation and Future Work 129

Chapter 5 Modelling Ground and Surface water Interaction using Machine Learning and MIKE FEFLOW Model 130

5.1 Identification of Groundwater Potential Zone using Hydrogeophysical Investigation, Machine Learning and MCDM Techniques 130

5.1.1 Introduction 130

5.1.2 Research Gap and Novelty of the Work 132

5.1.3 Objective of the research work 132

5.1.4 Area of Investigation 132

5.1.5 Research Design and Methodology 135

5.1.5.1 Field investigation: Vertical Electrical Resistivity Soundings (VES) and soil sampling 135

5.1.5.2 Estimation of Dar-Zarrouk and hydrogeological parameters 136

5.1.5.3 Laboratory experiments and soil hydraulic parameters 137

5.1.5.4 Development of groundwater potential model based on field investigation 138

5.1.5.4.1 Well inventory and model setup 138

5.1.5.4.2 Machine learning based models 138

5.1.5.5 Fuzzy set theory based models 139

5.1.5.6 Estimation of Groundwater Potential Index (GWPI) 141

5.1.5.7 Model assessment and validation techniques 141

5.1.6 Results and discussion 144

5.1.6.1 Hydrogeological and hydraulic prospects inducing groundwater potential in the river basin 144

5.1.6.2 Soil hydraulic prospects inducing groundwater potential in the river basin 146

5.1.6.3 Factor importance and model's output comparison 148

5.1.6.4 Model evaluation and validation 151

5.1.6.5 Relationship between groundwater level and groundwater potential models 152

5.1.7 Recommendations and sustainable plans 153

5.1.8 Conclusion and Reccomendations 156

5.1.9 Limitation and Future Work 157

5.2 Understanding the exchange process between ground and surface water using mini drive point piezometer and mathematical models to identify suitable Managed Aquifer Recharge sites 157

5.2.1 Introduction 157

5.2.2 Research Gap and Novelty of Work 159

5.2.3 Objective of the Research Work 159

5.2.4 Area of Investigation 160

5.2.5 Research Design and Methodology 160
5.2.5.1 Field investigation and mini drive point piezometer (MDP) installation 160
5.2.5.2 Mathematical algorithms to understand ground and surface water exchange 162
5.2.5.2.1 Vertical gradient 162
5.2.5.2.2 Hydraulic conductivity 163
5.2.5.2.3 Ex-situ hydraulic conductivity measurement 164
5.2.5.3 Determination of hydraulic parameters, including channel cross-sectional area, flow velocity, and water level 165
5.2.5.4 Groundwater flow modelling using MIKE-FEEFLOW model 166
5.2.5.5 Identification of suitable Manage Aquifer Recharge (MAR) sites using MCDM models 167
5.2.5.6 Statistical techniques for validation and accuracy 168
5.2.6 Results and Discussion 169
5.2.6.1 Comparative analysis of hydraulic conductivity between insitu and exsitu measurements 169
5.2.6.2 Identification of losing and gaining stream 173
5.2.6.3 Groundwater flow modelling using MIKE-FEFLOW 177
5.2.6.4 Identification of suitable sites for Managed Aquifer Recharge (MAR) 180
5.2.6.5 Efficacy of the MAR selected site for construction of radial collector well and infiltration gallery using pumping test 185
5.2.7 Conclusion and Recommendations 191
5.2.8 Limitation and Future Works 191
Chapter 6 Groundwater Vulnerability and pollution risk assessment 193
6.1 Groundwater vulnerability assessment for drinking water suitability using Fuzzy Shannon Entropy model 193
6.1.1 Introduction 193
6.1.2 Research Gap and Novelty of Work 194
6.1.3 Objectives of the Research Work 195
6.1.4 Area of Investigation 195
6.1.5 Research Design and Methodology 198
6.1.5.1 Data Source 198
6.1.5.2 Experimental and laboratory analysis 198
6.1.5.3 Fuzzy Shannon Entropy model 199
6.1.5.1 Hybrid groundwater vulnerable susceptibility mapping model 200
6.1.5.2 Water quality index (WQI) 200

6.1.5.3 Receiver Operating Characteristics (ROC) curve 201
6.1.6 Description of criterions for hybrid Fuzzy Shannon Entropy-groundwater vulnerable index (FSE-GVI) 202
6.1.6.1 Slope 202
6.1.6.2 Soil Media 202
6.1.6.3 pH level 203
6.1.6.4 Geology 203
6.1.6.5 Groundwater level 204
6.1.6.6 Aquifer depth 204
6.1.6.7 Specific yield 205
6.1.6.8 Hydraulic conductivity 205
6.1.6.9 Impact of the vadose zone 207
6.1.6.10 Groundwater recharge 207
6.1.6.11 Land use and land cover 208
6.1.6.12 Population density 208
6.1.6.13 Groundwater based schemes 209
6.1.7 Results and Discussion 209
6.1.8 Validation of the identified vulnerable zone 210
6.1.9 Discussion 215
6.1.10 Conclusion and Recommendation 220
6.1.11 Limitation and future work 221
6.2 Application of Fuzzy C means clustering and Fuzzy EDAS to assess groundwater irrigation suitability and prioritization for agricultural development 222
6.2.1 Introduction 222
6.2.2 Research Gap and Novelty of work 223
6.2.3 Objective of the Research Work 224
6.2.4 Area of Investigation 224
6.2.5 Research Design and Methodology 224
6.2.5.1 Sample collection and preparation 224
6.2.5.2 Geostatistical modeling and clustering techniques 226
6.2.5.2.1 Fuzzy C-means clustering of geochemical data 226
6.2.5.2.2 Fuzzy EDAS for suitable irrigation zone prioritization 229
6.2.6 Results and Discussion 230
6.2.6.1 Groundwater hydrogeochemical statistics 230

6.2.6.2 Hydrogeochemical facies and geochemical evolution process 238
6.2.6.3 Correlation analysis 243
6.2.6.4 Derivation of irrigation water quality indices and its spatial distribution 245
6.2.6.5 Fuzzy C-means clustering 247
6.2.6.6 Fuzzy EDAS basin prioritization based on irrigational suitability indices 251
6.2.7 Conceptual outcome of the study and recommendations 251
6.2.8 Conclusion and Recommendation 254
6.2.9 Limitation and Future Work 255
Chapter 7 Novel adsorbents in remediation of hazardous environmental pollutants: In light of fluoride, iron and phosphate 256
7.1 Enhanced fluoride removal from groundwater using red and white kaolinite lithomarge to develop a low cost eco-friendly defluoridation unit 256
7.1.1 Introduction 256
7.1.2 Research Gap and Novelty of work 257
7.1.3 Objective of the study 258
7.1.4 Area of Investigation 258
7.1.5 Research Design and Methodology 259
7.1.5.1 Chemicals and consumables 259
7.1.5.2 Collection and synthesis of the natural adsorbent 260
7.1.5.3 Batch experiment analysis 260
7.1.5.4 Adsorption isotherm 261
7.1.5.5 Adsorption kinetics 262
7.1.5.6 Fixed bed column studies 263
7.1.5.7 Modeling of breakthrough curves 264
7.1.6 Results and discussion 265
7.1.6.1 Point of zero charge (PZC) 265
7.1.6.2 Influence of particle size on fluoride adsorption 266
7.1.6.3 Influence of stirring/agitation speed on fluoride adsorption 267
7.1.6.4 Influence of contact time on fluoride adsorption 267
7.1.6.5 Influence of pH of the solution 268
7.1.6.6 Influence of absorbent dose on fluoride adsorption 268
7.1.6.7 Influence of temperature on fluoride adsorption 269
7.1.6.8 Influence of initial fluoride concentration 271
7.1.6.9 Adsorption kinetics of fluoride 271

7.1.6.10 Adsorption isotherm 274
7.1.6.11 Continuous column experiment: Experimental setup and kinetic modeling of fixed-bed column leaching test 275
7.1.6.12 Characterization of the kaolinite lithomarge laterite: Before and after adsorption 278
7.1.6.13 Regeneration studies on the used natural adsorbent 282
7.1.6.14 Performance comparison of the natural adsorbent with others 283
7.1.7 Future plan and development of community based filtration system 286
7.1.8 Conclusion and Recommendation 287
7.1.9 Limitation and Future Work 288
7.2 Probing adsorption efficiency of low surface area hardwood biochar and its modification for an enhanced cationic (Fe+) and anionic (PO_4^{3-}) nutrient removal from aqueous solution 289
7.2.1 Introduction 289
7.2.2 Research Gap and Novelty of Work 290
7.2.3 Objective of the study 291
7.2.3.1 Research Design and Methodology 291
7.2.3.1.1 Materials used 291
7.2.3.2 Synthesis of magnesium oxide loaded-hardwood biochar 292
7.2.3.3 Microstructural, textural and elemental analysis: Characterization and analytical method 292
7.2.3.4 Batch adsorption experiments 292
7.2.3.5 Point of zero charge (pHpzc) analysis 293
7.2.3.6 Adsorption isotherm dynamics 294
7.2.3.7 Adsorption kinetic study 295
7.2.3.8 Error analysis 296
7.2.4 Results and Discussion 296
7.2.4.1 Biochar screening for iron and phosphate adsorption 296
7.2.4.2 Micro-structural and physico-chemical characterizations of biochars 298
7.2.4.3 Effect of pH on iron and phosphate removal 301
7.2.4.4 Effect of adsorbent dose on iron and phosphate removal 302
7.2.4.5 Adsorption performance of HW and MgO-HW for iron and phosphate removal 303
7.2.4.5.1 Effect of initial concentration and adsorption isotherm studies 303
7.2.4.5.2 Effect of contact time and kinetics study 307
7.2.4.6 Plausible mechanism and after adsorption feedstock characterization 311

7.2.5 Economic analysis and future work 313
7.2.6 Conclusion and Recommendation 314
7.2.7 Limitation and Future Work 314
Chapter 8 Overall Conclusion and Recommendations 316
Chapter 9 Appendix…….. 319
Chapter 10 References 332

LIST OF TABLES

Table 1.1 Comparative assessment of groundwater resource of India from 2004-2022 (CGWB, 2022) 8

Table 3.1 Computational algorithm of the morphometric parameters of the basin 41

Table 3.2 Computation of morphometric parameters of the Sub-basins of Shilabati River 52

Table 3.3 Computation of Inter-correlation matrix of 14 selected geomorphic parameters 59

Table 3.4 Principal Component Unrotated and rotated loading matrix of 14 morphometric parameters 59

Table 3.5 Identification of the most influencing parameter for sub-basin clustering 60

Table 3.6 Computational table of ANOVA as extracted from SPSS software 61

Table 3.7 Classification of sub basin into cluster 61

Table 3.8 Prioritization of sub-basins using 18 morphometric parameters and MCDM models 63

Table 3.9 Selection of best model using SCCT 64

Table 4.1 Triangular Fuzzy Scale 75

Table 4.2 Normalized Fuzzy Direct Relation Matrix of the selected long term drought indices 77

Table 4.3 De-Fuzzified and Normalized Direct Relation Matrix of the selected long term drought indices 77

Table 4.4 Total Direct Relation Matrix of the selected long term drought indices 77

Table 4.5 Prominence and relation axis for cause and effect 78

Table 4.6 Percentage wise distribution of the drought risk zone in different blocks 92

Table 4.7 Yield anomaly index 92

Table 4.8 Calculated compound factor for block prioritization using long term drought indices 93

Table 4.9 Information of data acquired 101

Table 4.10 Locational description of wells 101

Table 4.11 Areal description of LULC class 112

Table 4.12 Locational description of wells based on LULC change from 1989-2018 113

Table 4.13 Results of Mann Kendall test statistics 122

Table 4.14 Details of the cluster analysis as executed from XLSTAT software 124

Table 4.15 Drought and non-drought years as analysed from Standard Groundwater Level Index 126

Table 5.1 Comparative analysis of the studies related to groundwater potential zone mapping/modelling 131

Table 5.2 Triangular Fuzzy Scale (Chang, 1996) 140

Table 5.3 Areal distribution of the groundwater potential zone using ML and MCDM techniques 150

Table 5.4 Areal distribution of the groundwater potential zone in different sub-basins 150

Table 5.5 Aquifer resistivity, thickness, groundwater potential from VES survey and models and Sustainable management plan for different groundwater potentiality and development sites 155

Table 5.6 Effective radius and pore function of estimating hydraulic conductivity from grain size analysis 165

Table 5.7 Soil particle size distribution of estimation of hydraulic conductivity from statistical grain size analysis 171

Table 5.8 Hydraulic conductivity measure and calculated using empirical algorithms 172

Table 5.9 Summarization of observed data mini-piezometer 176
Table 5.10 Boundary conditions for groundwater flow modelling using MIKE FEFLOW 178
Table 5.11 Conditioning factors for identification suitable sites for MAR. 182
Table 5.12 Ranking of sampling sites based on Fuzzy MCDM models 184
Table 5.13 Spearman's rank correlation among the fuzzy MCDM models 185
Table 5.14 Aquifer parameters as obtained from the pumping test 188
Table 6.1 Summary of past studies in aquifer vulnerability 197
Table 6.2 Triangular fuzzy scale (Bakeshlou et al. 2017) 200
Table 6.3 Pairwise comparison matrix of fourteen thematic layers for identification of soil loss susceptible zone 214
Table 6.4 Descriptive statistics of the water quality parameters 215
Table 6.5 Water quality status of the sampling village sites 217
Table 6.6 Geological scenarios of sampling sites 226
Table 6.7 Linguistic fuzzy scale 229
Table 6.8 Descriptive statistics of the groundwater quality parameters 232
T**able 6.9** Descriptive statistics of the irrigation suitability parameters 246
Table 6.10 Validity scores of the Fuzzy C-means clustering technique 251
Table 7.1 Groundwater sampling sites 260
Table 7.2 Thermodynamic parameters for the adsorption of Fluoride on Kaolinite lithomarge 270
Table 7.3 Results of rate kinetics model fit and correlation coefficients for fluoride adsorption 274
Table 7.4 Applications of the adsorption isotherms in the adsorption of fluoride 275
Table 7.5 Results of fixed bed column leaching test 277
Table 7.6 EDX elemental analysis of red and white kaolinite lithomarge laterite soil 278
Table 7.7 Comparison of various adsorbents and their potency for fluoride removal 284
Table 7.8 Surface area of different biochars 290
Table 7.9 Equilibrium isotherm models used for the iron and phosphate uptake onto hardwood and MgO hardwood 295
Table 7.10 Equilibrium kinetic models used for the iron and phosphate uptake onto hardwood and MgO hardwood 296
Table 7.11 Different error functions used for equilibrium isotherm/kinetics analyses 296
Table 7.12 BET Surface Area Analysis of Hardwood and MgO-Hardwood 298
Table 7.13 Elemental composition as revealed by EDX 301
Table 7.14 Adsorption isotherm parameters for the adsorption of iron and phosphate onto Hardwood and MgO-Hardwood 307
Table 7.15 Parameters for various kinetic models for iron and phosphate removal 311
Table 7.16 Comparative analysis of adsorbent cost 314

LIST OF FIGURES

Fig. 1.1 A flowchart depicting the interconnectedness of climate change, surface and groundwater water resources, land management, and food resilience, along with the key stakeholders engaged in the whole process. 2

Fig. 1.2 Impact of climate change on global hydrological system 3

Fig. 1.3 State wise Irrigation Draft Vs Domestic & Industrial (CGWB, 2022) 4

Fig. 1.4 Aquifer system around the world and distribution of global water (Taylor et al. 2013) 5

Fig. 1.5 Predicted groundwater level trends across India (Malakar et al. 2021) 6

Fig. 1.6 Comparison of groundwater resources of West Bengal (Data source: CGWB, West Bengal, 2022) 8

Fig. 1.7 Major groundwater polltants arround the world 10

Fig. 1.8 Graphical plot showing occurrences of main groundwater research objectives in India 10

Fig. 1.9 Graphical plot shows the research work done till date on the major pollutants in India 11

Fig. 1.10 Graphical plot showing the application of frequently used modelling techniques in groundwater studies 13

Fig. 1.11 Graphical Plot showing the collaborative behavior of major countries of the world conducting groundwater research 13

Fig. 1.12 Graphical plot showing the application of DRASTIC in groundwater vulnerability studies 14

Fig. 2.1 (a) Location of the Shilabati river basin; (b) deforestation of the river basin and rill ad gullies within the river basin 21

Fig. 2.2 Soil map of the river basin 22

Fig. 2.3 Geomorphology of the river basin 23

Fig. 2.4 Areal distribution of Land use and Land cover from 1989-2021 24

Fig. 2.5 Spatio-temporal distribution of the land use and land cover from 1989-2021 25

Fig. 2.6 Steps for the calculation of runoff using SCS-curve number 26

Fig. 2.7 Output from SWAT tool and validation of the results using the observed data from Kadam Deuli Dam 27

Fig. 2.8 Total runoff of the sub-basins for the year 2000, 2014, 2018 and 2021 using SCS-curve number 28

Fig. 2.9 Slope of the river basin 29

Fig. 2.10 Drainage Density of the river basin 30

Fig. 2.11 Relative relief of the river basin 31

Fig. 2.12 Geology of the river basin 32

Fig. 2.13 Average monthly of the river basin from 1998-2021 33

Fig. 2.14 Groundwater recharge of river basin based on GEC, 2007 methodology 34

Fig. 2.15 Index Map of the Study Area 37

Fig. 3.1 Location of the Shilabati river basin (A) Degrading condition of the Joypanda sub-watershed (B) Lateritic Ravine at the middle stretch 44

Fig. 3.2 Flowchart depicting the methodology of the study 49

Fig. 3.3 Stream ordering of the sub-basins 53

Fig. 3.4 Different morphological aspects of the basin (a) form factor; (b) elongation ratio; (c) circularity ratio; (d) stream frequency; (e) drainage density and (f) constant of channel maintenance 55

Fig. 3.5 Different morphometric aspects of the river basin (a) infiltration number; (b) length of overland flow; (c) drainage texture; (d) ruggedness index; (e) dissection index and (f) hypsometric integral 56
Fig. 3.6 Prioritization of the river basin based on MCDM techniques (A) TOPSIS (B) VIKOR (C) COPRAS (D) Condition of the Joypanda sub-basin 63
Fig. 3.7 Validation of the model using groundwater yield 65
Fig. 4.1 Location of the area of interest 69
Fig. 4.2 Adopted methodological flow chart of the present study 70
Fig. 4.3 Interaction between M2 and M1 75
Fig. 4.4 Average monthly rainfall (mm) from 1998 to 2018 of Shilabati river basin 79
Fig. 4.5 Spatio-temporal distribution of SPI 2000 80
Fig. 4.6 Spatio-temporal distribution of SPI 2009 81
Fig. 4.7 Spatio-temporal distribution of SPI 2018 82
Fig. 4.8 Spatio-temporal distribution of LST 84
Fig. 4.9 Spatio-temporal distribution of LST 84
Fig. 4.10 Spatio-temporal distribution of VCI and TCI 85
Fig. 4.11 Spatio-temporal distribution of NDWI 87
Fig. 4.12 Spatio-temporal distribution of SMI 87
Fig. 4.13 Spatio-temporal distribution of SAVI 88
Fig. 4.14 Seven selected long-term drought indices 90
Fig. 4.15 Delineated drought risk zone map 91
Fig. 4.16 Cause and effect relationship 91
Fig. 4.17 Calculated compound factor for block prioritization using long term drought indices 94
Fig. 4.18 Cropping pattern practiced within the study area 95
Fig. 4.19 Location of the study area 100
Fig. 4.20 Digital Elevation Model 103
Fig. 4.21 Geology of the study area 103
Fig. 4.22 Aquifer depth of the study area 104
Fig. 4.23 Geomorphology of the study area 104
Fig. 4.24 Soil map of the study area 105
Fig. 4.25 Slope map of the study area 105
Fig. 4.26 Cropping pattern of the study area 106
Fig. 4.27 Graphical representation of Average monthly rainfall and groundwater level (1998-2018) 111
Fig. 4.28 Land use and land cover map of 1989 114
Fig. 4.29 Land use and land cover map of 2000 114
Fig. 4.30 Land use and land cover map of 2009 115
Fig. 4.31 Land use and land cover map of 2018 115
Fig. 4.32 Groundwater level at Premonsoon, Monsoon and Post monsoon 1996 117
Fig. 4.33 Groundwater level at Premonsoon, Monsoon and Post monsoon 2001 117
Fig. 4.34 Groundwater level at Premonsoon, Monsoon and Post monsoon 2006 118
Fig. 4.35 Groundwater level at Premonsoon, Monsoon and post monsoon 2011 118
Fig. 4.36 Groundwater level at Premonsoon, Monsoon and post monsoon 2016 119
Fig. 4.37 Dendrogram of the clusters 124

Fig. 4.38 Map showing 4 clusters of Well 124
Fig. 4.39 The Box and Whisker plot of the fluctuation variation of well points 125
Fig. 4.40 Map showing Standard Groundwater Level Index of 2018 monsoon season 125
Fig. 5.1 Location of the study area with soil sampling and geophysical investigation sites 133
Fig. 5.2 Pseudo-sections and resistivity cross section of Guniada and Aralbara site (Upstream section) 134
Fig. 5.3 Pseudo-sections and resistivity cross section of Dumuria and Kantapal site (Middle stream section) 134
Fig. 5.4 Pseudo-sections and resistivity cross section of Sarai and Harisinghpur site (downstream section) 135
Fig. 5.5 Flowchart showing the methodology of the current research 143
Fig. 5.6 Conditioning factors as estimated from geophysical survey 146
Fig. 5.7 Aquifer parameters as estimated from geophysical survey 146
Fig. 5.8 Conditioning factors as estimated from soil sampling 148
Fig. 5.9 Importance of conditioning factors 149
Fig. 5.10 Groundwater potential map derived using machine learning models, (a) XGBoost model, (b) Random Forest model, (c) Naive Bayes model and (d) Fuzzy AHP 150
Fig. 5.11 Validation of different models through ROC curve 151
Fig. 5.12 Multiple Correspondance analysis between groundwater conditioing factors and groundwater potential zone using XGBoost 152
Fig. 5.13 Groundwater level map of the study area and (b) correlation coefficients between groundwater level and different models 154
Fig. 5.14 Location of the study and piezometer installation sites 162
Fig. 5.15 Flowchart for the determination of suitable MAR site for groundwater resource management 163
Fig. 5.16 Mini drive point piezometer (MDP) installation mechanism and sequential procedure for estimation of vertical gradient and slug test. (A) Using a hammer on the streambed, the steel cast is forged into the streambed. (B)The mini piezometer is slipped inside the steel casing. (C) In the streambed, the minipiezometer is held in place while the steel casing is removed. (D) Complete installation of minipiezometer for identification of gaining and losing stream 164
Fig. 5.17 Soil classification of the 19 sites plotted based on USDA soil classification 170
Fig. 5.18 Comparative analysis of hydraulic conductivity (K_h) from different estimation technique 170
Fig. 5.19 Losing and gaining stream conditions across the river basin 174
Fig. 5.20 Plotting of losing and gaining sites against hydraulic conductivity (K_h) 174
Fig. 5.21 Understanding the groundwater- stream water exchange under different hydro-environmental conditions 175
Fig. 5.22 Boundary conditions of the groundwater flow model with soil sampling sites and pumping wells 178
Fig. 5.23 Simulated hydraulic head and observation well in MIKE FEFLOW interface 179
Fig. 5.24 Groundwater head contours of the Shilabati river basin 179
Fig. 5.25 Observed vs. simulated hydraulic head for the period (2019-2022). 180
Fig. 5.26 Graphical representation and comparative analysis of rank obtained by sampling sites 184
Fig. 5.27 Drawdown (s) versus time data (t) Plotted on semi-log scale for aquifer Test (Neuman, 1972) 186
Fig. 5.28 Litholog of the main pumping well and the observation wells 188

Fig. 5.29 (A) Selected site, conductance of continuous pumping test and time vs. drawdown graph for main well; (B) time vs drawdown graph for observation wells (4) 190
Fig. 6.1 Location of the study and diagram of the stratigraphic profile (A–A') 201
Fig. 6.2 Modeling framework 202
Fig. 6.3 Maps of groundwater vulnerability conditioning factors (a) slope (b) soil cover (c) pH (d) Groundwater level (e) specific yeild (f) aquifer depth 206
Fig. 6.4 Geology of study area and litholog (A & B) 207
Fig. 6.5 Maps of groundwater vulnerability conditioning factors (a) hydraulic conductivity (b) impact of vadose zone (c) recharge (d) land use and land cover (e) population density (f) groundwater-based irrigation schemes 212
Fig. 6.6 (a) Importance of parameters (b) Groundwater Vulnerability Index (c) Areal distribution of groundwater vulnerable zone 213
Fig. 6.7 Spatial distribution of groundwater quality parameters (a) Total dissolve solids; (b) Electrical conductivity; (c) Iron; (d) Hardness; (e) Alkalinity and (f) Chloride 216
Fig. 6.8 Correlation between WQI and Groundwater Vulnerable Index 217
Fig. 6.9 Water Quality Index of different sites 218
Fig. 6.10 Validation of Groundwater vulnerable index using ROC curve showing area under the curve for hardness, alkalinity, iron and TDS 218
Fig. 6.11 Location of the study area and sampling sites 225
Fig. 6.12 Flowchart of the research methodology 227
Fig. 6.13 Spatial distribution of groundwater quality parameters (a) pH; (b) Temperature; (c) Electrical Conductivity; (d) Total Dissolve Solids; (e) Alkalinity and (f) Hardness 233
Fig. 6.14 Spatial distribution of groundwater quality parameters (a) Calcium; (b) Iron; (c) Magnesium; (d) Sodium; (e) Potassium and (f) ICP-OES 234
Fig. 6.15 Spatial distribution of groundwater quality parameters (a) Chloride; (b) Fluoride; (c) Bicarbonate; (d) Nitrate; (e) Phosphate and (f) Sulphate 235
Fig. 6.16 Box and Whisker plot for physicochemical parameters 236
Fig. 6.17 Box and Whisker plot for physicochemical parameters 237
Fig. 6.18 Scatter plot between Total Hardness (TH) versus Total Dissolve Solids (TDS) 238
Fig. 6.19 Piper diagram demonstrating the hydrochemical compositions of water 240
Fig. 6.20 Durov plot of the groundwater samples 240
Fig. 6.21 Gibbs diagram showing the natural mechanism of groundwater chemistry 241
Fig. 6.22 Gibbs diagram showing the natural mechanism of groundwater chemistry 241
Fig. 6.23 Chadha's diagram showing the water types for groundwater quality 242
Fig. 6.24 Ionic ratio of $Cl-$ versus $Na+/Cl-$ concentration in groundwater samples 242
Fig. 6.25 Correlation plot between the different hydrogeochemical parameters 243
Fig. 6.26 Correlation plot between different hydrogeochemical parameters 244
Fig. 6.27 Spatial distribution of irrigation suitability parameters over the basin. 248
Fig. 6.28 (a) USSL classification of the groundwater samples; (b) Wilcox classification of the groundwater samples; (c) Doneen's permeability index of the groundwater samples 249
Fig. 6.29 Fuzzy c-means clustering of the groundwater sampling sites 250
Fig. 6.30 Fuzzy EDAS based prioritization of the basin for groundwater management and the predominant crops within the river basin 253
Fig. 7.1 Location of the study area (a) Shilabati river basin in West Bengal with fluoride affected districts, (b) fluoride affected blocks within the river basin and groundwater sampling sites,

(c) evidences of skeletal fluorosis and bone deformation among villagers, (d) water sampling tube well and (e) collection site of natural adsorbent (Garbeta, Paschim Medinapore district)..... 259

Fig. 7.2 (a) Schematic diagram of the fixed bed column used in laboratory; (b) Particle size distribution of sand for determination of effective grain size 264

Fig. 7.3 Point of zero charge (P_{ZC}) for (a) red kaolinite lithomarge laterite soil and (b) white kaolinite lithomarge laterite soil. 266

Fig. 7.4 Influence of particle size in fluoride removal efficiency for (a) red and (b) white type 266

Fig. 7.5 Influence of agitation speed in fluoride removal efficiency for (a) red and (b) white type 267

Fig. 7.6 Influence of contact time in fluoride removal efficiency for (a) red and (b) white type 268

Fig. 7.7 Influence of ph of the solution (a) red and (b) white type; influence of adsorbent dose: (c) red and (d) white type and influence of temperature on fluoride adsorption: (e) red and (f) white type 270

Fig. 7.8 Influence of initial concentration in fluoride removal efficiency for red and white type 271

Fig. 7.9 Pseudo-first-order model for fluoride absorption onto (a) red and (b) white kaolinite lithomarge laterite soil; Pseudo-second-order model for fluoride absorption onto (c) red and (d) white kaolinite lithomarge laterite soil and Intra-particle diffusion model for fluoride absorption onto (e) red and (f) white kaolinite lithomarge laterite soil 273

Fig. 7.10 Langmuir model for fluoride absorption onto (a) red and (b) white kaolinite lithomarge laterite soil; Freundlich model for fluoride absorption onto (c) red and (d) white kaolinite lithomarge laterite soil and Temkin model for fluoride absorption onto (e) red and (f)white kaolinite lithomarge laterite soil 276

Fig. 7.11 FESEM characterizations of red and white type, (a) Red kaolinite lithomarge laterite-before adsorption; (b) Red kaolinite lithomarge -after adsorption; c) White kaolinite lithomarge –before adsorption and d) White kaolinite lithomarge – after adsorption 279

Fig. 7.12 EDX spectra of red and white laterite soil adsorbent, (a) Red laterite-before adsorption; (b) Red laterite-after adsorption (c); White laterite –before adsorption (d) and White laterite-after adsorption 280

Fig. 7.13 Fourier Transformation Infrared (FTIR) spectral data of (a) before and (b) after application of red kaolinite lithomarge laterite soil and (c) before and (d) after application of white kaolinite lithomarge laterite soil 281

Fig. 7.14 X-ray diffraction pattern of kaolinite lithomarge of (a) red and (b) white type and (c) possible mechanism of fluoride adsorption on Alpha Trigonal SiO_3 and Alpha Hexagonal Al_2O_3 pattern revealed from XRD data..... 282

Fig. 7.15 Reusability study of red and white kaolinite lithomarge-laterite 283

Fig. 7.16 Schematic diagram of the low-cost rural household filter for fluoride removal 287

Fig. 7.17 Point of zero charge (PCZ) of hardwood and (b) point of zero charge of MgO-Hardwood 294

Fig. 7.18 Biochar screening for selection of biochar for (a) iron and (b) phosphate removal..... 297

Fig. 7.19 Zeta potential distribution of hardwood and MgO-hardwood biochar..... 299

Fig. 7.20 (a) FESEM micrographs of hardwood; (b) FESEM micrographs of MgO-hardwood; (c) EDS spectrum of Hardwood; (d) EDS spectrum of MgO-Hardwood; (e) XRD Spectra of Hardwood and (d) XRD spectra of MgO-Hardwood biochar..... 300

Fig. 7.21 FTIR spectra of hardwood and MgO-Hardwood feedstock..... 301

Fig. 7.22 Effect of initial solution pH on (a) iron adsorption and (b) phosphate adsorption..... 302

Fig. 7.23 Effect of adsorbent dose on (a) iron and (b) phosphate removal 303

Fig. 7.24 Effect of initial concentration on (a) iron and (b) phosphate removal 304

Fig. 7.25 Adsorption isotherm of iron uptake by hardwood (a) Langmuir; (b)Freundlich (c)Temkin; (d) Elovich and (e) Dubinin-Radushkevich (D-R)..... 305

Fig. 7.26 Adsorption isotherm of phosphate uptake by MgO-hardwood (a) Langmuir; (b)Freundlich (c)Temkin; (d) Elovich and (e) Dubinin-Radushkevich (D-R)..... 306

Fig. 7.27 Adsorption kinetics of iron uptake by Hardwood (a) effect of time on adsorption; (b) Pseudo 1^{st} order (c) Pseudo 2^{nd} order; (d) Non-linear Elovich kinetic and (e) Non-linear IDPM..... 309

Fig. 7.28 Adsorption kinetics of phosphate uptake by MgO-Hardwood (a) effect of time on adsorption; (b) Pseudo 1^{st} order (c) Pseudo 2^{nd} order; (d) Elovich kinetic and (e) Non-linear IDPM..... 310

Fig. 7.29 Plausible Mechanism of (a) iron and (b) phosphate removal..... 312

LIST OF PICTURES

Picture 2.1 Drying condition of the Shilabati River 35
Picture 2.2 Fall in groundwater level in dug wells within the river basin 35
Picture 2.3 (a) Contaminated dug well used for domestic purpose and (b) people effected with bone deformation and skeletal fluorosis within the river basin..... 36

LIST OF ABBREVIATIONS

AHP Analytical Hierarchy Process
ANN Artificial Neural Networks
ANOVA Analysis of Variance
ARIMA Autoregressive Integrated Moving average
MSL Mean Sea Level
AUC Area under the ROC Curve
AVHRR Advanced Very High-Resolution Radiometer
AVI Aquifer Vulnerability Index
GOD G-Groundwater Hydraulic Confinement, O—Overlying Aquifer Strata
SI Susceptibility Index
BCM Billion Cubic Meters
BET Brunauer-Emmett-Teller
BIS Bureau of Indian Standards
HW Hardwood
CART Classification and Regression Trees
CD Community Development Block
CF Compounding Factor
CFCS Converting Fuzzy data into Crisp Scores
CGWB Central Ground Water Board
CHIRPS Climate Hazards Group InfraRed Precipitation with Station data
COPRAS Complex Proportional Assessment
DEM Digital Elevation Model
DEMATEL Decision Making Trial and Evaluation Laboratory
DGPS Differential Global Positioning System
DRASTIC Depth to Water, Net Recharge, Aquifer Media, Soil Media, Topography, Impact of the Vadose Zone, And Hydraulic Conductivity of the Aquifer
EDTA Edetic Acid and Etheylenediaminetetraacetic Acid
EIA Environmental Impact Assessment
EPIK Epikarst, Protective cover, Infiltration conditions and Karst network development
ERT Electrical Resistivity Tomography
GEP Gene Expression Programming
FAO Food and Agriculture Organization
FCM Fuzzy C-means Clustering
FPR False Positive Rate
FSE-GVI Fuzzy Shannon Entropy Groundwater Vulnerability Index
FTIR Fourier Transform Infrared
NAF Sodium Fluoride
GEC Ground Water resource Estimation Committee
GIS Geographical Information System
GMS Groundwater Modeling System
EDAS Evaluation Based on Distance from Average Solution
GMSL Global Mean Sea Level
GRACE Gravity Recovery and Climate Experiment.
GSI Geological Survey of India
GWL Groundwater Level
GWPI Groundwater Potential Index
GWPZ Groundwater Potential Zone
GWS Groundwater Storage
HCA Hierarchical Cluster Analysis
IBE Ionic Balanced Equation
ATSDR Agency for Toxic Substances and Disease Registry
IBM International Business Machines
ICAR-ATAR Indian Council of Agricultural Research -Agricultural Technology Application Research Institute
ICP-OES Inductively Coupled Plasma Optical Emission Spectroscopy
IFS Intuitionistic Fuzzy Sets
IMD India Meteorological Department
IPCC Intergovernmental Panel on Climate Change
IWD Inverse Distance Weighted
KNNK-Nearest Neighbor
LGWP Low Groundwater Potential

LST Land Surface Temperature
LULC Land use and Land Cover
MAE Mean Absolute Error
MAR Managed Aquifer Recharge
MCA Multiple Correspondence Analysis
SVM Support Vector Machine
MCDM Multi-Criteria Decision Analysis
MDP Mini Drive-Point Piezometer
MGWP Moderate Groundwater Potential
MH Magnesium Hazard
MLA Machine Learning Algorithm
MLD Million Liters per Day
NBSS LUP National Bureau of Soil Survey & Land Use Planning
MODFLOW Modular Three-Dimensional Finite-Difference Ground-Water Flow Model
MODIS Moderate Resolution Imaging Spectroradiometer
MRL Maximum Residue Level
MSE Mean Square Error
NABARD National Bank for Agriculture and Rural Development
CNN Convolutional Neural Network
NASA National Aeronautics and Space Administration
NB Naïve Bayes Classifier
NDVI Normalized Difference Vegetation Index
NDWI Normalized Difference Water Index
NIR Near Infrared
NOAA National Oceanic and Atmospheric Administration
NPK Nitrogen, Phosphorus, and Potassium
NTU Nephelometric Turbidity Unit
OLI Operational Land Imager
PCA Principal Component Analysis
PD Percentage Deviation
PEST Parameter Estimation and Uncertainty Analysis
PGWP Poor Groundwater Potential
PHED Public Health Engineering Department
PI Permeability Index
PS Potential Salinity
PSO Pseudo-Second-Order
PTEE Polytetrafluoroethylene
PVC Poly Vinyl Chloride
PFO Pseudo-First-Order
RAI Rainfall Anomaly Index
RF Random Forest
RMSE Root Mean Square Error
ROC Receiver Operating Characteristic Curve
RSBC Residual Sodium Bicarbonate
RSE Residual Sodium Carbonate
SAR Sodium Adsorption Ratio
SAVI Soil Adjusted Vegetation Index
SCCT Spearman's Rank Correlation Coefficient
SCS Soil Conservation Service
SGWI Standard Groundwater Level Index
SINTACS Water table depth (S), Effective infiltration (I), Unsaturated zone (N), Soil media (T), Aquifer media (A), Hydraulic conductivity zone (C), Topographic slope (S)
SMI Soil Moisture Index
SPI Standard Precipitation Index
SPSS Statistical Package for Social Sciences
SRTM Shuttle Radar Topography Mission
SSP Soluble Sodium Percentage
SWAT Soil & Water Assessment Tool
SWID State Water Investigation Directorate
RS Remote Sensing
GIS Geographical Information System
AHC Agglomerative Hierarchical Clustering
TCI Temperature Condition Index
TDS Total Dissolved Solids
TFN Triangular Fuzzy Number
TLC Temperature, Water Level and Conductivity Meter
ASTM American Society for Testing and Materials
TPR True Positive Rate
USBR United States Bureau of Reclamation
USDA U.S. Department of Agriculture

USGS United States Geological Survey
USSL US Salinity Laboratory
VCI Vegetation Condition Index
VES Vertical Electrical Sounding
VHG Vertical Hydraulic Gradient
VHGWP Very High Groundwater Potential
VHI Vegetation Health Index
VIKOR VlseKriterijumska Optimizacija I Kompromisno Resenje
VIS Visible Imagery Sensor
TOA Top of the Atmosphere
DN Digital Number
WBPCB West Bengal Pollution Control Board
WHO World Health Organization
YAI Yield Anomaly Index

ABSTRACT

The Shilabati river basin, situated in the southeastern part of West Bengal, India, is facing a severe groundwater crisis. This tropical plateau fringe region, originating from the Chotonagpur gneissic complex, experiences poor groundwater recharge and suffers from annual droughts, leading to prolonged water scarcity. Human activities, natural phenomena, and climate change have adversely affected the groundwater in the Puruliya, Bankura, and West Medinapore districts of West Bengal. These factors release harmful elements into the water, with high concentrations of fluoride (>2 mg/l) being particularly detrimental. The increased presence of fluoride in the Shilabati river basin has resulted in numerous cases of skeletal fluorosis and bone deformations in recent years. To gain insights into the groundwater and surface water interaction and facilitate contaminant remediation using eco-friendly materials, an integrated approach combining field and laboratory investigations was employed. This comprehensive study involved a thorough desk study, a field survey of all sub-basins, groundwater and soil sampling, geophysical surveys, pumping tests, piezometer installations, as well as laboratory-based experimental and instrumental analyses.

To achieve the research objectives, morphometric attributes of nine sub-watersheds within the Shilabati river basin, covering a total area of 3881 km^2, were estimated. Principal Component Analysis was utilized to group these attributes into three components, and K-means clustering was applied to categorize the sub-watersheds into three clusters based on morphometric asymmetry. Through statistical and decision-making models, the Donai sub-watershed emerged as the top-ranked area, displaying a greater amplitude in recharging its aquifer with well yield capacities ranging from 200-400 LPM (Litres per Minute). On the other hand, sub-watersheds like Betal and Joypanda require sustainable management at a priority level, as validated by groundwater yield data, with well yield capacities ranging from 10-100 LPM. To investigate groundwater degradation, 20 wells from the West Bengal river basin were selected for analyzing their seasonal groundwater level trends using the Mann Kendall test statistics from 1996-2018. The results revealed that 60% of the wells exhibited a decline in water levels, particularly during the post-monsoon season. By utilizing Fuzzy Decision-Making Trial and Evaluation Laboratory (DAMETAL), this study combined earth observation data with ancillary data to predict drought risk zones. Three years of rainfall deficit from the normal were selected using Standard Precipitation Index (SPI), Long-term Temperature Condition Index (TCI), Long-term Vegetation Condition Index (VCI), Vegetation Health Index (VHI), Long-term Soil Moisture Index (SMI), Long-term Soil Adjusted Vegetation Index (SAVI) and Long-term Normalized Difference Water Index (NDWI) for the fuzzy DAMETAL model. An increase in negative Standard Precipitation Index values in recent years serves as a primary indicator of drought within the river basin. This research introduced a novel approach by applying data generated from the field survey to identify groundwater potential zones using a comparative framework of machine learning and fuzzy logic techniques. Spatial associations between groundwater yield data and each conditioning factor were calculated using 197 wells (70%) as training data and 88 wells (30%) as testing/validation data. In comparison to the Random Forest (0.67), Naïve Bayes (0.71), and Fuzzy Analytic Hierarchy Process (AHP) (0.68) techniques, XGBoost achieved an AUC of 0.79. XGBoost also exhibited a correlation coefficient of 0.78 when compared with groundwater-level data.

In the current study, subsurface characteristics within the complex formation of the Shilabati basin system in West Bengal, India were estimated using a cost-effective piezometer and MIKE FEFLOW based on a steady-state numerical model. This study represents the first attempt to identify suitable sites for implementing Manage Aquifer Recharge (MAR) technology in West Bengal, India, aiming to manage extreme drought events. The hydraulic conductivity values, calculated from piezometer installations, range from 0.00206 to 6.765 m/day, with the highest value observed at the Dakshin Pairachali site. This study holds significant potential for researching the interaction between ground and surface water, thereby addressing the conditions of losing and gaining streams within the channel. Out of the 19 sites where piezometers were installed, 5 exhibit losing conditions, while 14 sites demonstrate gaining conditions, with Vertical Hydraulic Gradients (VHGs) ranging from -0.21 to -1.07 and 0.01 to 3.14, respectively. The presence of such losing stream systems makes them unsuitable for MAR sites due to the risk of polluted water seeping into adjoining aquifers, which would contaminate ecosystems, as well as irrigation and drinking water quality.

The MIKE FEFLOW model was successfully run and calibrated for four years (2019-2022) in steady-state mode, utilizing scarce datasets for the entire river basin. The groundwater head ranges from 160.33 to -0.32 m.a.s.l, providing valuable information on the direction of flow and aiding the identification of suitable MAR sites. The model results have shown competence and a reasonable level of accuracy (0.90) in matching the observed groundwater levels at 47 sites. Additionally, this study introduces a novel approach to identify groundwater vulnerable zones by combining Fuzzy Shannon Entropy (FSE) with a decision support algorithm, which replaces conventional methods such as DRASTIC and GOD. The groundwater in the river basin is rated on a scale ranging from excellent to unfit for consumption, and a comparison of the model with 74 groundwater quality data points reveals an excellent correlation with the water quality index (r=0.84), Total Dissolved Solids (70%), iron (72%), hardness (85%), and alkalinity levels (75%). The research findings indicate that 27.3% of the sampled sites (villages) have poor water quality, and 23.21% exhibit a very high vulnerability zone, emphasizing the need for competent planning, development, and managerial techniques to safeguard groundwater resources. Furthermore, this study focuses on identifying a river basin suitable for agriculture and prioritizing its management using a new clustering tool based on fuzzy logic techniques in R and Geographical Information System. The derived fuzzy C-mean clustering (FCM) method outperforms other commonly used hard computing techniques such as Hierarchical Clustering, K-means clustering, and Agglomerative Clustering. It divides the sampling sites into two clustering groups (FCM I & FCM II), which have been validated using fuzzy silhouette index (0.85), the partition coefficient (0.76), the partial entropy (0.68), and the modified partition coefficient (0.52). Additionally, hydrogeochemical analysis confirms the predominance of rock-water interaction, chemical weathering, and ion exchange processes in the aquifer system of the study area. According to the correlation plots, the studied groundwater samples largely evolved from Ca^{2+}-HCO_3^-, Mixed Ca^{2+}-Mg^{2+}-Cl^- types, and HCO_3^-–Ca^{2+}types. A Fuzzy EDAS priority map has been prepared based on all the irrigation suitability parameters concludes that the groundwater at the upstream and downstream section of the basin requires the most attention. Based on the highest priority for management, five zones have been delineated: very high (5.98%), high (22.31%), medium (16.39%), low (32.30%), and very low (23.02).

Based on the analysis of groundwater quality, it has been observed that iron, phosphate, and fluoride are the prominent pollutants within the river basin. This study focused on investigating fluoride adsorption on kaolinite

lithomarge (red and white laterite) from Paschim Medinapore (West Bengal, India). It explored both kinetic and equilibrium aspects through a series of batch tests and a fixed bed column study using natural water. The experimental results revealed that, among the pH values relevant to fluoride-enriched groundwater, the red type of kaolinite lithomarge exhibited the highest removal efficiency (98.32%) at pH 6.58, while the white type demonstrated a removal efficacy of 95.31% at pH 6.51. Water samples were collected from 11 sites within the fluoride-contaminated zone of the river basin, and natural groundwater was filtered using the red type of kaolinite lithomarge. The filtration process achieved a removal capacity of 97.13% within 30 minutes, for an initial fluoride concentration of 2.37 mg/l. The laboratory-tested prototype showed promising results in contaminant removal, offering a low-cost and time-saving natural filtration option that provides one liter of fluoride-free water for 0.0015 USD. Additionally, low-cost hardwood wastes (HW) ($4.46/kg) with a low surface area (6.87 m^2/g) and magnesium-impregnated hardwood modified (MgO-HW) biochar were developed for the removal of iron and phosphate from aqueous solutions. The HW and MgO-HW biochar exhibited excellent Dubinin-Radushkevich isotherm (D-R) maximum adsorption capacities of 289.45 mg/g and 828.82 mg/g for iron and phosphate, respectively. These capacities were attributed to the well-developed pore structures with high magnesium content in MgO-HW and the abundant oxygen-containing functional groups in HW biochar. This work highlights the potential of using natural adsorbents, especially for fluoride, iron, and phosphate removal at a low cost. It also opens up new opportunities for separating pollutants from the aquatic environment using eco-friendly materials. Increased investments and efforts should be directed towards implementing all the suggestions and recommendations highlighted in this study. These actions will benefit not only the local people of the basin but also the entire world, given the current era of water-related issues.

Chapter1

Research Background

1.1 Introduction

1.1.1 Issues and Challenges of Groundwater Water under Changed Climate Scenario

The rise in global temperatures and its subsequent effects on the climate system have a significant impact on water resources. These effects include rising sea levels, melting glaciers, changes in rainfall patterns, and soil moisture. The combination of a growing population, increasing water consumption demand, and the complex interplay with climate change further exacerbates the challenge of water scarcity (Swain et al. 2022). According to data from NOAA 2023, the globally averaged earth surface temperature in the year 2022 (including both land and ocean) was 0.86°C, making it the sixth warmest year on record since 1880 (Ouhamdouch et al. 2022). If current human actions continue to intensify global warming at the same rate, it is projected that the global temperature may reach a 1.5°C increase between 2030 and 2052. Such higher temperatures will disrupt the hydrological cycle by accelerating water evaporation, leading to droughts in certain regions, while other areas experience extreme precipitation events (Famiglietti, 2014). Overall, the worldwide precipitation rate over land areas has increased by 0.1 inches/decade. One long-term consequence of rising temperatures is the gradual rise in sea levels. Over the past 150 years, global mean sea level (GMSL) has increased by approximately 7.87 inches (around 3.3 mm/year) due to the melting of glaciers and thermal expansion caused by the accumulation of heat in the oceans (NOAA 2023). In addition to these long-term changes, scientists have observed a connection between climate change and compounded events such as floods and droughts. Such events have detrimental impacts on society and pose risks to water security (Li et al. 2022).

India experiences a diverse range of climatic conditions, characterized by extreme cold winters in the north and tropical weather conditions in the southern section. The northeastern sections of the country experience hot and humid climate, while the northwestern regions are dry and semi-arid/arid (Joshi et al. 2020). Agricultural yields in India heavily depend on rainfall during the southwest monsoon season, which occurs from June to September (Kumar et al. 2022). Agricultural production is severely impacted by extreme weather events such as floods, hailstorms, droughts, heat waves, cold waves, flash floods and cyclones. According to the 6th Assessment Report of the Intergovernmental Panel on Climate Change (IPCC, 2021), climate change has been reaffirmed as a significant factor affecting agriculture with far-reaching consequences. Rising atmospheric temperatures directly affect crop duration, process of photosynthesis, and eventually agricultural yield (Roy et al. 2022). They also influence the survival and spatial distribution of pest populations, accelerate mineralization of soil nutrient, decrease efficiency of nutrient use, and increase loss of water, leading to a greater demand for irrigation water and

nutrients from plants (Singh et al. 2020). Climate change indirectly impacts agricultural system through its effects on irrigational water accessibility, floods, droughts, soil fertility, and its respective erosion (Shah, 2009) (Fig.1.1)

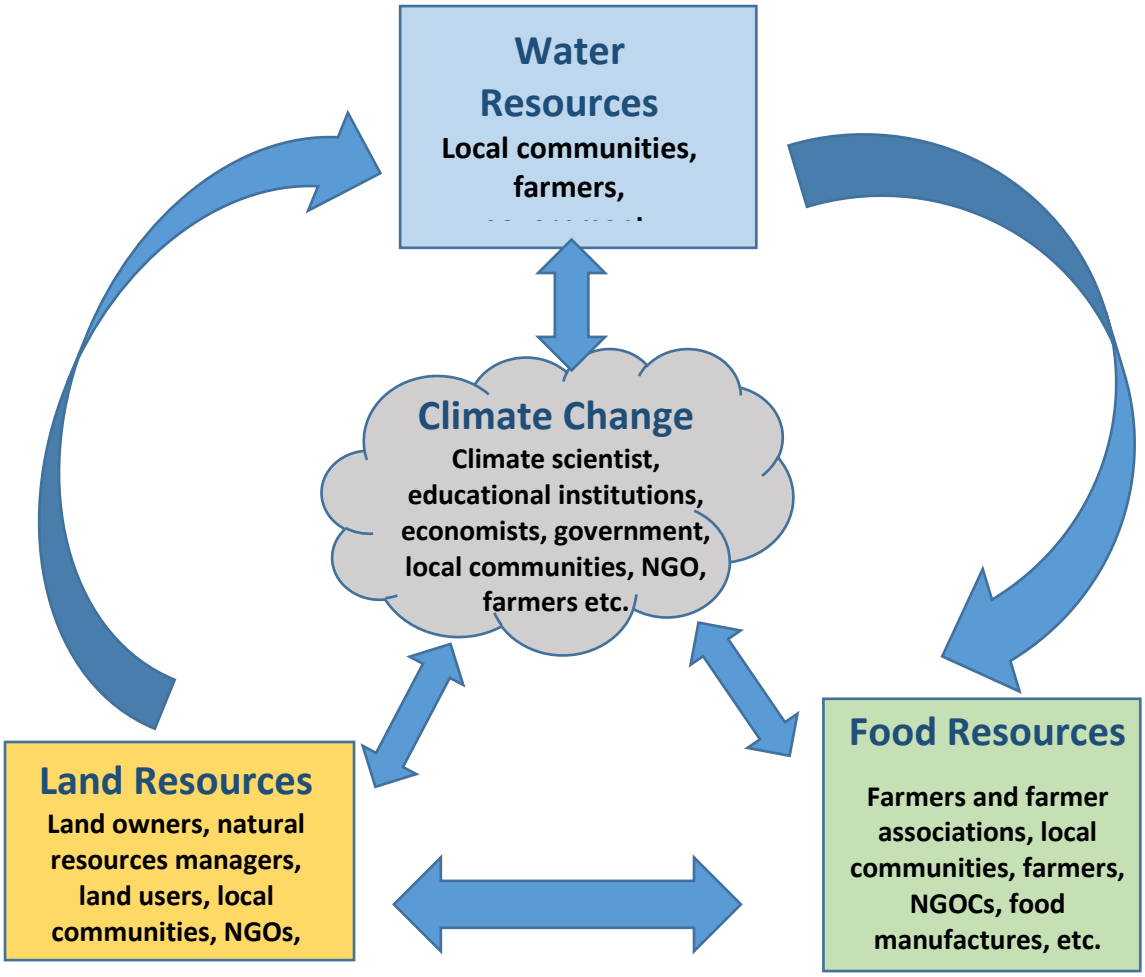

Fig. 1.1 A flowchart depicting the interconnectedness of climate change, surface and groundwater water resources, land management, and food resilience, along with the key stakeholders engaged in the whole process.

Groundwater recharge occurs when rainwater permeates through the soil, replenishing the groundwater table and serving as a decisive water source in arid/semi-arid areas. The demand for water in India's growing food, industry and domestic sectors is supplied by groundwater, which is extensively utilized by various users (Haq et al. 2021). Additionally, recharge from seepage losses in irrigation networks together with deep infiltration from farm irrigation contribute to the accumulation of groundwater (Patel et al. 2020). Irrigation from all available sources has played a significant role in enhancing agricultural yield in semi-arid and arid regions. Due to the seasonal nature of rivers in these areas, groundwater remains the only dependable water source (Pande et al. 2020) (Fig.1.2). Wells can be found in various parts of the semi-arid regions, particularly upstream of river basins. However, these regions face severe water issues, both in terms of quality and quantity, as evidenced by substantial seasonal declines in groundwater levels (Sithara et al. 2020).

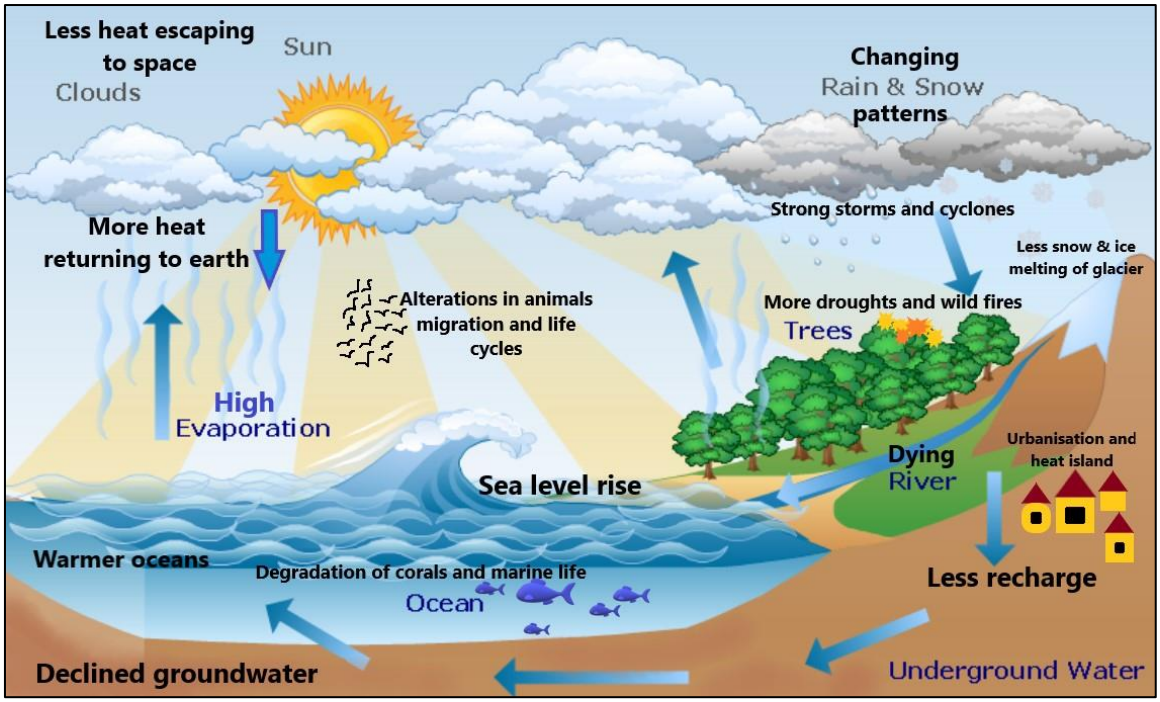

Fig. 1.2 Impact of climate change on global hydrological system

Irrigation system for agriculture in India has two major components one is surface or canal irrigational system and another is extraction from groundwater system (Das et al. 2020). Public investment is required for surface or canal irrigation, while private investment is required for groundwater resources management. Groundwater supply has grown to 62.4% of net irrigated areas from 28.7% (1950–1951), while canals have decreased to 23.6% of net irrigated areas (Sishodia et al. 2018). The introduction of mechanized pumping synergies in the mid-20th century resulted in significant drawdown expanse, leading to the overexploitation of groundwater resources and subsequent depletion of low or shallow aquifers (FAO, 2003). Increasing the implementation of engineering technologies can enhance water productivity and yield economic benefits. However, improving water productivity in crops without considering the economic viability may have limited significance for small and marginal agricultural farmers in developing countries of the whole world (Leng et al. 2015; Zaveri et al. 2016).

In most semi-arid regions, perennial provenance of river water is scarce. The groundwater table decreases when the amount of water extracted exceeds the amount being replenished (Mukherjee, 2022) (Fig.1.3). Deep water depth is identified in overexploited areas within these semi-arid regions. Specifically, there are two categories of deep confined aquifers: the first type varies in depth from 78 meters below groundwater level (mbgl), while the second type ranges from 154 to 274 mbgl, and is found in North Gujarat region (CGWB, 2018). The CGWB report indicates significant declines in North Gujarat over the past five years. Deeper aquifers experience an average annual decline of 2 meters in groundwater levels. Two important hydrogeological rock system have been identified: soft rock and hard rock (Robert et al. 2018).

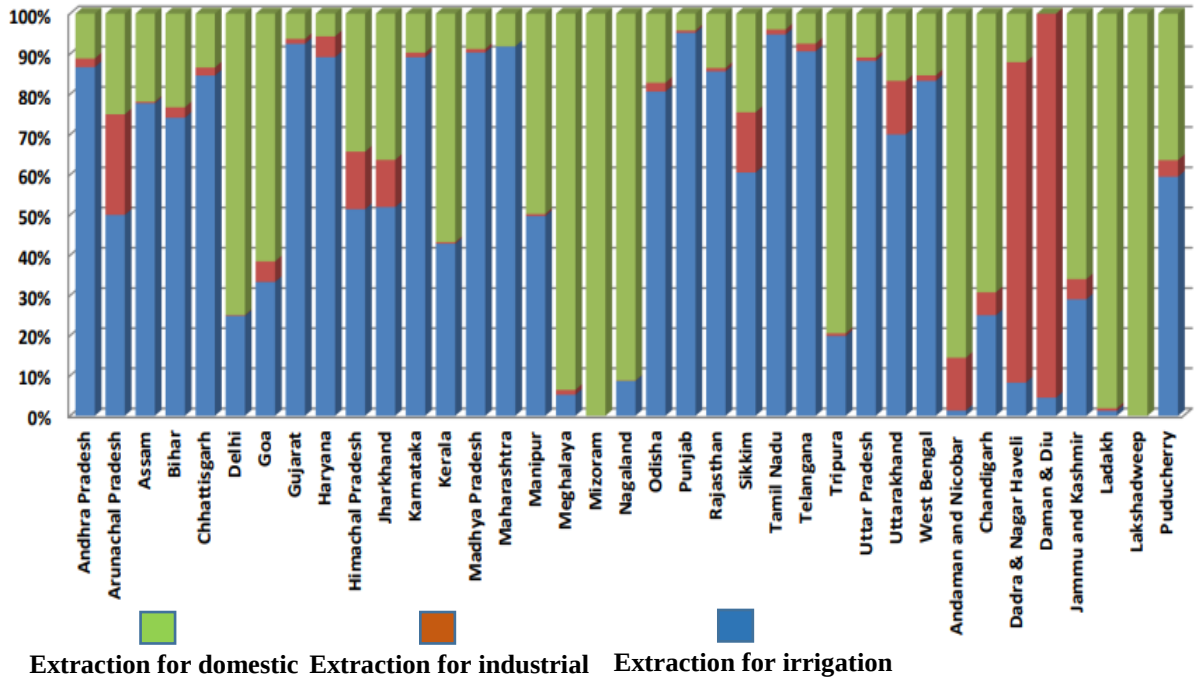

Fig. 1.3 State wise Irrigation Draft Vs Domestic & Industrial (CGWB, 2022)

Due to substantial increases in pumping capacity and the resulting groundwater level decline, the aquifer system has become susceptible to over abstraction. It is crucial to implement groundwater recharge and management/conservation programs in north parts of India (Fischer et al. 2022). Artificial recharging techniques should be employed to enhance groundwater recharge in these areas. Irrigation is the largest consumer of water globally, considering of 70% of developed water supplies (Sarkar et al. 2022). Negative consequences of groundwater exploitation include a decline in the groundwater level, harmful contamination, land subsidence, reduced crop yields, and diminished environmental flows.

According to the Food and Agriculture Organization (FAO, 2003), groundwater exploitation leads to various consequences:

i. Alterations in flow patterns within adjacent aquifers.
ii. Diminished water availability for ecological considerations, such as maintaining base flows in rivers, streams and wetlands, causing harm to ecosystems and downstream users.
iii. Escalated pumping costs and increased energy consumption.
iv. Land subsidence and damage to surface framework.

1.1.2 Global fresh water distribution and Appropriation

Approximately 79% of Earth's freshwater is locked in the polar ice caps, leaving about 99% of the remaining liquid freshwater as groundwater. With an approximate volume of 23.4×106 km^3, groundwater represents around 30% of the fresh water of the world or 2.5% of global water reserve, making it a crucial focus of research and a valuable resource for humanity (Bertosio et al. 2022). Groundwater itself plays a vital role in the process of global hydrological and global biogeochemical cycles, supporting ecosystem sustainability. It serves as a critical water source for fulfilling diverse human needs, including irrigation, domestic supply, and industrial growth. In regions

facing water scarcity, especially arid/semi-arid areas and heavily populated countries, groundwater often becomes the last available freshwater resource once surface waters are depleted (Zhang et al. 2022). Aquifers serve as the primary, safest and largest drinking water supply in many areas of the world. While agriculture accounts for roughly 25%-30% of global annual water use, certain regions like North America and Asia heavily rely on agricultural groundwater. Significant amounts of groundwater flow in vast sedimentary/alluvial aquifers, such as the High Plains aquifer in the central United States, the Great Artesian Basin in Australia, the Kalahari Sands in southern Africa, and the Nubian Sandstone Aquifer System in North Africa, which were recharged by rainfall events thousands/hundreds of years ago (Fig. 1.4) (Maasri et al. 2022; Taylor et al. 2013). Human activities, particularly irrigation, have greatly influenced the terrestrial water network. In the year 2000, irrigation was estimated for approximately 70% of global freshwater extractions and around 90% of human water use, leading to groundwater depletion in areas reliant on groundwater-fed irrigation, accumulation of groundwater from return flows in surface-water-fed irrigation, and changes in regional/local energy budgets due to increased soil moisture from agricultural irrigation (Cunillera et al. 2022). Irrigation has resulted in the depletion of groundwater storage in various arid and semi-arid systems, including the northwest India, North China Plain, and the United States High Plains, as well as in humid regions of Brazil, Pakistan, Afghanistan, Bangladesh etc., where groundwater abstraction is particularly intense (Qiu et al. 2022). An estimate suggests that, in addition to the prevailing statistically significant declining trends in groundwater levels in north western parts of India and the Gangetic river basin between the year 1996 and 2018 (Fig. 1.5), even much declining trends may potentially be witnessed in parts of northern central and southern India during the 5-year forecasting session from 2019 to 2023 (Xiong et al. 2022).

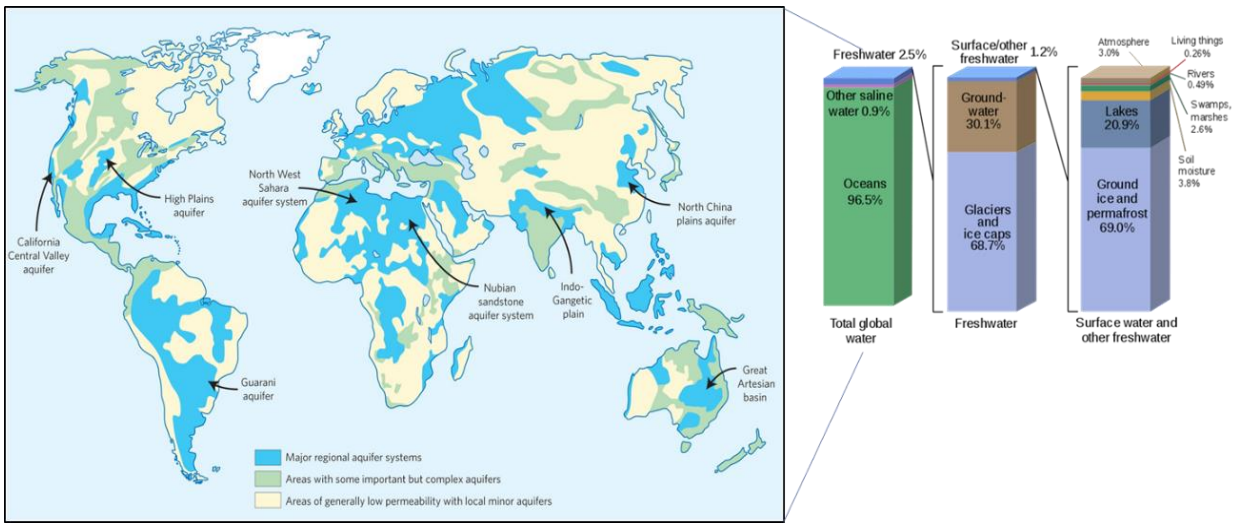

Fig. 1.4 Aquifer system around the world and distribution of global water (Taylor et al. 2013)

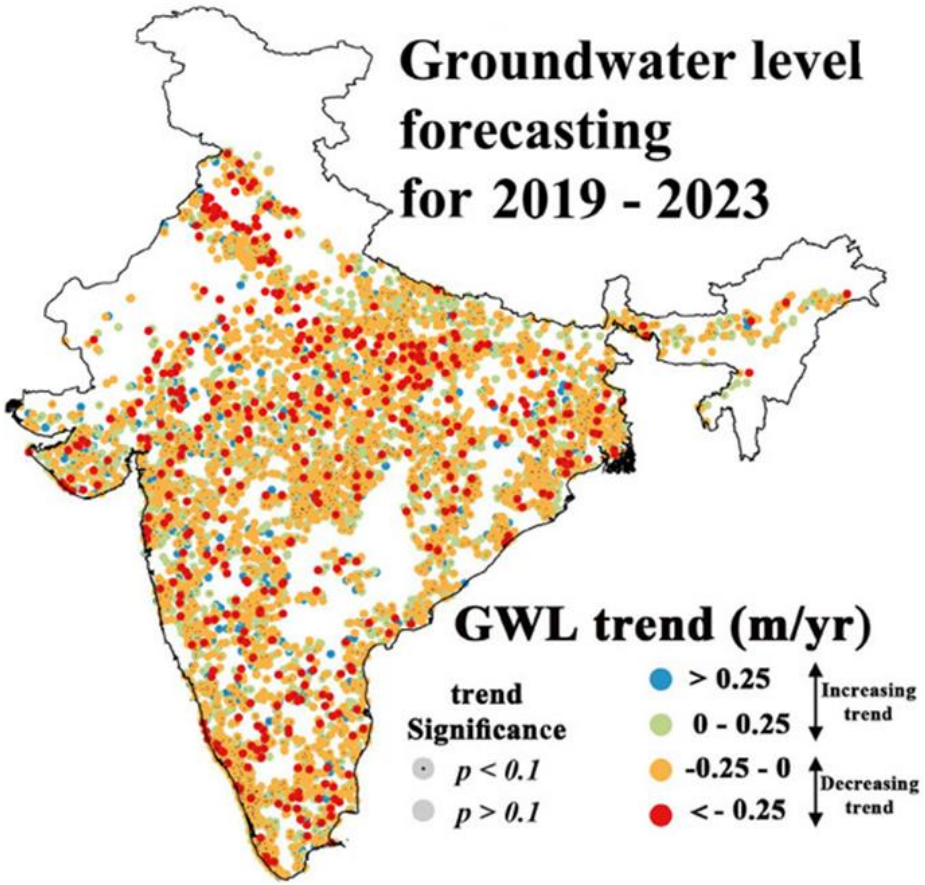

Fig. 1.5 Predicted groundwater level trends across India (Malakar et al. 2021)

1.1.3 Status of Groundwater in Rural and Urban areas of India

Groundwater accounts for approximately 35% of the global annual water supply. In India, the estimated convenience of groundwater is about 339 billion/m3, with a withdrawal rate of around 251 km^3. It plays a crucial role in meeting the water needs of rural (85%), urban (50%), and overall irrigation (65%) in India, making it closely intertwined with the bio-physical, human and ecological environment (Varma et al. 2017). The significance of groundwater extends to agro-based industries, agricultural activities, as well as urban domestic and rural uses in India. However, multi-cropping, intensive cropping, high-yielding cropping, and increased irrigation have led to a decline in groundwater levels. Previous studies indicate that India entered the water-stress zone by the year of 2015 and is projected to become water-scarce by 2050 (Shaji et al. 2021). The monsoon season (June to September) accounts for approximately 80% of India's annual rainfall and exhibits significant variations in groundwater storage (GWS) between the pre and post-monsoon period. Agriculture irrigation alone consumes about 85% of India's water, equivalent to around 1123 billion m^3 or roughly 28% of replenishing freshwater. It is estimated that by 2050, India will need to produce 250 million metric tons of food, resulting in a substantial demand for water (Yadav et al. 2021). Additionally, changes in terrestrial water, rapid urbanization, and the associated challenges with water resources have contributed to heterogeneous groundwater depletion. Therefore, it is essential to promote sustainable management and effective monitoring of groundwater to meet the growing water demand in a cost-effective manner. The mean groundwater level (GWL) depths for shallow and deep wells

vary significantly across the different states of the country (Ali et al. 2019). Over 65% of shallow wells have groundwater level less than 6 meters below ground level (mbgl), while more than 64% of deep wells have Groundwater levels deeper than 6 meters and over 30% deeper than 10 to 12 mbgl (Wu et al. 2021). The deepest groundwater levels are predominantly found in northwestern part of India, eastern part of India consisting of Bengal basin including the areas of the Gangetic basin, and certain parts of southern section of India including Pennar and Kaveri river basins (Jasechko and Perone, 2021). Noticeable depletion trends in groundwater level are observed in several regions, particularly in north western parts of India and parts of the Ganges river basin, where some observation wells have experienced exceptional annual level decline rates exceeding 1 meter (Lohani et al. 2023). These regions are also susceptible to high groundwater withdrawal due to cropping patterns and crop consumptive water requirements and drought events. In West Bengal, specifically Purulia, Bankura, and West Medinapore districts, are facing a decline in water table where the total annual groundwater recharge decreased since 2004 (Fig.1.6). Purulia district, an extension of the Chota Nagpur Plateau, is particularly known for its water scarcity and susceptibility to extreme drought (Senapati et al. 2021). This situation is further exacerbated by the lack of proper infrastructure and resources to store and conserve water. As a result, the local communities are struggling to access safe, clean drinking water (Sahoo et al. 2021). The government is taking steps to address this issue, but more needs to be done. The groundwater status according to Central Groundwater Report 2022 are as follows (CGWB, 2022)

- The annual recharge of groundwater is estimated to be 437.60 Billion Cubic Meters (BCM), while the extraction stands at 239.16 BCM (Table1.1).
- According to the assessment, there has been an increase in groundwater recharge compared to the previous assessment in 2020, which reported a recharge of 436 BCM and an extraction of 245 BCM.
- The 2022 assessment reveals that groundwater extraction is at its lowest since the year 2004 when it was recorded at 231 BCM. Among the total of 7,089 assessment units in the country, 1,006 units have been identified as 'Over-exploited.
- Irrigation accounts for about 87% of the total annual groundwater extraction, equivalent to 208.49 BCM. On the other hand, domestic and industrial use only accounts for 13% of the total extraction, which amounts to 30.69 BCM.
- In terms of state-wise groundwater extraction, the overall extraction level in the country stands at 60.08%. States such as Rajasthan, Punjab, Haryana, Dadra & Nagar Haveli, and Daman & Diu have a very high extraction level exceeding 100%.
- In Tamil Nadu, Delhi, Karnataka, Uttar Pradesh, and union territories like Lakshadweep, Chandigarh, and Pondicherry, the extraction level ranges between 60% and 100%. The rest of the states have a groundwater extraction level below the value of 60%.

Table 1.1 Comparative assessment of groundwater resource of India from 2004-2022 (CGWB, 2022)

Ground Water Resources Assessment	2004	2009	2011	2013	2017	2020	2022
Annual Ground Water Recharge (bcm)	433	431	433	447	432	436	438
Annual Extractable Ground Water Resource (bcm)	399	396	398	411	393	398	398
Annual Ground Water Extraction for Irrigation, Domestic & Industrial uses (bcm)	231	243	245	253	249	245	239
Stage of Ground Water Extraction (%)	58 %	61 %	62 %	62 %	63 %	62 %	60%

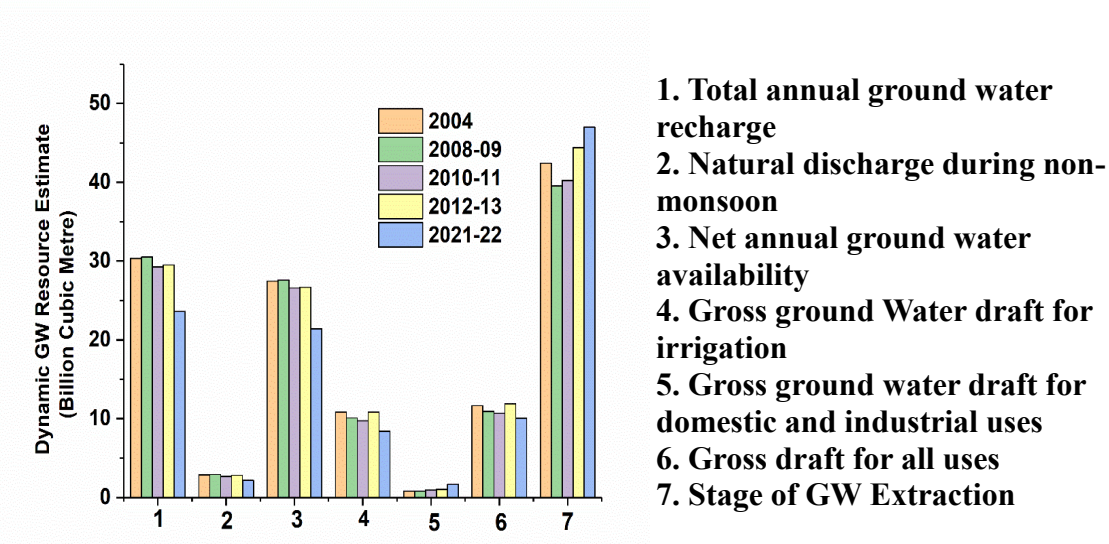

Fig. 1.6 Comparison of groundwater resources of West Bengal (Data source: CGWB, West Bengal, 2022)

1.1.4 Groundwater Vulnerability to pollution

Approximately 30% of the world's freshwater resources are stored as groundwater beneath the Earth's surface. Groundwater is accessed through dug wells, bore wells, and pumps for the human consumption and agricultural purposes (Wekesa, 2018). Apart from being a vital freshwater source, groundwater plays a crucial role in maintaining the balance of aquatic and terrestrial ecosystems and adapting to unpredictable monsoons and extreme summers in the era of climate change (Ran et al. 2022). However, industrial, agricultural practices, and mining activities, improper disposal of waste and related groundwater pollution have led to an increase in contamination in various parts of India. The 5th minor irrigational census as conducted by the Central Ground Water Board reported a 60% depletion of groundwater in India between the year 2007 and 2017, with irrigation accounting for about 90% of its usage (Ravindra et al. 2022). Water-intensive crops such as paddy and sugarcane have

significantly contributed to groundwater depletion, particularly in the northern sections of India, as observed by a satellite-based imagery study conducted by the National Aeronautics and Space Administration (NASA). Moreover, states with significant groundwater reserves also face water pollution issues, with various studies detecting toxic substances and heavy metals such as chromium, arsenic, lead, nitrate, cadmium, and pesticides (Fig.1.7). The quality problems of groundwater pollution can be broadly categorized into two types: geogenic and anthropocentric. Geogenic pollution can be defined as naturally occurring increased concentrations of certain elements in groundwater that have ill health hazards. Carcinogenic contaminants such as arsenic, uranium, cadmium, lead, radon, and pesticides have been primarily detected in Indian water sources and have been inspected and reported by numerous researchers (Panneerelvam et al. 2022. In India, contamination from fluoride and arsenic is predominantly geogenic in type and affects several parts of the country, posing significant health concerns and challenges for ensuring a safe water supply. In addition, iron, manganese, elevated levels of salinity, radon, uranium, selenium, chromium, and other major trace elements have been reported in certain areas and may also have geogenic origins (Rao et al. 2022). Approximately 50-40 million people in India reside within the very high-risk zone of arsenic contamination. The states of India where arsenic contamination have been inspected include Bihar, West Bengal, Jharkhand Uttar Pradesh, Manipur, Assam, Punjab, Haryana, Karnataka, and Chhattisgarh, Moreover, the highest concentrations are mainly found in the Indo-Gangetic Plains, prompting the Central Ground Water Board to recommend the utilization of arsenic-safe and free deeper aquifers in the region through well-regulated pumping system (Vig et al. 2022). West Bengal and Uttar Pradesh are the most affected states of India (Mishra et al. 2022). Fluoride contamination is also widespread in groundwater, with high levels occurring in various parts of the world. India alone accounts for approximately 12 million out of the 85 million tons of anionic fluoride deposits found in the Earth's crustic layer (De et al. 2022). Consequently, elevated fluoride levels (more than 1.5 mg/l) are frequently detected in groundwater across several states in India, including Telangana, Andhra Pradesh, Assam, Chhattisgarh, Bihar, Gujarat, Delhi, Jammu and Kashmir, Haryana, Jharkhand, Kerala, Madhya Pradesh, Karnataka, Maharashtra, Punjab, Odisha, Rajasthan, Uttar Pradesh, Tamil Nadu, and West Bengal. While there have been several pieces of research on groundwater contamination in India, there is a gap in research specifically addressing the presence of carcinogens in water to the best of our optimum knowledge. Therefore, this work aims to valuable provide insights into the various sources, distribution, and potential natural remedial measures for various carcinogenic elements found in groundwater in India, based on sustainable measures (Jaydhar et al. 2022). Based on 500-1000 data Bibliometric analysis was employed to trace the evolution of scientific literature and uncover unique characteristics pertaining to groundwater-related domains. The growth of publications in this bibliometric research was extracted from Elsevier's SCOPUS database. Over the period spanning from 2000 to 2022, a comprehensive collection of 1000 records, encompassing the keywords "groundwater vulnerability," "India," and "groundwater depletion," “major pollutants” were identified. The graphical plot has been done using VOSviewer software which shows that most of the groundwater studies in India were focused on pollutant identification (Fig.1.8) to curb out its harmful health hazards on human society where the major pollutants were Iron, Arsenic, Chromium, fluoride, nitrate, pesticides etc. (Fig.1.9).

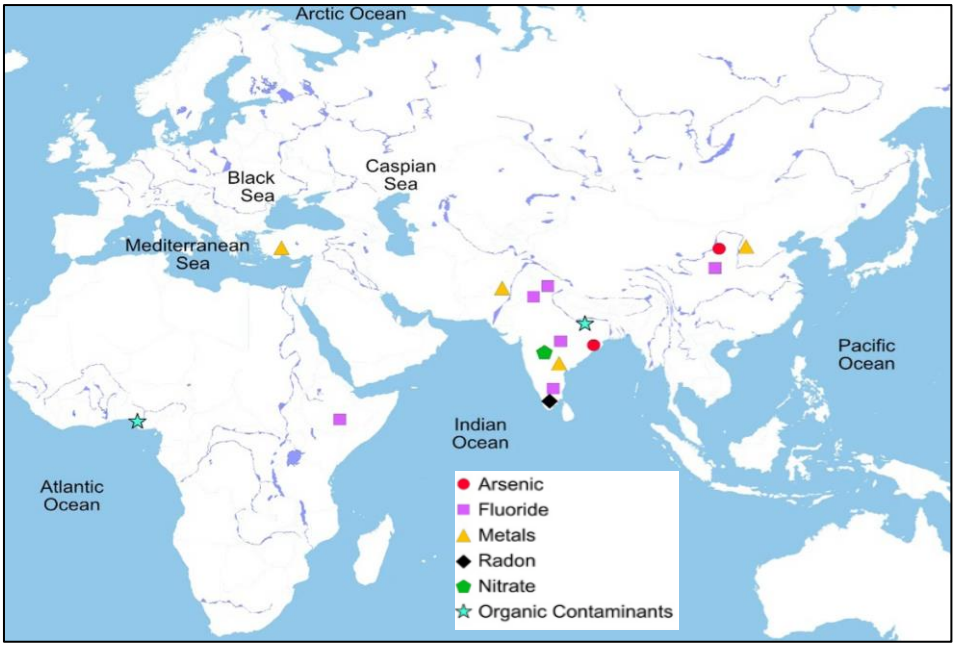

Fig. 1.7 Major groundwater polltants arround the world

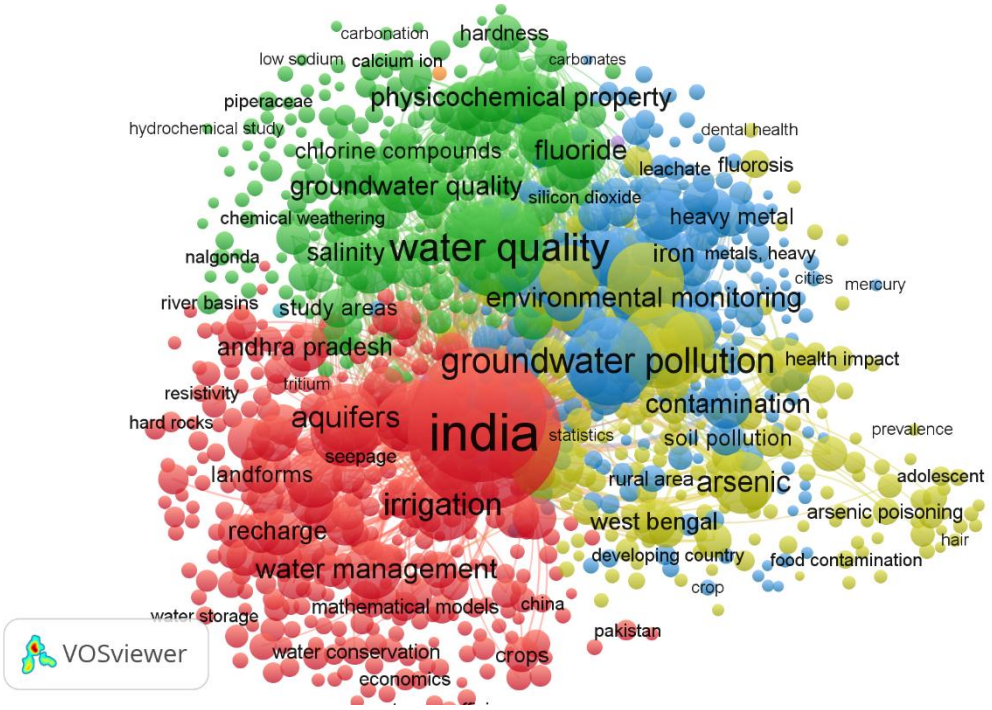

Fig. 1.8 Graphical plot showing occurrences of main groundwater research objectives in India

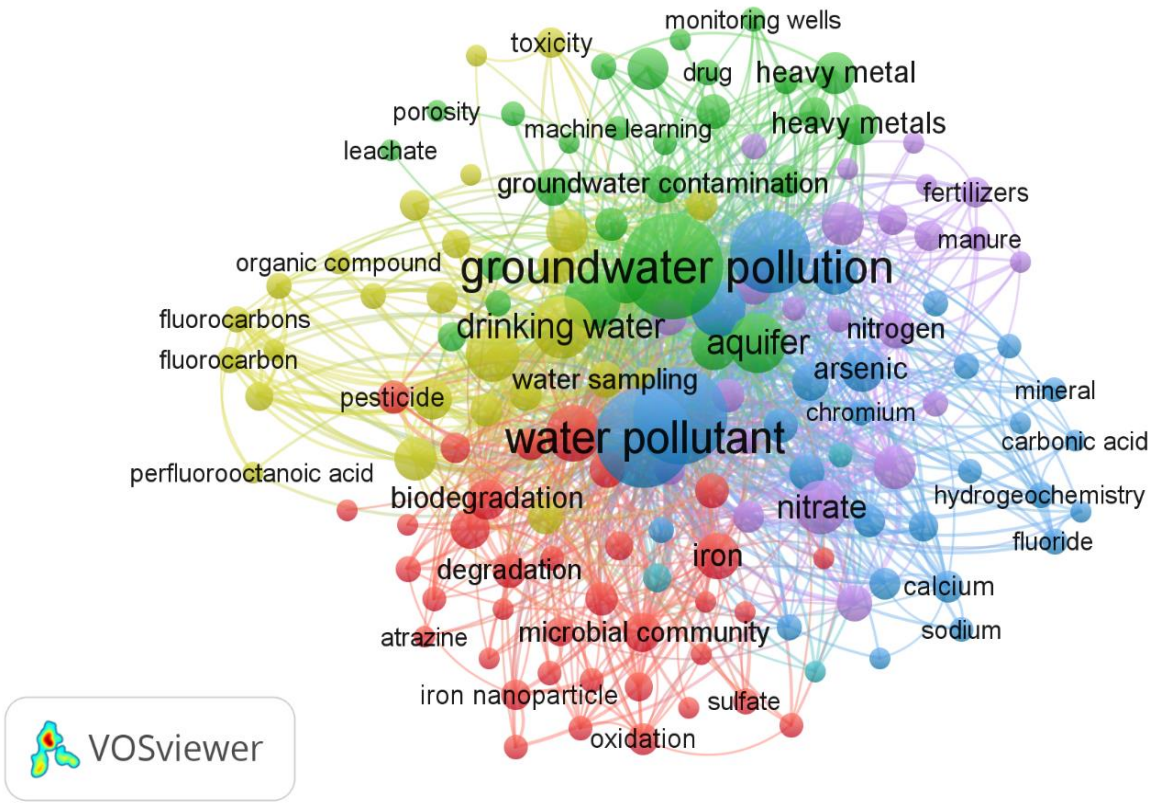

Fig. 1.9 Graphical plot shows the research work done till date on the major pollutants in India

1.1.5 Advances in Remote Sensing/Geographical Information System and modelling techniques in Groundwater potential and vulnerability studies

Advancements in remote sensing and groundwater modeling techniques have greatly contributed to groundwater studies. Researchers both in India and abroad, such as Ifedeigwu et al. 2022; Rahmati et al. 2015; Dar et al. 2021; Saranya and Saravanan, 2020, have successfully utilized remote sensing and geographic information system techniques to assess groundwater potential of an area at regional and local scale. However, the selection of thematic layers for delineating groundwater potential zones has been arbitrary, with weights assigned based on personal decisions. Recently, researchers such as Bera et al. 2020; Doke et al. 2021; Kaur et al. 2020, have effectively employed multi-criteria decision-making (MCDM) techniques, specifically Saaty's Analytical Hierarchy Process (AHP), to determine the relative weights for the groundwater potential mapping research. MCDM has gained global recognition as an efficient tool for addressing complex decision problems where application of fuzzy logic is less (Ghosh et al. 2022). In environmental studies, the processing of numerous data and their size often makes modeling studies complex. Geographic information system (GIS) tools and is spatial-temporal operations offer valuable opportunities for preprocessing various types of spatiotemporal information and datasets, facilitating researchers in achieving their core objectives (Raj et al. 2022)

Numerous studies have focused on assessing groundwater vulnerability to pollution using various methods. The DRASTIC approach, developed by Aller et al,1986 based on seven parameters (recharge, depth to water, soil media, aquifer media, topography, hydraulic conductivity and impact of the vadose zone), has shown promising results in many research cases and has been frequently used in current studies (Yu et al. 2022). There are, however, major limitations to the original DRASTIC method. Each aquifer, whether it is unconfined or confined, represents its own dynamic characteristics, making it difficult to apply the DRASTIC method in areas with both types of aquifers (Fannakh and Farsang, 2022). Furthermore, the lack of a standardized guideline for vulnerability index determination and the uncertainty surrounding the accuracy of the vulnerability index have led researchers to modify the original method using various techniques, such as frequency ratio, Analytical Hierarchy Process , Single-Parameter Sensitivity Analysis, Fuzzy-AHP model, Mamdani Fuzzy Logic model, Supervised Classification with Fuzzy Logic framework, projection/prediction pursuit dynamic clustering, and considerations of anthropogenic/ man made influence, such as population, land cover/land use alteration impacts etc. (Sresto et al. 2022; Chakraborty et al. 2022).

In recent studies, hybrid ensemble machine learning models, combining machine algorithm and statistical analysis, have shown promising results in environmental/ ecological hazard mapping, including landslide, flood, drought, forest fire susceptibility, groundwater level/trend prediction etc. (Nair et al. 2022). To date, no previous study has explored the potential of the comparative study of hybrid machine learning and MCDM algorithms in groundwater potential and pollution studies, making it a valuable avenue for future research (Patel et al. 2022).

The development of conceptual models is crucial in simplifying complex underground water systems. A reliable, simple and accurate conceptual modelling technique form the basis for numerical groundwater flow and transport models, reducing errors and enabling the analysis of groundwater system changes, flow directions, recharge, inflow, outflow, and aquifer depletion and storage (Xiang et al. 2020). The MODFLOW computer application is commonly used for solving groundwater flow issues using various numerical additional models (Arifjanov et al. 2021). Researchers worldwide have utilized MODFLOW to investigate groundwater flow and behavior in various regions of the world (Ameur et al. 2021; Karki et al. 2021).

Bibliometric analysis was employed to trace the evolution of scientific literature and uncover distinct characteristics pertaining to application of remote sensing, geographical information system and flow modeling domains. The growth of publications in this bibliometric analysis was extracted from Elsevier's SCOPUS database. Over the period spanning from 2000 to 2022, a comprehensive collection of 500-1000 records, encompassing the keywords "groundwater vulnerability," “world," and "groundwater flow”, “DRASTIC” and "MODFLOW" were identified. The graphical plot using VOSviewer software shows that most of the groundwater vulnerability and flow modelling studies were focused on the application of DRASTIC, MODFLOW model and Analytical Hierarchy Process (AHP). Fig. 1.10, Fig. 1.11 & Fig. 1.12 shows the collaborative studies on groundwater resources estimation around the world where India takes a major role by conducting many bilateral studies on the above concerned topic.

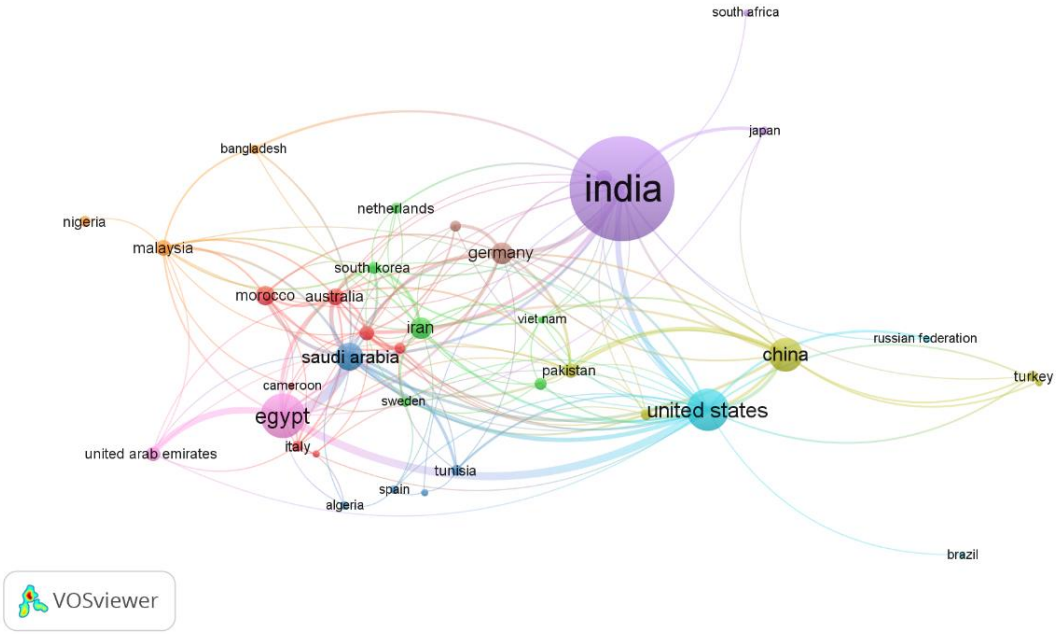

Fig. 1.10 Graphical plot showing the application of frequently used modelling techniques in groundwater studies

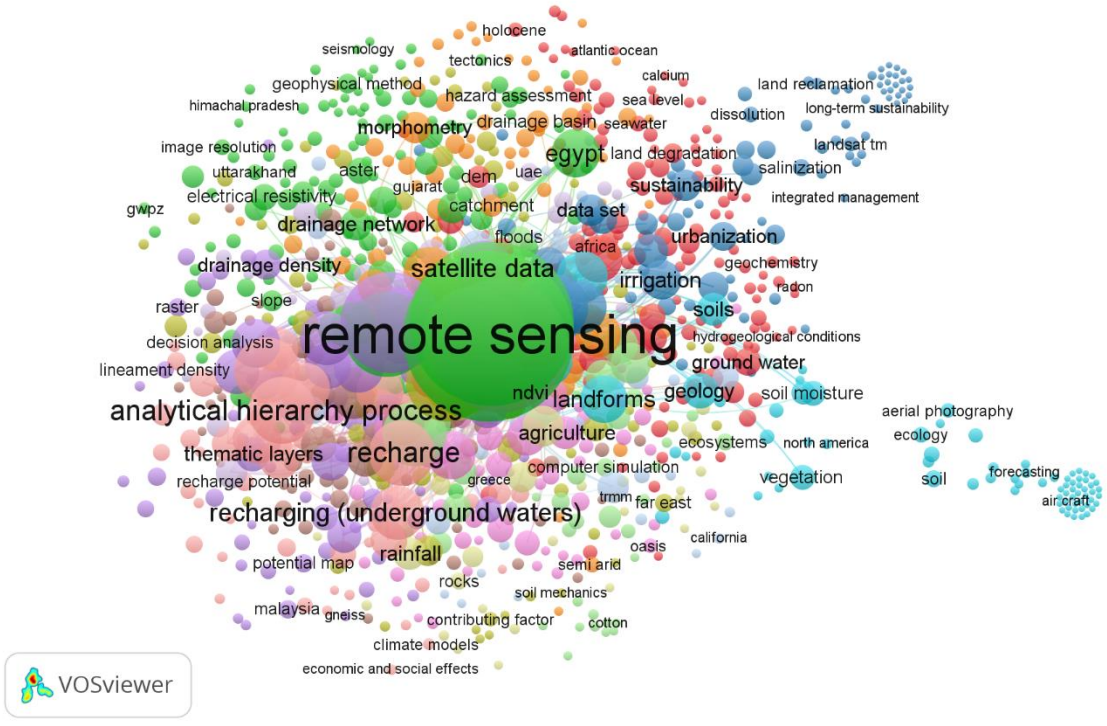

Fig. 1.11 Graphical Plot showing the collaborative behavior of major countries of the world conducting groundwater research

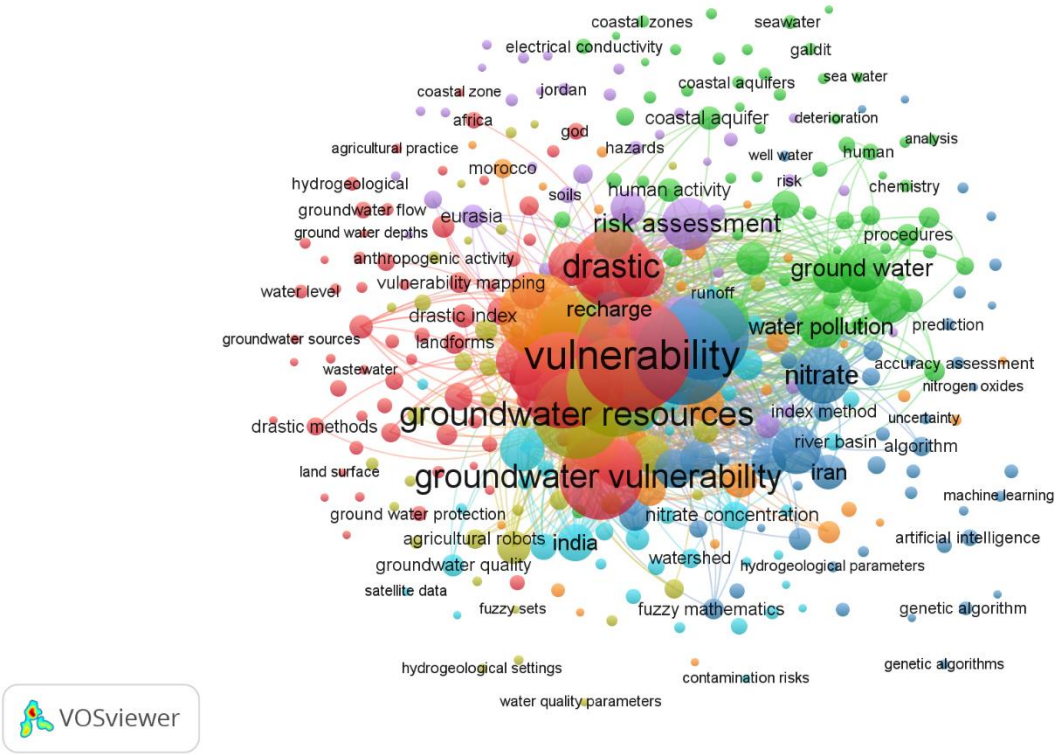

Fig. 1.12 Graphical plot showing the application of DRASTIC in groundwater vulnerability studies

1.1.6 General Framework of the Current Research

The general framework of my current research study typically follows a structured approach from chapter 3 to 7 to investigate various aspects related to groundwater resources, pollution and sustainable mitigation in hydrogeological river basin of West Bengal, India. Here is the outline of the general framework:

I. **Introduction:** a. Background: Provided an overview of the importance of groundwater as a vital water resource, its significance for human consumption, agriculture, and ecosystem sustainability. b. Research Problem: Identified the specific research gap or problem in the knowledge that my study aims to address. Explained the significance of studying groundwater in the context of local, regional, or global water challenges. c. Research Objectives: Clearly stated the objectives of my research, outlining the specific goals and outcomes that I intend to achieve through your study.

II. **Literature Review:** a. Reviewed previous studies: Summarized relevant literature on groundwater studies, including research on groundwater vulnerability, depletion, pollution, and eco-friendly management approaches. Highlighted the key findings, methodologies used, and any limitations or gaps in previous and current research. b. Theoretical Framework: Presented theoretical frameworks, conceptual models and established new frameworks/theories that underpin my research and guide my approach.

III. **Methodology:** a. Research Design: Described the overall research design and approach, such as whether it is a field study, laboratory experiment, modeling analysis, or a combination of methods. b. Data Collection: Explained the methods and techniques used for data collection, including groundwater

sampling, monitoring, remote sensing, numerical modeling and laboratory testing. Discussed the selection criteria for my study area, sampling locations, or datasets used. c. Data Analysis: Outlined the analytical methods, statistical techniques, or modeling approaches employed to analyze the collected data. Explained every software tools, GIS systems, or modeling platforms utilized.

IV. **Results**: a. Presented the findings of my research, organized according to the specific objectives and research questions. Used appropriate tables, figures, and maps to illustrate the results effectively. b. Discussed the outcomes of the data analysis, including groundwater trends, patterns, correlations, or significant findings related to groundwater vulnerability, depletion, or pollution. Compared the results with previous studies or established benchmarks.

V. **Discussion:** a. Interpretation of Results: Analyzed and interpreted the significance of my findings in relation to the research problem and objectives. Discussed any unexpected or contradictory results and provided possible explanations or hypotheses. b. Implications and Applications: Discussed the practical implications of my research findings for groundwater management, policy-making, or sustainable water resource planning. Highlighted how my research contributes to existing knowledge and addressed the research gap identified in the introduction. c. Limitations: Acknowledged the limitations of my research, such as data constraints, methodological limitations, or potential sources of bias. Suggested areas for future research to overcome these limitations.

VI. **Conclusion:** Summarized the key findings of my research and restated their significance in addressing the research problem. Emphasized the broader implications for groundwater management, sustainability, or policy development. Provided a concise conclusion that aligns with my research objectives.

1.1.7 Overall Research Gap

I. Analysis of ground and surface water interaction in complex terrain conditions within a river basin.
II. Evaluation of groundwater recharge patterns along different stretches of the river.
III. Assessment of groundwater drought in response to climate change and development of a groundwater level index.
IV. Utilization of MIKEFEFLOW modeling software to simulate groundwater flow under changing climate conditions and analyze the impact of drought intensity on groundwater resources.
V. Integration of new machine learning (ML) and Fuzzy MCDM techniques in groundwater research.
VI. Incorporation of field-based conditioning factors for estimating groundwater potential zones.
VII. Investigating the effectiveness of low surface area biochar and cost-effective earth materials for contaminant removal (in light of iron, phosphate and fluoride).

1.1.8 Over all Aims and Objectives

The main objective of the study is to make sustainable watershed management by analyzing groundwater and surface water flow interaction, estimation of recharge potential zone, and contaminant remediation using natural adsorbent.

Scope of the Study

- Documentation of hydro-meteorological, hydro-geological, and hydro-geomorphic status of the study area.
- Calculation of water budget and estimation of groundwater resources of the study area.
- Identification of the steady flow of groundwater and its interaction with the river channel through modeling techniques and piezometer installation.
- Selection of different landscape and channel patterns and its relation to subsurface aquifer recharge.
- Estimation of aquifer characteristics based on Dar Zarrouk Parameters at selected sites to analyse the groundwater flow of the study area.
- Multivariate risk assessment of ground water resource of the study area in view of groundwater quality assessment for irrigation and drinking water suitability.
- Estimation of recharge potential zone using field-based conditioning factors with different standard formulae and machine learning techniques.
- Develop an integrated watershed strategy plan for sustainable solution through identification of Managed Aquifer (MAR) Sites and recommendation for affected areas.
- Enhanced eco-friendly treatment of three major groundwater contaminants like iron, phosphate and fluoride using biochar and natural clay.

1.1.9 Novelty of the Current Research

I. Comparative analysis of four MCDM models in environmental studies.
II. Application of Fuzzy DEMATEL in Environment and climate studies.
III. Estimation of groundwater drought and level index which was not done before.
IV. This study introduces a novel methodological framework to compare fuzzy MCDM and machine learning techniques using field-based conditioning factors.
V. This study introduces a novel methodological framework to understand the exchange process using MIKE FEFLOW and Piezometer installation.
VI. A novel approach to identify groundwater vulnerable zones using the FSE-GVI model.
VII. This study focused on detecting a river basin suitable for agriculture and priority for management using a new clustering tool of groundwater quality with fuzzy logic technique in R and Geographical Information System.
VIII. Application of low-cost natural eco-friendly adsorbent for the enhanced removal of iron, phosphate, and fluoride.

1.1.10 Study Expectations

This research is expected to serve as a valuable guide for policymakers and stakeholders, particularly in drought-affected regions of Puruliya, Bankura, and West Medinapore in West Bengal, as well as for the entire country of India. It aims to support the development of sustainable water security plans, specifically addressing groundwater management in the context of climate change.

Furthermore, this research has the potential to enhance existing frameworks and interventions focused on safeguarding precious groundwater resources and enhancing the overall quality of wellbeing in local communities. The study also proposes strategies for the prevention, control, and eco-friendly remediation of groundwater contaminants, such as iron, phosphate, and notably fluoride, with global implications. The implementation of these strategies can significantly contribute to the health, well-being, and economic progress of rural populations in similar less-developed countries.

1.1.11 Overall Study Limitations

Although the issues covered in the overall research outline are undoubtedly wider and massive in context, this noteworthy study was undertaken specifying the following scope and concerned limitations:

i. While the findings of this research may have broader applicability, particularly in underdeveloped regions, the discussions and the outcome presented primarily focus on the case study conducted in the Shilabati river basin in West Bengal, India.
ii. Mapping recharge susceptibility at a micro scale proves challenging due to the unavailability of actual groundwater yield data, historic groundwater level data, and aquifer characteristics (such as specific yield, transmissivity, hydraulic conductivity). Remote sensing data, such as Landsat images, cannot provide this level of detail.
iii. The limited availability of soil and water chemical analysis, due to the constraints of COVID-19 and the distant location of the study area, restricts the ability to capture temporal compositional variations adequately.
iv. Although the application of low surface hardwood biochar and natural clay for contaminant removal is highly valued, their local availability may be restricted to specific sites.

1.1.12 Global Importance

The health of ecosystems relies heavily on the availability and quality of water resources. The research on the hydrological system in the Shilabati River basin will help in understanding how water flows through different layers, affecting the ecology of the area. By identifying risks to the ecosystem and developing eco-friendly remediation measures using biochar and kaolinite adsorbents, policymakers can contribute to the preservation and restoration of the natural environment and can bring smiles to the face of poor inhabitants by providing safe and clear water.

Research findings on hydrological systems and water security in the Shilabati River basin can contribute to global knowledge exchange and inform policy development. By sharing data (mostly field based valid data), methodologies (Modified Fuzzy MCDM and machine learning techniques), and best practices, researchers and policymakers from different regions can learn from each other and adapt successful approaches to their contexts. This collaboration can lead to improved water management strategies and the development of sustainable solutions to water-related challenges worldwide.

1.1.13 Comprehensive Thesis structure

The thesis comprises 8 interconnected chapters, each with its own distinct focus, which can be summarized as follows:

i. **Chapter 1** provides an overview of the study, including the problem statement, research gap, research justification, aim and objectives, novelty of the research, limitations, and study expectations.

ii. In **Chapter 2**, the focus is on the challenges related to water supply and the significance of groundwater resources in the Shilabati River basin, examining both micro and macro aspects. This chapter also delves into the physical and non-physical characteristics and the fundamentals of groundwater contamination and pollutants and fate in the sub-surface environment of the river basin.

iii. The research focus of **Chapter 3** is to address groundwater related issues through several statistical techniques and multi-criteria decision-making approaches (MCDM). To accomplish the research objectives morphometric attributes of 9 sub-watersheds of the Shilabati river basin having a total area of 3881 km2 have been estimated. Principle Component Analysis (PCA) has been used to group these attributes into three components and K-means clustering categorized the sub-watershed into 3 clusters based on morphometric asymmetry. Basin prioritization based on recharge and infiltration capacity using three MCDM techniques like Technique for Order of Preference by Similarity to Ideal Solution (TOPSIS), Complex Proportional Assessment (COPRAS), VlseKriterijumska Optimizacija I Kompromisno Resenje (VIKOR) ranked the sub-watersheds where TOPSIS has been selected as the best model using spearman rank correlation coefficient test.

iv. **Chapter 4** examines drought risk zones in Shilabati river basin by analyzing Landsat images captured during three specific years with precipitation deficits (2000, 2009, and 2018). The study evaluates seven parameters, including the Standard Precipitation Index (SPI), Long-term Temperature Condition Index (TCI), Long-term Vegetation Condition Index (VCI), Vegetation Health Index (VHI), Long-term Soil Moisture Index (SMI), Long-term Soil Adjusted Vegetation Index (SAVI), and Long-term Normalized Difference Water Index (NDWI). The Fuzzy DEMATEL model was utilized to identify drought risk zones and better understand the causative and effective factors represented through a causal diagram. To investigate groundwater degradation, 20 wells located in a river basin in West Bengal were selected. The study focuses on analyzing the seasonal trend of groundwater levels using Mann Kendall test statistics from 1996 to 2018. Results indicate that 60% of the wells exhibited a decline in water levels, particularly during the post-monsoon season. These wells are primarily situated near agricultural land, where extensive groundwater extraction occurs through submersible pumping wells, as observed from a socio-economic survey. To classify the wells based on fluctuation magnitude, an Agglomerated Hierarchical Cluster analysis was performed.

v. **Chapter 5** had a novel objective of creating groundwater potential maps by comparing machine learning techniques with a Fuzzy MCDM model, using only field-based conditioning factors. The process involved several steps. Initially, 285 wells were selected, with 70 percent allocated for model training and 30 percent for validation. Thirteen field-based conditioning factors were considered. The association between these factors and groundwater occurrences was analyzed. Subsequently, the XGBoost, Random Forest, and Naïve Bayes models were constructed using the training dataset, and weights were

determined using the Fuzzy Analytical Hierarchy Process of Extent Analysis method. To assess and compare the performance of the four models, ROC curves, AUCs, MCAs, and correlation plots were utilized. In the current study, the subsurface characteristics of the Shilabati basin system were determined using cost-effective piezometers and MIKE FEFLOW software, which employs a steady-state numerical model. The pore size and fine particle content of streambeds are influenced by two opposing flow conditions, which in turn affect the hydraulic conductivity of the streambed. However, there is limited documentation on the hydraulic conductivity (K_h) analogies for losing and gaining streams. This study also represents the first attempt to identify suitable sites for implementing Managed Aquifer Recharge (MAR) technology in West Bengal, India, particularly for managing extreme drought events. The identification of suitable sites was carried out using three fuzzy multi-criteria decision analysis methods.

vi. **Chapter 6** introduces a novel approach to identifying groundwater vulnerable zones by combining Fuzzy Shannon Entropy (FSE) with a decision support algorithm, as an alternative to DRASTIC, GOD, and similar methods. This study proposes the "FSE-GVI" framework, which expands and redesigns the original seven geological and hydrogeological parameters by incorporating geochemical and anthropogenic factors. Thirteen geo-environmental and hydrogeological factors are optimized using weighting techniques. The model is validated using 74 groundwater quality data points, demonstrating a strong correlation between the water quality index (r=0.84) and various indicators such as Total Dissolved Solids (70%), iron (72%), hardness (85%), and alkalinity levels (75%). To determine different hydrochemical zones, a fuzzy clustering-soft computing technique is employed, considering 13 essential parameters of groundwater quality. Fuzzy C-means clustering (FCM) outperforms other traditional hard computing techniques like Hierarchical Clustering (HCA), K-means clustering, and Agglomerative Clustering. The FCM divides the sampling sites into two clustering groups (FCM I & FCM II), which are validated with fuzzy silhouette index (0.85), partition coefficient (0.76), partial entropy (0.68), and modified partition coefficient (0.52).

vii. **Chapter 7** focused on investigating the adsorption of fluoride on kaolinite lithomarge (red and white laterite) from Paschim Medinapore in West Bengal, India. The study explored both kinetic and equilibrium aspects through a series of batch tests and a fixed bed column study using natural water. Analysis using X-ray Powder Diffraction revealed that the Alpha SiO_2 with a trigonal structure and Alpha Al_2O_3 with a hexagonal structure of the natural adsorbent played a crucial role in the mechanism of fluoride absorption. Additionally, a novel low-cost ($4.46/kg) and low surface area (6.87 m^2/g) hardwood waste (HW) was developed as a biochar, and it was modified with magnesium impregnation (MgO-HW). This modification proved to be economically advantageous compared to numerous alternative methods. The Hardwood and MgO-HW biochar were designed for the removal of iron and phosphate from aqueous solutions.

viii. **Chapter 8** provides a comprehensive overview of the thesis, including the synthesis of key findings, contribution to the existing body of knowledge, and offers recommendations for future research.

ix. **Chapter 9 & 10** provides the insights of appendixes, and references of the complete Ph.D. thesis work.

Chapter2

General Features of the study area

2.1 Locational description of the river basin: Shilabati River

Shilabati river basin is one of the important river basins located at the eastern part of West Bengal, India extended between 23º14'18.03" N to 22º26' 25.12" N latitude and 86º38' 46.08" E to 87º46' 36.65" E longitude. The river (Fig. 2.1a) originates from the dissected upland of Chotonagpur Plateau of Puncha block of Puruliya district, West Bengal and flows in south easterly direction through Simlapal, Taldangra, Indpur, Khatra and Hirabandh block of Bankura district and Garbeta I, II, III, Salboni, Keshpur, Chandrakona I, II, Daspur and Ghatal block of West Medinapore district, West Bengal, India where it joins with Rupnarayan river. The study area covers a total area of approximately 3880 km^2 and consists of nine sub-watersheds namely Silai, Joypanda, Tamal, Betal, Parang, Purander, Kubai, Donai and Silai Ketia Khal. The upper section of the basin particularly the parts of Puruliya and Bankura district is highly drought prone whereas the lower section is affected by high monsoonal discharge (Ghosh 2019). The river basin experiences semi-arid to humid climatic condition and receives an average monthly precipitation of 109 mm and average monthly temperature of 37º C. In the upper section the river is extensively dissected, undulating with irregular topography comprising bare and waste land where soil erosion by water action predominates (Shit et al. 2015; Sarkar and Mishra 2018). Parts of Puruliya district of West Bengal alone contributes 52.4% (328 thousand hectare) of land effected by water erosion among others (Sarkar and Mishra 2018) from where this river basin originates. In the middle section the basin is crisscrossed by numerous ephemeral rill and gullies (Fig.2.1c) caused by the accelerated removal of soil cover through surface runoff (Shit et al. 2013). The major inducing factors for land degradation in Shilabati river basin are deforestation (Fig.2.1b), degradation in soil quality, loosening of the topsoil and soil erosion through water action (Mahala 2020) which makes it inescapable to evaluate the soil erosion susceptible zone that servers the food and livelihood sustenance of the people inhabiting there. An upstream dam has also been constructed named Kadam Deuli dam which act as pick-up barrage of Kangsabati river canal system. The Geomorphic unit of the study area consist of buried pediments with lateritic capping and the lower sector is of alluvial origin. Soil textures includes clay, clay loam and sandy loam to fine loam. Bare soil with loosened top is prevalent over the study area which intensifies soil erosion because of the recent forest degradation activities related to the extension of human inhabitants and unscientific agricultural activities. Presence of rills and gullies (Fig.2c) also predominates within the study area which deepens during high runoff events.

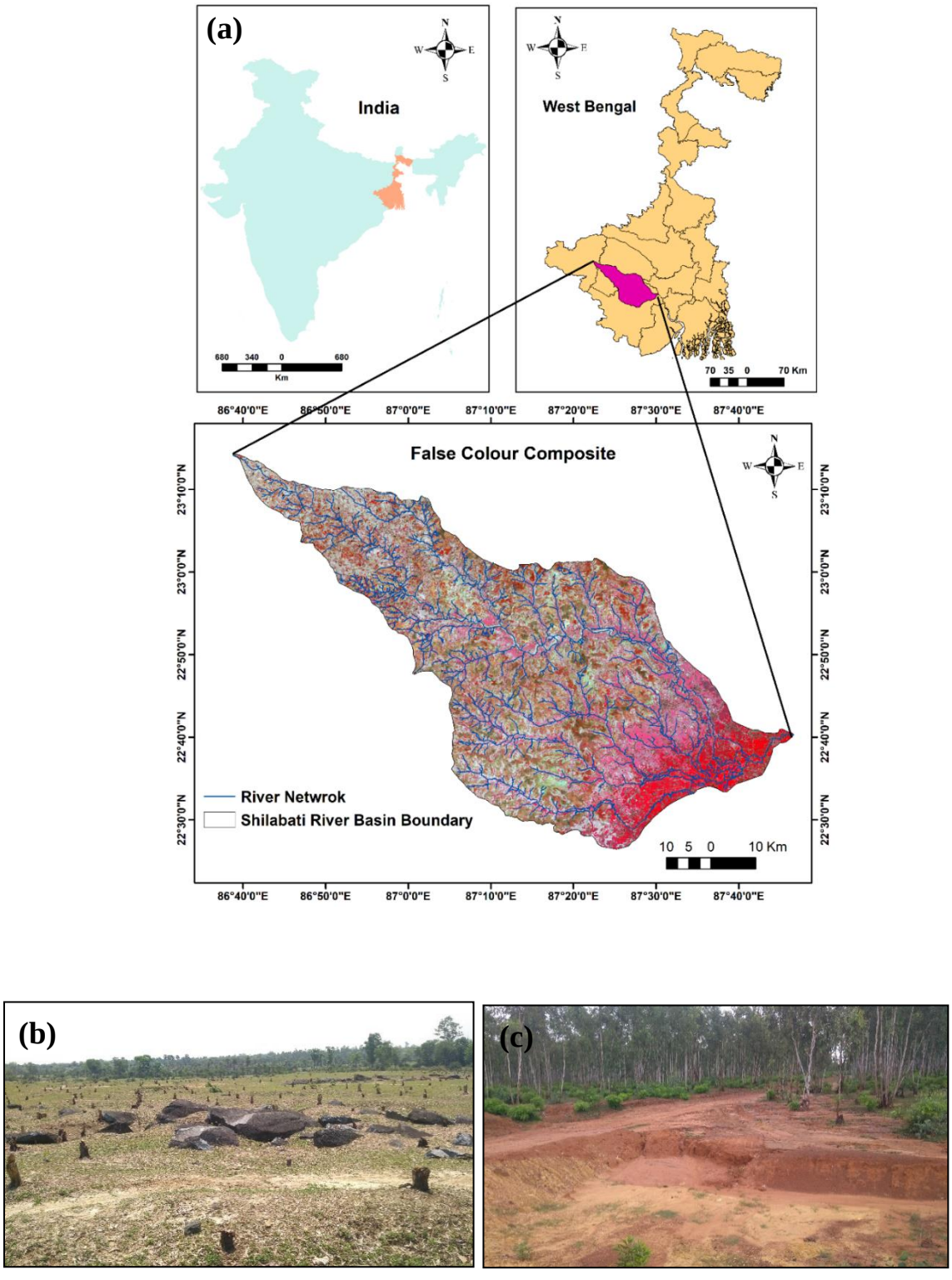

Fig. 2.1 (a) Location of the Shilabati river basin; (b) deforestation of the river basin and rill ad gullies within the river basin

2.2 General characteristics of the study area

2.2.1 Soil types

Soil erosion from an area depends on the type of soil and the nature of consolidation which depends on the influencing factors such as geology, climate and physiographical features (Arya et al. 2020). Eight soil texture types (Fig.2.2) has been identified within the basin namely fine (14.36%), fine loamy soil (38.11%), fine loamy to coarse loamy (13.34%), fine loamy to sandy (8.83%), fine- fine loamy (20.57%), fine to very fine (0.29%), Gravelly loam (2.33%) and gravelly loam to loam (2.18%). Areas predominant in sandy loam, sand and loamy texture soil are less susceptible to erosion than very fine sand and clay textured soil. Fine texture soil is predominantly found at the upper section of the basin which can lead to more soil erosion through water as the relief over the region is also higher. From a field survey conducted by the authors, intensive deforestation (Fig. 2.1b) has also been observed in the upstream part. The upper Shilabati basin exhibits coarse grained soil, predominantly sandy loam, with characteristics such as high silica content, poor humus content, and limited water carrying capacity. These attributes significantly impede land area productivity within the region. In the middle undulating plateau, known as the upland areas of the basin, the laterite soil possesses high percentage of iron, greater leaching potential, low pH, and inadequate water carrying capacity, leading to land and soil degradation. This degradation occurs as essential nutrient materials are get leached from these soils, aided by the formation of rills and gullies. Conversely, the soil in the lower sections of the river basin contains a substantial clay content, resulting in a heightened water-holding capacity and indirectly contributing to flood occurrences. Overall, the soils throughout most of the basin are prone to vulnerability due to their fragile characteristics.

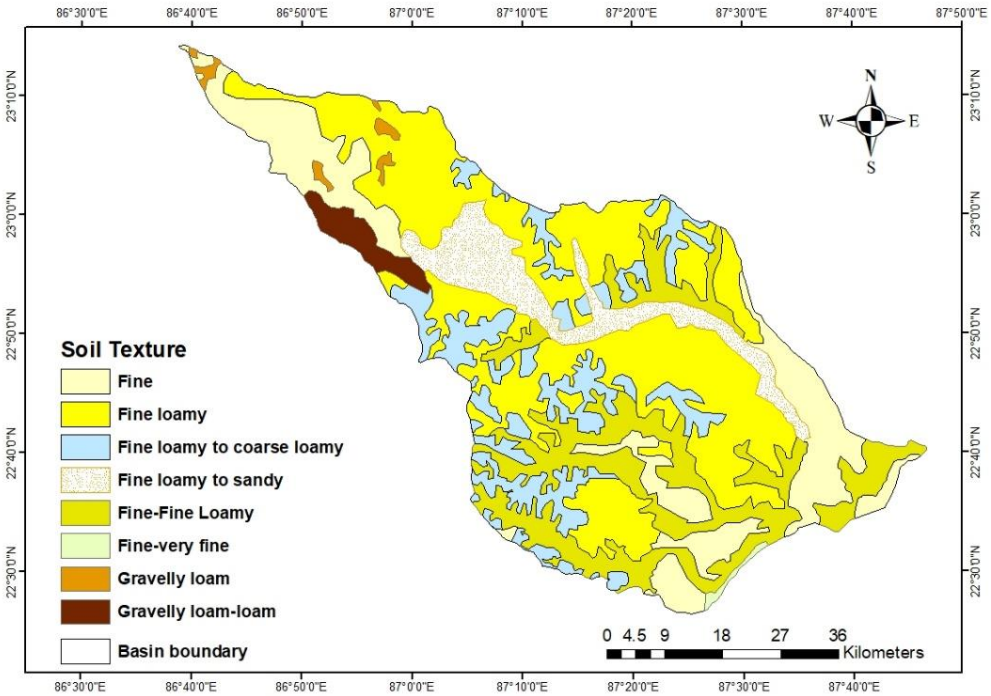

Fig. 2.2 Soil map of the river basin

2.2.2 Geomorphology

The geomorphological feature of a region depends on the composite interaction between the earth surface, climatic modifications, ecology and hydrology of an area (Dolui et al. 2016). Shilabati river basin represents a parallel drainage pattern between the Kasai and Dwarakeswar river basin covering the dissected lateritic Rarh regions with patches of deciduous forest and lateritic exposure (Ghosh et al. 2015). The lateritic exposure located within the region comprises alternative layers of lithomarge clays where tunnel erosion is predominant commonly known as soil piping (Ghosh and Bhattacharya 2012). Geomorphological features within the basin have been divided into 7 types namely denudational pediment-pediplain complex (6.22%), buried pediment shallow with laterite capping (12.29%), buried pediment moderate with laterite capping (34.12%), buried pediment shallow (13.18%), valley fill deposits (11.27%), fluvial origin older flood plain (10.92%) and fluvial origin active flood plain (12%) (Fig. 2.3). Buried pediment moderate with laterite capping is the predominant geomorphic feature within the study area and is highly susceptible towards soil erosion if not managed sustainably. Figure e illustrates the geomorphic features of the basin.

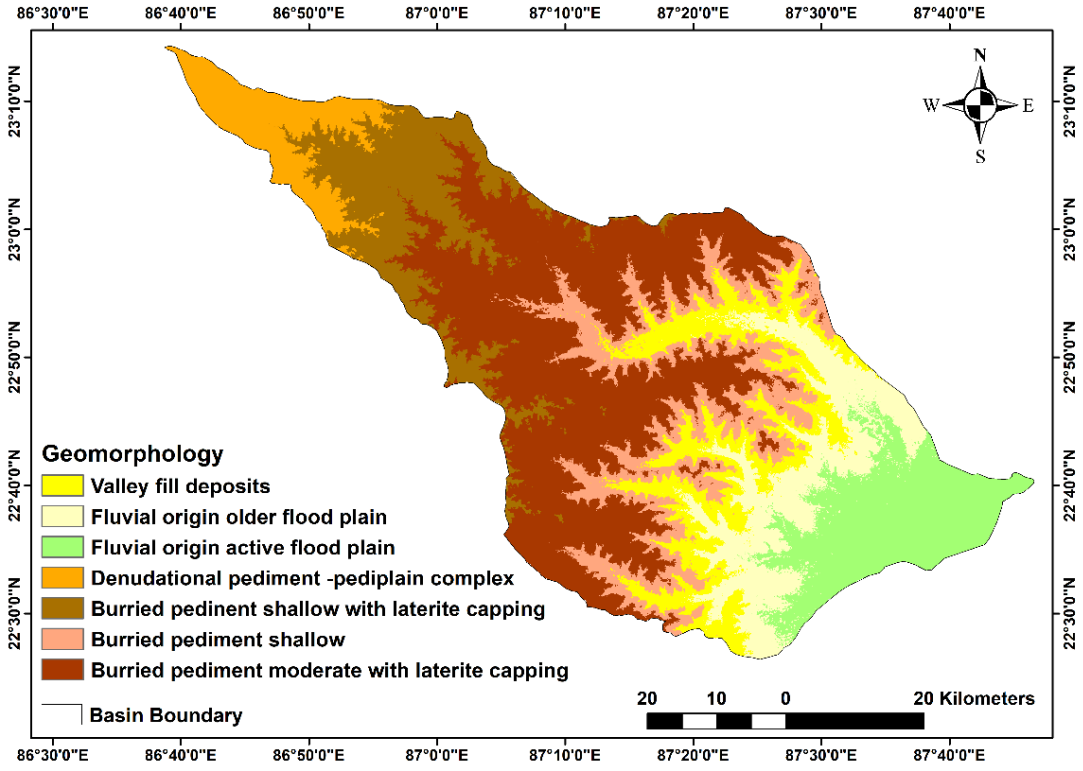

Fig. 2.3 Geomorphology of the river basin

2.2.3 Land use and Land cover

Land use and land cover plays an important role in effecting overall environmental health of a particular region if done in an unscientific way. Different type of land use and land cover play a different role in facilitating runoff capacities (Das et al. 2018) and hence control soil erosion. In this study Landsat satellite imagery has been downloaded from the year 1989-2021 and image atmospheric correction and geometric correction have been made

in QGIS software version 3.4.6. The corrected image has been used to prepare the land and land cover map in ErdAS Imagine 9.2 software using a supervised classification technique. The average accuracy of the classification has been calculated based on kappa co-efficient which came as 97%. The land use and land cover of the river basin has been classified into 9 classes namely water body, lateritic exposure, dry fallow, open forest, dense forest, sand bar, wet fallow, agricultural land and settlement (Fig.2.4). After agricultural land, dry fallow land dominates over the region and the areas under it are likely to increase as the forest cover of the region is decreasing year after year and decade after decade (Shit and Mondal 2019). Fig 2.5 shows the land use and land cover maps of the study area from 1989-2021. In order to conserve the soil surface, scientific land development, dry land agriculture and overall watershed management are needed. There has been an increase in the dry fallow land from 35.34% in 1989 to 39.12% in 2021 which in turn will have negative impacts on the groundwater recharge of the region (Fig.2.5).

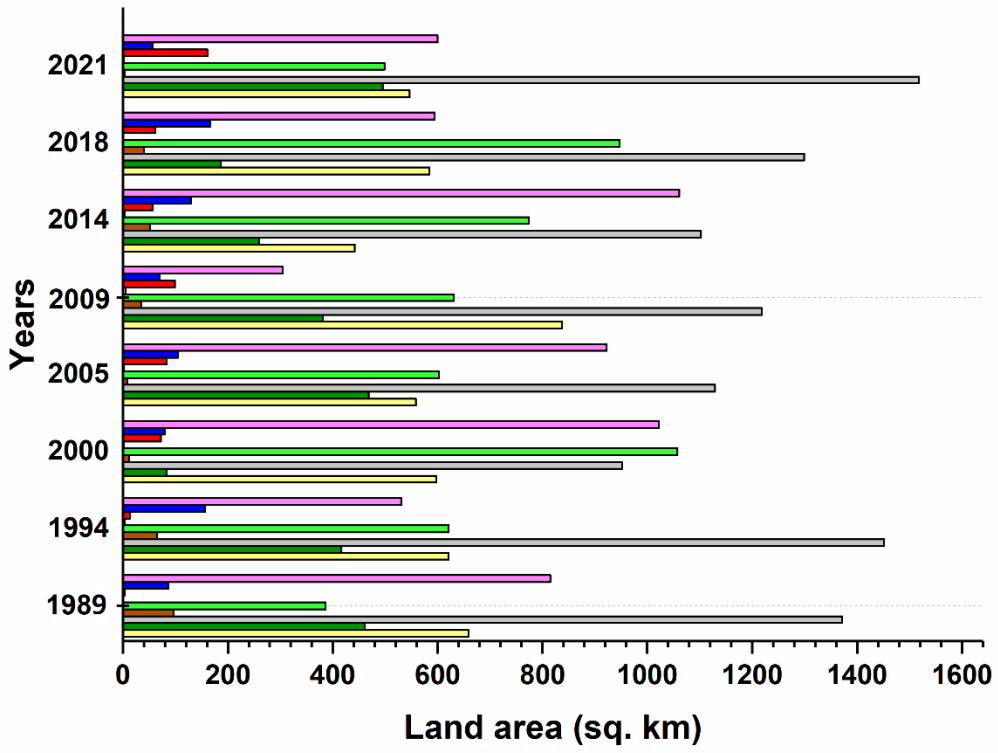

Fig. 2.4 Areal distribution of Land use and Land cover from 1989-2021

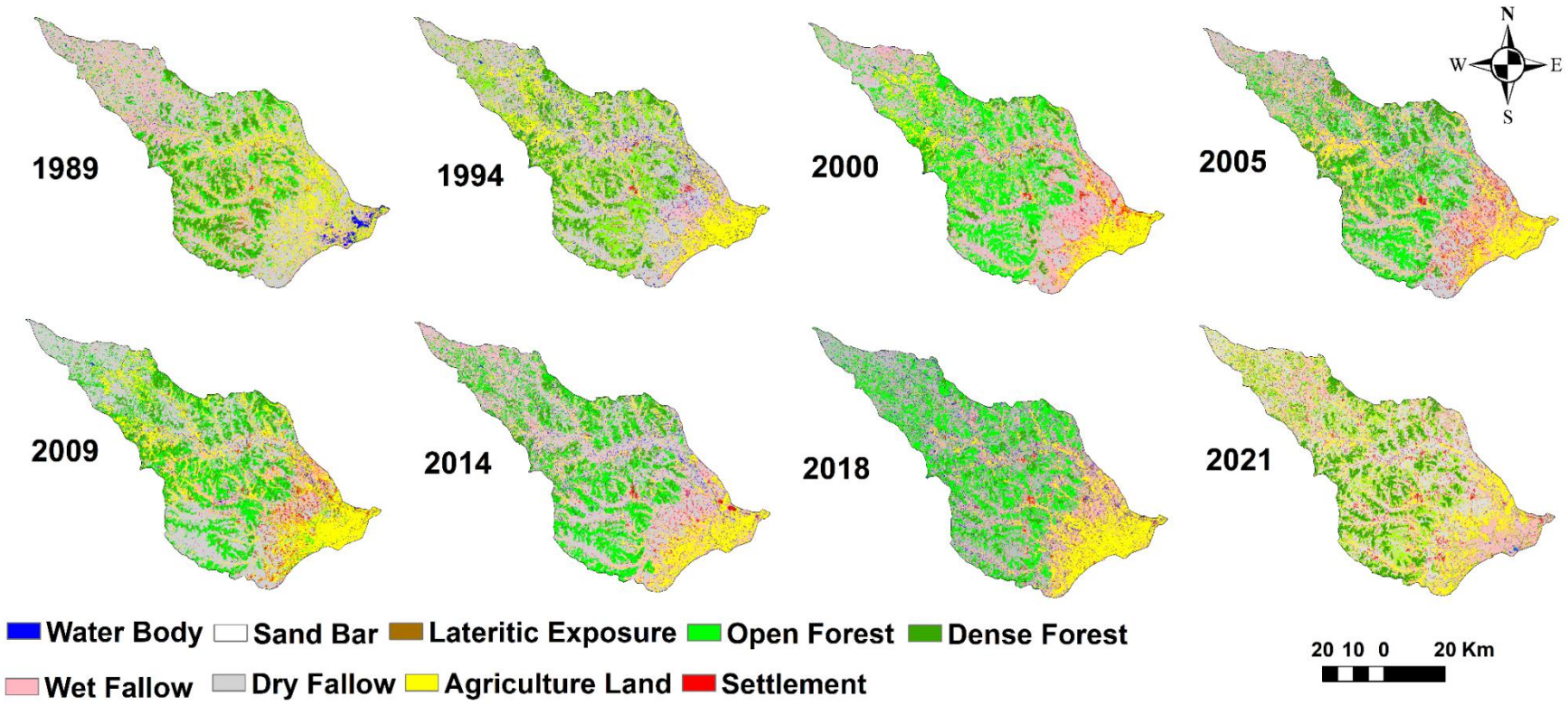

Fig. 2.5 Spatio-temporal distribution of the land use and land cover from 1989-2021

2.2.4 Runoff and Discharge

Runoff is one of the vital conditioning factors that controls the soil erosion of a particular region (Khatun, 2016). Runoff can be measured for a daily, monthly and yearly regime. The runoff and rainfall relationship can better be determined through USDA Soil Conservation Service (SCS) method (Fig.2.6) and the application of geospatial technology made it easier. The flow chart of the runoff estimation has been shown in fig. 2.6. The main input of the runoff estimation is land use and land cover and soil map. In the study area runoff has been estimated for the year 2000, 2014, 2018 and 2021 for each of the 9 sub-basins of River Shilabati. Runoff is higher in the upstream section of the basin where the presence of barren land is prevalent and therefore requires runoff control strategies. Based on the Soil and Water Assessment Tool (SWAT) model the average runoff of the basin is 1015.98 (Fig. 2.7a and b) which directly correlates with the runoff as calculated from SCS-Curve number. In the sub-basin Parang the runoff in the year 2000 was about 1178.1 which increased to about 2138.6 in the year 2021 (Fig.2.8). Therefore, sustainable water management strategies are required to enhance the water security plan for the rural inhabitants. The discharge of the basin has also been calculated from the SWAT model and has been validated well with the only Gauge station located at the Kadam Deuli dam located at the upstream of the river basin. There has been a major alteration in the flow velocity of the river basin since 1985 to 2014 because of the climate change effects.

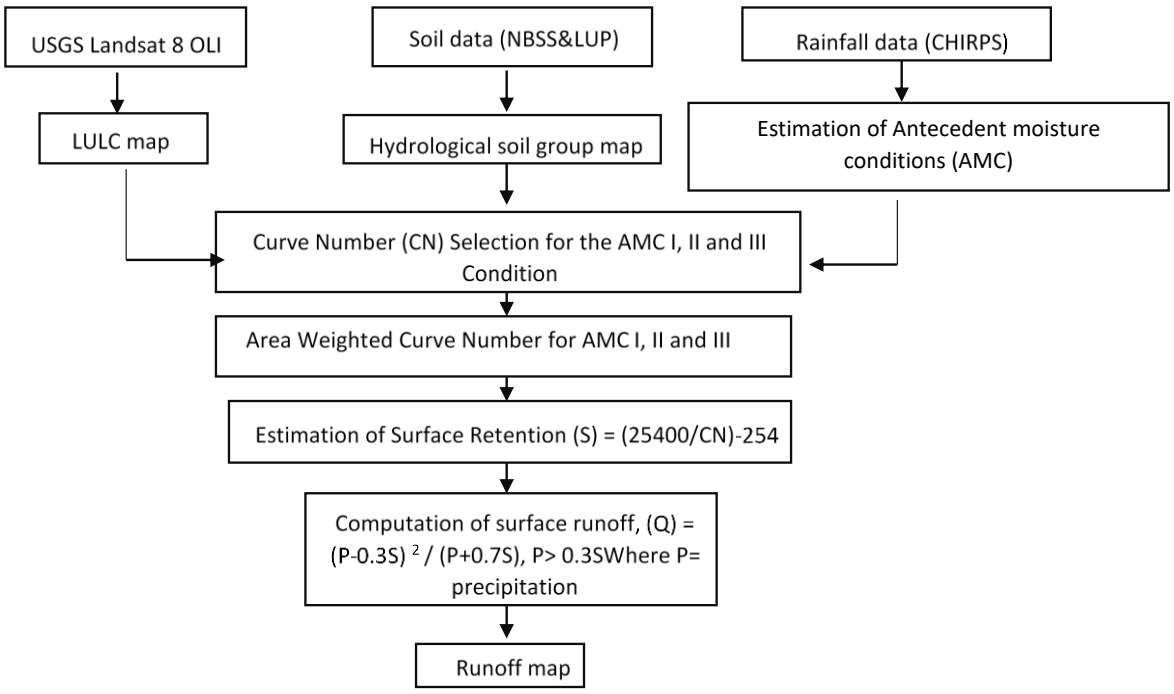

Fig. 2.6 Steps for the calculation of runoff using SCS-curve number

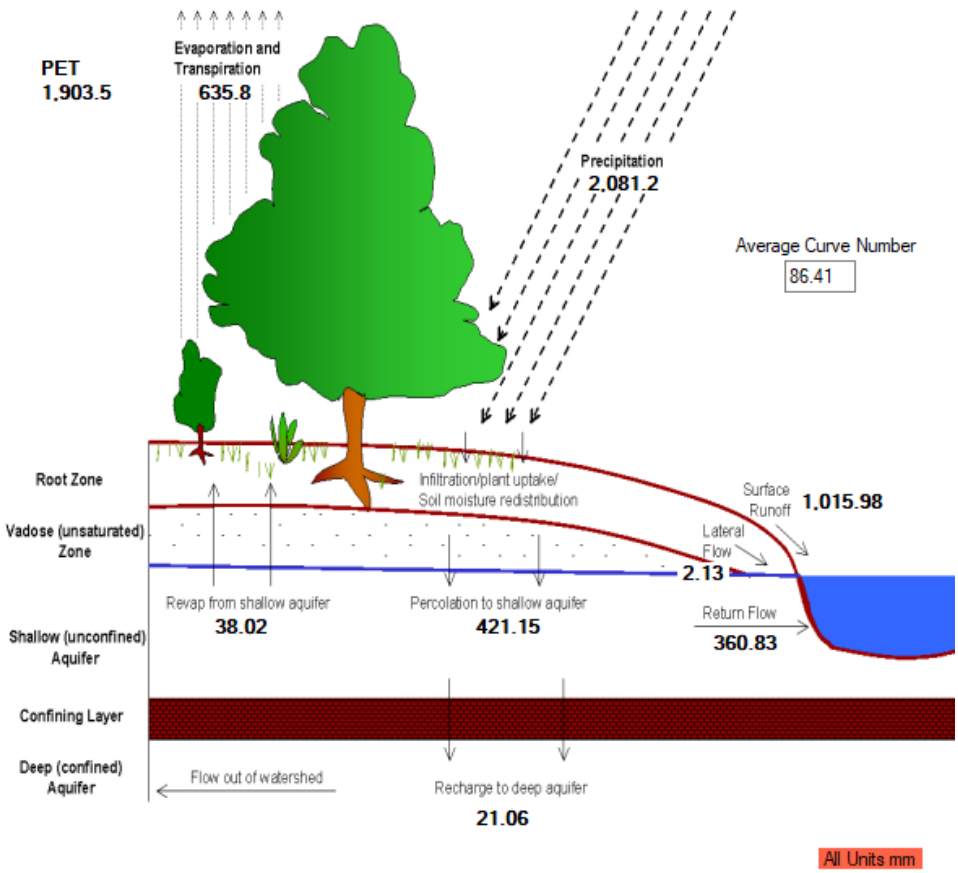

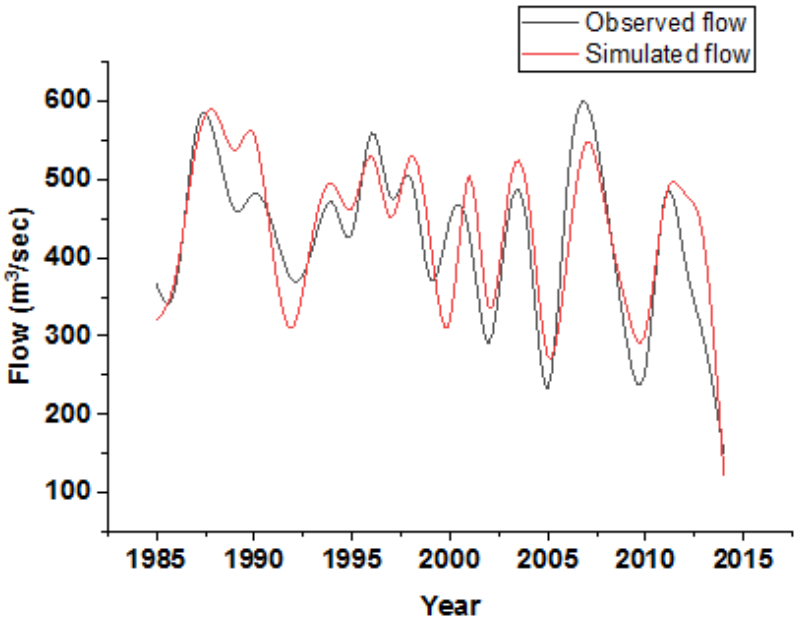

Fig. 2.7 Output from SWAT tool and validation of the results using the observed data from Kadam Deuli Dam

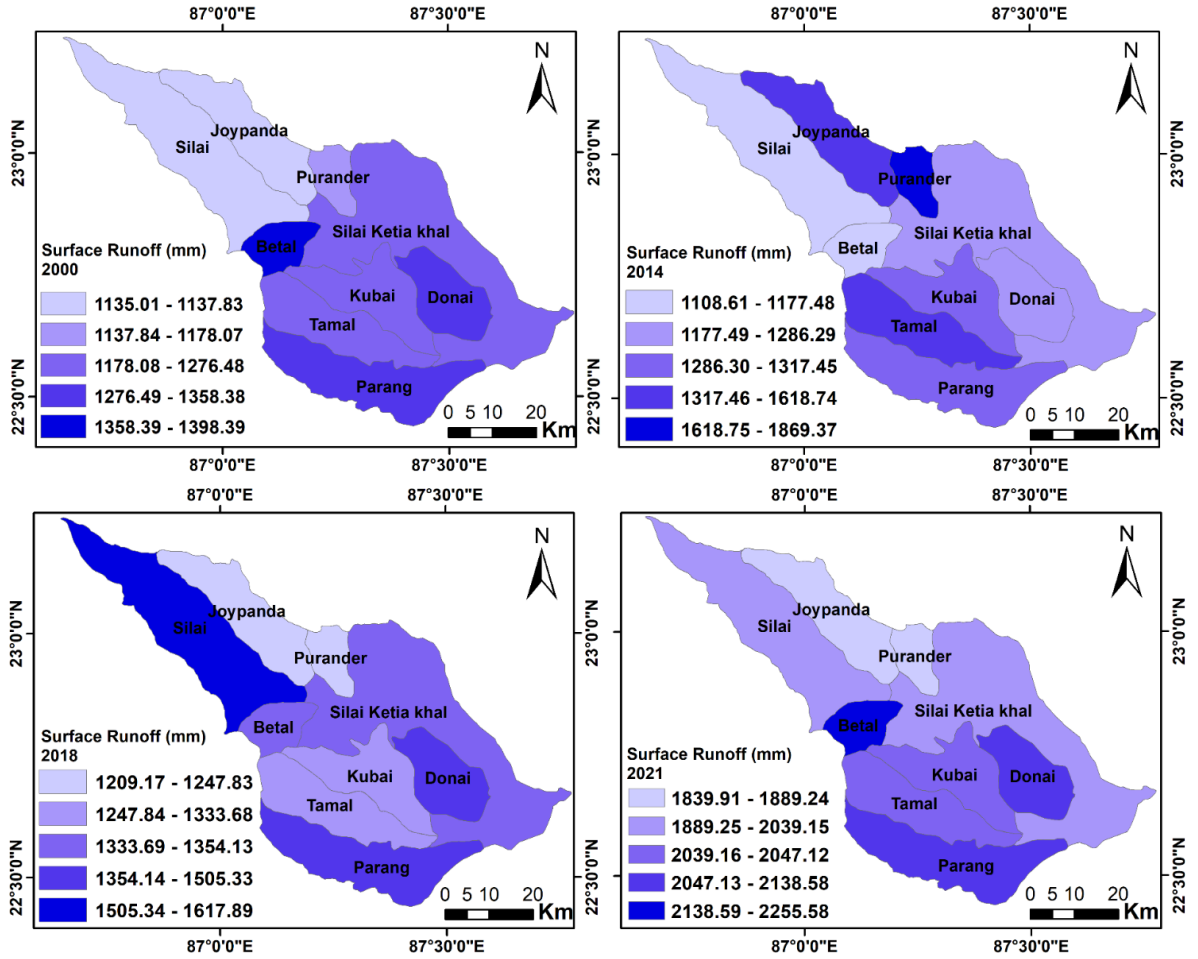

Fig. 2.8 Total runoff of the sub-basins for the year 2000, 2014, 2018 and 2021 using SCS-curve number

2.2.5 Slope

The slope is an important conditioning factor that engenders soil loss from a particular region based on its steepness. Greater the slope more will be the rapid surface runoff which will lead to an increase in the soil erosion rate (Magesh, 2012). The slope map of the river basin has been prepared using SRTM DEM of 30 m resolution through ArcGIS tool box version 10.3 (Fig.2.9). The slope has been calculated in degrees and is divided into 5 classes. The slope ranges from 0º - 0.56º (37.80%) is mainly concentrated at the lower section of the basin where the runoff is less and experiences less erosion. The areas having slope 0.57º -1.2º (34.23%) implies less susceptible for runoff and which is found scattered throughout the basin. The areas with 1.3º - 1.9º (21.33) slope signifying the areas with little undulation and this undulation increases with the slope ranging from 2º-5.5º (6.61%) mainly concentrated at the upper and middle section of the basin. The areas having the slope 5.6º - 20º (0.03%) are the areas associated with irregular topography, high surface runoff and greater soil erosion can be seen in few parts in the upper section of the basin. The Fig. 2.9 illustrates the slope map of the river basin.

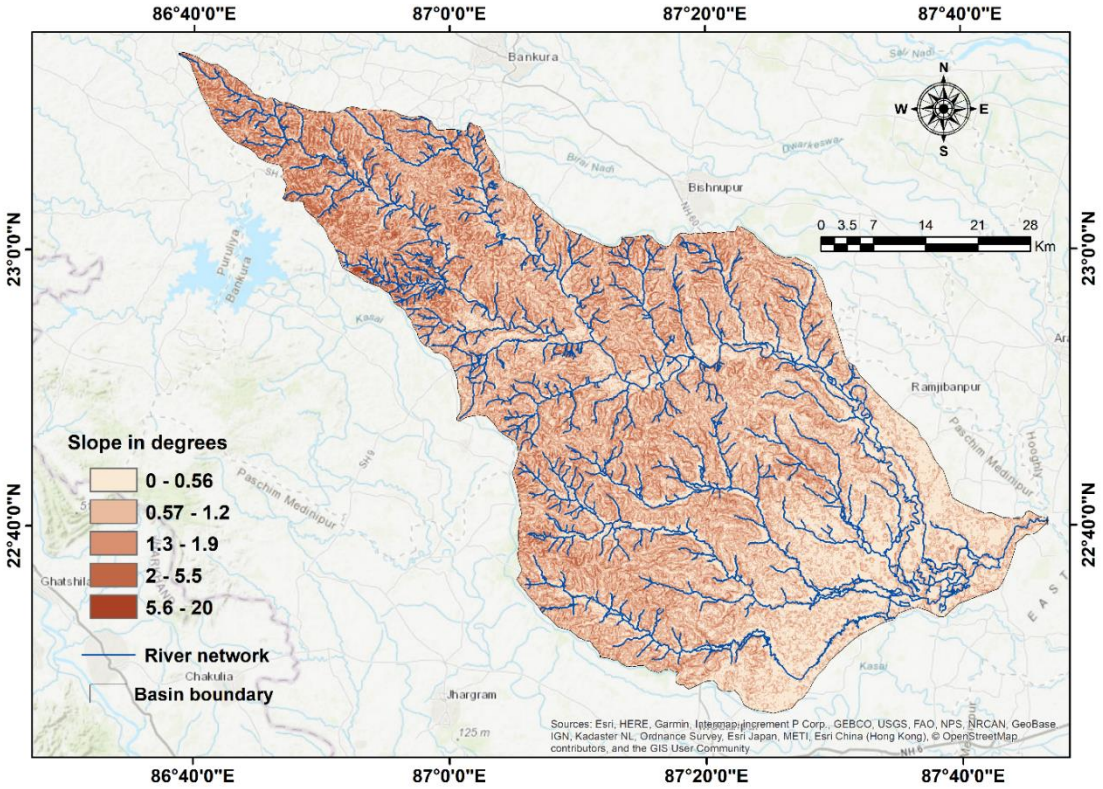

Fig. 2.9 Slope of the river basin

2.2.6 Drainage Density

Drainage density may be defined as the closeness in the spacing of the stream channels which can be defined as the total length of the stream segment of all orders per unit area. It indicates the density of stream channels in the river basin (Tiwari et al. 2019) and greater the density greater will be the dissection of the topography and more will be the soil erosion. The drainage density of the basin has been calculated using the Horton's method (1945) following Eq. (2.1)

$$Dd = L/A \tag{2.1}$$

Where L= Total length of the stream (km) and A is the Area (km^2)

The average drainage density of the basin is 0.338 km/km^2. The drainage density of the basin is divided into five classes (Fig 2.10) that is very high (38.87%), high (38.09) moderate (18.90%) low (4.10%) and very low (0.04%). The region is criss-crossed by the number of rills and gullies which initiate predominantly during the rainfall periods (Shit et al. 2015) and encourage greater runoff. It has a direct relation with runoff and hence soil erosion. Afforestation and scientific land use and land cover management are at an early need for sustainable development of the river basin.

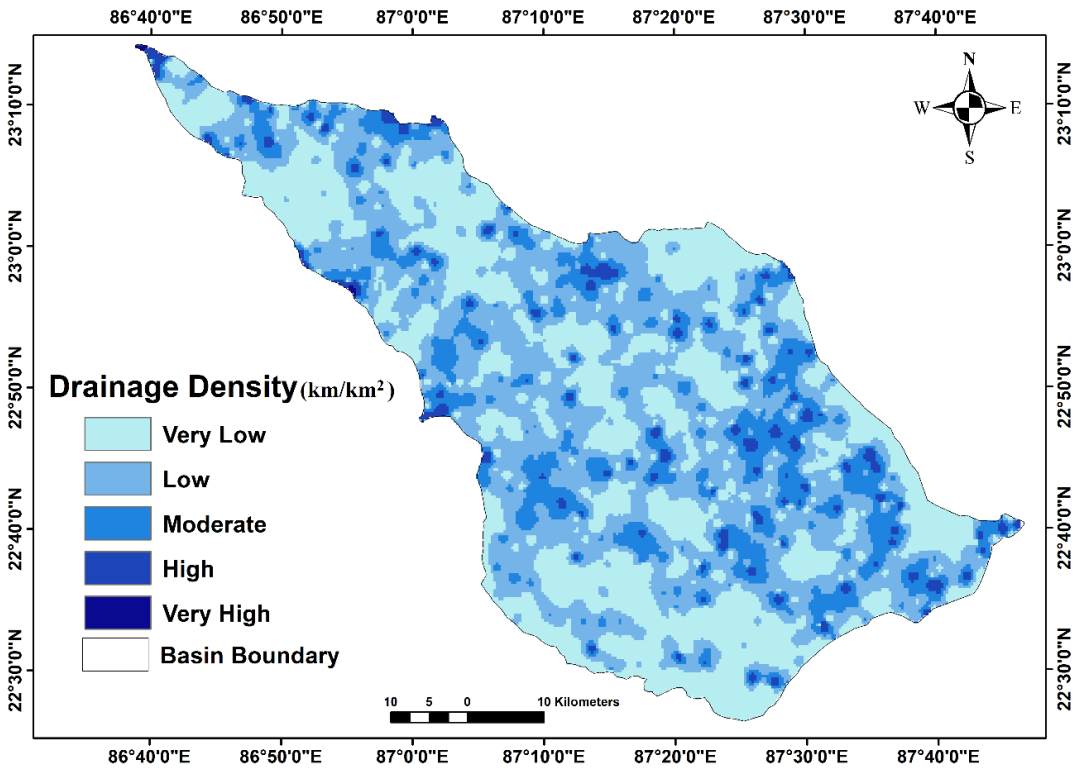

Fig. 2.10 Drainage Density of the river basin

2.2.7 Relative Relief

Relief is a significant conditioning factor that instigates the wasting away of the soil particle in a particular region. Greater the relief greater is the chances of soil loss if remain exposed to wind and water. Relative relief may be defined as the difference between the highest and the lowest point in the study area which gives a comprehensive morphometric assessment of the region and the degree of dissection (Thakurdesai and Pise, 2016). In the present study relative relief has been calculated using the Melton formula introduced in 1957. The algorithm used can be written as Eq. (2.2)

$$R_r = \Delta H/P \qquad (2.2)$$

Where, H is the difference between the highest and lowest point within the area and P is the basin perimeter. The relative relief of the region has been divided into 5 classes (Fig.2.11). The regions having very high relative relief of 40.22 -86.56 m (1.30%) is located at the upper section mainly covering Puruliya and Bankura district where soil erosion by water predominates (Sarkar and Mishra 2018). Whereas very low relative relief of 0.923-11.67 (22.92%) can be found at the lower section of the river where erosion is less.

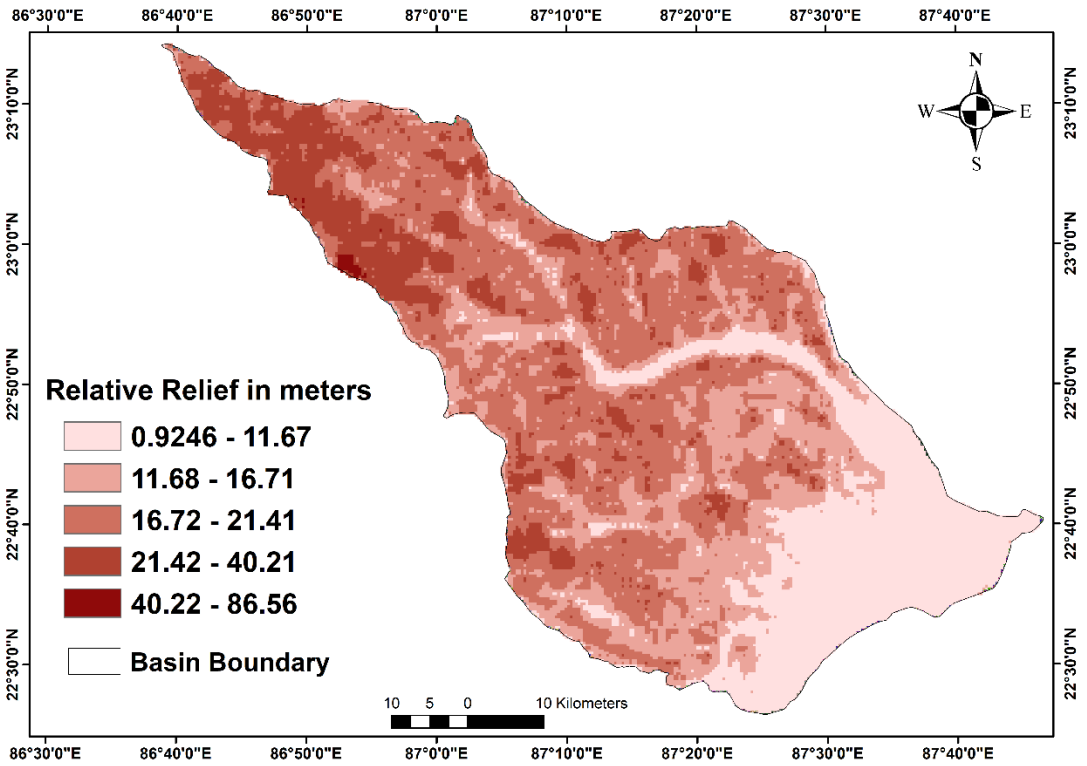

Fig. 2.11 Relative relief of the river basin

2.2.8 Geology and hydrogeology

Aquifer contamination can occur through surface runoff, seepage, and infiltration of polluted environments, which are highly influenced by the geological setting (Biswas et al. 2020). Delineation of the geology of the study area has been made from the map as provided by the Geological Survey of India (GSI) on GIS platform. Fig. 2.12 illustrates the geology map of the river basin. The upper section of the basin covering the Puruliya and Bankura district consists of a diverse group of rocks from different geological ages like intrusive Granites, meta-sedimentary of Singhbhum group, Chotonagpur gneissic complex, volcanic rocks of Dalma group and sediments of Quaternary ages and Gondwana plain and granite and gneissic crystalline complex of the Archean era (Das et al. 2019; Goswami and Ghosal, 2022). The most common are granitic and granitic gneiss (12.77%) (Das et al., 2018). In the complex rock terrain, contamination from the surface source is less as the infiltration is less than in the weathered and fractured areas. As a result of granite, pegmatites, fluorite, etc., fluoride contamination dominates in some parts of the upper basin (Saha et al. 2017). The middle section of the basin is primarily composed of fluvial-deltaic sediment covered by primary and secondary lateritic terrain where iron contamination is high (Bhunia et al. 2012). The lower part comprises younger alluvium of sand, silt and clay where groundwater is in unconfined condition with surface loamy clay. It is important to note that the downstream section has moderate infiltration with good chances of aquifer vulnerability from pollutant sources and a decline in groundwater levels due to extreme agricultural extraction by submersible pumps (Halder et al. 2020). A significant portion of the study area consists of granite gneiss (12.77%), lateritic soil/ laterite (41.38%), sand, silt & gravel (present-day deposit) (4.79%), yellowish-brown fine sand, silt, clay (7.59%), mica schist with hornblende.

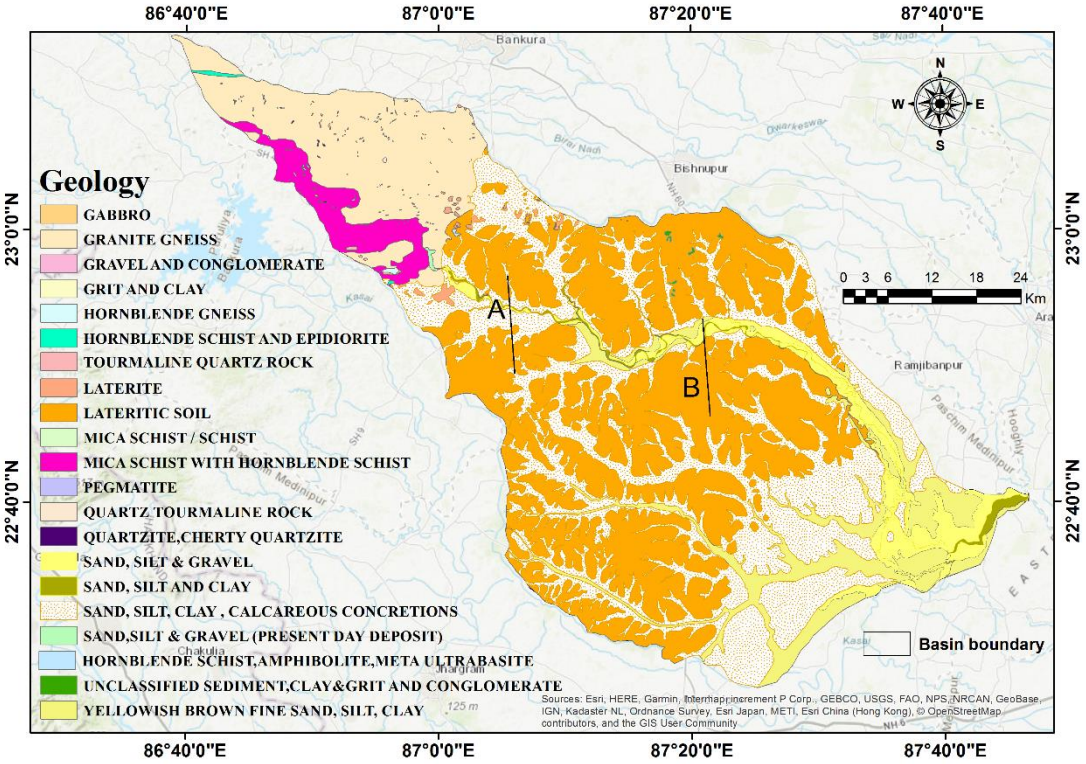

Fig. 2.12 Geology of the river basin

2.2.9 Climate and Vegetation

The river basin comprises diverse climatic scenarios with semi-arid conditions in the upper section and tropical monsoon type in the lowest part of the basin. It experiences drought in its upper part, threatening livelihoods, while flooding in its downstream section threatens human lives. A consequence of both of these events is the ruination of agricultural fields (Palchaudhuri and Biswas 2016). The average monthly rainfall of the basin varies from 100-190 mm (Fig. 2.13) and the maximum temperature ranges from 40-40^{o}C. Fig. 2.13 shows the average monthly rainfall of the basin from the year 1998 to 2021. Due to the climate change rainfall increased due to the increase in intensity of short duration events. Furthermore, a check dam in the upstream portion of the dam provides insufficient water, making the area more vulnerable to droughts. Global water demand, limited water supplies from existing reservoirs, regional inequalities, and climate change make water supply management very challenging under such terrain conditions (Bera and Das, 2021), resulting in poor agricultural output during dry seasons and summer months. In the central part of the basin, one can witness a dense forest canopy adorned with numerous clusters of Sal trees. Unfortunately, the expanding population has led to a decline in forest coverage. Nonetheless, efforts have been made annually through diverse afforestation schemes and programs to establish new forests on barren lands or government-owned areas. Additionally, certain forested regions underwent conversion into agricultural lands, and the introduction of irrigation in these areas resulted in the encroachment upon forested territories which will eventually lead to climate change inducing the magnitude of drought events in near future.

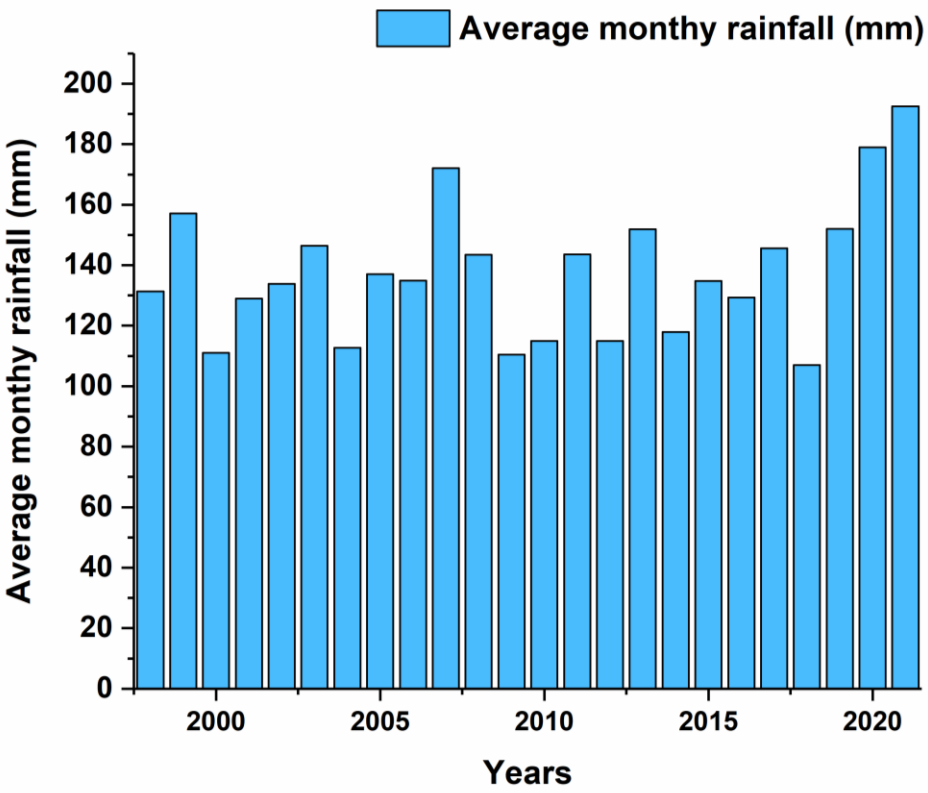

Fig. 2.13 Average monthly of the river basin from 1998-2021

2.2.10 Groundwater Recharge

In this study, groundwater recharge was assessed by collecting the pre and post monsoon groundwater levels from 20 observation wells using CGWB and CHIRPS rainfall data, as well as specific yield and infiltration factors based on the local geology. Under unconfined to semi-confined layers throughout the basin, groundwater is mainly concentrated in fractured and weathered zones (Sahoo et al. 2021). Over the basin, land use and land cover are changing rapidly, affecting groundwater recharge and reducing water table levels. It is therefore necessary to accurately estimate recharge in order to gain a better understanding of groundwater pollution and aquifer vulnerability (Robins, 1998). Based on the GEC, 1997 and 2015, groundwater recharge has been calculated using Eq. 2.3 (Prasad and Rao, 2018).

I. Groundwater recharge (ham) by water table fluctuation method (wfm) = Geographic area * Specific yield* Rise in the water table
II. Groundwater recharge (ham) by Rainfall infiltration method (rifm)= Area* Normal rainfall* Infiltration factor

According to the criteria as recommended by GEC, 1997 final recharge of the basin has been calculated using Percentage Deviation (PD) following the Eq. 2.3 (Siva Prasad et al. 2018).

$$PD = \frac{a(wfn) - b(rifm)}{b(rifm)} * 100 \quad (2.3)$$

The groundwater recharge has been divided into five classes namely 3.37-1293.4 (21.36%), 1293.5-2583.5 (41.57%), 2583.6-3873.5 (29.48%), 3873.6-5163.6 (3.66%) and 5163.6-6453.6 (3.93%).

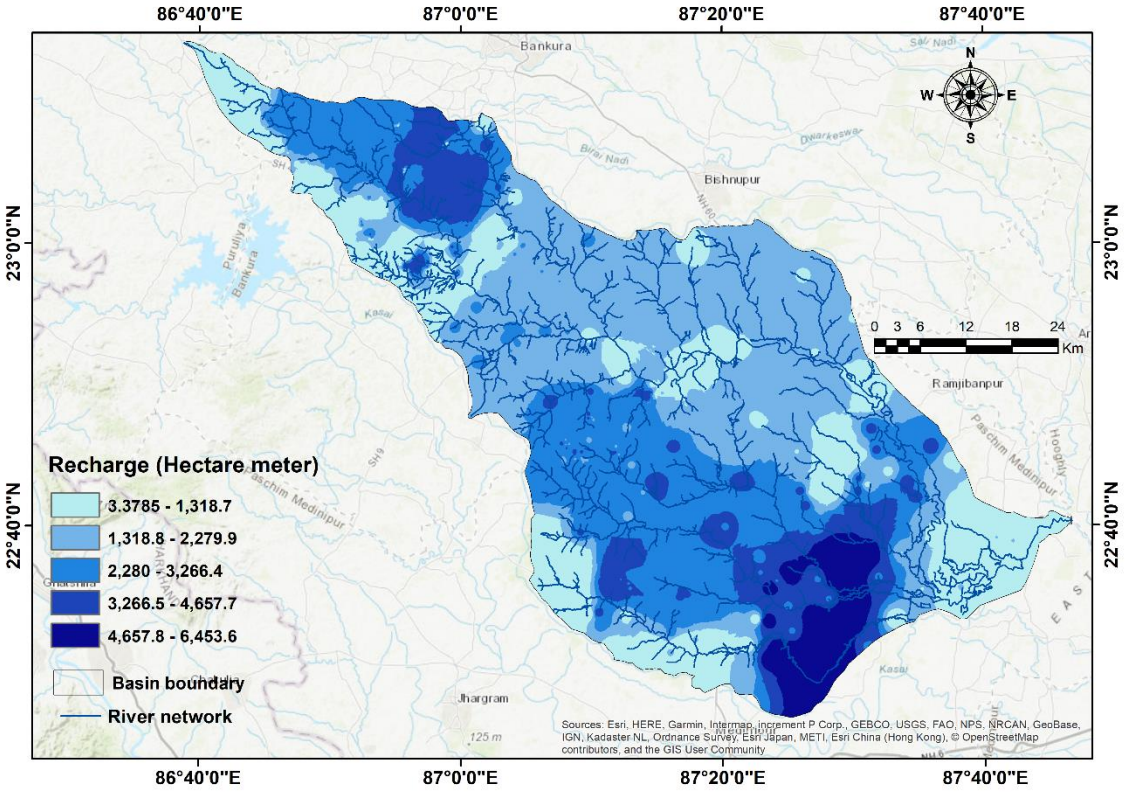

Fig. 2.14 Groundwater recharge of river basin based on GEC, 2007 methodology

2.3 Major Hydro-Environmental Problems within the Study Area

- In the lower section of the basin, the dominant factor is the impact of overland flow rather than channel flow, mainly due to the limited channel storage capacity of small watersheds. Additionally, small watersheds play a significant role in high-intensity precipitation events of short duration and can alter the landscape pattern. This area is characterized by high river banks and a narrow river channel. During the winter season, rainfall is minimal, further use by irrigation for the spring crops. However, in the monsoon season, the river becomes highly vulnerable, resulting in extensive flooding. The magnitude of river regulation impacts varies depending on the degree of channel modification, including straightening, widening, dredging, and the release of water from the storage for irrigation and for generation of hydroelectricity which can cause rapid and abnormal changes in water level and velocity.
- The Shilabati River is surrounded by unplanned markets and experiences various anthropogenic activities. Continuous direct dumping of untreated anthropogenic waste into the river deteriorates water quality, river shoreline basins, and causes severe pollution. The pollution status of the Shilabati River is progressively worsening, with phosphate and turbidity identified as major physicochemical parameters contributing to the pollution based on extensive literature reviews. Numerous pipelines connected to public toilets discharge waste directly into the lower reaches of the river. Additionally, small-scale industries and factories situated along the riverbank, such as battery and religious stick factories, discharge their untreated waste directly into

the river. Furthermore, various shops near the river dispose of waste products, including ashes from burnt religious sticks and used flowers, into the river water.

- The upper catchment area of the river has unfavorable soil conditions for agriculture. However, with increasing population demands and urbanization, the use of subsurface water in the study area has been growing. In the unconsolidated sandy sediments of recent alluvium, which primarily contain laterite and fine loamy soil in the middle and lower sections of the basin, the water table lies between 2 mbgl to 20 mbgl. Groundwater yield is significant and supports agriculture through shallow wells and deep tube wells. However, in the upper section, groundwater is mainly concentrated in cracks and fractures of rocks, and frequent drought events have led to a sharp decline in groundwater levels.
- Due to limited availability of fresh drinking water supply and the absence of centralized drinking water treatment facilities, people are compelled to consume fluoride-contaminated water in the upstream section of the river basin. The presence of skeletal fluorosis and bone deformations among local villagers was prominent during field surveys. High levels of iron contamination in groundwater in the middle and lower sections of the basin are also evident.

2.4 Evidences of the research problem from the study area

Picture 2.1 Drying condition of the Shilabati River

Picture 2.2 Fall in groundwater level in dug wells within the river basin

Picture 2.3 (a) Contaminated dug well used for domestic purpose and (b) people effected with bone deformation and skeletal fluorosis within the river basin

2.5 Index map of the study area

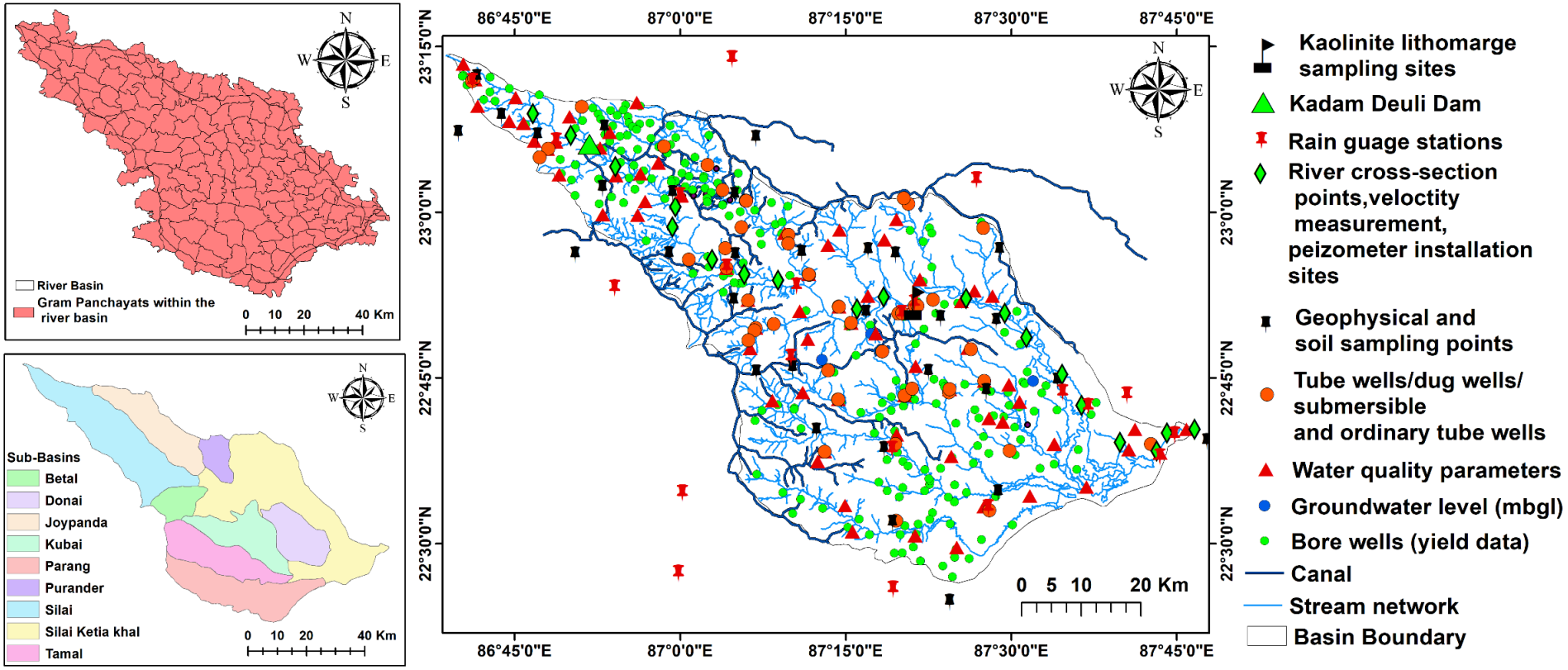

Fig. 2.15 Index Map of the Study Area

Chapter3
Basin Prioritization for Sustainable Groundwater Management

3.1 Introduction

Water scarcity is now one of the major issues at a global level largely driven by the enormous growth of the human population and exaggerated by impact of climate change through precipitation and temperature alterations. Drying of the river and water bodies is due to the increase in the magnitude and intensity of temperature anomalies which has become quite evident. The global temperature rose by 0.85ºC from 1800 to 2012 which may further trend to increase accelerating the current situation (Li et al. 2016). Beside the climatic impacts, geology, relief, geomorphic attributes, structural symmetry etc. are the foremost dominant factors controlling the water ecosystem at a basin scale (Mesa, 2006). To address numerous hydrological, hydrogeological and hydro-morphological scenarios acting within a basin requires a watershed management plan and strategies. Watershed is also a biophysical response unit as well as holistic ecosystem that highlights the material, information and energy flow through it (Wang et al. 2016). A watershed is a topographically demarcated area drained by a network of streams namely a river system. It is mainly the total area scaling from the originating point of a stream up to its mouth or draining point. Watersheds are the main source of navigation, drinking water supply, recreation, agriculture and irrigation, sustenance of the ecological habitat and disposal sites of waste water and materials (Russo, 2008). To study the behavioral attributes of a watershed morphometric analysis remains the prime concern as it controls the other related components. Understanding the conjunctive use of ground and surface management is the most important for integrated water resources management (Zhang, 2015) where the assessment of morphological parameter assessment is the primary aim and the preliminary investigation strategy. To ascertain the current status of the characteristics of a stream within a watershed like carrying capacity of water and sediments, recharge and runoff characteristics etc. morphometric analysis is at urgent need. According to Asfaw and Workineh (2019), analysis of morphometric parameters helps in the estimation and identification of the potential areas of the infiltration and runoff and other related hydrological phenomena of a watershed. Watershed morphology is therefore is a matrix of linear aspects, areal aspects and relief aspects of a basin which are the results of the interaction of climate lithology, geology and land use over a long-time frame (Aisuebeogun and Ezekwe, 2013). Incorporating all the components it is necessary to prioritize the sub-watersheds based on different issues for the sustainable watershed management at a micro-scale which is basically the ranking of the sub-basins in respect to their order as such one can implement soil and water conservation techniques accordingly (Abdeta et al. 2020). Several investigations have been carried out related to morphometric analysis which depends on the topography of the landform by which the drainage basin has been composed of and on the shape and the structure of river system within it (Horton, 1932). Horton in 1945 made the quantification of the drainage basin based on morphometric characteristics like drainage density, stream order, bifurcation ratio and stream length ratio. Fenta, 2017 analysed the morphometric parameters from four perspectives like drainage network, watershed geometry, relief character and drainage texture of Angula watershed in semi-arid region of North Ethiopia. Debelo et al. (2017) identified

the areas vulnerable to soil erosion using morphometric attributes and found linear and relief aspects having a positive association and areal aspects have a negative with soil erosion. Ayogu et al. 2019 applied the morphometric aspects to validate Horton's postulation in the Anambra drainage basin of Nigeria.

Remote sensing and GIS are now one of the emerging platforms which fastens such work within a short period and in a cost-effective manner and the works which are evaluated numerically can be mapped in GIS platform to make it more flexible for water resources management (El Garouani et al. 2020). Rahaman et al. 2015 identified the water scarce zone is Kallar watershed of Tamil Nadu, India using morphometric attributes together with remote sensing, GIS and Fuzzy Analytic Hierarchy process. Incorporation of MCDM (Multi-Criteria Decision-Making Technique) and statistical technique in watershed analysis is a new trend. Choudhari 2018 has used remote sensing and GIS for prioritization of the Mula river basin, Maharashtra, India to identify the areas requiring high priority to go under conservation measures. Before the application of various techniques of prioritization to find out the potential zone based on the occurrence of an event, it is important to find the inter co-relation between the morphometric attributes. Application of multivariate models is an important methodology useful while analysing the data consisting of the large number of variables (Meshram and Sharma, 2017) and to reduce the dimensionality in a data set (Malik et al.2019). Amparan et al. 2019 made a correlation analysis like Principal Component Analysis (PCA) and Group Analysis (GA) using morphometric parameter of 31 watersheds to identify soil erosion prone zones in the Conchos river basin of Northern Mexico. Now to witness the capability of morphometric attributes to prioritize the basin, Farhan et al. (2017) applied PCA over forty-three 4^{th} order sub-basin of Zerqua river in North Jordan. The need for such techniques is more in the going days as 159 million people are entirely dependent on surface water bodies as recommended by WHO (2017). Application of this methodology will help in the sustainable water resources management (Dusabe, 2019). Each of the tributaries within a river system borne certain individual hydro-morphological characterises in such cases cluster analysis plays an eminent role. Raju and Kumar, 2011 applied K- means cluster analysis, fuzzy cluster analysis and neural network to group 25 micro-watershed of Kuesthal watershed, Rajasthan, India based on the need of conservation and management practices. Such kinds of studies are fewer in number which is needed the most. Application of cluster analysis is quite visible in water quality monitoring assessment. In watershed management after analysing the variability of the morphometric aspect, the foremost work is to study the influence of these parameters in quantifying the recharge and runoff pattern of the basin through prioritization techniques. Groundwater recharge is one of dominant factor in case of groundwater withdrawal and identifies the groundwater development potential of a particular area or region (Doll and Florke, 2005). Groundwater recharge depends on the physiographic heterogeneity and climatic setting of the landscape. As such in mountain watershed groundwater is considered as a major contributor because of the shallow soil development and steep slopes (Somers and Mckenzie, 2019). Whereas in plateau region groundwater recharge depends on soil and local regional undulation at the prior level (Yin et al. 2011). At the downstream section groundwater infiltration is more as they are structured by fluvial outwash plain (Epting et al. 2021). Areas of higher groundwater recharge are the areas of low runoff and vice versa. The global aquifer depletion was reported to as 283 (±40) km^3/ year according to Wada et al. (2010). As such ranking of sub-watershed based on MCDM techniques is needed to conserve their valuable resource through priority wise basin management. MCDM is an effective tool in water resources management which depends on the structuring of decision problem which incorporates the choosing and selection of criteria and decision options (Machiwal et al. 2010; Onu et al. 2017). Ameri et al. 2017 applied three different MCDM techniques like TOPSIS, VIKOR, SAW and CF for ranking the sub-watershed of Ghaemshahr basin of Iran based on erodibility character. Makhduni and

Dwarakish (2019) applied TOPSIS and VIKOR for ranking the river basin of Netravati catchment, Karnataka, India. Dhan et al. 2016 applied MCDM and decision tree algorithm in the identification of groundwater potential zone and surveyed about 80 tube wells to validate the model. Therefore, for effective conservation prioritization of the watershed is important to identify top priority area (Meshram et al. 2020).

Morphometric attributes provide new a perception of the hydrological process operating within the basin which influence the water availability and the water scarcity in river basin. According to the Central Water Commission, Government of India report (2018-2019) more than 600 million people are facing a shortage in terms of water supply for drinking, agriculture, irrigation and in other sectors. Due to climate change most of the river are drying up during the summer months and extensive flood occurs in monsoon from short period precipitation events. According to Masood et al. (2015), for Ganga Brahmaputra Meghna basin the runoff will increase by 33.1%, 16.2% and 39.7% respectively by the end of the 21st century.

3.2 Research Gap and Novelty of Work

Groundwater crisis is playing a serious concern in the Shilabati river basin located in a tropical plateau fringe region of the south eastern part of West Bengal, India. The river rises from the geological structure of Chotonagpur gneissic complex where groundwater recharge is very poor and is affected by yearly drought scenarios with a prolonged shortage of water supply. Based on the literature reviews no research work has been done on the basin prioritization for understanding sustainable groundwater management. The present research is to address this issue through a number of statistical techniques and multi criteria decision making approaches (MCDM). Novelty of the research was reflected in the application of K- means clustering in basin prioritization studies and its validation using groundwater yield data.

3.3 Objectives of the Research Work

Based on the above conditions it is necessary to undertake watershed management strategies to cope with the situation to ensure uniform distribution of water resources within the basin and no such studies have been conducted earlier in the selected area of interest. Therefore, the objective of the study is (a) to analyses the correlation among morphometric parameters and their clumping using PCA (b) clustering of sub-basin based on morphometric asymmetry using K-means clustering (c) prioritization of sub-basin based on groundwater potential using TOPSIS, VIKOR and COPRAS (d) selection of the best model and validation with groundwater yield data. Such studies will provide valuable information regarding the water resources scenario of both the surface and groundwater availability to the policy makers and stake holders for sustainable watershed management at a micro scale and will contribute to various water resources engineering discipline.

3.4 Area of Investigation

The Shilabati river basin is an important river basin located in the south eastern part of West Bengal, India comprising three districts of Puruliya, Bankura and West Medinapore. It rises from the Chotonagpur plateau in Puruliya district and flows in a south easterly direction and joins the Rupnarayan river system in West Medinapore district. The latitudinal extent of the basin is 23º14'18.03" N to 22° 26' 25.12" N and the longitudinal extent is between 86° 38' 46.08" E to 87° 46' 36.65" E (Fig 1). The basin covers an area of 3881 km^2 approximately and the perimeter of the basin is 342.98 km and is divided into 9 sub basins namely Silai, Joypanda, Purandar, Betal,

Kubai, Tamal, Donai, Parang and Silai-Ketia Khal. The elevation of the river basin varies from 212 m to 4 m (meters). The basin experiences tropical climatic conditions with an average monthly rainfall of 109 mm which is mainly concentrated in the month of July and October (Ghosh and Mondal, 2018) and the average monthly temperature ranges between 35ºC to 40ºC. The basin experiences drought like condition in the upstream section whereas it receives occasional flash flood in the downstream section (Annual Flood Report, 2018). The basin is crisscrossed by numerous rill and gullies as located near the margin of Chotonagpur plateau comprising rolling land with dissected upland particularly at the middle section (Shit et al. 2015). Land degradation, groundwater depletion, drying of the surface water bodies and more intensively soil erosion through extensive runoff from the bare land are the main parameters driving and alternating the physical characteristics of the basin (Mahala, 2020). Such potential scenarios make it inevitable to evaluate the influence of morphometric parameters towards hydrological, topographical, hydro-geological and societal behavior of the drainage basin.

3.5 Research Design and Methodology

3.5.1 Data source

Watershed is a topographically demarcated area drained by a river system where after each precipitation event runoff initiate from a single point and joins the nearby stream. The Shilabati basin has been digitised from scanned topographical sheets (73I/12, 73I/16, 73J/13, 73 M/4, 73 M/8, 73N/1, 73N/10, 73N/14, 73N/2, 73N/5, 73N/6, 73N/7 and 73N/9) obtained from survey of India, Government of India. The basin has been sub-divided into nine sub-watersheds based on the contour line and flow direction of the streams. The elevation map of the study area has been obtained from SRTM (Shuttle Radar Topographic Mission) Digital Elevation Model (DEM) of 90m resolution as downloaded from USGS Earth Explorer website (https://earthexplorer.usgs.gov/). Software used in this study include ArcGIS 10.3 and ERDAS Imagine 9.2 for geospatial analysis and SPSS and XLSTAT for statistical analysis. The morphometric attributes like drainage network, basin geometry, drainage texture and relief aspects of the sub-basin have been calculated using different empirical algorithms as given in the tabular format (Table 3.1). The methodology of the study has also been shown in a schematic flowchart format (Fig 3.1).

Table 3.1 Computational algorithm of the morphometric parameters of the basin

Morphometric parameters		Algorithms	References
Drainage network	Stream order (S_u)	Hierarchical rank	Strahler (1964)
	Stream number (N_u)	$N_u = N_1+N_2+N_3\ldots..+N_n$	Horton (1945)
	Stream length (L_u) in km	$L_u=L_1+L_2+L_3+\ldots\ldots+L_n$	Strahler (1964)
	Stream length ratio (L_{ur})	$L_ur=L_u/L_{u-1}$ Where, L_u = Total stream length of the order S_u L_{u-1}= The total stream length of its next order	Horton (1945)
	Bifurcation ratio (R_b)	$R_b= N_u/N_{u+1}$ Where, N_u = the total number of stream segments of the order S_u N_{u+1} = Number of the stream segments of the next higher order	Schumm (1956)
	Mean bifurcation ratio (MR_b)	ΣR_b	Schumm (1956)
	Mean length of stream (L_{sm})	$L_{sm} = L_u / N_u$	Strahler (1964)
	Mean stream length ratio (L_{urm})	Summation of L_{ur}	Horton (1945)
	Rho coefficient (ρ)	$\rho = L_{ur} / R_b$	Horton (1945)

Basin Geometry	Basin area (A) in km^2	----	Schumm (1956)
	Basin perimeter (P) in km	----	Schumm (1956)
	Basin length (L_b)	----	Schumm (1956)
	Form ratio (R_f)	$R_f = A/ L_b^2$	Horton (1932)
	Elongation ratio (R_e)	$R_e = 2/ L_b \times (A/\pi)^{0.5}$	Schumm (1956)
	Circularity ratio (R_c)	$R_c = 4\pi A/P^2$	Miller (1953), Strahler (1964)
	Basin shape factor (B_{sf})	$B_{sf} = \frac{L^2}{A} = \frac{L}{W}$ Where L = length of the basin, W= width of the basin, A= area of the basin	Morisawa (1958), Horton (1945)
	Compactness Co-efficient (C_c)	$C_c = 0.2821 \times P/A^{0.5}$	Gravelius (1914)
	Lemniscate's value (k)	$K = L^2/ A$	Chorley (1957)
Drainage texture analysis	Stream frequency (F_s)	$F_s = N_u/ A$	Horton (1932)
	Drainage density (D_d) in km/km^2	$D_d = L_u /A$	Horton (1932)
	Drainage basin texture ratio (T)	$T= D_d \times F_s$	Horton (1945)
	Constant of Channel maintenance (C) in km^2/km	$C = 1/ D_d$	Schumm (1956)
	Infiltration number (I_f)	$I_f = F_s \times D_d$	Faniran (1968)
	Length of overland flow (L_g) in km	$L_g = A/2 \times L_u$	Horton (1945)
Relief aspects	Height of the basin mouth (z) in m	-----	
	Maximum height of the basin (Z) in m	-----	
	Total basin relief (H) in m	H = Z-z	Strahler (1952)
	Relief ratio (R_h)	$R_h = H / L_b$	Schumm (1956)
	Ruggedness number (R_n)	$R_n = H \times D_d$	Schumm (1956)
	Dissection index (D_{is})	D_{is} = H / Absolute relief (m)	Singh and Dubey (1994)
	Melton ruggedness number (M_{gn})	$M_{gn} = H/ A^{0.5}$	Melton (1965)
	Gradient ratio (G_r)	G_r = (elevation at source - elevation at mouth) / L_b	Sreedevi et al. 2005

3.5.2 Hypsometric Curve and Integral

Hypsometric analysis is the outcome of the relationship between the horizontal cross-section of the watershed in respect to its relief and it's dimensionless. It signifies the present stage of the drainage basin based on the landform development. In this paper hypsometric curve has been prepared using SRTM DEM of 90m resolution from where the basin area or elevation has been extracted. The hypsometric curve is calculated using the following equation (Strahler, 1952; Dikapa et al. 2017) (Eq.3.1).

$$Hc = \left(\frac{a}{A}\right) / \left(\frac{h}{H}\right) \quad (3.1)$$

Where Hc is the hypsometric curve, a/A means relative area and h/H means relative elevation.

One of the important aspects of the hypsometric curve is the hypsometric integral which is the relative area below the curve that is the ratio of the area under the curve to the area of the entire square (Meshram and Sharma, 2017). The ratio is estimated as the part of the area above a particular contour line to the total area of the drainage basin. Here the hypsometric integral has been calculated using the algorithm as devised by Pike and Wilson, 1971, which is as follows (Eq. 3.2)

$$HI = \frac{E_{mean} - E_{min}}{E_{max} - E_{min}} \quad (3.2)$$

Where, HI denotes elevation–relief ratio or hypsometric integral, E mean refers mean elevation of a watershed obtaining from identified contour demarcating area, E max and E min refer maximum and minimum elevation from this identified contour area. If the HI value is > 0.60 the watershed is regarded to be in the youthful stage, if the value ranges from 0.35-0.60 the watershed is designated to be under the equilibrium stage and lastly values < 0.35 depicts the watershed in old stage or the monadnock phase.

3.5.3 Principle Component Analysis

Multivariate statistical analysis of the parameter is a convenient tool while analysing large agricultural data set as it efficiently reduces the Skewness and dimensionality (Sharma et al. 2020). Principle Component Analysis is one of such statistical tools used in water resources studies in the recent days. It is a method that helps in identifying the similarities, patterns and differences within the dataset reducing the number of complexities in it (Le et al. 2017). A data set comprising of un-correlated variables with new orthogonal will be produced from a set of correlated variables (Olsen et al. 2012). The new variables are the principal components. In PCA the Eigen value are extracted and values greater than 1.0 are considered based on which the number of components is determined (Le et al. 2017). In this study PCA has been used to observe and group 14 morphometric parameters to find out the correlation among them. The PCA technique has been executed using SPSS software applying the equation as described by Sharma et al. 2015.

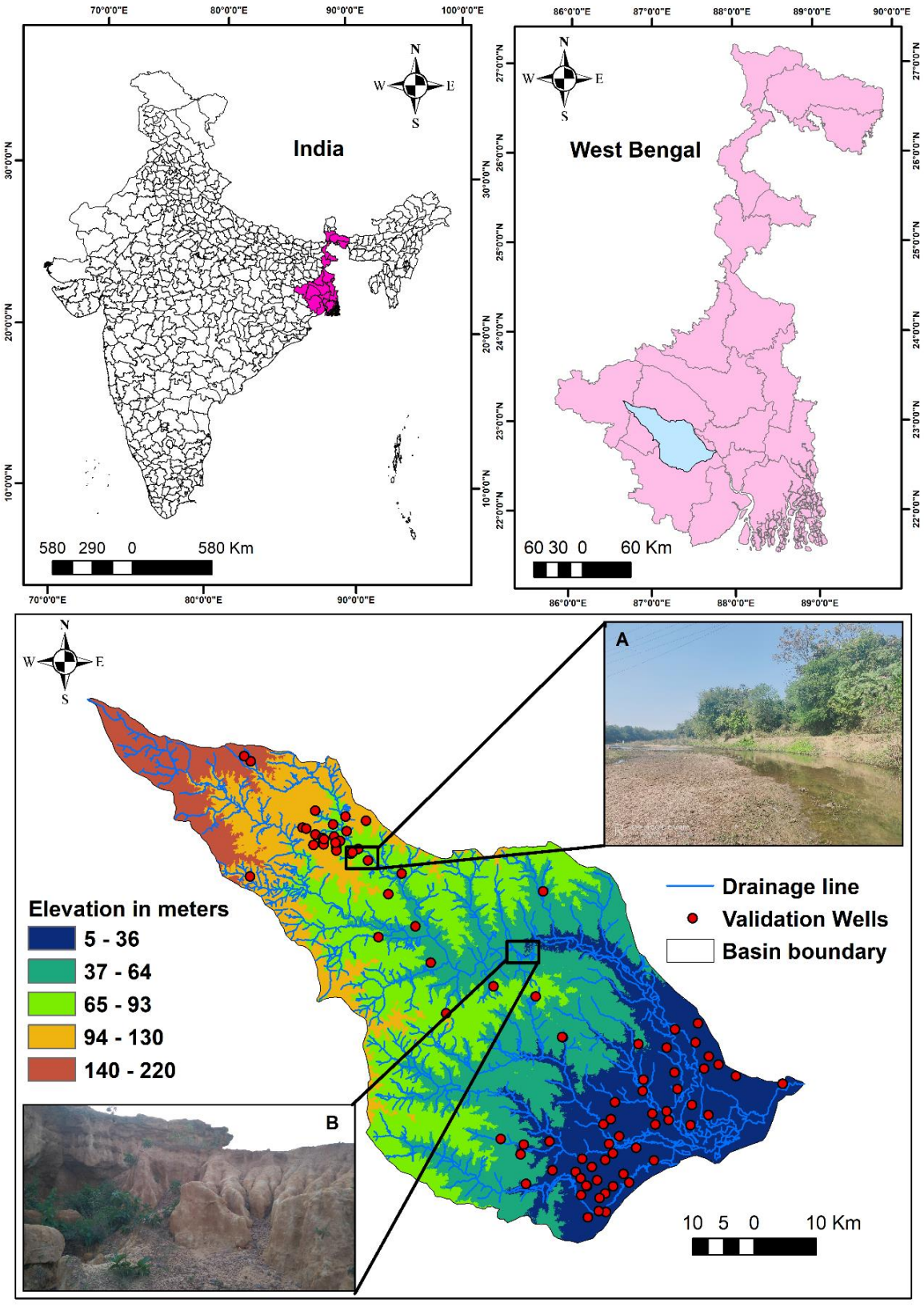

Fig. 3.1 Location of the Shilabati river basin (A) Degrading condition of the Joypanda sub-watershed (B) Lateritic Ravine at the middle stretch

3.5.4 K- Means Clustering Analysis

Clustering is a statistical technique where objectives are grouped based on certain criteria or characteristics showing similarities among them. K- means clustering, hierarchical clustering, model-based clustering are the common techniques used in different environmental studies which provide unbiased methods to understand the union among the variables using standardise data (Noiva et al. 2016; Rana et al. 2017). In this study use of K-means clustering has been made into consideration where there is a large set of data with numbers of clusters but the group they belong to is not known (Das, 2020). K- Means clustering is generally used to create clusters based on similarity which is quite applicable here (Zubair et al. 2020). The calculative procedure of the K-means clustering includes –first, the number of clusters is specified, second steps include the initialization of the centroids and random selection of the k data points for the centroid, the third steps includes the sum of the squared distance between the data points and all the centroids. The 4th step includes the computation of each data to its closet cluster or centroid and in the last the centroid for each cluster is calculated using the average of all the data points that correspond to each cluster or group. In the present study the K-means clustering has been executed using SPSS statistical software to group the sub-basins based on their morphological attribute to detect the nature of asymmetry among them.

3.6 Multicriteria Decision Making (MCDM) Technique

MCDM is a tool to solve complex problem by examining different alternatives having different criteria and looks out for the best alternative over certain objectives (Arabameri et al. 2018). There are numerous techniques of MCDM to calculate the weight of the alternatives and sub-alternatives used in environmental and water related studies. In this study four MCDM technique has been applied namely Entropy, TOPSIS, COPRAS and VIKOR to prioritise the sub-basins based on the infiltration and recharge capacity incorporating 18 basin morphometric parameters.

3.6.1 Entropy Method of weight calculation

Entropy is a method to remove disorders, uncertainties, instabilities and disturbances in a data set (Hagizadeh, 2017). The concept of information entropy was first introduced by Claude E. Shannon in the year 1948. It can measure the amount of useful information present in the dataset. The following steps have been used to compute the weight of each criterion (Maghsoodi et al. 2018; Dehdasht et al. 2020).

The 1st step include the normalization of the values of the morphometric attributes using Eq.3.3

$$X_{ij} = \frac{x_{ij}}{\sqrt{\sum_{i=1}^{m} x_{ij}}} \quad (3.3)$$

Where Xij is the normalized performance index of ith alternative respecting jth attribute i= 1,2,….m and j= 1,2,…n and xij presents the performance index of the ith alternative respecting jth attribute i=1,2,..m and j= 1,2,…n.

The 2nd step includes the calculation of entropy for each index (Eq.3.4)

$$E_j = -k \sum_{i=1}^{m} X_{ij} \ln X_{ij} \text{ , in which k= } \frac{1}{l(m)} \quad (3.4)$$

The 3rd step includes the calculation of the degree of deviation of the important information for each criterion. (Eq.3.5)

$$D_{j=}1\text{-}E_j, \text{ j=1,2….n} \quad (3.5)$$

Where Dj is the measure of the degree of deviation of the important information for the j[th] criterion.

The 4th step of the calculation includes entropy weight of the criteria

$$W_j = \frac{D_j}{\sum_{j=1}^{n} D_j} \quad (3.6)$$

Where Wj is the importance weight of the j[th] criteria.

3.6.2 TOPSIS model

TOPSIS is one of the widely used MCDM methods to determine the best alternative having the shortest distance from the ideal solution and farthest distance from the negative ideal solution (Velasquer and Hester, 2013). It is the distance-based method 1st introduced by Hwang and Yoon (1981). The method has been executed to prioritise and ranking the sub-basin based on the objective of the potential groundwater recharge capacity using the following algorithms.

The 1st step includes the construction normalized Decision Matrix (DM) and its normalization (Eq. 3.7)

$$R_{ij} = Xij \Big/ \sqrt{\sum_{i=1}^{m} X^2\ ij} \quad (3.7)$$

Where Rij is the normalized decision matrix and Xij is the i[th] alternative performance in the j[th] criteria.

The 2nd step includes the calculation of weights

Assuming that we have a set of weights for each of the criteria W_j for j = 1…..n. Now we have to multiply each column of the normalized decision matrix by its associated weight (Eq.3.8)

$$Vij = Wj \times Rij \quad (3.8)$$

Where Vij is the weighted normalized matrix, Rij is the normalized matrix and Wj is the weight of the criteria j.

The 3rd step includes the identification of Positive and negative Ideal solution (PIS & NIS)

The positive ideal (M+) and the negative ideal (M-) solutions are defined according to the weighted decision matrix via equations below (Eq.3.9-3.10)

PIS = M+ = {V1 +, V2 +…, Vn +}, where: Vj + = {(maxi (Vij) if j ∈J) ;(mini Vij if j ∈J')} (3.9)

NIS = M- = {V1 - , V2 -…, Vn -}, where: Vj - = {(mini (Vij) if j ∈J); (maxi Vij if j ∈J')} (3.10)

The 4th step includes the Calculation of the separation (S) distance of each competitive alternative from the ideal and non-ideal solution

The separation from the positive ideal alternative is (Eq.3.11)

$$S_i^+ = [\Sigma (vj^* - vij)^2]^{½} \quad i = 1, \ldots, m \quad (3.11)$$

The separation from the negative ideal alternative is (Eq.3.12)

$$S_i^- = [\ \Sigma (vj' - vij)^2]^{½} \quad i = 1, \ldots, m \quad (3.12)$$

The last step includes the calculation of the relative closeness to the ideal solution (P)

Now for each competitive alternative the relative closeness of the potential location with respect to the ideal solution has been computed (Eq.3.13)

$$P_i = S_i^- / (S_i^+ + S_i^-) \quad (3.13)$$

3.6.3 VIKOR Model

It is an MCDM model widely accepted and used in economical, technological, socio-economic and environmental studies. It is a method used to rank and select a set of alternatives from a group of criteria (Gao et al. 2019). The method has been calculated using the following steps (Ameri et al. 2017; Gao et al. 2019).

The 1st step includes the construction of a decision matrix and normalization similar as TOPSIS method.

The 2nd step includes the determination of the best value (V^+j) and the worst value (V^-j) of all the criteria (j = 1,2, …,n): if the i-th criterion is a profit criterion, its maximum value is more important to the purpose, then Vj +=maxVij and VJ −=minVij.

The 3rd step includes the calculation of the value of the utility measure (Si) and regret measure (Ri) (Eq. 3.14-3.15)

$$S_i = \sum_{i=1}^{n} W_j \, (V^+j - V_{ij}) / (V^+j - V^-j) \quad (3.14)$$

$$Ri = \max_i [\sum_{i=1}^{n} W_j \, (V^+j - V_{ij}) / (V^+j - V^-j)] \quad (3.15)$$

The 4th step include calculation of the VIKOR index (Q_j) (Eq. 3.16)

$$Q_j = \frac{v\,(S_i - S^-)}{(S^* - S^-)} + (1\text{-}v)\,\frac{(R_i - R^-)}{(R^* - R^-)} \quad (3.16)$$

Where, $S^- = \min S_i$, $S^* = \max S_i$, $R^- = \min R_i$, $R^* = \max R_i$, and v is introduced as a weight of the strategy of the maximum group utility or the majority of criteria, here v=0.5, now rank the order of the preference based on the value of Q. Here higher the Q value higher will be the rank denoting poor recharge capacity of the basin.

3.6.4 COPRAS

COPRAS is a MCDM technique introduced by Zavadskas and Kaklauskas in the year 1961 (Arabameri et al. 2018). It helps is assuming direct and corresponding affiliation of the level of the magnitude and practicality of the alternatives in the presence of the conflicting criteria (Chatterjee and Chakraborty 2013). The method has been executed in the following steps (Ayrim et al. 2018; Arabameri et al. 2018).

The 1st step includes the preparation of the decision matrix and normalization of the data set using the following equation (Eq. 3.17)

$$X_{ij} = \frac{x_{ij}}{\sum_{i=1}^{m} x_{ij}} \quad (3.17)$$

Where X_{ij} is the normalised quantity of the j^{th} criterion, x_{ij} is the i^{th} alternative of the j^{th} and m denotes the alternative numbers.

The 2nd step calculation of the normalised weighted decision-making matrix using the following algorithm (Eq.3.18)

$$d_{ij} = w_j \times X_{ij}, \quad (3.18)$$

Where Xij is the efficiency of the i^{th} and w_j is the weight of the criteria.

The 3rd step includes the computation of the maximum and the minimum values of the alternatives. The alternatives are classified as maximising and minimising indices using the following algorithm (Eq. 3.19-3.20)

$$S^+_j = \sum_{i=1}^{n} y + ij \quad j= 1, 2, 3….n \quad (3.19)$$

$$S^-_j = \sum_{i=1}^{n} y - ij \quad j= k+ 1, k+2….n \quad (3.20)$$

Where $y+ij$ and $y-ij$ are the weighted normalised values for the important and unimportant adjectives respectively.

The last step includes the computation of the relative weights of each of the alternatives using the following algorithm (Eq. 3.21)

$$Q_{i=} \ S^{+}_{j} + \frac{S^{-}_{min}\Sigma^{n}_{j=1}s^{-}_{j}}{s^{-}_{j}\ \Sigma^{n}_{=1}\frac{S^{-}_{min}}{s^{-}_{j}}} = S^{+}_{j} + \frac{\Sigma^{n}_{i=1}s^{-}_{j}}{s^{-}_{j}\ \Sigma^{n}_{=1}\frac{1}{s^{-}_{j}}} \quad (3.21)$$

Where S^{-}_{min} is the minimum value of S^{-}_{j} and S^{+}_{j} and S^{-}_{j} are the minimum and maximum indices.

3.7 Selection of Best Model through Nonparametric Correlation Test

The execution of the models in ranking the sub-basin based on MCDM technique produces a diverse outcome which is required to validate through some correlation test (Arabameri et al. 2018). Here nonparametric method of Spearman rank Correlation Coefficient test (SCCT) has been done used which can be calculated applying the following algorithm (Gust and D'journo 2014, Arabameri et al. 2018) (Eq.3.22).

$$r_{s}= 1- \frac{6\Sigma^{n}_{i=1}d^{2}_{i}}{n(n^{2}-1)} \quad (3.22)$$

Where d_i is the difference between the ranks of models for each alterative and n is the number of observations.

3.1 Results and Discussion

3.1.1 Analysis of morphometric parameters

The mathematical analysis of a drainage basin based on its shape, size and dimension provides the basis of investigation of any region while making any scientific exploration related to the hydrological behavior of the respective watershed. The basin attributes for such kind of investigation include the area, shape, size, attitude, volume and texture of the present landform. The Shilabati river basin comprises an area of approximately 3881 km^2 and has a total length of all streams of about 1310.44 km. The region is crisscrossed by a number of lineaments or faults. The geology of the upper section is composed of hard rocks while the downstream section is alluvial in origin. The basin is under both ground and surface water stress due to the continuous extension of agricultural land hence analysis of the morphometric asymmetries is needed to understand the recharge potential for sustainable conservation of aquifers for sustainable conservation.

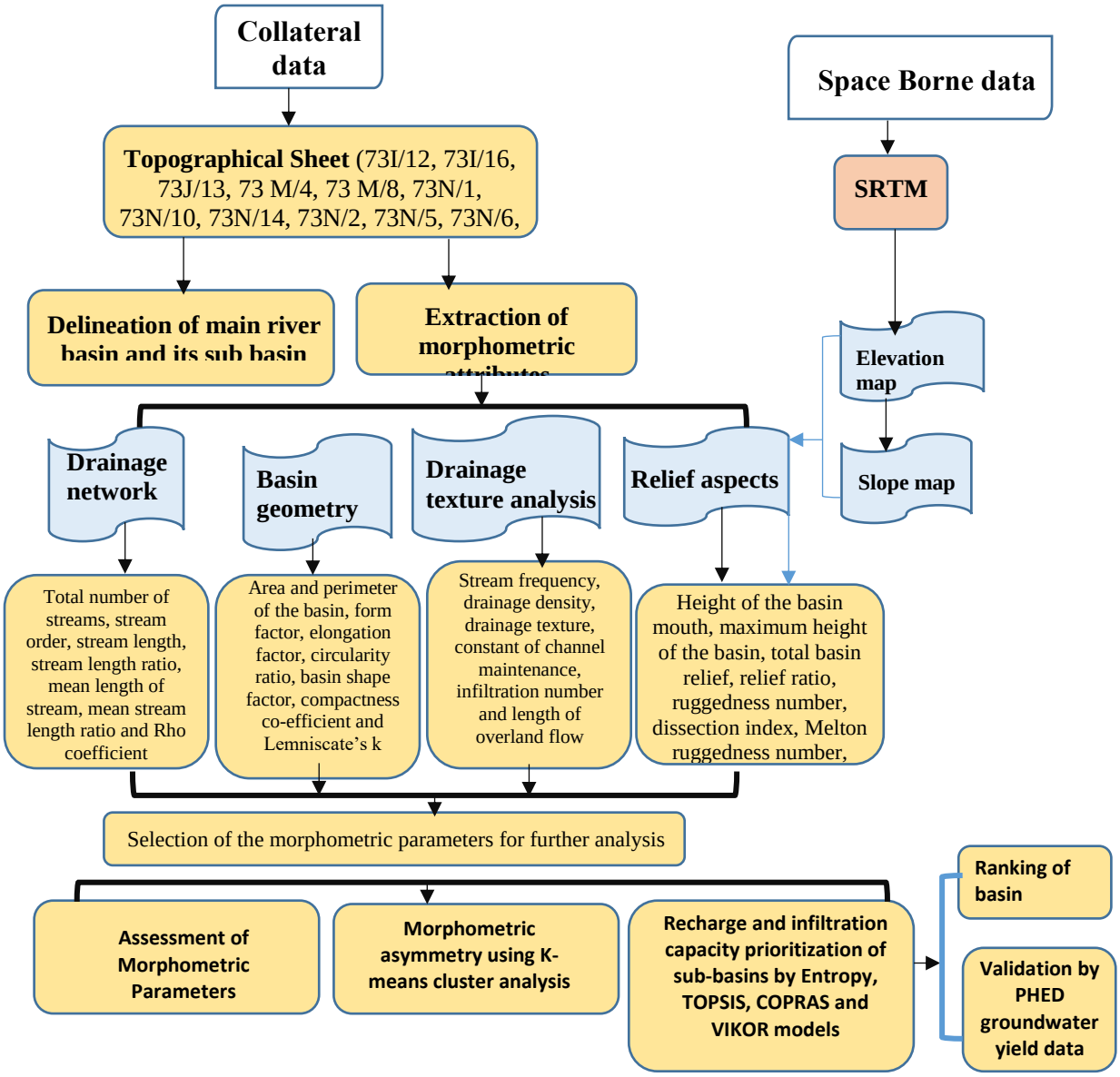

Fig. 3.2 Flowchart depicting the methodology of the study

3.1.2 Drainage Network

A first step towards understanding the hydrological behaviour of the watershed is drainage network analysis. Drainage network analysis includes the mathematical calculation of the total number of streams, stream order, stream length, stream length ratio, mean length of stream, mean stream length ratio and Rho coefficient (Table 3.2). The stream lines of the Shilabati basin have been digitized using Topographical sheets in ArcGIS software version 10.3. The algorithm used in the calculation of each parameter for each sub-basin has been given in the tabular format (Table 3.1). Stream order can be divided into three types that is first to third order streams are designated as headwater streams, fourth to sixth order as medium streams and above sixth order are regarded as the river (Prabhakaram and Raj, 2018). In the present study sub-basin, Paranag is a 3rd order stream means it is a head water stream and the sub-basin Jaypanda, Silai, Purandar, Betal, Kubai, Tamal, Donai, and Silai-Ketia Khal belongs to the group of medium streams. (Fig 3.3).

Stream number is mainly the number of stream segments within the watershed. Total stream number and stream number of each order for all the sub-basin have been estimated given in a tabular format (Table 3.2). The number of streams decreases with the increase in the stream order. The number of the 1st order streams are highest in the Silai sub-basin (199 numbers) and lowest in Donai sub-basin (23 number). A greater number of higher order streams signifies the active hydrological behaviour of the drainage basin in terms of runoff, recharge capacity and erodibility.

Stream length is the measure of the distance along the channel from its source and up to its draining outlet. The stream length of each order has been estimated and summed up to find out the actual length of the streams. The sub-basins like Joypanda (189.44 km), Tamal (221.158 km), Parang (183.58 km), Kubai (137.38 km), Silai (535.89 km) and Silai-Ketia Khal (600.39 km) (Table 3.2) has the highest stream length hence infiltration will be low and runoff will be higher during the rainfall events. Thus, the sub-basin having lower stream length (Donai, Purander and Betal) will be more prone to recharge its aquifer rather than runoff. Mean length of streams has also been calculated which signifies the characteristic size component of a drainage network and its contributing surfaces of sub-basin (Strahler, 1964). The mean stream length increases with the increase in stream order. But in few sub-basins anomaly can be seen which may be due to the nature of slope and topography. Like in sub-basin Silai the mean stream length of the 3rd order is 17.67 km, 4th is 57.25 km and it decreases to 27.12 km in case of 5th order (Table 3.2).

Stream length ratio is the ratio of the mean length of the stream of one order in respect to the next higher order. The stream length ratio and mean stream length ratio for all the sub-basin have been estimated. The mean stream length ratio of the sub-basins varies from 0.60 (Silai) to 2.41 (Betal). Greater value indicates more irregularities and unevenness of the topography and hence contributing greater runoff and poor groundwater recharge.

The bifurcation ratio is the index of relief and dissection as postulated by Horton (1945). It is a dimensionless property and shows the interaction and integration of streams within the basin. It is the number of stream segments of a given order to the number of stream segments to the next higher order. Greater the bifurcation ratio greater will be the runoff which will intensify soil erosion leading to poor infiltration and groundwater recharge. The mean bifurcation ratio ranges from 2.970 (Silai Ketia Khal) to 6.25 (Betal) and is higher at the upstream section and middle section where the rills and gullies are common having dendritic and trellis drainage patterns (Shit et al. 2015) (Table 3.2).

One of the significant parameters of drainage network analysis is Rho coefficient which is the ratio between stream length ratio and bifurcation ratio as defined by Horton (1945). The Rho coefficient determines the storage capacity of the basin on the degree of drainage development. The Rho coefficient is higher in Silai sub-basin (0.16) and lower in Purander (0.20). Greater the Rho coefficient signifies greater risk of soil erosion and poor recharge during extreme rainfall events.

3.1.3 Basin Geometry

The basin geometry is an association of structure, relief, shape, size, climate condition and denudational history of the river basin. The basin geometry includes a number of parameters like area and perimeter of the basin, form factor, elongation factor, circularity ratio, basin shape factor, compactness co-efficient and Lemniscate's k (Table

3.2). The total area and perimeter of the basin is 3881 km^2 and is 342.98 km and having the highest basin length of about 131.42 km. In regard to the sub-basins, Silai Ketia Khal has the largest basin area.

Form factor may be defined as the ratio of the basin area to the square of the basin length as defined by Horton (1932). Form factor controls the hydrological behaviour of the drainage basin. Higher the form factor higher will be the peak flow within a short duration and thereby greater runoff and less infiltration. The form factor ranges from 0.148 (Silai) to 0.444 (Betal) (Fig 3.4a) (Table 3.2). The flood discharge is mainly concentrated in the lower reaches of the basin where water holding capacity of the soil is high and basin geometry encourages the same (Mahala, 2019).

According to Schumm (1956) elongation ratio may be defined as the ratio of diameter of a circle of same area like that of the basin and the maximum basin length. It also determines the runoff and infiltration character of the basin. An elongated basin has lesser chance of runoff during extreme events. It ranges from 0.55 (Joypanda) to 0.85 (Betal) (Fig 3.4b) (Table 3.2).

One of the predominant factors that controls the flood discharge of the basin is circulatory ratio. It is the ratio of the area of the basin to area of the circle having the same perimeter of the watershed (Miller, 1953). The circulatory ratio is mainly influenced by length and the frequency of the streams, land use and land cover, climatological aspects, relief, slope and geological characteristics of the basin. The circulatory ratio of the sub-watershed ranges from 0.20 (Silai-Ketia Khal) to 0.67 (Betal and Donai) (Table 3.2). More circular the basin more efficient for the runoff and hence poor groundwater recharge (Fig 3.4c).

Compactness coefficient is the ratio of the perimeter of the watershed to the circumference of the circular area which equals to the area of the watershed. The compactness coefficient of the basin ranges from 1.218 (Betal) to 2.030 (Silai Ketia Khal). Thereby the sub-basin having higher compactness coefficient is more prone to runoff. Another important parameter is the Lemniscate's k which is an important determinant of the slope of the basin (Chorley 1957). Lemniscate's k has a direct relationship with runoff and indirect relationship with the recharge character of the basin. The Lemniscate's k of the basin ranges from 2.25 (Betal) to 5.61 (Silai Ketia Khal) (Table 3.2).

Table 3.2 Computation of morphometric parameters of the Sub-basins of Shilabati River

Parameters		Silai	Joypanda	Purander	Betal	Parang	Tamal	Kubai	Donai	Silai Ketia Khal
Drainage network	Highest S_u	5	4	4	4	3	4	4	4	5
	MR_b	6.22	4.37	3.01	3.65	6.25	4.96	3.71	2.94	2.97
	L_{urm}	0.61	0.96	0.99	0.78	2.41	1.01	1.26	2.37	1.03
	ρ	6.22	0.22	0.33	0.21	0.39	0.20	0.34	1.08	2.88
Basin Geometry	A	723.46	375.85	118.93	139.91	479.33	363.89	335.81	266.38	1077.49
	P	166.27	106.39	47.44	51.05	133.16	105.08	105.64	70.55	263.26
	L_b	69.85	45.33	18.17	17.76	50.77	44.22	39.63	27	63.71
	R_f	0.15	0.18	0.36	0.44	0.19	0.19	0.21	0.37	0.27
	R_e	0.49	0.55	0.77	0.85	0.55	0.63	0.59	0.77	0.66
	R_c	0.33	0.42	0.66	0.67	0.32	0.41	0.38	0.67	0.20
	B_{sf}	6.74	5.46	2.77	2.25	5.58	5.37	4.68	2.74	3.77
	C_c	1.75	1.55	1.23	1.22	1.72	1.55	1.63	1.22	2.03
	k	4.53	5.47	2.78	2.25	5.38	5.37	4.68	2.74	4.53
Drainage texture analysis	F_s	0.24	0.29	0.31	0.37	0.10	0.24	0.17	0.12	0.23
	D_d	0.74	0.50	0.58	0.72	0.38	0.61	0.41	0.53	0.56
	T	0.18	0.15	0.18	0.27	0.37	0.24	0.07	0.07	0.13
	C	1.35	1.98	1.74	1.39	2.61	1.64	2.43	1.88	1.79
	I_f	0.18	0.15	0.18	0.27	0.03	0.14	0.07	0.06	0.13
	L_g	0.37	0.25	0.29	0.36	0.19	0.30	0.21	0.06	0.28
Relief aspects	z	48	47	39	42	10	13	13	13	5
	Z	219	165	104	114	111	109	104	66	112
	H	171	118	65	72	101	96	91	53	107
	R_h	0.06	0.11	0.14	0.08	0.14	0.09	0.09	0.08	0.07
	R_n	0.23	0.06	0.04	0.05	0.04	0.06	0.03	0.14	0.19
	D_{is}	0.78	0.72	0.63	0.63	0.91	0.88	0.88	0.80	0.96
	M_{gn}	0.006	0.006	0.006	0.006	0.005	0.005	0.005	0.003	0.003
	G_r	0.002	0.003	0.004	0.004	0.002	0.002	0.002	0.002	0.001
	HI	0.440	0.410	0.520	0.490	0.400	0.480	0.430	0.400	0.390

*Stream order (S_u), Mean bifurcation ratio (MR_b), Mean stream length ratio (L_{urm}), Rho coefficient (ρ), Basin area (A) in km^2, Basin perimeter (P) in km, Basin length (L_b), Form ratio (R_f), Elongation ratio (R_e), Circularity ratio (R_c), Basin shape factor (B_{sf}), Compactness Co-efficient (C_c), Lemniscate's value (k), Stream frequency (F_s) Drainage density (D_d) in km/km^2, Drainage basin texture ratio (T), Constant of Channel maintenance (C) in km^2/km, Infiltration number (I_f), Length of overland flow (L_g) in km, Height of the basin mouth (z) in m, Maximum height of the basin (Z) in m, Total basin relief (H) in m, Relief ratio (R_h), Ruggedness number (R_n), Dissection index (D_{is}), Melton ruggedness number (M_{gn}) , Gradient ratio (G_r) and Hypsometric Integral (HI).

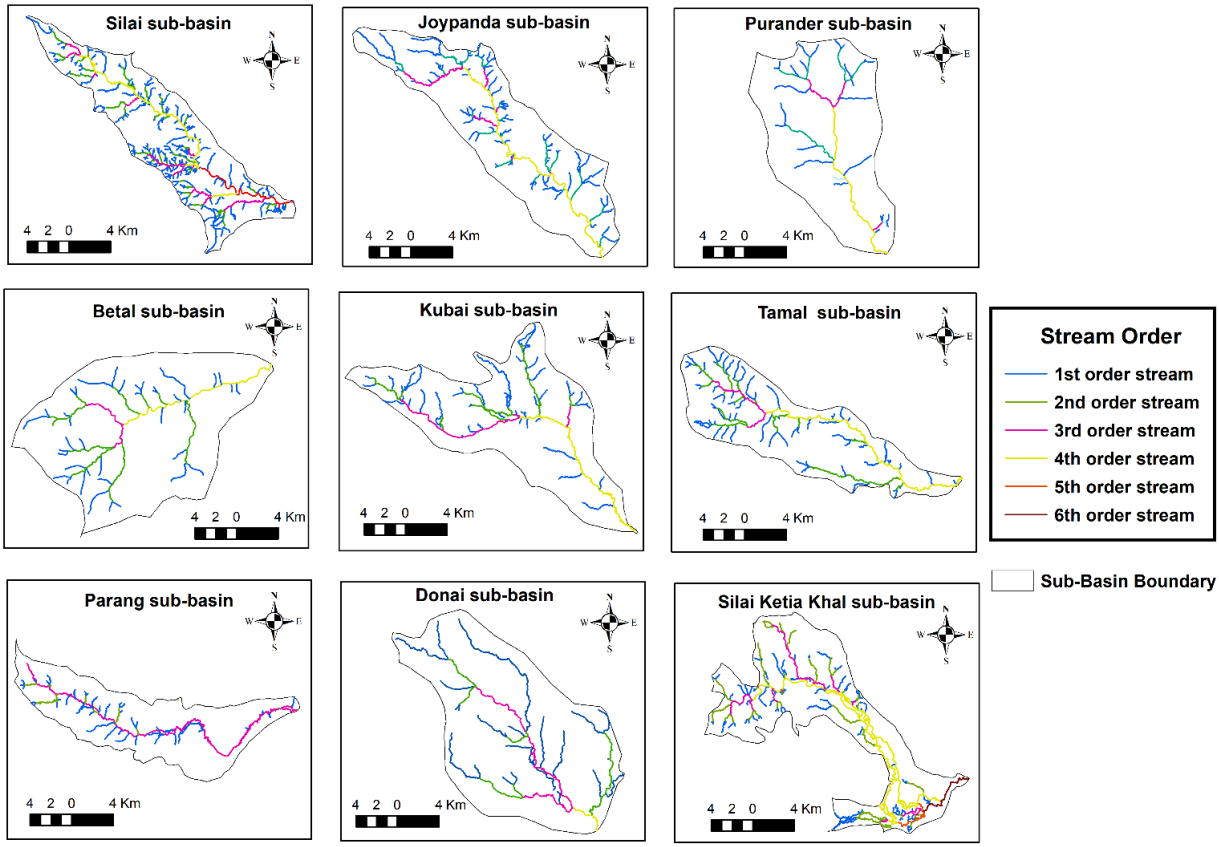

Fig. 3.3 Stream ordering of the sub-basins

3.1.4 Drainage Texture Analysis

Drainage Texture analysis of the basin indicates the magnitude and the intensity of landscape dissection by a channel network. The parameters of drainage texture analysis include stream frequency, drainage density, drainage texture, constant of channel maintenance, infiltration number and length of overland flow (Table 3.2).

Stream frequency is the foremost character that dignifies infiltration capacity and permeability of a river basin. It can be defined as the total number of stream segment irrespective of all the orders in per unit basin area (Horton 1945). It depends on the geology, relief, slope and rainfall character of a region. Stream frequency is higher in Betal (0.372) signifying more runoff and less in case of Parang (0.096) where the infiltration may be higher (Fig 3.4d) (Table 3.2).

Drainage density is one of the predominant factors that indicate the relative spacing of the stream lines. It is the mean length of the stream segment of all orders per unit area (Horton, 1945). Hydrological behaviour like runoff intensity, infiltration capacity and soil water action depend on the drainage density while it depends on the soil character, relief, slope, geological character, geomorphology climatic etc. of drainage basin. Drainage density is higher in mountain areas or highlands where slope is high and presence of impermeable surface material predominates. The drainage density of the basin ranges from 0.383 (Parang) to 0.741 (Silai) (Fig 3.4e) (Table 3.2).

According to Schumm (1956) constant of channel maintenance is the inverse of the drainage density and is expressed in km^2. It is the ratio of the area of the drainage basin to the total length of all the channels. Higher the value of the channel maintenance higher will be the permeability of rocks and hence more recharge. In the present study channel maintenance of the basin ranges from 1.35 (Silai) to 2.61 (Parang) (Fig 3.4f) (Table 3.2).

Infiltration number depends on the climate, natural vegetation, relief and stage of the development of the drainage basin. It is one of the products of drainage density and signifies the infiltration character of the drainage basin (Pareta and Pareta, 2012). The infiltration number of the basin ranges from 0.066 (Donai) to 0.267 (Betal) (Fig 3.5a). Higher value of the factor higher will runoff and poor groundwater recharge.

Length of the overland flow is another important determinant of the hydrological behaviour of the drainage basin. It is the horizontal length of the flow of the precipitated water that moves over the land surface and reaches the first order stream of the basin. Sub basin having shorter length of overland flow will flash flood even if the rainfall is less and hence poor aquifer recharge (Prabhakaran and Raj, 2018). The length of the overland flow is higher in case of Silai sub-basin (0.37) and lower in Paranag (0.19) (Fig 3.5b).

The next comes the texture ratio which depends on the lithological aspect of the drainage basin (Meshram and Sharma, 2017). It has a significant contribution towards the infiltration character of the drainage basin. Greater the texture ratio greater will be the runoff and low infiltration. The texture ratio of the basin ranges from 0.066 (Donai) to 0.267 (Betal) (Fig 3.5c).

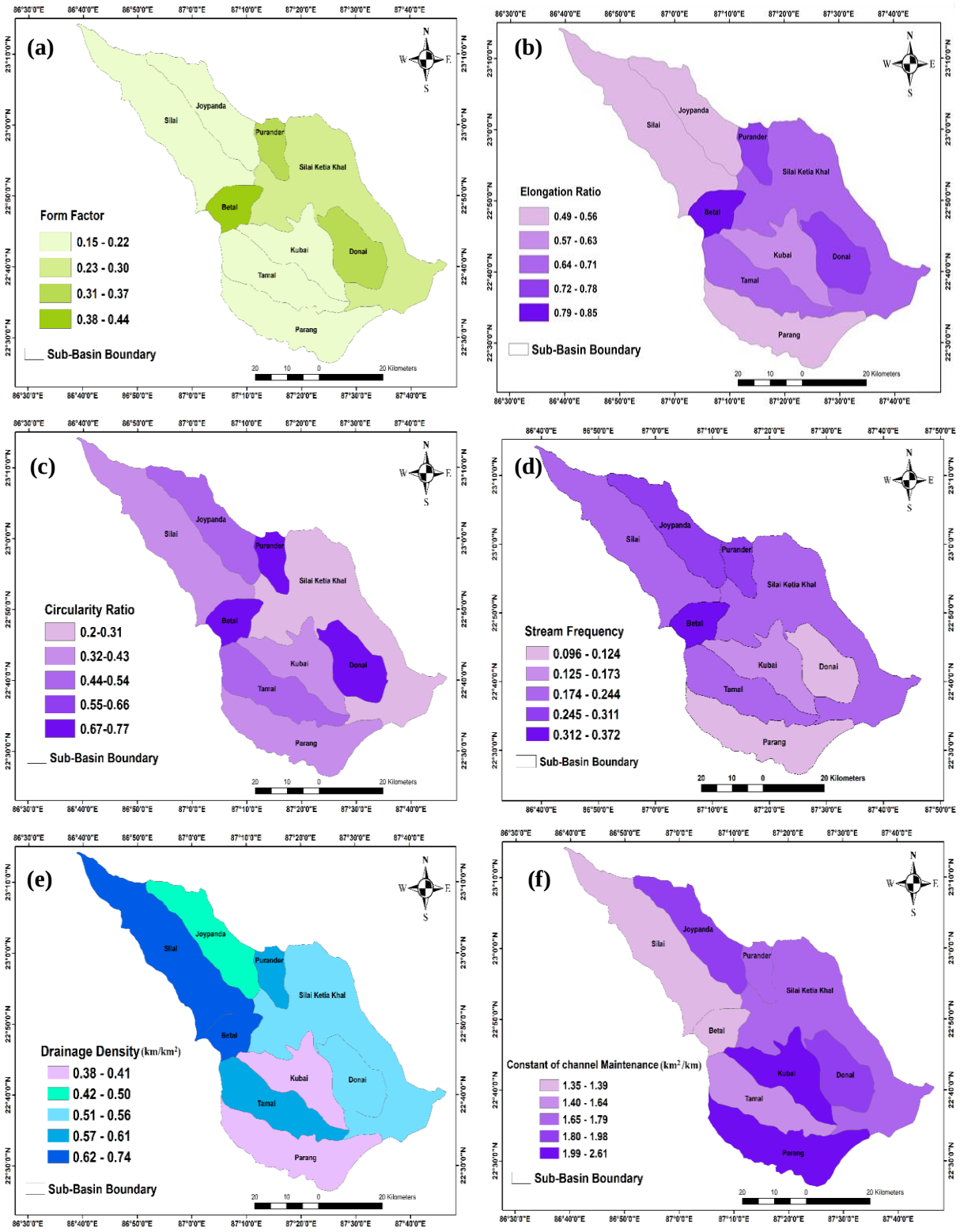

Fig. 3.4 Different morphological aspects of the basin (a) form factor; (b) elongation ratio; (c) circularity ratio; (d) stream frequency; (e) drainage density and (f) constant of channel maintenance

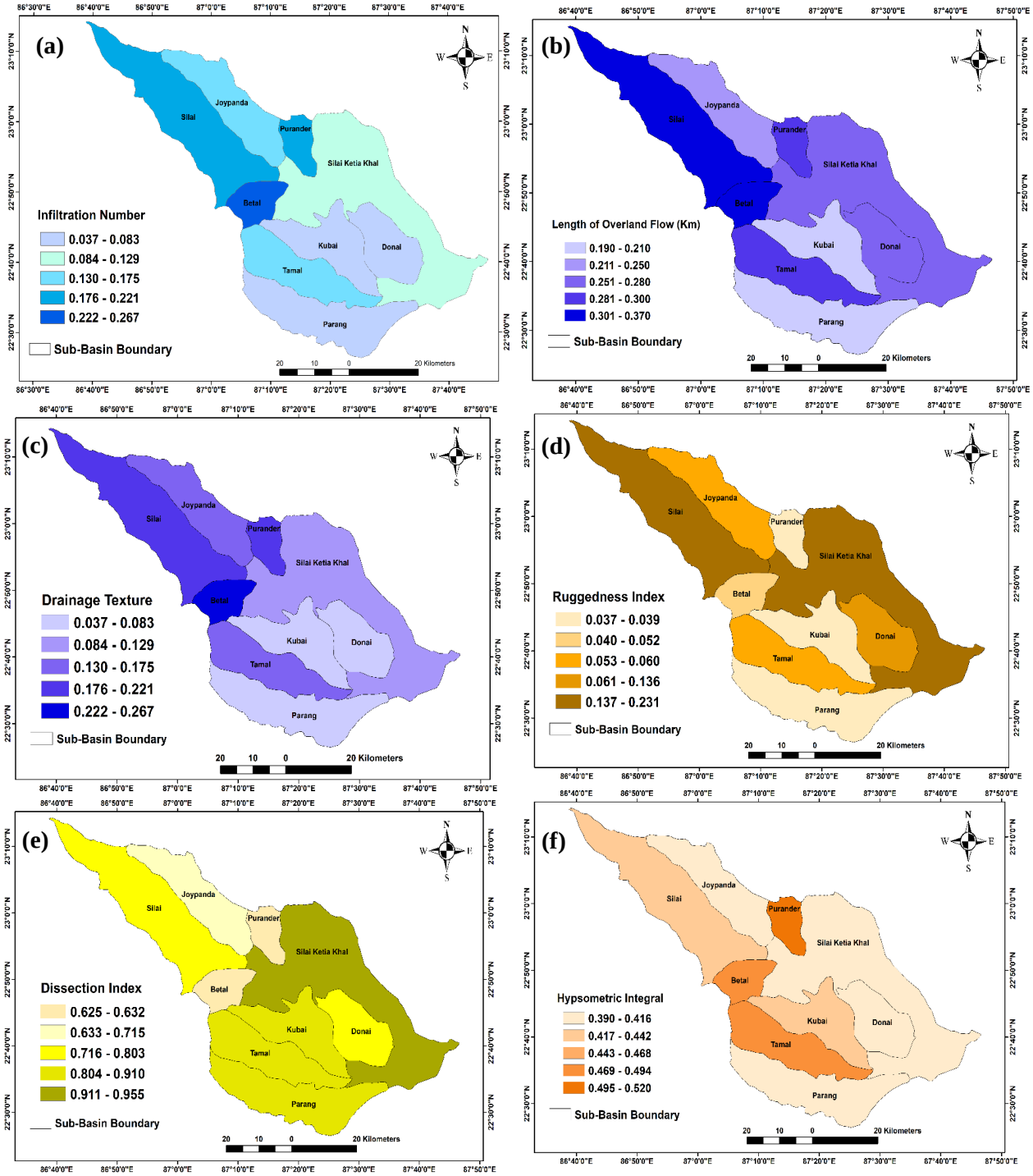

Fig. 3.5 Different morphometric aspects of the river basin (a) infiltration number; (b) length of overland flow; (c) drainage texture; (d) ruggedness index; (e) dissection index and (f) hypsometric integral

3.1.5 Relief Aspects

The three-dimensional aspects of the drainage basin include the volume and altitude of the vertical components of the drainage basin (Prabhakaran and Raj, 2018). The hydrological behaviour of the drainage basin is highly influenced by the gradient characteristics. The relief aspects of the drainage basin include height of the basin mouth, maximum height of the basin, total basin relief, relief ratio, ruggedness number, dissection index, Melton ruggedness number and gradient ratio. The upper reaches of the Shilabati river basin is characterised by undulating topography, steep sloping upland and presence of pediment at the foot hill zone which hinders both the land and groundwater development of the area (Mahala, 2020).

The maximum relief of the Shilabati basin is 219 m and 5 m at the mouth of the basin which has been extracted from STRM DEM of 90 m resolution. According to Schumm (1956) relief ratio is the ratio between total relief of the basin and the longest dimension of the basin parallel to the main drainage line. Higher values are related to higher channel gradient and steep slope leading to more runoff, soil erosion and poor groundwater recharge. The relief ratio of the basin ranges from 0.0017 (Silai Ketia Khal) to 0.004 (Betal) (Table 3.2).

The ruggedness index signifies the irregularities and steepness of the basin. It is the product of the basin relief and drainage density of the watershed according to Patton and Baker (1976). Higher values of ruggedness number higher will be the soil erodibility, low infiltration and poor groundwater recharge. Within the Shilabati basin Purander (0.231) has the highest ruggedness index and lowest can be found in Kubai (0.037) and Purander (0.037) (Fig 3.5d) as shown in table 3.2.

Basin can be differentiated into two types namely basin with debris flow potential and basin with bed load sediment transport potential (Melton, 1965). This potentiality can be determined through Melton ruggedness index. Higher the value higher is the soil erodibility from the basin. The Melton ruggedness number of the basin ranges from 0.003 (Donai and Silai Ketia Khal) to 0.006 (Joypanda, Purander, Betal and Silai) (Table 3.2).

Dissection index of the basin presents the degree and intensity of the vertical erosion within the basin. It is one of the important measures of the soil erosion where the lower value signifies flat surface and complete absence of vertical erosion hence greater infiltration of surface flow where the case is opposite for higher values. Silai Ketia Khal (0.955) has the highest dissection index value and Purander (0.632) has the lower the value (Fig 3.5e). The sub-basin where Silai Ketia Khal is located is characterised by dissected plateau fringe particularly the upper section where the soil development is also poor signifying poor recharge capacity (Shit and Maity, 2012).

Gradient ratio is also the most important contributor to the sub-surface recharge. It is the indicator of the channel slope and hence plays an important role in the assessment of runoff (Pareta and Pareta, 2011). Higher values indicate poor infiltration capacity of the basin. The gradient ratio of the basin ranges from 0.0017 (Silai Ketia Khal) to 0.0041 (Betal). In the present study hypsometric integral has also been calculated following equation 1 and 2 which shows most of the sub-watershed have HI values between 0.39 and 0.52 which clearly signifies their equilibrium stage as shown in table 2. But the river Shilabati has a HI value of 0.28 signifying the old stage or dying condition criss-crossed by a number of tributaries having low sediment transport potential (Fig 3.5f). But extensive anthropogenic interference, forest degradation and lithological character make it prone to soil erosion at the upstream course. While the downstream section is highly vulnerable to periodic floods due to its distinctive basin-shaped topography and thereby requires a sustainable management plan (Kar and Das, 2020).

3.1.6 Assessment of Inter-Relationship among Morphometric Parameters using Principal Component analysis

To curb out which morphometric parameters are inducing the next other parameters is much important while analysis the hydrological and geomorphological independencies of a river basin. In this study inter-correlation matrix has been calculated (Table 3.3) using 14 morphometric attributes namely bifurcation ratio, drainage density, texture ratio, stream frequency, circularity ratio, form factor, elongation ratio, length of over land flow, relief ratio, ruggedness number, compactness ratio, hypsometric integral, dissection index and length of channel maintenance. The correlation matrix has been prepared using IBM SPSS Statistics 23 software. The matrix significantly reveals that bifurcation ratio has a very strong correlation with ruggedness number (0.842), Drainage density has very strong correlation with Texture ratio (0.851), length of overland flow (0.999) and length of channel maintenance (-0.976), Stream frequency has a strong correlation with (Correlation coefficient more than 0.6) length of overland flow, dissection index and length of channel maintenance (Table 3). Strong correlation (more than ± 6.0) exists between circularity ratio, form factor, elongation ratio, and compactness ratio and dissection index). Length of overland flow is showing a strong negative correlation with length channel maintenance. Next the relief ratio is showing a very strong correlation with the ruggedness index (0.878), compactness ratio has a strong correlation with dissection index (0.763) and lastly hypsometric integral has a strong correlation with dissection index of the basin. Based on this correlation matrix it is not quite evident to conclude the grouping of the parameters on physical significance (Meshram and Sharma, 2017). For technical and scientific grouping of the parameters and to find out the most effective one, principal component analysis (PCA) has been executed where correlation matrix is subjected to the PCA (Nikam et al. 2014)

The extraction method of component transformation matrix has been done using PCA and varimax with Kaiser (1974) normalization has been used for rotation method. The Unrotated loading matrix (Table 3.3) shows the first three components whose Eigen values are greater than 1, together contributes 90.465 of the total variances explained. From the table 3.3 it can be observed that the first component has a strong correlation with drainage basin texture ratio, stream frequency, hypsometric integral, dissection index (greater than ± 0.80), good correlation with circulatory ratio, form ratio, elongation ratio, compactness co-efficient (greater than ± 0.70) and a moderate correlation with drainage density, length of overland flow and constant of channel maintenance. The second component shows a strong correlation with mean bifurcation ratio and ruggedness number (greater than ± 0.80) and good correlation with drainage density, length of overland flow and constant of channel maintenance (greater than ± 0.70). The third component has a moderate or poor correlation among the parameters. Under such circumstances it can be observed that some components have a strong some have moderate or poor correlation. Therefore, it is not possible to conclude under such variability and uncertainty which will enforce to rotate the first factor loading matrix to obtain a well-grounded correlation (Arefin et al. 2020)

Utilizing the selected components of the 1st factor unrotated loading matrix the rotated factor loading matrix has been executed by post multiplying the transformation matrix. The parameters have been grouped into three components (Table 3.4). The 1st component shows a strong correlation (greater than ± 0.80) with drainage density, texture ratio, stream frequency, length of overland flow, length of channel maintenance which mainly falls under the drainage component. The 2nd component shows a strong correlation (greater than ± 0.80) with circularity ratio, form factor, elongation ratio, and compactness ratio and are easily be dignify them as the shape component of the

basin. In the 3rd component bifurcation ratio, ruggedness number and compactness ratio are showing strong correlation which groups them as the relief or slope component where elevation and gradient dominates.

Table 3.3 Computation of Inter-correlation matrix of 14 selected geomorphic parameters

Morphometric parameters	Inter- Correlation matrix													
	MR_b	D_d	T	F_s	R_c	R_f	R_e	L_g	R_h	R_n	C_c	HI	D_{is}	C
MR_b	1.000	.388	-.071	-.253	-.486	-.529	-.531	.374	.688	.842	.487	-.435	.420	-.353
D_d	.388	1.000	.851	.678	.257	.276	.273	.999	.291	.343	-.223	.501	-.473	-.976
T	-.071	.851	1.000	.949	.364	.423	.410	.849	-.123	-.072	-.333	.678	-.704	-.839
F_s	-.253	.678	.949	1.000	.347	.393	.392	.675	-.272	-.256	-.324	.676	-.734	-.706
R_c	-.486	.257	.364	.347	1.000	.798	.787	.279	-.183	-.477	-.990	.569	-.779	-.303
R_f	-.529	.276	.423	.393	.798	1.000	.975	.306	.038	-.281	-.720	.405	-.568	-.325
R_e	-.531	.273	.410	.392	.787	.975	1.000	.297	-.009	-.349	-.724	.467	-.500	-.345
L_g	.374	.999	.849	.675	.279	.306	.297	1.000	.309	.345	-.241	.501	-.484	-.976
R_h	.688	.291	-.123	-.272	-.183	.038	-.009	.309	1.000	.878	.273	-.493	.303	-.326
R_n	.842	.343	-.072	-.256	-.477	-.281	-.349	.345	.878	1.000	.548	-.501	.385	-.306
C_c	.487	-.223	-.333	-.324	-.990	-.720	-.724	-.241	.273	.548	1.000	-.597	.763	.263
HI	-.435	.501	.678	.676	.569	.405	.467	.501	-.493	-.501	-.597	1.000	-.667	-.502
D_{is}	.420	-.473	-.704	-.734	-.779	-.568	-.500	-.484	.303	.385	.763	-.667	1.000	.485
C	-.353	-.976	-.839	-.706	-.303	-.325	-.345	-.976	-.326	-.306	.263	-.502	.485	1.000

Table 3.4 Principal Component Unrotated and rotated loading matrix of 14 morphometric parameters

Morphometric parameters	Unrotated matrix			Rotated matrix		
	Component			Component		
	1	2	3	1	2	3
MR_b	-.383	.855	.071	.195	-.500	.772
D_d	.667	.729	-.077	.932	.123	.315
T	.841	.378	-.317	.945	.197	-.139
F_s	.814	.194	-.422	.859	.172	-.332
R_c	.796	-.349	.392	.217	.902	-.217
R_f	.742	-.229	.550	.188	.933	-.015
R_e	.744	-.251	.512	.191	.916	-.056
L_g	.678	.723	-.046	.924	.154	.327
R_h	-.219	.700	.645	.001	.050	.975
R_n	-.364	.847	.300	.116	-.329	.905
C_c	-.771	.396	-.312	-.203	-.848	.294
HI	.813	-.129	-.347	.641	.336	-.523
D_{is}	-.871	.120	.085	-.588	-.547	.366
C	-.694	-.701	.022	-.913	-.188	-.322
Eigen value	6.833	4.091	1.741	5.155	4.159	3.350
% of total factor covariance	48.807	29.220	12.438	36.825	29.709	23.931
Cumulative % of total factor covariance	48.807	78.027	90.465	36.825	66.534	90.465

3.1.7 Morphometric asymmetry using K-means cluster analysis

K means clustering has been applied for separating the sub-watershed into k-groups or clusters. The sub-watershed has been grouped into three clusters based on the morphometric asymmetry. Application of K-means clustering is new in watershed morphometric analysis and is significant while working with numerous variables to group the sub-watershed based on its hydrologic behavior. The techniques select certain centroids and group the objects lying closest to the centroids based on Euclidean distance. The sub-watersheds have been clustered based on 14 parameters namely bifurcation ratio, drainage density, texture ratio, stream frequency, circularity ratio, form factor, elongation ratio, length of overland flow, relief ratio, ruggedness index, compactness ratio, hypsometric integral, dissection index and length of channel maintenance. The whole calculation procedure has been executed in SPSS Statistics Version 23. First, the morphometric attributes of all the sub-watershed have been normalised and final cluster centroids are calculated using the morphometric attributes. After calculating the cluster centres, the sub-basin has been group based on the closest distance to the cluster centre. From the Table 3.5 it can be seen that the cluster centre 1 is mostly highly influenced by slope parameters (Higher values), cluster centre 2 is mainly influenced by shape parameters and cluster 3 is moderately influenced by both the slope and shape parameters to some extent. In K-means clustering an ANOVA table is also calculated (Table 3.6) to curb out which variable contribute more to the cluster separation. Bifurcation ratio (7.348) is the most important parameter which act a strong separator of each sub-basin. The basins which have been designated as cluster 1 (Tamal, Silai and Silai Ketia Khal) (Table 3.7) depends upon the influence or similar in terms of morphometric parameters having highest calculated z score like bifurcation ratio, stream frequency, circularity ratio, form factor, relief ratio, ruggedness index, compactness ratio, hypsometric integral and dissection index thus the dominance of slope and relief aspects can be reflected. The cluster 2 (Purandar and Betal) show similarity in drainage density, stream frequency, circularity ratio, form factor, elongation ratio, length of overland flow, hypsometric integral and texture ratio where the basin geometrical shape predominates and cluster 3 (Joypanda, Parang, Kubai and Donai) show similarity in respect to the length of channel maintenance. Therefore, the clustered basins will show likeness in terms of flood character, infiltration character, soil erosiveness etc. which will help in the formulation of a strategic wise basin management plan in a sustainable way.

Table 3.5 Identification of the most influencing parameter for sub-basin clustering

Morphometric parameters	Calculated Z-score for final cluster centre		
	Cluster 1	Cluster 2	Cluster 3
MR_b	0.987	-1.150	-0.165
D_d	0.635	0.721	-0.837
T	0.219	1.235	-0.782
F_s	0.065	1.250	-0.673
R_c	-0.792	1.229	-0.020
R_f	-0.596	1.356	-0.230
R_e	-0.474	1.305	-0.296
L_g	0.609	0.747	-0.830
R_h	0.619	-0.633	-0.147
R_n	0.847	-0.783	-0.244
C_c	0.799	-1.153	-0.022
HI	-0.071	1.401	-0.647
D_{is}	0.625	-1.410	0.236
C	-0.641	-0.719	0.840

Table 3.6 Computational table of ANOVA as extracted from SPSS software

Morphometric parameters	Cluster		Error		F statistic	Significance level
	Mean square	Degree of freedom	Mean square	Degree of freedom		
MR_b	2.840	2	0.387	6	7.348	.024
D_d	2.529	2	0.490	6	5.158	.050
T	2.822	2	0.393	6	7.189	.026
F_s	2.478	2	0.507	6	4.884	.055
R_c	2.454	2	0.515	6	4.760	.058
R_f	2.481	2	0.506	6	4.899	.055
R_e	2.219	2	0.594	6	3.737	.088
L_g	2.494	2	0.502	6	4.969	.053
R_h	1.022	2	0.993	6	1.029	.413
R_n	1.811	2	0.730	6	2.482	.164
C_c	2.289	2	0.570	6	4.015	.078
HI	2.810	2	0.397	6	7.085	.026
D_{is}	2.689	2	0.437	6	6.156	.035
C	2.549	2	0.484	6	5.269	.048

Table 3.7 Classification of sub basin into cluster

Sub basin	Cluster
Silai	1
Joypanda	3
Purander	2
Betal	2
Parang	3
Tamal	1
Kubai	3
Donai	3
Silai Ketia Khal	1

3.2 Recharge and infiltration capacity prioritization of sub-basins by TOPSIS, COPRAS and VIKOR models

The prioritization of the sub-basin focusing the objective to rank them according to the recharge and infiltration capacity has been done using the MCDM techniques. After the computation of the attributes related to drainage network, basin geometry, drainage texture and relief aspects among them 18 morphometric parameters namely stream length of 1st order, mean stream length ratio, bifurcation ratio, drainage density, basin texture ratio, stream frequency, circularity ratio, form factor, elongation ratio, length of over land flow, relief ratio, dissection index, compactness co-efficient, infiltration number Lemniscate's value, hypsometric integral, dissection index, gradient ratio and length of channel maintenance has been used to prioritize the sub-basin. To remove the unitary influence over the methodology method of data normalization has been executed. In this study linear method of data normalization technique has been performed before the computation of decision matrix for the each MCDM method (TOPSIS, COPRAS and VIKOR). The weight of each morphometric attribute has been calculated before the execution of each MCDM model using Shannon (1948) Entropy model (Equation 3.4-3.7). The Entropy weight calculation of the effective morphometric attributes effecting the infiltration capacity showed that stream length of 1st order, basin texture ratio, infiltration number, mean stream length ratio and hypsometric integral with scores 0.123,0.121,0.089, 0.076 and 0.074 have the highest effect on the recharge and infiltration capacity of the sub-basins. After the determination of the weight of the morphometric attributes weight normalized decision matrix has been calculated for TOPSIS, VIKOR and CORPAS. In TOPSIS the identification of Positive and negative Ideal solutions, calculation of the separation distance of each competitive alternative from the ideal and non-ideal solution ($S_i^+ and\ S_{\bar{i}}$) and the relative closeness of the potential location with respect to the ideal (P_i) has been formulated using the equation from 3.10 to 3.14. Higher the value of P_i lower will be the rank (1) of the sub-basin hence greater recharge capacity (Table 8). Subsequently in VIKOR the calculation of the value of the utility measure (S_i) and regret measure (R_i) and the VIKOR index (Q_i) has been executed using the equation 3.15, 3.16 and 3.17. Here higher the value of Q_i higher will be the rank (9) and poor the recharge capacity of the sub-basin. (Table 8). The computation of the maximum (S^+_j) and the minimum (S^-_j) values of the alternatives and the calculation of the relative weights (Q_i) of each of the alternatives for the COPRAS model has been done using the equation from 3.20-3.22 (Table 3.8). The results of sub-basin prioritization (Fig 3.6) on the basis of their sensitivity towards the recharge and infiltration capacity showed that in TOPSIS model sub-basin Donai, Silai and Kubai ranked 1, 2 and 3 and is more susceptible towards good recharge and infiltration capacity whereas sub-basin Betal, Joypanda and Purander ranked 9, 8 and 7 are susceptible to poor groundwater recharge. According to the VIKOR model sub-basin Silai, Donai and Tamal ranked 1, 2 and 3 and are more sensitive towards groundwater recharge whereas sub-basin Silai-Ketia Khal, Betal and Purander ranked 9, 8 and 7 and least sensitive towards recharge and infiltration. The COPRAS model showed that the sub-basin Parang, Donai and Silai ranked 1, 2 and 3 which has greater recharge capacity whereas sub-basin Purander, Betal and Silai Ketia Khal ranked 9, 8 and 7 have poor capacity in terms of recharge and infiltration.

Table 3.8 Prioritization of sub-basins using 18 morphometric parameters and MCDM models

Sub basin	TOPSIS				VIKOR				COPRAS			
	S^+_j	S_i^-	P_i	Rank	S_i	Ri	Q_i	Rank	S^+_j	S^-_j	Q_i	Rank
Silai	0.103	0.145	0.585	2	0.938	0.149	0	1	0.087	0.038	0.110	3
Joypanda	0.123	0.128	0.511	8	2.381	0.966	0.277	6	0.076	0.032	0.103	5
Purander	0.109	0.115	0.515	7	2.618	1.596	0.387	7	0.065	0.039	0.088	9
Betal	0.128	0.106	0.453	9	4.313	1.781	0.613	8	0.078	0.063	0.092	8
Parang	0.121	0.148	0.550	4	2.210	0.572	0.206	5	0.064	0.015	0.123	1
Tamal	0.118	0.132	0.527	6	2.024	0.445	0.168	3	0.074	0.032	0.101	6
Kubai	0.111	0.139	0.555	3	2.106	0.569	0.193	4	0.065	0.020	0.108	4
Donai	0.086	0.138	0.617	1	1.768	0.487	0.142	2	0.074	0.020	0118	2
Silai Ketia Khal	0.114	0.138	0.546	5	5.140	4.009	1	9	0.078	0.030	0.107	7

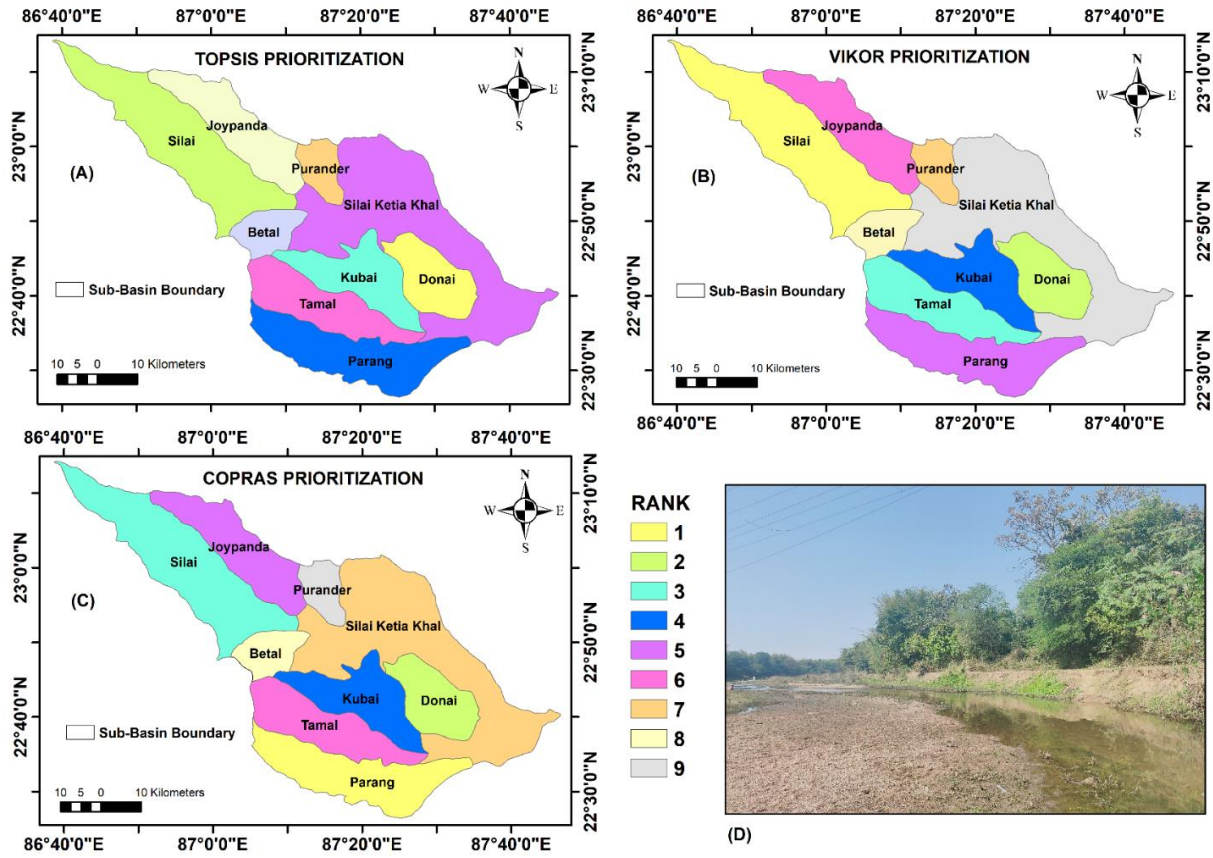

Fig. 3.6 Prioritization of the river basin based on MCDM techniques (A) TOPSIS (B) VIKOR (C) COPRAS (D) Condition of the Joypanda sub-basin

3.3 Selection of the best model and validation using yield data

MCDM techniques have great diversity and this diversity stimulate the flexibility in the selection of the appropriate technique and each technique has its strengths and shortcoming (Singh and Malik, 2014). Therefore, the selection of the best model is necessary to achieve the objectives of the study and to implement the conservation techniques accordingly. In the present research the results of the model have been compared based on the SCCT technique (Table 3.9) which shows the TOPSIS model has the highest co-relation among the other MCDM tools that is 0.750 with COPRAS and 0.717 with VIKOR. The rank map of the sub-basin according to the TOPSIS model has been validated using groundwater yield data as obtained from the Public Heath Engineering Department (PHED), government of West Bengal, India (Fig 3.7). The application of groundwater yield data is more sustainable and appropriate than groundwater level data as it has been calculated through pumping tests properly judging the efficiency of the aquifer. The groundwater yield data has been grouped into four classes <10 LPM (Litre per Minute), 50-100 LPM, 100-200 LPM and 200-400 LPM. According to TOPSIS rank, sub-basin Donai ranks 1st in recharging its aquifer where most the wells are having the yield from 200-400 LPM whereas sub-basins like Betal and Joypanda ranks 9 and 8 respectively having most of the wells with yield rate between 50-100 LPM and < 10 LPM indicating poor recharge. The sub-basin like Betal and Joypanda is located at the upstream section where the geology is mainly comprising of granitic gneiss and bare land is the prime land use class inducing the watershed towards more groundwater level depletion. Hard rocky terrain over the regions is a hindrance in the infiltration process only the areas of weathered and fractured zone show good potential for groundwater (Das et al. 2018). The sub-basin Donai is located at the downstream part particularly in the flood plain area comprising of sand, silt and clay with calcareous concretions acting as the good aquifer (Bhunia et al. 2012). The lower part of the river basin has also strong potential. The applied approach of the study has merits that provided significantly well-grounded results and can be applied elsewhere with necessary modifications. The lower part of the basin has also a strong potential for groundwater recharge where the runoff volume induces groundwater storage through stream flow (Bhunia et al. 2021). The upper and middle part of the basin are affected by climate change, alterations in land use and land cover and scare surface and groundwater resources and thereby requires sustainable management (Halder et al. 2020).

Table 3.9 Selection of best model using SCCT

	Models	COPRAS	TOPSIS	VIKOR
SCCT	COPRAS	1	0.750	0.683
	TOPSIS		1	0.717
	VIKOR			1

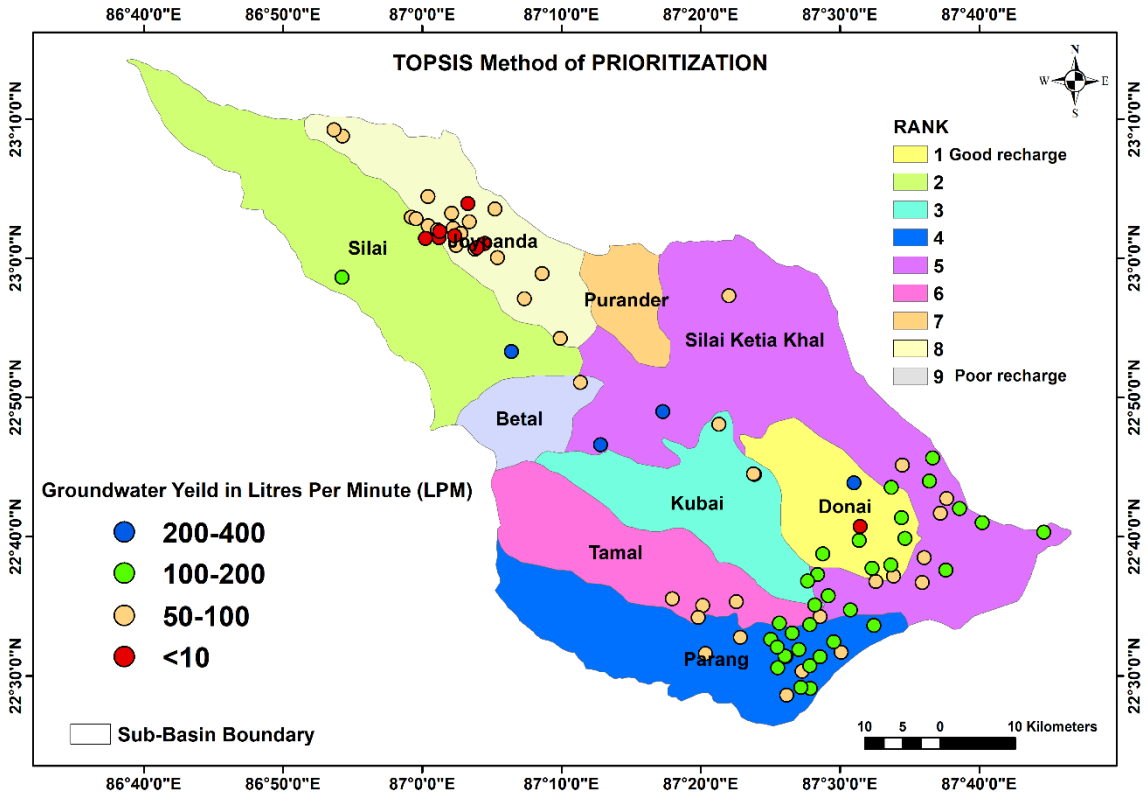

Fig. 3.7 Validation of the model using groundwater yield

3.4 Conclusion and Recommendations

There is a lack in groundwater development in India and the parts of West Bengal occupying the Indo-Gangetic Plain which is highly irrigated with extensive practice of groundwater withdrawals through pumping sets than any other parts of the country (Bhanja et al. 2019). This makes it inevitable to quantify the recharge and infiltration capacity of the river basins and their sub-basins for its effective management and groundwater development. The current research describes the analysis of the morphometric attributes of the Sub-basin of Shilabati River with an objective to analyze the recharge capacity as those attributes represent the underlain geomorphology, geology, slope, relief, climate and hydrological phenomenon as well. The quantitative morphometric parameters of the nine watersheds have been calculated using remote sensing and GIS and their interactions have been fabricated using statistical model and techniques like PCA and K-means clustering. Basin prioritization has been done using various MCDM approaches like TOPSIS, VIKOR and COPRAS. PCA analysis shows that the bifurcation ratio has a very strong correlation with ruggedness number, drainage density has a very strong correlation with texture ratio, length of overland flow and length of channel maintenance, next the stream frequency has a strong correlation with length of overland flow, dissection index and length of channel maintenance which clearly specifies the co-existence of relationship among the generic parameters influencing groundwater recharge. From K-means clustering has been estimated to divide the basin into groups based on their morphological significance and unevenness. 3 clusters have been identified where the cluster 1 consists of Tamal, Silai and Silai Ketia Khal which are mainly controlled by the slope aspects signifying more soil erosion and thereby requires sustainable management. The 2nd cluster consists of Purander and Betal are mainly controlled by the shape parameters of the

basin and the cluster 3 consisting of Joypanda, Parang, Kubai and Donai are mainly influenced by both shape and slope aspects. Next the prioritization of the basin has been conducted using three MCDM techniques where TOPSIS has been selected as the best model through SCCT technique. The model prioritizes the Donai basin as the most influential one towards good infiltration and recharging its underground layers where the groundwater yield ranges from 200-400 LPM.

The model prediction has also been well validated with the yield data. The sub-basins which are having low potential for groundwater recharge require the implementation of management techniques such as rejuvenation of surface water bodies, rain water harvesting, artificial recharge, construction of check dams etc. Based on the analysis areas of optimum recharge can be used for the construction of wells for drinking water supply. The adopted methodology of the present study of basin prioritization based on groundwater recharge potential can be used by the land use planners and policy makers as a prime study for the sustainable management of the river basin. The techniques followed in the study are simple and cost effective but are bit lengthy as the combination of different models is necessary to obtain the results more precisely (Mohamed et al, 2015). Above all, it will help to formulate sustainable conservation strategies at the different levels of the watershed management programme.

3.5 Limitation and Future work

Through morphometric analysis, groundwater recharge mapping overcomes some of the limitations associated with typical hydrological models, which are time-consuming to construct and difficult to apply to a larger area. There are some limitations to this study. However, since actual groundwater yield data are not available everywhere, mapping recharge susceptibility at a micro scale is difficult. In addition, remote sensing data (such as Landsat images) are not capable of providing this type of information. Thus, the study will continue to focus on the collection of groundwater yield data in situ using pumping tests and hydrogeological surveys in order to improve its relevance and accuracy.

Chapter4

Impact of Climate Change on Hydrometeorological events and hydrogeological system using Fuzzy and statistical techniques

4.1 Modelling drought vulnerability tracts of the river basin under climatic scenario

4.1.1 Introduction

Drought is the inevitable consequence of climate change inclusive of precipitation and temperature variability at an extreme stage. Dearth of precipitation events over a long period is the foremost cause of occurrence of the drought (Dalezios, 2011). There is a direct connection between meteorological drought, hydrological drought, and agricultural drought; imbalances in one have an impact on the other. Consequences of drought are diverse in nature and damage cost is hard to estimate (Mladjen, 2013). Due to poor rainfall over a period, agricultural regions in arid or semi-arid regions are mainly affected by the vicious cycle of drought, which reduces soil moisture conditions. Drought modulates the soil moisture condition as soil wetness controls the lateral and sensible heat flux on the earth surface leading to the initiation and maintenance of convection (Mavromatis, 2009). Incapability of land discourages cultivation and creates serve and hostile environmental situation towards plants, animals, livestock potential, biomass potential which ultimately dismantle the economic, financial and food security of human being (Silvestri et al. 2012). At a global scale one-fifth of the damages caused by natural events is mainly drought which estimates an expense of around USD 80 billion per year (White 2003; Carlowicz, 1996). According to IPCC report of 2007, an increase of temperature by 2 to 3^{o} C will disrupt the crop and livestock productivity in the tropical areas as a consequence of desertification and effected area will be Asia, Sub-Saharan Africa and Latin American countries (FAO, 2017). It was estimated that 42% of the land area under the Indian continent has suffered severe drought in the year 2019 and was 6% dry compared to previous years. Estimation of the drought severity, extent and circumstances related to it should clearly be understood by the decision makers and accordingly can strengthen the proactive mainframe of the water resources management at a regional scale (Mishra and Singh, 2009). Prediction of drought and identification of drought prone regions are urgently needed to combat such a global issue. In the present day, satellite and geospatial information systems are used to monitor drought-related extremes over land and to quantify the impacts of drought (Aghakouchak, 2014). Different hydrological, vegetational and climatological variables can be regarded as drought indicators, whose anomalies or departure rates from long-term environmental baseline will help to quantify drought severity. Satellite images from different sources such as Landsat, Sentinel, MODIS etc. can be used to calculate drought indices by applying numerous algorithms as formulated by populous authors. Seasonal forecast of temperature and precipitation anomalies by various centres and satellite platforms inclusive of National Climate research Centre of United States, European Centre for medium range weather forecast, Tropical Rainfall Measuring Mission by NASA, Indian Meteorological

Department (IMD) are the provenience of high-quality data which can be used to assess drought (Jeyaseelan, 2003). Murad and Islam (2011) investigated the agricultural drought risk zones using Normalised Difference Vegetation Index of Bangladesh using 250m resolution data from MODIS satellite from 2000-2008. Through the application of monthly NDVI (1989-2000) data acquired from Advanced Very High-Resolution Radiometers (AVHRRs), Ji and Peters (2003) optimized the relationship between vegetation potency and moisture availability. Rojas et al. (2001) applied similar methodology in order to identify drought prone areas in agriculture intensive tracts of Africa by using Vegetation Health Index (VHI) as calculated from NDVI defining the period of seasonal advent and end of grain filling stage date. These drought indices are frequently used by numerous authors as these are time consuming and cost effective in predicting the results in the nutshell. NDVI, VHI, Vegetation Condition Index (VCI), NDWI etc. are useful tools of drought recognitions and are globally accepted for monitoring vegetational drought in different regions under varying ecological implications (Wang, 2005). Dutta et al. (2015) applied NOAA-AVHRR NDVI data and calculated Standard Precipitation Index (SPI), Rainfall Anomaly Index (RAI) etc. to monitor agricultural drought in Rajasthan which is one of the most drought effected region of North Western India. Extremities of the surface heating can be estimated using Land Surface Temperature (LST) as such Sruthi and Aslam (2015) applied both NDVI and LST using MODIS data in defining agriculturally and hydrological drought prone regions of Raichur district of Karnataka. Thus, the efficiency of effective use of remote sensing indices has been proved by numerous authors as Gumma et al. (2015) mapped and monitor rice cultivated areas using MODIS 250 m resolution 8-day time series data and validated it with rice ecosystem map and statistical analysis. Meteorological drought in due respect to the precipitation variability can be detected by computing SPI of different time scale to assume the frequency of the event occurrence (Ganapati, 2018). Drought identification using multi-criteria decision-making tool incorporating all the above parameters with individual weightage is an innovative approach to conduct instantaneous indications of vital zones and to take conservation measures accordingly. Aher et al. (2017) took eight hydro-meteorological and vegetational parameters and applied Analytical Hierarchy Process (AHP) and Artificial Neural Network (ANN) model to identify drought prone regions of India. Palchandhuri and Biswas (2016) investigated the drought prone region of Puruliya districts of West Bengal, India applying fourteen parameters and AHP which formed 70% of the area is under severe drought. In some cases, AHP method of MCDM does not provide adequate results because it is highly dependent on crisp set modelling. Fuzzy approaches are suitable to overcome this issue.

4.1.2 Research Gap and Novelty of Work

In the eastern part of India, Gangetic West Bengal is the largest producer of agricultural output, which is likely to be affected by 1°C of temperature rise between 2020 and 2029, and about 4.5°C between 2030 and 2099 (Ghosh, 2019). The western districts of West Bengal, India are located around the extended Chotonagpur plateau and are affected by semiarid climate conditions. These regions include Puruliya, Bankura, Paschim Medinapore, Burdwan and parts of Birbhum which are experiencing droughts because of poor preparedness and ineffective water management, thereby reducing the agricultural yields of the state. Till now no studies have been conducted on this river basin and also the application of the Fuzzy DEMATEL on environmental studies where the stake holders and decision makers can have a better understanding of the drought scenario of the basin.

4.1.3 Objective of the Research Work

A fuzzy environment is considered in this study to identify zones prone to drought based on remote sensing derived indices. The general scope of the paper aims a) to analyse the spatio-temporal variability of drought indices with long term effects where three drought years have been selected (2000, 2009 and 2018) b) application of Fuzzy DAMETAL to find out the drought risk prone zones and c) identification of the causal and effect groups from all the drought parameters and d) validation of the identified zone with Yield Anomaly Index (YAI).

4.1.4 Area of Investigation

The river basin comprises diverse climatic scenarios with semi-arid condition in the upper section and tropical monsoon type in the lower most section (Fig.4.1). It experiences drought in its upper part, threatening livelihoods, while flooding in its downstream section threatens human lives. A consequence of both of these events is the ruination of agricultural fields (Palchaudhuri and Biswas, 2016). The average monthly rainfall of the basin varies from 100-170 mm and the maximum temperature ranges from 40-40°C. Furthermore, a check dam at the upstream portion of the dam provides insufficient water, making the area more vulnerable to droughts. The global water demand, limited water supplies from existing reservoirs, regional inequalities, and climate change make water supply management very challenging under such terrain conditions (Bera and Das, 2021), resulting in poor agricultural output during dry seasons and summer months. Thus, the study deals with the identification of the drought prone zone and its severity towards the mankind.

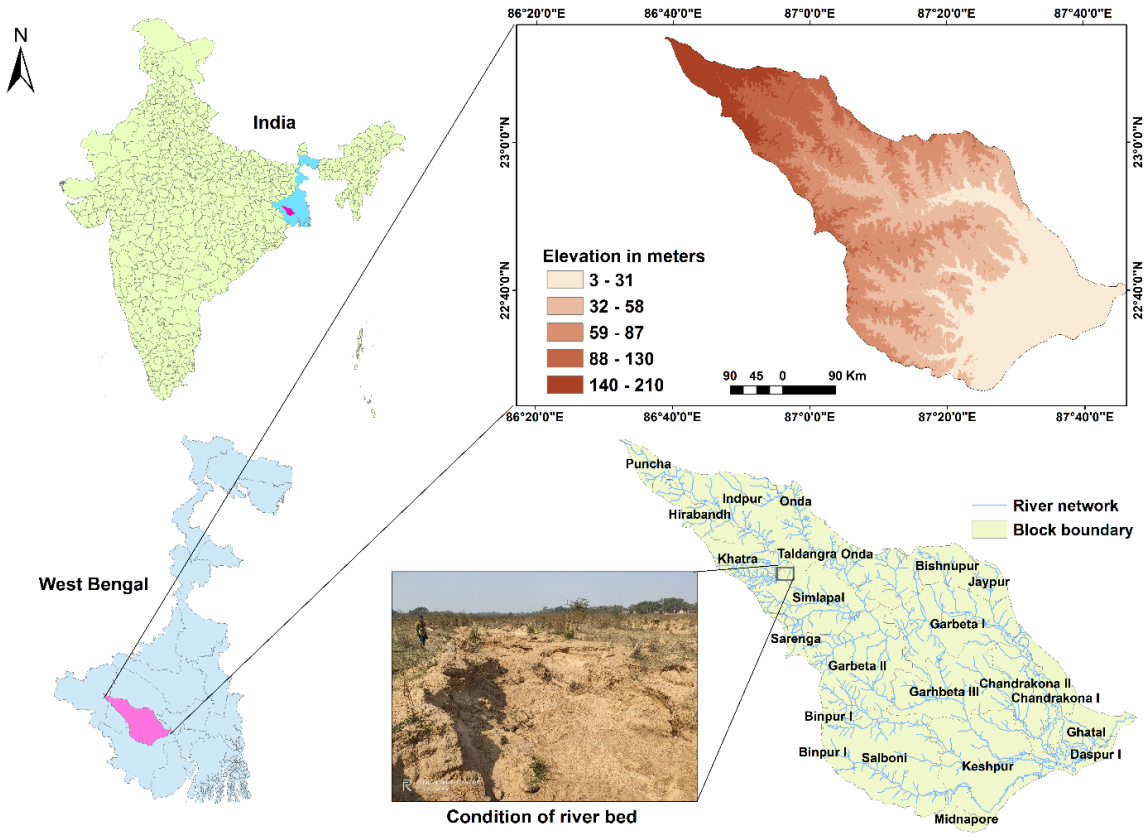

Fig. 4.1 Location of the area of interest

4.1.5 Materials and methods

4.1.5.1 Data source

In the present study identification of the drought risk zone has been done applying Multiple-criteria decision-making (MCDM) tool coupling Fuzzy DEMATEL (Decision making trial and evaluation laboratory) using seven global long-term conditional factors or parameters namely Normalised Difference Water Index (NDWI), Vegetation Condition Index (VCI), Temperature Condition Index (TCI), Soil Moisture Index (SMI), Soil Adjusted Vegetation Index (SAVI), Standard Precipitation Index (SPI). Monthly gridded rainfall data of TRMM 3B43 (0.25^{o} x 0.25^{o}) (Brasil Neto et al. 2021) from 1998-2018 have been downloaded from the GESDISC website (https://disc.gsfc.nasa.gov/) used in this study to estimate the precipitation parameter. Based on the precipitation scenario within this time frame, three years (2000, 2009 and 2018) have been selected having the lowest rainfall. In the later section, the importance of selecting the three years has been discussed further. For other parameter estimation, Landsat 5, Landsat 7 and Landsat 8 OLI (Operational Land Imager) images (Arekhi et al. 2020) of path 139 and row 40 have been retrieved from the USGS Earth Explorer website (https://earthexplorer.usgs.gov/) for the year 2000, 2009 and 2018 at a monthly time scale. Because of cloud coverage, data has been downloaded for the months of summer and dry period, when the severity of drought and poor water supply is at its greatest. All the remote sensing indices and their global long-term effect have been calculated applying different algorithms discussed under the head conditioning factors. For the calculation of Yield Anomaly Index (YAI) agricultural data (2000-2019) has been collected from the Directorate of Agriculture, Government of West Bengal (Fig.4.2).

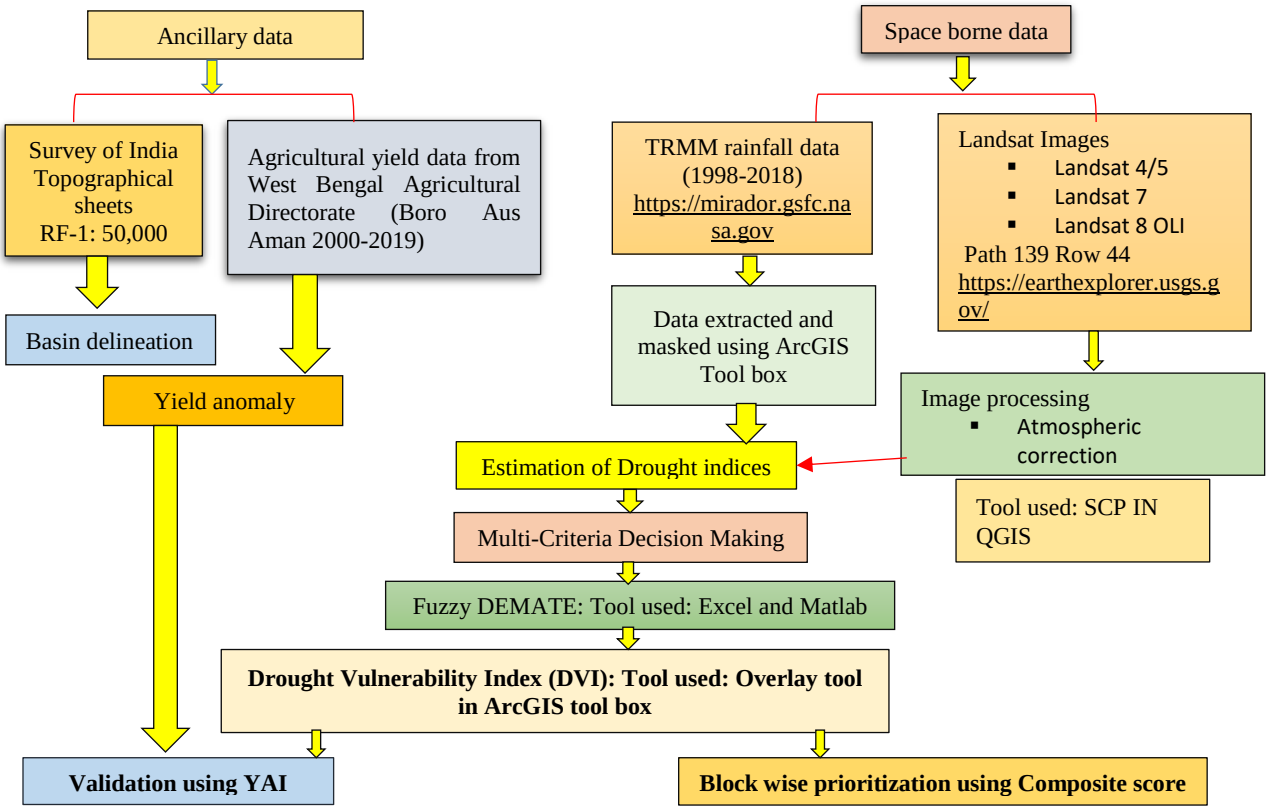

Fig. 4.2 Adopted methodological flow chart of the present study

4.1.5.2 Conditioning factors/ criteria

4.1.5.2.1 Normalised Difference Vegetation Index (NDVI)

NDVI is one of the important tools which identifies the vegetation proportion obtained by measuring the difference between infra-red portion and red light which the vegetation strongly reflects and absorbs (Mohammad et al. 2019). NDVI of the different months of the drought years i.e. are 2000, 2009 and 2018 has been calculated using the following algorithm (Mc Feeters, 1996; Dutta et al. 2015) (Eq.4.1)

$$NDVI = (NIR- VIS) / (NIR+VIS) \quad (4.1)$$

Where NIR is near infra-red and VIS is visible red and the value ranges from -1 to +1 where negative value indicates proportion of water and positive values are associated with vegetation content.

4.1.5.2.2 Vegetation Condition Index (VCI)

VCI is an important remote sensing index that compares the NDVI value of the current year with the range of values that has been observed in the same period in the previous year within the observation tenure. It was developed by Krogan in year 1995 to distinguish the weather aspect from the environment aspects in the NDVI values (Du et al. 2018). It is expressed in percentage. Low values signify drought. The algorithm has been expressed in the following (Krogan 1995) (Eq. 4.2)

$$VCI = (NDVIj - NDVI_{min}) / (NDVI_{max} - NDVI_{min}) \quad (4.2)$$

NDVI min and NDVI max are the minimum and maximum values of each pixel calculated within the observed period and NDVIj is the mean of the months of the current year.

4.1.5.2.3 Land Surface Temperature (LST)

LST is the remotely sensed radiative skin temperature of the surface of the earth whose estimation depends upon the vegetation cover, soil moisture condition and Albedo. Thermal band of the Landsat group of the imageries has been used to determine LST where the sensors measure TOA (Top of Atmosphere) and by using Plank's law of brightness temperature (Ghaleb et al. 2015; Dash et al. 2002). The factor has been calculated using the following set of algorithms (Kumar et al. 2020; Ghaleb et al. 2015)

The 1st step includes the conversion of DN (Digital Number) to satellite brightness temperature (Eq. 4.3)

$$BT = K_2 / \ln (K_1/L\lambda) + 1 \quad (4.3)$$

Where BT is the brightness temperature K_1 is band-specific thermal conversion constant (in watts/meter squared × ster × μm), K_2 is the band-specific thermal conversion constant (in kelvin), Lλ is the Spectral Radiance at the sensor's aperture, measured in watts/ (meter squared × ster × μm), λ = wavelength of emitted radiance, $\rho = h \times c/\sigma$ (1.438×10^{-2} m·K) , h = Planck's constant (6.626×10^{-34} J·s)

The 2nd step include the calculation of the land surface temperature in Kelvin (K) (Eq. 4.4)

$$T = TB / [\ 1 + (\lambda \times TB / \rho)\ \ln\varepsilon \quad (4.4)$$

λ = wavelength of emitted radiance, ρ = h × c/σ (1.438 ×10−2 m·K), h = Planck's constant (6.626 ×10−34 J·s), σ = Boltzmann constant (1.38 ×10−23 J/K), c = velocity of light (2.998 ×108 m/s), ε = emissivity, which is given (Van de Griend and Owe, 1993) by ε = 1.009 + 0.047 ln (NDVI)

The 3rd step include the Conversion from Kelvin to Celsius (Eq. 4.5) (4.5)

$$Tc = T - 273$$

Where T = land surface temperature in Kelvin and Tc is the land surface temperature in Celsius

4.1.5.2.4 Temperature Condition Index (TCI)

TCI is a useful tool to measure the severity of drought. It has been measured to estimate the response of vegetation towards temperature. Using LST for the current year, it has been calculated in relation to the range of values observed within the same season/month during the period of observation. It has been calculated using the algorithm as suggested by Krogan (1995) (Eq.4.6)

$$TCI = (LST_{max} - LST_{i}) / LST_{max} - LST_{minx} \quad (4.6)$$

Where Lst_{min} and LST_{max} are the maximum and minimum value of the current year with the range of values that has been observed in the same period in the previous year within the observation tenure. Low values depict the extremity of drought over the region and is expressed in percentage.

4.1.5.2.5 Vegetation Health Index (VHI)

VHI is an important tool for measuring agricultural drought. It is mainly applied in arid, semi-arid and sub-humid climatic region where there is a scanty of water (Gidey et al. 2018). Both the parameters VCI and TCI are used in the calculation of VHI. Both the conditioning factors have an equal contribution in addressing the vegetation stress over the region. The VHI has been calculated using the following equation (Wang and Yu, 2021) (Eq. 4.7)

$$VHI = a \times VCI + (1- a) \times TCI \quad (4.7)$$

Where a = 0.5 (It is the contribution from VCI and TCI)

4.1.5.2.6 Normalized Difference Water Index (NDWI)

The extent of the surface water can be analyzed using Normalized Difference Water Index which was introduced by Mc Feeters in the year 1996. NDWI of three years i.e. 2000, 2009 and 2018 has been calculated using Landsat images using the following mathematical algorithm (Eq. 4.8)

$$NDWI = (Green - NIR)/ (Green + NIR) \quad (4.8)$$

After calculating the NDWI of different months for each year its long-term anomaly has been estimated using the following algorithm (Eq. 4.9)

Long term anomaly of NDWI = (NDWI*i* – NDWI *min*) / (NDWI *max* – NDWI *min*) (4.9)

Where NDWI*i is* the mean of all the months of the current year*;* NDWI *max* and NDWI *min* are the minimum and maximum values of each pixel calculated within the observed period.

4.1.5.2.7 Soil Moisture Index (SMI)

To quantify the suitability of a land based on surface water conditions for agricultural growth soil moisture index is an important tool of concern. Soil moisture index can be measured insitu but they are expensive and time consuming (Saha et al. 2018). SMI takes an important part while discussing climate, vegetation and drought. Here soil moisture index has been calculated based on the distribution assemblage of the soil moisture condition in NIR Red spectral reflectance space as formulated by Zhan et al. 2007. The algorithm can be written as follows (Eq.4.10)

$$SMI = 1-\frac{1}{\sqrt{a^2+1}}(NIR + a \times Red) \quad (4.10)$$

Where a is the slope of the line correlation between NIR and Red band. The value ranges from zero to 1 and values close to 1 represents high soil moisture condition. After calculating the SMI for each months of the three different year long term SMI anomaly has been estimated using the equation 4.11.

(SMI*i* – SMI*min*) / (SMI*max* –SMI*min*) (4.11)

Where SMI*i is* the mean of all the months of the current year*;* SMI*max* –SMI*min* are the minimum and maximum values of each pixel calculated within the observed period.

4.1.5.2.8 Soil Adjusted Vegetation Index (SAVI)

Reflectance of the bare soil is prevalent over the study area because of the deforestation in regard to the expansion of anthropogenic activities. SAVI is an efficient tool that helps to minimize the influence of soil brightness from spectral vegetation indices which includes the application of red and near infrared (NIR) wavelength (Huete 1988). Therefore, SAVI has been applied here to detect vegetational variation over the region where poor vegetational cover persists with greater dominancy of dry fallow and bare lands. The following algorithm has been used to calculate SAVI (Huete 1988) (Eq. 4.12).

$$SAVI = \frac{NIR+RED}{NIR-RED} * (1+L) \quad (4.12)$$

L is the brightness correction factor. The value of L varies with the amount or cover of the vegetation, here L = 0.5 has been used. SAVI value ranges -1 to + 1 where positive value indicates healthy vegetation. After calculating the SAVI of the months for the years 2000, 2009 and 2018, long term effects have been calculated using the following algorithm (Eq. 4.13).

(SAVI*i* – SAVI*min*) / (SAVI*max* –SAVI*min*) (13)

Where SAVI*i is* the mean of all the months of the current year*;* SAVI*max* –SAVI*min* are the minimum and maximum values of each pixel calculated within the observed period.

4.1.5.2.9 Standard Precipitation Index (SPI)

In order to assess drought, it is important to calculate the standard precipitation index based on the uniformity of precipitation over a period of time. This can be considered a standard deviation of observed cumulative precipitation from average. It is possible to identify dry and wet periods in the monthly precipitation using SPI (Cavus and Aksoy 2019; Mahamoudi et al. 2021). The precipitation has been obtained from TRMM (Tropical Rainfall Measuring Mission: https://gpm.nasa.gov/missions/trmm) with product number 3B43 at a monthly scale having resolution of 0.25 x 0.25 degree (Jiang et al. 2020). A total of 13 grids cover the whole basin, and the data are in NETCDF format. Using the above dataset SPI has been calculated applying the following algorithm (Biag et al. 2021) (Eq. 4.14).

$$SPI= \frac{x_j+\mu_j}{\sigma_j} \quad (4.14)$$

Where x is the precipitation of the month j (1, 2, 3,…12), μ is the average precipitation and $\boldsymbol{\sigma}$ is the standard deviation of the dataset. Positive values of SPI indicate period of wet and negative values represents dry or drought condition (Malakiya and Suryanarayana 2016). For the calculation of long-term SPI, the following equation has been used (Eq.4.15)

$$(SPI_i - SPI_{min}) / (SPI_{max} - SPI_{min}) \quad (4.15)$$

Where SPI*i is* the mean of all the months of the current year*;* SPI*max* –SPI*min* are the minimum and maximum values of each pixel calculated within the observed period.

4.1.5.2.10 Yield Anomaly Index (YAI)

Yield anomaly Index can be defined as the index for calculating the deviation of crop yield for a particular year from its long-term trend. YAI has been used here to validate the drought risk zone map. The region is dominated with paddy cultivation (Halder et al. 2020) under such circumstances crop statistics of Aman, Aus and Boro for the three seasons (Pre-monsoon, monsoon and post-monsoon) has been collected from Directorate of Agriculture, Evaluation Wing, Government of West Bengal. YAI has been calculated using the following algorithm (Dutta et al., 2015) (Eq. 4.16).

$$YAI= (Y-\mu)/\boldsymbol{\sigma} \quad (4.16)$$

Where, Y is crop yield, μ is the long-term average yield and $\boldsymbol{\sigma}$ is the standard deviation.

4.1.5.3 Fuzzy DAMETAL

Decision-Making Trial Evaluation Laboratory (DEMATEL) is a useful technique for the assessment of cause and effect relationship for a set a criteria or parameters (Muhammad and Cavus 2017). The model has been developed by Geneva research Centre of Battelle Memorial Institute to visualise the structure of complicated causal relationship between race, hunger, environmental protection and energy, etc. problem (Chin et al., 2018). But the application of this model in water related studies are fewer in number. Shahi et al (2018) applied fuzzy DAMETAL in the analysis of business intelligence performance. In 2017 Muhamnad and Cavus (2017) applied this technique

in the assessment of the learning management system. Tsai (2015) made environmental evaluation of high technology product manufacture using this fuzzy DAMETAL model. In the present study drought risk zone has been using Fuzzy DAMETAL and will be the effective one. As drought is an event which is induced by certain conditional factors (temperature, rainfall etc.) and is reflected through the analysis of effect parameters (vegetational growth, soil moisture condition etc.). The model has been executed using a number of mathematical algorithms in SPSS and Matlab. The steps have been given below (Seker et al. 2017).

Step 1: Define the conditioning factors

Step 2: To eradicate the vagueness of the human assessment a triangular fuzzy scale having the linguistic variable of 'influence' has been used which is a five-level scale (No influence, very low influence, low influence, high influence and very high influence) as proposed by Li (1999). The fuzzy numbers of these linguistic variable have been given in table 4.1 and the membership function among the fuzzy number has been shown in fig. 4.3.

Table 4.1 Triangular Fuzzy Scale

Linguistic scale for importance	Triangular Fuzzy scale
No Influence	(0,0,0.25)
Very low influence	(0,0.25,0.5)
Low influence	(0.25,0.5,0.75)
High influence	(0.5,0.75,1)
Very high influence	(0.75,1,1)

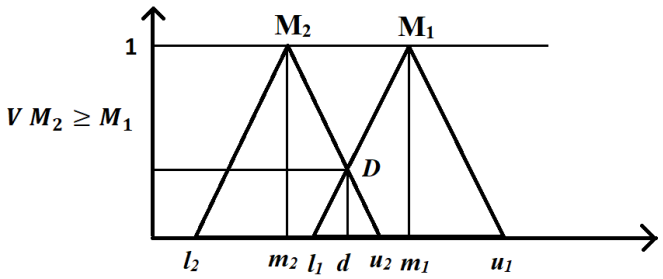

Fig. 4.3 Interaction between M2 and M1

Step 3: Now for converting these fuzzy numbers defuzzification techniques has been considered. It is the method of the selection of the specific crisp component based on the fuzzy set and also converts the fuzzy numbers into crisp score (Opricovic and Tzeng 2003). In this study CFCS type of defuzzification method has been used and is executed in the following sub steps (Eq. 4.17- 4.26)

I. Let us suppose that $\boldsymbol{Z_{ij}^k}=(\boldsymbol{l_{ij}^k}, \boldsymbol{m_{ij}^k}, \boldsymbol{u_{ij}^k})$ stands for fuzzy assessments of evaluator (k=1,2,3…p) about the degree to which the criterion i influences over criterion j

II. Normalisation of fuzzy direct relation matrix and computation of all alternatives (Table 4.2)

$$\Delta_{Min}^{Max} = max u_{ij}^k - \min l_{ij}^k \quad (4.17)$$

$$Xl_{ij}^k = \frac{l_{ij}^k - \min l_{ij}^k}{\Delta_{Min}^{Max}} \quad (4.18)$$

$$Xm_{ij=}^{k} \frac{m_{ij}^{k} - \min l_{ij}^{k}}{\Delta_{Min}^{Max}} \quad (4.19)$$

$$Xu_{ij=}^{k} \frac{u_{ij}^{k} - \min l_{ij}^{k}}{\Delta_{Min}^{Max}} \quad (4.20)$$

III. Calculation of right (us) and left (ls) normal values. For j = 1....j (Table 4.3)

$$xls_{ij}^{k} = \frac{xm_{ij}^{k}}{1+xm_{ij}^{k}-xl_{ij}^{k}} \quad (4.21)$$

$$xus_{ij}^{k} = \frac{xu_{ij}^{k}}{1+xu_{ij}^{k}-xm_{ij}^{k}} \quad (4.22)$$

IV. Calculation of total crisp normalized value, For j = 1....j

$$xus_{ij}^{k} = \frac{xls_{ij}^{k}\left(1-xls_{ij}^{k}\right)+xus_{ij}^{k}*xus_{ij}^{k}}{1-xls_{ij}^{k}-xus_{ij}^{k}} \quad (4.23)$$

V. Compute crisp values, For j = 1....j

$$Z_{ij}^{k}=minl_{ij}^{k} + x_{ij}^{k} * \Delta_{min}^{max} \quad (4.24)$$

Step 4: Calculation of the total relation matrix (Table 4.4)

$$T = N(I - N)^{-1}$$

Step 5: Calculation of sum of rows and the sum of columns which are separately represented by D and R in the total-relation matrix. (Table 4.5)

$$D= [\sum_{i=1}^{n} t_{ij}]_{n*1} \quad (4.25)$$

$$R= [\sum_{i=1}^{n} t_{ij}]_{n*1} \quad (4.26)$$

Step 6: In the last step a cause and effect diagram are being prepared where the horizontal axis (D+R) is estimated by adding R and D and the vertical axis (D-R) is calculated by subtracting R from D. Now (D+R) can be defined as the 'prominence' which signifies the importance of the degree of criterion, (D-R) may be denoted as the 'relation' which signifies the degree of influence. The negative values of (D-R) is grouped into the effect group which implies the influence from other criteria and the positive values of (D+R) mean that it has a consequential impact.

Table 4.2 Normalized Fuzzy Direct Relation Matrix of the selected long-term drought indices

Criteria	Standard Precipitation Index (SPI)			Soil Moisture Index (SMI)			Vegetation Condition Index (VCI)			Temperature Condition Index (TCI)			Soil Adjusted Vegetation Index (SAVI)			Vegetation Health Index (VHI)			Normalized Difference Water Index (NDWI)		
SPI	0.00	0.00	0.25	0.75	1.00	1.00	0.75	1.00	1.00	0.50	0.75	1.00	0.50	0.75	1.00	0.75	1.00	1.00	0.75	1.00	1.00
SMI	0.25	0.50	0.75	0.00	0.00	0.25	0.50	0.75	1.00	0.25	0.50	0.75	0.50	0.75	1.00	0.50	0.75	1.00	0.50	0.75	1.00
VCI	0.25	0.50	0.75	0.25	0.50	0.75	0.00	0.00	0.25	0.25	0.50	0.75	0.25	0.50	0.75	0.75	1.00	1.00	0.25	0.50	0.75
TCI	0.25	0.50	0.75	0.75	1.00	1.00	0.75	1.00	1.00	0.00	0.00	0.25	0.50	0.75	1.00	0.75	1.00	1.00	0.75	1.00	1.00
SAVI	0.25	0.50	0.75	0.25	0.50	0.75	0.50	0.75	1.00	0.25	0.50	0.75	0.00	0.00	0.25	0.50	0.75	1.00	0.50	0.75	1.00
VHI	0.33	0.67	1.00	0.33	0.67	1.00	0.33	0.67	1.00	0.33	0.67	1.00	0.33	0.67	1.00	0.00	0.00	0.33	0.33	0.67	1.00
NDWI	0.25	0.50	0.75	0.50	0.75	1.00	0.50	0.75	1.00	0.25	0.50	0.75	0.50	0.75	1.00	0.50	0.75	1.00	0.00	0.00	0.25

Table 4.3 De-Fuzzified and Normalized Direct Relation Matrix of the selected long-term drought indices

Criteria	SPI	SMI	VCI	TCI	SAVI	VHI	NDWI
SPI	0.007	0.183	0.183	0.130	0.130	0.183	0.183
SMI	0.077	0.007	0.130	0.077	0.130	0.130	0.130
VCI	0.077	0.077	0.007	0.077	0.077	0.183	0.077
TCI	0.077	0.183	0.183	0.007	0.130	0.183	0.183
SAVI	0.077	0.077	0.130	0.077	0.007	0.130	0.130
VHI	0.103	0.103	0.104	0.104	0.103	0.100	0.104
NDWI	0.077	0.130	0.130	0.077	0.130	0.130	0.007

Table 4.4 Total Direct Relation Matrix of the selected long-term drought indices

Criteria	SMI	VCI	TCI	SAVI	VHI	NDWI	SPI
SPI	0.540	0.592	0.409	0.483	0.693	0.564	0.280
SMI	0.271	0.418	0.276	0.372	0.489	0.398	0.263
VCI	0.305	0.270	0.253	0.296	0.491	0.320	0.240
TCI	0.515	0.564	0.280	0.461	0.660	0.537	0.329
SAVI	0.320	0.398	0.263	0.245	0.466	0.379	0.250
VHI	0.383	0.421	0.318	0.371	0.489	0.401	0.301
NDWI	0.380	0.418	0.276	0.372	0.489	0.289	0.263

Table 4.5 Prominence and relation axis for cause and effect

Criteria	D (sum of row)	R (sum of column)	D- R	D+R	Normalised values	Rank
SPI	3.560	1.926	1.634	5.486	0.144	2
SMI	2.487	2.713	-0.226	5.200	0.136	6
VCI	2.175	3.080	-0.905	5.255	0.138	5
TCI	3.345	2.076	1.269	5.421	0.142	3
SAVI	2.323	2.600	-0.277	4.923	0.129	7
VHI	2.684	3.779	-1.095	6.463	0.169	1
NDWI	2.487	2.887	-0.400	5.374	0.140	4

4.1.5.4 Model prioritization using Compound factor (CF)

Compound factor model is a predominant statistical tool used to rank certain criteria, parameters, condition factors based on specific objectives and sometimes to collate performance and accuracy of models (Namous et al. 2021). It rather implies a knowledge-based structure in the alteration of rational interpretation of portentous event in quantitative estimation (Sadhasivam et al. 2020). In the current study the tool has been used in ranking the conditioning parameters and the average value of the assigned rank of each CD blocks determine its respective priority among others (Altaf et al. 2014). The algorithm has been executed using the following equation (Eq. 4.27).

$$CF = \frac{1}{n} \sum_{i=1}^{Pn} R \quad (4.27)$$

CF is the compound factor; R is the rank of the parameters and Pn is the total number of conditioning factors.

In the current study after the identification of the drought risk prone zone CD (Community Development) blocks has been prioritised based on the extracted values of 7 conditioning factors. The lower values of the selected conditioning factors signify the occurrence of drought, poor vegetation health, low moisture content etc. Lower values from each CD blocks has been taken under consideration and higher weightage has been entrusted. The study area comprises 22 CD blocks as such the lower values have been ranked with 22 and the 2nd lower values has been ranked 21 and so on. Higher CF values denote higher the priority to eliminate drought and providing sustainable solutions towards water resources management over the region.

4.1.5.5 Estimation of Drought Vulnerability zone

Identification of the drought risk zones using remote sensing indices has been increasing in the recent days due the advancement of the earth-observation satellite system (Dalezios et al., 2014) and is also time consuming. Accounting 40% of the Indian land surface is affected by drought where failed monsoon rains are the primary cause. The North-East monsoon (October-December) that provides 10-20% of India's rainfall, was deficient by 44% in 2018 from the long-term normal of 127.2 mm according to the India Meteorological Department (IMD, 2018) and regarded 2018 as one of the warmest year. Such rainfall variability caused a deficit in the South-West monsoon (June-September) which often provides 80% of rainfall fell short by 9.4% in the year 2018 which is near

about the 10% deficit range as declared by drought. Therefore, in this study drought risk zone of a river basin of West Bengal, India has been calculated using the following equation (Eq. 4.28)

$$Drought\ risk\ zone = SPI\ anomaly * weight + VCI\ anomaly * weight + TCI\ anomaly * weight + NDWI\ anomaly * weight + VHI\ anomaly * weight + SMI\ anomaly * Weight + SAVI\ anomaly * weight \quad (4.28)$$

Where, SPI is Long -tern Standard precipitation index; VCI is Long -term vegetation Condition Index; TCI is Long-term Temperature condition index; NDWI is Long-term Normalized Water Index; SMI is Long term Soil Moisture Index; SAVI is Long term Soil Adjusted Vegetation Index.

4.1.6 Results

4.1.6.1 Drought Monitoring through Standard Precipitation Index (SPI)

In order to recognize the deficit of precipitation on the different usable water sources like stream, river, wetland, soil moisture condition, reservoir storage and groundwater application of multi time scale SPIs will help to identify the nature of drought (Moghbeli et al. 2020). TRMM satellite rainfall data for 2000, 2009 and 2018 has been used to calculate SPI. According to the average monthly rainfall of the river basin from 1998 to 2018, these three years are selected based on the lowest rainfall and also have an interval of nine years (Fig. 4.4). The SPI has been calculated for the drier and summer months (January, February, March, April, May, October, November and December) of each three years when the basin consisting of Puruliya, Bankura and West Medinapore District experiences extreme drought-like conditions (Ghosh 2019). SPI (Fig.4.5) values in 2000 are negative in a few regions, indicating a deficit in rainfall, particularly in March (-0.68 to -0.99), April (0.34 to -0.11), October (1.29 to -0.77) and November (-0.35 to -0.77). In 2009 (Fig. 4.6), drought conditions primarily persist during March (0.08 to -0.44), April (-0.76 to -1.60), October (0.97 to -0.19), November (0.79 to -0.19) and December (0.17 to –0.66). As shown in Fig 4.7, drought in 2018 saw mainly in January (0.53 to -0.62), February (0.30 to -0.72), March (0.32 to -0.61), October (0.33 to -0.61), November (0.10 to -0.67) and December (2.7 to -0.67). The drought-affected months are increasing, which in time will result in vegetation degradation, a decrease in agricultural production and hydrological changes in the upper section and south eastern region of the river basin. In the upper section of the basin vegetation growth is scarce and forest degradation is quite relevant in the recent years (Manna and Mondal 2017) which can also have an adverse effect on the changing patterns of precipitation scenario.

Fig. 4.4 Average monthly rainfall (mm) from 1998 to 2018 of Shilabati river basin

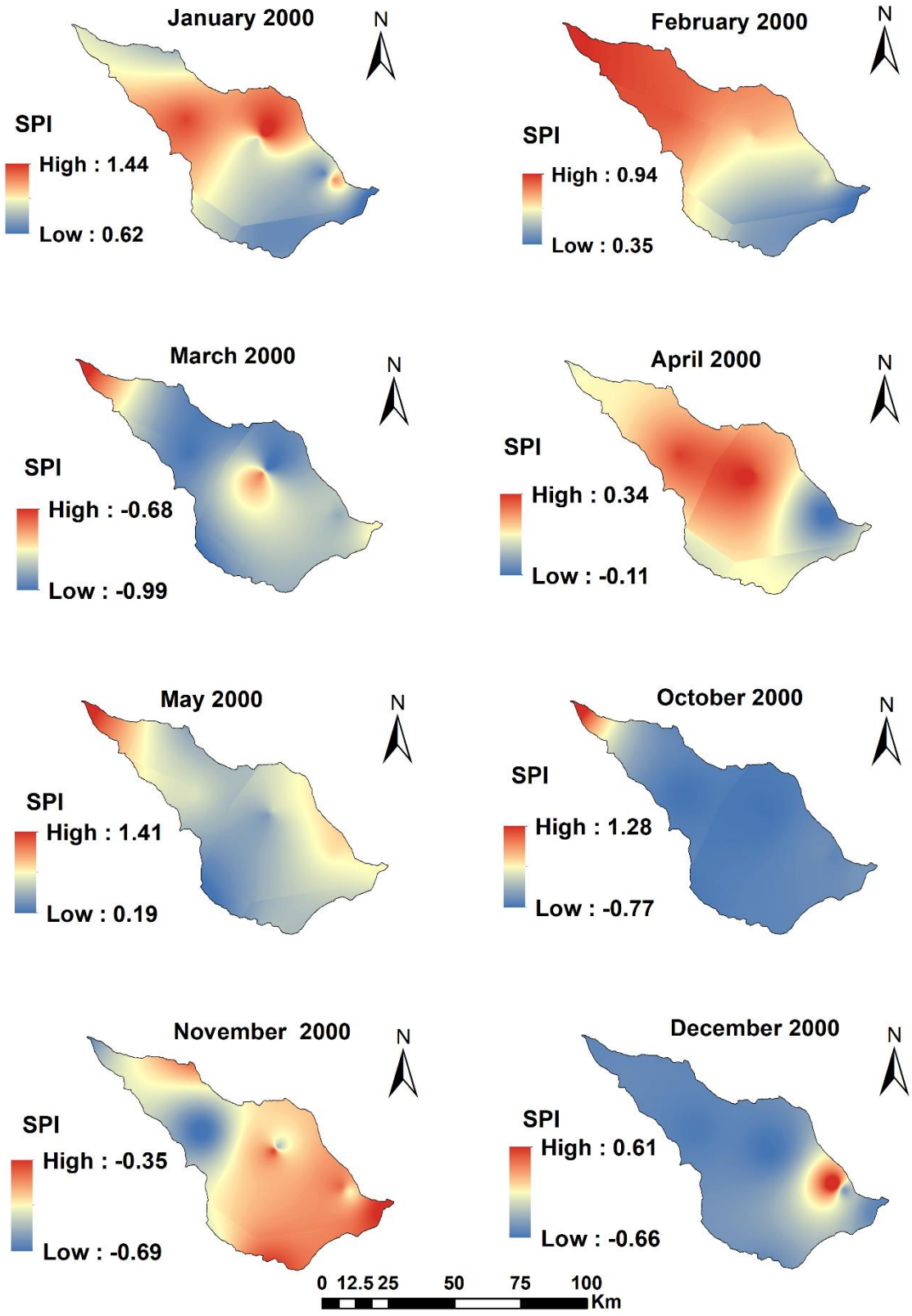

Fig. 4.5 Spatio-temporal distribution of SPI 2000

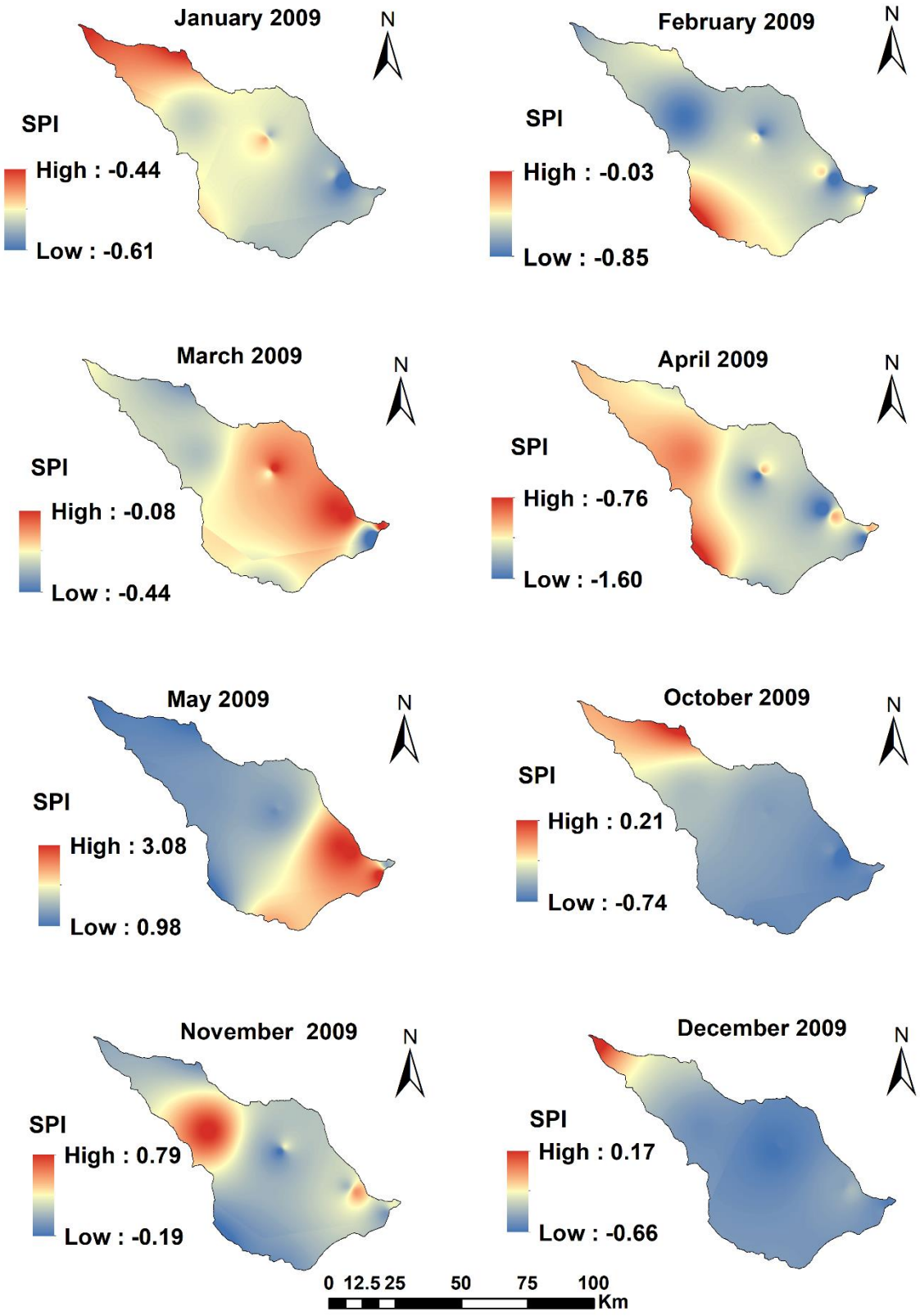

Fig. 4.6 Spatio-temporal distribution of SPI 2009

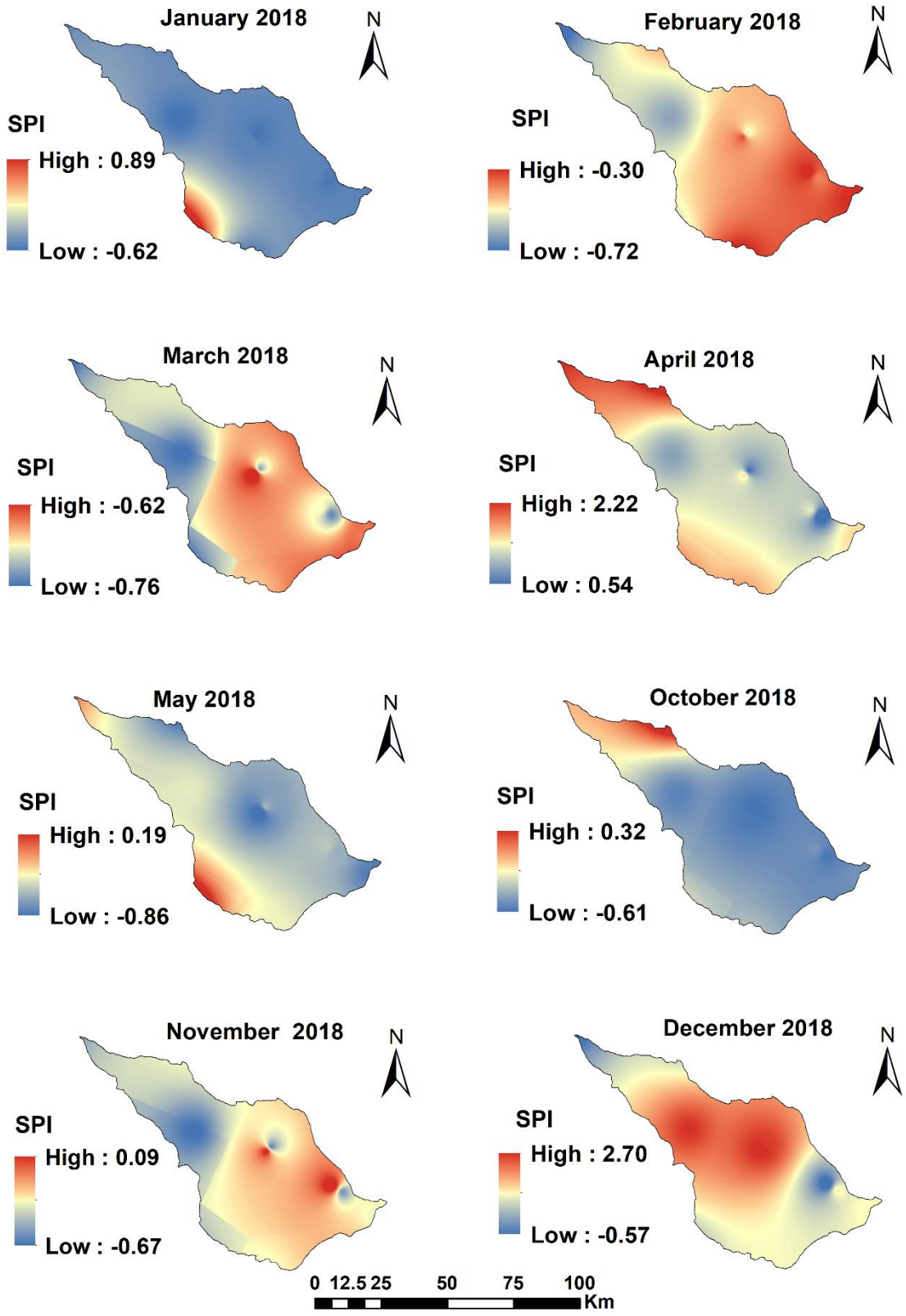

Fig. 4.7 Spatio-temporal distribution of SPI 2018

4.1.6.2 Long term drought analysis using LST and NDVI derived indices

Land surface temperature is an important parameter that plays an important role in identifying the drought prone region. Figure 4.8 shows the spatial-temporal distribution of LST for the years 2000 (January, March, November, and December), 2009 (January, February, March, April, November and December) and 2018 (January, February, March, April, November, and December). In 2000, the highest temperature was found in March (41.50°C), in 2009 it was mostly observed in April (44.10°C), and in 2018 it reached 57.140°C. There has been a continuous rise in the skin surface temperature over the river basin. Deforestation and changes in precipitation trends are the main causes of the temperature rise. The red zones indicate high LST values and is mainly concentrated in the upper most section of basin over the three years. In order to quantify the drought risk in long term surveillance with the help of LST derived index, TCI has been used in the present study. It is a thermal stress criterion used for the drought translocational assessment of a particular area/zone (Gidey et al. 2018). TCI values ranged from 22.6-55% in 2000, 21-57.9% in 2009, and 22.9-40.8% in 2018. For three consecutive years, TCI values have been lower upstream. Low TCI values indicate vegetation stress caused by dehumification or severe weather associated with high temperature conditions (Karneieli et al. 2006). As the river basin is located in the western degraded part of the Chotonagpur plateau, the river basin has been experiencing extreme and acute long-lasting droughts for a long time (Ghosh, 2019) due to the late advent of monsoon. The basin also comprises three major districts of West Bengal like Puruliya, Bankura and West Medinapore where drought is a recurrent problem particularly for the first two (Aktar et al. 2015). In terms of the vegetational cover, dense and open forest together with extensive extension of agricultural land can be observed over the entire basin. Agricultural is the unavoidable and worst drought hit economic sector of the basin (Senapati and Das, 2021). For the three selected years, NDVI has been calculated to quantify overall vegetational stress and related health hazards (Fig.4.9). It reached a low value of -0.47 in March 2000, and vegetational stress was observed throughout the basin. In 2009 the lowest NDVI value is observed in June where it becomes -0.26, and in November it reaches -0.33. In 2018 further deterioration in vegetation health observed in March (-0.91). Upstream and middle sections of the basin suffer from moisture deficiencies and vegetational stress, restricting cropping practices there while downstream appears healthier. As can be seen from the year's water scarcity, water scarcity is concentrated in high temperature months. Long term observation of the drought scenario from the light of vegetational stress has been observed using Vegetation Condition Index (VCI). Comparatively, 2009 observed the lowest VCI value of 1.17% indicating severe vegetational trauma. Similar nature is witnessed for the spatial vegetation Health Index (VHI) derived from both VCI and TCI (Fig. 4.10) (Gidey et al. 2018; Masitoh and Rusydi 2019). VHI value for the study area ranged from 2.37-57.6 clearly indicating the patches of extreme drought condition leading to vegetational strain due to its poor adaptive capability under climate change condition. Local residents also expressed their distress about irrigation scarcity and poor crop production during the field survey. Drying up of the surface water sources and decease in groundwater level are continuously exaggerating the situation (Halder et al. 2020) and thereby requires sustainable management at an urgent basis.

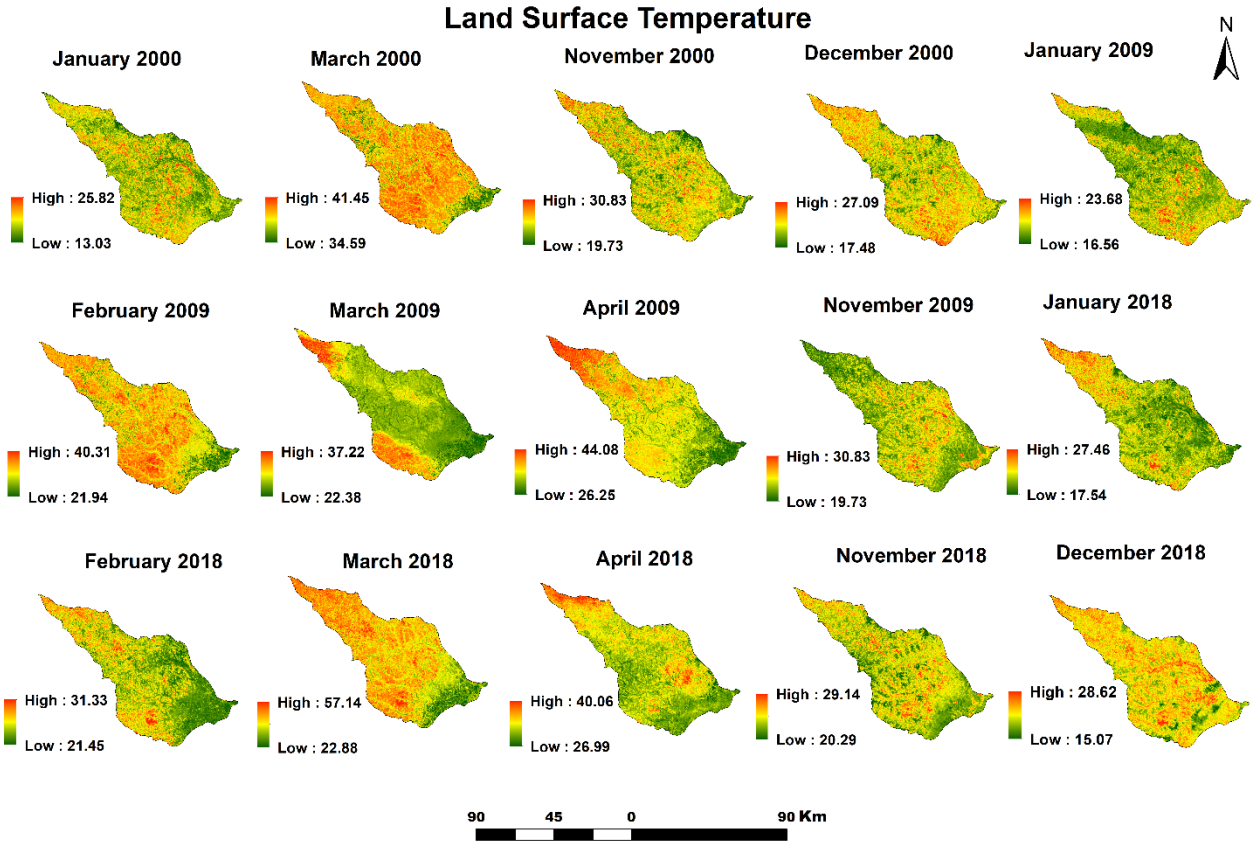

Fig. 4.8 Spatio-temporal distribution of LST

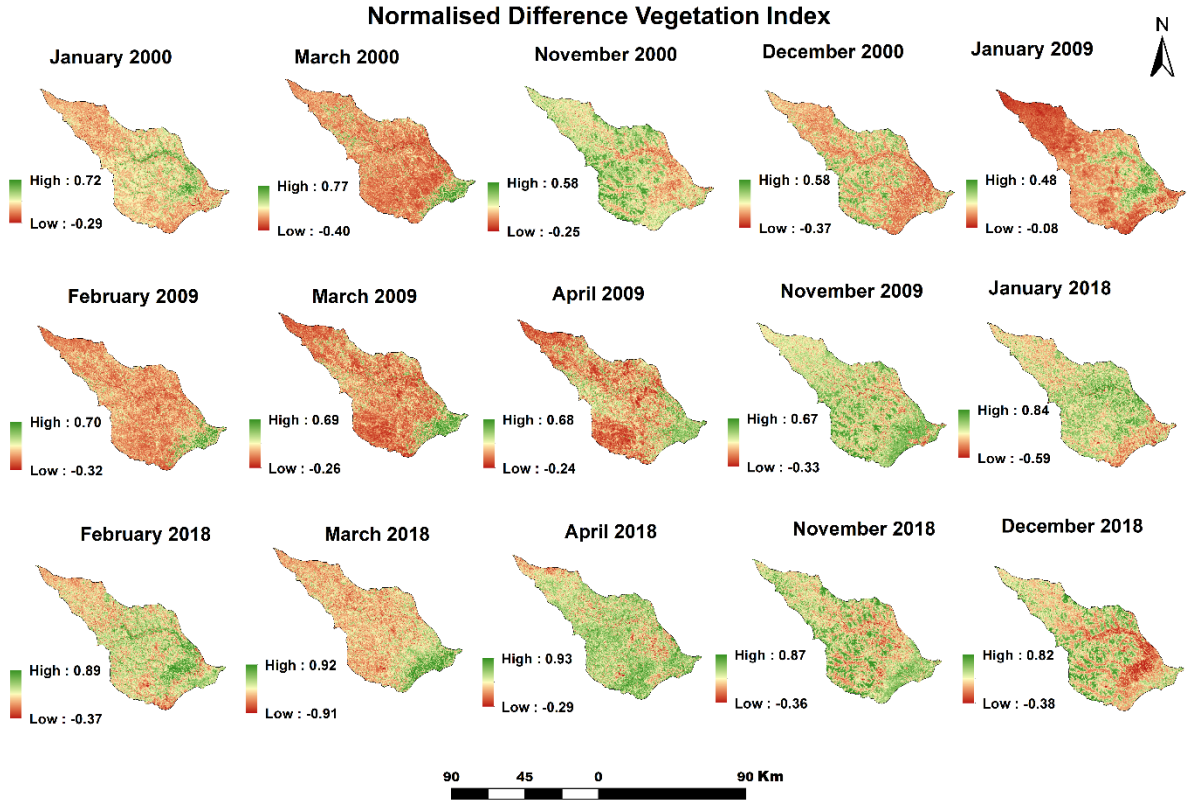

Fig. 4.9 Spatio-temporal distribution of LST

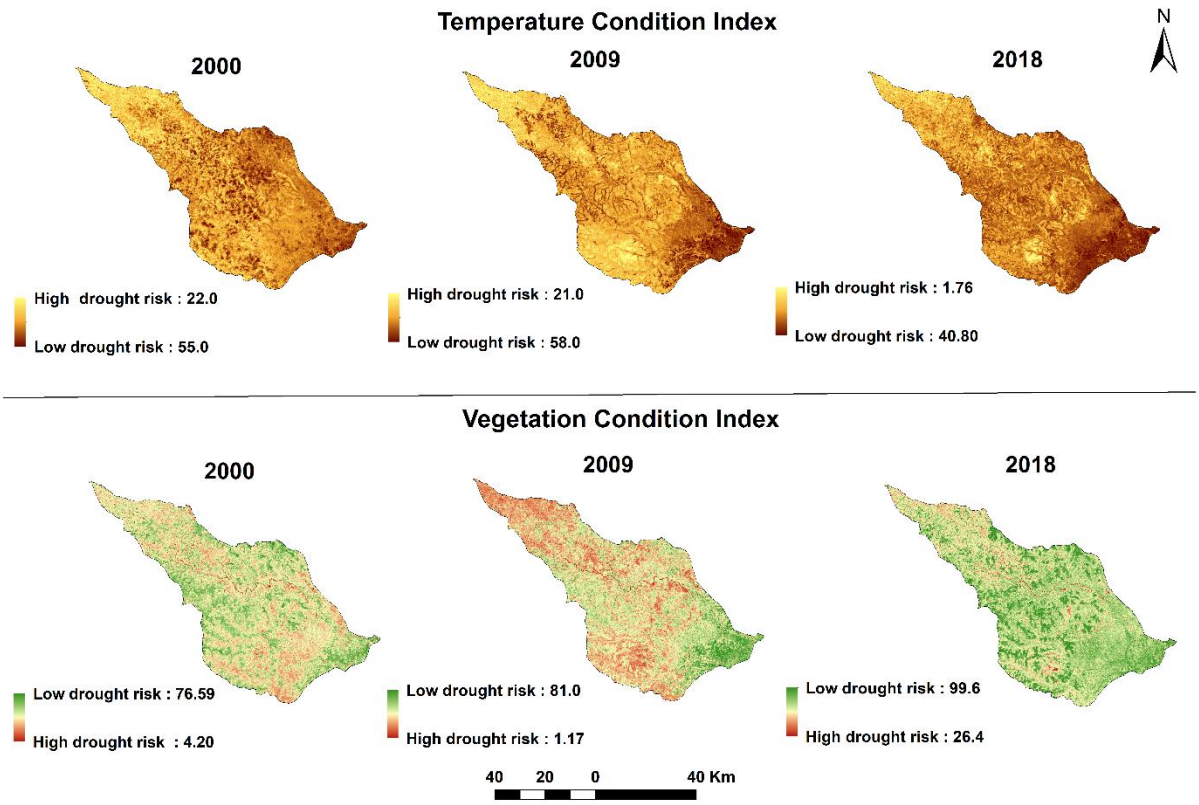

Fig. 4.10 Spatio-temporal distribution of VCI and TCI

4.1.6.3 Long term drought and water stress analysis using NDWI

The upstream section of the basin is a part of the Chotonagpur plateau, which is mostly affected by drought scenarios (Raha and Gayen 2020). The basin and its associated region are predicted to receive scanty rainfall during the monsoon and the temperature will rise by one degree Celsius between 2055 and 2099 (Ghosh 2016; Datta and Das 2019). As a result of poor rainfall and temperature rise, the basin is experiencing drastic water shortages and face severe challenges to socio-economic development (Das et al. 2018). NDWI has been estimated to identify the extent of drying up of surface water bodies (Fig 4.11). In 2000, the NDWI value reached -0.72 in March and similar scenarios are observed in 2009. The value further decreases to -0.88 in March and -0.92 in April. Throughout the basin, the scenarios clearly show surface water shortages. Ultimately, this surface water crisis is leading to the unscientific extension of groundwater for irrigation, which will lead to water scarcity over the entire basin (Halder et al. 2020). Calculating long-term NDWI indexes for the basin reveals a reflection of water crises, with values ranging from 0.72-0.064. According to Sahoo et al. 2021, Puruliya and Bankura districts experience high water stress, and proper surface water management is needed to mitigate it before it aggravates.

4.1.6.4 Drought monitoring through SMI and SAVI

In order to understand how the earth surface and its atmosphere exchange energy during a drought scenario, soil moisture has to be considered as an important parameter to consider (John et al. 2001). With a higher concentration of soil moisture in the soil, groundwater recharge will be reduced and surface runoff will increase, whereas with a lower concentration of soil moisture, drought will be imminent and will affect the growth of vegetation. Numerous techniques are there to estimate this parameter such as time domain reflectometry, gravimetric methods

and other exsitu and insitu techniques which is quite laborious to execute for the entire basin (3881 Sq.km) (Zhang et al. 2014). Thus, the application of remote sensing proves a unique technology to estimate the concentration of soil moisture at a regional and global scale (Lakshmi, 2013). It is evident from Figure 4.12 that a low SMI value is observed during the pre-monsoon season in March. 2009 observed the lowest SMI value of 0.096 during the month of November when the rainfall is also less. Lack of soil moisture condition is a hurdle in the downstream sections of the basin where triple cropping is practised (Biswas et al. 2006). There was an increase in SMI across the basin throughout the year 2018, with the lowest SMI (0.34) to be found in April. Long term SMI ranges from 1-0.47 and is lowest almost throughout the basin because of the deforestation, bare soil condition and extensive evapotranspiration form the surface cover (Mahala 2020). SAVI (Figure 4.13) is calculated to understand vegetation sensitivity incorporating soil and atmospheric parameters. It showed similar trends over three observation years. In 2000 SAVI value is lowest in March (-0.15), in 2009, lowest in February (-0.08) and in 2018, April showed the lowest value of -0.20. The long-term SAVI ranged from 0.61-0.11, which shows vegetation stress in the upstream and middle sections of the river. A major crop cultivated during the study period is Boro, which is shown in December-January and harvested in April-May. According to the agriculture statistical database, Boro crop areas declined from 1401.8 thousand hectares in 2000-2001 to 1290.0 thousand hectares in 2014-2015, with Puruliya having the lowest concentration (Biswas, 2020). Das et al. (2016) report that potato is a major crop cultivated through October-November and harvested during February-March in the basin, but it suffers from enormous losses due to frequent droughts. As a result of water storage on both the surface and the ground, Puruliya ranked last in potato production for the 2014-2015 season (Biswas 2020). During the field survey, there were reports of poor irrigation facilities, inadequate canal water supply, and scarce rainfall events, which led to poor agricultural and production results. In this way, these indices are useful for assessing and identifying long-term drought effects in vegetation areas that require sustainable water management.

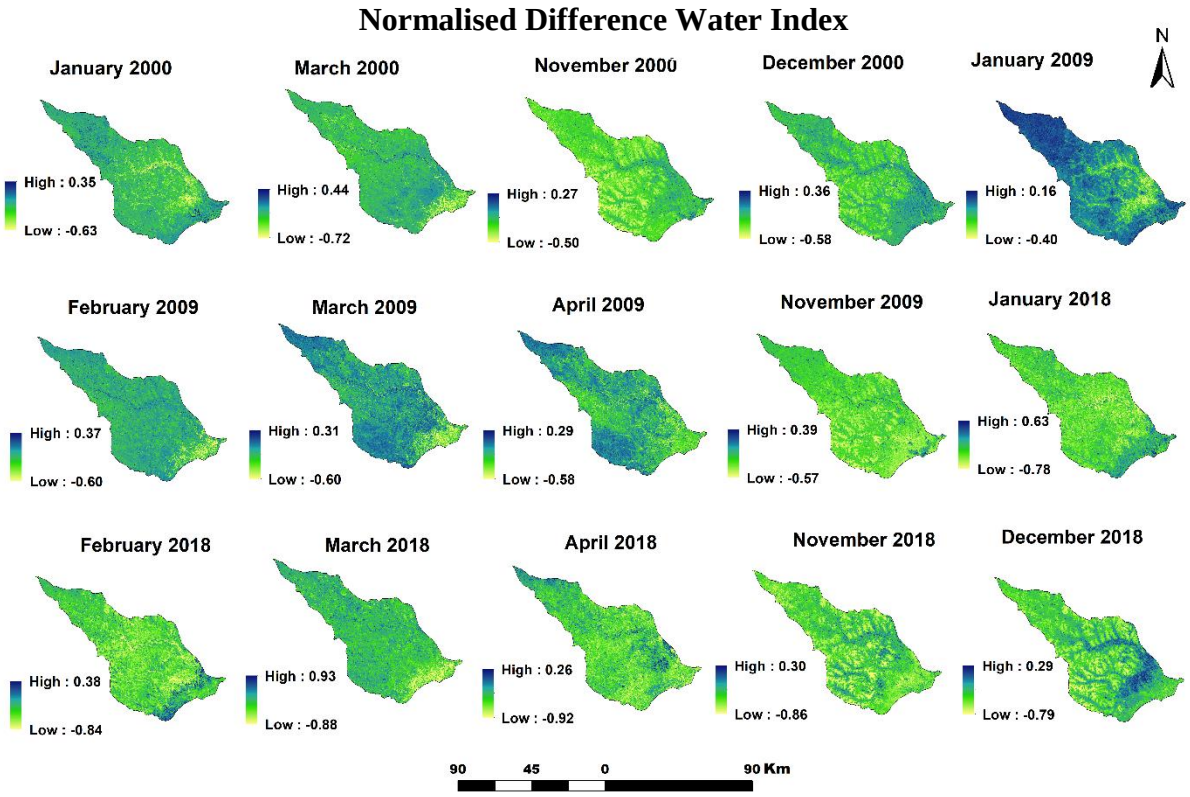

Fig. 4.11 Spatio-temporal distribution of NDWI

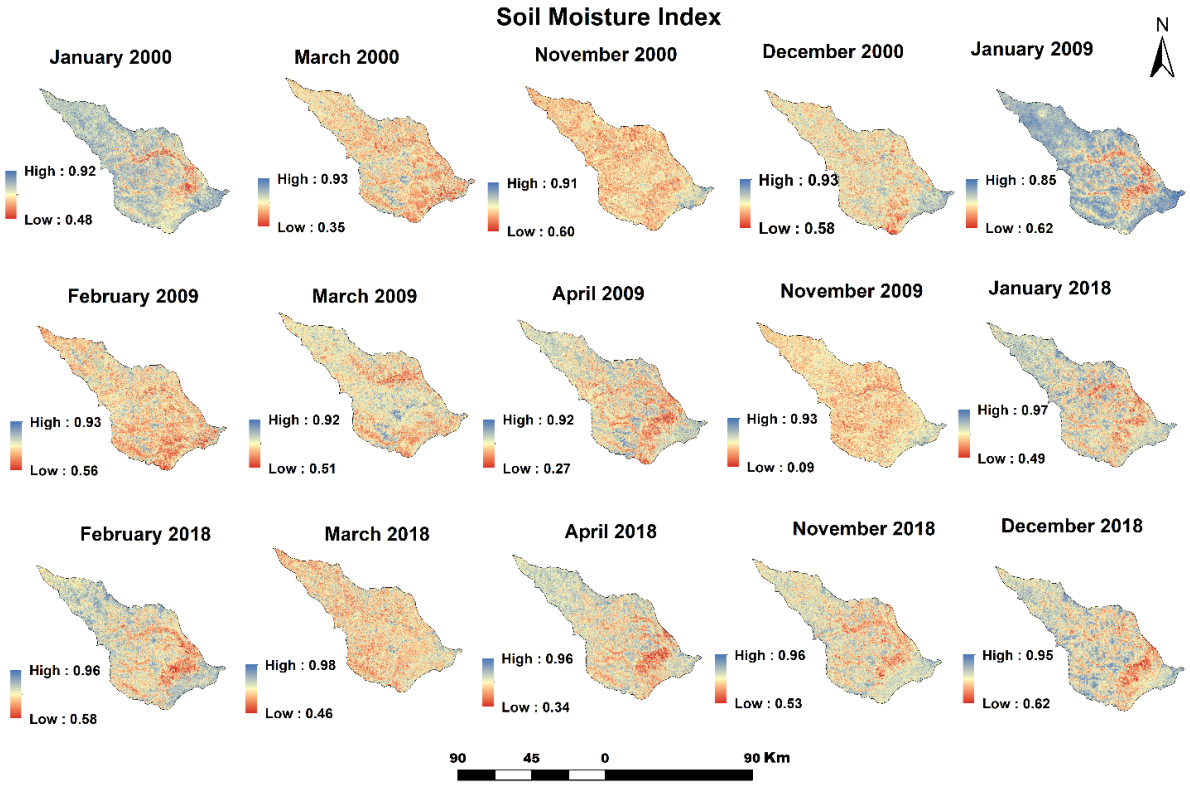

Fig. 4.12 Spatio-temporal distribution of SMI

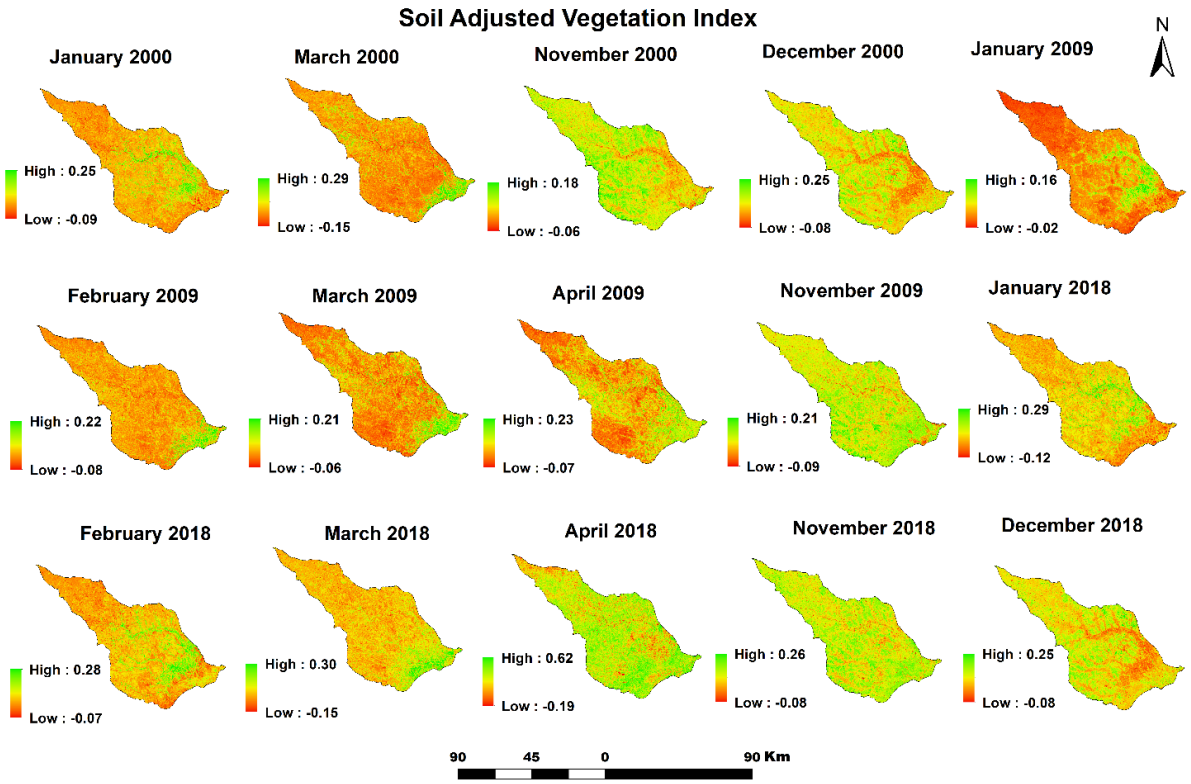

Fig. 4.13 Spatio-temporal distribution of SAVI

4.1.6.5 Identification of Drought risk prone zone using Fuzzy DAMETAL and causal diagram

Intensity, spatial coverage and duration of drought changes from one scenario to another. The zones affected by harsh drought condition and the region having the maximum vigour switch from season to season (Wilhite et al. 2014). Drought risk in any region is the combined outcome of the both region's susceptibility towards the event and its inescapable effect on the society. Parts of Puruliya, Bankura and the areas in the degraded plateau of West Bengal are reported to suffer from long drought duration and thereby require identification of risk zones (Ghosh, 2019). Forecasting drought is a critical phenomenon in the dry parts of West Bengal but the risk zones can be identified based on the previous recession and using remote sensing/GIS (Bhunia et al. 2020). The drought risk map in this study has been prepared applying the fuzzy DAMETAL calculated weights to seven long term meteorological, hydrological and vegetational parameters (Fig 4.14). A triangular fuzzy number has also been used to calculate the weights. The long term VHI scored the highest in predicting drought risk zone (0.169) followed by the long-term SPI (0.144) and long-term TCI (0.142) (Table 4.5). VHI is extensively used in the validation of severe agricultural drought parameters as it shows high correlation with drought scenarios and moisture content of the study area (Sandeep et al. 2021). The other parameters like long term NDWI, VCI, SMI, and SAVI has been ranked consecutively which promulgate far reaching caliber in identifying drought risk zones. All the estimated parameters have been reclassified in the ArcGIS spatial analyst tool. The final drought risk map has been divided into 5 classes (Fig 4.15). This study shows that very high- and high-risk zones contribute 34.7% to the area and are concentrated in the upper and middle sections of the basin, which fall under the western degraded plateau and

lateritic ravines known for drought proneness (WBPCB, 2009; Ghosh, 2019). The drought condition in this zone particularly in Puruliya and Bankura is strongly distressed by soil moisture paucity inducing soil erosion and poor agricultural opportunities (Santra et al. 2020). The moderate risk zone covers 25.7% of the basin. Low and very low risk zone contributes 40% of the basin and is mostly concentrated in the lower most section or at the mouth of the basin where agricultural production is highest. Akram et al. (2019) also found Keshpur, parts of Salboni block and lower most part of Medinapore block of West Medinapore district has more suitable area for paddy and potato production. A percentage-wise distribution of the drought risk zones in the three districts (Puruliya, Bankura, and West Medinapore) is shown in Table 4.6. The Puncha block of Puruliya covers 25.43% and 39.54% of the high and very high-risk zones, whereas Daspur and Ghatal block of West Medinapore district cover 80.65% and 77.33% of very low/no risks. This district (Daspur and Ghatal) has much higher crop intensity, but is at risk of floods, so water basin management plans are needed (Bera and Chatterjee 2019). Figure 4.16 illustrates a causal diagram by (D+R) on the horizontal axis and (D-R) on the vertical axis. Higher values of (D+R) indicate greater importance of the parameter in identifying drought risk zones. In the current study the most important three criteria are the long term VHI, SPI and TCI. The values of (D-R) divides the drought inducing parameters into a cause group and effect group. Long term SPI and TCI are having the positive value and are under the cause group whereas long term SAVI, NDWI, SMI, VCI and VHI are under the effect group. This scenario which is clearly depicted here is that the poor rainfall condition together with temperature rise is creating water scarcity over the basin that will ultimately bring distress to the vegetational growth and other related socio-economic activities. As of now, there is no study or approach that combines remote sensing indices and fuzzy DAMETAL to predict drought risk zones and validates these zones with agricultural data. A method to identify the drought risk zone in this data scarce river basin is also missing. The study concluded that meteorological, hydrological, and agricultural drought are frequently common in this basin, providing baseline information for adapting mitigation strategies to such a large geographic area.

4.1.6.6 Validation of drought prone zone using YAI and prioritization of CD blocks using Composite score method

Validation of the drought risk map should be done by either field survey or by using statistical techniques to verify the areas based on the level of risk persistent in the region (Dayal et al 2018). In the present study the final map has been validated using yield anomaly index (YAI) calculated using long term yield data (2000-2019) of the Boro crop. Table 4.7 shows the YAI for the period of 2000-2001, 2009-2010 and for the year 2018-2019 based on the data availability. As the work has been conducted based on the months with cloud-free satellite images from the end of the year to the beginning of the year, boro crops yields, which are shown in winter (November/December) and harvested in March/April (Tiwari et al 2001), were selected for validation. Most districts showed negative values in 2000-2001. Among the other blocks, Puncha has the highest negative value (-2.79). A similar trend can be observed in almost all blocks with negative values in 2009-2010. The negative value further deviates to -4.71 in Puncha block signifying poor agricultural production followed by Bishnupur block (-1.42). According to the final risk map, Puncha block covers the largest percentage (25.43%) of very high risk zones within the basin. YAI is highest in Ghatal (3.33) and Daspur I block of West Medinapore district in 2000-2001, demonstrating the accuracy of fuzzy DAMETAL model. Daspur I have the highest positive value of 0.179 in 2018-2019. CF model has also been used to prioritize blocks based on the extracted lower values of the long-

term drought indices, which indicate drought and poor moisture content (Dutta et al., 2015). According to Table 4.7, the lower values of the parameters were ranked with a score of 21 as the highest rank. With the CF value calculated using eq. 4.27, higher values will be prioritized for conservation. Simlapal (1), Garbeta I (2) Salboni (3), Garbeta II (4), Taldangra (5) Puncha (6) are the most stressed block where urgent attention is required or drought intervention strategies and preparedness measures (Fig 4.17). Daspur (21), Mindapore (20), Binpur (19) requires less attention in this respect and are producing quantifiable agricultural output to be meet the local demands (Bera and Chatterjee 2019). Disparity in precipitation trend and its pattern in the different blocks within the basin is quite evident leading to drinking water scarcity, poor agricultural production, and shortage of food, fodder, and thereby affecting employment opportunities (Raha and Gayen 2019). Almost all the blocks are suffering from low river regime and decline in groundwater level in the recent years (Sahoo et al. 2021). Not only the specified study area India as a whole contributes 50% of the area having under serve drought and climate change will further accelerate the scenario (Kamble et al. 2010; Ghosh, 2019).

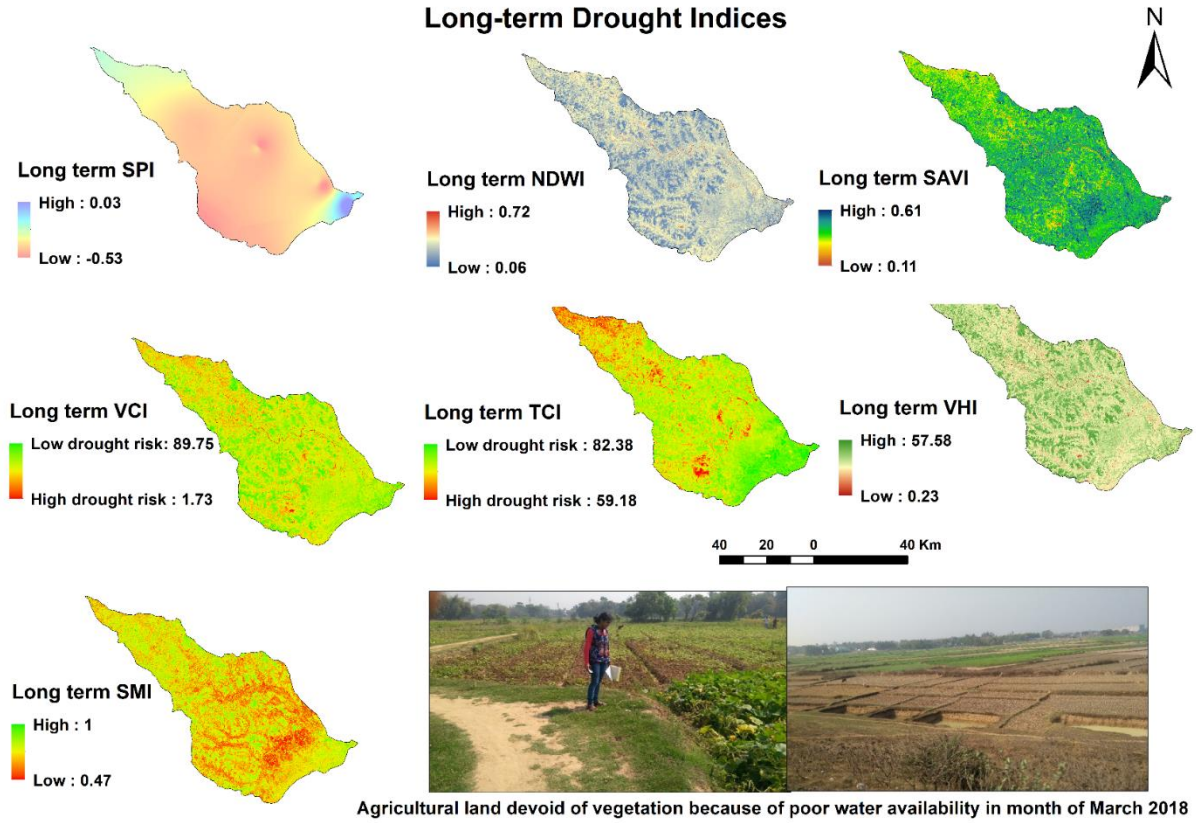

Fig. 4.14 Seven selected long-term drought indices

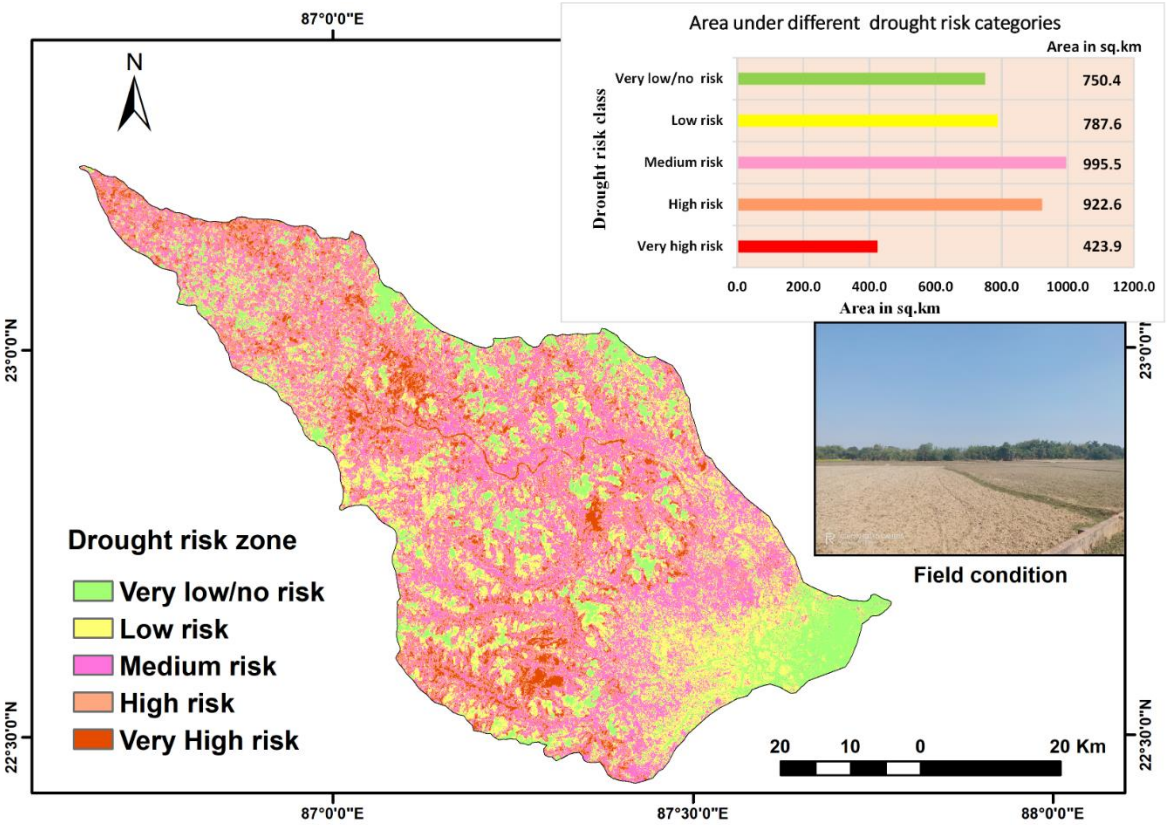

Fig. 4.15 Delineated drought risk zone map

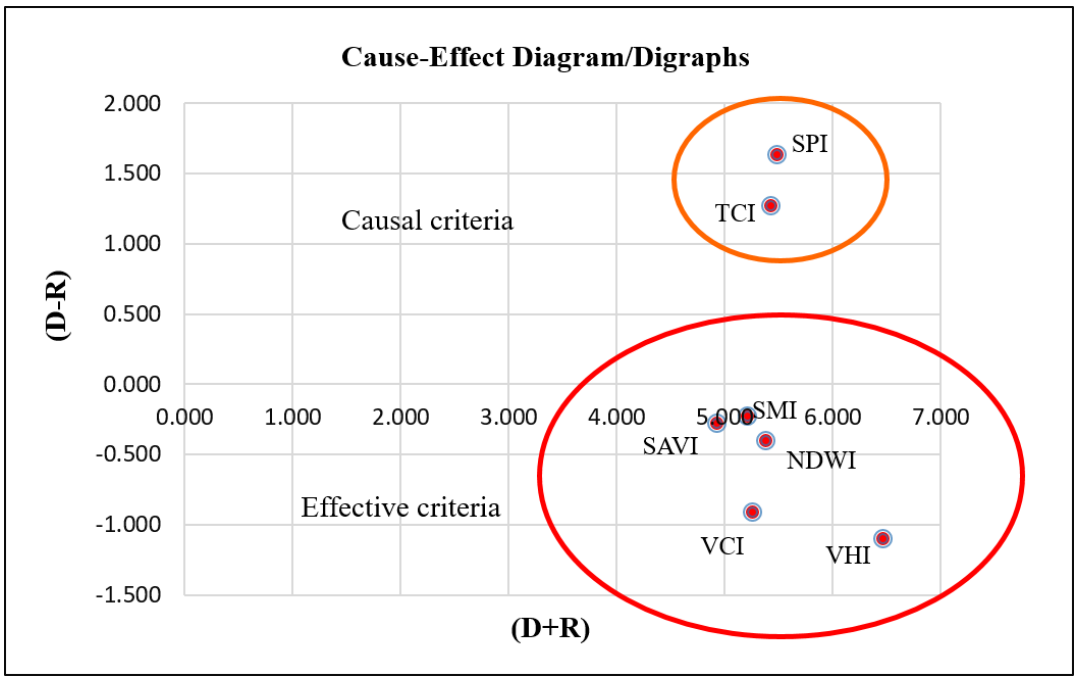

Fig. 4.16 Cause and effect relationship

Table 4.6 Percentage wise distribution of the drought risk zone in different blocks

Districts	Blocks	Total area in sq.km	Area in percentage				
			Very high risk	High risk	Medium risk	Low risk	Very Low/ /No risk
Puncha	Puncha	48.84	25.43	39.54	21.38	9.03	4.63
Bankura	Bishnupur	113.27	7.41	20.82	22.29	20.67	28.82
	Onda	52.27	10.20	28.41	24.18	17.93	19.28
	Indpur	241.89	16.88	30.24	25.74	15.26	11.87
	Khatra	102.94	13.33	31.68	22.04	17.83	15.13
	Hirabandh	108.53	6.43	23.09	25.94	20.64	23.90
	Simlapal	302.91	20.14	29.01	23.01	15.52	12.32
	Taldangra	336.88	13.03	28.48	24.19	15.75	18.54
	Jaypur	55.68	5.05	17.40	23.65	26.63	27.26
	Sarenga	32.15	5.72	17.54	22.12	26.10	28.52
West Medinapore	Mindapore	36.26	16.24	31.41	29.81	15.31	7.23
	Keshpur	416.49	2.92	11.74	31.58	36.21	17.55
	Chandrakona I	135.82	1.32	11.04	32.20	39.63	15.82
	Chandrakona II	171.32	4.78	20.18	36.29	28.69	10.05
	Daspur I	51.44	0.12	0.19	1.96	17.07	80.66
	Ghatal	135.15	0.04	0.84	3.60	17.99	77.54
	Garbeta I	308.60	12.31	15.81	35.91	19.27	16.70
	Garbeta II	312.46	13.36	28.10	26.56	16.15	15.83
	Garbeta III	384.84	8.05	23.22	29.26	19.65	19.82
	Binpur I	10.02	16.67	29.34	20.26	12.18	21.56
	Salboni	471.74	20.13	29.00	21.16	14.79	14.91

Table 4.7 Yield anomaly index

Districts	Blocks	2000-2001	2009-2010	2018-2019
Puruliya	Puncha	-2.79	-3.11	-4.71
Bankura	Bishnupur	0.32	-1.75	-1.42
	Onda	-1.42	-1.58	-0.51
	Indpur	0.38	-0.79	0.35
	Khatra	-0.05	-0.19	-0.10
	Hirabandh	1.09	-0.03	-0.89
	Simlapal	-0.37	-0.91	-0.35
	Taldangra	-0.40	-0.47	-0.93
	Jaypur	0.31	-0.92	0.60
	Sarenga	0.21	-0.85	0.21
West Medinapore	Mindapore	-0.80	-1.62	-0.09
	Keshpur	-0.90	-1.67	-0.08
	Chandrakona I	0.11	-0.23	0.07
	Chandrakona II	0.22	-0.14	-0.89
	Daspur I	3.00	-0.08	0.18
	Ghatal	3.43	-0.07	0.09
	Garbeta I	0.90	0.29	0.44
	Garbheta II	-0.96	-1.00	-0.59
	Garbeta III	-0.59	-1.36	0.10
	Binpur I	-0.13	-0.85	0.82
	Salboni	-1.55	-1.38	-0.81

Table 4.8 Calculated compound factor for block prioritization using long term drought indices

Districts	Blocks	VCI	Rank	TCI	Rank	VHI	Rank	SPI	Rank	NDWI	Rank	SMI	Rank	SAVI	Rank	Sum	Compound parameter	Final Priority
Puruliya	Puncha	33.05	20	62.26	17	0.12	16	-0.30	1	0.08	11	0.59	12	0.17	16	93.00	13.29	6
Bankura	Bishnupur	39.41	11	64.09	10	0.14	10	-0.44	8	0.08	12	0.57	14	0.20	13	78.00	11.14	13
	Onda	36.60	14	62.46	16	0.13	11	-0.43	6	0.08	10	0.60	9	0.14	19	85.00	12.14	10
	Indpur	33.62	18	59.85	20	0.13	13	-0.39	3	0.08	18	0.59	10	0.21	9	91.00	13.00	7
	Khatra	40.89	10	63.13	12	0.16	7	-0.42	5	0.07	20	0.62	8	0.22	6	68.00	9.71	15
	Hirabandh	34.85	17	63.08	13	0.11	19	-0.37	2	0.06	21	0.64	5	0.20	12	89.00	12.71	8
	Simlapal	30.30	21	59.92	19	0.02	21	-0.45	11	0.08	16	0.57	15	0.11	21	124.00	17.71	1
	Taldangra	38.68	12	62.13	18	0.12	15	-0.45	9	0.08	14	0.55	16	0.21	10	94.00	13.43	5
	Jaypur	36.24	15	64.87	8	0.13	12	-0.44	7	0.09	5	0.63	7	0.16	17	71.00	10.14	14
	Sarenga	37.11	13	66.43	6	0.11	18	-0.45	10	0.09	8	0.58	13	0.19	15	83.00	11.86	11
West Medinapore	Mindapore	46.02	4	68.46	3	0.20	2	-0.47	16	0.10	1	0.66	3	0.24	3	32.00	4.57	20
	Keshpur	43.04	6	65.67	7	0.17	6	-0.46	13	0.09	7	0.52	18	0.21	8	65.00	9.29	16
	Chandrakona I	45.69	5	69.76	2	0.20	4	-0.51	18	0.09	4	0.64	6	0.23	5	44.00	6.29	18
	Chandrakona II	42.09	7	62.53	14	0.12	17	-0.48	17	0.10	2	0.59	11	0.19	14	82.00	11.71	12
	Daspur I	51.98	1	73.15	1	0.24	1	-0.39	4	0.08	9	0.68	2	0.27	1	19.00	2.71	21
	Ghatal	46.14	3	67.97	4	0.19	5	-0.46	12	0.08	17	0.70	1	0.24	4	46.00	6.57	17
	Garbeta I	33.47	19	63.61	11	0.07	20	-0.53	21	0.09	6	0.54	17	0.12	20	114.00	16.29	2
	Garbeta II	36.20	16	64.09	9	0.12	14	-0.47	15	0.08	15	0.50	19	0.16	18	106.00	15.14	4
	Garbheta III	41.35	9	62.48	15	0.16	8	-0.46	14	0.08	13	0.47	21	0.21	7	87.00	12.43	9
	Binpur I	47.65	2	67.17	5	0.20	3	-0.51	19	0.09	3	0.64	4	0.24	2	38.00	5.43	19
	Salboni	41.53	8	59.18	21	0.16	9	-0.52	20	0.08	19	0.49	20	0.20	11	108.00	15.43	3

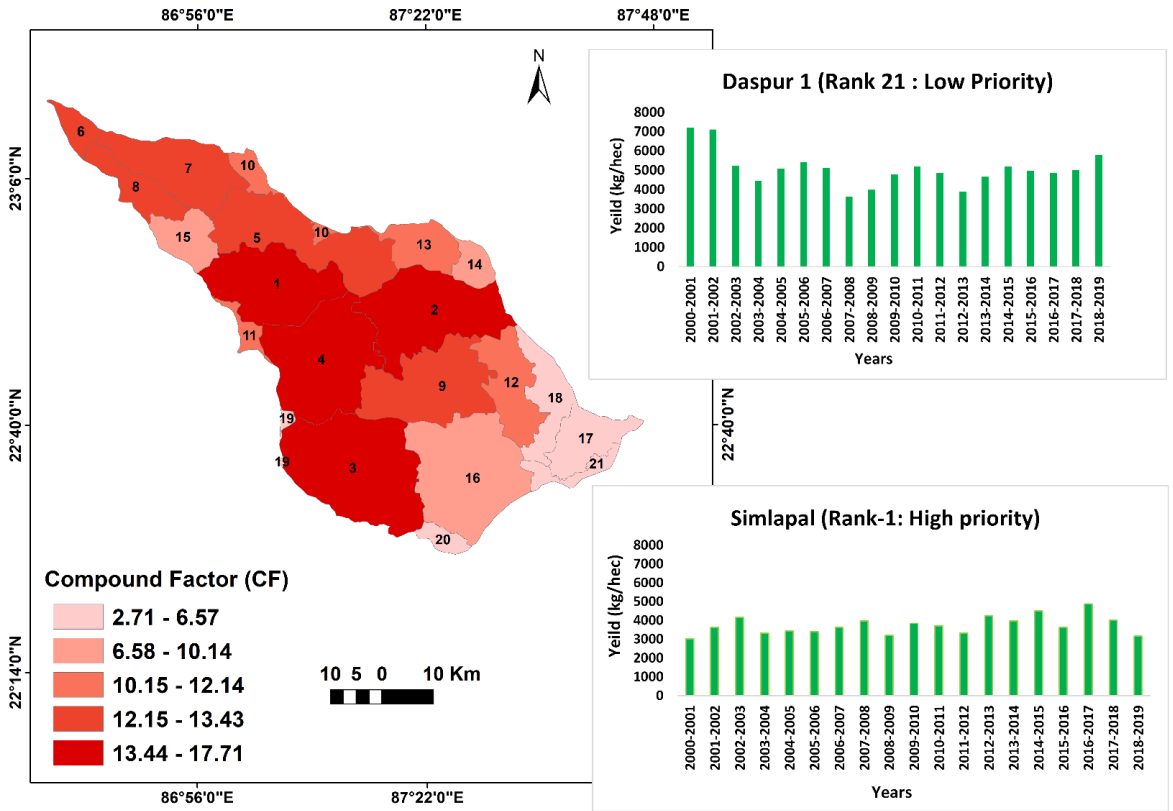

Fig. 4.17 Calculated compound factor for block prioritization using long term drought indices

4.1.6.7 Association of drought prone zone and cropping pattern practiced

Figure 4.18 shows that in the upstream and the middle section of the basin, single and double cropping is mostly practiced. The farmers in this section of the basin practice rice cultivation mainly in the Kharif season depending on the rainfall only (Roy and Jana 2019). From the field survey it has been reported by the local inhabitants about water scarcity and crop failure. They are forced to do single or double cropping in the wet months because of a lack of irrigation facilities and pre- and post-drought conditions. A large portion of the area under the basin remains uncropped and uncultivated during the dry months and summer seasons subjected to soil erosion (Halder et al. 2021). The downstream section is primarily cropped with Aman rice, potatoes, and sesame, primarily in the blocks of West Medinapore (CIP progress report, 1997-1998; Rajwade and colleagues, 2015). Therefore, the analysed technique can be used to demarcate vulnerable zones to aid fanatical planning for coping with future drought incidents.

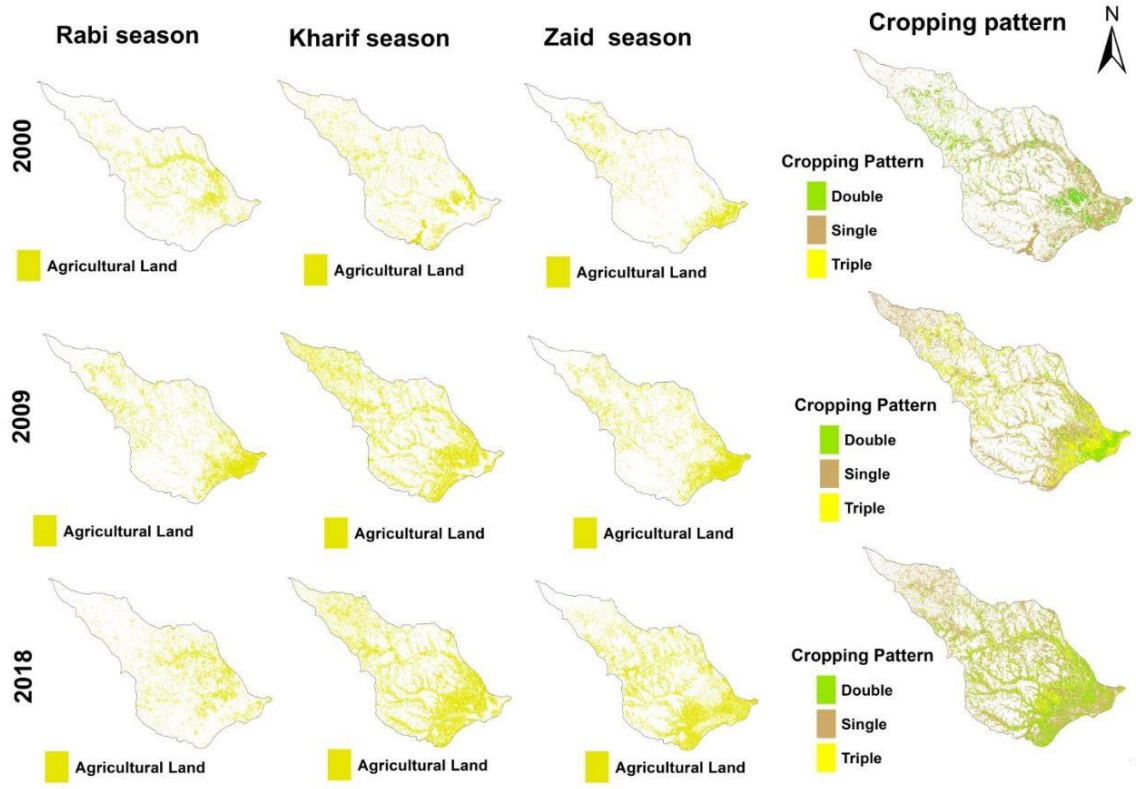

Fig. 4.18 Cropping pattern practiced within the study area

4.1.7 Discussion

Drought is a contemptuous natural phenomenon and the result of the rainfall deficit where substantial impact can be observed in hydrology and vegetation (Ghosh 2019). A complete drought management plan should consist of two important aspect one is contemplative factors like duration, intensity, severity, magnitude etc. and another is eventual planning which includes risk assessment. As a primordial step towards sustainable solutions, the present research not only aimed to identify the risk zone using drought indices, but also to critically assess the overall conditions in each distinct area of the basin. Most of the studies critically assessed the spatio-temporal trends of the precipitation and temperature impacts only (Schilling et al. 2020) which are regarded as the most relevant parameter for pragmatic simulations (Hao et al. 2018); Raha and Gayen, 2020). Drought are sometimes analysed using simple one dimension to critical earth models of global and regional origin having lowbred spatial resolution, limit in understanding micro and meso scale drought progression (Saharwardi et al. 2021). Beside the rainfall and temperature parameters an extensive range of significant criteria for drought risk mapping like NDWI, NDVI, VCI, TCI, VHI, SAVI, SMI, YAI has been taken into consideration to accomplish the study. Decision making system is the main light of focus in this study which is complex and enigmatic and requires multiple criteria to decode a real-world situation (Arabameri et al. 2018). This study introduces a new approach by applying fuzzy DAMETAL technique to identify drought-prone zones by analyzing long term trends or the influence of each of the seven criteria discussed above. This method is most commonly used in computer science, mathematics, and industrial studies, but it is effective in resolving inbred phonological ambiguity with hydrological and meteorological factors (Sathyan et al. 2020). No studies have been conducted using this integrated fuzzy-GIS

approach incorporating the long-term indices in drought studies both at a national or international scale and the indices selected here have advantage than conventional datasets which can cover large areas and data scare basins (Alahacoon et al. 2021). The framework of the study will therefore be able to identify drought risk zones validated by the use of agricultural production, which will highlight this neglected basin in government policies and drought preparedness efforts. It is estimated that 75% of the region receives monsoonal rainfall within less than 100 hours, which results in drought in the upstream section as water rolls back downstream due to steep slopes and fragile soils, causing high flows in lower reaches (Bhunia et al. 2020). And if this continues water balance scenario within the whole watershed will get disturbed (Kar et al. 2012). Most of the studies in the basin are conducted using SPI only. Ghosh, (2019) found that the drought duration over the region increased after 1950s by applying SPI trends and is district specific. Bhunia et al. (2020) found negative SPI values are frequent in the districts of Puruliya, Bankura and West Medinapore which requires an intensive study on hydrological drought before executing any plan of action. Thus, the study aimed at the integration of the satellite-based weather and ecological condition to portray drought patterns spatially and temporally (Jain et al. 2009).

The seven long-term parameters assessed in this study are effective in determining vulnerability and can be applied to any terrain condition around the world since they are the consolidation of remote sensing and GIS, making it time consuming and cost-effective in the current pandemic situation. By using these indices vulnerability level of different sites can be evaluated and compared but sometimes the local environment may affect the frame and design (Panthi et al. 2016). The validation technique is also well justified and proves the accuracy of the model portraying the actual scenario of the river basin. The present results of the study are also authenticated with the previous studies conducted by murthy et al. (2015), Dayal et al. (2018), Thao et al. (2019) and Wang et al. (2020).

4.1.8 Conclusion and Recommendations

Indian water demand is expected to increase by 32% by 2050, reaching 1450 km^3 a year (Ghosh, 2019). In Puruliya, Bankura and West Medinapore, intermittent drought is highly prevalent, and residents have become accustomed to it as part of their lives (DRCSC, 2017). In light of this scenario, it is essential to identify the drought risk zone within the Shilabati river basin comprising the above districts for drought preparedness. To effectively manage drought, water resources need to be allocated based on a risk assessment plan, otherwise it may ruin agricultural production in the river basin. Using fuzzy DAMETAL, the current study combines earth observation data with ancillary data to predict drought risk zones. Using long term trends of VCI, TCI, VHI, NDWI, SPI, SMI, and SAVI for the fuzzy DAMETAL model, three years of rainfall deficit from the normal have been selected. There has been an increase in the negative SPI values in the past few years, which can be considered a primary indicator of drought. The 1st three factors instigating the model to predict drought hotspot zone are VHI (0.169), SPI (0.144) and TCI (0.142). Water scarce and poorly vegetated sites are explained by the complex interplay of these three factors. An explanatory causal diagram has been drawn between the cause group (SPI, TCI) and effect group (SMI, SAVI, NDWI, VCI and VHI). Using the model assumptions, the risks were divided into five groups: very high risk (10.9%), high risk (23.8%), medium risk (25.7%), low risk (20.3%) and very low/no risk (19.3%). There is a serious risk of drought in the upstream and middle sections of the basin, and it is most noticeable in March and April. In April 2000, SPI reached -1.60, indicating drought. There are low/negative values or drought

conditions in all sections of the basin where surface water bodies have dried up and groundwater drought has been observed (Halder et al. 2020). The upstream section has a slope of 5.6 degrees to 20 degrees with mostly bare land, resulting in poor moisture conditions and low groundwater recharge (Halder et al., 2020). Meanwhile, the downstream section has saturated alluvial deposits that favour vegetable growth. The predicted map is validated with YAI values as calculated from Boro crop yield. In the upstream section of the basin, Puncha block has highly negative YAI values for 2000-2001 (-2.69), 2009-2010 (-3.11), and 2018-2019 (-4.71). A block-wise distribution of the final risk zone also showed Puncha (25.43%), Simlapal (20.14%), Salboni (20.13%), and Indpur (16.88%) having most of the high-risk zones upstream and middle. Thus, the risk zones for each block have been prioritized using seven long-term indices, where Simlapal (1) Garbeta I (2) Garbeta II (3) Taldangra (4), Puncha (6) and others are ranked according to their highest priority. ICAR-ATAR, 2018-2019 reported, that these areas suffer from poor rainfall, elevated temperatures, coarse soil and poor water retention capacity, and less vegetable growth. The reflectance of the drought is also witnessed in the cropping pattern of the basin. An increase in dry spell and a decrease of wet spell can lead to a water crisis within 6-12 hours of moderate intensity. Therefore, sustainable strategies include rainwater harvesting, constructing check dams, planting drought-resistant crops, controlling runoff, and limiting grazing.

4.1.9 Limitation and Future Work

An interesting and unique approach is presented in this study by using spatio-temporal indices to simulate drought risk zone in Shilabati basin. Methodology is interesting and valuable, time-consuming, easy to use, cost-effective, and has high computing demands. Hydro-meteorologists should adapt the methodology to conduct reconnaissance surveys in these sites for drought management. Drought mitigation plan includes predictability, monitoring, impact assessment, and response, which are clearly framed in this study and can serve as a preparatory deliberation for stakeholders and policy makers. However, there are few limitations of the study which includes the availability of the cloud free high-resolution images, unavailability of the detailed reports and statistics of the agricultural output and yield data at the village and block level. Thus, the future studies aim at the inclusion of the various others field based conditioning factors into the model and field-based validation.

4.2 Analysis of Groundwater Level Trend and Groundwater Drought using Standard Groundwater Level Index

Variability of precipitation, temperature and evapotranspiration as predicted from various climate change scenarios will affect the aquifers which depend on physical properties of recharge areas (Green, 2016). Recharge in the arid and semi-arid regions sometimes changes due to the minimal changes in the precipitation volume (Green, 2016).The rise in mean global temperature will have a 30% decrease in groundwater recharge for 4% of the land area and 70% of the decrease in recharge in 1% of the land area globally (Portmann et al. 2013).Thus, vivid understanding of the impacts of climate change on global hydrological cycle including groundwater should be clear to undertake adaptation strategies (Engelenburg et al. 2017).This scenario of groundwater shortage can be termed as groundwater drought. The groundwater drought has an adverse effect on public, agricultural and industrial water supply as well as on groundwater dependent ecosystem and water bodies (Bloomfiled et al. 2013) According to Zekter and Everett (2004) about 50% of the domestic water, 40% of the industrial supply and 20%

of the irrigation supply is mainly sourced from groundwater. Thus, with an increase in the population density, the groundwater recharge as well as level will decrease more in shallow aquifer (Doll, 2009). Since the 20th century, the groundwater extraction explosively increased around the world. According to a database of 2010, the groundwater extraction is about 1000 km^3/ year and the major consumers are from Asia including India, China, Pakistan, Bangladesh and extraction rate has been tripled over the 50 years and still rising (Gun, 2012). Major parts of the Indian aquifer system are showing a declining trend due to alteration in the pattern of precipitation. The emergence of the modern pumping system and electrification in rural areas has led to the increase in groundwater extraction from 312 km^3/ year in 1960s to about 743km^3/ year in 2000 (Wada et al. 2010). Sustainable management of the groundwater resources is now challenging and complex in the areas of climate change and extensive anthropogenic activities, thus modern tool and decisions are needed to sustain long term groundwater extraction strategies (Carmona et al. 2013). Engelenburg et al. (2017) applied hydrological modelling to study the projected impact of climate in Veluure aquifer of Netherland to observe the effect of extensive groundwater extraction on groundwater dependent ecosystem nearby. Salem et al. (2018) studied the impact of climate change in irrigation cost for a groundwater dependent region of North West Bangladesh by using general circulation model and hydrological model based on support vector machine to simulate the groundwater level from meteorological variables. Before the simulation of groundwater level, analysis of present and future trend through evaluation of past data are needed. Sishodia et al. (2016) analyzed groundwater trend of 23 wells of a crystalline aquifer in semi-arid South India to observe whether the trends are due to physical or non-physical factors. Tiwari el at. (2011) employed GRACE satellite data and groundwater level to observe the groundwater storage in Andhra Pradesh and found an overall increase which may be due to inter annual variability of rainfall. Kumar and Rathnam (2019) applied four variation of Mann Kendal and Auto Regressive Integrated Moving Average (ARIMA) for prediction and trend analysis of forty observational wells of Warangal district and found three well showing positive trend and another 37 wells showing a negative trend. Positive trends in the groundwater level is a serious concern and needs supervision at an early stage. A positive trend means a decrease in groundwater level below surface level and such can be due to poor recharge because of changes in land use and land cover of a particular region. Rapid urbanization and increase in built up areas increase the fluctuation of groundwater level due to environmental degradation and concretion of soil surface. Patra et al. (2018) applied Normalised Built-up Index and estimated the land use and land cover change to identify the effects of extensive urban sprawl on groundwater recharge. Based on the trend analysis groundwater level and recharge pattern of wells can be grouped into numerous clusters to manage them specifically. Pathak and Dodamani (2019) applied hierarchical clustering method to group the fluctuation level of the wells in the Ghataprabha river basin of India and found that the cluster 1 and cluster 3 wells have high fluctuation due to groundwater drought. Ganapuram et al. (2016) conducted a study to identify spatio-temporal groundwater drought and drought prone regions using Standard Water Level Index and spline interpolation in geographical information system. Bloomfield et al. (2018) studied groundwater drought in the chalk aquifer of United Kingdom and found evapotranspiration associated with anthropogenic activities are the prime reason inducing the changing nature of drought. But till date studies related to groundwater drought are fewer in number, but this situation needs a strategic long-term action plan.

4.2.1 Research Gap and Novelty of Work

In India, according to Central Ground Water Board (CGWB) report of 2017- 2018 the overall stage of groundwater extraction increased from 62% to 63%. The over exploited region of India are parts of Punjab, Haryana and Delhi where indiscriminate withdrawal has been observed. According to CGWB, the annual replenishable groundwater resources was 432 Billion Cubic Meters (BCM), Net annual groundwater availability is also 393 BCM and annual groundwater draft is about 249 BCM. According to the report, 60% of the wells in India witnessed a declining trend in water level. Recent drying up of the water bodies due to an increase in the magnitude of the temperature graph in the parts of West Bengal, India, particularly in the districts of Bankura, Puruliya and West Medinapore led to the decline of water level in wells. Agricultural practice here solely depends on the extraction of groundwater through submersible pumping sets from shallow aquifer system leading to further decline in the water level. Land use and land cover change have also put a significant effect on the recharge pattern over the regions. After effects of the South West Monsoon shows poor recharge and slow increase in the post monsoon water level due to poor precipitation consistency. No comprehensive scientific assessment of groundwater wells has been done over the selected river basin under study.

4.2.2 Objectives of the Research Work

Thus the Objective of the study includes (i) to analyse the groundwater level variability through seasonal (Pre-monsoon, Monsoon and Post-monsoon) trend analysis using non parametric statistical method of Mann Kendall test for 20 wells within the study area (ii) to understand the impact of land use and land cover change of each of the well location to visualize the controlling factor for groundwater recharge (ii) application of Agglomerated Hierarchical Cluster analysis (HCA) to group the wells based on fluctuation scenario and lastly (iv) to understand the impact of climatological variability on water level or groundwater drought by using the Standard Groundwater Level Index for three seasons from 1996-2018. Such studies will incur valuable information and will give a reflection of the groundwater scenario of the basin to the stakeholders and policy makers for sustainable water resources management.

4.2.3 Area of Investigation

The Shilabati river basin is an important eastern river basin of West Bengal, India, which originates from Chotonagpur Plateau in Puruliya district of West Bengal and flows in a south easterly direction through the districts of Bankura, West Medinapore and joins Rupnarayan River at Ghatal block of West Medinapore, West Bengal, India. The river is positioned between 23^{o}32'N to 23^{o}14' latitude and 86^{o}40'E to 87^{o}46'E longitude (Fig.4.19). The elevation of the basin varies from 212 to 4 Mean Sea Level (MSL). The total catchment area is about 3,881 km^2. The river is divided into eight sub-basins namely Tamal, Kubai, Joy Panda, Parang, Purandar, Silai and Betal. The study area falls under semi-arid to humid climatic condition and receives an average monthly rainfall of 107 mm which is mainly concentrated in the monsoon season. The main land use and land cover of the region is agriculture and irrigation which are mainly practised using groundwater where extraction occurs through the shallow submersible pumping set. The study area covers three different terrain condition that is hard rock at the upper section, lateritic in the middle and the lower section is alluvial in origin. Here water bodies dry up every year mainly in the summer season during which people depend on the groundwater for various activities and

worsens the situation (Das et al. 2019) which makes it inevitable to evaluate the groundwater resource available within the region.

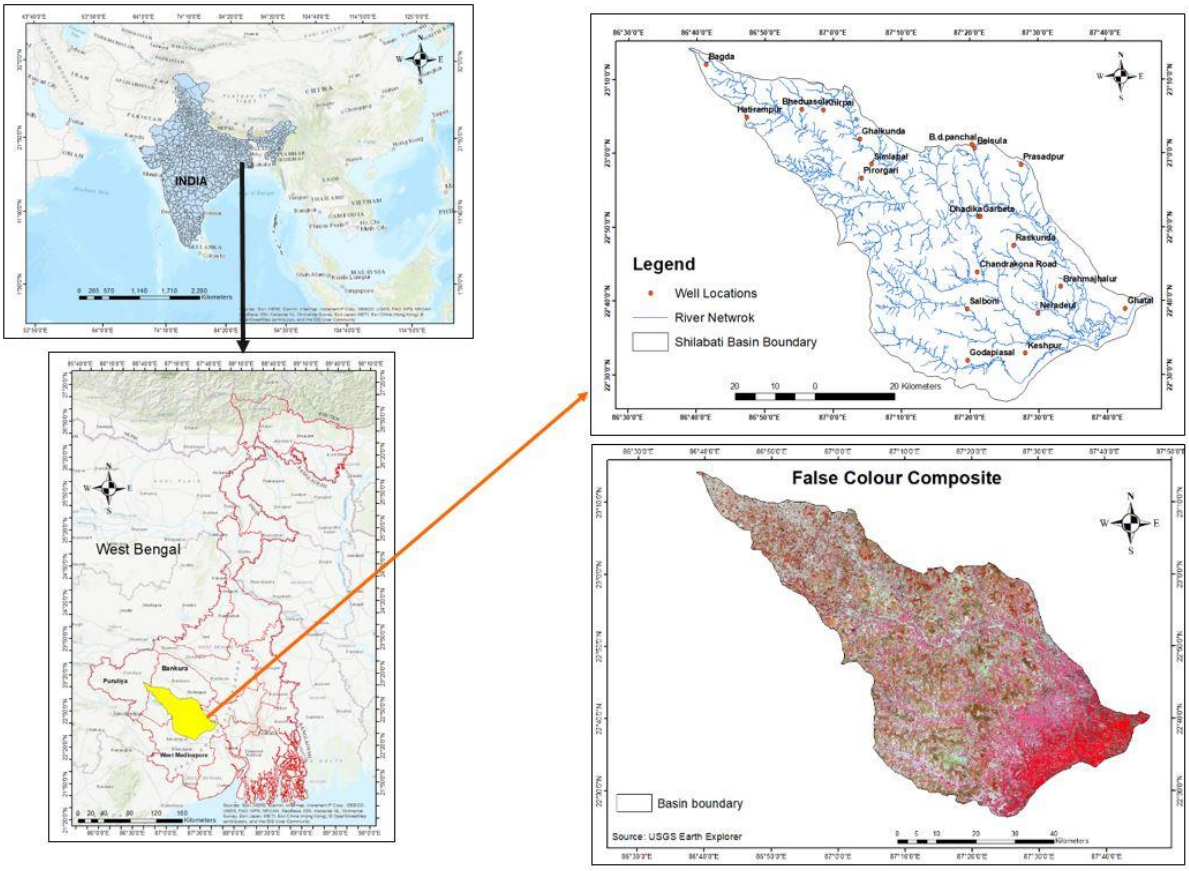

Fig. 4.19 Location of the study area

4.2.4 Research Design and Methodology

4.2.4.1 Date source

In order to fabricate the groundwater resource assessment groundwater level data of 20 monitoring wells (Fig.4.19) has been downloaded from Central Groundwater Board, Government of India for the period of 22 years (1996-2018) of three different seasons that is pre-monsoon, monsoon and post-monsoon. Gridded monthly rainfall data of TRMM 3B43 (0.25 degree * 0.25 degrees) have been downloaded for the GESDISC website (https://disc.gsfc.nasa.gov/) for the year 1998-2018. Land use and land cover classification maps have been prepared using Landsat images for four different years that is 1989, 2000, 2009 and 2018. The satellite images have been downloaded from UGSC Earth Explorer (https://earthexplorer.usgs.gov/) for path of 139 and row of 44 (Table 4.9). The locational description based on physical features (Fig. 4.20, 4.21, 4.23,4.24,4.25,4.26) of each of the 20 wells has also been made given in a tabular format (Table 4.10). In order to identify the agricultural cropping pattern prevalent in the study area, satellite image of three months leading to the cultivation of Rabi (January) Kharif (October) and Zaid (March) has been downloaded from USGS website. False Colour Composite of year 1989, 2000, 2009 and 2018 has been prepared and agricultural land has been extracted for the three different time period to understand the cropping pattern (Rabi, Kharif and Zaid. The extracted vector of the three images is superimposed to witness the cropping pattern (Fig 4.26).

Table 4.9 Information of data acquired

Date of acquisition	Path and row	Satellite
23.03.1989	139/44	Landsat 5
29.03.2000	139/44	Landsat 7
30.03.2009	139/44	Landsat 5
20.03.2018	139/44	Landsat 8 OLI

Table 4.10 Locational description of wells

Parameters	Soil	Geology	Geomorphology	Slope in degrees	Elevation in meters	Aquifer Depth in mbgl	Cropping pattern
Source Wells location	NBSSLUP	GSI	Prepared by author based on different source	SRTM DEM 30m resolution	SRTM DEM 30m resolution	SWID	Prepared by author using RS/ GIS
Badga	Gravelly loam	Granite Gneiss	Denudational pediment-Pedi plain complex	0.14	177	20	Non-cropped area
Chandrakona road	Fine loamy	Laterite	Valley fill deposits	1.41	44	30	Single cropping
Brahmajhalur	Fine sand	Sand, silt, clay, calcareous concretions	Fluvial origin older flood plain	0.76	20	40-50	Double cropping
Dhadika	Fine loamy to sandy	Laterite	Buried pediment shallow	3.62	47	30	Non-cropped area
Salboni	Fine-fine loamy	Yellowish brown fine sand, silt, clay	Fluvial origin older flood plain	1.36	27	30	Single cropping
Godapaisal	Fine loamy	Sand, silt and clay, calcareous concretions	Valley fill deposits	2.60	34	30	Single cropping
Keshpur	Fine sand	Sand, silt, clay, calcareous concretions	Fluvial origin older flood plain	1.08	17	40-50	Double cropping
Neradeul	Fine sand	Laterite	Fluvial origin older flood plain	0.97	16	40-50	Non-cropped area

Raskhunda	Fine loamy	Laterite	Buried pediment shallow	0.3	49	30	Single cropping
Belsula	Fine loamy	Laterite	Buried pediment moderate with laterite capping	2.16	66	45-80	Single cropping
B.D. Panchal	Fine loamy	Laterite	Buried pediment moderate with laterite capping	0.34	63	45-80	Double cropping
Pirorgari	Fine loamy to sandy	Laterite	Buried pediment shallow with laterite capping	1.23	84	45-80	Non-cropped area
Prasadpur	Fine loamy to sandy	Laterite	Buried pediment shallow	1.02	49	30	Double cropping
Simlapal	Fine loamy to sandy	Laterite	Buried pediment moderate with laterite capping	2.91	68	45-80	Single cropping
Khirpai	Fine loamy	Granite genies	Buried pediment shallow with laterite capping	2.07	115	5-15	Single cropping
Hatirampur	Fine sand	Mica schist with Hornblende schist	Denudation pediment-Pedi plain complex	1.02	164	5-15	Double cropping
Bheduasol	Fine sand	Granitic gneiss	Buried pediment shallow with laterite capping	2.41	116	5-15	Single cropping
Ghalkunda	Fine loamy	Sand, silt, clay, calcareous concretions	Buried pediment moderate with laterite capping	3.05	84	45-80	Single cropping
Garbeta	Fine loamy to sandy	Laterite	Valley fill deposits	1.36	39	30	Single cropping
Ghatal	Fine to fine loamy	Sand, silt & gravel	Fluvial origin active flood plain	0.1	8	40-50	Single cropping

** NBSSLUP: The National Bureau of Soil Survey and Land Use planning, GSI: Geological Survey of India, SWID: State Water Resources Investigation Directorate, SRTM: Shuttle Radar Topography Mission

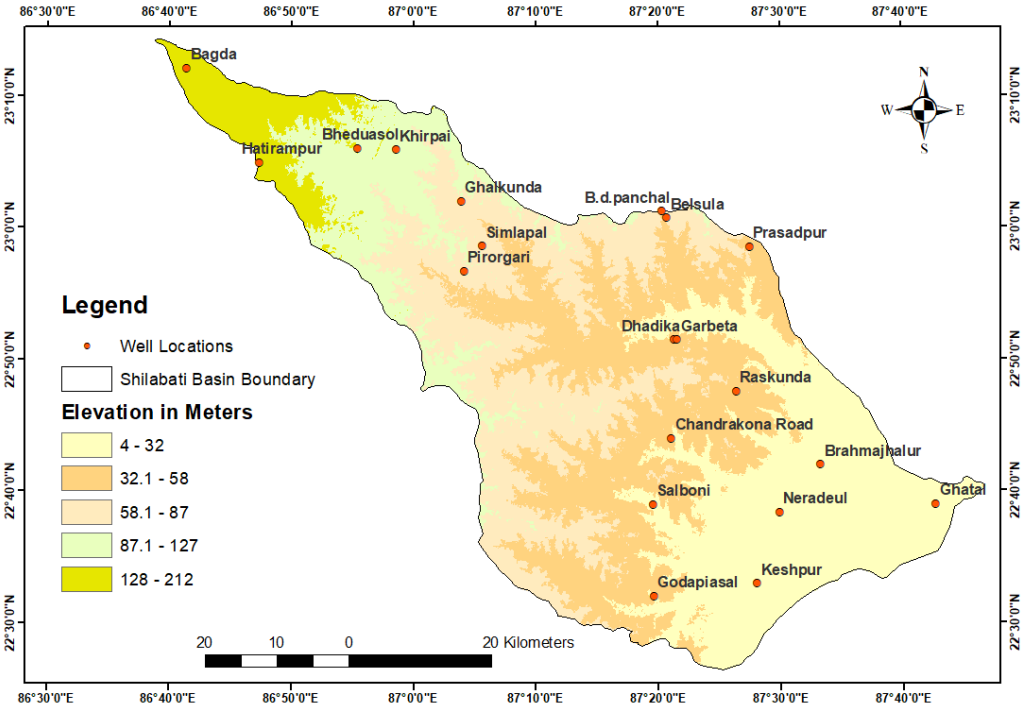

Fig. 4.20 Digital Elevation Model

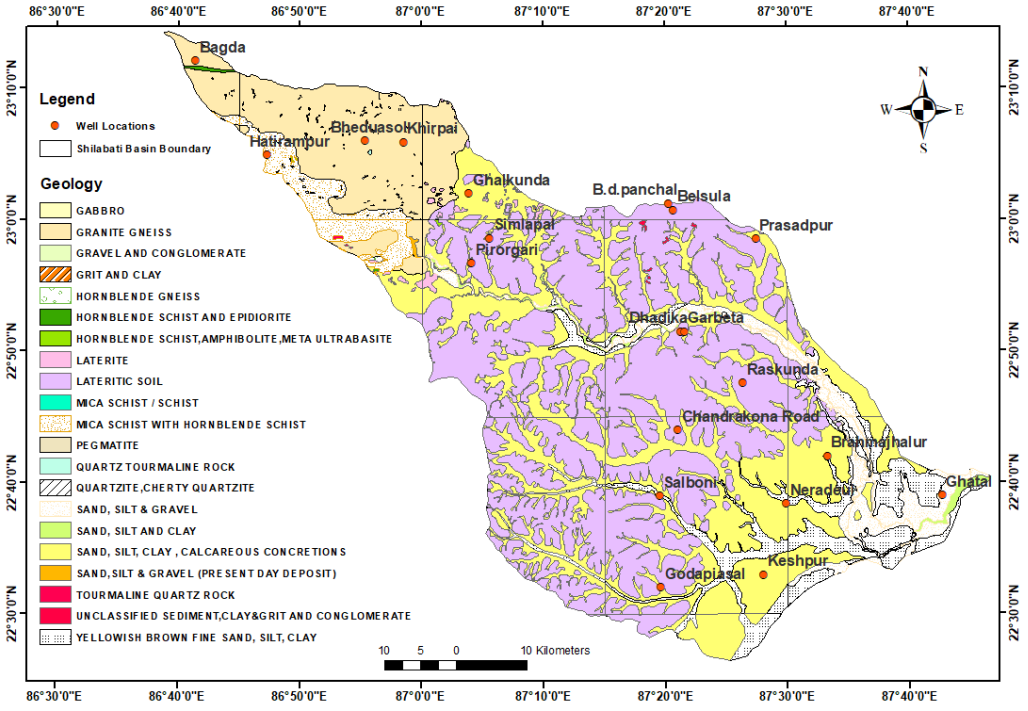

Fig. 4.21 Geology of the study area

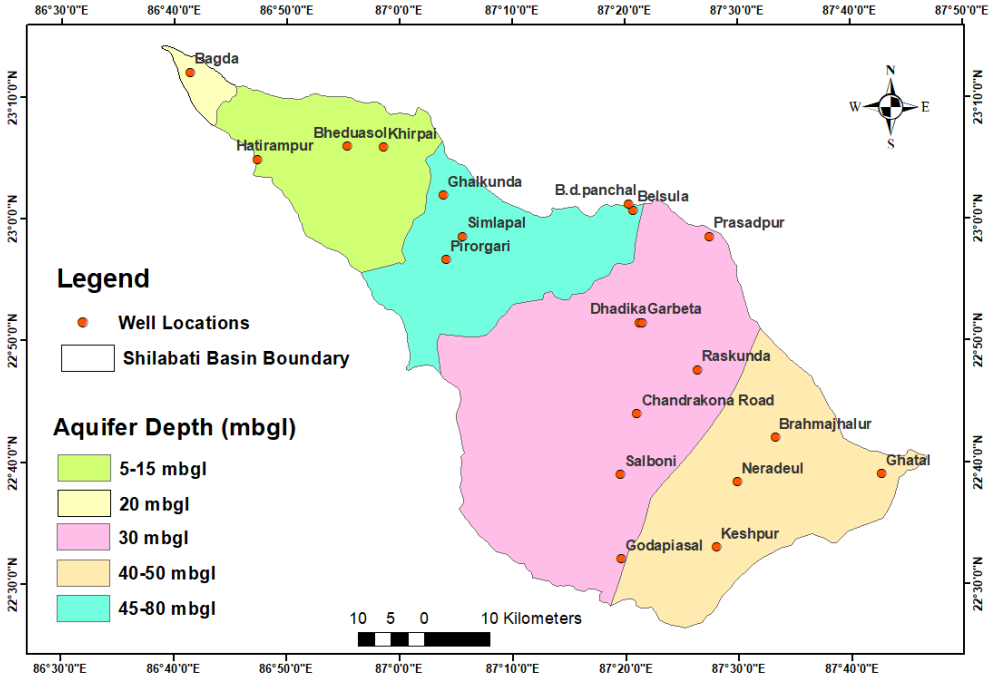

Fig. 4.22 Aquifer depth of the study area

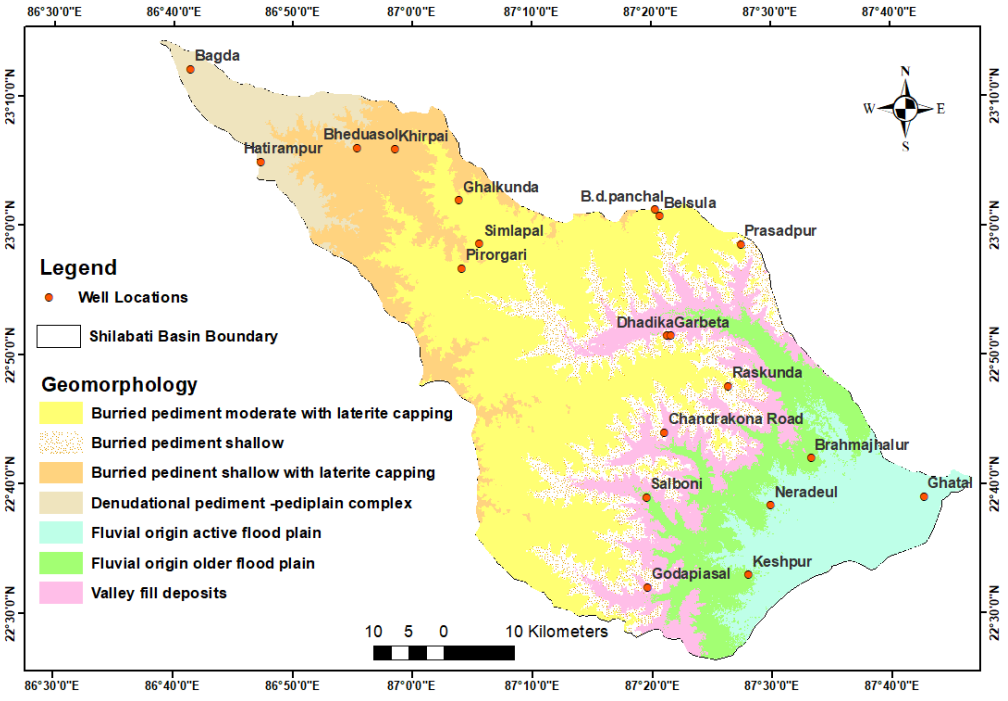

Fig. 4.23 Geomorphology of the study area

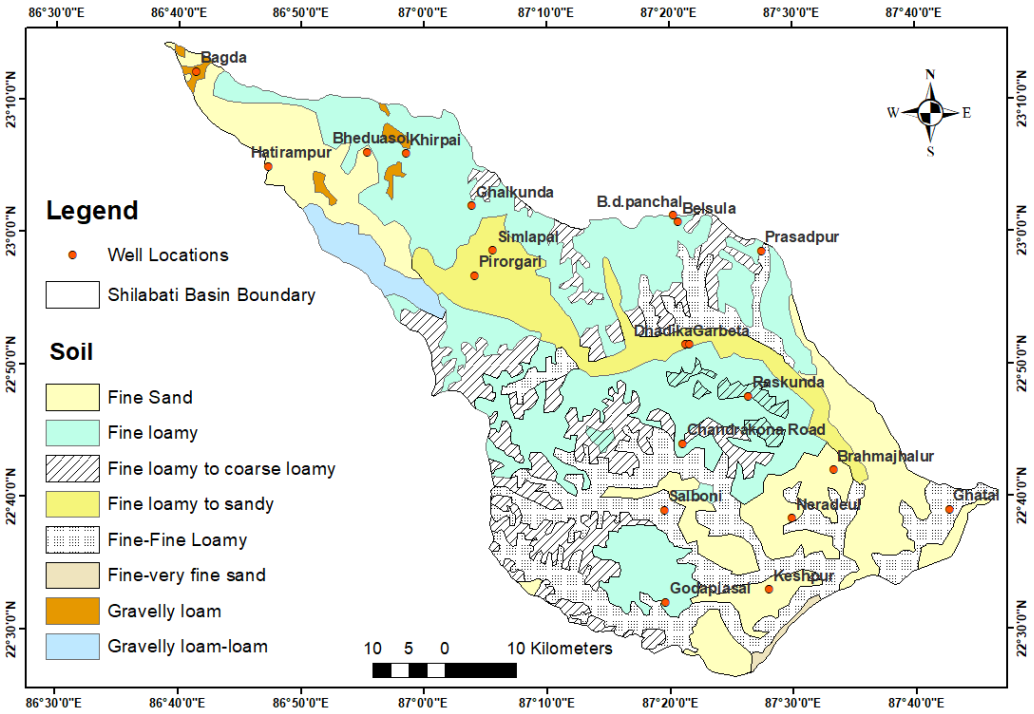

Fig. 4.24 Soil map of the study area

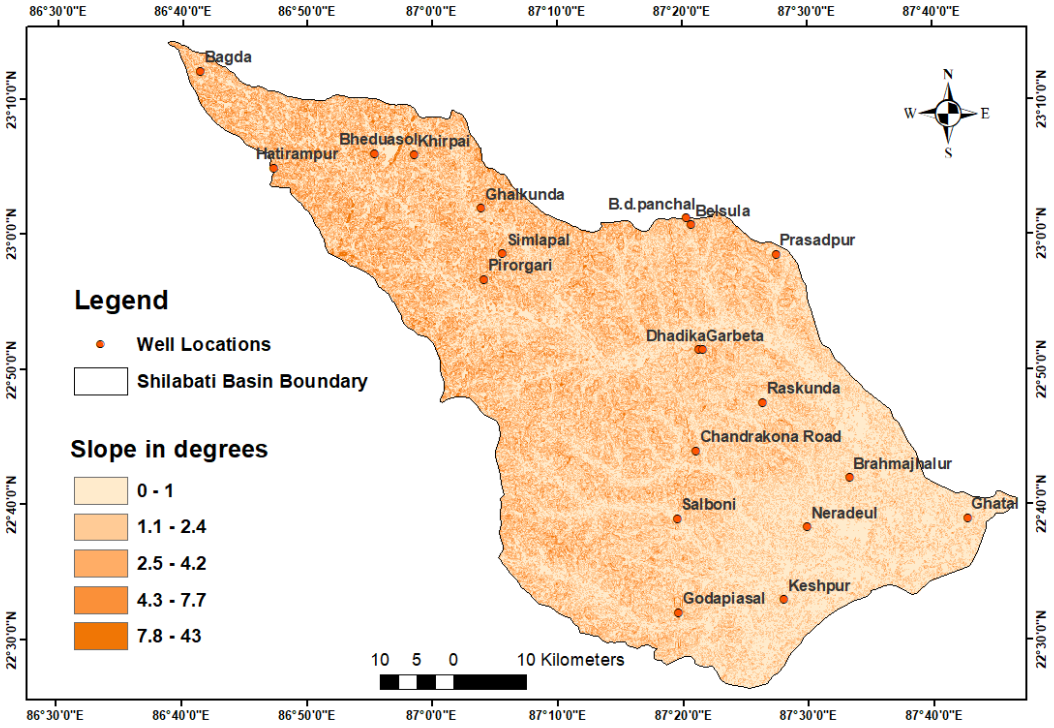

Fig. 4.25 Slope map of the study area

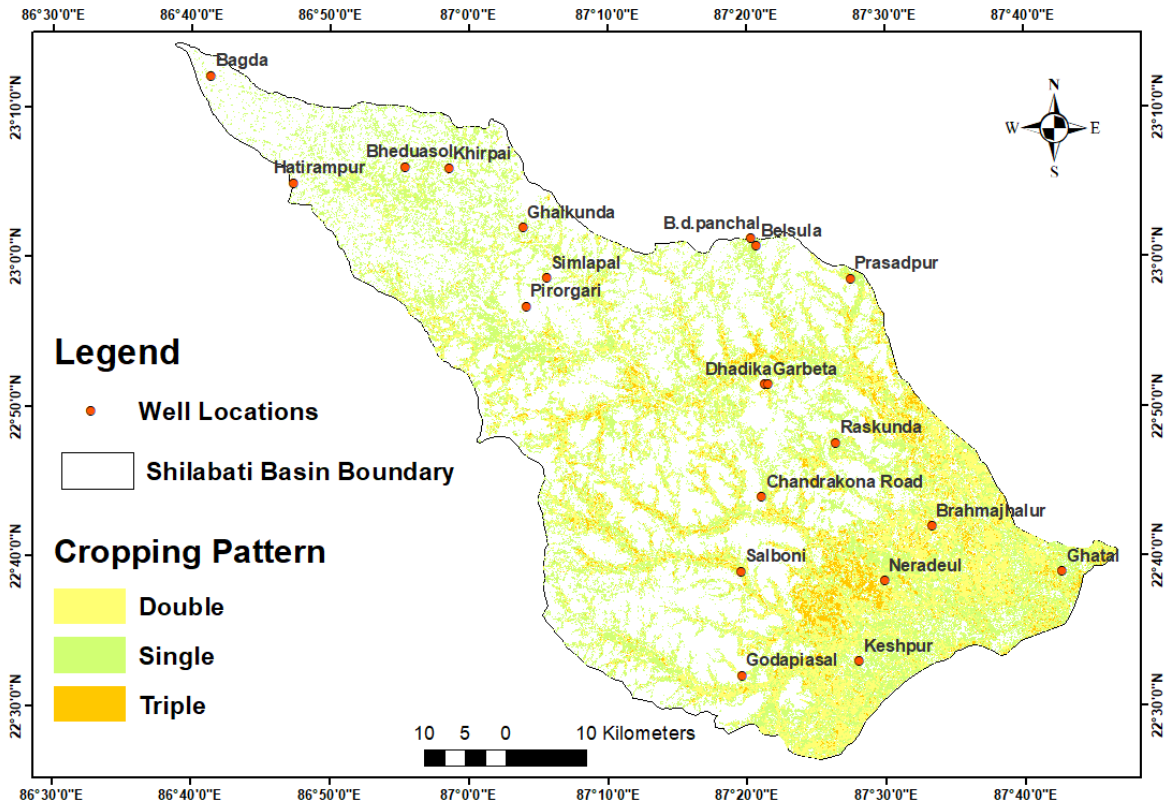

Fig. 4.26 Cropping pattern of the study area

4.2.4.2 Mann Kendall Test

Mann Kendall is a useful non- parametric statistical analysis to determine spatio-temporal trend within a dataset. The presence of outliers is common within a dataset of extreme events of such a non-parametric Mann Kendall is useful as it based on significance of difference but not on random value (Sulaiman et al. 2015). The test has been formulated by Mann Kendal (1945) and is mainly applied while handling environmental time series (Panda and Sahu, 2019). In this test there are two hypotheses, the null hypothesis (H_o) signify no trend in the data set and the alternative hypothesis (H_A) signifies a presence of increasing or decreasing trend within the data set. Here Mann Kendall test method has been applied to a long term (1996-2018) seasonal groundwater level data of Premonson, monsoon and post monsoon periods for 20 wells to detect statistically significant trend within it. Algorithm used for Mann Kendall test statistics S, Var and standardised test statistics Z are as follows,

$$S=\sum_{i=1}^{n=1}\sum_{j=i+1}^{n} sig(X_j - X_i) \quad (4.29)$$

$$\text{Sgn}\,(X_j - X_i) = \begin{cases} +1 \text{ if } (X_j - X_i) > 0 \\ 0 \text{ If } (X_j - X_i) > 0 = 0 \\ -1 \text{ If } (X_j - X_i) > 0 \end{cases} \quad (4.30)$$

$$\text{Var (S)} = 1/8\,[n\,(n-1)\,(2n+5) - \sum_{P=1}^{a} t_o(t_o - 1)\,(2t_o+5) \quad (4.31)$$

$$Z = \begin{cases} \frac{S-1}{\sqrt{VAR\ (S)}} \text{ If } S>0 \\ 0 \text{ if } S = 0 \\ \frac{S+1}{\sqrt{VAR\ (S)}} \quad \text{If } S< 0 \end{cases} \tag{4.32}$$

In these equations X_i and X_j are the time series monitoring data in sequential order, n is the length of the time series, t_o is the number of the tie in the p^{th} value and m is the numbers of tied variables. V is the Variance within the data set if $|Z|> Z_{1-\alpha/2,}$ (H_o) is rejected and a significant trend exist within the data. The positive value of the Z means upward rising and a negative value means downward trend. Here the test has been performed at a significance level of 0.05 in XLSTAT software.

4.2.4.3 Sen's Slope Estimator

The magnitude of the trend has been analyzed using the Sen's slope estimator as developed by Sen, 1968. It has been widely applied in numerous hydro-meteorological time series analysis (Gocic and Trajkovic, 2013) here it has been used to observe the groundwater level trend. The algorithm used in the calculation is given in the following

$$T_i = \frac{x_{i+x_k}}{j-k} \tag{4.33}$$

In this equation, the X_i and X_k represent the values of the data at the time j and k respectively. Let's consider

$$Q_s = \begin{cases} T_{(N+1)/2} \text{ N is odd} \\ ½\ (T_{N/2} + T_{(N+2)/2} \text{ N is even} \end{cases} \tag{4.34}$$

A positive Q_s value represents an increasing trend; a negative Q_s value represents a decreasing nature of the trend.

4.2.4.4 Agglomerated Hierarchical Clustering

In this study Agglomerated Hierarchical Clustering (AHC) has been applied to group the wells into the clusters based on the fluctuation pattern with 22-year time period data. It is a method that organize the data according to the hierarchical structures based on proximity matrix (Tian et al. 2014). There are two types of Hierarchical; clustering one is the Agglomerated and another is the Divisive method base on how the hierarchical decomposition performed. Here AHC has been used which is based on the definition of distance between two clusters. Five types of agglomerative techniques are there which include Complete Linkage, single Linkage, Average Linkage, Median Linkage and lastly Ward's Linkage method. In this paper Ward's method has been applied. The whole procedure has been performed using XLSAT.

4.2.4.5 Standard Groundwater Level Index (SGWI)

The Standard Groundwater Level Index is similar to that of the Standard Precipitation Index. It is a quantitative technique for the evaluation of groundwater level deficit in various time scale which signifies or reflects the

influence of extreme drought event on the water resources scenario. Based on the SGWI number of drought years signifying groundwater scarcity and its temporal variation can be observed (Pathak and Dodamani, 2019). Here SGWI has been calculated for each of the 20 wells from 1996-2018 and for each season i.e. premonsoon, monsoon and post monsoon. SGWI has been calculated using the following equation

$$X=\frac{K-M}{\sigma} \quad (4.35)$$

Where K= value of the respective year; M is the mean of 22 years and $\boldsymbol{\sigma}$ is Standard Deviation

4.2.5 Results and Discussion

4.2.5.1 Influence of Climate Variable on Groundwater Level

Groundwater recharge of a region depends on the precipitation which infiltrates through the soil surface. Association of groundwater and rainfall is better reflected through hydrograph. The groundwater level is highly sensitive towards the changes in the precipitation scenarios. An increase in the rainfall will lead to the increase in the groundwater well and vice versa. Gridded TRMM rainfall data from 1998-2018 has been downloaded and mean groundwater level of three season premonsoon, monsoon and post monsoon for the 20 wells has been shown graphically to understand the association between. All the graphical figures of the 20 well have been grouped in one (Fig.4.27) where the line shows the groundwater level and bar graph shows rainfall. Rainfall and groundwater level have been shown graphically from year 1998 to 2018 because of the non-availability of data from 1996.The graph shows the spatio-temporal distribution of the two variables. From the graph it can be seen that when the rainfall is low groundwater level decreased. From the well location Dhadika it can be observed that in the recent years from 2009 to 2016 the groundwater level rose upward. In well locations like Ghatal, Ghalkunda, Belsula, Neradeul, Salboni, Brahmajhalur and Badga groundwater level did not rise up even if the rainfall is high. Such temporal variation will give a preliminary idea of groundwater recharge whereas it also depends on the land use/land cover characteristics of the region which should be assessed parallelly. Recently this part of the West Bengal is facing a decline in rainfall particularly in the early monsoonal month of June and middle monsoonal month of August (Ghosh, 2018). Dong et al. (2016) also witnessed that a number of climatic model-based studies are suggesting a delayed monsoonal onset in the eastern part of Tropical Indian Ocean. For this reason, the summer is getting longer and villagers are more focusing on the extraction of sub-surface water rather than surface water resources. To curb such a situation rainwater harvesting during the wet spells is urgently required.

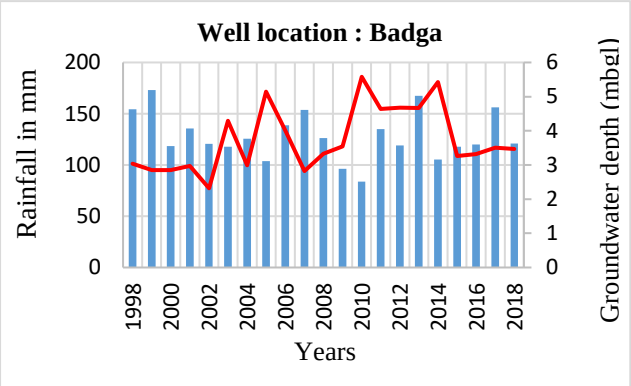
Well location : Badga
Rainfall in mm
Groundwater depth (mbgl)
Years

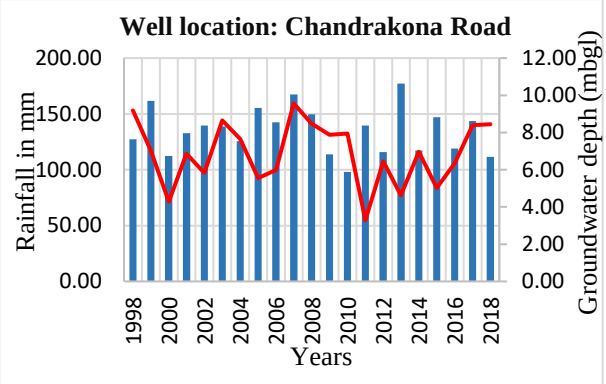
Well location: Chandrakona Road
Rainfall in mm
Groundwater depth (mbgl)
Years

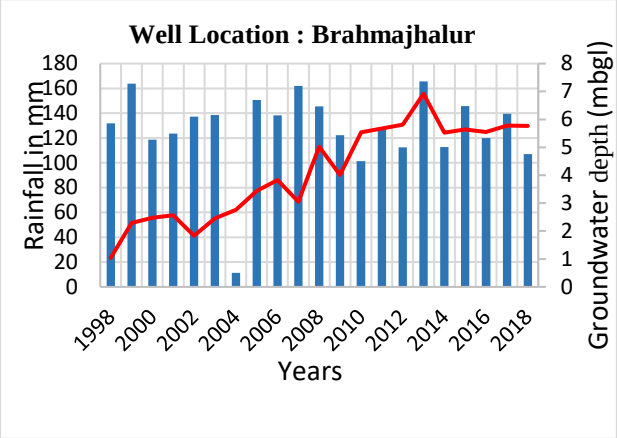
Well Location : Brahmajhalur
Rainfall in mm
Groundwater depth (mbgl)
Years

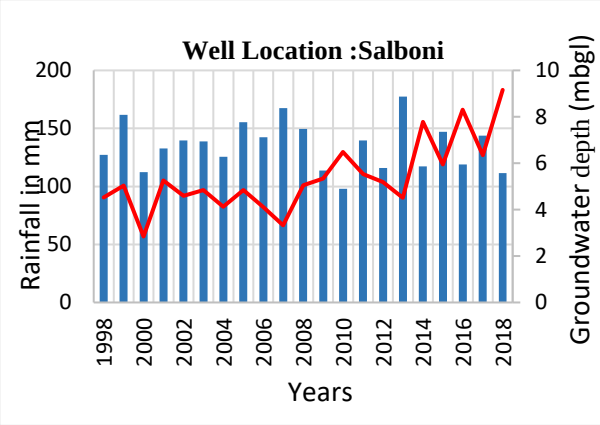
Well Location :Salboni
Rainfall in mm
Groundwater depth (mbgl)
Years

Continued….

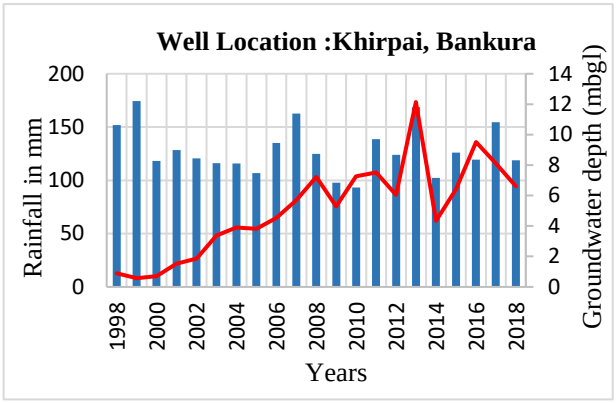
Well Location :Khirpai, Bankura
Rainfall in mm
Groundwater depth (mbgl)
Years

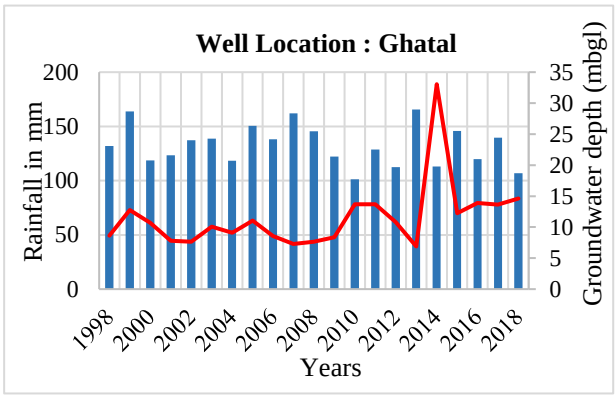
Well Location : Ghatal
Rainfall in mm
Groundwater depth (mbgl)
Years

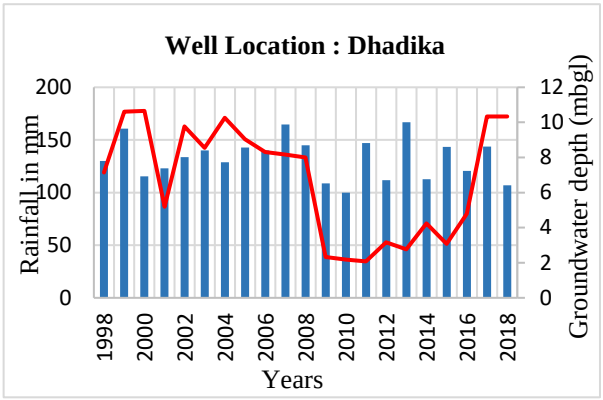
Well Location : Dhadika
Rainfall in mm
Groundwater depth (mbgl)
Years

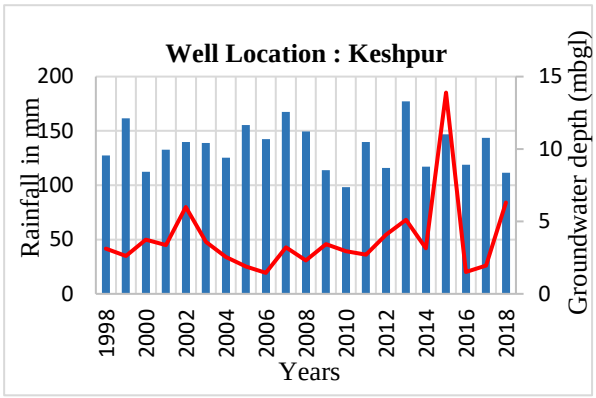
Well Location : Keshpur
Rainfall in mm
Groundwater depth (mbgl)
Years

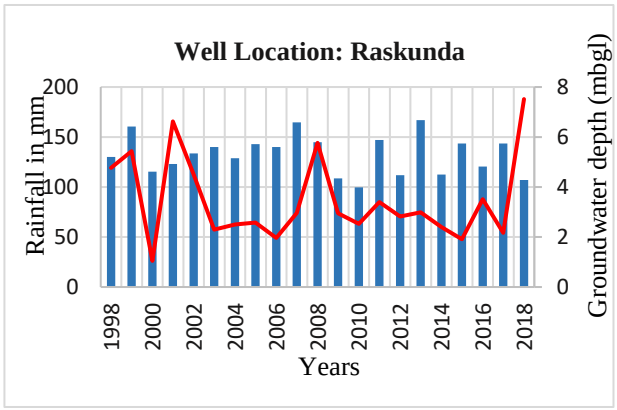
Well Location: Raskunda
Rainfall in mm
Groundwater depth (mbgl)
Years

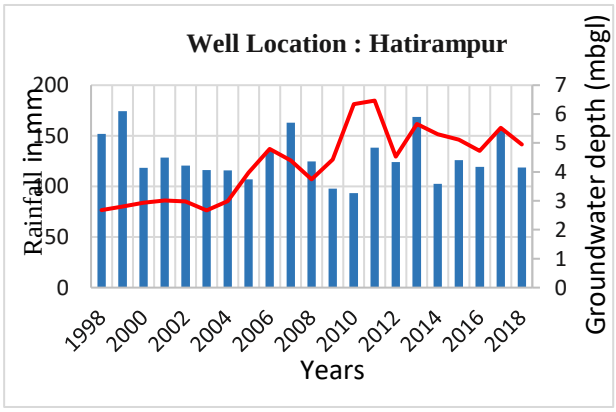
Well Location : Hatirampur
Rainfall in mm
Groundwater depth (mbgl)
Years

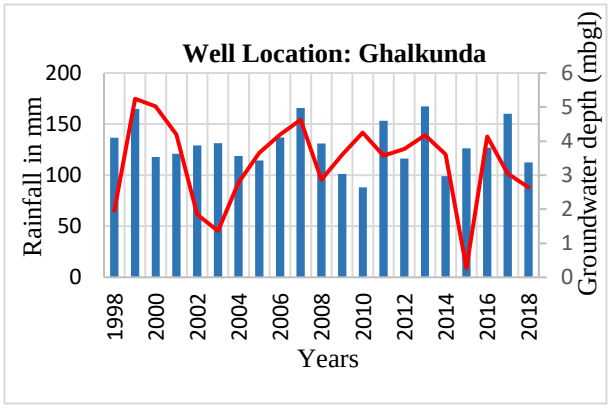
Well Location: Ghalkunda
Rainfall in mm
Groundwater depth (mbgl)
Years

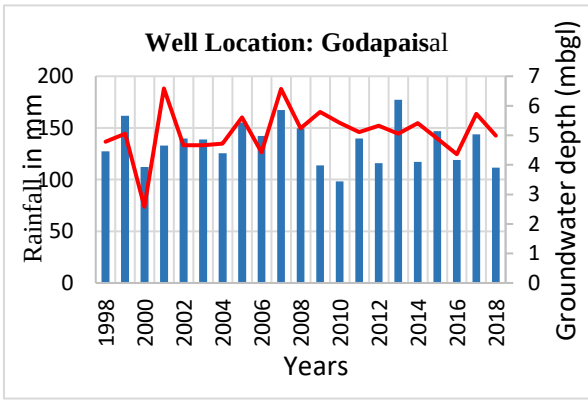
Well Location: Godapaisal
Rainfall in mm
Groundwater depth (mbgl)
Years

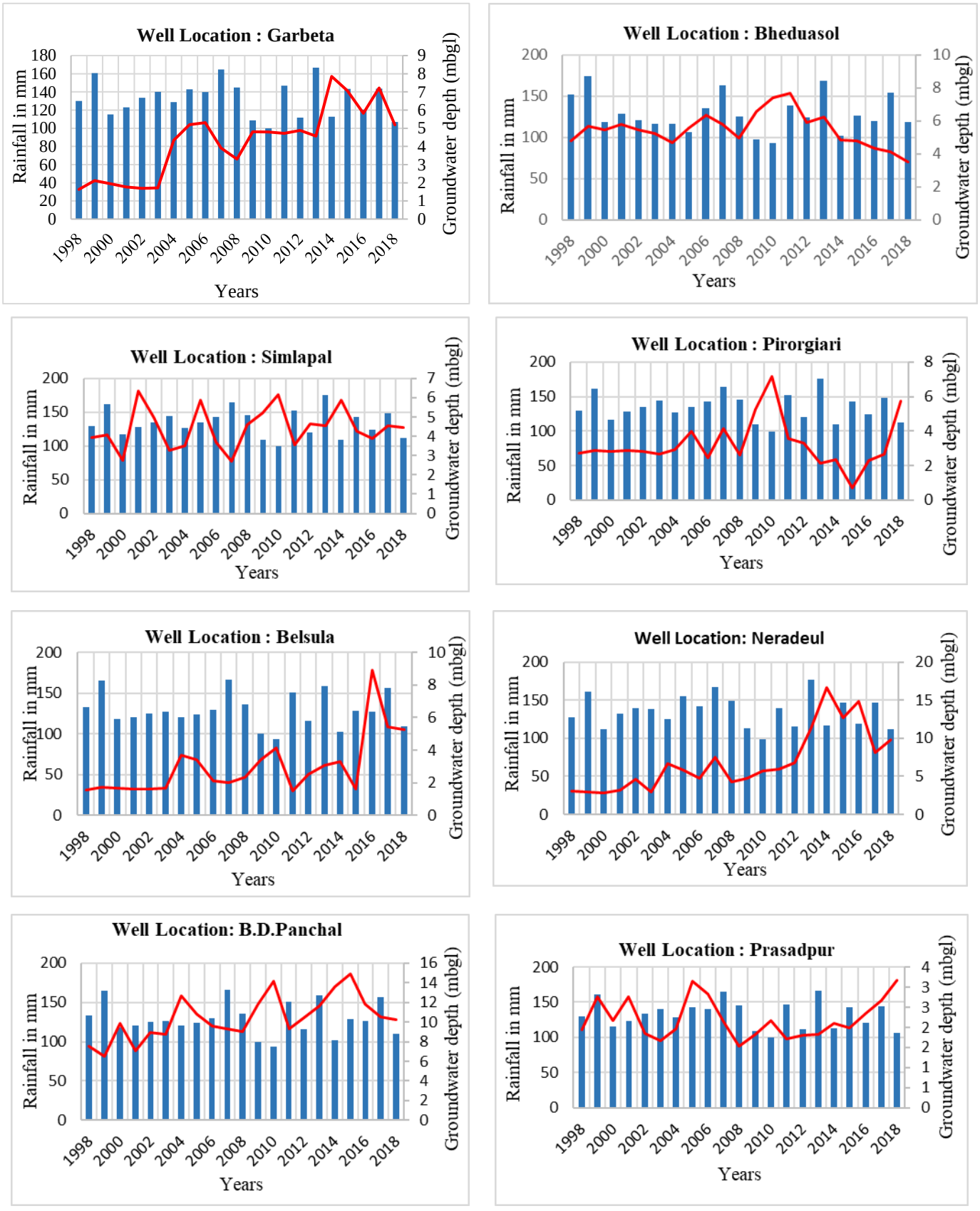

Fig. 4.27 Graphical representation of Average monthly rainfall and groundwater level (1998-2018)

4.2.5.2 Impact of Land Use and Land Cover change (LULC) on Groundwater level

Land use and land cover control the groundwater recharge of a region. The utilization of the soil surface for anthropogenic activities such as settlement, construction of road impedes the surface water infiltration in a region. Conversion of forested land into bare land increases surface runoff and hence decreases recharge. Here land use and land cover practice around the 20 wells have been analyzed for the year 1989, 2000, 2009 and 2018 (Fig.4.28, 4.29, 4.30 and 4.31). Classified maps have been prepared using supervised classification. Nine different classes of land use and land cover has been made and their accuracy assessment has been calculated using Kappa Index. The calculated accuracy of year 1989, 2000, 2009 and 2018 are 94%, 96%, 97.2% and 95.2% respectively. From the analysis of the classified maps it can be seen that the areas under different LULC classes has been changed over the years (Table 4.11). One of the predominant LULC in the river basin is bare land which covered 35.24% in 1989, 24.53 % in 2000, 38.76% in 2009 and 33.11 % in 2018 among all the other classes. Presence of bare land can be found scattered throughout the regions which indicates poor groundwater recharge, higher peaks of surface runoff and soil erosion that is quite predominant over the basin. Soil erosion also discourages groundwater recharge for this suitable cropping pattern and crop rotation technique should be adopted for its sustainable management (Shit et al. 2015). Percentage of dense forest cover over the region has also decreased from 1989 i.e. from 10.88% of the total area to 4.93 % in 2018. This decrease in natural vegetation has far reaching effect on the groundwater potential of the study area. But the percentage of water bodies (like ponds) increased over the study area may be to irrigate the agricultural land as the rainfall amount decreased. A locational description of the (Table 4.12) wells has also been done based on the LULC of the four years to identify the LULC class in and around the wells controlling the recharge pattern. Well location at Chandrakona road, Keshpur and Neradual which has been surrounded by agricultural land and fallow land in 1989 changed to settlement in 2018 which implies poor infiltration scenario of the basin. From the census report of 2011 it can also be found that Chandrakona has developed into a town as such concretion increased and groundwater level decreased due to poor recharge. The majority of the well locations has been transformed into bare land where sustainable management, afforestation and artificial recharge is needed to increase the stock of sub-surface water resources.

Table 4.11 Areal description of LULC class

Class	1989		2000		2009		2018	
	Area in km^2	Area in percentage	Area in km^2	Area in percentage	Area in km^2	Area in percentage	Area in km^2	Area in percentage
Agriculture land	649.61	16.71	598.11	15.41	829.92	9.86	577.16	14.87
Dense forest	422.96	10.89	84.65	2.18	382.79	38.76	191.36	4.93
Bare land	1369.25	35.24	951.87	24.53	1504.41	0.97	1285.18	33.11
Lateritic exposure	100.18	2.58	12.28	0.32	37.65	16.36	45.33	1.17
Open forest	431.89	11.12	1057.55	27.25	635.02	16.36	944.51	24.34
Sand Bar	1.19	0.031	2.54	0.065	5.40	0.14	0.74	0.019
Settlement	3.55	0.091	72.29	1.86	102.67	2.65	63.15	1.63
Water body	91.04	2.34	79.38	2.05	72.93	1.88	173.69	4.48
Fallow	816.00	21	1022.17	26.34	310.28	7.99	599.93	15.46

Table 4.12 Locational description of wells based on LULC change from 1989-2018

Well location	1989	2000	2009	2018
Badga	Bare land	Bare land	Bare land	Bare land
Chandrakona road	Agricultural land	Settlement	Fallow land	Settlement
Brahmajhalur	Bare land	Bare land	Fallow land	Fallow land
Dhadika	Lateritic exposure	Open forest	Open forest	Bare land
Salboni	Bare land	Open forest	Fallow land	Fallow land
Godapaisal	Fallow land	Fallow land	Fallow land	Agricultural Land
Keshpur	Fallow land	Fallow land	Settlement	Settlement
Neradual	Fallow land	Settlement	Settlement	Settlement
Raskhunda	Bare land	Fallow land	Fallow land	Agricultural land
Belsuda	Open forest	Open forest	Open forest	Bare land
B.D. Panchal	Fallow land	Agricultural land	Agricultural land	Fallow land
Pirorgairi	Dense forest	Fallow land	Bare land	Open forest
Prasadpur	Agricultural land	Open forest	Bare land	Open forest
Simlapal	Bare land	Bare land	Bare land	Bare land
Khirpai	Bare land	Fallow land	Bare land	Bare land
Hatirampur	Dense forest	Bare land	Open forest	Bare land
Bheduasol	Bare land	Open forest	Bare land	Dense forest
Ghalkunda	Bare land	Open forest	Dense forest	Dense forest
Garbeta	Agricultural Land	Agricultural land	Agricultural land	Fallow land
Ghatal	Fallow land	Agricultural land	Agricultural land	Agricultural land

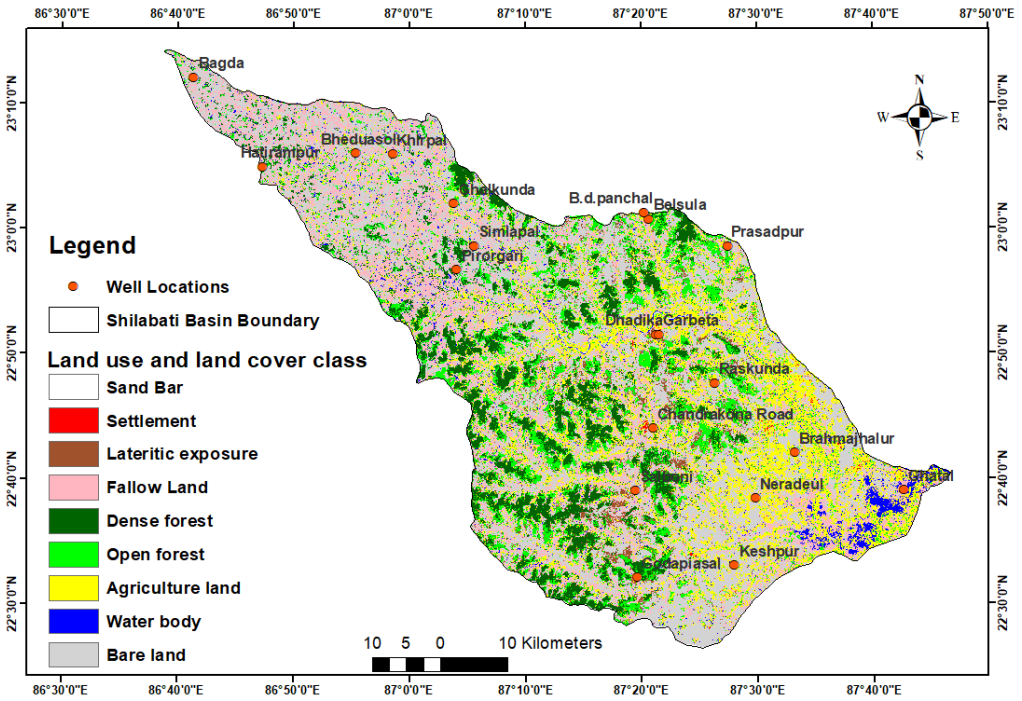

Fig. 4.28 Land use and land cover map of 1989

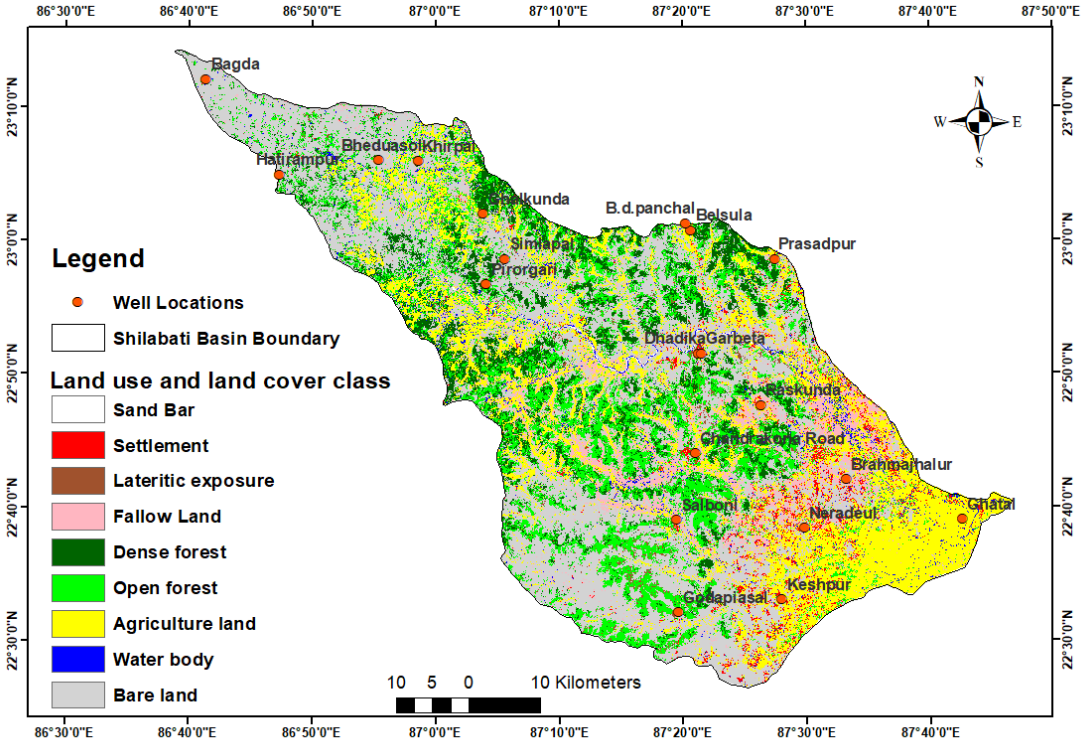

Fig. 4.29 Land use and land cover map of 2000

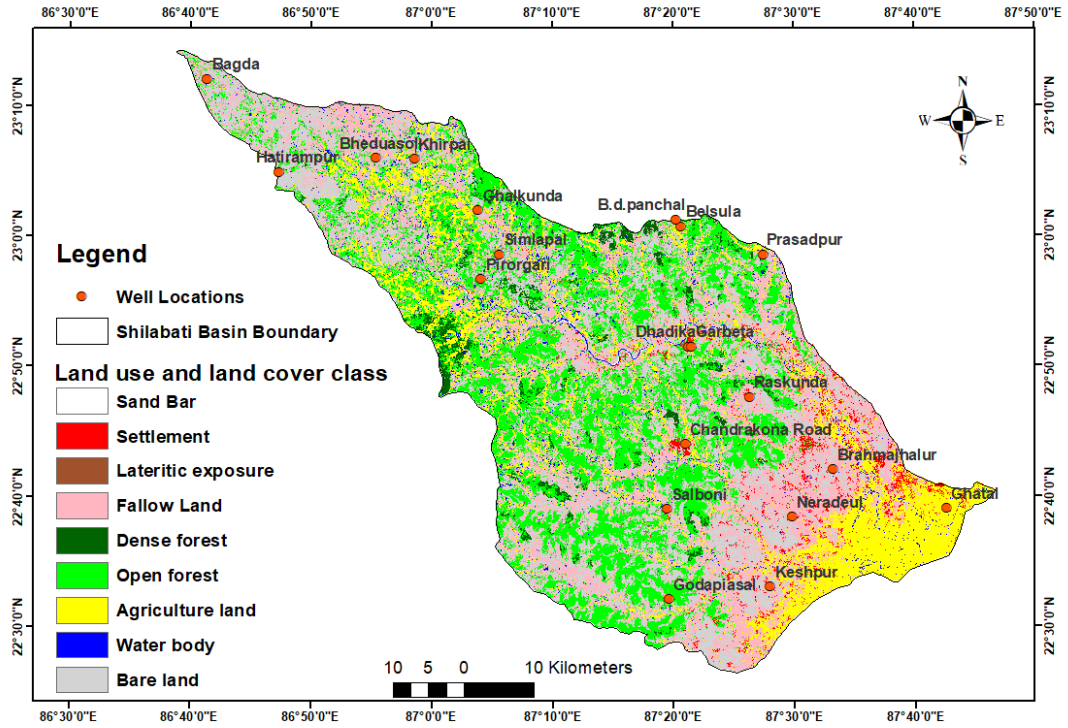

Fig. 4.30 Land use and land cover map of 2009

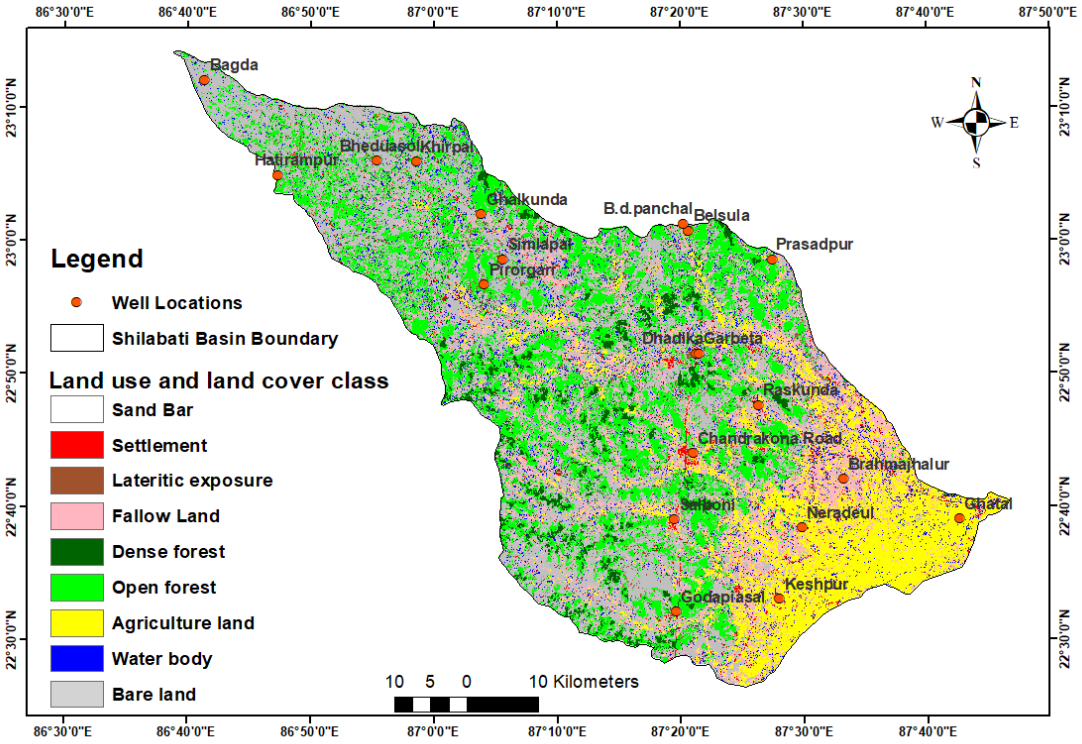

Fig. 4.31 Land use and land cover map of 2018

4.2.5.3 Spatio- Temporal Distribution of Groundwater Level Since 1996

To determine the spatio-temporal distribution of groundwater level of each of the wells, data from 1996-2018 has been downloaded for three seasons premonsoon, monsoon and post monsoon to calculate the descriptive statistics such as Mean, Standard Deviation, Skewness, Kurtosis, Variance, Median, Quartile 1, Quartile 2 and Quartile 3 and their Inter Quartile range which has been discussed in table 4. A1, 4. A2 and 4. A3 (Appendix). From the computed table 4. A1 (Appendix) it can be found that the mean water level of 22 years at premonsoon in Chandrakona and B.D. Panchal is 11.813 mbgl (meter below groundwater level) and 12.733 mbgl respectively which is quite low. Huge extraction of groundwater for agricultural activities and other domestic purpose may be the prime reason of concern. Standard Deviation of the premonsoon water level depth is also high where high value is witnessed at Neradual which is 6.405 mbgl. During the monsoon the mean groundwater level slightly, improved which ranges between 2-7 mbgl that is mainly due to the effect of recharge through precipitation. During the post monsoon season the mean ranges from 1.56-8.6 mbgl which also reflects the replenishment of aquifers through infiltration. Most of the values of the premonsoon, monsoon and post monsoon are highly skewed and showing asymmetrical distribution. 5 wells of premonsoon, 5 wells of monsoon and 4 wells of monsoon are showing highly skewed values. Inter quartile range denotes the measure of variability. The inter-quartile range is higher in case of well location at Dhadika, B.D Panchal and Ghatal for monsoon season, Dhadika, Neradeul, and Ghatal for premonsoon and B.D Panchal and Khirpai for post monsoon. The computed table will help to understand the variability of the groundwater level. Spatio – temporal distribution of the groundwater level of the three seasons has been shown in Fig 4.32, 4.33, 4.34, 4.35 and 4.36. From the distribution it can be seen that the mid-section of the basin is having lower groundwater level during the post monsoon season where the development of the settlement can be observed. In other words, most of the depth of the groundwater level is lowered after the offset of the monsoonal season. As the volume of precipitation in the monsoonal months decreased farmers are utilizing groundwater for paddy and vegetable cultivation effecting the sub-surface water stock of drier periods. From the socio-economic survey conducted by the authors also revealed the increased use of submersible pumping system in the recent days due to the poor and irregular water supply from the canals, drying up of the river beds and most of dug wells has become obsolete. More than 50-70 such pumps operate in the villages falling within the basin for agriculture and domestic purposes. On a global scale this kind of spatio-temporal change analysis is fewer in number because of the lack of groundwater monitoring systems (Bui et al. 2012) but are needed for sustainable river basin management.

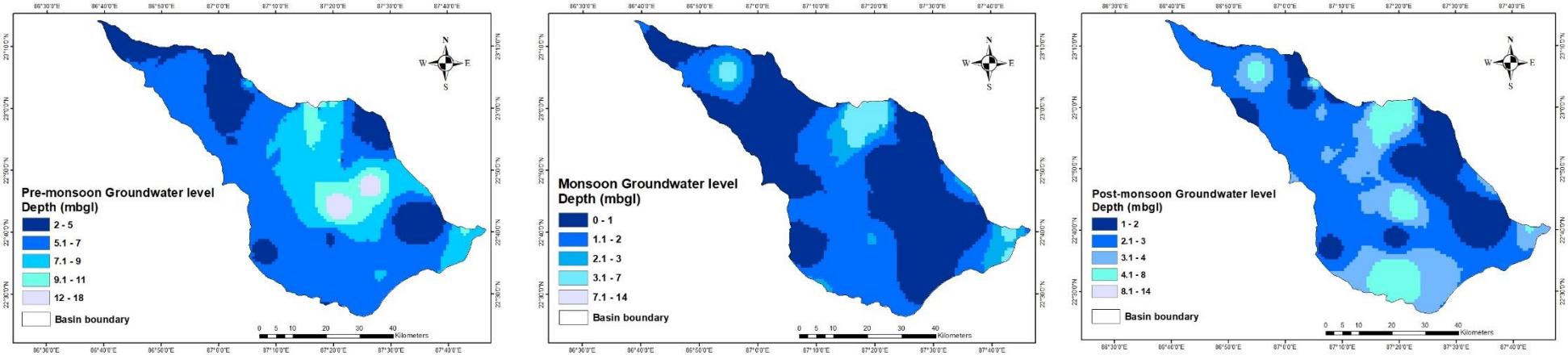

Fig. 4.32 Groundwater level at Premonsoon, Monsoon and Post monsoon 1996

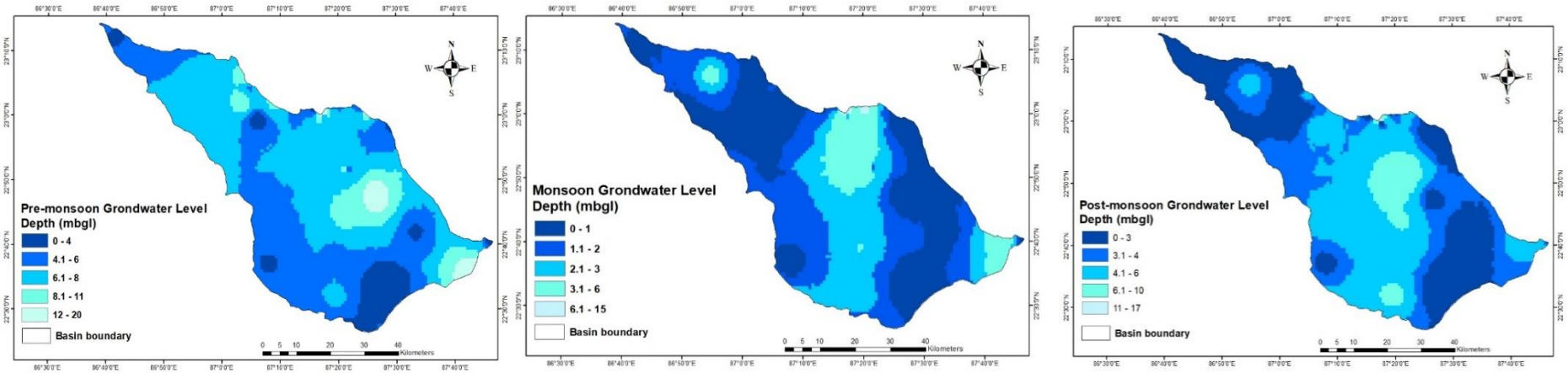

Fig. 4.33 Groundwater level at Premonsoon, Monsoon and Post monsoon 2001

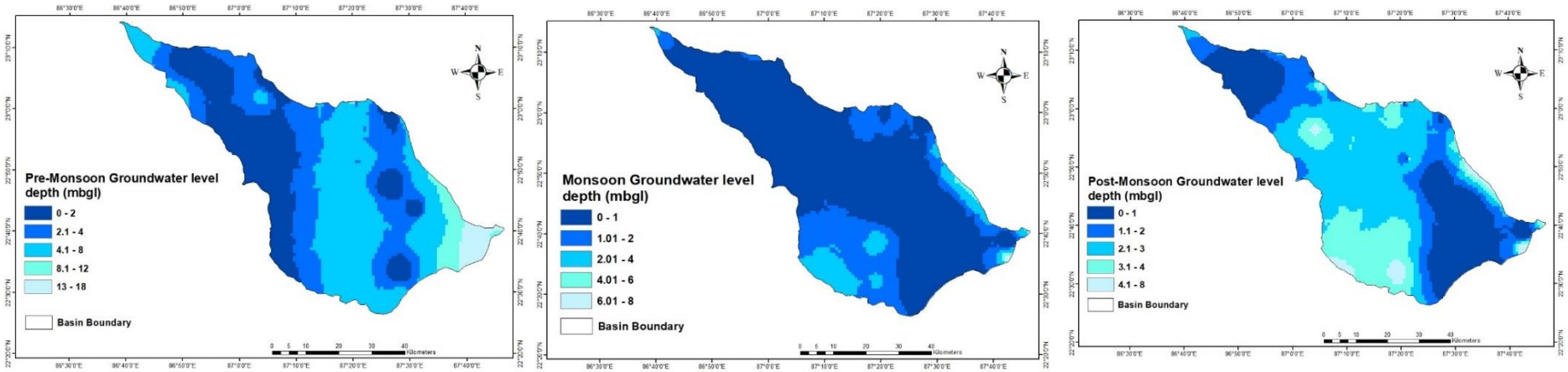

Fig. 4.34 Groundwater level at Premonsoon, Monsoon and Post monsoon 2006

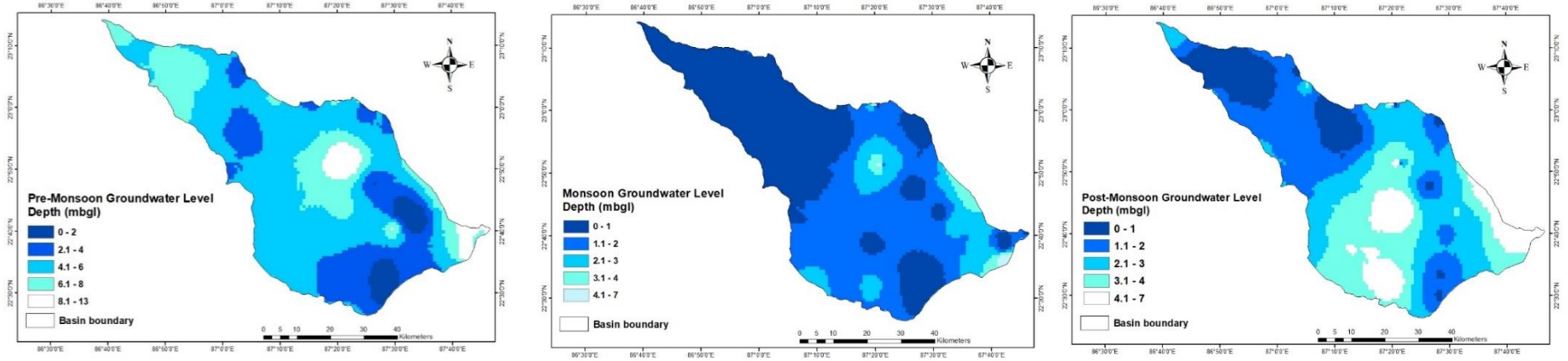

Fig. 4.35 Groundwater level at Premonsoon, Monsoon and post monsoon 2011

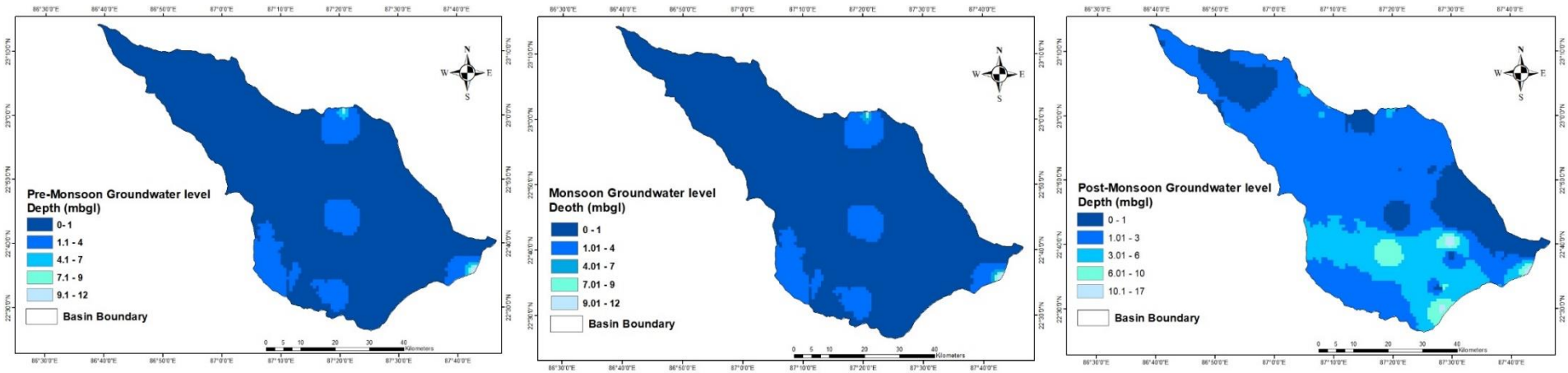

Fig. 4.36 Groundwater level at Premonsoon, Monsoon and post monsoon 2016

4.2.5.4 Groundwater Level Trend Analysis

The Asymmetrical distribution as observed from the statistical analysis substantiate the need for the application of the non-parametric trend method to identify the trends in the data sets. The time series data form 1996-2018 for the premonsoon, monsoon and post monsoon has been taken under the study. The seasonal variability and groundwater crisis are observed in the study area. Which can be due to the following a) influence of the uneven distribution of precipitation and its deficit in the recent years b) conversion of bare land c) heavy extraction of groundwater through submersible pumping system for agricultural activities and domestic purpose d) extensive sand mining in the river bed hampering the conjunctive system between groundwater and surface water resources. From the field studies, extensive sand mining in various sections of the river has been observed disturbing the interaction of the two most important hydrological system. At the best of our knowledge, no reference studies have been done till date within the basin using the groundwater level data whereas reference studies are available related to the soil erosion. Mann Kendall test statistics has been applied in this paper to witness the trend. In this method each monitoring wells visualise the groundwater dynamics of the adjoining areas and each trend gives an idea of the extent of the fluctuation over the period of time (Vousoughi et al. 2013). The method has been executed using XLSTAT software. The trend has been analysed at a significance level of 0.05 or 5% of confidence level. Two hypotheses have been considered, H_o (Null hypothesis) denotes the absence of trend and H_A denotes the presence of trend within the data set. To understand the magnitude and intensity of the trend Sen's slope estimate has also been calculated. The Kendall's tau, S, VAR, P and slope of each of the wells of three seasons has been given in a tabular format (table 4.13). Under premonsoon condition, out of the 20 wells 9 wells are showing an increasing trend which means the groundwater level is declining at a higher rate. Higher value of groundwater level indicates greater decline as the level is calculated or measure from surface as zero. During the monsoon 5 wells namely Brahmajhalur, Salboni, Simlapal, Belsula and Garbeta are showing increasing trend i.e. groundwater level is declining and others showed no significant trend. In post monsoon season increasing trend is observable in 12 wells and 1 well (Dhadika) is showing a decreasing trend. Groundwater level in post monsoon period is important as it signifies the quantity of recharge after monsoonal precipitation. Most of the wells showing upward trend are located near the agricultural land as reflected from the LULC analysis where extensive extraction is going on. A field survey is also conducted to inspect the groundwater crisis where most of the inhabitants informed about the extensive withdrawal using higher energy utilization and at the higher cost. In the summer months villagers experience drought like condition particularly in the upstream and the middle section because of poor rainfall and practice single crop cultivation using sub-surface water reducing the sustainability of aquifers. One of the major problems of the study area includes over-abstraction from the aquifers and river and increasing demand of the water by the growing population. Under such situation this paper contributes in identifying the hotspot areas in terms of water level decline that will help to undertake watershed management techniques likewise.

4.2.5.5 Cluster Analysis of Wells Based on Their Fluctuation Scenario

Agglomerated Hierarchical Cluster (AHC) has been applied to classify the wells according to their fluctuation variability. It is an important statistical tool that determines each case into a separate group or cluster and connects each cluster until one cluster remains (Salah et al. 2012). Here Hierarchical Clustering based on the Ward's linkage method has been applied. Fluctuation of the groundwater has been calculated subtracting the pre-monsoon from

post monsoon groundwater level for the period of 22 years. This statistical tool has been applied to observe long term variability of fluctuation of groundwater level in wells and grouping them which are showing similar trends for sustainable management. Groundwater fluctuation helps in understanding the vulnerability of aquifers in terms of recharge potential controlled by climatological and anthropogenic factors the wells have been grouped into four clusters and the details of the analysis generated from the software has been given in tabular format (Table 4.14). The dendrogram (Fig 4.37) shows the cluster hierarchy of the wells located in the study area. It has been observed from the spatio temporal variation of the wells of different clusters (Fig.4.38) that 15 wells showed similar fluctuation variation are in cluster 1 where the mean fluctuation ranged between 1.8 to 4.329 m. The second cluster consists only 1 well whose mean fluctuation is 6.305m and the 3rd cluster and 4th cluster consist of 2 wells each with mean fluctuation between 4.52 to 4.01 m and 3.46 to 2.861 respectively. The fluctuation is higher in cluster 2 and 3. Cluster 3 consists of well location of Chandrakona road and mean fluctuation is about 6.305 m. The box and whisker plot (Fig.4.39) give the indication of fluctuation of each of the wells with their respective variability. The reason for the higher fluctuation at well location Chandrakona Road can be due to change in land use and land cover which was mainly surrounded by agricultural land in 1986 and transformed into a built-up area in 2018. Thus, concretion has changed the recharge scenario. Another reason for the increased fluctuation witnessed in the wells is mainly due to the precipitation variability and time taken by the aquifer to replenish as groundwater extraction overdrafts the recharge. According to CGWB published report of West Bengal (2015-2016) (CGWB-2015-2016) 28.30% of the wells in Bankura district, 38.9% of the wells in Puruliya district and 38.6% of the wells in West Medinapore district are having a water table depth of 5-10 m in the month of November. A part of all the three districts fall under the basin area. Such type of cluster analysis is also new in this river basin. Towards efficient planning for sustainable groundwater management grouping of the wells will help in the adoption of cluster wise management strategies (Vishwajith et al. 2015).

Table 4.13 Results of Mann Kendall test statistics

Well Location	Premonsoon					
	Kendall tau	S	VAR	P	Slope	Trend
Badga	0.198	50	1432.67	0.195	0.061	No
Chandrakona road	-0.079	-20	1432.37	0.616	-0.087	No
Brahmajhalur	-0.721	182.00	1432.67	<0.0001	0.322	Increasing
Dhadika	-0.210	-53	1431.67	0.19	-0.222	No
Salboni	0.467	118	1432.67	0.002	-0.165	Increasing
Godapaisal	-0.325	-82	1432.67	0.032	-0.039	Decreasing
Keshpur	-0.341	-86	1432.67	0.025	-0.169	Decreasing
Neradeul	0.459	116	1432.67	0.002	.609	Increasing
Raskhunda	-0.238	-60	1432.37	0.119	-0.114	No
Belsula	0.214	54	1432.67	0.161	0.039	No
B.D. Panchal	0.726	183	1431.67	<0.0001	0.425	Increasing
Pirorgairi	0.293	74	1432.67	0.054	0.081	Increasing
Prasadpur	-0.143	-36	1432.67	0.05	-0.037	No
Simlapal	-0.178	-45	1432.67	0.245	-0.061	No
Khirpai	0.290	73	1432.37	0.057	0.26	Increasing
Hatirampur	0.663	167	1432.67	<0.0001	0.215	Increasing
Bheduasol	-0.139	-35	1431.67	0.369	-0.023	No
Ghalkunda	-0.087	-22	1432.67	0.579	0.579	No
Garbeta	0.420	106	1432.67	0.289	0.289	Increasing
Ghatal	0.412	104	1432.67	0.404	0.404	Increasing
Well Location	Monsoon					
	Kendall tau	S	VAR	P	Slope	Trend
Badga	-0.020	-5.0	1433.67	0.916	-0.002	No
Chandrakona road	0.225	57	1433.67	0.139	0.073	No
Brahmajhalur	0.433	109	1431.67	0.004	0.046	Increasing
Dhadika	-0.158	-40	1432.67	0.303	-0.224	No
Salboni	0.502	127	1433.67	0.001	0.119	Increasing
Godapaisal	0.135	34	1432.67	0.383	0.020	No
Keshpur	0.289	73	1433.67	0.057	0.031	No
Neradeul	-0.143	-36	1432.67	0.355	-0.033	No
Raskhunda	0.176	44	1428	0.255	0.024	No
Belsula	0.320	81	1433.67	0.035	0.030	Increasing
B.D. Panchal	-0.099	-25	1433.67	0.526	-0.172	No
Pirorgairi	-0.182	-46	1432.67	0.234	-0.006	No
Prasadpur	-0.147	-37	1431.67	0.341	-0.018	No
Simlapal	-0.115	-29	1433.67	0.460	-0.024	No

Khirpai	0.826	209	1433.67	<0.0001	0.395	Increasing
Hatirampur	-0.028	-7.6	1431.67	0.874	-0.005	No
Bheduasol	-0.115	-29	1433.66	0.460	-0.100	No
Ghalkunda	0.166	42	1432.67	0.279	0.031	No
Garbeta	0.375	95	1433.67	0.013	0.049	Increasing
Ghatal	0.217	55	1433.67	0.154	0.257	No
Well Location	Post-monsoon					
	Kendall tau	S	VAR	P	Slope	Trend
Badga	0.512	129	1431.67	0.001	0.086	Increasing
Chandrakona road	-0.036	-9.00	1433.67	0.833	-0.036	No
Brahmajhalur	0.510	129	1433.67	0.001	0.261	Increasing
Dhadika	-0.383	-97	1433.67	0.011	-0.244	Decreasing
Salboni	0.628	159	1433.67	<0.0001	0.176	Increasing
Godapaisal	0.067	17	1433.67	0.673	0.045	No
Keshpur	0.143	36	1432.67	0.355	0.046	No
Neradeul	0.562	142	1432.67	0.001	0.486	Increasing
Raskhunda	0.127	32	1432.67	0.413	0.033	No
Belsula	0.436	110	1432.67	0.004	0.060	Increasing
B.D. Panchal	0.499	126	1432.67	0.001	0.384	Increasing
Pirorgairi	0.293	74	1432.67	0.054	0.081	Increasing
Prasadpur	0.350	88	1430.67	0.021	0.068	Increasing
Simlapal	0.218	55	1431.67	0.154	0.110	No
Khirpai	0.689	174	1432.67	<0.0001	0.309	Increasing
Hatirampur	0.737	186	1432.67	<0.0001	0.251	Increasing
Bheduasol	0.234	59	1431.67	0.125	0.035	No
Ghalkunda	0.345	87	1431.67	0.023	0.134	Increasing
Garbeta	0.483	122	1432.67	0.001	0.292	Increasing
Ghatal	0.269	68	1432.67	0.077	0.144	No

Table 4.14 Details of the cluster analysis as executed from XLSTAT software

Class	Cluster 1	Cluster 2	Cluster 3	Cluster 4
Objects	15	1	2	2
Sum of weights	15	1	2	2
Within-class variance	113.076	0.000	189.891	140.186
Minimum distance to centroid	6.173	0.000	9.744	8.372
Average distance to centroid	9.772	0.000	9.744	8.372
Maximum distance to centroid	16.271	0.000	9.744	8.372

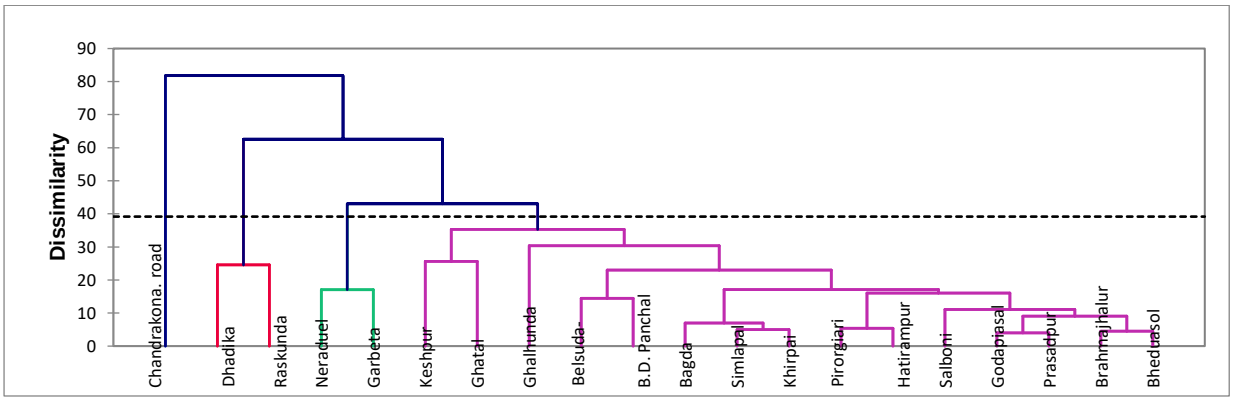

Fig. 4.37 Dendrogram of the clusters

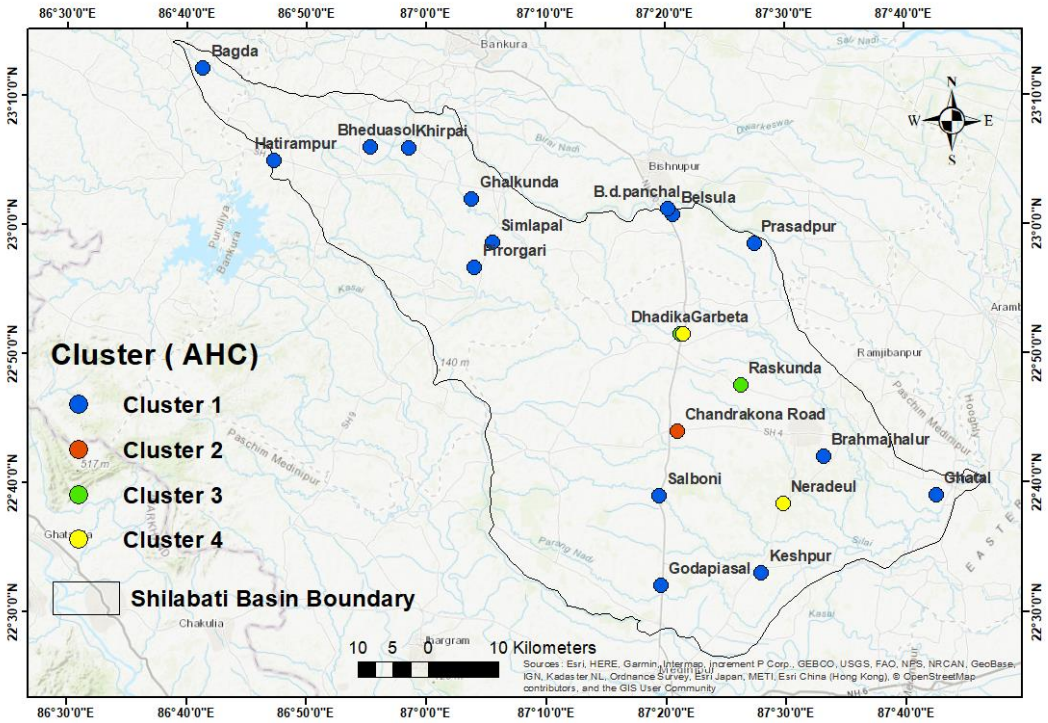

Fig. 4.38 Map showing 4 clusters of Well

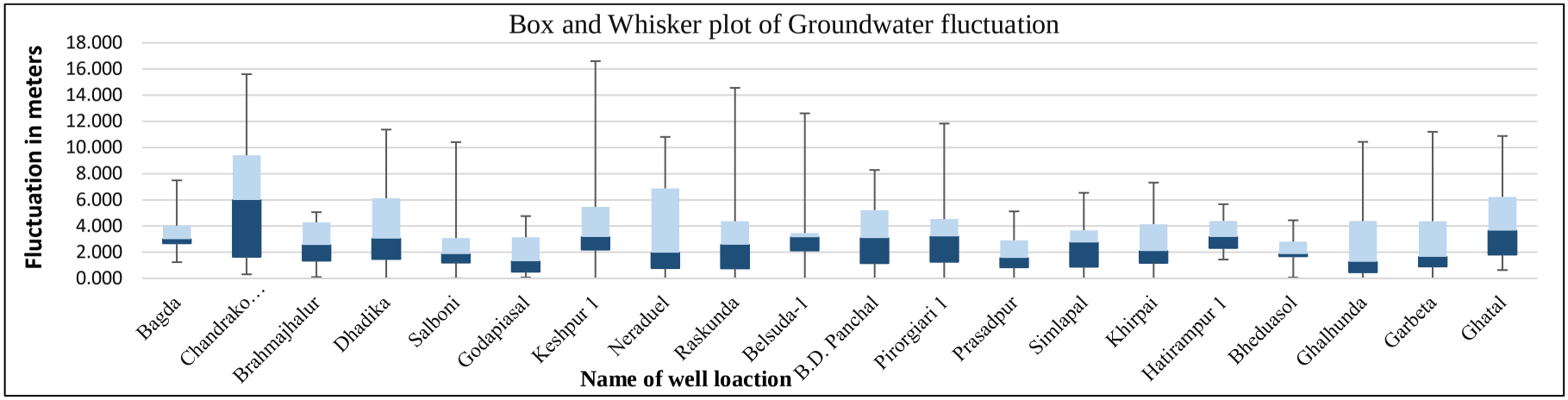

Fig. 4.39 The Box and Whisker plot of the fluctuation variation of well points

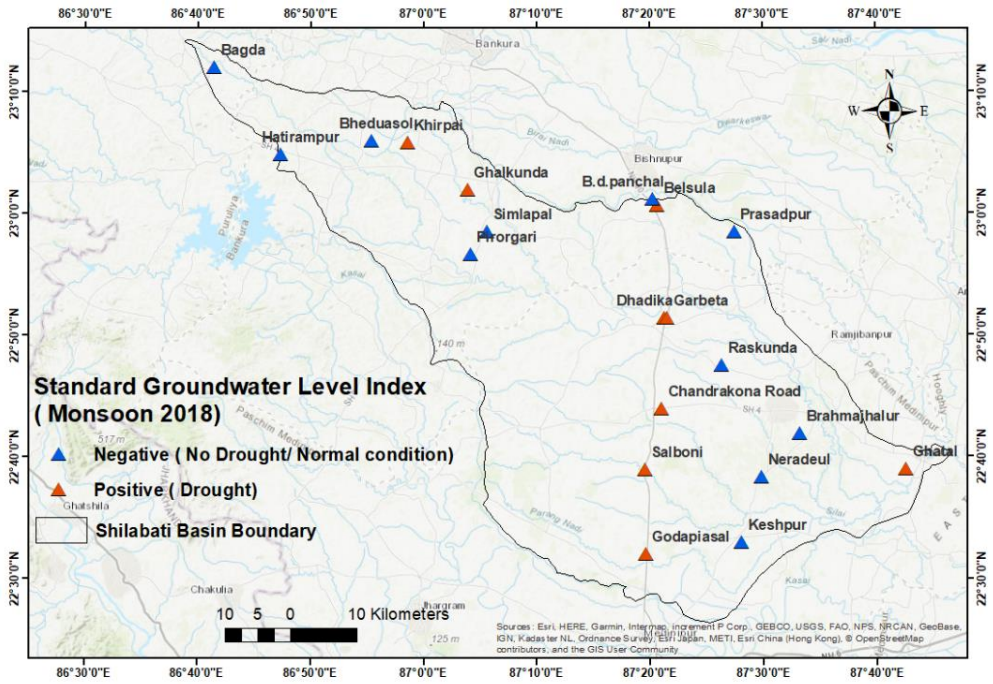

Fig. 4.40 Map showing Standard Groundwater Level Index of 2018 monsoon season

Table 4.15 Drought and non-drought years as analysed from Standard Groundwater Level Index

Well Location	Premonsoon		Monsoon		Post monsoon	
	Drought year	Non Drought year	Drought year	Non Drought year	Drought year	Non Drought year
Badga	1996-2002, 2004, 2005 ,2007,2008, 2016,2017,2018	2003,2006,2009,2015	2005,2010,2012,2013,2014	1996-2004,2005,2006-2009,2011,2015-2017	2001,2006,2008-2011,2013,2014,2017,2018	1996-2000,2002-2005,2007,2012,2015,2016
Chandrakona road	1996,1999,2003-2005,2008-2010,2015,2016	1997,1998,2000-2002, 2006,2007,2011-2014,2017,2018	1998,2001,2003,2007,2009,2010,2013,2016-2018	1996,1997,1999,2000,2002,2004-2006,2008,2001-2012,2014,2015	1996-1998,2001,2006-2010,2012,2014,2016-2018	1999,2000,2002-2005,2011,2013,2015,2016
Brahmajhalur	2010-2018,	1996-2009	2005-2008,2012,2013,2015	1996-2004,2009-2011,2014,2016,2018	2008-2018	1996-2007
Dhadika	1996-2000,2002-2008 ,2016,2017,2018	2001,2009-2015	1998-2004,2006-2008,2017,2018	1996,1997,2005,2009-2016	1997,1999-2008,2014,	1996,1998,2009-2013,2015-2018
Salboni	1999,2010,2011 ,2014-2018	1996-1998,2000-2009,2012,2013	1998,2001,2003-2005,2009,2010,2013-2018	1996,1997,1999,2000,2002,2006-2008,2011,2012	2001,2006,2008-2012,2014-2018	1996-2000,2002,2005,2007,2013
Godapaisal	1996-1996, 2001-2005, 2007-2010, 2012, 2013, 2014, 2016,2017	2000,2006,2011,2015, 2018	1998,1999,2001,2003,2005, 2010,2013,2015,2017,2018	1996,1997,2000,2002,2004,2006-2008,2011,2012,2014,2016	1996,1997,2001,2206-2009,2012,2014,2017,2018	1998-2000,2002-2005,2010-2011,2013,2015,2016
Keshpur	1996-2002,2007,2001-2013, 2018	2003-2006,2008-2010,2014-2017	2003,2009,2013,2015	1996 -2002,2004-2008,2010-25012,2014,2016-2018	2002,2014,2015,2018	1997-2001,2003-2013,2016,2017
Neradeul	2004-2007,2009-2011,2013-2016, 2018	1996-2003, 2008,2012,2017	1996-1998,2002-2004,2005-2013,2017-2018	1999-2001,2005-2013,2017,2018	2007,2011-2018	1996-2006,2008-2010
Raskhunda	1996,1999,2001 ,2002,2008,2016,2018	1997,1998,2000,2003-2007,2009-2015,2017	2002,2007-2009, 2011, 2012,2015	1996-2001,2003-2006, 2010, 2013,2014,2016-2018	1997,2001,2007,2009,2011,2013,2014 ,2016-2018	1996,1999,2000,2002-2006,2008,2010,2012

Belsula	2004,2005,2008,2012,2013,2016	1996-2003, 2006,2007,2009-2011,2014,2015,2017, 2018	2010,2016,2017,2018	1996-2009,2011-2015	2005,2009,2010,2013,2014,2017,2018	1996-2004,2006,2008,2011,2012,2015,2016
B.D. Panchal	2004,2007,2009--2018	1996-2003,2005-2006, 2008	2000,2001,2003-2006, 2010,2013-2015	1996-1999,2002,2007,2009,2011,2012,2016-2018,	2002,2004,2009,2010,2012,2014-2018	1996-2001,2003,2005-2008,2011,2013
Pirorgairi	1996-2000,2003,2004,2007,2018	2001,2002,2005,2006. 2008-2017	2002,2005,2007-2010	1996-2001,2003-2004,2006,2011-2018	2005,2008,2010-2012,2016,2017	1996-2004,2006,2007,2009,2013-2015,2018
Prasadpur	1996,1998-2002 ,2005,2006,2016,2017,2018	1997, 2003,2004, 2007-2015	1998-2002, 2004, 2005,2007,2010, 2014,2015	1996,1999,2002-2004,2006-2008,2011,2012,2016-2018	1997,2001,2004,2005,2006,2009,2010,2012,2014,2016,2017,2018	1996,1997,2000,2002,2003,2007,2008,2011,2013,2015
Simlapal	1996-1999,2001-2003.2005,2008,2012-2014	2000,2004,2006,2007, 2009,2010,2011, 2015-2018	1997,1998,2000,2001,2005,2009,2010,2012,2014,2015	1996,1999,2002-2004,2006-2008,2011,2013,2016,2018	1996,1997,2001,2002,2008-2012,2014,2016-2018	1999-2000,2003-2007,2013,2015
Khirpai	2003-2013,2017,2018	1996-2002,2014-2016	2010-2013,2015-2018	1996-2009,2014	2006-2011,2013-2017	1996-2005,2012,2018
Hatirampur	2009-2011.2013-2018	1998-2008,2012	2005-2007,2010-2013	1996-2004,2008,2009,2014-2018	2006-2018,	1996-2005
Bheduasol	1996,1999-2003,2006-2008,2015-2019	1997,1998,2004,2005, 2009-2014,2018	1996,1998-2001,2003-2006,2009-2013	1997,2002,2007,2008,2014-2018	2000,2006,2007,2009,2010,2011,2017,2018	1997-2001,2003-2005,2008,2012-2016
Ghalkunda	1999-2001,2004-2006,2008,2011-2013,2016	1996-1998, 2002, 2003, 2007, 2009,2010,2014,2015, 2017,2018	1998,1999,2002,2005,2007,2009,2010,2013,2017,2018	1996,1997,2000,2001,2003,2004,2008,2011,2012,2014-2016	2005-2007,2009,2010,2012-2014,2016-2018	1996-2004,2008,2011,2015
Garbeta	2004-2006,2010-2017	1996-2003,2007,2009	2005,2009,2013,2017,2018	1996-2004,2006-2008,2010-2012,2014-2016	2007-2012,2014-2015	1996-2006,2003,2016
Ghatal	1999,2005,2010,2011,2013-2018	1996-1998,2000-2004,2006-2009,2012	1999-200,2010-2012,2014-2018	1996-1998,2001-2009,2013	2000,2003,2014	1996-1999,2001,2002,2004-2013,2015-2018

4.2.5.6 Identification of Groundwater Drought Years using Standard Groundwater Level Index

One of the natural disasters that results in the loss of life and economic destruction is drought (Tan et al. 2020). Now a days groundwater crisis has become a global problem. Drought respective of groundwater is a need of concern as it is one of the fresh water reserves and an important source of drinking source for people. Due to climate change a deficit in precipitation can be reflected in water crisis particularity in groundwater. Analysis of the hydro-geological drought using groundwater level data helps in stabilizing all the ecosystem services (Krogulec, 2018). Here groundwater drought has been analysed using Standard Groundwater Level Index (SGWI). SGWI has been calculated for year 1996-2018 of each of the wells for three seasons. It is not possible or feasible to graphically represent the calculated data of each to present SGWI within the manuscript. The identified drought and non-drought year have been given in tabular format (Table 4.15). In pre-monsoon periods wells like Dhadika, Godapaisal, Keshpur, Chandrakona have more drought years, in monsoon well location like Prasadpur, Simlapal, Raskhunda has greater drought years where as in post monsoon Simlapal, Bheduasol, Neradeul has a higher frequency of drought years. The identification of drought years along with the trend analysis will help in micro-watershed conservation served by the water source locations. In 2018 (Fig.4.40) the wells located in the lower middle section faced groundwater drought in terms of lowering of the water level. This section of the basin experience high temperature variations and uneven distribution of rainfall all-round the year. According to Ghosh (2019), the chances of extreme drought attack are more prone to the western degraded plateaus comprising parts of Puruliya, Bankura and West Medinapore districts of West Bengal and some parts of Rarh Bengal. Beside the climate anomalies these wells are mainly located near the settlement centre where the current anthropogenic activities are leading to the poor recharge. In a region of rapid urbanization and scarce surface water, detailed investigation of the effects of land use and land cover on groundwater recharge is needed (Pan et al. 2011). Fewer studies have been conducted on the regional as well as global characterization of the groundwater drought and its regular monitoring and it is also new to this study area.

4.2.6 Conclusion and Recommendations

The present study provided the results of the groundwater vulnerability in a river basin of West Bengal, India in context climate change and extensive anthropogenic activities. The basin is dominated by agricultural practice but in the recent years production has been decreasing because of a deficit in precipitation and decline in the groundwater level. The study has been conducted in Shilabati river basin of West Bengal, India located at the extension of Chotonagpur plateau. A number of statistical techniques like descriptive test statistics, Mann Kendall trend test, cluster analysis and SGWI has been applied to highlight the scenario. The land use and land cover analysis made here showed a decrease in dense forest cover from 10.88 % in 1989 to 4.93% in 2018. Such decrease in the forest cover increases bare land and reduces the water holding capacity of soil which increases greater runoff and poor aquifer recharge. The groundwater level trend has also been observed using Mann Kendall test statistics where 25 % of the wells showing declining trend in monsoon period, 45% showing declining trend in pre-monsoon period and 60% in case of post-monsoon period. Extensive pumping of the sub-surface water and drying of the river beds is the main cause of such decline. From the field level study, the villagers also informed about the water scarcity in the recent years due to lack of precipitation which eventually led to the decline in groundwater level

and drying of surface water bodies and giving a threat to food security. Well location at Chandrakon Road has been showing higher fluctuation about 6.305m which is mainly due to the effect of land use and land cover change and alteration of precipitation dynamics. An increase in the settlement cover here has led to increase in built-up area encouraging overland flow and replenishment of the aquifer takes longer time. Standard Groundwater Level Index has been calculated to observe the groundwater drought within the study area. Well located at the populated centres are showing positive values that is greater deviation from the normal depth and is signifying more decline in water level. In 2018 the wells located at the lower middle section mainly faced groundwater drought. Every year this river basin faces extreme meteorological, hydrological and agricultural drought in the month of April and March which sometimes extends to the month of June due to the delayed onset of monsoon. Discharge from the wells does not reach the satisfactory level and the majority of the wells goes dry during the hot and humid summer season (Dey et al. 2018).

4.2.7 Limitation and Future Work

Researchers may encounter challenges due to the limited availability of historic groundwater data. There is also the possibility that the quality and accuracy of the available data may vary, resulting in potential inaccuracies in the results of the study. More detailed study to explore the cumulative effects of the trend and pattern of the groundwater quantity and quality is essential. The outcome of the study can be an elementary step to improve the sustainable groundwater management strategy. To mitigate such groundwater problem Managed Aquifer Recharge (MAR) and aquifer yield testing can be the important solution together with rainwater harvesting techniques. Continuous monitoring of groundwater level and quality is also important to protect and increase the stock of water in the aquifer layers and will be focused on the future studies.

Chapter5

Modelling Ground and Surface water Interaction using Machine Learning and MIKE FEFLOW Model

5.1 Identification of Groundwater Potential Zone using Hydrogeophysical Investigation, Machine Learning and MCDM Techniques

5.1.1 Introduction

Over the last few decades, precipitation totals have been decreasing and the distribution of storm events has been irregular, which has resulted in a greater dependence on groundwater. This reliance was exacerbated by the growing population, which led to more wells being drilled to meet the growing agricultural and domestic water demand (Ouatiki et al. 2022). It is estimated that groundwater supplies 80% of the nation's drinking water in rural areas, 50% of the nation's urban water needs, and over 50% of the nation's irrigational demand (National Remote Sensing Agency, 2008). The estimated depletion of groundwater in the world between 1900 and 2008 was summed up as 4,500 km^3, which corresponds to a sea level rise of 12.6 mm (more than 6% of the total) (Konikow, 2011). Since 1950, groundwater depletion has increased significantly, with a maximum rate in the last decade (2000–2008), with 145 km3/yr on average (or 0.40 millimeters of sea level rise per year, or 13% of 3.1 millimeters per year during this recent period). Groundwater depletion contributed to the global sea level by 0.035 millimeters per year in 1900, 0.57 millimeters per year in 2000, and is projected to be 0.82 millimeters per year by 2050 as a result of groundwater depletion (Wada et al. 2012). According to recent studies, India's Indo-Gangetic plains have seen a drastic drop in groundwater levels. The alarming depletion rate is caused by a dual combination of reduced groundwater recharge and extensive abstraction due to a variety of hydrogeological and human-induced reasons (Joseph et al. 2022). There has been a decrease in groundwater levels in several states of India between 1 meter per year to 3 meters per year, which has increased the cost of well drilling and pumping (Devineni et al. 2022). Considering these challenges, understanding the groundwater potential zone is crucial for sustainable management and optimal water resource planning. Additionally, such valuable information is essential in planning socio-economic development and environmental sustainability, particularly in countries where a significant portion of their Gross Domestic Product is derived from agricultural production, like India, Bangladesh, Pakistan, etc. (Chand, 2022). A number of factors determine the movement and appearance of groundwater, including geology, geomorphology, fractures and lineaments, drainage, land use, soil, climate conditions, and their mutual relationship (Elvis et al. 2022). Researchers have reported that such parameters are the most critical and commonly used variables in the estimation of groundwater potential (Ponnusamy and Elumalai, 2022). These secondary databases, which can be used to support groundwater water resource determinations by providing various thematic details, are often not readily available and are inaccurate (Kumar et al. 2016). Depending on the specific data layer, DEM-derived data layers may provide low classification accuracy in most cases (Yu et al. 2012). Data

collection and output generation using remote sensing and secondary information are subject to uncertainty due to a variety of factors, including sparse statistics, noise and limitations of remote sensing sensors used for data collection (Shirmard et al. 2022). According to Mosavi et al. (2021), a major limitation of their study was the absence of comprehensive maps of the soil cover in the study area. In most cases, geomorphological/geological features are misinterpreted and require confirmation via high-resolution satellite images (Pani et al. 2016). The current study thus uses primary field data to identify the potential groundwater zone, based on geophysical investigation and actual soil characteristics to ensure authenticity. It is therefore imperative to know the aquifer conditions, including their geometrical and hydraulic parameters, to effectively explore, exploit, and manage groundwater resources (Oli et al. 2022; Lge et al. 2022). These aquifer hydraulic parameters include hydraulic conductivity, transmissivity values, water-holding capacity, moisture content, etc. An alternative method for estimating the hydraulic properties of aquifer systems is vertical electrical sounding (VES), which is cost-effective and can be used before drilling. By incorporating secondary geoelectrical parameters, geophysical studies can overcome the above uncertainties and create more realistic results. Anisotropy, transverse resistance, longitudinal conductance, and average longitudinal resistivity, are the secondary geoelectrical characteristics that can be determined from the main geoelectrical parameters (Sankar et al. 2023; Metwaly et al. 2021). The advantage of acquiring these parameters is that they are nonlethal to the subsurface, cost-effective, take less time, and are less ambiguous in interpretations (Todd, 1980). Thus, the novelty of this research lies in the application of the field-based data as demonstrated in Table 5.1.

Table 5.1 Comparative analysis of the studies related to groundwater potential zone mapping/modelling

Methodological reference	Models used in Groundwater potential zone				Selection of conditional parameters for identification of GWPZ			Validation technique/parameter used
	MCDM/Fuzzy MCDM and GIS	ML and Fuzzy MCDM both and GIS	ML and GIS	Statistical models	Field based factors	Secondary data-based factors	Remote Sensing based factors	
Anh et al. 2023	×	×	√	×	×	√	√	ROC and AUC/ Spring locations
Kundu et al. 2023	×	×	√	√	×	√	√	ROC and AUC/ Groundwater yield
Choudhary et al. 2022	√	√	√	√	×	√	√	ROC and AUC/Groundwater level
Goswami and Ghosal, 2022	√	×	×	√	×	√	√	ROC and AUC/Groundwater level
Rahaman et al. 2022	√	×	×	×	×	√	√	ROC and AUC/ Perennial water bodies
Pande et al. 2021	√	×	×	√	×	√	√	ROC and AUC/Groundwater level
Kumar et al. 2021	√	√	×	×	×	√	√	ROC and AUC/ Groundwater yield
Akbari et al. 2021	√	×	×	×	×	√	√	ROC and AUC/Groundwater level ×
Ahmed et al. 2021	√	×	×	√	×	√	√	ROC and AUC/Groundwater level
Jesiya and Gopinath, 2020	√	×	×	×	×	√	√	×
Panahi et al. 2020	×	×	√	×	×	√	√	ROC and AUC/Groundwater level
Husen et al. 2020	×	×	√	×	×	√	√	×
Arabameri et al. 2019	√	×	×	√	×	√	√	ROC and AUC/ Groundwater yield
Current study	√	√	√	×	√	×	×	ROC, AUC and MCA/Groundwater yield

5.1.2 Research Gap and Novelty of the Work

In recent years, multi-model approaches and ensemble models have become effective in understanding vulnerability, susceptibility, potentiality, hazards, and so on. (Das et al. 2022; Shirmard et al. 2022; Mosavi et al. 2021; Elvis et al; Pal et al. 2020). A variety of machine learning algorithms, including XgbooST (Barzegar et al. 2021), RF (Tasan et al. 2023), Naive Bayes (Pham et al. 2021), and MCDM techniques like Fuzzy AHP (Doke et al. 2021; Das et al. 2022), have not been extensively applied for the detection of groundwater availability under specific topographic and hydrological conditions. These two methods for predicting groundwater potential zones have never been compared well in previous research. Further, the performance of these ML models has never been explored in the river basins of West Bengal, India, where the secondary database is very scarce. Each of the models aims to reduce the economic cost of GW potential mapping by finding the most economical and accurate methodological framework. Additionally, MLAs' and Fuzzy AHP's prediction rates are very accurate, in part due to their capacity to include a wide range of predictors and their ease in constructing appropriate connections among them (Malllick et al. 2021; Singha et al. 2021). This study, therefore, introduces a novel methodological framework to compare fuzzy MCDM and machine learning techniques. Machine learning models were trained and tested on existing well yield data, and groundwater potential maps were created based on predicted well yield classes. The proposed framework uses fuzzy-AHP to assign weights to the different conditions, and its accuracy was compared to that of a machine learning approach. To make the comparison, 13 influencing factors soil permeability, porosity, bulk density, hydraulic conductivity, transmissivity, soil moisture content, water holding capacity, fracture porosity, the resistivity of formation, anisotropy, transverse resistance, longitudinal conductance, and longitudinal resistivity were considered and made an efficient validation using ROC, AUC and MCA approaches.

5.1.3 Objective of the research work

Based on the above the research gap the main objective of the study includes (a) estimation of the Hydrogeophysical parameters and soil characteristics using Geophysical survey and soil sampling; (b) identification of the groundwater potential zone using Machine learning algorithms and Fuzzy MCDM techniques and their comparative analysis and (c) model validation and testing using ROC and AUC curve and correlation coefficient using MCA framework.

5.1.4 Area of Investigation

The river basin is located between the transition zone of Western Plateau and Eastern plain with large textured sandy soil of granitic gneiss and schist series at the upstream section with laterite soil in the middle and alluvial soil at the downstream section deposited under inter fluvial condition (Sarkar et al. 2022) (Fig.5.1). In the upstream section undulating mountainous characteristics of the soil impedes water to percolate unground leading to the decline in groundwater level and depletion simultaneously (Mahala, 2021). As far as physiography is concerned, it is characterized by a dissected pedimental landscape with skeletal soil and lateritic terrain, both these factors are contributing to the region's barrenness and unproductiveness (Bera and Das, 2021; Sharma, 2009). Gneiss and schist from the Archean period of this basin are characterized by infertile and immature soil, vast barren land and rock outcrops. A broad range of rock types are found in the basin, including granite, gneiss, quartzite, and schist

which are prevalent mostly upstream and in the upper middle section. According to our geophysical investigation, groundwater is mostly tapped through open wells (2-15 mbgl) in such areas and through cracks and joints (Fig.5.2). During the Holocene period, vast amounts of alluvium and laterite were deposited around the middle section of the basin. The primary and secondary laterite is commonly found within this section (Ghosh and Kundu, 2022). The massive upper interfluvial undulating surface covered with lateritic materials in this section of the basin is subjected to gully and hill erosion (Goswami and Ghosal, 2022). Groundwater recharge is also affected by this phenomenon, resulting in high overland flow. A near surface aquifer is located in this section where the ground water table depth varies between 4.5-22 mbgl (Fig.5.3) (CGWB, 2022). The downstream section includes two major geological units; the Lalgarh formation, composed of granite pebbles, quartz, and sometimes lateritic materials (Das and Pal, 2019). The second formation is the Sijua formation, with low slopes, soft unconsolidated sediments and a high proneness to flooding. Along the floodplains of the river, recent or younger alluvium has been deposited. Clay-sand aquifers are present at depths of 10-20 meters, but they provide less water due to a high proportion of fine-grained sands (Fig.5.4). Therefore, in a favorable location, the ideal fabrication of a dug well, tube well, and submersible well will yield a good quantity of water throughout the entire year, transforming the basin from dehydrated to hydrate and ensuring greater water, energy and food security as an alternative to rainfall-led subsistence agriculture. In this case, a comprehensive identification of groundwater potential zones is necessary.

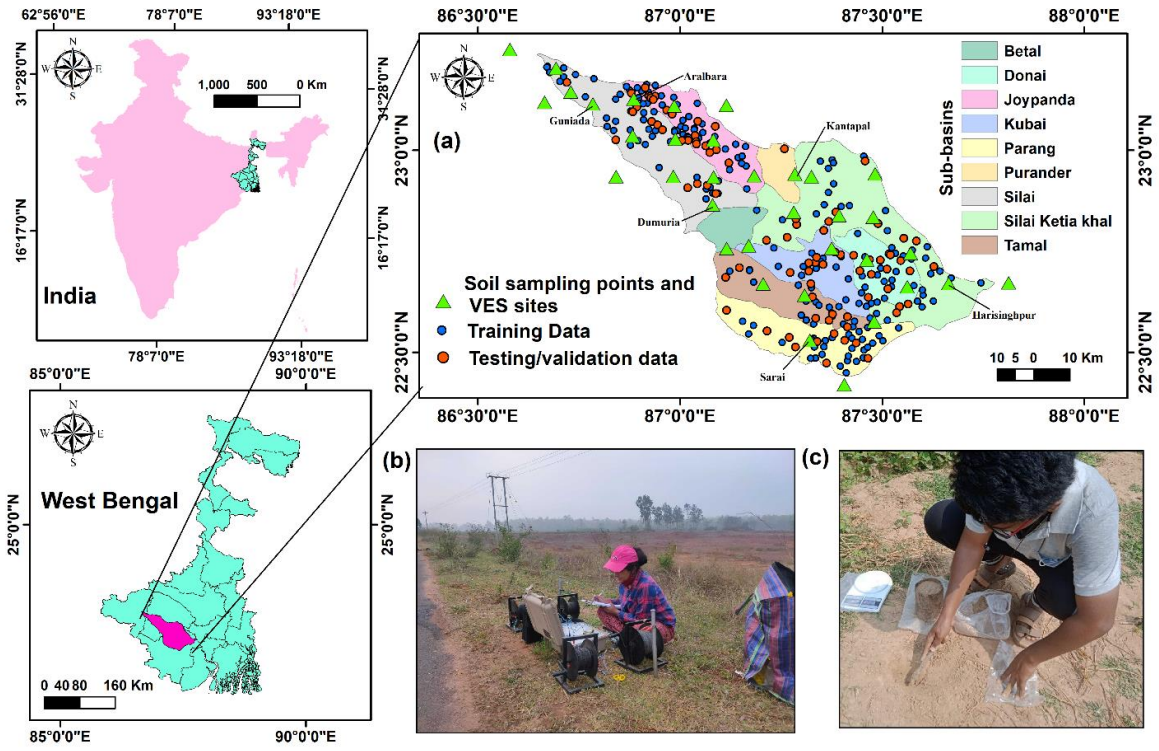

Fig. 5.1 Location of the study area with soil sampling and geophysical investigation sites

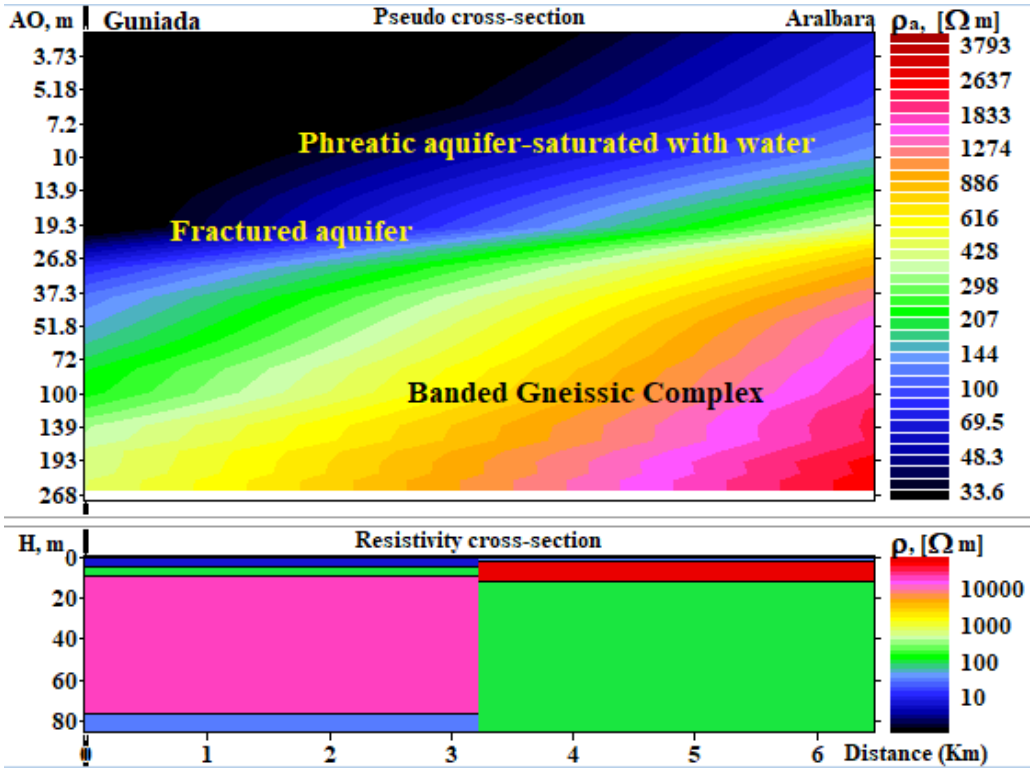

Fig. 5.2 Pseudo-sections and resistivity cross section of Guniada and Aralbara site (Upstream section)

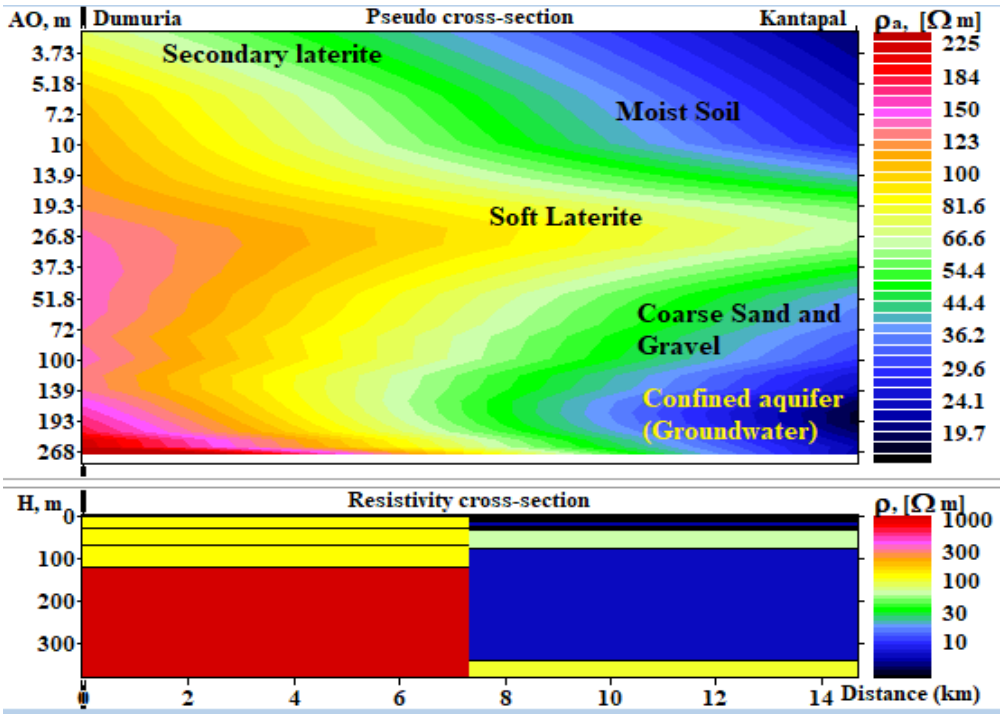

Fig. 5.3 Pseudo-sections and resistivity cross section of Dumuria and Kantapal site (Middle stream section)

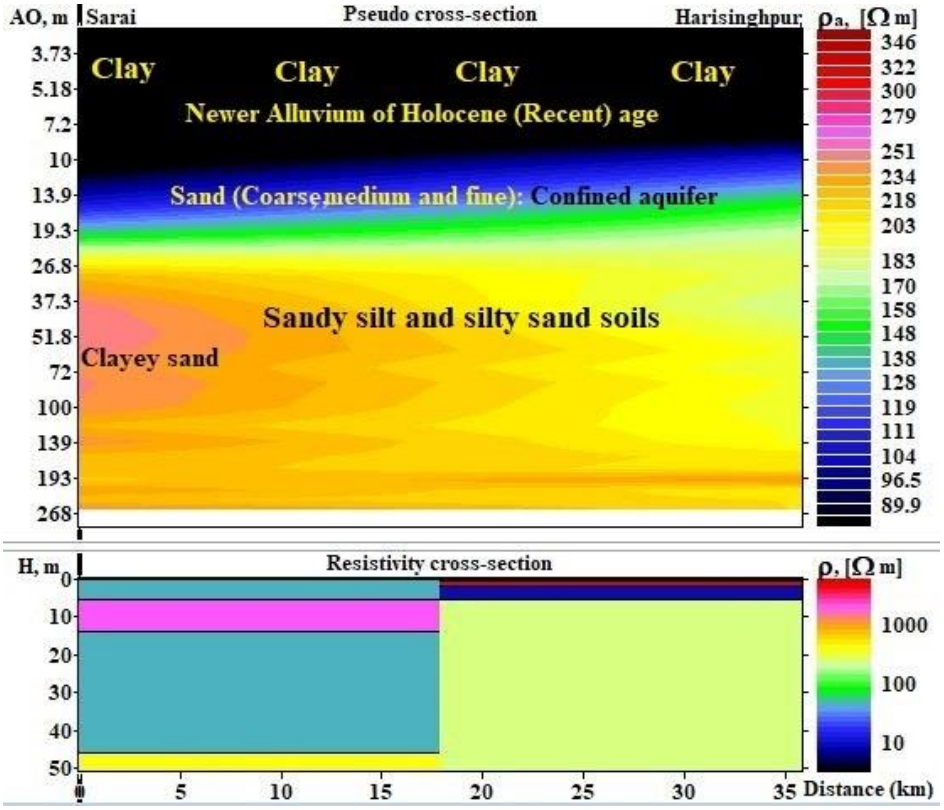

Fig. 5.4 Pseudo-sections and resistivity cross section of Sarai and Harisinghpur site (downstream section)

5.1.5 Research Design and Methodology

5.1.5.1 Field investigation: Vertical Electrical Resistivity Soundings (VES) and soil sampling

Using Schlumberger electrode arrays (Fig.5.1), groundwater availability was geophysical investigated at 34 village locations. In this study, the groundwater prospective areas were identified based on VES data collected by IGIS Microprocessor based Signal Enhancement Resistivity Meter Model SSR-MP1-SL in order to estimate conditioning factors. Schlumberger's arrangement provides a number of practical, allegorical, and operational, advantages. To increase the depth of the electrical current penetration, current electrodes and potential electrodes were gradually moved apart on each side of the investigation sites as per the standard plan of action (Sankar et al. 2022). A majority of the measurements were conducted along village mud roads/agricultural fields, with electrodes moved in a straight line. The Schlumberger array of current electrodes (A and B), potential electrodes (M and N) and the apparent resistivity (ρa) is calculated using the following algorithm (Bhatnagar et al. 2022) (Eq. 5.1).

$$\rho a\ (\Omega m) = 2\ \pi\ R^* [\{(AB/2)\} + (MN/2)\}^*\{(AB/2) - (MN/2)\}]/MN \qquad (5.1)$$

Where, R (Ω) is the Resistance obtained from ΔV/I; I is the current introduced in the earth material; V is the Voltage; AB is the distance between A and B current electrode and MN is the distance between M and N potential electrode.

For the fabrication of the sounding curves, a bi-logarithmic graph is used in which data is plotted showing the apparent resistivity (a) and the half electrode spacing (AB/2) respectively. This estimate of resistivity is used to distinguish layers between the different subsurface materials since it depends on the various physical properties of the lithological units and the type/amount of water present in the pore spaces (Mahmud et al. 2022). In order to obtain the Dar-Zarrouk parameters, a computer-based 1-D automatic modeling scheme IPI2WIN program (lite) was used to interpret the sounding curves and to prepare pseudo cross section and resistivity cross sections (Fig. 2-4) (Naidu et al. 2021). Using the software, a minimization of the RMS error between the measured and predicted resistivity values was achieved between (5-10%) for the input resistivity data. In addition, soil sampling and exploration were conducted by core drilling from a depth of 15-30 cm based on the ground surface and weighted at field. To measure the bulk density of soil, a cylindrical core cutter with a diameter of 10 cm and a height of 12.7 cm was used. Bulk density was calculated by dividing the soil mass by the volume of the core cutter. A sand replacement method was used for soils containing a high percentage of gravel and hard rock. The water displacement method has been applied to lump samples of cohesive soil. A core cutter method was used to determine in-situ bulk density for fine-grained cohesive soils without stones, and approximately one kilogram of soil was packed in zip lock pockets and transferred to the laboratory for further analysis. All VES and soil sampling locations were recorded using a global positioning system (GPS) receiver (Etrex 10 Garmin) for further analysis in ArcGIS 10.4 and Origin 2017 software.

5.1.5.2 Estimation of Dar-Zarrouk and hydrogeological parameters

An assessment of the groundwater prospect for an area can be better performed by using geoelectrical field curves that frequently indicate the character of consecutive lithological succession in a river basin (Alarifi et al. 2022). Based on the above discussed approach, the interpreted resistivity data and the curves from the survey demonstrate the presence of multi-geoelectrical layers in different geological sections of the river basin. By using these curves, thematic maps were created in ArcGIS platform expressing the thickness of surface soils, fractured and deep weathered zones (Agyemang, 2022). The Dar-Zarrouk attributes, including longitudinal conductance (SC), longitudinal resistance (ρ_t), transverse resistivity (ρ_t), transverse resistance (TR), coefficient of electrical anisotropy (λ), resistivity of formation (ρ_m), fracture porosity (φf), reflection coefficients (r) were computed based thickness ($fi_1, fi_2, fi_3, \ldots fin$) and resistivity ($\rho_1, \rho_2, \rho_3 \ldots \rho_n$) of the N layer as obtained from geophysical investigation. The hydraulic properties (Hydraulic conductivity and transmissivity) of the study area were also determined using the above primary aquifer parameters. All the conditioning factors based on the geophysical investigation have been calculated using the following equation (Eq. 5.2-5.11) (Nugraha et al. 2023; Nwachukwu et al. 2019; Lge et al. 2022; Naidu et al. 2021).

(i) Longitudinal resistivity (ρ_l)= $\frac{T}{H} = \frac{\sum h_i}{\sum(\frac{h_i}{p_i})}$ (5.2)

(ii) Longitudinal conductance (SC)=$\sum_{i=1}^{n}(\frac{h_i}{p_i}) = \frac{h_1}{p_1} + \frac{h_2}{p_2} + \frac{h_3}{p_3} + \cdots \frac{h_n}{p_n}$ (5.3)

(iii) Transverse resistivity (ρ_t) = $\frac{T}{H} = \frac{\sum(h_i.p_i)}{\sum h_i}$ (5.4)

(iv) Transverse resistance (TR) =$\sum_{i=1}^{n} h_i.p_i = h_1.p_1 + h_2.p_2 + h_3.p_3 \ldots\ldots h_n.p_n$ (5.5)

(v) Coefficient of electrical anisotropy (λ)= $\sqrt{\frac{\rho_t}{\rho_I}}$ (5.6)

(vi) Resistivity of formation (ρ_m) = $\sqrt{\rho_I TR}$ (5.7)

(vii) Fracture porosity ((φf) = $\frac{3.41\times10^4(N-1)(N^2-2)}{N^2C\,(\rho_{max}-\rho_{min})}$, (5.8)

(viii) Reflection coefficient (r)= ($\frac{\rho_n-\rho(n-1)}{\rho_n+\rho(n-1}$) (5.9)

(ix) Hydraulic Conductivity (K) m/day =386.40 $R_{rw}^{-.93283}$ (5.10)

(x) Transmissivity (T_r) = KσT=$\frac{KSC}{\sigma}$ = Kh (5.11)

Where, N is the vertical anisotropy corresponding to the coefficient of electrical anisotropy (λ), C is the specific conductance of groundwater (371 µS/cm), ρ_{max} and ρ_{min} are the maximum and minimum apparent resistivity (Ωm) respectively and σ = electrical conductivity (inverse of resistivity).

5.1.5.3 Laboratory experiments and soil hydraulic parameters

The soil samples were pretreated by removing plant debris and small particles and then oven dried at 105°C for 24 hours before being analyzed. Upon preparation, soil samples were passed through a mechanical sieve from 11.2 mm to 38µm following the Indian Standard code: 1498-1970. Additionally, hydrochloric acid was applied to eliminate inorganic carbon and to obtain accurate results. Using the hydrometer method and the above mechanical sieve, the mean percentage of sand, silt, and clay particles was determined after preparing the samples. Soil permeability is a function of grain size distribution, which was typically determined by estimating equivalent particle diameters D_{10}, D_{17}, D_{20}, D_{30}, D_{50}, D_{60}, D_{75}, and D_{90}. The coefficient of curvature (Cc) and the coefficient of uniformity (Cu) are also commonly used indices. A curvature coefficient describes the concavity (or curve) of a grain size distribution curve, and a uniformity coefficient is defined as the ratio between D_{60} and D_{10}. In addition to particle shape and arrangement, permeability is also affected by void ratio and interconnectivity between voids (porosity). To measure the water-holding capacity in the laboratory, filter papers, funnels, and two measuring cylinders were used. Finally, the moisture content of the soil was determined by oven drying technique. To calculate soil hydraulic parameters, the following empirical equations were used (Shamsuddin et al. 2019; Yu et al. 2013) (Eq.5.12-5.18)

I. Bulk density (g/cm^3) = Soil weight (g) / Soil volume (cm^3) (5.12)

II. Curvature coefficient (Cc)= $\frac{(D_{30})^2}{(D_{10})(D_{60})}$ (5.13)

III. Coefficient of uniformity (Cu) =$\frac{D_{60}}{D_{10}}$ (5.14)

IV. Porosity (n) = $\frac{V_v}{V}$ × 100% (5.15)

V. Permeability by Kozeny-Carman (1956) (m/day) = $\frac{g}{v}\times 8.30\times10^{-3}[\frac{n^3}{(1-n)^2}]d_{10}^2$ (5.16)

VI. Moisture content (%) = $\frac{w_1-w_2}{w_2}\times 100$ (5.17)

VII. Water holding capacity= $\frac{v_1-v_2}{w_1}\times 100$ (5.18)

Where, V_v is the volume of void; V is the total volume of the soil; g is acceleration due to gravity; v is the kinematic viscosity; W_1 of wet soil; W_2 weight of dry soil; V_1 ml of water poured into the funnel and amount of water (V_2) collected in the measuring cylinder.

5.1.5.4 Development of groundwater potential model based on field investigation

5.1.5.4.1 Well inventory and model setup

The inventory yield data for the wells were obtained from the Public Health Engineering Department, Government of West Bengal, India. In order to train the machine learning models, wells with flow rates greater than 50 LPM (liter/minute) are regarded as having good groundwater potential (1), and wells with flow rates less than 50 LPM as being poor (0). In total, 285 wells yield data were collected. The points were split into training and validation points based on a proportion of 70:30 on the ArcGIS 10.4 platform.

The Feature Importance Plot and built-in feature function were applied in R Studio to calculate the importance of the above calculated conditioning factors for Groundwater Potential Zone (GWPZ). In the first step, we used the Inverse Distance Weighting (IDW) interpolation technique to generate thematic maps of all 13 field-calculated conditioning factors. Using ArcGIS conversion toolbox, the conditioning factors were resampled into the spatial resolution of 30 x 30 m. Within the ArcGIS platform, the 'extract multi-values to points' tool under the spatial analyst toolbox was applied to extract values of conditioning factors. CSV files containing the extracted values of the points were imported into R software for machine learning applications. After applying different machine learning models to the training set, ROC curves and AUCs were generated based on the predicted values as plotted and calculated in Origin software using testing/validation datasets. In the final step, the predicted values from the trained models were imported into ArcGIS for further analysis and final potential map preparation. Correlation analysis was performed using the collected groundwater level data for the year 2021-2022 in order to validate and to prove the accuracy of the models.

5.1.5.4.2 Machine learning based models

a. Extreme gradient boosting (XGBoost)

In conjunction with gradient boost trees, Extreme Gradient Boosting (XGBoost) is an ensemble learning approach. This algorithm was proposed by Chen and Guestrin (2016) as a further improvement on gradient-boosting decision trees (Li et al. 2022). As part of the XGBoost model, several weak learners (each tree) are combined to create a strong learner (Ali et al. 2023) through additive learning. Each XGBoost decision tree must depend on the other trees, and the model built for each upcoming tree must be based on the most recently calculated residuals or errors from the previous tree. A sample's expected value is thus determined by adding the values of the leaves in each tree. XGBoost incorporates continuous addition of regression trees into the prior model, and then uses the CART ensemble (classifier and regression tree) to fit the residuals of the prior model (Jamei et al. 2022). In order to prevent over fitting, it has several regularization features. XGBoost's final prediction is comprised of a weighted sum of the weighted contributions of each decision tree. Based on Kilinc et al.'s (2023) findings, the XGBoost model was highly recommended for use with hydrological datasets. The whole model was run using the R statistical software package "xgboost".

b. Random Forest

In this study, we used random forest model to identify the groundwater potential zone in the Shilabati river basin. This algorithm captures nonlinear dependencies through regression trees (continuous data) or enhanced classification trees (discrete data) and is fast to process, performs well, and can easily be optimized with minimal

input (Tyralis et al. 2019). By using different data subsets, different decision trees are developed and trained using bootstrapping. In random forests models, the primary hyper parameters are mtry (the number of variables per tree node) and 'ntree' (the number of trees). The cross-validation error was minimized using a fivefold cross-validation procedure, and 'mtry' was suggested to be used as two thirds of the number of predictors (Giri et al. 2023).In several studies, the method was shown to be capable of ranking the important variables/conditioning factors at the training and testing stages (Kathirvelu et al. 2023; Guo et al. 2023).A significant benefit of the RF ML algorithm is that there is no need to perform cut processing, a large number of trees can be considered, and automatic feature selection can be performed. Tyralis et al. 2019 provided a detailed description of RF and its application in GPM. In addition to its ability to manage large datasets with different levels of dimensionality, random forest models do not require any hypotheses regarding the explanatory variables or response variable (Ruidas et al. 2022). This model was run using the R statistical software package "Caret". The posterior probabilities ($P_t(C|f)$ for a tree of each class was estimated using the following algorithm (Eq.5.19) (Miraki et al. 2018)

$$(P_t(C|f_j) = \frac{1}{T}\sum_{t=1}^{T}((Pt(C|f) \qquad (5.19)$$

In a training dataset f, the posterior probability ($Pt(C|f)$ is the probability that a selected case belongs to class Ci.

c. Naive Bayes

Naive Bayesian (NB) classifiers are probabilistic graphical algorithms for classifying datasets. Constructing a probability curve for each class in the dataset is based on the Bayesian theorem. This is based on independent distributions and discretization of continuous distinct values (Pham et al. 2021). A naive Bayesian classifier assumes, in simple terms, that the absence or presence of a specific feature cannot be related to other features. NB classifiers could be trained efficiently with supervised learning frameworks relating to the precise essence of the probability model (Aburub and Hadi, 2016; Arabameri et al. 2021; Rasool et al. 2022). NB classifiers offer the advantage of being extremely simple to construct and do not require parameter estimations. To implement the Naive Bayes model, the caret package and "naive Bayes" were used in the R environment. For modeling and mapping the groundwater potential of the Shilabati River basin, let X = (x_1, x_2, ...x_n) represent a vector of independent explanatory variables. The groundwater potential ($P(Cj|x_1, ...,x_n)$) is thus estimated using the following algorithm (Pham et al. 2021) (Eq.5.20).

$$P(Cj|X) = \frac{P(C_j)P(X|C_j)}{P(X)} \qquad (5.20)$$

5.1.5.5 Fuzzy set theory-based models

The traditional AHP is accompanied by uncertainty and unclear determination. Therefore, it can't accurately reflect human thinking. Unlike conventional AHP, the fuzzy logic algorithm is based on advanced logical principles (Shao et al. 2020). In terms of ambiguity, vagueness, and imprecision, fuzzy logic is remarkably easy to employ in drawing specific conclusions from scientific information (Mallik et al. 2019). When spatial planning is concerned, fuzzy logic is normally used to make decisions regarding the execution of spatial objects on a map as members of a set of objects (Githinji et al. 2022). Using the Fuzzy-AHP technique, hierarchical analysis is fuzzified with fuzzy numbers, and pairwise comparisons are supervised to evaluate the Fuzzy weights (Das and Pal, 2019). A triangular fuzzy number (TFN) is used to represent the matrix element in the normalization method (Table 5.2). It is possible to avoid inaccuracy, ambiguity, and uncertainty by using TFN (Shao et al. 2020; Sener,

2023). In the current research, the extent analysis method in fuzzy AHP as formulated by Chang (1996) was applied (Halder et al. 2020).

Assume, X = {x_1, x_2, x_3…. xn} is an object set, and G = {g1, g2, g3… gn} as a goal set. According to this method, each object was considered, and each goal was assessed in terms of its extent. In order to determine the weights of conditioning factors using Fuzzy-AHP, the following steps were considered (Saha et al. 2023; Chang, 1996; Halder et al. 2020). TFNs (Table 5.2) was demonstrated as M^1_{gi}, M^2_{gi},……M^m_{gi}, i= 1, 2, 3……n where M^j_{gi} (j = 1, 2, …, m)

The first step includes the value of a fuzzy synthetic extent (Si) based on the ith object (Eq.5.22)

$$Si = \sum_{i=1}^{m} M_{gi}^{j} * [\Sigma_{i=1}^{n} \sum_{j=1}^{m} M_{gi}^{j}]^{-1} \quad (5.22)$$

In order to estimate the $\sum_{j=1}^{m} M_{gi}^{j}$, the fuzzy addition operation of the m extent analysis was done using the following Eq. (5.23)

$$\sum_{j=1}^{m} M_{gi}^{j} = \sum_{j=1}^{m} lj, \sum_{j=1}^{m} mj, \sum_{j=1}^{m} uj \quad (5.23)$$

where, l is the lower limit,m is the middle value and u is the upperlimit of the entire dataset.

In oder to obtain this equation $[\Sigma_{i=1}^{n} \sum_{j=1}^{m} M_{gi}^{j}]^{-1}$ the calculation has been performed using Eq. (5.24)

Table 5.2 Triangular Fuzzy Scale (Chang, 1996)

Linguistic scale for importance	Triangular Fuzzy scale	Triangular Fuzzy Reciprocal scale
Just equal	(1,1,1)	(1,1,1)
Equally important (EI)	(1/2,1,3/2)	(2/3,1,2)
Weakly more important (WMI)	(1,3/2,2)	(1/2,2/3,1)
Strongly more important (SMI)	(3/2,2,5/2)	(2/5,1/2,2/3)
Very strongly more important (VSMI)	(2,5/2,3)	(1/3,2/5,1/2)
Absolutely more important (AMI)	(5/2,3,7/2)	(2/7,1/3,2/5)

$$[\Sigma_{i=1}^{n} \sum_{j=1}^{m} M_{gi}^{j}] = \sum_{j=1}^{m} li, \sum_{j=1}^{m} mi, \sum_{j=1}^{m} ui \quad (5.24)$$

Now the reverse of the formula has been done using Eq. (5.25)

$$[\Sigma_{i=1}^{n} \sum_{j=1}^{m} M_{gi}^{j}]^{-1} = 1/\sum_{i=1}^{n} u_1, 1/\sum_{i=1}^{n} m_1, 1/\sum_{i=1}^{n} l_1, \quad (5.25)$$

The step 2 includes the estimation of the degree of possibility of $M_2 = (l_2, m_2, u_2) \geq M_1 = (l_1, m_1, u_1)$ and was defined as Eq. (5.26)

$$V(M_2 \geq M_1) = \sup_{y \geq x} [\min (\mu_{M1}(x), \mu_{M2}(y))] \quad (5.26)$$

The above algorithm can also be written as Eq. (5.27)

$$V\begin{cases} (M_2 \geq M_1) = 1, & \text{if } m_2 \geq m_1 \\ 0, & \text{if } m_2 \geq m_1 \\ \dfrac{l_1 - u_2}{(m_2 - u_2) - (m_1 - l_l)} & \text{otherwise} \end{cases} \quad (5.27)$$

The 3rd step includes the formulation of possible degree for convex fuzzy number to be greater than k convex fuzzy numbers Mi = (i= 1, 2, 3… k) using the following Eq. (5.28)

$$V= (M\geq M_1, M_2\ldots\ldots Mk) = (V [(M\geq M_1) \text{ and } (M\geq M_2) \text{ and } (M\geq M_k)] = \min V (M\geq M_i), \quad i= 1, 2, \text{ and } 3\ldots..k \tag{5.28}$$

$$\text{It can be assumed that the equation (5.29), } d_1 (A_1) = \min V (S_1\geq S_k) \tag{5.29}$$

For k = 1 , 2, ……., n; k≠I, and thus the weight vector can be obtained by following the Eq. (5.30)

$$W' = (d' (A_1), d' (A_2) ,\ldots\ldots., d' (A_n))^T \tag{5.30}$$

Where the Ai = (1, 2, 3,…….,n) are m elements.

In the last step the normalized weight was estimated by using Eq. (5.31)

$$W' = (d (A_1), d (A_2)\ldots\ldots d (A_n))^T \tag{5.31}$$

Where W is a non-fuzzy number.

The pairwise comparison matrix and the respective calculated weights of all the thirteen parameters using the above equations has been shown in Table 5. A1.

5.1.5.6 Estimation of Groundwater Potential Index (GWPI)

To calculate the groundwater potential index, we used a weighted linear combination method based on the weightage estimated from the Fuzzy AHP extent analysis method (Table 5. A2). In the GIS environment, the weights of conditioning factors and sub-factors/classes were linearly combined as per Eq. 5.32.

GWPI= *Longitudinal conductance * Weight + Longitudinal Resistance * Weight + Transverse Resistivity * Weight + Transverse Resistance * Weight + Coefficient of Electrical Anisotropy * Weight + Resistivity of Formation * Weight + Fracture Porosity * Weight + Reflection Coefficients * Weight + Hydraulic Conductivity * Weight + Transmissivity * Weight + Bulk Density * Weight + Porosity * Weight + Permeability * Weight + Soil Moisture Content * Weight + Water Holding Capacity * Weight* (5.32)

5.1.5.7 Model assessment and validation techniques

To evaluate the performance of the ML techniques and Fuzzy AHP model in delineating the groundwater potential zone, the ROC curve, AUC, and MCA were used. It is possible to compare the models using such techniques in terms of their deterministic and probabilistic prediction and acceptance (Ghosh et al. 2023). Based on the ROC and AUC, we can determine whether the anticipating power of this model is accurate in producing a probability map that harmonize with the highly ranked variables with the actual transition (Ikirri et al. 2023).The ROC curve was applied to plot the true positive rates (TPR or Sensitivity) against the false positive rates (FPR or 1-specificity), and the area under the curve (AUC) was calculated as a measure of the fit (Biswas et al. 2022). Following are the algorithms used to calculate the sensitivity and specificity of the model (Eq. 5.33 and 5.34) (Masror et al. 2023)

$$X = \text{FPR (1-specificity)} = \frac{FP}{TN+FP} \quad (5.33)$$

$$Y = \text{TPR (sensitivity)} = \frac{TP}{TP+FN} \quad (5.34)$$

Where FP is false positive; TP true positive; FN is false negative and TN is true negative.

The current study also introduces a validation method based on multiple correspondence analysis (MCA), which identifies conditioning factors that are linked to similar responses as usual. Using MCA, it is possible to map both variables and individuals, enabling a complex visual map to be constructed whose structural features can be interpreted (Rosmadi et al. 2023; Grochowalski and Hendrickson, 2023). Associations between the conditioning factors and the model-predicted groundwater potential zone were assessed by such correlation analyses (Baeumler et al. 2023). The flowchart of the methodology of the current study was shown in Fig.5.5.

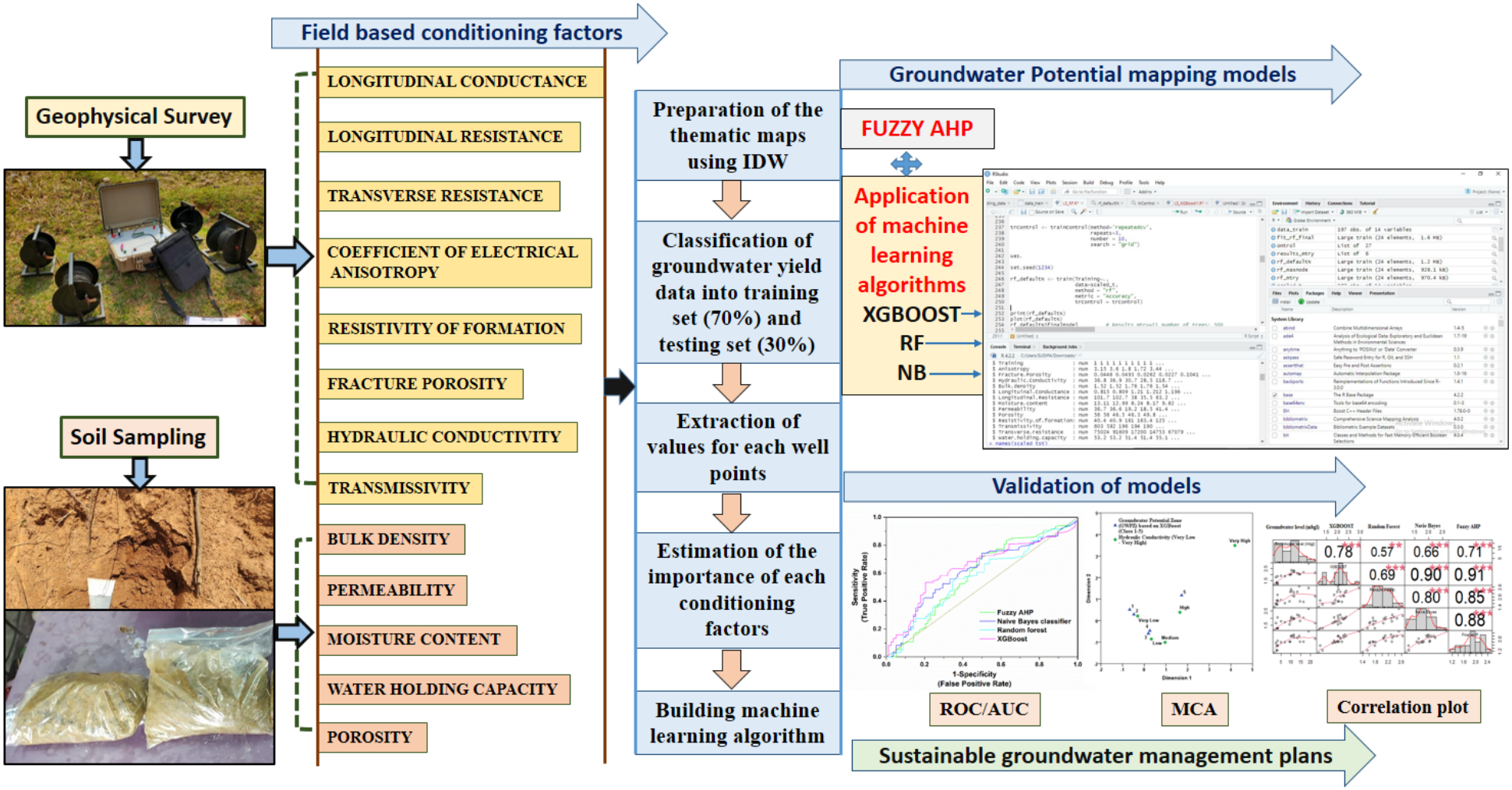

Fig. 5.5 Flowchart showing the methodology of the current research

5.1.6 Results and discussion

5.1.6.1 Hydrogeological and hydraulic prospects inducing groundwater potential in the river basin

Groundwater potential was evaluated based on the hydrogeophysical parameters including aquifer resistivity (ρ), aquifer thickness (h), longitudinal conductance (SC), longitudinal resistance (ρl), transverse resistance (TR), coefficient of electrical anisotropy (λ), resistivity of formation (ρm), fracture porosity (φf), reflection coefficients (r), hydraulic conductivity (K) and transmissivity (T*r*). Figure 6 and 7 illustrates the spatial distribution of these parameters. Due to the heterogeneity of the sub-surface layer and the compactness of the study area, there is a large variation in the value of aquifer resistivity throughout the basin. Longitudinal conductance is used as a measure of the resistance of geological strata to surface and subsurface pollution, as well as the potential for groundwater recharge (Nugraha et al. 2022). The longitudinal conductance of the basin ranges from 0.048 to 2.122 mho. In accordance with the values they exhibit (Table.5. S2), the map (Fig.5.6) can be classified into 5 groundwater dominant zones. Upstream and downstream areas with low SC are considered good groundwater potential zones, and are transmissive when compared to the rest of the basin. However, the aquifer is vulnerable to contamination (Mohammed et al. 2023). There is a lack of groundwater and poor water quality in the upstream section of the basin, where trace elements and fluoride have been reported frequently. The downstream section, on the other hand, consists mainly of agricultural land where the chemical contaminants quickly dissolve into surface water and are absorbed underground by the vadose zone (Bera et al. 2021; Ruidas et al. 2022).In the middle section of the basin, where the lateritic clay varies from shallow to deep, yellowish to reddish, loamy to clayey in texture, and with imperfect drainage, the aquifer shows a greater protective capacity but poor groundwater potential (Sarkar et al. 2020). The longitudinal resistance (Ωm) of the river basin ranges from 0.006-238.75, and it is lowest in the downstream section. Freshwater zones are mainly concentrated in the upstream section where groundwater remains in cracks and joints, resulting in higher longitudinal resistance values. Groundwater here is largely confined to the fracture matrix and the weathered mantle due to the geology and structure of the area, which lacks primary porosity in the upstream section (Nayak et al. 2020). High-resistance materials and their transverse resistance (TR) are studied using transverse resistance. An increase in TR values indicates that the thickening of the high-resistivity materials is evident. The transverse resistance of the river basin ranges from 48.66 to 1222000 ohms. Considering the greater values of TR, it can be concluded that the groundwater zones of the study area are freshwater zones. In the upstream and downstream sections of the basin, Tr values are highest. The groundwater at the upstream section is a source of freshwater available even during the driest seasons, unlike surface waters which may have scarce or no water during severe droughts (Sahoo et al. 2021). Rock age strongly influences Tr values, and a higher Tr value indicates a zone permeable to groundwater movement and flow and serves as region of high transmissivity (Nugraha et al. 2022).

To investigate the possible influence of anisotropy on flow through unconsolidated sediments, the coefficient of anisotropy was measured (Qin et al. 2023). Based on the results of the analysis of this integrated geophysical dataset, anisotropy appears to play a significant role in controlling the flow and movement of groundwater in unconsolidated aquifers. All over the basin, the coefficient of anisotropy ranges from 0.592 to 2358.25. The majority of the basin falls within the range of 0.592-120.79. It is hypothesized that greater coefficients of

anisotropy are caused by intrusive rocks that normally have higher resistivities than the host rock, which creates an unconformity in resistance (Batayneh, 2013). Due to the existence of thick sequences of silt, sand and clay in the elevated laterite tracts, anisotropy values increased downstream. During the premonsoon period, the water level in facile phreatic aquifers of porous older alluvium range from 5 to 10 mbgl. In deep aquifers under confined or semi-confined strata and piezometric surfaces, water levels vary between 5 and 10 mbgl (Bhattacharya et al. 2020). The formation resistivity factor measures how pore structure influences material resistance (Nwachukwu et al. 2019). The formation resistivity in the study area ranges from 0-2970. Resistance of formation values in the middle section of the basin is very high, suggesting that the groundwater in that zone was contaminated with detrimental pollutants and the existence of basement rock is deeper (Gaikwad et al. 2022). Here, the aquifer is generally contaminated with fluoride due to the presence of fluoride-bearing minerals and rocks in the sub-surface layers (Mondal and Kumar, 2017). Due to an increase in clay content, formation resistivity decreases in the downstream section (Mahmud et al. 2022) In general, the downstream section occurs within an unstable floodplain environment, with moderate drainage conditions having sandy loam with clay content with swelling characteristics on the upper horizons. It is found that the organic carbon content is higher in the uppermost horizons, along with higher clay content and a decrease in formation resistance (Sarkar et al. 2020). Fracture porosity is associated with tectonic fractures in rocks and minerals (Naidu et al. 2021). The fracture porosity (φf) of the river basin ranges from 0 to 5.611. The high value of fracture porosity identifies the layer of substantial groundwater potential within the water-bearing rock formation (Tahama et al. 2022). Because of the presence of alluvium lithology in the downstream section, the formation over this area contains fine to very fine grain-sized sediments and unlithified materials that result in high porosity levels (Adhikary et al. 2020). Because of jointing and fracturing, primary porosity in the upstream section is inconsequential and secondary porosity plays a significant role in groundwater circulation. From the fig. 5.6, it is also visually evident that fracture porosity and electrical anisotropy are positively correlated.

The fig. 5.7 illustrates the spatial distribution of hydraulic conductivity (K) in the study area (K values range from 1.553 to 440.11 m/day). The wide range of hydraulic conductivity in the basin aquifer system may be attributed to the heterogeneity of the geological formations (Chowdhury et al. 2022). Middle and downstream sections of the study area exhibit low K values, whereas upstream sections exhibit higher values. The low hydraulic conductivity of such areas indicates a lower permeability of the earth system (Amiri et al. 2022). In the north eastern section of the basin, ground water exists beneath a clay horizon of locally varying thickness and below an alluvium of a single thick saturation zone (Oli et al. 2022). Furthermore, the aquifer's capacity to transmit groundwater within the river basin ranges between 10.152 and 2253.4 m^2/day. Fine-grained sediments are characterized by very low hydraulic conductivity, low transmissivity, and a formation factor. In sandy terrain conditions, these fine-grain sediments consist primarily of sand with some silt and clay. In the northeastern and middle sections of the basin, high values of transmissivity are observed. Transmissivity values for the downstream section of the basin are well consistent with those reported in Chowdhury et al. (2010). Therefore, the results obtained from the geophysical investigation are reliable which have been estimated considering the isotropy and the heterogeneity of the field environment and by combining all field-based data and not by costly pumping tests (Amiri et al. 2022; Akhter et al. 2022).

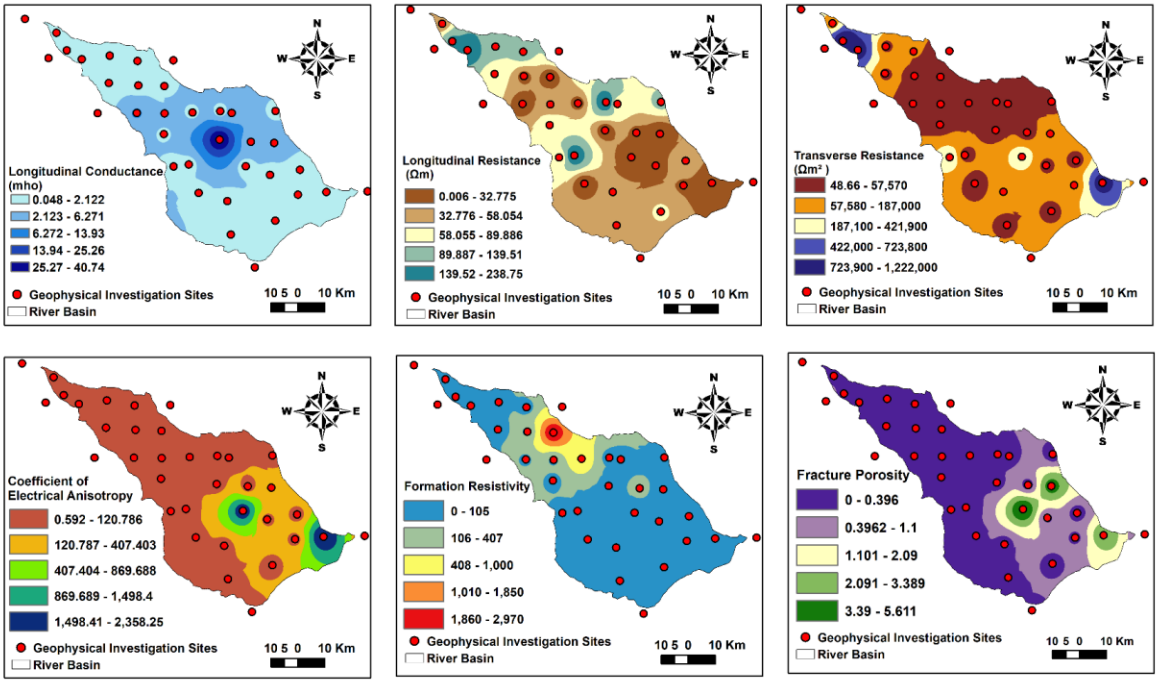

Fig. 5.6 Conditioning factors as estimated from geophysical survey

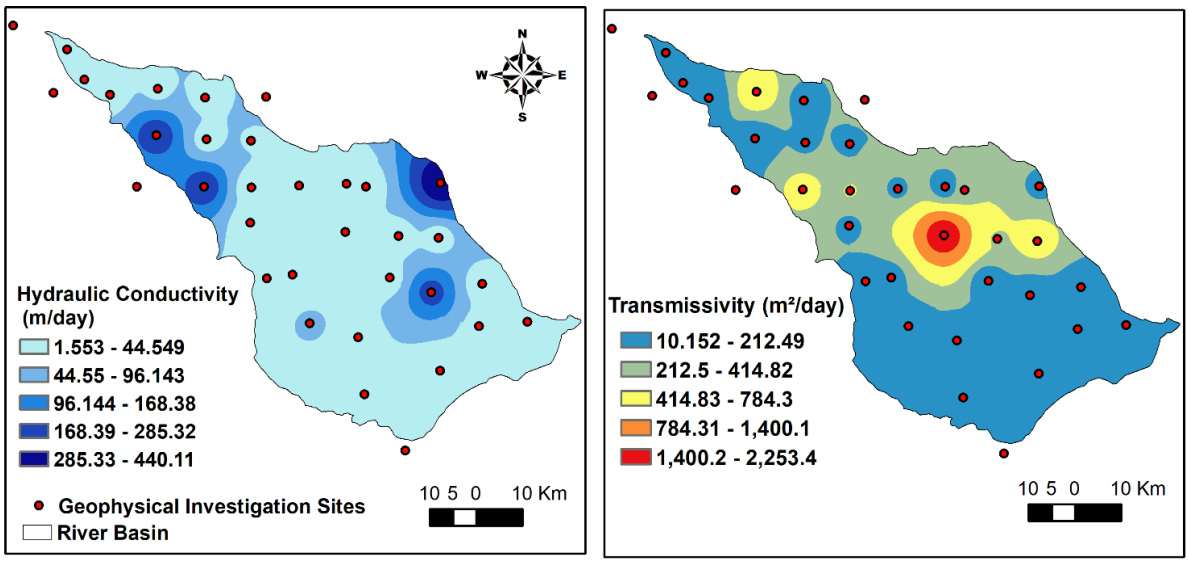

Fig. 5.7 Aquifer parameters as estimated from geophysical survey

5.1.6.2 Soil hydraulic prospects inducing groundwater potential in the river basin

Hydraulic properties of saturated and unsaturated soils must be accurately characterized in order to address a number of issues related to hydrogeological and groundwater studies (Durner and Fluhler, 2009). Groundwater potential of the study area was also determined using 5 soil hydraulic parameters including bulk density, porosity, permeability, soil moisture content and water holding capacity. Bulk density is a measure of soil's ability to function as a structural support, a transport medium for water and solutes, and a means for aerating soil (Liu et al. 2022). It has a significant influence on soil productivity and processes by affecting rooting depth, infiltration,

soil porosity, water holding capacity, aeration and biological activities of micro-organisms. The bulk density of the river basin ranges from 0.08 to 2.197 grams per cubic centimeter. Soil samples that contain a greater proportion of clay than sand have the potential to influence a region's groundwater recharge. In the downstream and middle sections of the basin, bulk density is higher, but it does not vary greatly throughout the basin (Fig.5.8). Clay possesses the property of retaining water molecules since it has pores; therefore, the density of soil mass decreases as clay content increases, whereas soils with more compact pore spacing have a higher bulk density (Kadam et al. 2021) and thereby increases groundwater recharge. Porosity is calculated on the basis of bulk density. Soils having low bulk density is characterized by innumerable pore spaces and loose aggregates, and thus it discourages groundwater transmission (Zhang et al. 2018). The porosity of soil is thus determined by the proportion of pore spaces in the soil (Liu et al. 2023). The porosity of the basin ranges from 26.83 to 76.67 (%) and is lowest in the north-eastern part of the basin. In this complex hydrogeological basin, aside from meteorological and hydraulic conductivity, soil porosity is the most significant factor influencing groundwater recharge. When algal blooms occur in the forest cover of the laterite soil in the middle section of the basin, groundwater recharge occurs followed by an increase in infiltration rate (Singh et al., 2021). Groundwater seepage through the topsoil is also affected by the soil condition of an area, including both the porosity and permeability (Maqsoom et al. 2022). The permeability of the basin ranges from 3.41 to 122.7 m/day. In the river basin, the quaternary thick alluvial deposits and structures with high permeability and productivity are commonly found at the northeastern and southwestern edges of the river basin (Mengistu et al. 2022) having good groundwater potential. A majority of infiltration occurs in plateaus with thick alluvial deposits, which affects permeability (Mezni et al. 2022). The soil moisture content plays a significant role in controlling deep percolation (Stafford et al. 2022), and within the basin, it ranges from 0.099 to 51.13 %. Agricultural activities constitute the sole economic activity in the downstream section of the basin, where soil moisture is high. During the 2021 irrigation season, a greater frequency of irrigation events was observed in the downstream section of the basin, resulting in greater infiltration and aquifer recharge (Das and Panda, 2022). Soil water holding capacity (storage) is an indicator of our last inspected soil hydraulic parameter, and it is often referred to as a water retention capacity (Tang et al. 2022). The water-holding capacity of the soil in the basin ranges from 17.26-83.84 (%). The downstream section of the basin consists of loamy clay-clayey soil characterized by clay horizons that severely restrict percolation, have low permeability, and are high water-holding capacity (Parihari et al. 2023).

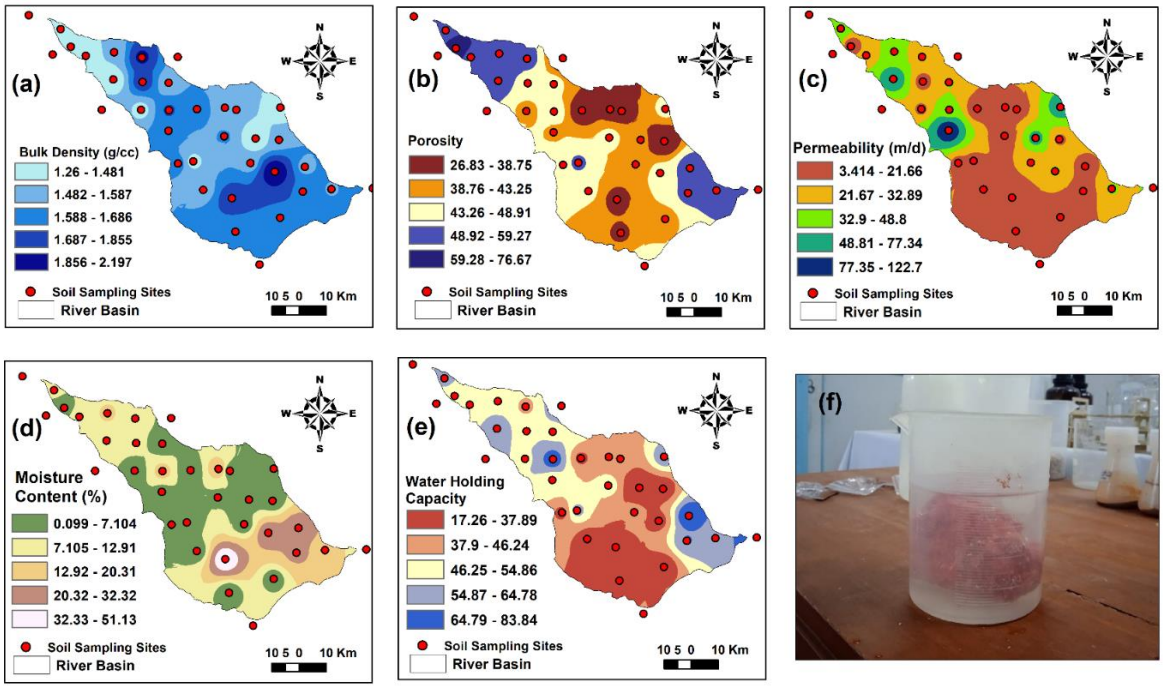

Fig. 5.8 Conditioning factors as estimated from soil sampling

5.1.6.3 Factor importance and model's output comparison

Based on the previously discussed XGBoost, RF, Naive Bayes, and Fuzzy AHP methods, the uncertainty/weightage of the GWPI results and conditioning factors of importance were estimated. Upon training the ML techniques, the values of each feature are transposed to determine the importance of each feature class, as proposed by Breiman (2001). The fig. 5.9 illustrates the importance ranking of conditioning factors as determined by the above algorithm in the R platform. Accordingly, all predictor significance levels were scaled to a maximum value of 1, which indicated that the most strongly relatable conditioning factor was the one having the largest summation. Concerning the fuzzy logic approach, the weights of the conditioning factors have been estimated after the fuzzification of the datasets. As shown in Fig. the most significant conditioning factor for groundwater flow, occurrence, and direction, according to Fuzzy AHP and Naive Bayes, is the hydraulic conductivity. At any given scale, hydraulic conductivity represents the most important aquifer parameter controlling groundwater flow within an aquifer (Sanchez-Vila et al. 2006). As indicated by XGBoost, permeability is the most significant factor and RF indicates that bulk density has the greatest influence on the aquifer recharge in a particular area. The groundwater potential zones were determined by deciphering several distinct feature classes of thirteen conditioning factors. The values of the entities are expressed in a dimensionless form which is used to index probable groundwater potential zones. The GWPZ maps were predicted based on well yield positions, and the mapping of GWPI values was performed using the XGBoost, RF, NB, and Fuzzy AHP methods. GWPI values range from 0 to 1 for these four models. To construct the GWPZ maps, the values were classified into five distinct classes (very low, low, moderate, high, and very high potential) (Fig. 5.10) using the commonly used classification method popularly known as "natural break" (Jenks) (Rahman et al. 2022). The very high and high groundwater potential zones are scatteredly distributed within the river basin, mostly around

the main river channel which agrees with the study conducted by Arunbose et al. 2021. In the XGBoost model, most areas are associated with moderate (28.74 %), very low (22.61 %), and high (20.58 %) potential, and the remaining area is characterized by low (19.98 %) and very high (8.07 %) potential. In the RF model, most areas are associated with low (25.01 %), very low (24.81 %), and high (20.75 %) GWP, and the remaining area is defined with medium (19.91 %) and very high (9.52 %) potential. In the NB model, most locations are defined by very low (25.93 %), moderate (23.04 %), and low (22.19 %) potential, and the rest of the area is correlated with high (20.57%) and very high (8.25 %) GWP. Lastly, In the Fuzzy AHP model, most regions are associated with moderate (27.25 %), high (22.18 %), and low (21.89 %) potential, and the rest of the area is correlated with very low (20.03 %) and very high (8.40 %) GWP (Table 5.3). The downstream end and the upstream northwestern part of the river basin revealed promising results as majority of the high potential zones were concentrated along the main river channel having coarse to fine texture sandy soils. Due to the presence of cracks and joints, high hydraulic conductivity, and high permeability in a few patches of the upstream section and older alluvium, flat terrain that remains flooded during the monsoon seas in the downstream section has a very high tendency to infiltrate surplus water (Kundu et al. 2023). The central part of the area has a moderate groundwater potential, interspersed with zones of high groundwater potential. Though very low and low groundwater potential zones are scatteredly found over the whole river basin in small sections but are more prominent in the south-western to the central-north region where transverse resistance, permeability, and moisture content are low as it is mainly covered with laterite soil (Osinubi et al. 2009). Table 5.4 shows the sub-basin wise distribution of groundwater potential zone with sub-basin Silai having the highest area under very low groundwater occurance (87.27 Km^2) located at the central-northern section of the basin.

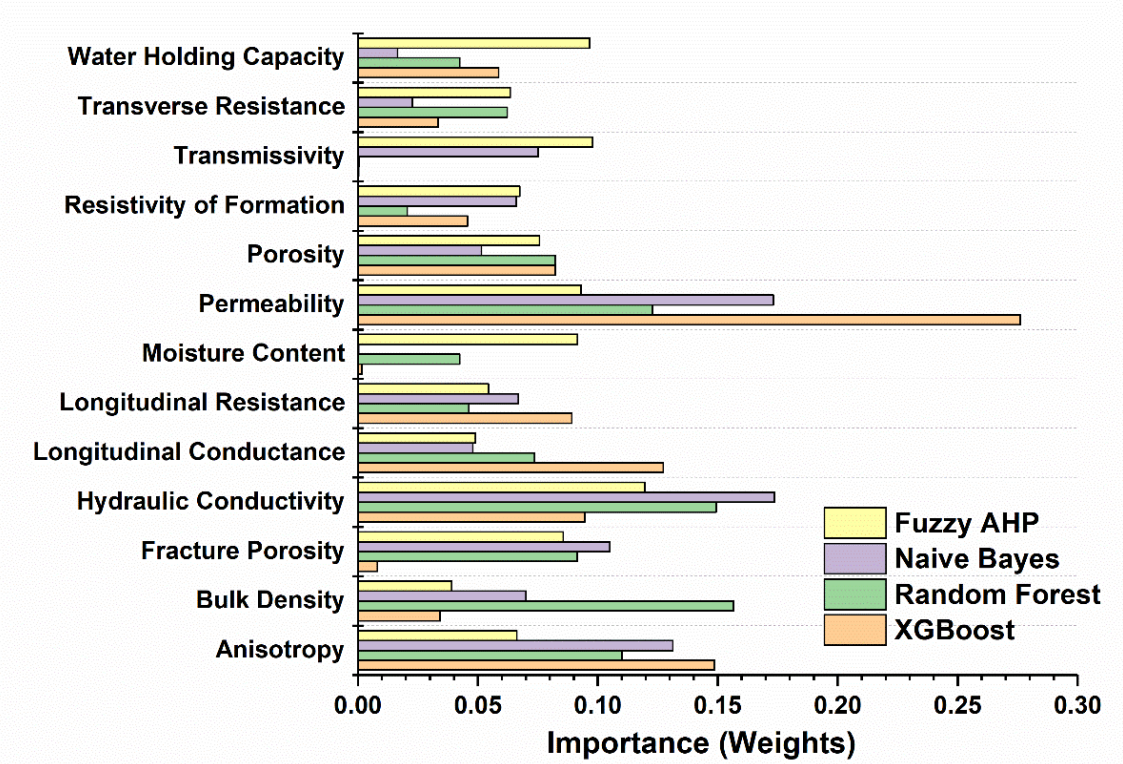

Fig. 5.9 Importance of conditioning factors

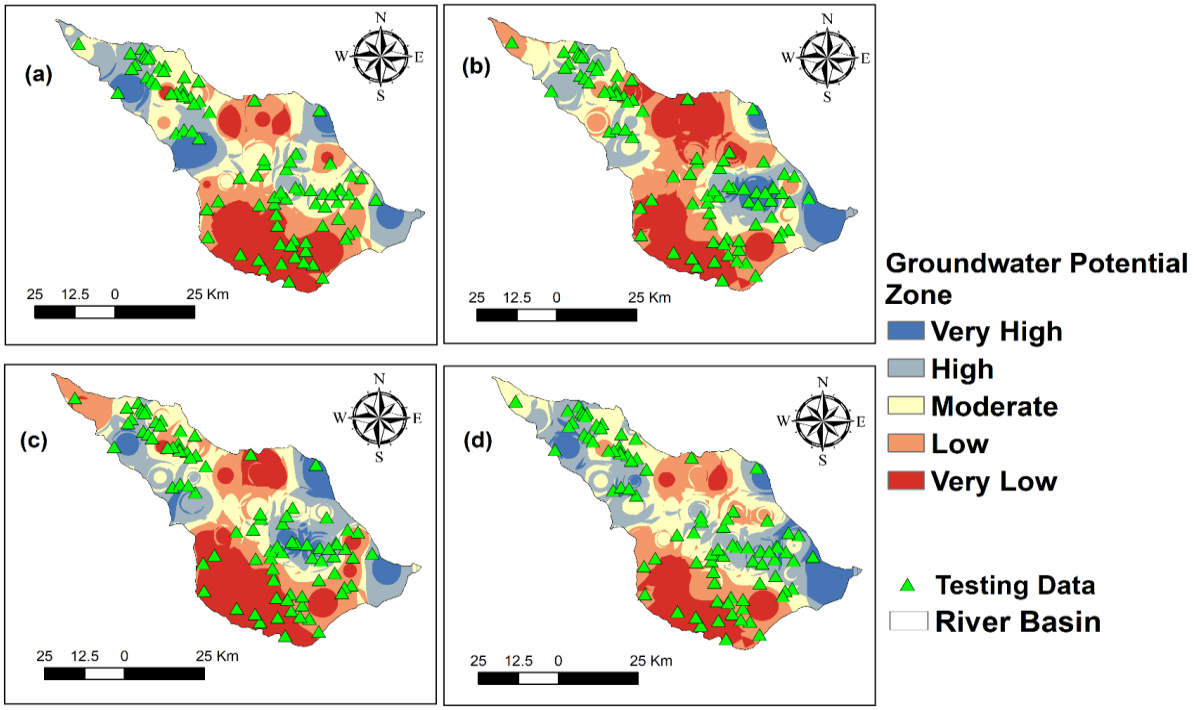

Fig. 5.10 Groundwater potential map derived using machine learning models, (a) XGBoost model, (b) Random Forest model, (c) Naive Bayes model and (d) Fuzzy AHP

Table 5.3 Areal distribution of the groundwater potential zone using ML and MCDM techniques

Methodology	Model	Very Low		Low		Moderate		High		Very High	
		Area in Km^2	Area in %	Area in Km^2	Area in %	Area in Km^2	Area in %	Area in Km^2	Area in %	Area in Km^2	Area in %
ML Techniques	XGBOOST	877.69	22.61	775.46	19.98	1115.51	28.74	798.96	20.58	313.47	8.07
	RF	962.85	24.81	970.79	25.01	772.82	19.91	805.14	20.75	369.49	9.52
	NB	1006.50	25.93	861.22	22.19	894.39	23.04	798.48	20.57	320.49	8.25
MCDM	Fuzzy AHP	777.52	20.03	849.83	21.89	1057.53	27.25	860.80	22.18	335.42	8.4

Table 5.4 Areal distribution of the groundwater potential zone in different sub-basins

Models	Class	Areal distribution (Km^2) of GWPZ of Sub-basins using different models								
		Betal	Donai	Joypanda	Kubai	Parang	Purander	Silai	Tamal	Silai Ketia Khal
XGBOOST	Very good	3.26	0.00	45.44	33.26	411.56	93.22	17.05	258.76	86.64
	Good	13.47	68.41	21.82	168.19	65.25	4.12	22.25	101.22	221.26
	Medium	46.67	168.68	237.71	74.67	2.32	4.12	178.53	3.93	397.94
	Low	40.19	29.30	70.58	59.66	0.00	0.00	324.18	0.00	274.61
	Very low	36.23	0.00	0.22	0.00	0.00	0.00	180.86	0.00	96.21
RANDOM FOREST	Very good	0.00	0.00	94.97	17.12	336.01	114.49	1.32	178.78	219.98
	Good	53.71	7.11	84.67	88.63	122.75	4.42	145.72	155.99	306.94
	Medium	44.49	52.00	100.51	93.75	20.37	0.00	254.05	29.13	178.11
	Low	41.63	95.24	95.63	100.22	0.00	0.00	314.10	0.00	158.00
	Very low	0.00	112.05	0.00	36.06	0.00	0.00	7.68	0.00	213.62
NAIVE BAYES	Very good	20.23	16.39	22.00	38.02	382.64	58.25	21.66	310.93	135.97
	Good	33.91	64.20	129.53	112.93	96.49	58.38	151.36	52.97	160.91
	Medium	49.46	45.01	206.80	76.84	0.00	2.28	189.68	0.00	323.82
	Low	35.95	98.88	17.44	59.03	0.00	0.00	288.39	0.00	298.45
	Very low	0.28	41.91	0.00	48.97	0.00	0.00	71.78	0.00	157.51
FUZZY MCDM	Very good	5.15	0.00	45.05	25.87	410.67	9.41	0.00	208.79	72.69
	Good	43.24	1.94	66.24	116.05	64.84	96.77	43.02	155.11	261.76
	Medium	62.37	86.94	178.24	138.60	3.63	12.33	234.76	0.00	340.05
	Low	29.07	162.62	83.91	55.21	0.00	0.39	357.83	0.00	171.32
	Very low	0.00	14.89	2.33	0.07	0.00	0.00	87.25	0.00	230.83

5.1.6.4 Model evaluation and validation

To verify the groundwater potential zone maps, the groundwater well yield data of the river basin was utilized, which represent the actual aquifer recharge characteristics and groundwater potential for a particular site. The model training was conducted with approximately 70% of the wells (197 wells), while the succeeding action on the framework validation was conducted with 30% of the wells (88 wells). All models have been compared using ROC and AUC curves. Values less than 0.55 are considered negligible, values greater than 0.56 are considered small, values greater than 0.64 are considered moderate to good, and values greater than 0.71 are considered strong predicted values (Hamilton and Wormer, 2015). As shown in Fig. 5.11, the prediction-rate curves of the XGBoost, the RF, the NB, and the fuzzy AHP models were determined based on the AUC. The ROC-AUC curves show (Fig.5.11) that all four MLAs and Fuzzy AHP techniques had moderate to strong prediction accuracy where XGBoost is the best model with an AUC of 0.79 indicating a strong performance of the classifier than RF (0.67), NB (0.71) and Fuzzy AHP (0.68).In addition, the XGBoost model resulted in more consistent results as compared with the ANN, SVR, KNN and NB models as observed from the studies by Osman et al. 2021 and Rasool et al. 2022.

In this research, Multiple Correspondence analysis was also employed to explore the association between the first 4 significant conditioning factors (hydraulic conductivity, permeability, longitudinal conductance and anisotropy) as optimized by XGBoost and XGBoost classified GWPZ map. This analysis was conducted to ensure that the XGBoost model is precise and adequate so that it can be used more frequently in groundwater studies around the world. An association between the datasets was visually represented in a perceptual plot to demonstrate the overall relationship between them, indicating that the areas with the highest values of the four parameters have the highest groundwater potential (Fig.5.12). Based on the above-mentioned reasons and validation reports, it can be stated that the XGBoost model is capable of manifesting the relationship between hydro-geophysical and hydraulic parameters with groundwater occurrences.

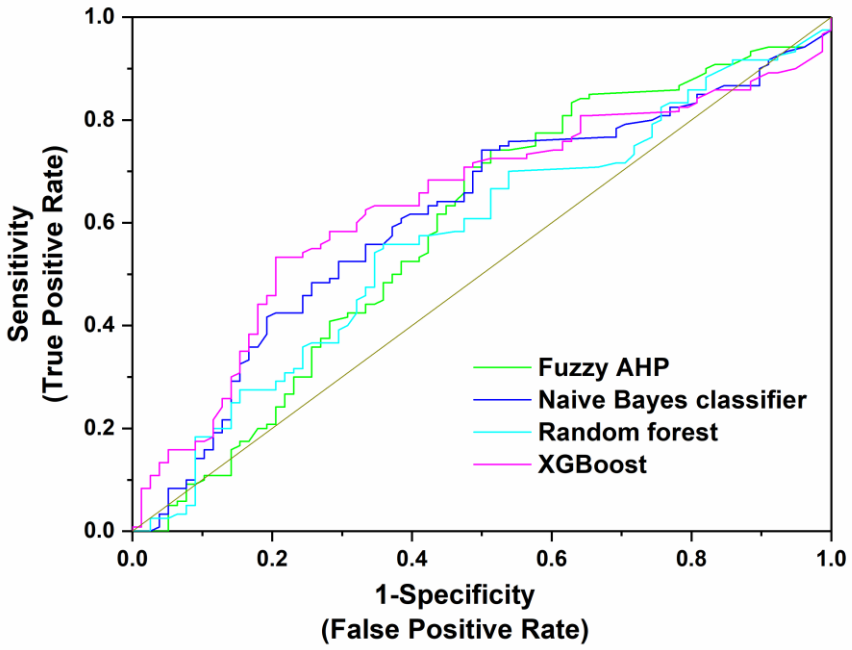

Fig. 5.11 Validation of different models through ROC curve

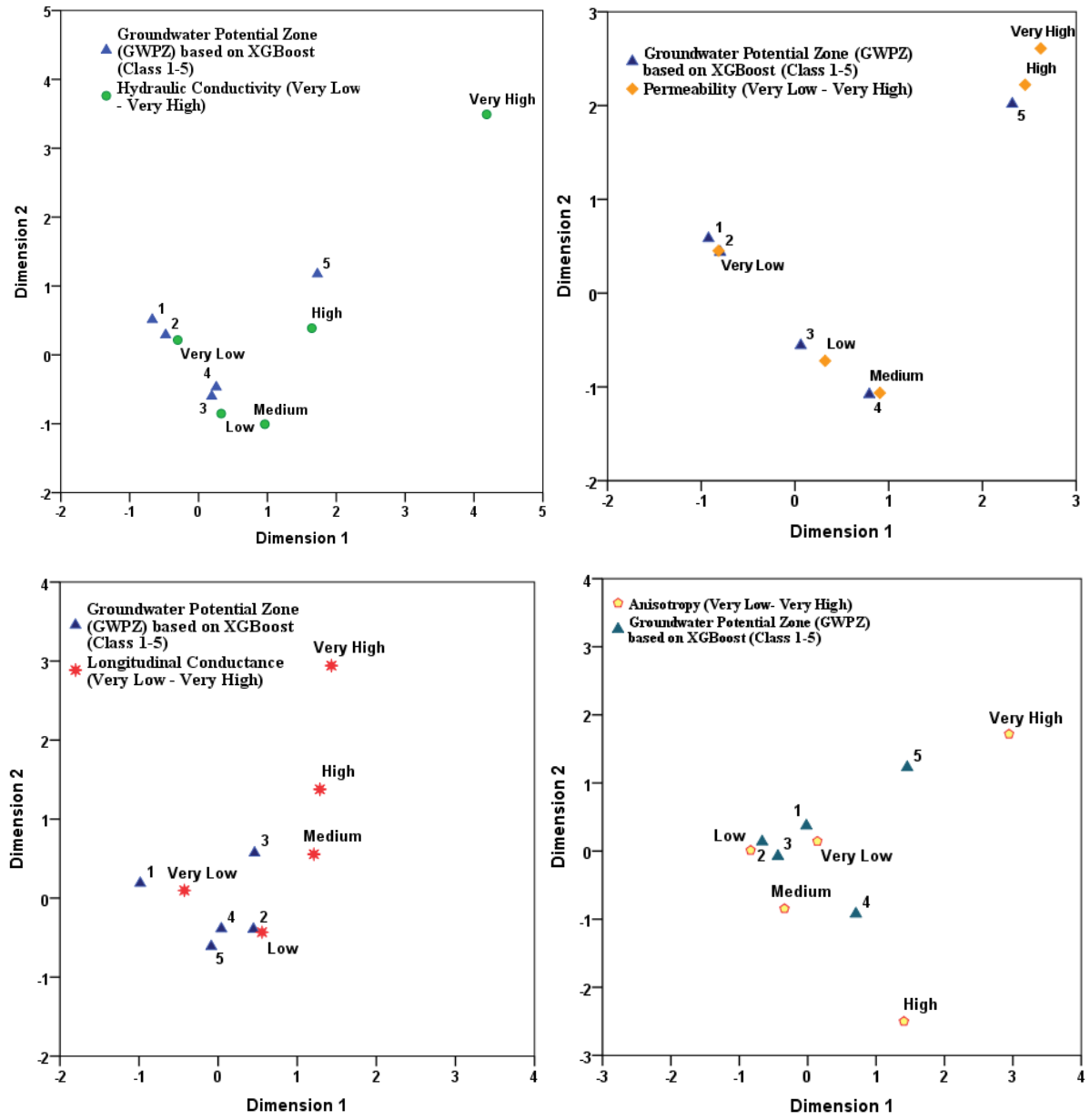

Fig. 5.12 Multiple Correspondance analysis between groundwater conditioing factors and groundwater potential zone using XGBoost

5.1.6.5 Relationship between groundwater level and groundwater potential models

According to the groundwater level survey conducted from November 2021- February 2022 throughout the river basin, the groundwater level ranges between 0.86 to 20.6 mbgl. During the field survey, it was perceived that groundwater is the primary source for irrigation, domestic, and drinking and is extracted through dug wells in the upstream section and submersible wells in the downstream section of the basin. As a result, groundwater management is of paramount importance for the study area.1/3 of the upstream population relies on irrigation-based agricultural activities, and most of the irrigation supply is sourced from shallow aquifer systems, which leads to rapid aquifer diminishing (Goswami and Ghosal, 2022). Thus, an accuracy assessment was carried out to

determine the correlation between the predicted groundwater potential zones map based on XGBoost, RF, NB, and Fuzzy AHP and the observed groundwater level data of 53 wells. For calculating classification accuracy, groundwater level measurements were used as reference points. A correlation matrix is generally used to assess accuracy in the R platform (Fig.5.13). XGBoost achieved a linear regression coefficient of 0.78, which was followed by Fuzzy AHP (0.71), NB (0.66), and RF (0.57), demonstrating the reliability of XGBoost methodology in accurately determining the groundwater potential zone of the Shilabati river basin.

5.1.7 Recommendations and sustainable plans

The present study compares the groundwater potential zones estimated from geophysical studies across the villages located within the river basin with the map derived from the XGBoost model. Evaluation units are classified as very high, high, moderate, low, and very low groundwater potential. The groundwater yield potential areas of each village site were identified based on reflection coefficients as estimated from geophysical surveys. Generally, potential aquiferous zones are found in basement complex terrain where there is thick overburden material and a low reflection coefficient of <0.8. According to the VES survey (Bayewu et al. 2018), promising groundwater potential was evaluated using four basic criteria; high groundwater potential occurs in areas where overburden material thickness exceeds 13 m with a reflection coefficient < 0.8; moderate groundwater potential occurs in areas where overburden material thickness exceeds 13 m with a reflection coefficient $\geq$ 0.8; low groundwater potential occurs in areas where overburden material thickness is <13 m with a reflection coefficient > 0.8 and poor groundwater potential occurs in areas where overburden material thickness is <13 m with a reflection coefficient < 0.8. The extent of the aquifer protective ability of the village sites was estimated using the ratings of aquifer protective capacity (El Mountassir et al. 2022) where transverse resistance and longitudinal conductance were used. Based on aquifer protection capacity, the village sites were classified as moderate, weak and poor (table 5.5). In the current research village site-wise sustainable planning is recommended for the river basin to mitigate the “critical” stage of groundwater depletion which also validates the applicability of the XGBoost Model. Village sites in the upstream section of the river basin, including Aralabara, Baladghata, Bansidi, and so on, match the groundwater status as estimated from both the field and software analyses.

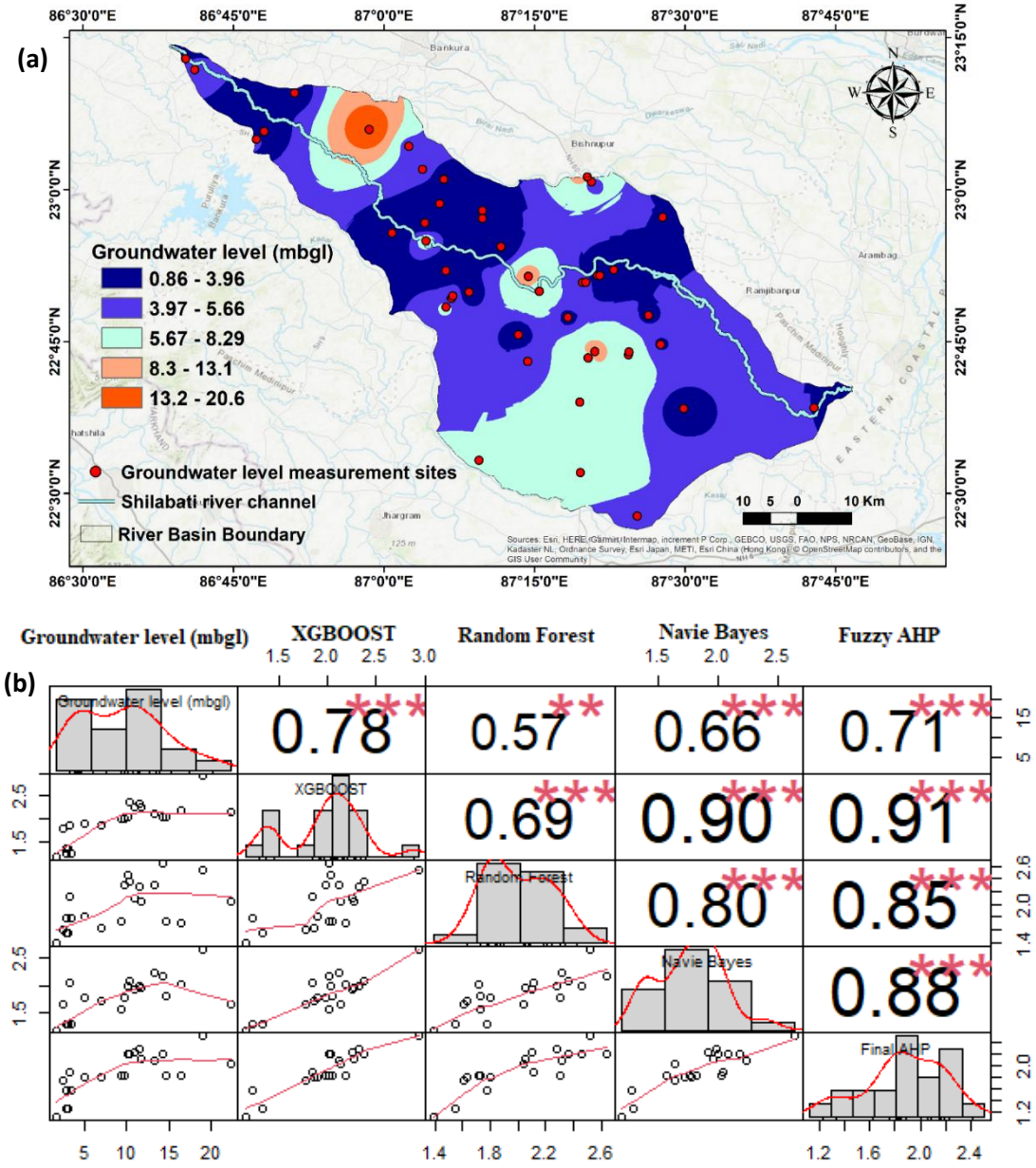

Fig. 5.13 Groundwater level map of the study area and (b) correlation coefficients between groundwater level and different models

Table 5.5 Aquifer resistivity, thickness, groundwater potential from VES survey and models and Sustainable management plan for different groundwater potentiality and development sites

Geophysical investigation sites (Villages) within the basin	Layer 1		Layer 2		Layer 3		Layer 4		Layer 5		Layer 6		Layer 7		Layer 8		GWPZ based on VES study	GWPZ based on XgBOOST model	Protective capacity and remarks
	$ħ_1$	ρ_1	$ħ_2$	ρ_2	$ħ_3$	ρ_3	$ħ_4$	ρ_4	$ħ_5$	ρ_5	$ħ_6$	ρ_6	$ħ_7$	ρ_7	$ħ_8$	ρ_8			
Aralbara	1.53	31.90	9.93	98805	-	110	-	-	-	-	-	-	-	-	-	-	LGWP	LGWP	Poor and needs sustainable plan to increase groundwater recharge
Baladghata	7.60	522	9.05	74	34.10	3583	77.4	16.10	-	18.50	-	-	-	-	-	-	HGWP	VHGWP	Good
Bansidi	4.42	20.50	8.46	15.50	7.15	411	10.1	411	50.90	6.33	-	16.50					HGWP	HGWP	Good
Baramesya	3.95	9.45	1.97	5.60	-	16616	-	-	-	-	-	-	-	-	-	-	LGWP	MGWP	Good
Bhagirathpur	1.52	5.02	7.93	7537	-	301	-	-	-	-	-	-	-	-	-	-	PGWP	HGWP	Moderate and aquifers require water conservation measures to increase its sustainability.
Chandabil	2.5	1155	22	139	40.80	17	-	3526	-	-	-	-	-	-	-	-	MGWP	LGWP	Good
Dumuria	0.77	30.20	27.20	127	41	127	49	135	-	5582	-	-	-	-	-	-	MGWP	MGWP	Moderate and aquifers require water conservation measures to increase its sustainability.
Gharpathar	4.55	9.57	62.90	986	-	22.30	-	-	-	-	-	-	-	-	-	-	HGWP	MGWP	Moderate and aquifers require water conservation measures to increase its sustainability.
Godapaisal	6.16	19.70	9.24	19.70	22.60	1654	-	939	-	-	-	-	-	-	-	-	HGWP	VHGWP	Good
Gopalpur	6.29	35	12.20	88.20	-	542		-	-	-	-	-	-	-	-	-	PGWP	LGWP	Moderate and aquifers require water conservation measures to increase its sustainability
Guniada	4.23	9.43	4.54	128	68.20	17914	-	38.20	-	-	-	-	-	-	-	-	HGWP	MGWP	Moderate and aquifers require water conservation measures to increase its sustainability
Jadavnagar	2.28	408	11.50	160	77	99.70	-	0.198	-	-	-	-	-	-	-	-	MGWP	VLGWP	Good
Kantapal	5.07	19.30	3.90	281	1.92	281	12.4	5.47	2.78	5.47	4.17	5.47	45.4	66.4	266	7.34	MGWP	LGWP	Excellent
Kharjuria	0.27	13.30	0.42	0.53	0.284	0.53	4.88	4069	27.30	4.77	-	227	-	-	-	-	MGWP	MGWP	Very good
Kolaboti	3.15	510	8.56	113	13.30	272	53.1	83.60	47.90	69.20	-	229	-	-	-	-	HGWP	HGWP	Good
Kusumdunri	3.76	466	3.77	466	33	149	54.4	22	-	516	-	-	-	-	-	-	MGWP	LGWP	Good
Mamra	1.80	94.46	13.58	150.10	48.50	388.10	66.3	31.52	-	267.40	-	-	-	-	-	-	MGWP	VHGWP	Good
Metyal	1.79	15.10	4.37	85559	-	133	-	-	-	-	-	-	-	-	-	-	PGWP	VLGWP	Weak and Groundwater extraction levels should be minimized
Mulgram	1.95	11.20	10.50	92274	-	97.60	-	-	-	-	-	-	-	-	-	-	PGWP	VLGWP	Weak and Groundwater extraction levels should be minimized
Niasa	4.22	16.50	1.76	7.47	0.68	7.47	1.22	7.47	11.80	7689	-	7689	-	-	-	-	PGWP	MGWP	Good
Pachaparar	0.96	4.79	1.03	9023	14.90	17.9	-	13904	-	-	-	-	-	-	-	-	MGWP	VHGWP	Good
Pathaisol	1.02	5.16	0.19	11.80	4.70	5019	-	0.48	-	-	-	-	-	-	-	-	PGWP	LGWP	Moderate and aquifers require water conservation measures to increase its sustainability
Rampur	1.05	40.90	7.56	40.30	16	17.30	-	872	-	-	-	-	-	-	-	-	MGWP	VGGWP	Good
Rautara	1.14	1.72	0.34	9304	3.25	165	0.907	124	-	23.90	-	-	-	-	-	-	PGWP	MGWP	Moderate and aquifers require water conservation measures to increase its sustainability
Salboni Road	0.52	1345	0.42	1345	1.53	769	1.46	119	47.60	217	-	1092	-	-	-	-	HGWP	VHGWP	Moderate and aquifers require water conservation measures to increase its sustainability
Salboni Station	2.90	16.50	4.49	18937	-	6.14	-	-	-	-	-	-	-	-	-	-	PGWP	VHGWP	Weak and Groundwater extraction levels should be minimized
Sankarkata	0.49	381	2.55	31.40	2.01	19	10.2	35270	-	9.49	-	-	-	-	-	-	PGWP	LGWP	Poor needs sustainable plan to increase GW recharge
Sarai	5.44	46.60	8.39	1809	32	55.10	-	396	-	-	-	-	-	-	-	-	MGWP	HGWP	Good
Uppar Maity Bandh	0.09	0.24	0.13	200	2.54	11	0.992	11	35.50	798	-	57.80	-	-	-	-	HGWP	VLGWP	Moderate and aquifers require water conservation measures to increase its sustainability

*HGWP= High Groundwater Potential; MGWP= Moderate Groundwater Potential; PGWP= Poor Groundwater Potential; LGWP= Low Groundwater Potential; VHGWP= Very High Groundwater Potential; VLGWP= Very Low Groundwater Potential

Village sites such as Kharjuria, Kolaboti, Metayal, and so on located in the middle section correspond to the results of both the analyses, where the stage of groundwater development ranges from 4-42%, but there is limited scope for artificial recharge in laterite soils having low permeability. Open-dug wells are feasible in this section in areas of hard rock terrain within the depth of 10-15 meters which again falls under the critical-semi critical zone as defined by the CWGB, 2022. In the downstream section, the stage of groundwater development exceeded more than 60% where village sites namely Salboni Road, Pathaisol, and Rampur, and so on have moderate to good aquifer protective capacity because of the overburden thick clay deposits.

Village-wise sustainable groundwater planning of the river basin must emphasize promoting surface/subsurface water conservation, considerate use, accelerating water tariff procedures, alternative cropping/cultivation patterns, promoting positive sustainable awareness to the community, implementing appropriate scientific planning, normalizing water retaining practices in domestic, agricultural and industrial environments, etc. Measuring the abstraction of water yield from all wells should be the primary objective. Secondly, the objective was to prompt the farmers that the amount of water that can be abstracted is limited to the volume that is specified based on the well drilling depth (Naqa and Al-Shayeb, 2009). In addition to providing significant implications for rivers, wetlands, lakes, and aquatic ecosystems that depend on groundwater system, sustainable groundwater planning will be convenient for long-term groundwater management and development etiquettes in the Shilabati River basin of West Bengal, India.

5.1.8 Conclusion and Reccomendations

The Shilabati River basin relies primarily upon groundwater for agricultural, industrial, and domestic activities. In most parts of the study area, overexploitation and unscientific extraction have resulted in a decrease in groundwater levels, which exaggerates water problems in dry periods. To ensure the successful and sustainable management of this valuable natural resource, detailed investigations must be conducted in the river basin.

- In most cases, secondary data or remote sensing data were used to generate groundwater potential maps, which are not always reliable for specific situations or needs. Secondary datasets, such as past soil maps, geological maps, etc., provide a great deal of information, but quality does not always imply relevance. Accordingly, the novelty of the present work lies in the application of the data generated from the field survey for identifying the groundwater potential zone using a comparative framework of ML and MCDM. In contrast to traditional cost-effective and invasive methods such as pumping tests, this method provides accurate quantitative information regarding groundwater resources. VES data (resistivity) and its derived parameters and various soil hydraulic parameters have been used in this work to ascertain the current field situation. Topsoil thickness varies across the research area. The upstream area consists of a low-thickened weathered zone, while the middle and lower sections of the basin consist of a high-thickened weathered and alluvium zone. Weathered geological fractures in upstream and middle sections act as phreatic aquifers with few fractured zones acting as semi-confined systems.
- Concerning groundwater yield data and each conditioning factor, spatial associations were calculated using 197 wells (70%) as training data and 88 wells (30%) as testing/validation data. In comparison to the RF (0.67), the NB (0.71) and the Fuzzy AHP (0.68) techniques, XGBoost achieved an AUC of 0.79. XGBoost also displayed a correlation coefficient of 0.78 when compared with groundwater-level data.

Further, a new validation approach, the MCA method, was introduced, which showed a strong correlation of XGBoost with the condition parameters.

- The predicted groundwater potential areas were classified into five groups, from very high to very low. According to the XGBoost model, GWPZ map of the entire river basin, 313.47 km^2 (8.07%) was categorized as very high groundwater potential areas, 798.96 km^2 (20.58%) were classified as high groundwater potential areas, and 1115.51 km^2 (28.74%), 775.46 km^2 (19.98%), and 877.69 km^2 (22.61%) were classified as moderate, low, and very low. However, fractured zones (upstream) and alluvial deposits (downstream) possess the greatest potential for groundwater occurrence within the study area.

5.1.9 Limitation and Future Work

One of the major limitations of the methodological framework includes the inability to generate hydrodynamic behavior of subsurface geology using geophysical surveys in isolated/remote areas, although can be counterchecked with the proposition that those places will be less populous. The incorporation of such ML techniques and decision trees into Fuzzy MCDM models should be emphasized in future studies. Thus, the purpose of this study is to establish a basic basis for drafting a field-based management plan for groundwater and to provide feasibility for additional research on developing a conscientious groundwater extraction policy that can be applied in different parts of the world with appropriate accommodations.

5.2 Understanding the exchange process between ground and surface water using mini drive point piezometer and mathematical models to identify suitable Managed Aquifer Recharge sites

5.2.1 Introduction

Over land and ocean, the surface temperature of 2021 has been 1.51 °F (0.84 °C) warmer than the twentieth-century average of 57.0 °F (13.9 °C) and 1.87 °F (1.04 °C) warmer than the pre-industrial period (1880-1900) (NOAA, 2022). There have been several management practices proposed and implemented that can meet water demand without negatively impacting groundwater (Kim et al. 2017; Harb et al. 2016). In most cases, these projects are carried out at regional scales and involve the construction of check dams, reservoirs and ring tanks at a small scale (Poff and Olden, 2017). In addition of providing drinking water, rainwater harvesting (RWH) has also attracted interest as a method for replenishing groundwater (Wadi et al. 2022). Nevertheless, these surface works also result in significant water losses and are influenced by climate change and anthropogenic activities as found in Australia where loss of water using these structures have reach up to 40% of their storage capacity/year (Crag et al. 2005). One of the best alternatives for water harvesting and management is the managed aquifer recharge (MAR). During times of surface water surplus, it allows the replenishment or maintenance of groundwater levels, as well as storage of water during droughts (Standen et al. 2020) without increasing evapotranspiration losses (Dillon and Arshad, 2016). Modification of in-channel segments, installing floodwater spreading systems, infiltration gallery, collector wells etc. balances and recovers groundwater resources and enables cyclical water management by storing surplus surface water in aquifers during rainy seasons. A majority of MAR research and projects are conducted in Europe, where 224 MAR sites are active in 23 European countries

as of 2013. Most of the active MAR sites are located in Germany, followed by the Netherlands, France, Finland, Sweden, Switzerland, and Spain, with less than ten active MAR sites found in the other countries. Induced bank filtration ranks first among all MAR types with 127 sites (57% of total active sites); surface-spreading methods rank second with 77 sites (34% of total active sites) (Sprenger et al. 2017). In India, few or no researchers have investigated Managed Aquifer Recharge (MAR) (Gowrisankar et al. 2017) where the value of MAR sites are less or nil. As a part of the Managing Aquifer Recharge and Sustaining Groundwater Use through Village-level Intervention (MARVI) project, a village-level participatory approach has been developed to measure groundwater levels in groundwater-stressed regions of India and to improve water-use efficiency. However, it has not been intensively implemented (Maheshwari et al. 2014; Dillion et al. 2019). Using radial collector wells, infiltration gallery and pumping to inject water into an aquifer as a technique of Aquifer Storage and Recovery (ASR) in an unconfined aquifer near a stream bed can be best implemented when the river is under gaining conditions (Alam et al. 2022) which has been highlighted in the current study.

MAR implementation is gaining attention, but selecting sites and methods is challenging and costly (Casanova et al. 2016; Dillon et al. 2020). Subsurface factors such as hydraulic conductivity (K_h), transmissivity, aquifer saturated thickness, storage coefficients or specific yields (Sy) of the aquifer, land use type, hydraulic heads, vegetation cover, geology, rock type and soil type, stream conditions that are losing or gaining, etc., play a major role in determining MAR sites. Hydraulic conductivity (K) is the most important among them that can be measured using mini piezometers in a cost-effective manner (Alkhatib et al. 2021).Typically, mini-piezometers include an open end or a perforated interval of a few centimeters with slots or drilled holes near the bottom end of a metal or PVC pipe (Woessner, 2017).There are many ways to install mini-piezometers, including driving them into floodplain sediments with shallow water tables (Rivett et al. 2008; Brodie et al. 2007) and, less commonly, drilling holes in bedrock stream bottoms (Kennedy, 2017).They can be used to investigate hydraulic conductivity and gain/lose stream conditions in shallow sediment aquifers, lake shorelines, and wetland features and can be validated using classical algorithms. The validation of acquired data can be carried out using several grain-size methods proposed by Beyer (1964), Hazen (1893), Kozeny (1927), Schlichter (1899), Sauerbrei (Kasenow, 2002) and Shepherd (1989). An experimental study conducted by Indelman et al. (1999) determined the K_h value for sand layers at Chalk River, Ontario, Canada, by using grain size methods and compared the results with radiotracer data. Their study, however, revealed that the differences between tracer tests and K_h estimates from grain-size analysis has been rather insignificant. Results from slug and bail tests can also provide streambed horizontal hydraulic conductivity (K_h) values, but when compared to grain-size analysis, they provide irrelevant results (Vienken and Dietrich, 2011; Kalbus et al. 2006; Cheng and Chen, 2007). Therefore, a mini piezometer can be used within countries where resources are limited to estimate hydraulic conductivity and can identify gaining and losing streams on a low-budget and with minimal resources. The current study is the first to investigate this research problem, which has not been explored before.

Despite adaptive approaches, such as trial and error, modeling is an important tool for estimating the feasibility of MAR methods. The hydraulic heads can provide information on groundwater flow and stream-aquifer interaction and are therefore required to identify a MAR site (Bresciani et al. 2022). Most models used to estimate hydraulic head and flow direction have not been developed specifically for MAR applications. In addition to MODFLOW (Behera et al. 2022), SEAWAT (Diersch et al. 2002), HST3D (Kipp and Kenneth, 1997), and

PHAST (Parkhust et al. 2004) are also frequently used for modeling saturated flows. It is possible to substitute MODFLOW packages and its long processing times with MIKE FEEFLOW, a finite element subsurface flow and transport simulation system that provides graphics-based and interactive user interfaces, data interfaces with GIS systems, and programming interfaces that can solve complex problems (Khalid Awan et al. 2015; Glass et al. 2022;). There has only been one study published to date that estimates and optimizes three-dimensional groundwater-surface models using FEFLOW models for managing seawater intrusion in Pingtung Plain, Taiwan (Dibaj et al. 2020). Although, no paper has examined FEFLOW model applications specifically for estimating hydraulic head and validation for identification of MAR locations.

5.2.2 Research Gap and Novelty of Work

In addition, MAR projects require feasibility studies before implementation (Ringleb et al. 2016). In particular, choosing suitable sites for the location of a project requires combining and prioritizing different criteria. Numerous studies have documented the benefits of MAR implementation. The main goal of these studies was to find out which areas are the most suitable for artificial recharge. In order to assess the suitability of a site, multi criteria decision analysis (MCDA) is most commonly used (Malczewski and Riner, 2015; Wadi et al. 2022). The MCDA involves the selection and assignment of weights to defined criteria, which introduces some subjectivity into the decision-making process (Afrasiabi et al. 2022; Buchanan et al. 1998). Fuzzy TOPSIS, Fuzzy COPRAS, and Fuzzy EDAS are among the most widely used MDCA alternatives, since they allow for a consistency check in the MCDA, so the bias is reduced and the problems of fuzziness are resolved (Mulubrhan et al. 2014). Over the past decade, a variety of new fuzzy MCDA techniques have been developed (Kansara et al. 2022; Sequeira et al. 2022), some of which have proved to be more effective for certain cases (Jozaghi et al. 2018; Kolios et al. 2016), while others show the opposite results (Dozic and Kalic, 2015; Gul et al. 2021). As a result, in the end, the goals of the different MCDA projects determine the usefulness and performance of the methods (Krishankumar et al. 2021). Asadabadi et al. 2019 have reported that Fuzzy TOPSIS, Fuzzy COPRAS, and Fuzzy EDAS do well when applied to simple problems, and much of the criticism of these methods has been based on misunderstandings of their function and applicability (Dhiman and Deb, 2020). They are easy to use, flexible, intuitive, and has a strong appeal to users, which makes fuzzy TOPSIS, fuzzy COPRAS, and fuzzy EDAS, one of the most popular MCDA techniques (Tavana et al. 2021). Few studies are there on artificial recharge site suitability using fuzzy TOPSIS (Malekian and Reza, 2018) but no studies has been conducted to rank suitable sites for MAR using Fuzzy COPRAS and Fuzzy EDAS.

5.2.3 Objective of the Research Work

A significant increase in water demand has been caused by rapid urbanization, industrialization, and agricultural expansion in India. Having 16% of the world's population, India has only 4% of the world's freshwater resources. It has been estimated that 2%, 9% and 89% of the groundwater consumed here is used by the industrial, domestic and agricultural sectors (Bhunia, 2020; Richard-Ferroudji et al. 2018). The net annual groundwater availability for West Bengal is 27.58 BCM (Billion Cubic Meters) after allowing 2.92 BCM of natural discharge. There is a gross draft of 10.91 BCM for all uses. As a result, there is only 16.75 BCM of groundwater available for irrigation in the future, leaving around 1.02 BCM for industrial and domestic use to 2025. In West Bengal, groundwater has dropped 11 meters since 2013, especially in the central and western parts, including Puruliya, Bankura, West

Medinapore, and Burdwan (State of Environment Report-West Bengal, 2016). This implies the implementation of MAR in West Bengal but no related studies have been there. This research is a breakthrough in the field of MAR in West Bengal where the objective of the study mainly focused on a) estimation of hydraulic conductivity and identification of losing and gaining streams using mini-piezometer and gain size analysis; b) understanding groundwater head and flow modelling using MIKE FEFLOW; c) selection of suitable site for MAR using Fuzzy MCDM techniques and d) validation and efficacy of the MAR site using statistical approaches and pumping test for designing infiltration gallery and radial collector well.

5.2.4 Area of Investigation

The river basin is generally undulating and has a mean elevation of 4 m above sea level (m.a.s.l.) with the highest point at 212 m (Halder et al. 2020). The historical daily records obtained from synoptic meteorology stations of the Indian Meteorological Department within the study area have been used to collect hydroclimate variables, such as minimum and maximum temperature and precipitation. On average, the annual precipitation across the Shilabati river basin is around 190 mm however, their average varies spatially from 200 mm for the downstream section of the basin to 180 mm in the upstream section. The river is approximately 250 km long and 100-200 m wide; its average depth is 15 m, and the stream bed sediments are mainly coarse sand to gravely in the upstream stretch and medium-fine sand in the downstream section (Pal, 2016).

At the upstream section of the study area, the geological strata primarily consist of condensed stratigraphic successions of archacan granite gneiss, Precambrian massive granites, permo-cambriferous sandstone shale, quartzite and active alluvium sediments (Dolui et al. 2016). Granitic gneiss, Pink Granite, and phylite & mica schist are the dominant rocks. In the upstream section of the basin covering the parts of Puruliya district, amphibolites, hornblende, mica schist, intrusive granite, and crystalline limestone are the major rock systems of this unconfined aquifer zone. As these aquifers formed between Palaeozoic and Jurassic times, the groundwater potential and permeability are high in this kind of water bearing layers (Bera et al. 2022). The yield of the wells within this section ranges from 50-100 litre/min. Groundwater movement in granitic gneiss terrain is entirely controlled by lithological characteristics such as joints, topography, fractures, and weathered zone depth (Acharya and Prasad, 2017). The middle section is mainly composed of ferruginous sediments with rock fragments, laterites and sand silt clay having Pleistocene lateritic upland of riverine origin (Mandal and Chakrabarty, 2021). In the downstream section the geological structure is mainly dominated by sand, silt and clay of fluvial origin. In this section, valley-fill deposits generally consist of sand, silt, gravels, pebbles, and other unconsolidated materials and the yield from the tube wells/submersible pumps range from 100-200 litre/min. The groundwater in the study area is mainly stored in a shallow unconfined aquifer in the Quaternary gravel layer with cracks and fractures having a thickness of 50-60 m depth in the upper sections and more than 100 m in the downstream section.

5.2.5 Research Design and Methodology

5.2.5.1 Field investigation and mini drive point piezometer (MDP) installation

In the current research nineteen (19) study sites (Fig.5.14) have been selected along the Shilabati river basin at a distance of 10-15 km from each based on the locational accessibility. To convert the sampling sites in geospatial platform Garmin eTrex® 10, EGNOS-enabled GPS receiver has been used to record the geographical

information. The field investigation has been conducted from November 2021- February, 2022. It is critical to understand how gaining and losing conditions persist over time in order to understand how the stream health is maintained. Thus, such studies are particularly relevant during low flow conditions when water scarcity is high, affecting water resources and its end users as well as the hydro-ecological impacts within the stream and its surrounding ecosystems (Frye, 2013). Among the 19 sites, seven sites are located in the upstream section, seven at the middle and five sites has been chosen at the lower course of the river. The sediments in the upstream section comprises of coarse grain sand and gravel, in the middle section sediments are of sandy-silty type and in the lower section sediments are clayey to sandy clay in origin. The regional groundwater flow is from the west to east of the basin. In-situ hydraulic conductivity and hydraulic gradient has been measured using mini drive point piezometer (MDP) installed in those 19 sites on the stream bed. The installation mechanism of MDPs has been shown in the figure 3. The length of the driver or the steel cast is about 2m, the length of the PVC pipes is about 4m, length of the perforation is 17 cm, radius of the perforated interval is 0.5 cm and the radius of the piezometer is about 1cm. The MDPs used in the current research are less time consuming and cost effective (Chen et al. 2013) with minor river disturbance to the sedimentary structure of the region. All the materials for the fabrication of MDPs are readily available in market with a total cost less than $12/MDP. The steel cast is drilled into the river bed with a disposable drive point cap at the end made up of wood which is an environment benign material (Martinez, 2010). Traditional cross-sectional survey and river water level measurement has been done using a tape, level staff and Trimble® R10 GNSS System and stream flow measurement has been done using a propeller stream flow meter commonly called current meter (Koutalakis et al. 2022). Groundwater level measurement from 47 dug well across the has been done using Solinst TLC (Temperature, Water Level and Conductivity) Meter during the pre-monsoon, monsoon and post monsoon season during the period from 2019-2022. Soil samples have been collected from the MDPs installation sites and 37 sites across the river basin and are sealed in air tight bags for the laboratory analysis. Bulk density has been tested in-situ using sand replacement and core cutter method. The rest of the parameters like grain size analysis, dry density, moisture content, water holding capacity etc. has been analysed in the laboratory. The samples have been dried for 15 days and are placed in a mechanical sieve shaker using a standard ASTM Erode colt sieve at half phi intervals (Bhattacharya et al. 2016). Further analysis, plots, curves and triangular diagram has been done using Origin 2022b software. The flowchart of the complete methodology of current study has been given in Fig. 5.15.

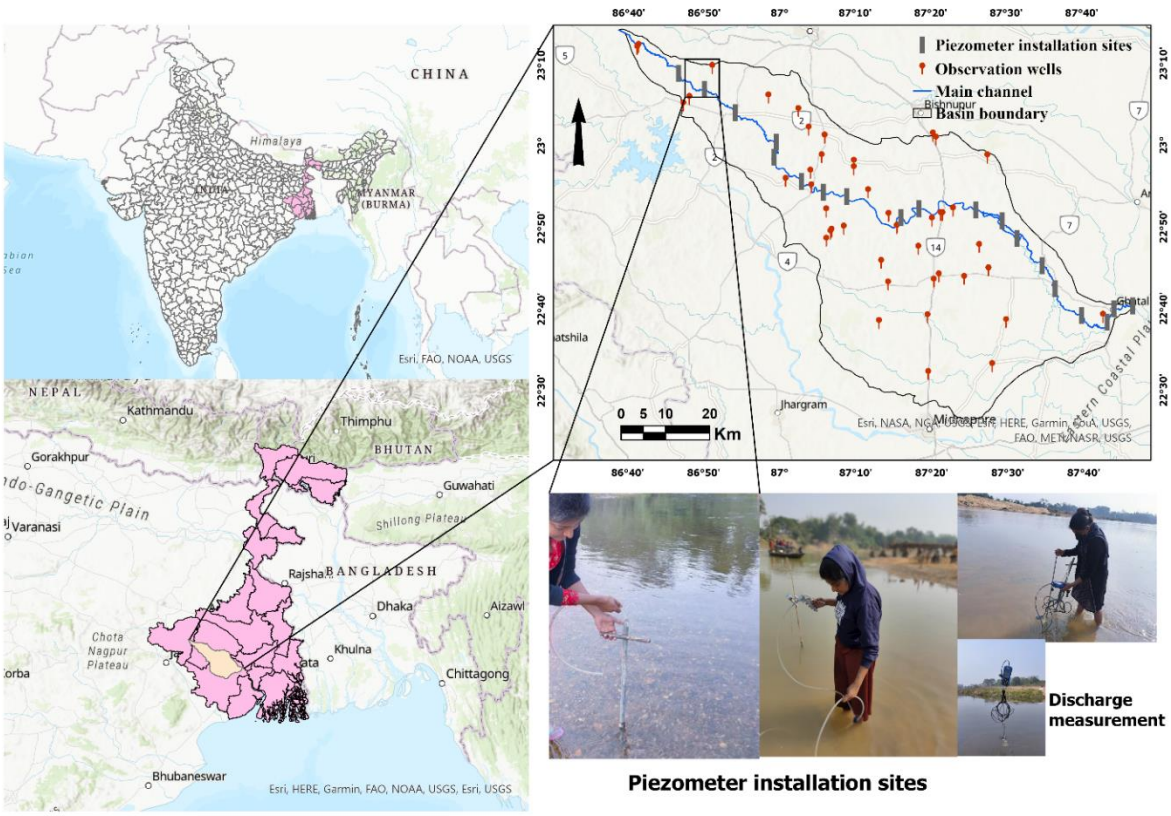

Fig. 5.14 Location of the study and piezometer installation sites

5.2.5.2 Mathematical algorithms to understand ground and surface water exchange

5.2.5.2.1 Vertical gradient

The vertical gradient of the groundwater flow has been determined by installing the MDPs in to the stream bed. Figure 3 shows the driving mechanism for analyzing the hydraulic head where the tube is inserted into the river bed and another tube is submerged into the water being sure to hold it above the stream bottom. A hand vacuum pump has been attached at the top with a 'T' connector to draw water level up in both the tubes (Martinez, 2010). The vertical groundwater gradient has been calculated using the following algorithm (Woessner, 2017; Martinez, 2010; Baxter and Hauer, 2003) (Eq.5.35).

$$\text{Vertical hydraulic gradient } (V_H) = \frac{\Delta h}{\Delta l} \tag{5.35}$$

Where, Δh is the difference between groundwater level measured in MDPs and surface water level in the tube which is divided by the depth to which the MDP penetrates into the streambed (Δl) (Fig. 5.16 D). A positive gradient (+) indicates groundwater level higher than the river water level signifying the effluent stream or gaining condition, whereas negative gradient (-) indicates groundwater level below the river stage signifying influent or losing stream (Simonds and Sinclair, 2002; Woessner, 2017; Woessner, 2000; Winter et al. 1988)

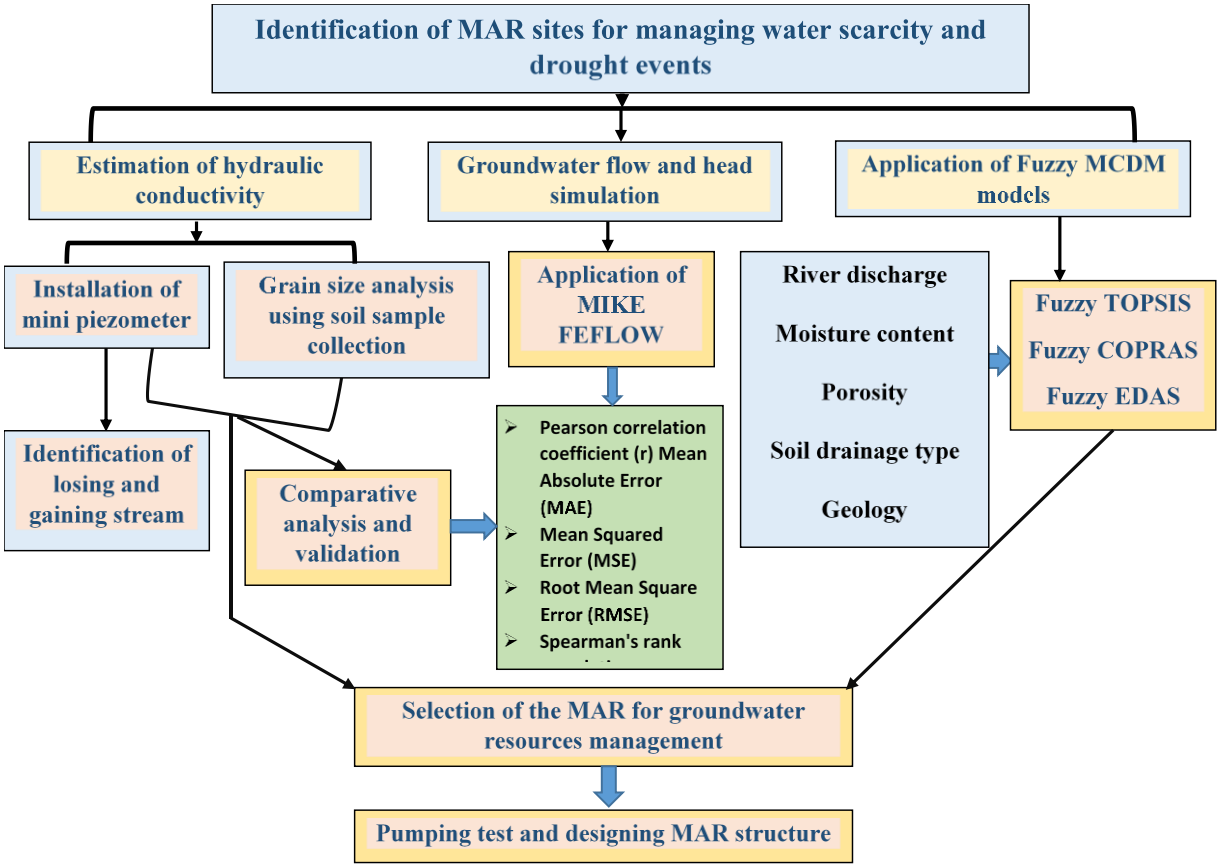

Fig. 5.15 Flowchart for the determination of suitable MAR site for groundwater resource management

5.2.5.2.2 Hydraulic conductivity

a. In-situ permeability test

The in-situ permeability test has been conducted according to the falling head test (Chen, 2000; Chen, 2004). To measure the hydraulic conductivity (K_h) MDPs has been installed in 19 sites within the river bed (Fig.5.14) at varying depth up to the stream bed sediments (Shamsuddin et al. 2019). After installing the MDP, water has been poured in from the top opening within a specific time period until it has been overflowing and reading has been noted (Fig.5.16). The values of in-situ hydraulic conductivity have been calculated using the following algorithm (Rivett et al. 2007; Baxter and Hauer, 2003; Hvorslev, 1951).

$$K_h = \frac{r^2 log_e(\frac{L}{R})}{2LT_o} \qquad (5.36)$$

Where, r is the radius of the mini-piezometer; L is the length of the perforation; R is the radius of the perforated interval; T_o is the basic time lag, a time value (t) as calculated from a plot of field

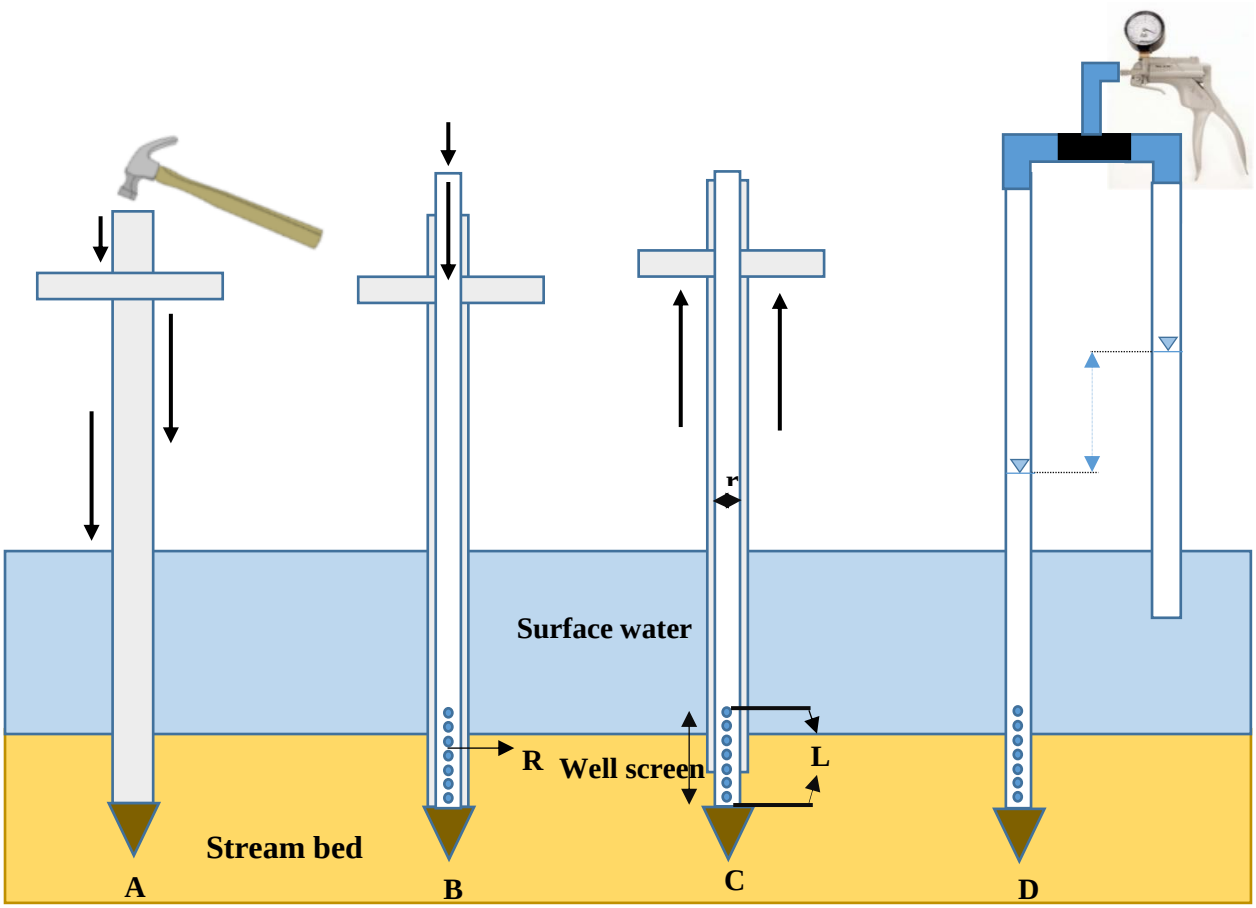

Fig. 5.16 Mini drive point piezometer (MDP) installation mechanism and sequential procedure for estimation of vertical gradient and slug test. (A) Using a hammer on the streambed, the steel cast is forged into the streambed. (B)The mini piezometer is slipped inside the steel casing. (C) In the streambed, the minipiezometer is held in place while the steel casing is removed. (D) Complete installation of minipiezometer for identification of gaining and losing stream

5.2.5.2.3 Ex-situ hydraulic conductivity measurement

To compare and validate the generated data from MDPs, hydraulic conductivity has also been measured using the grain size analysis of the collected soil samples from the 19 sites along the river bed and 37 sites (Fig.5.22) across the river basin. From the sieve analysis the cumulative percentage of weight has been obtained and the results has been plotted on a semi log arithmetic graph in Excel to estimate the parameters including D_{10}, D_{17}, D_{20}, D_{30}, D_{60}, D_{90}, effective grain diameter (de), structure coefficient etc. for calculating hydraulic conductivity using various empirical equations (Fabian et al. 2022). In the current research the classical algorithms of Hazen (1893), Slichter (1898), Beyer (1964), Sauerbrei (Kasenow, 2002), USBR (1990), Kozeny (1953) and Chapuis (2005) has been used. The summery of these algorithms has been outlined in Table 5.6. The calculated hydraulic conductivity from these equations are dimensionally homogeneous which facilitates comparison and analysis as well as practical application (Pliakas and Petelas, 2011). The parameters like porosity and coefficient of grain uniformity required

for the application of these empirical equations has been calculated using the following algorithm (Milan and Andjelko, 1992) (Eq. 5.37 and 5.38).

$$\text{Porosity (n)} = 0.255\ (1+0.83)^{U_c} \quad (5.37)$$

$$\text{Coefficient of grain uniformity} = U_c = \frac{U_{60}}{U_{10}} \quad (5.38)$$

Table 5.6 Effective radius and pore function of estimating hydraulic conductivity from grain size analysis

Name	Equation Type	Structure coefficient (α)	Porosity function θ (n)	Relevant parameter	Applicable conditions
Hazen (1893)	Empirical	6×10^{-4}	[1+10 (n-0.26)]	d_{10} in mm	0.01 cm < d_{10} < 0.3 cm U_c < 5
Slichter (1898)	Empirical	1 ×10-2	n3.287	d_{10}	0.01 cm < d_{10} < 0.5 cm
Beyer (1964)	Empirical	$5.2\times10^{-4} \log\frac{500}{U}$	1	d_{10}	0.006 cm < d_{10} < 0.006 cm 1< U_c < 20
Sauerbrei (Kasenow, 2002)	Empirical	3.75×10^{-3}	$\frac{n^3}{(1-n)^2}$	d_{17}	Sandy and sandy clay d_e < 0.5 mm
Kozeny (1953)	Empirical	8.3×10^{-3}	$\frac{n^3}{(1-n)^2}$	d_{10} or $\frac{1}{d_e} = \frac{3}{2}\frac{\Delta_{g1}}{d_1} + \sum \Delta_{g1} \frac{d_i^g + d_i^d}{2 d_i^g d_i^d}$	Coarse sand/ Large-grain sands
US Bureau of Reclamation (1990)	Empirical	$(4.8\times10^{-4})\ (10^{0.3})$	1.0	$d_{10}^{1.15}$	Medium-grained sand with U < 5; derived for T = 15 °C
Chapuis et al. 2005	Empirical	1.412	$\frac{n^{2.35}}{(1-n)^{1.565}}$	$d_{10}^{1.565}$	0.03 mm ≤ d_{10} ≤ 3 mm

5.2.5.3 Determination of hydraulic parameters, including channel cross-sectional area, flow velocity, and water level

The elevation of the river channel bed above the mean sea level (MSL) has been determined by employing a tape, level staff, and the Trimble® R10 GNSS System. To assess the river cross section and water velocity (V) at each station, several hydrological instruments have been utilized, including a current meter, depth measuring standard, measuring tape, and stake. The discharge value (m^3/s) (Q) is calculated as the product of velocity and cross-section area (A) (m/s). The cross-section area, which can be trapezoidal or triangular in shape, is derived from multiplying the depth (d) and width (w), as indicated in Eq.5 and 6 (Kamarudin et al. 2017). These values consider the factors such as the limitations of the current meter, the variability of river flow velocity across the cross section, and the uncertainty in calculating the cross-sectional geometry. The river flow gauge was determined using the velocity-area method, which involved using a current meter to measure specific point velocity at specified intervals of 20%, 40%, 60%, and 80% of the river flow depth at multiple verticals across the channel cross-sections. The flow depths and specific point velocities have been measured with an accuracy of 0.0002 m (0.2 mm) and 0.0002 m/s, respectively. The data from each vertical point has been collected and averaged to obtain the mean point velocity, reducing approximate errors resulting from variations in water flow.

$$\text{Cross-section area (CSA)} = w \cdot d\ (m^2) \quad (5.39)$$

$$\text{Discharge } (Q = w \cdot d \cdot V)\ m^3/s \quad (5.40)$$

5.2.5.4 Groundwater flow modelling using MIKE-FEEFLOW model

A two-dimensional variable density finite groundwater model of Shilabati river basin has been developed using MIKE FEFLOW software (Dibaj et al. 2021). FEFLOW is a new user-friendly groundwater modelling software which uses a finite triangular element mesh to represent the model platform that provide more efficient refinement around the boundaries and wells than MODFLOW, GMS, Groundwater Vistas, PEST etc. (Kumar, 2019). FEFLOW can easily construct complex grids embedded with GIS packages making it a powerful tool for critically analyzing groundwater scenarios (Trefy and Muffels, 2007). Groundwater data has been extracted from 27 pumping wells (Fig.5.22) within the river monitored by Public Health Engineering Department (PHED), West Bengal having a yield range from 50-200 liter per minute. 47 Observation wells (Fig.5.14) located within the basin has been monitored by the authors within the time frame of 2019-2022. Firstly, the 2D domain of the river basin has been generated as a polygon shape file in ArcGIS platform with main river channel and 27 pumping well location has been imported into the FEFLOW model (Dibaj et al. 2020). Secondly, a super mesh has been generated as an intermediate stage incorporating the outer and inner geometrics. Based on the super mesh, a finite triangular element mesh has been generated following a two-step procedure. First the triangular mesh has been generated to discretize the irregular internal and external geometry of the super mesh and then the triangular mesh has been converted into a quadrangular mesh (Fig. 5. A1) to reduce the number of elements by maintaining the representation of geometrical input features of the super mesh (Dhi-wasy, 2010). The model domain covers an area of 3888 km^2 with 42,526 elements and 20,500 nodes. The elevation of the model varies from 5-210 m above mean sea level. The current model consists of a single layer which has been conceptualized based on the input parameters including boundary conditions (Table 5.10), groundwater level, geology, land use, river stage, discharge etc. The summary of the model parameters has been given in table. Hydraulic conductivity and porosity required for the model has been estimated from the grain size analysis of 37 soil samples as collected from different sections of the basin (Fig.5.22). The river flows from the west to east and is non-perennial that remains dry almost throughout the year and as such the recharge has been estimated using the Groundwater Estimation Committee (GEC, 2015), which has been used in the model as material properties (Sridhar et al. 2018). Infiltration rate has been estimated using the minidisk infiltrometer during the field study. Such infiltrometer has been fabricated using a polycarbonate tube with semi-permeable stainless steel with an attached porous disk at the bottom (AL Sulaiman and Aboukaima, 2016). Initially at time zero, infiltrometer has been placed on the soil surface at the depth of 15cm from the ground. Infiltration rate has been determined by estimating the volume of water infiltrating into the ground over time. The model has been simulated in steady state conditions to identify the groundwater flow direction and has been calibrated with a number of trial and errors (Pande et al. 2022). The model has been reasonably calibrated and validated after a number of runs and estimated the groundwater head using the groundwater level data of 47 observation wells from 2019-2022. The groundwater flow in the current research has been simulated using the following two-dimensional equation of finite difference method (Su et al. 2018; Todd and Mays, 2005) (Eq.5.41).

$$\frac{d}{d_x}\left(K_{xx}\frac{d_h}{d_x}\right)+\frac{d}{d_y}\left(K_{yy}\frac{d_h}{d_y}\right)=S_s\frac{d_h}{d_t}+\mathrm{Q} \qquad (5.41)$$

Where, $K_{xx,}$ K_{yy} are the hydraulic conductivity in x and y direction, h is the hydraulic head, S_s is the specific storage coefficient and Q here indicates the source/sink (pumping, recharge etc.). The model output provided the contours of the head equipotential lines and graphs of calculated verses observed head.

5.2.5.5 Identification of suitable Manage Aquifer Recharge (MAR) sites using MCDM models

Induced infiltration of water into the adjacent aquifer using riverbank infiltration and recharge can result in positive changes in water quality and quantity as a result of filtration, biodegradation, and adsorption (Hoang et al. 2022). Although MAR is a growing technology, the successful and cost-effective operation of large-scale schemes relies on rigorous site investigation due to hydrogeological variables that vary from site to site. For decades, riverbank filtration (RBF) has been widely used in Europe (Hubbs, 2006; Grischek, 2020) and in the USA as a low-cost pretreatment method (Kruc et al. 2020; Dillon et al. 2019) and currently in countries like China, India (Ronghang et al. 2019), and Egypt (Hu et al. 2016; Sandhu et al. 2011; Ghodeif et al. 2016). A site investigation for MAR can be expensive and time-consuming that involves boring, logging, pumping tests, and hydrochemical sampling (Sandhu, 2015). It is therefore important to develop a methodology for pre-selecting and pre-evaluating suitable sites across a wider area, making use of available databases and multi-criteria decision analyses, particularly in regions where MAR is not widely applied but can have a significant impact on water supply and management system. In the current study hydrogeological characteristics of aquifer for 19 different sites has been estimated using the installation of MDPs and field survey. For the current work, nine conditioning parameters have been considered for the selection of suitable site for MAR namely hydraulic conductivity, river discharge, moisture content, porosity, drainage type, rainfall, land use type, geology and aquifer material. Three fuzzy system incorporated with MCDM techniques like Fuzzy EDAS, Fuzzy TOPSIS and Fuzzy COPRAS has been applied to rank the 19 different sites as the best river bank infiltration site. The development of fuzzy decision-making models along with MCDM methods is gaining traction rapidly. Evidence from research groups shows the crucial importance of fuzzy decision models (Kahraman et al. 2017). A fuzzy model is created by combining different MCDMs and related techniques which includes Fuzzy TOPSIS, fuzzy VIKOR, fuzzy COPRAS, fuzzy EDAS etc. It was Ghorabaee et al. (2015) who developed the classic EDAS method for multi-criteria inventory problems. In a subsequent study, Ghorabaee et al. (2016) used the EDAS approach for selecting suppliers. Kahraman et al. (2017) applied a new EDAS approach to solving solid waste disposal site choice problems. It is based on the distances between each alternative and the average solution based on each criterion. EDAS has also been shown to be an efficient method of handling MCDM problems. The influence of maximizing and minimizing criteria on evaluation results is considered separately in fuzzy COPRAS method. It considers both ideal and anti-ideal solutions when selecting a best alternative. A fuzzy COPRAS approach has been used by Chatterjee and Bose (2013) to select wind farm sites, Fouladgar et al. (2012) evaluated the working strategies at a construction company and the risk analysis of critical infrastructure has been carried out by Yazdani et al. (2011). As fuzzy linguistic variables are used to give weights to attributes and ranking to alternatives (Akram et al. 2022), the fuzzy COPRAS would be appropriate in this study. Chen (2000) proposed the Fuzzy TOPSIS method for solving MCDM problems. The fuzzy TOPSIS decision model includes incomplete, unquantifiable and vague data (Masdari and Khezri, 2020; Dhiman and Deb, 2020). This method has been used in many fields, such as site selection (Beskese et al. 2015), renewable energy (Rani et al. 2020), sustainability, supplier assessment and

selection (Kumar et al. 2018) and locational problems. Through considering real-life uncertainties and linguistic human decisions, the intuitionistic fuzzy numbers (IFS) based TOPSIS model can reflect approval or rejection, and ambiguity displayed by decision-makers and thus it has been used in this study to select RBF sites. The location which obtained the highest value have been regarded as the site which has the potential and the need for the implementation of MAR to manage water scarcity during drought events.

5.2.5.6 Statistical techniques for validation and accuracy

To evaluate the accuracy of the in-situ and ex-situ hydraulic conductivity, three error metrics has been used for the current research including Mean Absolute Error (MAE), Root Mean Square Error (RMSE), and Mean Squared Error (MSE**).** The methods are useful for comparing the predictions of two different forecasting methods based on the same data or series. (Amar et al. 2019). In order to calculate these error metrics, the following equations (5.42–5.44) have been used where n is the number of data points, y is the actual output vale (observed) and $\hat{y}$ is the predicted output value. The smaller the value of these metrics, the more accurate the technique (Rinne et al. 2022).

$$\text{Mean Absolute Error (MAE)} = \frac{1}{n}\sum_{i=1}^{n}|y - \hat{y}| \tag{5.42}$$

$$\text{Mean Squared Error (MSE)} = \frac{1}{n}\sum_{i=1}^{n}(y - \hat{y})^2 \tag{5.43}$$

$$\text{Root Mean Square Error (RMSE)} = \sqrt{\frac{\sum_{i=1}^{n}(y-\hat{y})^2}{n}} \tag{5.44}$$

Spearman's rank correlation

The Spearman rank correlation coefficient (Spearman ρ) is a nonparametric correlation coefficient (Dodge, 2008). In light of the popularity of Spearman's rank correlation coefficient, it has been further developed into a weighted variant that reflects differences between rankings better, as the alternatives ranked best are more significant than the rest of them (Paradowski and Szyjewski, 2022; Arabameri et al. 2018). Each observation from the fuzzy MCDM model for each site has been assigned a rank according to its position relative to the others in its own group. Spearman's rank correlation coefficient between the kth and ith MCDM methods has been calculated by the following equation (Gang et al. 2012) (Eq.5.45).

$$r_s = 1 - \frac{6\sum_{i=1}^{n} d_i^2}{n(n^2-1)} \tag{5.45}$$

Where d_i is the difference between the ranks of Fuzzy MCDM models for each alterative and n is the number of observations.

5.2.6 Results and Discussion

5.2.6.1 Comparative analysis of hydraulic conductivity between insitu and exsitu measurements

Aquifer parameters such as hydraulic conductivity, porosity, transmissivity, permeability etc. play a crucial role in groundwater assessment (Lachassagne et al. 2021). In most common cases these parameters are best estimated by pumping test which is expensive and time consuming (Oli et al. 2022). Hydraulic conductivity estimated using the MDP and gain size analysis provides a cost effective, less time consuming and efficient alternative. A total of 19 sites along the main Shilabati river from source to mouth has been selected for the installation of piezometer from where soils samples has been collected from the depth of about 20-30 cm. The key parameters of grain size distribution namely D_{10}, D_{17}, D_{20}, D_{30}, D_{60}, D_{90}, Coefficient of grain uniformity, porosity and soil textural and hydrological characterization including percentage of gravel, sand, silt and clay, bulk density, moisture content and dry density has been summarized in table 5.8. The textural characteristics of soil for each location has also been shown using figure 5.17. With the variable geological environment, gravel content (50.30 %) has been the highest in the upper Shilabati basin near Bangopalpur and almost zero near the mouth. The percentage of sand shows a progressive increase from the upper section of the basin at Chhotakeehanda (89.30 %) with its peak at the middle section (Raghunathbari-99.3 %) and thereafter decreases. The silt content revealed an opposite trend to that of the sand percentage. The clay content in the lower section of the basin has been the highest near the outlet (29.20 %) followed by Shyampur (24.1%), Dharmmapur (19.30%) and Radhakantapur (10 %). Due to the channel transportation, the sand content decreased from the upstream to downstream section in the river basin whereas the clay and silt content increased (Bhattacharya et al. 2016) due to flood deposits and tidal action (Maity and Maiti, 2013). A general insight can be gained from the hydrologic-process-based soil textural classifications (Fig 5.17), where clay-rich soils have low infiltration and drainage capacities, while low-clay soils have the opposite characteristics (Groenendyk et al. 2015). The bulk density of the river stretches ranges from 1.65 to 1.86 g/cm^3 and dry density varies from 1.36 to 1.76 g/cm^3. The area where the bulk density increased porosity decreased resulting in the decrease in the soil infiltration capacity (Zhou et al., 2009). The soil moisture content ranges from 3.10% to 36.10% and is lowest in the upstream and middle section because of the high evaporation rate and poor retention capacity of laterite soil (Rong et al. 2017). The other parameters from the grain size analysis have been used to calculate the K_h values using 7 classical algorithm including Hazen (1893), Slichter (1898), Beyer (1964), Sauerbrei (Kasenow, 2002), USBR (1990), Kozeny (1953) and Chapuis (2005). The K_h obtained from the MDPs and grain size analysis has been summarized in table 5.8 with comparative analysis in figure 5.18. The K_h values from the MDPs across all the study sites ranges from 0.00206 (Shyampur) to 6.765 m/day (Dakshin Pairachali). The values obtained from the different classical methods differed greatly based on their individual constraints but followed a similar trend and patterns (Fig.5.18). The error metrics including MAE (0.03), MSE (0.01) and RMSE (0.06) between the estimated value and MDP observed value has been lowest in case of Slichter equation giving a better fit and validating the accuracy of field investigation. In the light of the domain applicability of the empirical algorithms, K_h values from Shilabati river basin are mostly deviated from the Chapuis method due to its theoretical and locational implications. The K_h values from MDP is higher in the upstream section and middle because of the presence of gravel, coarse grain to fine grain sand and lowest in the downstream part. In soil with high sand content, non-capillary pores are likely to increase, improving the saturated hydraulic conductivity (Dingle et al. 2021). In contrast, soil with a higher clay and silt content have a lower hydraulic conductivity due

to the reduced water transmission in soil profile (Momin et al. 2018). Based on the above observations made, it can be concluded that the upper and mostly the middle section of the basin has higher potential for groundwater recharge and surface infiltration which will thereby increase the water quality of the aquifer below. Thus, the estimation of K_h for the initial assessment of stream-aquifer interaction and identification of MAR sites are proven necessary and application of MDPs can be an alternate technique suitable for such analysis (Wolny et al. 2018). Such studies are also beneficial for the rejuvenation of dying river basins globally as the number of such well-documented field illustrations are quite limited.

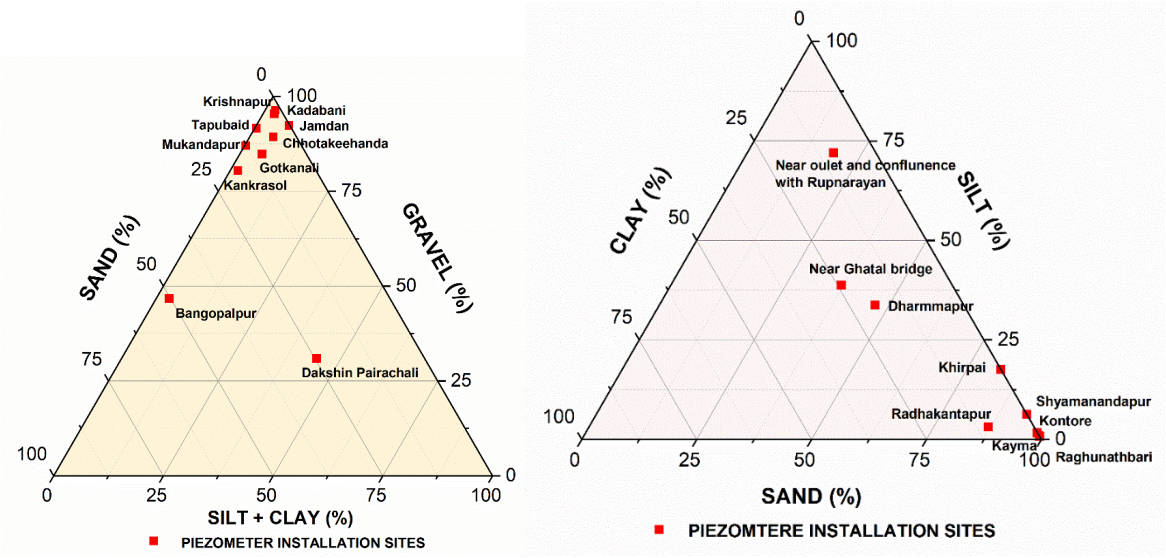

Fig. 5.17 Soil classification of the 19 sites plotted based on USDA soil classification

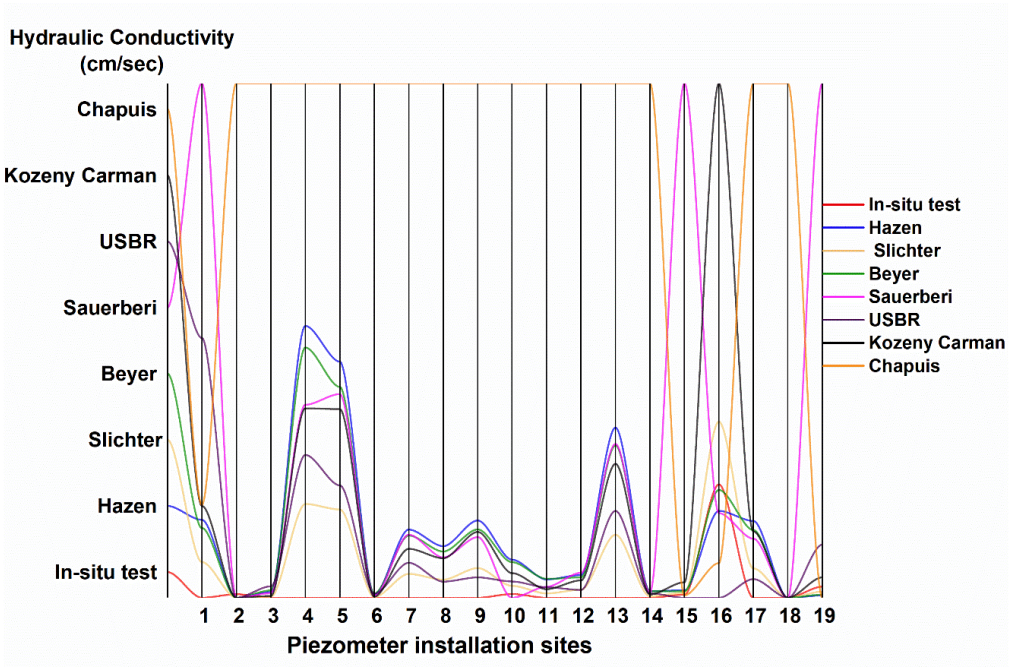

Fig. 5.18 Comparative analysis of hydraulic conductivity (K_h) from different estimation technique

Table 5.7 Soil particle size distribution of estimation of hydraulic conductivity from statistical grain size analysis

Sites	Gravel (%)	Sand (%)	Silt (%)	Clay (%)	Bulk density ($g/cm^{3)}$	Moisture content (%)	Dry Density ($g/cm^{3)}$	D_{10}	D_{17}	D_{20}	D_{30}	D_{60}	D_{90}	U_C	Porosity
Bangopalpur	50.30	48.70	3	0	1.75	4.70	1.67	0.29	0.83	1.04	2.01	0.20	0.00	0.69	0.48
Dakshin Pairachali	34.60	60.90	3.60	0.90	1.75	10.20	1.44	0.001	0.011	0.02	0.04	0.20	0	118.47	0.26
Chhotakeehanda	5.30	89.30	5.40	0	1.65	14.40	1.44	0.139	0.25	0.30	0.62	1.37	3.94	9.88	0.30
Mukandapur	12.70	87	0.30	0	1.80	2.40	1.76	0.648	0.80	0.84	0.98	1.91	0	2.94	0.40
Tapubaid	8.0	91.60	0.40	0	1.75	12.60	1.55	0.493	0.62	0.66	0.71	1.11	4.06	2.25	0.42
Gotkanali	10.10	84.80	5.10	0	1.93	13.20	1.71	0.104	0.17	0.19	0.25	1.10	4.82	10.54	0.29
Kayma	0	99.20	0.80	0	1.85	13.20	1.63	0.226	0.31	0.34	0.42	0.63	1.01	2.78	0.41
Kontore	0	98.3	1.70	0	1.62	13.30	1.43	0.157	0.19	0.21	0.23	0.38	0.68	2.41	0.42
Raghunathbari	0	99.30	0.70	0	1.80	12.40	1.60	0.164	0.19	0.20	0.21	0.32	0.69	1.95	0.43
Kadabani	2.0	95.40	2.60	0	1.78	5.40	1.67	0.180	0.05	0.25	0.32	0.59	1.16	3.27	0.39
Kankrasol	17.80	80.40	1.80	0	1.77	8.90	1.62	0.174	0.24	0.26	0.31	0.91	0	5.21	0.35
Shyamanandapur	0	93.70	6.30	0	1.79	5.60	1.70	0.084	0.12	0.12	0.15	0.21	0.28	2.46	0.42
Krishnapur	1.30	96.30	2.40	0	1.76	3.10	1.71	0.386	0.50	0.55	0.63	0.90	1.84	2.32	0.42
Jamdan	0.20	92.30	7.50	0	1.80	5.60	1.76	0.087	0.13	0.15	0.19	0.41	0.76	4.71	0.36
Khirpai	0	82.5	17.50	0	1.755	23.90	1.42	0.083	0.58	0.08	0.10	0.18	0.27	0.00	0.51
Dharmmapur	0	47	33.70	19.30	1.84	25.20	1.47	0.002	0.001	0.002	0.03	0.07	0.16	0.00	0.51
Radhakantapur	0	86.90	3.10	10	1.80	26.40	1.69	0.156	0.18	0.19	0.21	0.30	0.49	1.89	0.43
Shyampur	0	37.20	38.70	24.10	1.86	29.50	1.43	0.002	0.00009	0.001	0.02	0.04	0.13	16.50	0.27
Near outlet and confluence with Rupnarayan	0	18.80	52	29.20	1.86	36.10	1.36	0.001	0.01	0.013	0.02	0.07	0.20	0.00	0.51

Table 5.8 Hydraulic conductivity measure and calculated using empirical algorithms

Sites	In-situ Permeability (cm/sec)	Hazen cm/sec	Slichter cm/sec	Beyer cm/sec	Sauerberi cm/sec	USBR cm/sec	Kozeny Carman cm/sec	Chapuis cm/sec
Bangopalpur	0.0018700	0.156345	0.072722	0.140052	1.020945	0.516564	0.183944	0.185671
Dakshin Pairachali	0.0078300	0.000002	0.00000032	0.000001	0.000014	0.000040	0.00000047	1.099912
Chhotakeehanda	0.0006260	0.015336	0.003429	0.019297	0.012082	0.029407	0.005446	1.296902
Mukandapur	0.0001300	0.597462	0.206056	0.549822	0.424152	0.313987	0.416154	1.130084
Tapubaid	0.0001080	0.374538	0.140172	0.334608	0.323258	0.178431	0.299173	0.816014
Gotkanali	0.0000652	0.008401	0.001846	0.010768	0.005112	0.010161	0.002907	1.279651
Kayma	0.0001040	0.074248	0.026089	0.067806	0.068621	0.038164	0.053337	0.559471
Kontore	0.0008350	0.037598	0.013789	0.033803	0.029605	0.012332	0.029018	0.367444
Raghunathbari	0.0003470	0.043111	0.016748	0.038142	0.033869	0.011573	0.036711	0.284686
Kadabani	0.0055300	0.044697	0.014877	0.041795	0.001341	0.019872	0.029369	0.586130
Kankrasol	0.0016900	0.034229	0.009586	0.035414	0.021049	0.020235	0.017098	0.915346
Shyamanandapur	0.0001690	0.010729	0.003915	0.009662	0.011745	0.003783	0.008212	0.238853
Krishnapur	0.0001390	0.228036	0.084627	0.204246	0.206207	0.116577	0.179561	0.689327
Jamdan	0.0006660	0.008980	0.002615	0.009050	0.007582	0.006250	0.004768	0.652680
Khirpai	0.0055500	0.011420	0.007772	0.010146	0.676136	0.001447	0.021816	0.004686
Dharmmapur	0.0000044	0.000003	0.000007	0.000004	0.000003	0.000000	0.000019	0.000002
Radhakantapur	0.0006520	0.039286	0.015396	0.034693	0.030404	0.010038	0.033963	0.259269
Shyampur	0.0000024	0.000004	0.000001	0.000006	0.000000	0.000000	0.000001	1.017432
Near outlet and confluence with Rupnarayan	0.0000051	0.000002	0.000003	0.000002	0.000202	0.000022	0.000009	0.000001
MAE (In-situ and classical algorithms)	-	0.09	0.03	0.08	0.15	0.07	0.07	0.10
MSE (In-situ and classical algorithms)	-	0.03	0.01	0.03	0.10	0.02	0.02	0.20
RMSE (In-situ and classical algorithms)	-	0.18	0.06	0.16	0.31	0.15	0.13	0.60

5.2.6.2 Identification of losing and gaining stream

MDPs installed within the stream bed also provide with the information of losing and gaining stream condition by comparing the water level in piezometer and river water level (Kalbus et al. 2006; Freeze and Cherry, 1979). Many studies have been conducted earlier to identify gaining and losing condition using stream bed temperature profile (Schmidt et al. 2007), water budget method (Larned et al. 2015), flow gauging method (Vincent, 2005; Riegler, 2012), steady state groundwater budget method (White et al. 2012) but the estimation procedure of MDPs is straight forward and easy to install (Kennedy, 2017). MDPs are therefore appropriate for such data scarce basin which provided a detailed scenario of sub-surface flow condition at 19 different locations within Shilabati river basin. The mechanism related to the exchange process between the surface and groundwater interaction can be better understood in two theoretical concepts: groundwater infiltrates through the sediments into the stream (gaining stream), and stream water recharges the aquifer below (losing condition) (Cardevas, 2009). In some parts of a stream, it may act as a gaining medium, while in other sections, it may lose. In gaining conditions, the groundwater table level is higher than the river stage, whereas in losing conditions, the groundwater table level is lower than the river stage (Krause et al. 2011). In the current research, vertical hydraulic gradients (VHGs) have been calculated using piezometer data to identify gaining and losing streams. A positive VHG represents a gaining stream or effluent condition, while a negative VHG represents a losing stretch, where surface water recharges the aquifer beneath (Woessner, 2017; Simonds and Sinclair, 2002). Figure 5.19 and table 5.9 shows the gaining and losing stretch of the Shilabati river basin from source to mouth with K_h values (Fig.5.20). Among the 19 sites, 5 have influent conditions and 14 have effluent conditions with VHGs ranging from -0.21 to -1.07 and 0.01 to 3.14 respectively. Losing streams are most common in the dry climate and the locations at Bangopalpur and Chhotakeehanda fall under the drought prone region where the temperature ranges from 7°C in winter to as high as 47°C in summer, increasing the rate of evaporation (Patra, 2020). The districts namely Puruliya, Bankura and West Medinapore covering the river basin are experiencing extreme decline in water table whereas the uppermost section of the river basin is known for its scarcity of water and is considered as a drought-prone region (Bera et al. 2022). Losing stream condition is also observed in the downstream section at Radhakantapur, Shyampur and near the outlet of the Shilabati basin where the main channel meets the Rupnarayan River which is tidal in nature. Additionally, tidal stretches may change the pattern from losing to gaining and vice versa as the height of the water in the channel rises and falls twice daily (Cao et al. 2020). The effect of tide in the River Hugli impacts the lower section of the river near Bandar point which may be the reason of concern (Maity and Maiti, 2013). The fig. 5.21 shows a dramatic comparison between losing and gaining conditions under three different environmental conditions, including groundwater level, river discharge, and rainfall. An example of tidal influence can be seen in the downstream section of the basin where the groundwater level in the nearby well is high under the losing condition. Losing condition in the lower section of the basin is also influence by extensive pumping from the irrigation wells when the zone of drawdown in the aquifer intersect the surface water body nearby (Halder et al. 2020). There has been an increase in groundwater pumping in recent years, and such abstraction trends are predicted to continue in the near future, transforming gaining to losing conditions (Mukherjee et al. 2018). While the middle part of the basin has gaining conditions, where upward flow drives away fine particles, increasing pore space near the stream bed, resulting in higher hydraulic conductivity (Chen et al. 2013). A high K_h value is also caused by the high carbon content of the surface soil as compared to the subsoil due to the limited downward leaching of crop residues and incorporation of organic matter (Momin et al. 2018). These pore spaces of sediments

also decrease under losing stream conditions because of physical, chemical, and biological processes (Hancock, 2002). Clogging thus reduces K_h values of the losing stream by 10-100 times and thereby interrupting hydrological connection between stream and adjacent aquifer and cannot be selected for a MAR site.

Fig. 5.19 Losing and gaining stream conditions across the river basin

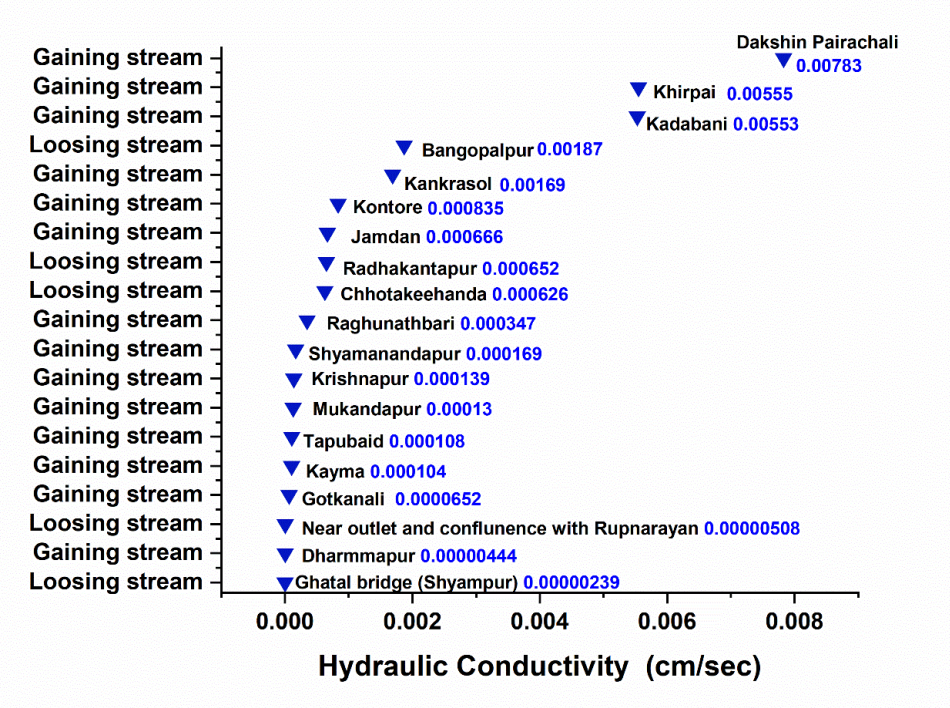

Fig. 5.20 Plotting of losing and gaining sites against hydraulic conductivity (K_h)

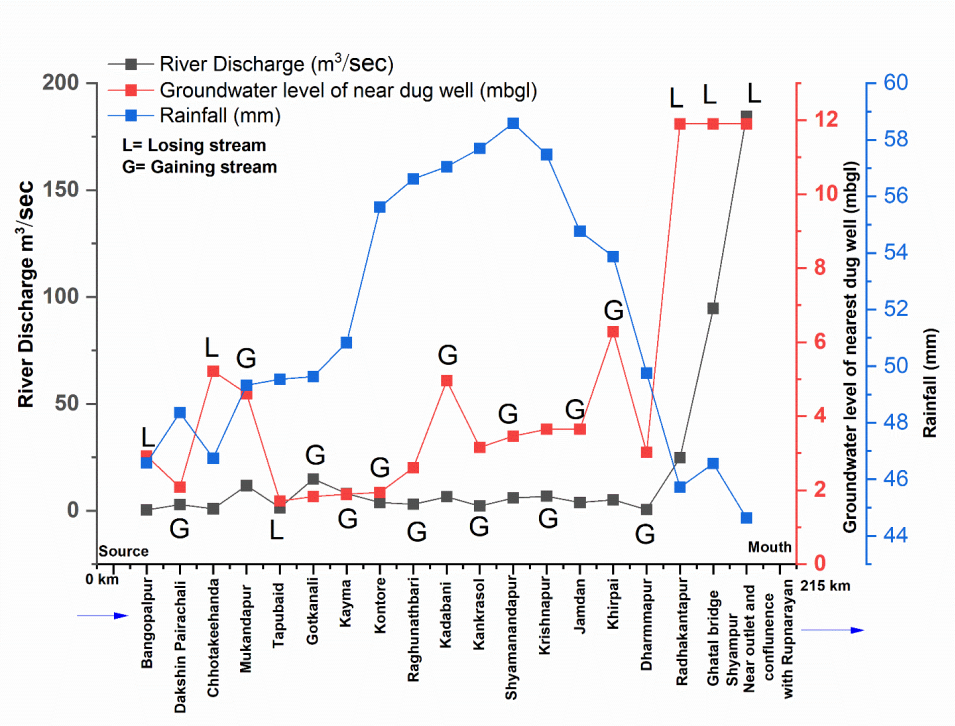

Fig. 5.21 Understanding the groundwater- stream water exchange under different hydro-environmental conditions

Table 5.9 Summarization of observed data mini-piezometer

Location	Latitude (North)	Longitude (East)	Elevation (m)	Vertical groundwater gradient	Losing/ gaining stream	In-situ Permeability (cm/sec)	In-situ Permeability (m/day)
Bangopalpur	23.14858056	86.77734722	135	-0.33	loosing stream	0.0018700	1.61568
Dakshin Pairachali	23.11579444	86.83453611	120	1.68	gaining stream	0.0078300	6.76512
Chhotakeehanda	23.06836389	86.90185548	96	-0.7	loosing stream	0.0006260	0.540864
Mukandapur	23.00806944	86.99255899	79	0.82	gaining stream	0.0001300	0.11232
Tapubaid	22.97702222	86.98856389	70	1	gaining stream	0.0001080	0.093312
Gotkanali	22.92847522	87.04892558	62	1.94	gaining stream	0.0000652	0.0563328
Kayma	22.90585833	87.09648056	55	0.59	gaining stream	0.0001040	0.089856
Kontore	22.89682222	87.14722589	50	2.05	gaining stream	0.0008350	0.72144
Raghunathbari	22.85430278	87.26718333	36	0.64	gaining stream	0.0003470	0.299808
Kadabani	22.87198056	87.30687222	34	0.74	gaining stream	0.0055300	4.77792
Kankrasol	22.88113056	87.38485556	24	2.6	gaining stream	0.0016900	1.46016
Shyamanandapur	22.86696667	87.43955556	22	0.36	gaining stream	0.0001690	0.146016
Krishnapur	22.81056389	87.52245893	16	0.84	gaining stream	0.0001390	0.120096
Jamdan	22.75507778	87.57656389	11	0.97	gaining stream	0.0006660	0.575424
Khirpai	22.70825833	87.60583611	12	3.14	gaining stream	0.0055500	4.7952
Dharmmapur	22.6527837	87.66388133	8	0.01	gaining stream	0.000004440	0.00383616
Radhakantapur	22.63927778	87.71961667	5	-1.07	loosing stream	0.0006520	0.563328
Shyampur	22.66616944	87.73495899	12	-0.21	loosing stream	0.000002390	0.00206496
Near outlet and confluence with Rupnarayan	22.67119167	87.77787222	3	-0.49	loosing stream	0.0000051	0.00438912

5.2.6.3 Groundwater flow modelling using MIKE-FEFLOW

In the current research, groundwater simulation has been carried out for the Shilabati River basin to highlight a possible scenario of the hydraulic head (metres above sea level - m.a.s.l). The general elevation of the basin varies between 210 to 5 meters from upstream to downstream. In the basin, groundwater levels range from 0.86 to 15.6 mbgl, with hydraulic conductivity ranging from 7.66 - 45.62 m/day and porosity varying from 38.7 - 76.67 (Fig.5.24), having groundwater under unconfined to semi confined in condition. During the pre-monsoon and post-monsoon seasons, most tube wells and dug wells within the basin experience severe groundwater decline (Bera et al. 2022). As a result of deforestation, unscientific groundwater extraction, and rapid settlements, extreme drought events occur more frequently in Western districts of West Bengal, particularly Puruliya, Bankura, and West Medinapore (Gupta and Patel, 2021; Halder et al. 2022). Within the basin, wells are often drilled and water is supplied to agricultural fields during rainless months for the cultivation of Rabi and Kharif crops. The majority of dug wells within the basin are operated manually or with mechanical power, and open channels are commonly used to irrigate crops. As compared to the upstream section of the basin, the middle and downstream sections utilize more groundwater, which requires the implementation of MAR along the Shilabati river basin (Chakraborty et al. 2022; Das et al. 2021). Discharge/yield from the pumping wells within the river basin ranges from 73m^3/day to 576 m^3/day. Groundwater discharge is higher in the parts of upper, middle and parts of downstream section, where it occurs in shallow, moderately weathered areas of older alluvium under unconfined conditions, as well as joints, fissures, and fractures beyond a semi-confined weathered zone. In this region, groundwater transmission, movement, and occurrence are influenced primarily by secondary porosity, namely fluvio-deltaic sediments (Bhunia et al. 2012; Mukherjee, 2016). Based on the fine gradation of soil particles to coarse-grained soil, the soil infiltration rate within the basin ranges from 0.5 mm/hr to 210.1mm/hr (Das et al. 2018). The river discharge is also very low near the source of the river basin with only 0.410 m^3/sec at Bangopalpur, whereas it is the highest near the outlet (184 m^3/sec) (Table 5.11). In the upper catchment of the channel, ephemeral flows occur during storm events, while downstream sections experience perennial flows and flood discharge during the monsoon (Choudhury, 2022). The hydraulic head has been simulated using MIKE FEFLOW (Fig.5.25 & 5.26) incorporating all the boundary conditions (Table.5.10) and material properties mentioned above. Groundwater in the Shilabati river basin has a regional flow governed by the spatial distribution of hydraulic conductivity and thus it flows from the areas of recharge (North and south edges of the basin covered with forest) to the areas of discharge (near the main channel lines) (Alfy et al. 2019). The net annual groundwater flow as simulated by MIKE FEFLOW has been directed towards the main channel. Groundwater velocity vectors indicate that the flow path is predominantly southward in the upstream section, and there is a complex flow condition in the middle and again southward in the downstream section. In the upper and middle sections of the stream, where the hydraulic conductivity of the streambed is high, groundwater flows with increased velocity near higher K_h values (Bresciani et al. 2018; Ge, 2003). As measured, the groundwater head in the basin ranges from 157 m.a.s.l. to 39.8 m.a.s.l., whereas the calibrated head from the model ranges from 157.5 m.a.s.l. to 38.9 m.a.s.l. for the selected observation wells. Observed groundwater head and calibrated groundwater head showed a reasonable agreement with Pearson's R of 0.90 (Fig.5.27) under steady state conditions. Accordingly, the equal potential lines indicate zones of high hydraulic conductivity near the main channel, which correspond to a rising infiltration capacity and an appropriate recharge site. Thus, it is necessary to conduct such studies before examining, suitable MAR sites, which have not yet been highlighted earlier.

Table 5.10 Boundary conditions for groundwater flow modelling using MIKE FEFLOW

Model setup	Model Domain name	Parameter	Source
Boundary condition (Fluid flow)	Hydraulic head BC	River stage and water table at mouth (m)	Collected from field survey
	Fluid- flux BC	Infiltration rate (m/day)	Collected from field survey using minidisk infiltrometer
	Fluid transfer BC (Min. hydraulic- head constant)	River stage and discharge along the channel at different locations (m)	Collected from field survey
	Well BC	Discharge from pumping wells (m^3/day)	Public Health Engineering Department (PHED, Government of West Bengal)
Materials properties	Conductivity	Hydraulic conductivity of aquifer materials (m/day)	Collected from field survey and laboratory analysis
	Drain-/fillable porosity	Porosity of aquifer materials	Collected from field survey and laboratory analysis
	Bottom elevation	Elevation of the river basin (m)	Shuttle Radar Topography Mission (30m resolution) USGS-govhttps://www.usgs.gov and elevation as measured from field (DGPS survey)
	Source/sink/recharge	Recharge (mm/acre)	Calculated using GEC 2015 methodology (http://cgwb.gov.in/GW-Assessment/2020-11-17_Detailed_Guidelines_GEC2015.pdf)
Model validation	Observation well	Groundwater level (mbgl)	Collected from field survey using Solinst Model 107 Temperature Level Conductivity (TLC) meter

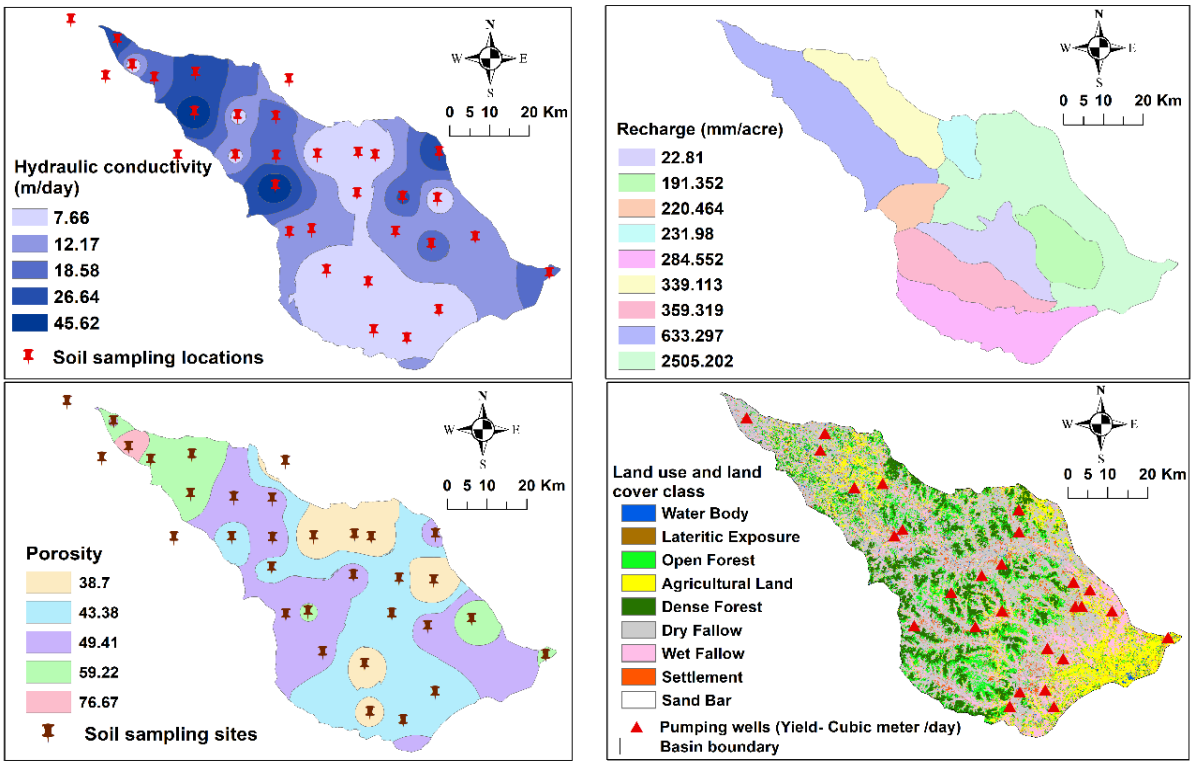

Fig. 5.22 Boundary conditions of the groundwater flow model with soil sampling sites and pumping wells

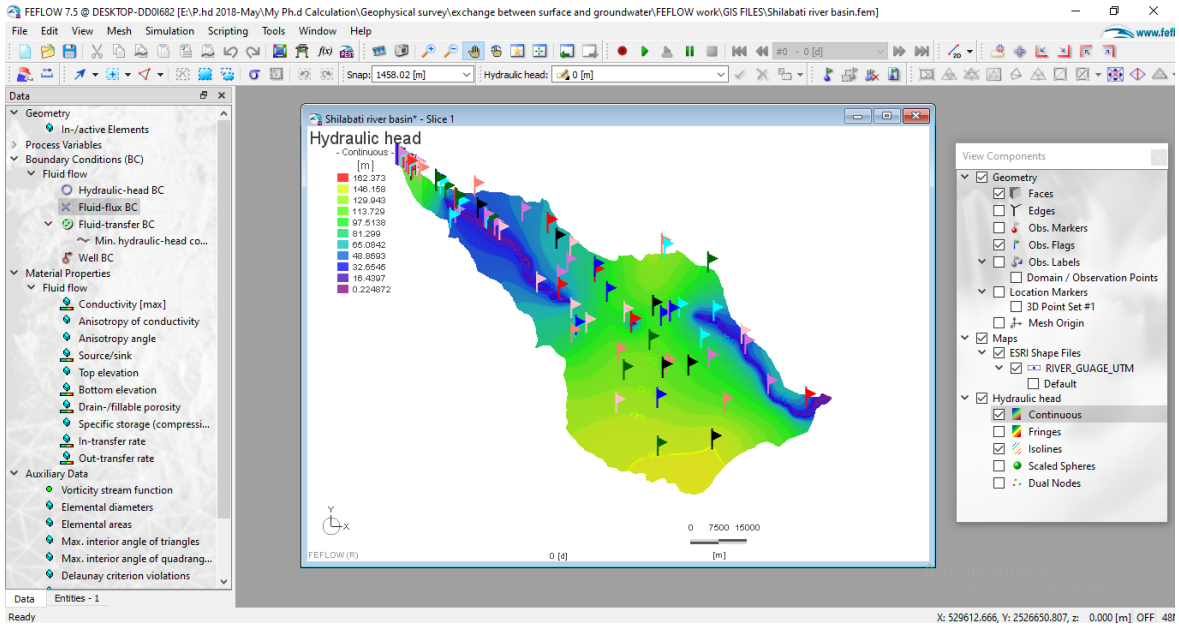

Fig. 5.23 Simulated hydraulic head and observation well in MIKE FEFLOW interface

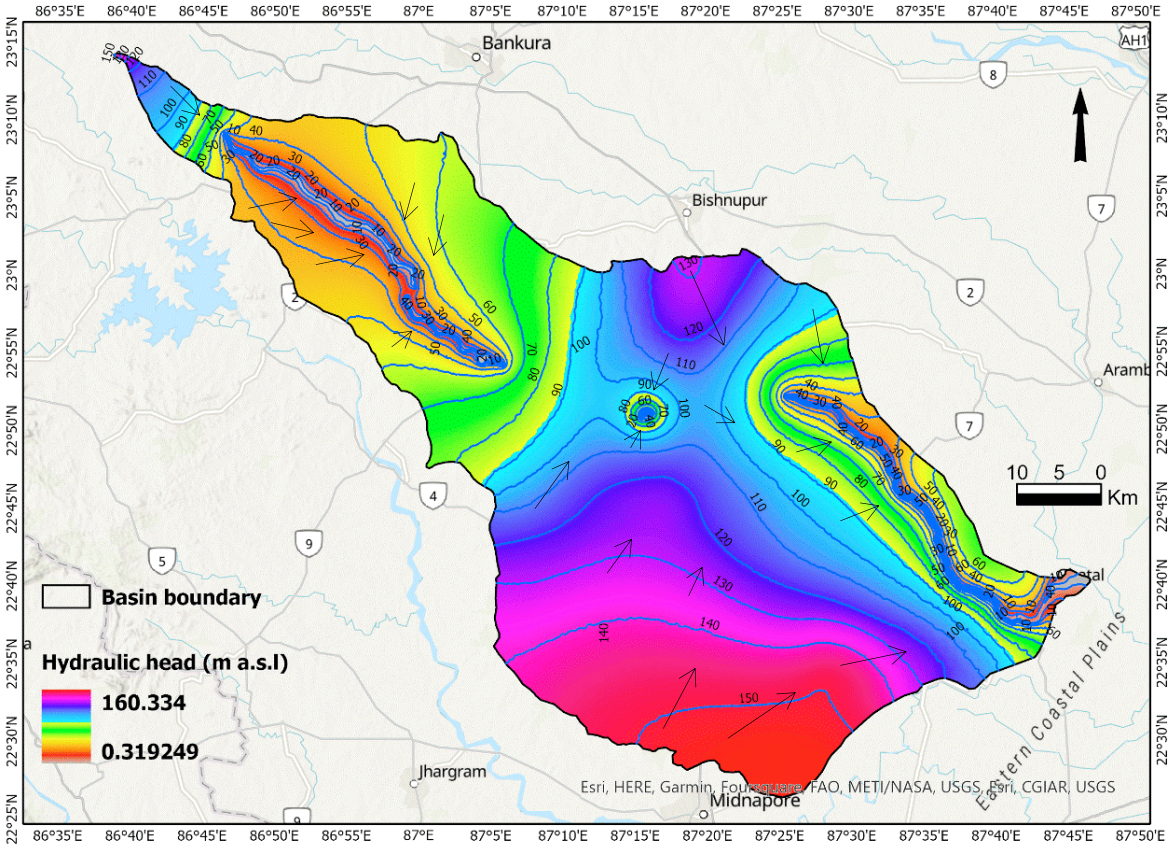

Fig. 5.24 Groundwater head contours of the Shilabati river basin

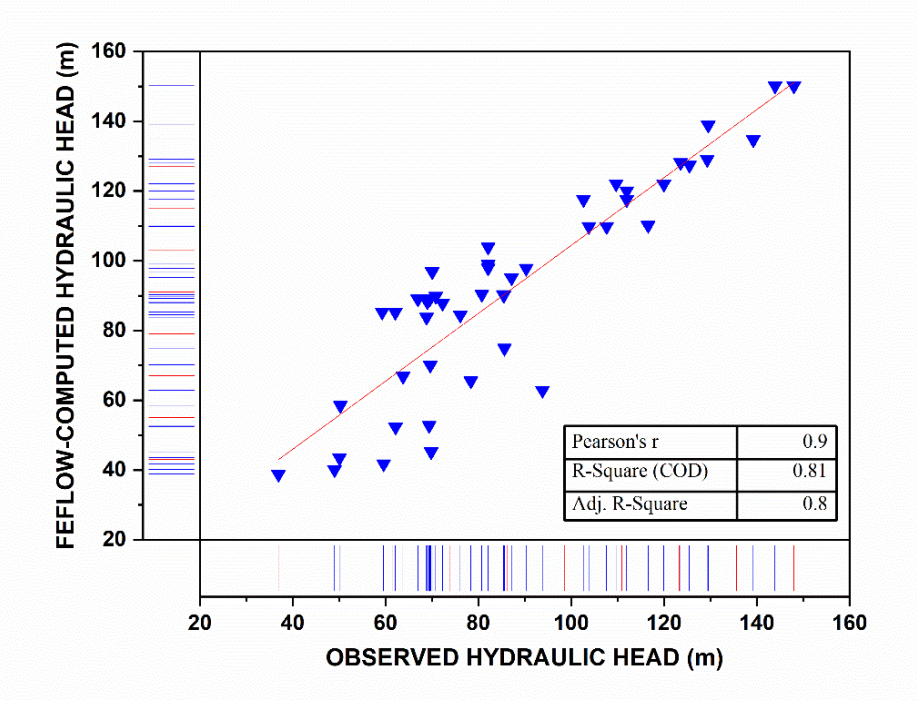

Fig. 5.25 Observed vs. simulated hydraulic head for the period (2019-2022).

5.2.6.4 Identification of suitable sites for Managed Aquifer Recharge (MAR)

The application of MAR is the emergent and the cheapest form of safe and sustainable water supply (Kazakis, 2018) technique that can be applied both in the rural and urban sector. In order to evaluate the feasibility of MAR, it is important to consider the availability of suitable sites, the optimal hydrodynamic condition of the aquifer, the presence of sufficient water sources, and a favorable hydrogeological environment (Karnath, 1994). As a part of the current study, nine primary and secondary parameters, including river discharge, moisture content, porosity, drainage type, rainfall, land use type, geology, aquifer material and hydraulic conductivity, has been used to identify suitable MAR sites among the 19 locations in the Shilabati river basin (Table 5.11). In the basin, river discharge ranges from 0.410 m^3/sec to 184 m^3/sec, while soil moisture ranges between 2% and 36.1%. Areas with high soil moisture contribute substantially to groundwater recharge (Mathias et al. 2017). Among the 19 sites, porosity ranges from 0.255 to 0.510, and hydraulic conductivity ranges from 0.00000239 cm/sec to 0.00783 cm/sec. In accordance with the soil physical characterization, soil drainage has been categorized as either good or poor. Additionally, this natural process supplies water for seeps, springs, stream baseflow, and aquifer recharge (Fausey, 2005). Daily gridded rainfall data (0.05º x 0.05º) has been downloaded from Climate Hazards Group Infrared Precipitation (CHIRP) and CHIRP combined with station observations (CHIRPS) (https://www.chc.ucsb.edu/data/chirps) from November 2021 - March, 2022 and it ranges from 46.561 mm to 58.583 mm. Land use and land cover around the main channel have been identified during the field investigation including bare land, agricultural dry fallow, agricultural cropped land and settlement. The areas covered with vegetation contribute largely to soil infiltration and therefore prevent soil erosion and runoff; these are regarded as suitable sites for MAR, while settlements and road networks are regarded as sources of groundwater pollution (Kazakis, 2018; Kamangar et al. 2019). Detailed information about the geological structure, rock type, and aquifer material has been obtained from the Geological Survey of India. Geological structure for the 19 locations can be

classified into granitoid gneiss, laterite (Ferricrete-hard crust, laterite nodules and lithomarge clay), alluvium sand dominant, alluvium sand and slit, old alluvium sand, silt and clay and alluvium slit and clay and the aquifer material can be classified into Weather and fractured rock, fractured rock, loose sediments underlain by weather and fractured rock and loose sediments. In the lower upstream and middle section of the basin, which cover parts of laterite soil and older alluvium, groundwater is mainly found in moderately thick to thin weathered and loose aquifer material under semi confined to unconfined condition can be regarded as a suitable site for MAR (Chatterjee, 2018; Paul et al. 2022). This section of the paper describes the results of the final investigation of the hydrogeological parameters and processes and their implications for MAR sites. The most appropriate site has been selected using three MCDM models, fuzzy EDAS, fuzzy COPRAS, and fuzzy TOPSIS. The location with the highest rank (19) has been identified as the suitable site that need MAR implementation to manage water scarcity. The table.5.12 and figure 5.26 show the ranking of the different sites based on the three different models. Based on fuzzy TOPSIS and fuzzy COPRAS, the location at Dakshin Pairachali achieved the highest rank (19), as well as having a high hydraulic conductivity (6.76 m^3/day), as observed by MDPs. The hydrogeological condition of this part of the channel has the potential for the groundwater recharge, but extensive exploitation of the groundwater for agricultural purposes has resulted in drastic lowering of the groundwater level in the summer months that needs to be addressed and managed sustainably (Goswami and Ghosal, 2022). Managed aquifer recharge includes a variety of methods, including dry wells, injection wells, infiltration ponds, or radial collector wells. These methods, which has proven successful in many parts of the world, including South Africa, India, Australia and the USA, can also be used in this river basin (Saleh et al. 2019). MAR can help this section of the basin in artificially recharging and storing water into an aquifer to recover it during drought events. A site suitability for MAR project is complicated and thus requires validation of the appropriate method of selection (Fuentes and Verroort, 2020). Spearman's rank correlation has been used here to identify the most effective method among the three where the ranks from fuzzy TOPSIS and fuzzy COPRAS proved nearly identical (0.928) results (Table 5.13).

Table 5.11 Conditioning factors for identification suitable sites for MAR.

Conditioning factors	River discharge (m^3/sec)	Moisture content	Porosity	Hydraulic conductivity (cm/sec)	Drainage type	Rainfall (mm)	Nearby land use type	Geology structure rock type	Aquifer material
Date source ► / Village name ▼	Field investigation	Field investigation	Field investigation	Field investigation	Field investigation	CHRIPS data	Field investigation	Geological survey of India	Geological survey of India
Bangopalpur	0.410	4.7	0.479	0.00187	Good	46.581	Bare land	Granitoid Gneiss	Weather and fractured rock
Dakshin Pairachali	2.940	21.2	0.255	0.00783	Good	48.359	Agricultural dry fallow	Granitoid Gneiss	Weather and fractured rock
Chhotakeehanda	0.930	14.4	0.295	0.000626	Good	46.747	Agricultural dry fallow	Granitoid Gneiss	Fractured rock
Mukandapur	11.800	2.4	0.402	0.00013	Good	49.328	Agricultural dry fallow	Granitoid Gneiss	Weather and fractured rock
Tapubaid	1.444	12.6	0.423	0.000108	Good	49.536	Agricultural cropped land	Laterite (Ferricrete-hard crust, laterite nodules and lithomarge clay)	Loose sediments underlain by weather and fractured rock
Gotkanali	14.870	13.2	0.291	0.0000652	Poor	49.635	Agricultural cropped land	Alluvium sand dominant	Loose sediments
Kama	8.050	13.2	0.407	0.0001040	Good	50.828	Agricultural cropped land	Alluvium sand and slit	Loose sediments
Kontore	3.920	13.3	0.418	0.0008350	Good	55.622	Agricultural cropped land	Alluvium sand and slit	Loose sediments
Raghunathbari	3.040	12.4	0.432	0.0003470	Good	56.620	Agricultural cropped land	Alluvium sand and slit	Loose sediments

Kadabani	6.520	5.4	0.394	0.0055300	Good	57.048	Agricultural cropped land	Alluvium sand and slit	Loose sediments
Kankrasol	2.200	8.9	0.352	0.0016900	Good	57.697	Agricultural cropped land	Alluvium sand and slit	Loose sediments
Shyamanandapur	6.000	5.6	0.416	0.0001690	Medium	58.583	Agricultural cropped land	Alluvium sand and slit	Loose sediments
Krishnapur	6.830	3.1	0.421	0.0001390	Medium	57.482	Agricultural cropped land	Alluvium sand and slit	Loose sediments
Jamdan	3.850	2	0.361	0.0006660	Medium	54.769	Agricultural cropped land	Alluvium sand and slit	Loose sediments
Khirpai	5.140	23.9	0.510	0.0055500	Medium	53.876	Agricultural cropped land	Older alluvium sand, silt and clay	Loose sediments
Dharmmapur	0.539	25.2	0.510	0.0000000444	Impervious	49.755	Agricultural cropped land	Older alluvium sand, silt and clay	Loose sediments
Radhakantapur	24.816	6.4	0.434	0.0006520	Medium	45.722	Settlement	Alluvium slit and clay	Loose sediments
Shyampur	94.620	29.5	0.267	0.0000000239	Impervious	46.561	Settlement	Alluvium slit and clay	Loose sediments
Near outlet and confluence with Rupnarayan	184.510	36.1	0.510	0.0000000508	Impervious	44.639	Agricultural cropped land	Alluvium slit and clay	Loose sediments

Table 5.12 Ranking of sampling sites based on Fuzzy MCDM models

Sites	FUZZY EDAS	FUZZY TOPSIS	FUZZY COPRAS
Bangopalpur	7	9	6
Dakshin Pairachali	18	19	19
Chhotakeehanda	4	7	12
Mukandapur	10	1	3
Tapubaid	13	4	4
Gotkanali	5	12	13
Kayma	9	10	9
Kontore	1	13	11
Raghunathbari	8	11	8
Kadabani	16	16	17
Kankrasol	2	14	14
Shyamanandapur	11	6	7
Krishnapur	12	3	5
Jamdan	6	8	10
Khirpai	14	17	16
Dharmmapur	15	5	1
Radhakantapur	3	2	2
Shyampur	17	15	15
Near outlet and confluence with Rupnarayan	19	18	18

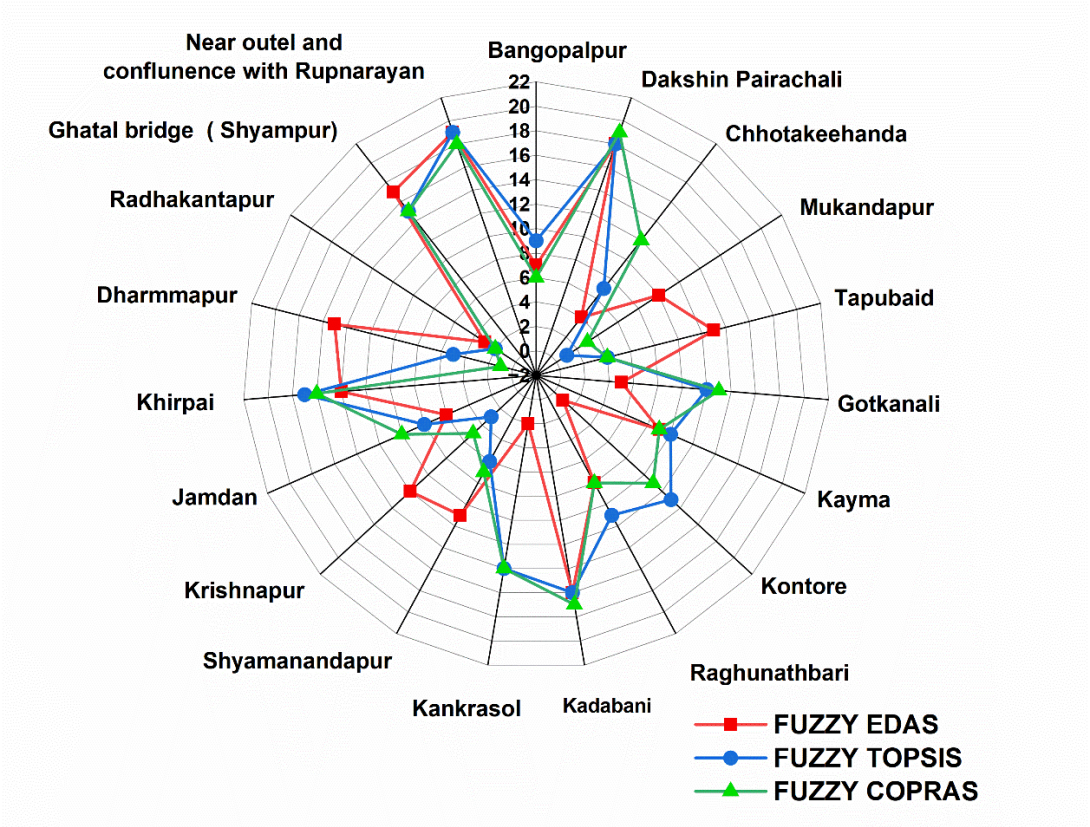

Fig. 5.26 Graphical representation and comparative analysis of rank obtained by sampling sites

Table 5.13 Spearman's rank correlation among the fuzzy MCDM models

MCDM techniques	Fuzzy EDAS	Fuzzy TOPSIS	Fuzzy COPRAS
Fuzzy EDAS	1.00	0.346	0.305
Fuzzy TOPSIS	0.346	1.00	0.928
Fuzzy COPRAS	0.305	0.928	1.00

5.2.6.5 Efficacy of the MAR selected site for construction of radial collector well and infiltration gallery using pumping test

To validate and ensure the construction of the radial collector well and infiltration gallery at locations that received the highest value (Dakshin Pairachali) has been done using long duration pumping test (4440 min or 76 hours). A radial collector well and infiltration gallery are typically designed and used for collecting water from a nearby stream, so a gaining stream condition is required in order to refill the aquifer (Huang et al. 2012). As single site pumping test are cost effective and requires huge man power thus it has been conducted only in the 1st selected site i.e., Dakshin Pairachali of Indpur block of Bankura district, West Bengal (Hasan et al. 2021) which require effective water management to cope up with the major drought events in near future. Aquifer parameters including transmissivity, storativity, specific yield, and confined storativity must be calculated under the real field conditions to prove the capacity of groundwater extraction and recharge (Bobrowsky & Marker, 2018). The pumping test has been conducted on the Shilabati river bed which remains in unconfined condition where groundwater is also released from the storages/ aquifer when extraction is made under the influence of gravity and when hydraulic heads are lowered (USGS, 1998). Using an analytical solution, Neuman (1972) predicted the time-drawdown relationships for unconfined aquifer in order to account such gravity induced withdrawal that has been considered in the current research. Slim boring of main pumping well and four observation wells has been done up to the depth of 20 m. The radius of the main well is about 102.5 mm and the outer radius of the well casting skin is about 152.5 mm. The radius of the observation wells is 38 mm. The pumping test has been conducted at the stream bed where the channel width is about 100-150 m, located at a distance of 40 km from river source. The water level has been observed to drop below the static water level in the pumping well and 4 observation wells (radially located) with a constant and steady discharge of 80 m^3/h. Following the start of the pump, water levels have been measured in each well for three days (4440 min) until saturation has been reached. As the pump stopped water level has been measured again to visualize the recuperate capacity of the aquifer. Utilizing the time-drawdown curves and Neuman straight line method (Fig.27), the following equations (Eq.5.46-5.48) have been used to compute the aquifer parameters (Schwartz and Zhang, 2003) for observation wells at a distance (r) of 80 m, 30 m, 20 m, 10 m when the main well pumped at a rate of 80 m^3/h (Q is the pumping rate in m^3/day) for a duration of 4440 min.

$$\text{The transmissivity of the aquifer (T)} = \frac{2.3Q}{4\pi\Delta s} \quad (5.46)$$

$$\text{The specific yield (Sy)} = \frac{2.25Tt_{oy}}{r^2} \quad (5.47)$$

$$\text{The confined storativity (S)} = \frac{2.25Tt_{os}}{r^2} \quad (5.48)$$

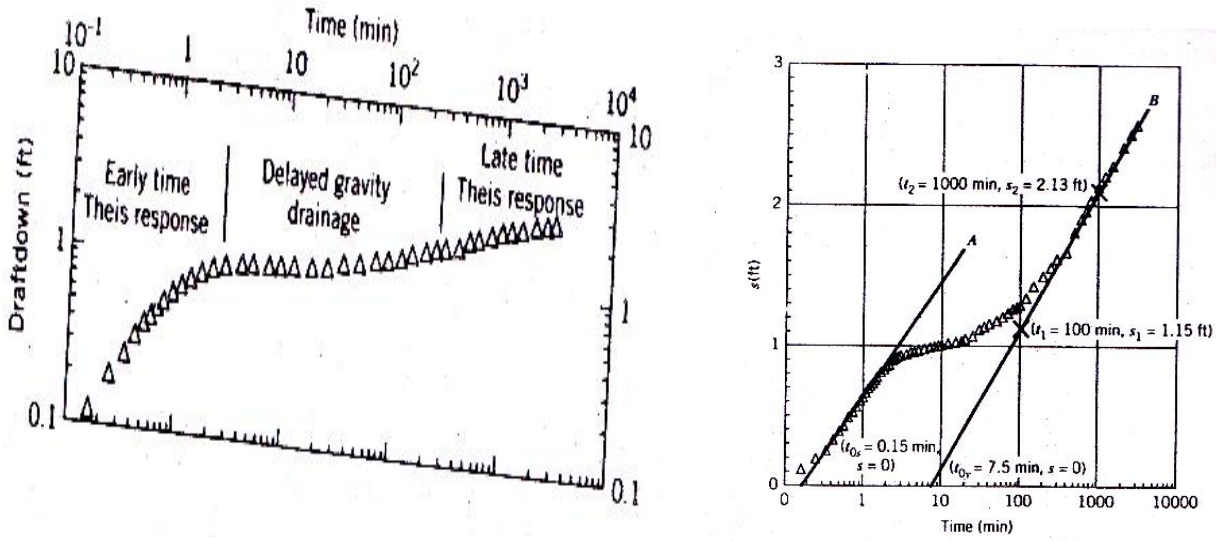

Fig. 5.27 Drawdown (s) versus time data (t) Plotted on semi-log scale for aquifer Test (Neuman, 1972)

Based on borehole data and soil sampling, the subsurface strata have been constrained into a number of distinct hydro stratigraphic units for all the wells (Fig.5.28). The litholog of the main well shows coarse sand with gravelly particles up to the depth of 3 m from top followed by fine sand with silt up to 7 m, followed by fine reddish sand up to 9 m, followed by coarse grained sand with pebbles and whitish clay up to 10 m, followed by fine sand with silty clay up to 14 m, followed by coarse sand with white clay (kaolinite) and pebbles up to 18 m followed by fine to coarse sand up to the boring limit (20 m). Based on the litholog it can be concluded that the site has a good potential for groundwater extraction and storage with the transmissivity of 2147.45 m^2/day. Table 5.14 shows the summarized results of all the aquifer parameters for the well as calculated from time vs. drawdown plots (Fig.5.29). Based on the above discussion a collector well and infiltration gallery can be designed at the Dakshin Pairachali site which will offer the best combination of high capacity from a single location and improved water quality by filtration through aquifer materials. In a variety of hydrogeological situations, such as in thin aquifers, horizontal wells (HWs), such as radial collector wells (RCWs), covered drainage trenches, and horizontal directionally drilled wells, are suitable alternatives to vertical wells from a hydraulic and economic point of view (Collins and Houben, 2020). Models have shown that collector wells produce smaller maximum drawdowns since drawdown is distributed over a larger area and fouling occurs at a slower rate, so wells need to be cleaned less frequently (Božović et al. 2020). Radial collector wells are also inexpensive and a simple method of obtaining high quality water (Spiridonoff et al. 1964) which can be easily implemented within the Shilabati river basin. Beside the radial collector well, infiltration galleries can also be constructed, which are essentially percolation trenches buried beneath the surface and filled with porous structural fill (Marazeula et al. 2022). Such porous fill can store a large amount of water, which can be used in drought events within the river basin (Godwin et al. 2022). Additionally, infiltration galleries can be used for flood water management and wastewater treatment by filtering the water through the soil profile as successful MAR systems rely on a substantial reduction in chemical and pathogenic contaminants as well (Casanova et al. 2016). In the current research depth of the porous media has been found around 20 m which can be optimum for the implementation of radial collector well and infiltration gallery at Dakshin Pairachali site. The quality of porous media and lack of obstruction from all the directions will facilitate the physical drilling of the strainers conveniently. Infiltration gallery can also be installed in similar

location but designed capacity should be minimal with single gallery due to the narrow width of the river. In current study, radial collector wells have been designed using the algorithm proposed by Huisman (1972) and validated using the Image Well Method (Kuo et al. 1994). The estimated maximum available yield came as 29.38 MLD at an allowable drawdown of 2.57 mbgl (though maximum allowable drawdown is 3.535 mbgl as obtained from pumping test) and maximum safe yield has been calculated as 12.096 MLD with 6 number of radial wells. The pumping shall be done for 18 hours in three shifts per day with horizontal strainers of 40 m length and 0.30 m diameter. In cases where aquifers are enclosed by rectangular boundaries, it is imperative to use the image well method to validate the design otherwise inaccurate values may arise (Butler and Tsou, 2003). An image well method calculates the impact of barriers or infinite sources of water on pumping well water levels. Image well representations create hydraulic systems that are equivalent to the effect of physical boundaries on flow systems, such as imaginary discharging or recharging wells. The maximum allowable entrance velocity according to the Huisman (1972) has been 0.000611m/sec whereas according to the image well method it is 0.002045. As per Raghunath (1987), the maximum allowable entrance velocity should not exceed 0.177 m/sec, thus the design for radial collector wells are accurate and effective according to image well theory. Where there is a reliable water supply, one or more infiltration galleries are often installed in conjunction with a collector well. Water enters the gallery from alluvium tract and is discharged from the gallery through the hydraulic head. As the length of the Shilabati river basin in this section is about 100 meters, the full width of the river has been considered to determine the Infiltration Gallery length. Infiltration galleries have been designed based on Raghunath (1987) and Ferris (1950) which came out to be 1170 meters with 16 galleries for this site. The details of other constructional design have been highlighted in the supplementary file.

The work on finding out a MAR site is not any new for the other countries (Fuentes and Vervoot, 2020; Sprenger et al. 2017) but doing this using low cost equipments and user-friendly modeling techniques has presented very robust results and will subside the water scarcity problem under any geological conditions. Sustainable planning mainly focuses on the prudent use of groundwater, conservation of surface water, limited extraction, progression of the water structure, awareness of water, alternative cropping practices, and the conservation of domestic and industrial water. Thus, for groundwater improvement in respect to long term such sustainable groundwater planning can be very beneficial. It is equally significant for implications on the rivers which are groundwater based, wetlands and for the benefit of entire ecosystem.

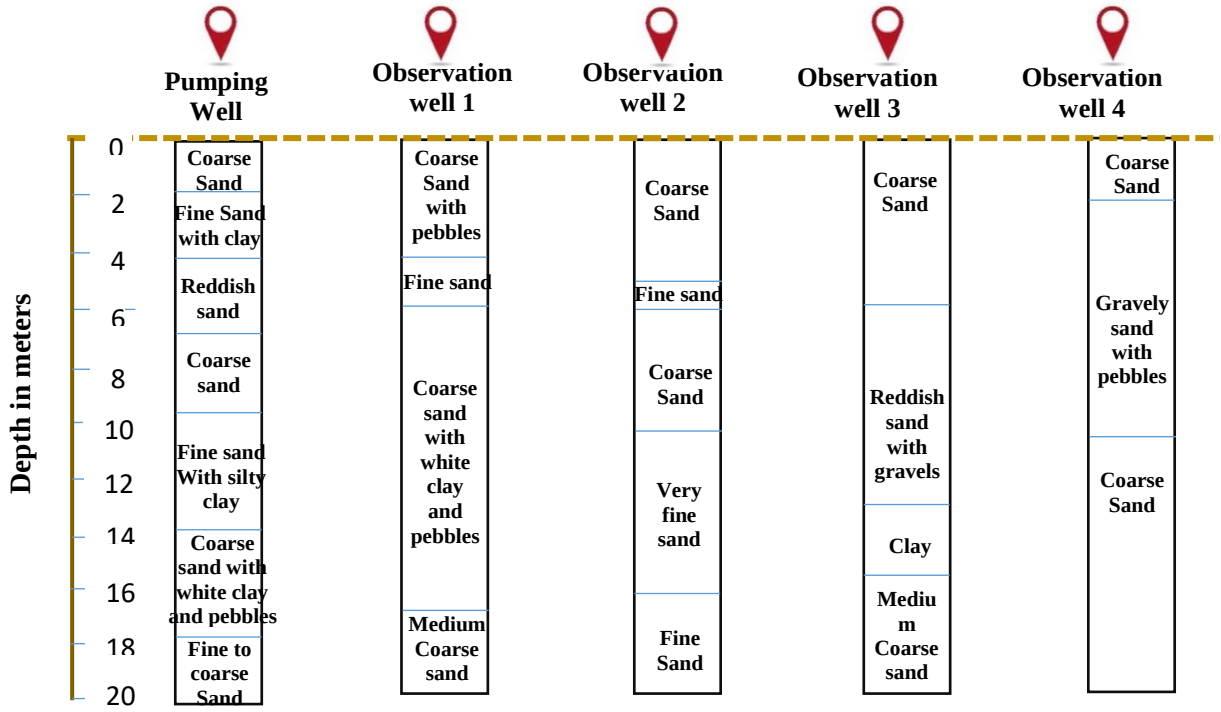

Fig. 5.28 Litholog of the main pumping well and the observation wells

Table 5.14 Aquifer parameters as obtained from the pumping test

Dakshin Pairachal, Indpur Bankura Well	Distance (m)	Latitude (North)	Longitude (East)	Discharge (m^3/hr)	Confined Storativity	Specific yield	Transmissivity (m^2/day)	Static water level (mbgl)	Maximum drawdown (m)	Recovery time to the static water level (min)
Main well		23°3'37.16"	86°54'24.67"				2147.45	0.695	3.535	120
OB-well I	80	23° 3'37.10"	86°54'27.72"		0.009	0.01	3253.83	0.01	0.154	90
OB-well II	20	23° 3'36.67"	86°54'24.88"	80	0.029	0.15	2080.99	0.366	1.088	85
OB-well III	30	23° 3'37.49"	86°54'23.70"		0.005	0.27	2196.34	0.799	1.495	85
OB-well IV	10	23° 3'37.58"	86°54'25.35"		0.002	0.27	1757.07	1.23	1.70	70
			Average Transmissivity (m^2/day) →				2322.06			

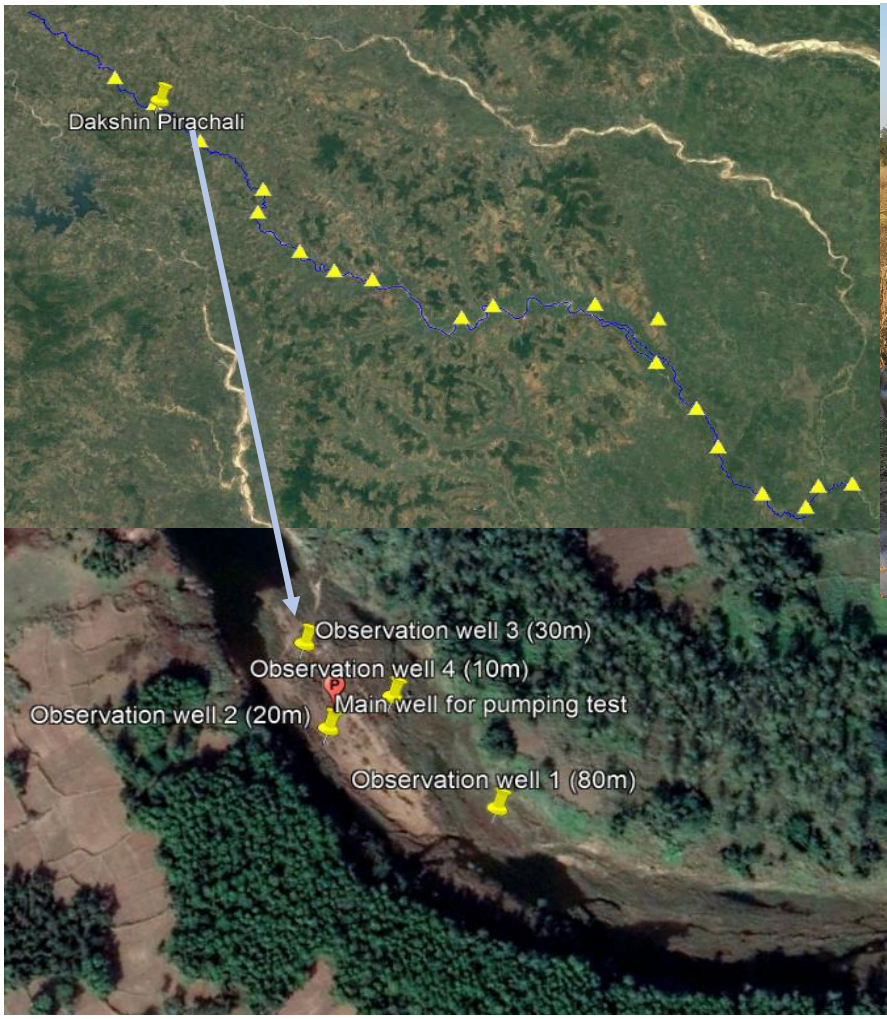
Dakshin Pirachali
Observation well 3 (30m)
Observation well 4 (10m)
Observation well 2 (20m)
Main well for pumping test
Observation well 1 (80m)

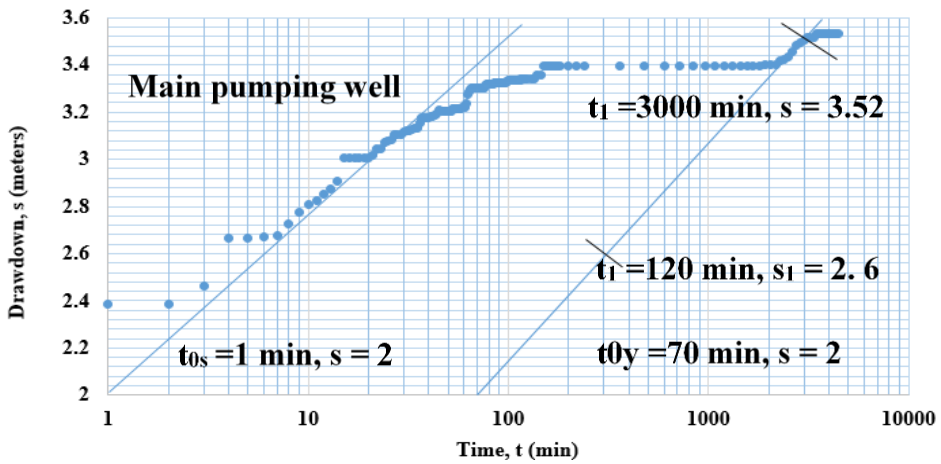
Main pumping well
t1 =3000 min, s = 3.52
t1 =120 min, s1 = 2. 6
t0s =1 min, s = 2
t0y =70 min, s = 2
Drawdown, s (meters)
Time, t (min)
3.6
3.4
3.2
3
2.8
2.6
2.4
2.2
2
1
10
100
1000
10000

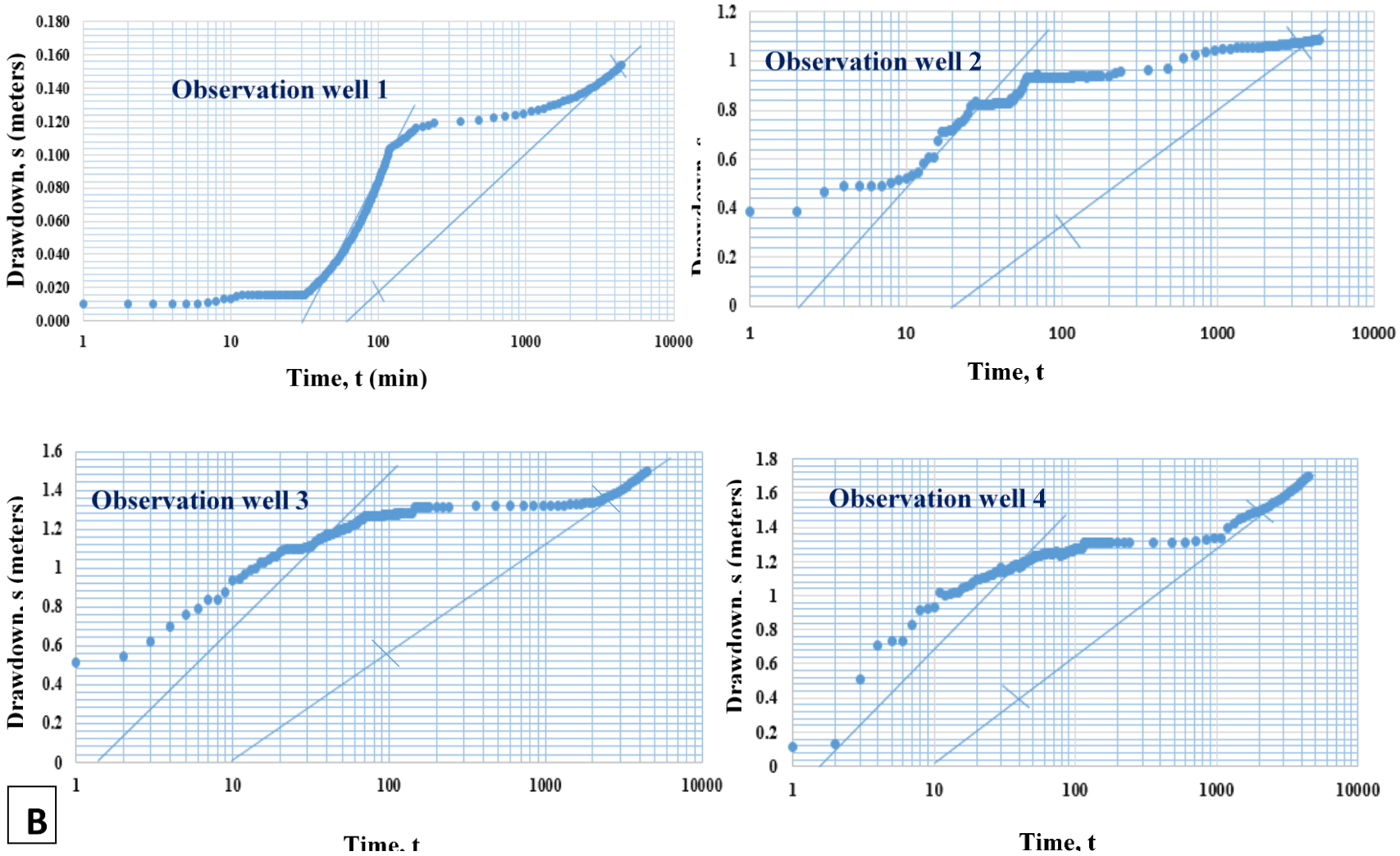

Fig. 5.29 (A) Selected site, conductance of continuous pumping test and time vs. drawdown graph for main well; (B) time vs drawdown graph for observation wells (4)

5.2.7 Conclusion and Recommendations

This study has been undertaken to investigate suitable site for Managed Aquifer Recharge (MAR) in Shilabati River Basin to cope with water scarcity during extreme drought events. To understand the hydrological science dealing with groundwater-surface water interaction in a cost-effective way, mini drive point piezometers (MDPs) have been used to estimate the hydraulic conductivity and to identify losing and gaining stretches within the 250 km long channel. Mini drive point piezometers have produced more impressive outcome for hydraulic conductivity when compared with the results from grain size analysis. Almost all the empirical equations followed the similar trend with field acquired data. The K_h values as calculated from MDPs ranges from 0.00206 to 6.765 m/day with highest at Dakshin Pairachali site. This study has a significant potential for research on GW–SW interaction which helped to address the losing and gaining stream conditions of the channel. Of all the 19 sites, 5 are showing losing conditions and 14 sites are having gaining conditions with VHGs ranging from -0.21 to -1.07 and 0.01 to 3.14 respectively. Such losing stream systems, cannot be selected as the MAR site as the polluted water seeps into the adjoining aquifers which contaminates both ecosystems as well as irrigation and drinking and water quality. The MIKE FEFLOW model was successfully run and calibrated for four years (2019-2022) in steady state mode for the whole river basin with scare datasets. The groundwater head ranges from 160.33 -0.32 m.a.s.l which will provide information on the direction of flow and help identify as suitable MAR site. The model results have been found to be competent and are seen to match the observed groundwater water levels of 47 sites to a reasonable level of accuracy (0.90).

MAR applications are generally driven by two factors: a suitable aquifer and an available water source. As long as these two factors are met, MAR can be applied. This study has also curved out the most suitable areas for managed aquifer recharge (MAR) application based on various fuzzy multi-criteria decision analysis (Fuzzy EDAS, Fuzzy COPRAS and Fuzzy TOPSIS). The overall study concept involves the integration of nine parameters: including river discharge, moisture content, porosity, drainage type, rainfall, land use type, geology, aquifer material and hydraulic conductivity. Based on fuzzy TOPSIS and fuzzy COPRAS, Dakshin Pairachali achieved the highest rank (19) which has hydrogeological suitability and foremost need for MAR implementation for managing extreme drought condition. In order to ensure dependable water supply and sustainable groundwater utilization over the long run, planners, decision makers, and hydrogeologists can use the results of the present study as guidelines for implementing MAR structures like radial collector wells and infiltration galleries in the study area. Based on the pumping test and drawdown estimation, a design for a radial collector well and infiltration gallery has been suggested for the selected site with a maximum safe yield of 12.096 MLD.

5.2.8 Limitation and Future Works

Climate change has contributed to a decline in the groundwater table in the Shilabati river basin as a result of reduction in groundwater recharge. Furthermore, reduced recharge and extended periods of drought have resulted in a rising demand for groundwater extraction. As a consequence, more streams are turning from gaining to losing, increasing the risk of aquifer contamination by the intrusion of polluted surface water. To date, there is little public and socio-political and environmental awareness of this problem and its related implementation of MAR as data on groundwater-surface water- interactions are scarce. The limitation of the study includes the non-availability

abundant data related to aquifer parameters like specific yield, transmissivity, hydraulic conductivity etc. of different geological layers. It will be an appeal to all government and non-government organizations to generate such data and make them available to vast researchers. We strongly encourage implementation of the current research to understand groundwater-surface water exchange process and their spatio-temporal development on a local and catchment scale globally.

Chapter6

Groundwater Vulnerability and pollution risk assessment

6.1 Groundwater vulnerability assessment for drinking water suitability using Fuzzy Shannon Entropy model

6.1.1 Introduction

The concept of groundwater management refers to a broad range of activities that include the prevention of contamination of groundwater (Li & Wang, 2022; Pandey et al. 2020). To develop useful strategies to protect groundwater contamination, vulnerability identification is the first important step. Idea of groundwater vulnerability has been dealt with by many authors (Aller et al. 1985; Oroji, 2019; Novinpour et al. 2022) across the different climatic regions of the world namely humid tropical regions (Nugraha et al. 2021; Saravanan et al. 2020), sub-tropical region (Tomer et al. 2019), arid and semi-arid region (Pourkhosravani et al. 2021) Mediterranean region (Vrouhakis et al. 2022) and in the temperate region (Oke and Fourie, 2017). Scientists and managers have implemented such techniques in different hydro-geocritical zones, including coastal tracts (Brodbar et al. 2022), alluvial zones (Fusco et al. 2020), hard rock terrains (Kumar and Krishna, 2018), and karstic aquifers (Hamdan et al. 2016). The factors that determine the vertical and horizontal transport of contaminants, such as the area of recharge, slope, soil texture, soil structure, soil depth, geology, flow rate, hydraulic conductivity, unscientific pumping from shallow aquifers, and poor land-use practices, which need to be assessed in order to prevent further degradation of water quality. A variety of natural pollutants can be transported through sedimentary soil and rock, including fluoride, arsenate, nitrate, iron, etc. The effects depend on their concentration and human interference (Sharma and Bhattacharya, 2017). Thereby it is necessary to differentiate protection zones from vulnerability using different colors so that they can be easily categorized and interpreted (Meerkhan et al. 2022). As a result of various scale approaches, there are various intrinsic aquifer vulnerability indexes that can be implemented in fissured media such as DRASTIC (Antonaleous and Lambralies, 2007; Thirumalaivasan et al. 2003), SINTACS, AVI, SI (Sharadqah, 2017) and GOD (Corneillo et al. 1997). They are mostly index-based methods that aid in the assessment of risky sections on a regional, global and local scale by ranking or rating them based on hydrogeological, hydro meteorological, and hydro-morphological criteria (Zare et al. 2022). In general, such models assume vertical transport of contaminants in deeper aquifers, with an area of approximately 0.45 square kilometers or greater (Kazakis and Voudouris, 2015). The problem with such models is that they are less accurate, omitting the important variables, and therefore they need to be modified and optimized (Bordbar et al. 2019). Based on a recent review of groundwater vulnerability index (GVI) methods, four categories can be distinguished: process-based prediction models (Guo et al. 2023), overlay analysis and index-based methods (Wu et al. 2018), AI-based hybrid methods (Nadiri et al. 2022), and statistical frameworks (Omeje et al. 2023). As shown in the table 6.1, there have been a variety of reviews for GVI methods. Additionally, there are other methods and techniques used to estimate groundwater or aquifer vulnerability zones, such as HEAVEN, ISIS, EPIK, COP etc. (Duarte et al. 2019). Datasets used in these methods

and approaches are heterogeneous, which may not be available at the basin, watershed, or catchment scale and are also time-consuming, computationally demanding and expensive. According to some researchers, water contaminant concentrations (mostly nitrate) have shown infirm correlation with the calculated DRASTIC index (Kwon et al. 2022). In the long run, these aquifer systems may face difficulties in managing groundwater contaminant risks, as well as in protecting and managing groundwater resources.

Such types of models, however, are weakened by three major limitations: (i) subjectivity in the selection of criterion (ii) subjectivity in the determining rates and weights values for the criterion (Kwon et al. 2022); and (iii) they are not the most appropriate models to be applied to a complex environment (urban, semi-urban, rural fringes and urban fringes) since they ignore human influences. The combined subjectivity of these limitations creates uncertainty when evaluating potential vulnerabilities. In the current study, model ranking and weighting have been done using the Fuzzy Shannon Entropy method, which combines mathematical and MCDM techniques with GIS applications. In reclassifying the values, fuzzy transformation method is more flexible and produces less sensitivity to outliers (Dastorani, 2022). Thus, for groundwater vulnerability susceptible prediction, the triangular fuzzy number is used to remove the vagueness or subjectivity of the relative preferences (Gorai, 2022). Data in different forms and magnitudes can be stored, manipulated, and analyzed by the integration of RS/ GIS and fuzzy logic into groundwater vulnerability mapping (Shao et al. 2020).

In West Bengal, particularly in semi-arid and arid areas, over exploitation of water, and low recharge, groundwater depletion has become a serious environmental problem, causing not only the loss of available water, but also the degradation of water quality. According to the Central Groundwater Board (CGWB) report (2017-2018), groundwater extraction increased to about 62%-63% in India. Fluoride concentrations exceeding 1.5 mg/l have been detected in 43 blocks covering seven districts in West Bengal (PHED report, 2009), with the highest concentrations in Puruliya, Bankura, Birbhum, etc. (Samal et al. 2020). According to Farooq et al. (2018), 40% of groundwater samples in Puruliya were fluoride-contaminated due to weathering and decadence of biotite. In some parts of Bankura, Nag and Das (2017) found that iron, calcium, sodium, chloride, bicarbonate, sulfate, and magnesium levels exceeded the permissible levels. Among the dug wells here, most are shallow and are typically left open, and most of the hand tube wells lack a concrete base, making them more susceptible to contamination from human activities and surface runoff (Kundu and Nag, 2018).In this research, a detailed study on groundwater vulnerability has been conducted within a river basin covering the districts Puruliya, Bankura, and West Medinapore of West Bengal.

6.1.2 Research Gap and Novelty of Work

Referring to the literature reviews on aquifer vulnerability studies and the highlighted advantages of FSE-GVI framework, the novelties of the study can be outlined as follows-(i) The available frameworks for mapping aquifer vulnerability suffer from subjectivities associated with the prescribed rate and weight values, which can be decreased using fuzzy MCDM techniques. FSE- GVI method takes the advantages of sealing impression problem and applies them to measure the subjective value of information under uncertainties and thereby increases model fidelity (Chaghooshi et al. 2012). (ii) FSE-GVI framework is developed for mapping intrinsic, total and specific vulnerabilities for confined, unconfined and semi-confined aquifer and (iii) inclusion of pH, population density and groundwater based irrigation schemes into the FSE-GVI framework would help in

acquiring the clear pictures of in-depth aquifer vulnerability as the determination of pH could serve as a sensitive indicator for contamination while population growth, irrigation and industrial expansion are exaggerating water pollution to a next level (Chapagain et al. 2022; Liyanage and Yamada, 2017). Although the framework for generating FSE-GVI framework is conventional in design, but the study takes a novel approach to incorporate it into aquifer vulnerability analysis.

6.1.3 Objectives of the Research Work

The main objective of this study is to generate aquifer information and identification of groundwater vulnerable zone using both qualitative and quantitative approaches in fuzzy logic and GIS environment. The study is also focused on developing a novel index to assess and map groundwater vulnerability towards contaminants that meets all the above requirements. Thus, the overarching objective of this research is a) to assess groundwater vulnerability using Fuzzy Shannon Entropy based groundwater vulnerability index (FSE-GVI) framework using 13 hydrogeological and anthropogenic criterions, this technique has been chosen because it can provide rugged and economically viable ways to assess groundwater vulnerability more accurately than old traditional methods incorporating new criterions and b) to validate the accuracy of vulnerability map with 74 drinking water quality parameters, the Water Quality Index (WQI), ROC and AUC curves. In this study, the expected results will provide valuable information regarding groundwater status across the river basin area, which can be an efficient resource for decision-makers while determining land use plans and groundwater resource management.

6.1.4 Area of Investigation

The study focused on the Shilabati river basin of West Bengal, India. In Puruliya District, it passes through complex rock terrain, while in Bankura and West Medinapore districts, it passes through laterite and alluvial terrains. It is the right bank tributary of Rupnarayan River with a total area of 3881 sq. km. Geographically the river basin is located between the latitudinal extents of 22º 14´ 03˝ N to 22º26´25.12˝ N and longitudes of 86º38´46.08˝ E to 87º46´36.65˝ E (Fig. 6.1). The river emerges from the Chotonagpur Plateau, flows east towards the West Medinapore district, and joins the masters stream Rupnarayan. The basin comprises 9 sub-basins namely Silai, Joypanda, Purander, Betal, Kubai, Tamal, Donai, Parang and Silai Ketia Khal. The upper, middle, and lower basins are hydro-geologically and hydro-geomorphologicaly different. The upper basin covering the Puruliya district is geologically dominated by granitic gneiss (Fig. 6.1) with soft phyllite and the mica schist of Singhbhum (Dolui et al. 2016). There is a rolling land of laterite and alluvium terrain in the middle stretch, which is unfavorable for recharge due to the occurrence of impervious geological setting under the surface (Pal Majumder et al. 2021). In the lower stretch, there is a significant concentration of younger and older alluvium, fluvial-deltaic sediment cloaked in primary and secondary laterite, where medium recharge can be observed (Bhunia et al. 2012).

From the hydrogeological scenario, aquifers in the hard rock at the upstream part of the basin have very low yield prospects and high drawdowns (Kundu and Nag, 2018). Within a depth of 12 mbgl, unconfined aquifers are mainly composed of semi-consolidated Gondwana sedimentaries (CGWB, 2022). Fractures can be found within 20 mbgl of this zone, and the prospect for yield is moderately low, along with the prospect for very high drawdown (up to 20m). Drilling and explorations in consolidated formations have revealed that fractures can be encountered more likely in the zone 0-50 mbgl. In these shallow fracture zones, the aquifers are usually unconfined or semi-confined. Groundwater sustainability in the middle section is adversely affected by the presence of crystalline impervious

rocks near the surface and highly permeable lateritic residual meta-sediment (Palmajumder et al. 2021). An unfavorable geohydrological condition for groundwater sustainability is the inundated nature of the surface drainage system. In general, there is a persistent hydrogeological scenario that affects groundwater availability and quality for a long time. In areas with old alluvial cover, there are medium to good prospects for producing groundwater through tube wells and dug wells. In the downstream section, valley-fill deposits generally consist of sand, silt, gravels, pebbles, and other unconsolidated materials (Bhunia et al. 2012). Tube wells or submersible pumps typically yield 100-200 litres/min. Groundwater here is under confined conditions with depth of the water ranging from 3 to 18 meters below ground level.

Nevertheless, extensive groundwater extraction for agricultural and domestic purposes is causing water levels to decline and geochemistry to change, making the water more vulnerable to consumption (Halder et al. 2021). Blocks like Puncha and Puruliya II of Puruliya district, Taldangra, Simlapal, Indpur, and Khatra of Bankura district are highly affected by Fluoride contamination (more than 1.5 mg/l) (Bera et al. 2021). It has also been found that the river basin is affected by iron contamination and high levels of Total dissolved solids (TDS) (790 to 1330 mg/l) are also observed in the river basin (Ghosh and Mondal, 2019). Agricultural land use and irrigation return flows, particularly in the downstream section, and sewage discharges in the upstream section, can cause higher TDS concentrations in groundwater (Nag and Das, 2017). Furthermore, during the field investigation the villagers reported the application of nitrogen, potash, and urea to the soil for agricultural growth, which can leach and contaminate the groundwater and can increase TDS (Paul et al. 2022). Over the past few decades, there has been a growth in medium-sized iron-based industries and secondary activities within the river basin which can be the sources of high iron concentration in groundwater (Chakraborty et al. 2022) beside the geogenic origin. Thus, the study area has been assessed for groundwater vulnerability to delineate the zones at risk from mild contamination to extensive contamination.

Table 6.1 Summary of past studies in aquifer vulnerability

Methodological reference	Groundwater vulnerability Index			Number of criteria	Newly added criteria	Type of aquifer			Validation technique/ parameter
	MCDM/Fuzzy MCDM and GIS	AI and GIS	Traditional model and GIS			Un-confined	Confined	Semi - confined	
Koon et al. 2023			Modified-DRASTIC	7	Lineament density	√			Fluoride
Taghavi et al. 2023			Modified DRASTICL and DRASTIC	8	Land use and land cover	√			Scatter plot/secondary data-bicarbonate, calcium, carbonate, chloride, magnesium, nitrate, potassium, sodium, sulfate, total dissolved solids, salinity
Elzain et al. 2023		KNN, ERT, BA	Modified DRASTIC-LU	9	Land use and land cover	√	√		Scatter plot/ nitrate
Saravanan et al. 2022	DRASTIC-AHP		DRASTIC	7		√		√	ROC/ nitrate
Yu et al. 2022	AHP-DRASTIC,AHP-DRASHCL,VWM-DRASHCL			7	Aquifer thickness, hydraulic resistance of the vadose zone, and land use.	√			ROC/ Field survey-nitrate, magnesium and
Lakshminarayanan et al. 2022	SE, SWARA and BBO		DRASTIC	7		√			ROC/ secondary data-nitrate
Chakraborty et al. 2022			DRASTIC	7			√	√	ROC/field survey-potassium
Gharekhani et al. 2022		ANN, GEP, SVM, BMA		7		√			
Rajput et a. 2020			Modified-DRASTIC	7				√	Correlation Index/secondary data-Chromium
Asfaw and Mengistu, 2020			Modified DRASTIC	8	Land use and land cover	√			pH, TDS and Nitrate
Nadiri et al. 2019	Fuzzy DRASTIC	AIMF		7			√		Scatter plot/ nitrate
Jhariya et al. 2019	DRASTIC-AHP			10	Land use and land cover, lineament buffer		√		Correlation plot/ Nitrate
Nadiri et al. 2017		SICM, SVM, NF, GEP.		7		√			
Lima et al. 2011			Drastic and Dyna-Clue Model	7		√			
Current study	Fuzzy Shannon Entropy (FSE-GVI)			13	Specific yield, pH, land use, land cover, population density, groundwater-based schemes for irrigation	√	√	√	Correlation Index -Water quality index (WQI) ROC and AUC/ field surveyed data-alkalinity, hardness, TDS and iron

6.1.5 Research Design and Methodology

6.1.5.1 Data Source

Primary and secondary sources, as well as satellite-derived observations, have been used in the study. Gridded rainfall data (Daily) has been obtained from Climate Hazards Group Infrared Precipitation (CHIRPS) (0.05º× 0.05º) combined with station observations (https:// www. chc.ucsb.edu/ data/ chirps) in tiff (Tagged Image File Format). It provides long-term precipitation records from 1981 and is useful for hydrological modeling and simulation (Luo et al. 2019). From USGS Earth Explorer website (https://earth explorer. usgs.gov/) Landsat 8 OLI (Operational Land Image) has been downloaded (path number 139 and row number 44) to prepare the land use and land cover map of the study area using GIS (Geographical Information System) tools. SRTM (Shuttle Radar Topographic Mission) Digital Elevation Model of 30m resolution has also been downloaded from the above website (https://earthexplorer.usgs.gov/) to prepare the slope map. From the secondary sources Topographical sheet numbers 73I/12, 73I/16, 73 J/13, 73 M/4, 73 M/8, 73 N/1, 73 N/10, 73 N/14, 73 N/2, 73 N/5, 73 N/6, 73 N/7 and 73 N/9 of scale 1:50,000 has been collected, scanned and geo-referenced in ArcGIS version of 10.4 to delineate the drainage basin. In order to prepare soil media maps and hydraulic conductivity maps, the soil texture map was obtained from the National Bureau of Soil Survey and Land Use Planning (NBSS & LUP) in raw format. To calculate the specific yield, a geological map has been acquired from the Geological Survey of India (GSI). The groundwater level has been obtained from the Central Groundwater Board (CGWB) of India. In order to prepare the Impact of Vadose Zone map, an aquifer depth map has been retrieved from the State Water Investigation Directorate (SWID), West Bengal. Data on groundwater-based irrigation schemes from SWID and census India have been collected to analyze the anthropogenic impact. Based on the above data and information, 13 thematic maps have been prepared to generate the final output using the MCDM technique and fuzzy logic approach (Fig. 6.2). Using Arc Toolbox in ArcGIS, the thematic maps with the varied resolution have been resampled (30m*30m) and reclassified for model precision.

6.1.5.2 Experimental and laboratory analysis

In order to validate the aquifer vulnerability model, water samples have been collected from different locations within the basin. To conduct accuracy analysis, GARMIN eTrex 10 was used to track waypoints at 74 well locations (dug wells, tube wells and submersibles). In order to validate the model, seven major drinking water quality parameters were evaluated, namely pH, Electrical Conductivity (EC), Total Dissolve Solids (TDS), Hardness, Alkalinity, Chloride, and Iron. Due to the high level of iron contamination throughout the basin, particularly in West Medinapore and its surrounding districts, this parameter should be well considered (Das et al. 2016). Using probes connected to Hach Series Portable Meters, pH, TDS and EC were measured in the field. For hardness, chloride, and alkalinity tests, 500 ml of groundwater samples have been collected and refrigerated. Tests of hardness were conducted in the laboratory using EDTA (Ethylenediamine Tetraacetic Acid). Salt nitrate ($AgNO_3$) solution was used as a titrant to determine alkalinity, and silver nitrate (H_2SO_4) to determine chloride. Separate acid fixed samples of 50ml have been collected for iron test using Inductively Coupled Plasma Atomic Emission Spectroscopy (ICP-OES). The analyzed data were used to prepare a Water Quality Index (WQI) and spatial distribution maps for assessing the model's accuracy.

6.1.5.3 Fuzzy Shannon Entropy model

To implement the proposed methodology, we divided the hybrid model into three steps: in step 1, fuzzy set theory is used for data standardization in the ArcGIS environment. A triangular fuzzy number (TFN) (Table 6.2) has been assigned to all the selected criteria to create the matrix following preprocessing. Step 2 involves determining the significance of each criterion in the overall susceptibility using fuzzy Shannon entropy. In this phase, SPSS (Statistical Package for Social Science) software was used to conduct the analysis. An objective-weighting scheme that incorporates Shannon entropy can help understand events. In the third step, ArcGIS version 10.4 software was used to integrate the results obtained in the previous steps. In the last step, receiver operating characteristics (ROC) curves and AUC calculations were used to validate the results. To deal with all the uncertainty in fuzzy information, a fuzzy Shannon entropy is an important mathematical tool (Yuan and Zheng, 2022). It is based on quantitative extraction of the expected information that is enclosed in a message, and has been widely applied to studies of integrated assessment of physical-environmental processes as well as natural hazards identification (Roodposhti et al. 2016; Garcia and Martin, 2018).

Construction of fuzzy decision matrix using TFN (Eq. 6.1)

$$\begin{matrix} F_1 & F_2 & \cdots & F_N \end{matrix}$$

$$\begin{matrix} \widetilde{X_{11}} & \widetilde{X_{12}} & \cdots & \widetilde{X_{1n}} \\ \widetilde{X_{21}} & \widetilde{X_{22}} & \cdots & \widetilde{x_{2n}} \\ \vdots & \vdots & \ddots & \vdots \\ \widetilde{X_{m1}} & \widetilde{x_{m2}} & \cdots & \widetilde{x_{mn}} \end{matrix} \qquad \text{i = 1,2….,m ; j= 1,2…..n} \qquad (6.1)$$

$$\tilde{X}_{ij} = \frac{1}{k}\left(\tilde{x}_{ij}^{1} + \tilde{x}_{ij}^{2} + \ldots..\tilde{x}_{ij}^{k}\right)$$

In the above equation (1) $\tilde{x}_{ij}^{k}$) is the rating of the alternative A_i with respect to the factor F_j analyzed during decision making and $\tilde{x}_{ij}^{k} = (a_{ij}^{k} + b_{ij}^{k} + c_{ij}^{k})$

a. Calculation of factor weight using Shannon entropy (Zongji et al. 2010) (Eq. 6.2)

$$E_j = - \quad k \sum_{1=i}^{m} P_{i,j} \; In \; P_{i,j} \qquad (6.2)$$

In the above equation E_j is the entropy value, $P_{i,j}$ is the value of the intensity of events in j^{th} factor and k is the positive constant, it is basically the choice of unit of count which is given by, (Eq. 6.3)

$$k = (\ln m)^{-1} \qquad (6.3)$$

Where m is the intensity of the factors in causing the event.

b. Creation of the normalized decision matrix $P_{i,j}$ for each factor using the following equation (6.4)

$$P_{i,j} = \frac{r_{i,j}}{\sum_{i=1}^{m} r_{i,j}} \qquad (6.4)$$

c. Weights play an important role which the factors play in simulating assessment where greater the value indicates greater functional role of that factor in the index system (Eq.6.5)

$$w_j = \frac{v_j}{\sum_{i=1}^{m} v_j} \qquad (6.5)$$

In the above equation W_j is the weight of the j^{th} factor and V_j can be defined as

$$v_{j=}1\text{-}E_j \qquad (6.6)$$

Table 6.2 Triangular fuzzy scale (Bakeshlou et al. 2017)

Linguistic scale for importance	Triangular Fuzzy scale	Triangular Fuzzy Reciprocal scale
Just equal	(1,1,1)	(1,1,1)
Equally important (EI)	(1/2,1,3/2)	(2/3,1,2)
Weakly more important (WMI)	(1,3/2,2)	(1/2,2/3,1)
Strongly more important (SMI)	(3/2,2,5/2)	(2/5,1/2,2/3)
Very strongly more important (VSMI)	(2,5/2,3)	(1/3,2/5,1/2)
Absolutely more important (AMI)	(5/2,3,7/2)	(2/7,1/3,2/5)

6.1.5.1 Hybrid groundwater vulnerable susceptibility mapping model

An aquifer vulnerability index can be divided into two categories: intrinsic vulnerability, in which the system's inherent properties are considered, and specific vulnerability, in which a particular group of contaminants is considered (Vrouhakis et al. 2022). However, models like DRASTIC, SINTACS, GOD, etc., consider only surface impressions (Bera et al. 2021). Equation 6.7 is used to calculate the hybrid aquifer vulnerability susceptibility mapping combining FSE calculated weights (w_i), which combines intrinsic, specific and total vulnerability.

$$\text{Groundwater Vulnerable Index (GVI)} = \sum_{i=1}^{n} w_i \otimes x_i \quad (6.7)$$

6.1.5.2 Water quality index (WQI)

To validate the model outcome, the water quality index of the groundwater samples was calculated using Brown et al. (1972)'s weighted arithmetic method. It is one of the most effective methods for analyzing the water quality of a particular region. In order to determine the quality of the drinking water, a mathematical equation was applied, which included several water quality parameters (Akter et al. 2016). In this study, WQI has been calculated using seven drinking water parameters. The Bureau of Indian Standards has been used to assess the quality of different water samples. The following equation has been used to perform the analysis (Tyagi et al. 2014) (Eq.6.8)

$$Q_i = \frac{C_i}{S_i} * 100 \quad (6.8)$$

Where Q_i, C_i, and S_i are regarded as quality rating scale, concentration of ith parameter, and standard value

Relative weight has been calculated using the following equation 6.9.

$$w_i = 1/S_i \quad (6.9)$$

Where the standard value of the ith parameter is inversely proportionate to the relative weight of the parameters

Final rating has been calculated using the following equation 6.10.

$$\text{WQI} = \sum Q_i w_i / \sum w_i \quad (6.10)$$

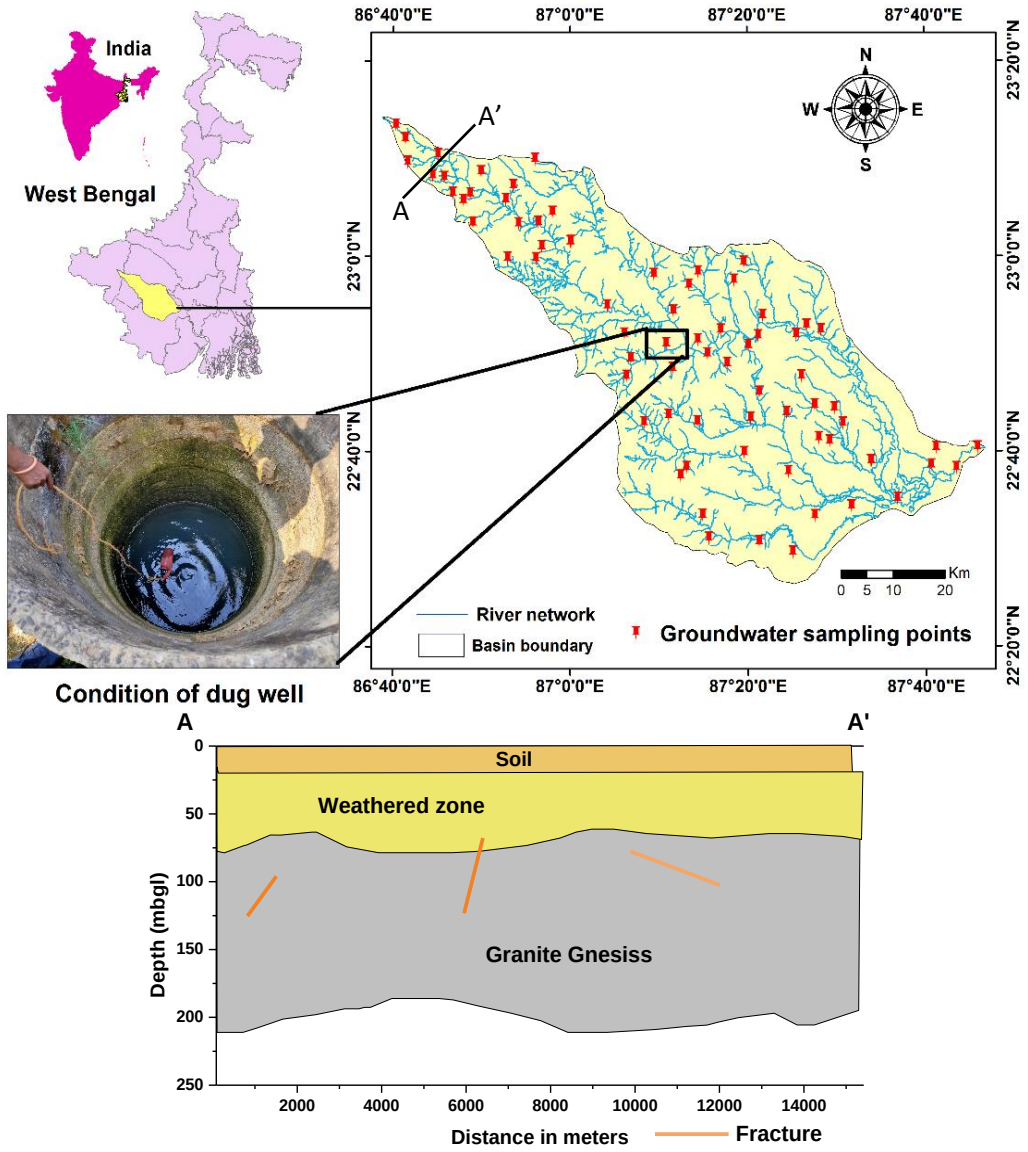

Fig. 6.1 Location of the study and diagram of the stratigraphic profile (A–A')

6.1.5.3 Receiver Operating Characteristics (ROC) curve

ROC curves were used to evaluate the efficacy of the hybrid aquifer vulnerability map using the Fuzzy Shannon entropy model. An essential statistical technique that enables deterministic and probabilistic prediction and acceptance of a simulation system (Hembram and Saha, 2019). It proves the accuracy by pointing out the system's predictive power to generate a probability map incorporating the highly ranked probabilities with the true intensity transition (Mas, 2018). According to the curve, the true positive rates (TPR or Sensitivity) are plotted against the false positive rates (FPR or 1-specificity). As a measure of the quality of the fit, the area under the curve (AUC) is considered (Saha et al. 2019). The sensitivity and the specificity of the Fuzzy Shannon entropy model have been evaluated using the following equations (Eqs. 6.11 and 6.12) (Saravanan et al. 2023).

$$X = \text{FPR (1-specificity)} = \frac{FP}{TN+FP} \quad (6.11)$$

$$Y = \text{TPR (sensitivity)} = \frac{TP}{TP+FN} \quad (6.12)$$

Where FP is false positive; TP true positive; FN is false negative and TN is true negative

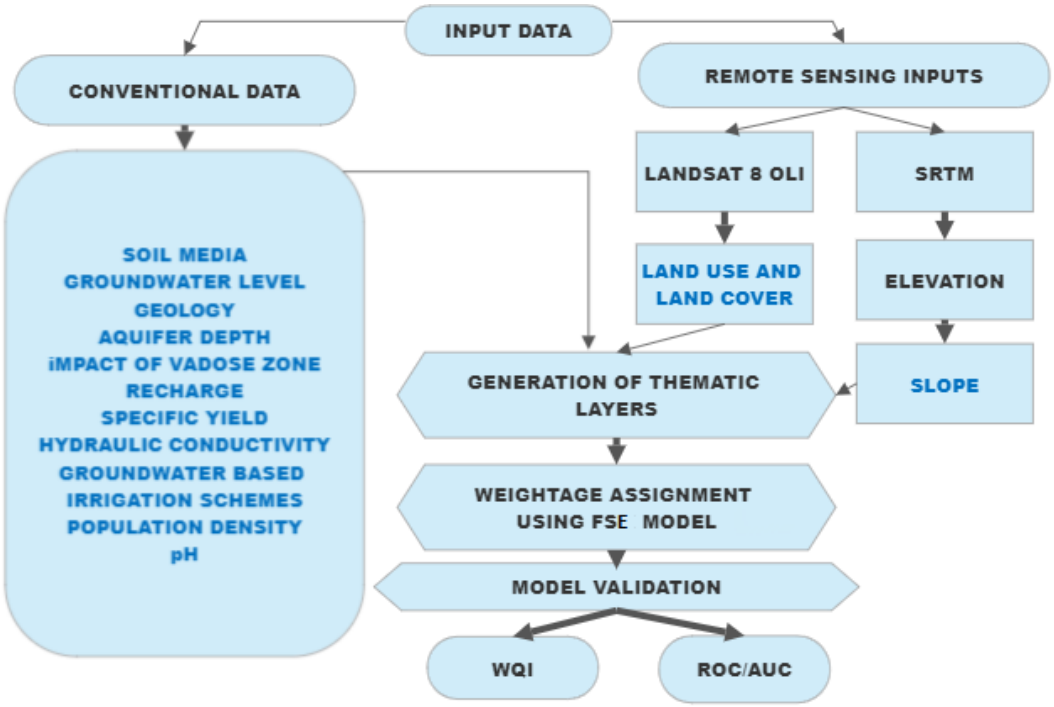

Fig. 6.2 Modeling framework

6.1.6 Description of criterions for hybrid Fuzzy Shannon Entropy-groundwater vulnerable index (FSE-GVI)

6.1.6.1 Slope

In terms of determining the contaminant vulnerability of an aquifer, slope plays an important role in controlling recharge. The steepness of a slope increases runoff flows, reduces recharge, and prevents infiltration (Abdullateef et al. 2021). The slope map in this study was prepared using SRTM DEM of 30m resolution. The slope has been grouped ranging from 0- 20º. Fig. 3a illustrates the slope map of the river basin. The weight assigned to this conditioning factor has been shown in table 6.3 and table 6. A1 (appendix). The slope ranging from 0-0.56º (30.91%) is mainly observed in the middle and lower section of the basin where runoff is less and hence more vulnerable to the surface contaminants to recharge the deeper layers. The slope of 0.57-1.2º (41.10%) and 1.3 - 1.9º (21.60%) is mainly concentrated in the middle section of the basin. The basin's upper section, ranging from 2-5.5º (6.35%) and 5.6-20º (0.04%) slope, is associated with irregular topography and higher surface runoff which are less susceptible to contaminant transportation compared to the downstream section (Fig. 6.3a).

6.1.6.2 Soil Media

Soil media actively participate in the recharge process and the transportation of contaminants through the stratification. The decomposition process, evaporation, fluid motion and other chemical reaction are continuously taking place on soil media (Muhammad et al. 2015) which helps in cation exchange and sometimes removal of heavy metals (Bera et al. 2021). Sometimes harmful contaminants slow down the permeability making the soil infertile. In this research, soil map has been restricted and digitized from the National Bureau of Soil Survey and

Land Use Planning (NBSS & LUP) where eight classes covered the drainage basin namely Fine-fine loamy (18.69%), Fine (21.01%), Fine loamy (34.05%), Fine loamy- coarse loamy (14.13%), Fine loamy- sandy (8.86%), Gravelly loam-loam (2.16%), Fine- very fine (0.30%) and Gravelly loam (0.80%). The fine loamy to sand, gravelly loam areas are the most vulnerable to contamination, since they have a high infiltration rate. The fine loamy to sandy soil concentrated in the middle section of the basin along the river course is the most susceptible zone. Downstream, fine-fine loamy soil is found, which has a low infiltration rate. Figure 6.3b depicts the soil media of the river basin and table 6.3 and table 6. A1 (appendix) present the weight assigned to each conditioning factor.

6.1.6.3 pH level

Soil water interaction, chemical reaction and ionic exchange greatly influence the pH (Kros et al. 2016). It is an important factor that is influenced by the biological and chemical parameters of the water and the toxicity of various chemical compounds (Saha et al. 2019). The pH of the 74 sampling village sites has been measured on-site using a portable pH meter. The raw data has been used to prepare the spatial distribution map using IDW in the GIS platform. pH level has been classified into 5 different classes namely 5.6-6.1 (8.86%), 6.2-6.4 (9.62), 6.5-6.7 (13.51%), 6.8-6.9 (45.19%),7-7.4(22.82%). The pH level of the basin is slightly alkaline to acidic in nature (Fig. 6.3c). The areas where hardness (magnesium or calcium) is high can affect the pH of water and soil, leading to the loss of phosphorus in water. Fig. 3c demonstrates the pH of the river basin and the weight assigned to this parameter is shown in table 6.3 and table 6. A1 (appendix).

6.1.6.4 Geology

Aquifer contamination can occur through surface runoff, seepage, and infiltration of polluted environments, which are highly influenced by the geological setting (Biswas et al. 2020). Delineation of the geology of the study area has been made from the map as provided by the Geological Survey of India (GSI) on GIS platform. Fig. 6.4 illustrates the geology map of the river basin. The weight assigned to this conditioning factor is shown in table 6.3 and table 6. A1 (appendix). The upper section of the basin covering the Puruliya and Bankura district consists of a diverse group of rocks from different geological ages like intrusive Granites, meta-sedimentary of Singhbhum group, Chotonagpur gneissic complex, volcanic rocks of Dalma group and sediments of Quaternary ages and Gondwana plain and granite and gneissic crystalline complex of the Archean era (Das et al. 2019; Goswami and Ghosal, 2022). The most common are granitic and granitic gneiss (12.77%) (Das et al., 2018). In the complex rock terrain, contamination from the surface source is less as the infiltration is less than in the weathered and fractured areas. As a result of granite, pegmatites, fluorite, etc., fluoride contamination dominates in some parts of the upper basin (Saha et al. 2017). The middle section of the basin is primarily composed of fluvial-deltaic sediment covered by primary and secondary lateritic terrain where iron contamination is high (Bhunia et al. 2012). The lower part comprises younger alluvium of sand, silt and clay where groundwater is in unconfined condition with surface loamy clay. It is important to note that the downstream section has moderate infiltration with good chances of aquifer vulnerability from pollutant sources and a decline in groundwater levels due to extreme agricultural extraction by submersible pumps (Halder et al. 2020). A significant portion of the study area consists of granite gneiss (12.77%), lateritic soil/ laterite (41.38%), sand, silt & gravel (present-day deposit) (4.79%), yellowish-brown fine sand, silt, clay (7.59%), mica schist with hornblende. Groundwater level. In unconfined

conditions, the distance between the groundwater and the water table is measured in meters below groundwater. In other words, it refers to the distance between surface pollutants reaching the groundwater (Yu et al. 2022). Groundwater level plays an important role in determining contaminant attenuation time. The greater the water level from the surface, the longer the travel path of the contaminant, and the longer it takes to attenuate (Shamsuddin et al. 2021). According to Halder et al. (2021), the groundwater level in Puruliya, Bankura, and West Medinapore has been declining over the past few years due to extensive extraction of groundwater to meet agricultural demands (Halder et al. 2021). In this study, groundwater level data for 2020 has been collected from CGWB and mapped in GIS platform using the inverse distance weighted (IDW) method. The groundwater level has been divided into 5 classes namely 1.5-5.16 (30.80%), 5.17-7.09 (42.61%), 7.10-9.56 (14.17), 9.57-13.1 (7.65%) and 13.2-21.2 (4.78%). In the upper and middle section of the basin groundwater is quite shallow where the chances of contamination are at their highest (Nag et al. 2021). Fig. 6.4 demonstrates the groundwater level of the river basin and table 6.3 and table 6. A1 (appendix) shows the weights.

6.1.6.5 Groundwater level

In unconfined conditions, the distance between the groundwater and the water table is measured in meters below groundwater. In other words, it refers to the distance between surface pollutants reaching the groundwater (Yu et al. 2022). Groundwater level plays an important role in determining contaminant attenuation time. The greater the water level from the surface, the longer the travel path of the contaminant, and the longer it takes to attenuate (Shamsuddin et al. 2021). According to Halder et al. (2021), the groundwater level in Puruliya, Bankura, and West Medinapore has been declining over the past few years due to extensive extraction of groundwater to meet agricultural demands (Halder et al. 2021). In this study, groundwater level data for 2020 has been collected from CGWB and mapped in GIS platform using the inverse distance weighted (IDW) method. The groundwater level has been divided into 5 classes namely 1.5-5.16 (30.80%), 5.17-7.09 (42.61%), 7.10-9.56 (14.17), 9.57-13.1 (7.65%) and 13.2-21.2 (4.78%). In the upper and middle section of the basin groundwater is quite shallow where the chances of contamination are at their highest (Nag et al. 2021). Fig. 6.3d demonstrates the groundwater level of the river basin and table 6.3 and table 6. A1 (appendix) shows the weights.

6.1.6.6 Aquifer depth

The unconfined level of groundwater is more vulnerable to contamination from the surface than the confined or semi-confined layer (Adebaya O and Abraham A, 2017). Generally, confined layers are thick deposits that encrust the underlying aquifer and shield it from the surface processes. Since heavy metals take a long time to percolate down, deep tube wells are popular in this section, which can pose a risk to itself at times (Shamsudduha et al. 2019). In shallow wells, Ximenes et al. (2018) found elevated levels of microbial contaminants and dissolved solids. The study area has 5 different aquifer depth classifications, namely shallow aquifer with weathered residium of 5-15 mbgl (meters below ground level) (23.63%) (Block like Puncha) and semi-confined aquifer in pediplain area with near surface weathered zone within 20 mbgl (43.25%) covering the upper section of the stream (Blocks like Hiraband, Indpur, Bankura, Khatra, Onda), unconfined to confined condition with primary aquifer from 30-85 mbgl (18.30%) at the middle section (Blocks like Simlapal, Taldangra, Onda, Sarenga, Garbeta I, II, III, Salboni, Keshpur) and unconfined condition with primary aquifer at 40-50 mbgl (14.82%) at the downstream section (Blocks like Ghatal, Chandrakona, Mindapore). Due to sewage discharge and natural sources, TDS in

groundwater in the middle section covering the Bankura district sometimes increases (Nag and Das, 2017). The depth of the aquifer in the river basin is shown in figure 6.3e. Table 6.3 and table 6. A1 (appendix) show the weights assigned to this conditioning factor.

6.1.6.7 Specific yield

To assess aquifer vulnerability and effectively manage groundwater, it is necessary to estimate recharge of groundwater and pumping volume (Chinnasamy et al. 2018). According to Johnson (1967) specific yield is the proportion of water that a saturated stratum produces by gravity in relation to its total volume. It is possible to estimate the specific yield (Sy) of different structures using geophysical methods, pumping tests, and soil moisture measurements, but due to the lack of access to such tests, Sy values for this study have been based on the values proposed by the Groundwater Estimation Committee (GEC, 1997) in accordance with the local geology. It has been found that groundwater recharge directly depends on the Sy of a particular lithology; therefore, the greater the yield, the greater the transport of contaminants into the deeper aquifer (Zhang et al. 2018a). Specifically, yield has been grouped into 5 categories based on local geology (GEC, 1997), namely 0.015 (0.05%) and 0.025 (41.34%) in the middle section of the basin, 0.03 (16.13%) in the upper section of the basin, 0.06 (4.84%) and 0.1 (37.64%) along the river course which is prone to aquifer vulnerability from surface contaminants (Fig. 6.3e). The weight assigned to this factor has been given in table 6.3 and table 6. A1 (appendix) and fig. 6.3f demonstrates the specific yield of the region.

6.1.6.8 Hydraulic conductivity

Aquifer hydraulic conductivity determines the rate of transport of groundwater into deeper aquifers. As a result, hydraulic conductivity reflects downstream movement of contaminants as well as the rate at which polluted water enters the deeper aquifer under specific head loss conditions. This depends on the hydraulic gradient of the aquifer (Chakraborty et al. 2022). The higher the hydraulic conductivity, the greater the degree of contamination (Alamne et al. 2022). Due to unavailability of pumping test data in this study area, hydraulic conductivity was determined based on the soil media covering the basin based on the U.S. Department of Agriculture (USDA) classification (Naseef et al. 2016; USDA). Based on the database hydraulic conductivity (micrometer/sec) has been ranged from 0.42-141 (21.30%), 1.41- 4.23 (61.6%), 14.11- 42.34 (14.13%) and 42.34-141.14 (2.95%). Throughout the main river, hydraulic conductivity is higher from the middle to the downstream where aquifer vulnerability is greater. Figure 5a illustrates the hydraulic conductivity map of the river basin (Fig. 6.5a). The weight assigned to this conditioning factor has been shown in table 6.3 and table 6. A1 (appendix).

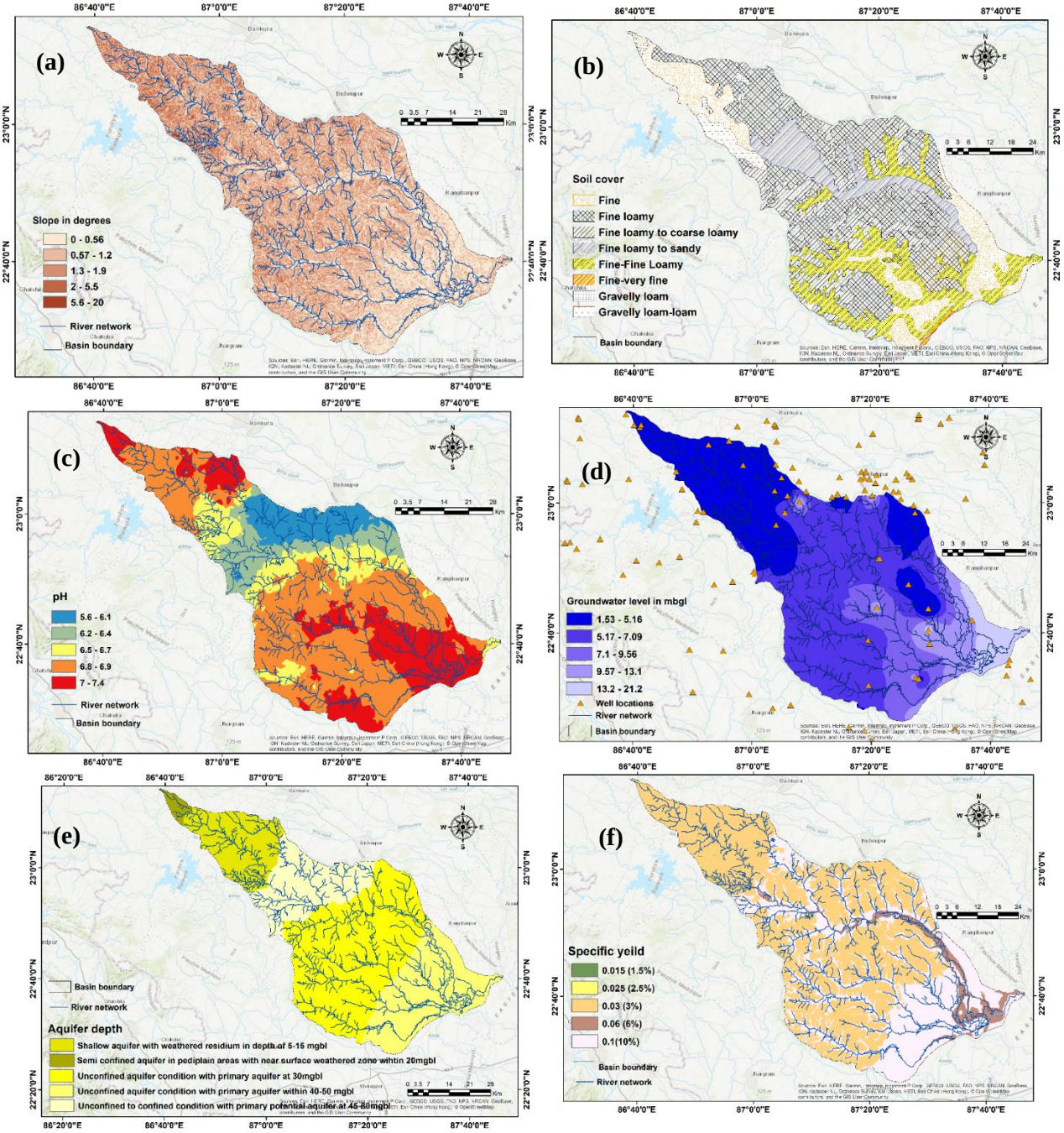

Fig. 6.3 Maps of groundwater vulnerability conditioning factors (a) slope (b) soil cover (c) pH (d) Groundwater level (e) specific yeild (f) aquifer depth

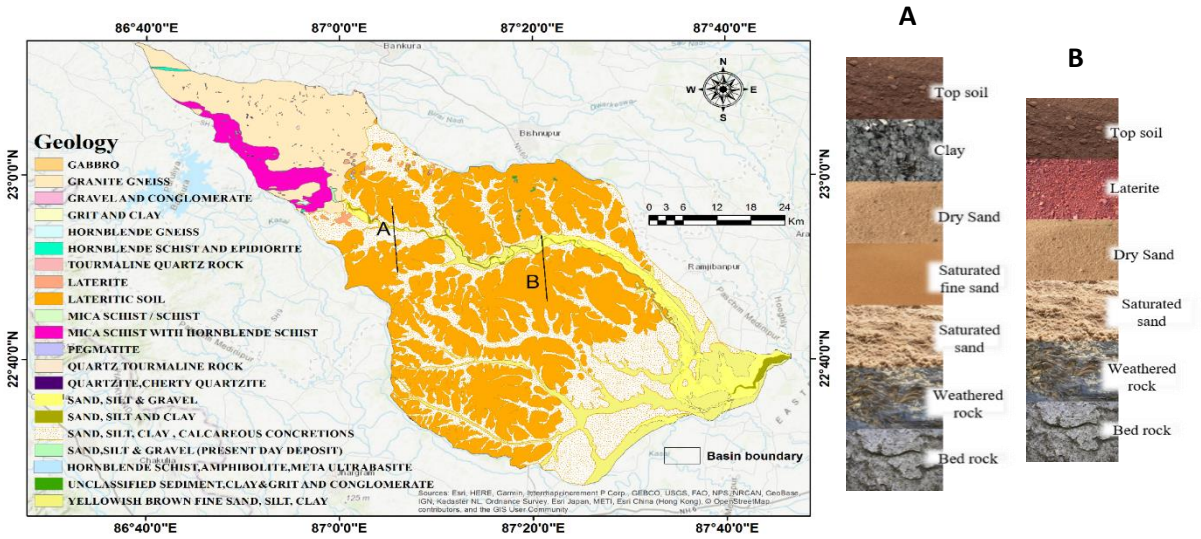

Fig. 6.4 Geology of study area and litholog (A & B)

6.1.6.9 Impact of the vadose zone

Vadose zones are unsaturated layers above the water table that play an important role in the percolation of contaminants into deeper layers (Kesuma et al. 2017). This layer serves as a pass way for contaminants migrating toward the water table, supporting the biogeochemical and biochemical degradation processes (Bera et al. 2021). In the summer, the zone remains dry, which leads to more contaminant transport, and this condition is reversed in the rainy season. Based on the hydrogeological map by the Geological Survey of India (GoI) layers for the study area have been demarcated and digitized in the GIS platform. The upper section of the basin mainly covers pink granite/biotite-granite gneiss (11.39%), mica schist, occasionally garnetiferrous (2.91%), metamorphosed basic rocks (0.07%), granite gneiss, migmatite (1.33%), granite gneiss (0.41%), ferruginous sediments with rock fragments (0.13%) remain mostly unsaturated throughout the year as they are located in the drought affected zones of Puruliya and Bankura districts (Ghosh et al. 2019) thus less vulnerable to the surface contaminants. In the middle and lower sections, laterite (0.19%), sands and silts in alternate layers (34.80%), sands, silts, clays impregnated with caliche nodules (19.78%), sands with silts, clays associated with fe-nodules (8.81%) are more vulnerable to surface contaminants during the dry and summer season when extensive groundwater extraction makes the situation worse (Thapa et al. 2019). Fig. 6.5b illustrates the impact of the vadose zone of the river basin. The weight assigned to this conditioning factor has been shown in table 6.3 and table 6. A1 (appendix).

6.1.6.10 Groundwater recharge

In this study, groundwater recharge was assessed by collecting the pre and post monsoon groundwater levels from 20 observation wells using CGWB and CHIRPS rainfall data, as well as specific yield and infiltration factors based on the local geology. Under unconfined to semi-confined layers throughout the basin, groundwater is mainly concentrated in fractured and weathered zones (Sahoo et al. 2021). Over the basin, land use and land cover are changing rapidly, affecting groundwater recharge and reducing water table levels. It is therefore necessary to accurately estimate recharge in order to gain a better understanding of groundwater pollution and aquifer

vulnerability (Robins, 1998). Based on the GEC, 1997 and 2015, groundwater recharge has been calculated using equations 6.13 to 6.15 (Prasad and Rao, 2018).

a. Groundwater recharge (ham) by water table fluctuation method (wfm) = Geographic area * Specific yield* Rise in the water table (6.13)

b. Groundwater recharge (ham) by Rainfall infiltration method (rifm)= Area* Normal rainfall* Infiltration factor (6.14)

According to the criteria as recommended by GEC, 1997 final recharge of the basin has been calculated using Percentage Deviation (PD) following the equation 15 (Siva Prasad et al. 2018).

$$PD = \frac{a(wfn) - b(rifm)}{b(rifm)} * 100 \quad (6.15)$$

The groundwater recharge has been divided into five classes namely 3.37-1293.4 (21.36%), 1293.5-2583.5 (41.57%), 2583.6-3873.5 (29.48%), 3873.6-5163.6 (3.66%) and 5163.6-6453.6 (3.93%). The weight assigned to this factor has been given in table 6.3 and table 6. A1 (appendix) and fig. 6.5c demonstrates the groundwater recharge distribution of the region.

6.1.6.11 Land use and land cover

Groundwater recharge is strongly influenced by land use and land cover, which act as sources of harmful pollutants. The forest cover helps in the recharge of groundwater by flashing out pollutants, while the buildup and fallow land discharge fresh recharge (Das et al. 2019). Urbanization, mining, agriculture, and industrial development pose a high pollution risk to groundwater. Desertification and areas that don't support agriculture are more likely to have groundwater contamination (Ahmad et al. 2021). In this research Landsat 8 OLI satellite image has been downloaded from https://earthexplorer.usgs.gov/. QGIS version 3.22 is used to preprocess the images for atmospheric, geometric and radiometric corrections. By using the supervise classification tool in ERDAS Imagine 9.2, land use and land cover maps were prepared. The kappa coefficient for the classification was 97.84%, proving the accuracy of the classification. The map has been classified into nine groups namely sand bar (0.15%), water body (0.75%), lateritic exposure (1.69%), open forest (1.87%), dense forest (5.91%), dry fallow (28.52%), wet fallow (25.40%), agricultural land (34.13%) and settlement (1.58%). The majority of the area is under the agricultural land in the downstream and middle sections along the river banks which have greater chances to recharge the contaminants because of the application of herbicides, pesticides and nitrogenous fertilizer into the soil (Xu et al., 2019). Additionally, low alkalinity in water will increase the effectiveness of pesticides (Fishel and Ferrell, 2019). Fig. 6.5d demonstrates the river basin's land use and cover. The weight assigned to this parameter has been shown in table 6.3 and table 6. A1 (appendix).

6.1.6.12 Population density

Global population growth is placing tremendous pressure on natural resources such as fresh water and soil. Direct discharge from the domestic wastes, leakage from the septic tank and poor management of the farm waste can lead to intrusive groundwater pollution (Zhang et al. 2018b). Locals reported during the field survey that most people practice open defecation and there is no sewerage system for household blue and gray water. In some

villages, pit latrines are used, but improper management can cause excreta to leak into groundwater, posing health hazards (Graham et al. 2013). Population density has been considered in this research to understand its influence on the aquifer system. Milledge et al. 2018 found a strong correlation between population density and ground and surface water contamination while studying the effect of microbial contamination across the Ganga Catchment. The current study used village wise population datasets from the district census handbook 2011 to create a population density map using ArcGIS software 10.4. Population density (person/sq.km) has been grouped into five groups namely 153.38-386.44 (30.98%), 386.45-571.04 (30.97%), 571.05-809.49 (24.05%), 809.50-1155.60 (11.54%) and 1157.70-2124.80 (2.46%). Middle and lower areas of the basin have a higher population density and are more susceptible to aquifer vulnerability (Fig. 6.5e). The weight assigned to this factor has been given in table 6.3 and table 6. A1 (appendix) and figure 5e demonstrates the groundwater recharge distribution of the region.

6.1.6.13 Groundwater based schemes

Water resides in the cracks and fractures of the jointed weathered rocks in the upper section of the basin. While the basin's lower section is semi-confined, extensive extraction occurs and water scarcity is observed (Bhunia et al. 2012). Groundwater-based irrigation schemes like tube wells, pumped dug wells, medium and high duty tube wells, and shallow tube wells are plentiful in downstream sections, putting additional pressure on aquifers. To maintain an optimal water level in the aquifer at a needed depth, extraction should not outpace recharge (Humphreyes, 2010). A GIS platform was used to prepare the final map of groundwater-based schemes based on block-wise data gathered from SWID (State Water Investigation Directorate). The groundwater-based schemes have been classified into 5 classes namely 4-251 (12.95%), 252-771 (8.07%), 772-1347 (27.09%), 1348-2527 (30.57%) and 2528-3681 (21.32%). According to the questionnaire survey, the most vulnerable aquifers are in Paschim Medinapore blocks where extensive groundwater extraction is made for potato, rice, and other crops (Akram et al. 2018). In table 6.3 and table 6. A1 (appendix), this factor is given a weight and fig. 6.5f shows the groundwater recharge distribution.

6.1.7 Results and Discussion

Effective use of groundwater requires proper management. The research focuses on identifying groundwater vulnerable tracts in the Shilabati river basin of West Bengal using a numerical model. In the first part of the study, the generation and application of the model was illustrated, followed by the identification of the vulnerability zones with respect to the suitability of drinking water, and finally, validation of the model was conducted. Based on the fuzzy Shannon entropy technique in ArcGIS 10.4 environment, the final map has been prepared and classified according to natural breaks (Jenks) (Fig. 6.6a-c). Data classification using Jenks natural breaks, also known as Jenks optimization, is an approach to determining the most appropriate classification of values. The goal is to minimize the average deviation of each class from the class mean while maximizing the deviation of each class from the means of the other groups (Chen et al. 2013). A higher index value indicates a higher probability of contamination of the aquifer (IIammurugan et al. 2022). Using 13 thematic parameters, vulnerable zones were delineated and their importance was determined based on the field survey. In terms of weighting and ranking, groundwater level (0.121) had the highest importance (1) since shallow aquifer depth is more likely to be contaminated. Following groundwater level is hydraulic conductivity (0.117), recharge (0.104), and specific

yield (0.102). A total of five categories have been identified in the final output map, which include very high values from 3.97-4.93 (10.82%), high values from 3.60-3.96 (23.20%), moderate values from 3.29-3.59 (29.29%), low values from 2.92-3.28 (25.02%) and very low values from 1.79-2.91 (11.64%). An area of very high to high vulnerability can be found in the middle of the basin. Anthropogenic activity and prevailing hydrogeological conditions are two major factors contributing to such vulnerability. The main problem in this zone is iron contamination (more than 1 mg/l) in drinking water (Chakraborty and Daspattanayak, 2019). Low to very low vulnerable zone is mainly concentrated in the upper section of the basin and in the areas covered by forest fringes along the middle edges of the basin. These forest acts as the filter towards the pollutants. All the detrimental chemical pollutants are under the permissible limit in this section. From the map it can an area of very high to high vulnerability can be found in the middle of the basin. Anthropogenic activity and prevailing hydrogeological conditions are two major factors contributing to such vulnerability. The main problem in this zone is iron contamination (more than 1 mg/l) in drinking water (Chakraborty and Daspattanayak, 2019). Low to very low vulnerable zone is mainly concentrated in the upper section of the basin and in the areas covered by forest fringes along the middle edges of the basin. These forest acts as the filter towards the pollutants. All the detrimental chemical pollutants are under the permissible limit in this section. From the map it can be seen that moderate zone is scatteredly found throughout the basin and covering majority of it.

6.1.8 Validation of the identified vulnerable zone

In order to achieve authentication and reliability, it is necessary to perform a model validation check (Chakraborty et al. 2022). To verify the accuracy and reliability of the applied model, water quality index correlation and ROC/AUC were used with four important drinking water parameters. To determine the effectiveness of this model in assessing the pollution scenario of groundwater and its suitability for drinking purposes (Hamza et al. 2017), WQI was calculated using equation 6.8-6.10. Local residents reported numerous problems with stomachs, reddish-brown stains on dishes, utensils and fixtures during the field investigation (Ortiz-Lopez et al. 2018). A total of seven drinking water parameters, including pH, Hardness, Total Dissolve Solids (TDS), Electrical Conductivity (EC), Alkalinity, Chloride and Iron, have been analyzed from 74 village sites (Table 6.4). The pH of the study area fell within 5.6-7.4 as discussed earlier and is alkaline to acidic in nature. The TDS value of the sampling sites ranges from 100-910 mg/l (Fig. 6.7a). Due to rock-water interactions, agricultural waste, and domestic waste, TDS concentrations are higher in the upper, central, and extreme lower parts of the basin. The presence of TDS above the desirable limit (500 mg/l) can be irritating to the stomach (Jain et al. 2003). According to Acharya et al. (2008), EC is directly proportional to mineral content in a dissolved state. EC values of the study area range from 104 -690 µs/cm (Fig. 6.7b) and are higher in the upstream section due to the hard rock's minerals dissolution and in the downstream section due to the dissolution of salts from kitchen waste as an anthropogenic source. The hardness value of the groundwater varies from 26- 1100 mg/l (Fig. 6.7c) within the basin. Water exceeding the limit of 300 mg/l is regarded as hard water causing skin irritation, eczema etc. The groundwater samples' alkalinity values (Fig. 6.7d) range from 10-1200 mg/l. The low alkalinity values in the central part of the basin can lead to corrosion of the pipeline system and increase the likelihood of heavy metals being released into the soil (Ma et al. 2020). High alkalinity can cause respiratory acidosis and alkalosis in the human body. Iron values of the samples range from 0.01- 15.6 mg/l. Fe content is higher in the basin's middle section (Fig. 6.7e), which may be due to the weathering of the rocks and overburden laterization (Ghosh et al. 2015). The concentration of chloride varies (Fig.

6.7f) from 5.67-187.94 mg/l and is within the permissible limit (250 mg/l). The descriptive analysis of the water quality parameters has been executed in the SPSS (Statistical Package for the Social Sciences) software (Table 6.4). The WQI index using the above parameters ranges from 9.83-475.05 where 33.78% are excellent, 21.62% are good, 8.11% are poor, 9.46% are very poor and 27.03% are unfit for drinking (Table 6.5). Fig. 6.8 and 6.9 show an excellent correlation between WQI and model output with Pearson's r of 0.83. Besides the WQI, ROC and AUC have been used to represent the precision of the model (Das and Mukhopadhay, 2020). AUC values can be classified into 5 groups based on the success rate of the prediction accuracy namely 0.5-0.6 (low/poor), 0.6-0.7 (good), 0.8-0.9 (very good) and 0.9-1 (excellent) (Yesilnscar and Topal, 2005). AUC values for hardness, alkalinity, iron, and TDS were 85%, 75%, 72%, and 70%, demonstrating the model's applicability in various environments and hydrogeological studies (Fig. 6.10). In this context, the WQI and the ROC/AUC were both highly effective and deserve future research adaptation (Hamza et al. 2017). This research will boost awareness of the groundwater pollution problem and the water management planners' inaccessibility of safe drinking water among the villagers.

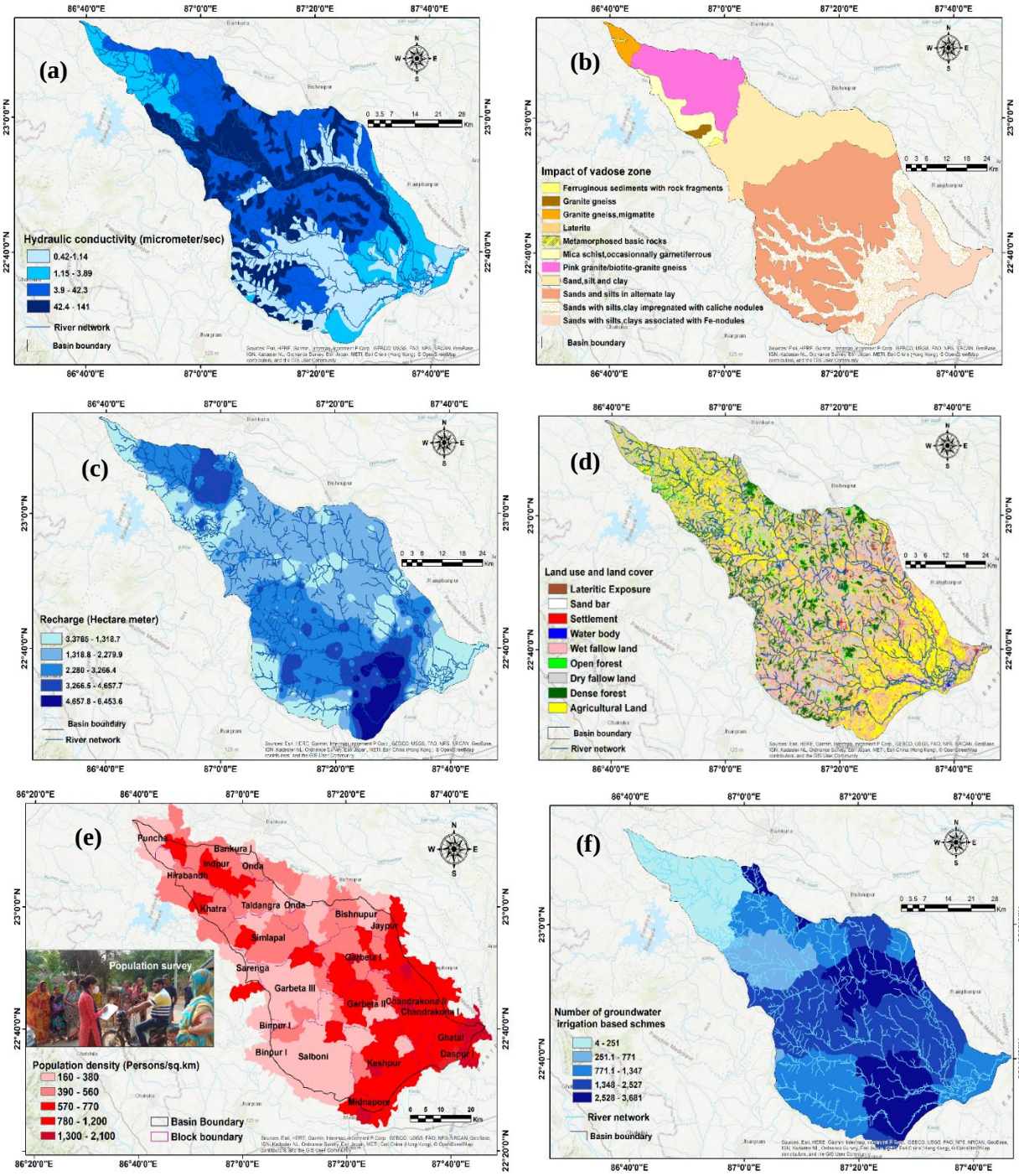

Fig. 6.5 Maps of groundwater vulnerability conditioning factors (a) hydraulic conductivity (b) impact of vadose zone (c) recharge (d) land use and land cover (e) population density (f) groundwater-based irrigation schemes

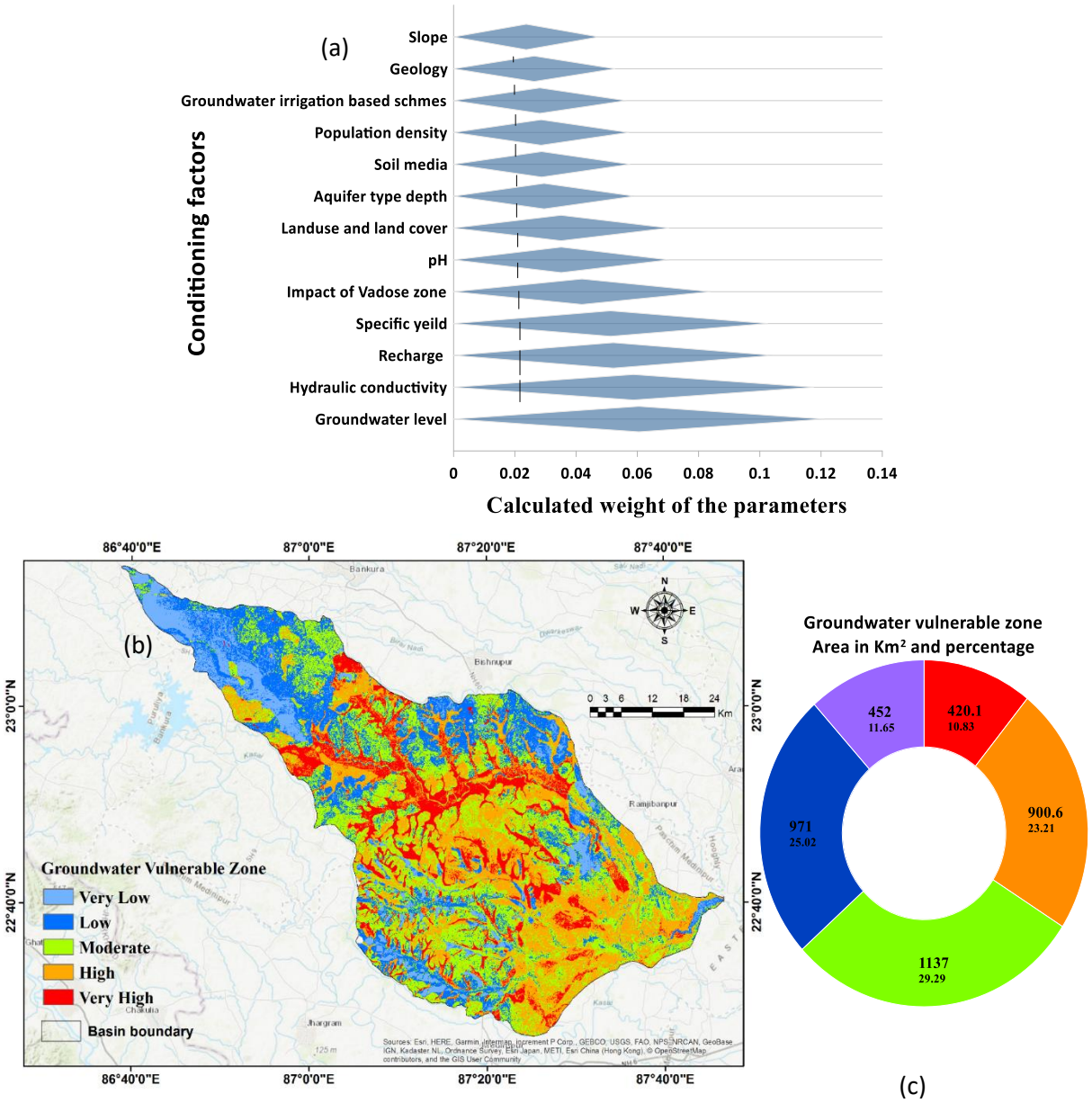

Fig. 6.6 (a) Importance of parameters (b) Groundwater Vulnerability Index (c) Areal distribution of groundwater vulnerable zone

Table 6.3 Pairwise comparison matrix of fourteen thematic layers for identification of soil loss susceptible zone

Parameters	Geology	Groundwater level	Soil media	Impact of vadose zone	Land use and land cover	Recharge	Specific yield	Aquifer depth	Hydraulic conductivity	Slope	Population density	pH	Groundwater based irrigation schemes	Fuzzy weight	Rank
Geology	1,1,1	2/5,1/2,2/3	1/2,2/3,1	1/2,2/3,1	2/5,1/2,2/3	2/5,1/2,2/3	2/5,1/2,2/3	1/2,2/3,1	1/2,2/3,1	3/2,2,5/2	3/2,2,5/2	2/5,1/2,2/3	2/5,1/2,2/3	0.053	12
Groundwater level	3/2,2,5/2	1,1,1	2,5/2,3	3/2,2,5/2	1,3/2,2	3/2,2,5/2	3/2,2,5/2	1,3/2,2	1/2,2/3,1	3/2,2,5/2	3/2,2,5/2	1,3/2,2	3/2,2,5/2	0.121	1
Soil media	1,3/2,2	1/3,2/5,1/2	1,1,1	2/5,1/2,2/3	2/5,1/2,2/3	1/3,2/5,1/2	2/5,1/2,2/3	1,3/2,2	2/5,1/2,2/3	1,3/2,2	1,3/2,2	1/2,2/3,1	1,3/2,2	0.058	9
Impact of Vadose zone	1,3/2,2	2/5,1/2,2/3	3/2,2,5/2	1,1,1	1,3/2,2	2/5,1/2,2/3	1/2,2/3,1	2,5/2,3	2/5,1/2,2/3	3/2,2,5/2	1/2,1,3/2	3/2,2,5/2	3/2,2,5/2	0.084	5
Land use and land cover	3/2,2,5/2	2/5,1/2,2/3	3/2,2,5/2	1/2,2/3,1	1,1,1	1/2,2/3,1	2/5,1/2,2/3	1/2,1,3/2	2/5,1/2,2/3	3/2,2,5/2	1/2,1,3/2	1/2,1,3/2	1/2,1,3/2	0.070	7
Recharge	3/2,2,5/2	2/5,1/2,2/3	2,5/2,3	3/2,2,5/2	2/5,1/2,2/3	1,1,1	1/2,1,3/2	3/2,2,5/2	1/2,1,3/2	3/2,2,5/2	3/2,2,5/2	1,3/2,2	3/2,2,5/2	0.104	3
Specific yield	3/2,2,5/2	2/5,1/2,2/3	3/2,2,5/2	1,3/2,2	3/2,2,5/2	2/5,1/2,2/3	1,1,1	3/2,2,5/2	2/3,1,2	3/2,2,5/2	3/2,2,5/2	3/2,2,5/2	3/2,2,5/2	0.102	4
Aquifer type depth	1,3/2,2	1/2,2/3,1	1/2,2/3,1	1/3,2/5,1/2	2/5,1/2,2/3	1/2,2/3,1	1/2,2/3,1	1,1,1	2/5,1/2,2/3	2/5,1/2,2/3	1,3/2,2	1/2,1,3/2	1,3/2,2	0.059	8
Hydraulic conductivity	1,3/2,2	2/3,1,2	3/2,2,5/2	3/2,2,5/2	3/2,2,5/2	2/3,1,2	1/2,1,3/2	3/2,2,5/2	1,1,1	3/2,2,5/2	3/2,2,5/2	3/2,2,5/2	3/2,2,5/2	0.117	2
Slope	2/5,1/2,2/3	2/5,1/2,2/3	1/2,2/3,1	2/5,1/2,2/3	2/5,1/2,2/3	2/5,1/2,2/3	2/5,1/2,2/3	3/2,2,5/2	2/5,1/2,2/3	1,1,1	1/2,1,3/2	1/2,1,3/2	2/5,1/2,2/3	0.047	13
Population density	2/5,1/2,2/3	2/5,1/2,2/3	1/2,2/3,1	2/3,1,2	2/3,1,2	2/5,1/2,2/3	2/5,1/2,2/3	1/2,2/3,1	2/5,1/2,2/3	2/3,1,2	1,1,1	2/3,1,2	2/3,1,2	0.057	10
pH	3/2,2,5/2	2/5,1/2,2/3	1,3/2,2	2/5,1/2,2/3	2/3,1,2	1/2,2/3,1	2/5,1/2,2/3	1,3/2,2	2/5,1/2,2/3	1,3/2,2	1/2,1,3/2	1,1,1	3/2,2,5/2	0.070	6
Groundwater irrigation-based schemes	3/2,2,5/2	2/5,1/2,2/3	1/2,2/3,1	2/5,1/2,2/3	2/3,1,2	2/5,1/2,2/3	2/5,1/2,2/3	1/2,2/3,1	2/5,1/2,2/3	3/2,2,5/2	1/2,1,3/2	2/5,1/2,2/3	1,1,1	0.056	11

Table 6.4 Descriptive statistics of the water quality parameters

Drinking Water Parameters	N	(BIS) (IS - 10500: 2012)/WHO (2003)	Range	Minimum	Maximum	Mean	Standard Deviation	Variance	Skewness	Kurtosis
pH	74	6.5-8.5	5.92	5.60	7.4	6.3797	.80725	.652	.065	-.066
TDS (mg/l)	74	500	812.0	102.0	914.0	238.081	126.8256	16084.733	2.618	10.906
Hardness (mg/L)	74	200	1100.0	26	1100	185.838	157.3214	24750.028	3.340	16.910
Alkalinity (mg/L)	74	200	1200.0	10.0	1200.0	152.514	164.5137	27064.774	4.056	23.970
Iron (mg/L)	74	1	14.6	.001	15.016	2.11005	6.158649	37.929	5.204	29.600
Chloride (mg/L)	74	250	182.27	5.67	187.94	45.1927	42.80995	1832.692	1.790	2.812
EC (µs/cm)	74	300*	586.0	104.0	690.0	373.189	158.4971	25121.334	.438	-.890

*Desirable limit for EC has been taken from WHO (2003), BIS Bureau of Indian Standards

6.1.9 Discussion

In the Bengal Basin, groundwater demand for irrigation and drinking has increased due to rapid population growth and anthropogenic activities (Das and Saha, 2022). Surface and groundwater resources within the Shilabati river basin are polluted by various anthropogenic activities, such as unplanned market growth beside the main channel, and the discharge of domestic waste (Roy et al. 2021). There was an increase in risk and vulnerability due to the unscientific and unrestricted withdrawal of groundwater in this region (Basu and Bera, 2010). As a result of this burden on the groundwater, the current methodology has been utilized where significant parts of the basin that show a high to very high likelihood of contamination of the groundwater. In the river basin, areas with shallow groundwater levels have been identified as having the highest level of contamination (Sophocleous, 2002).

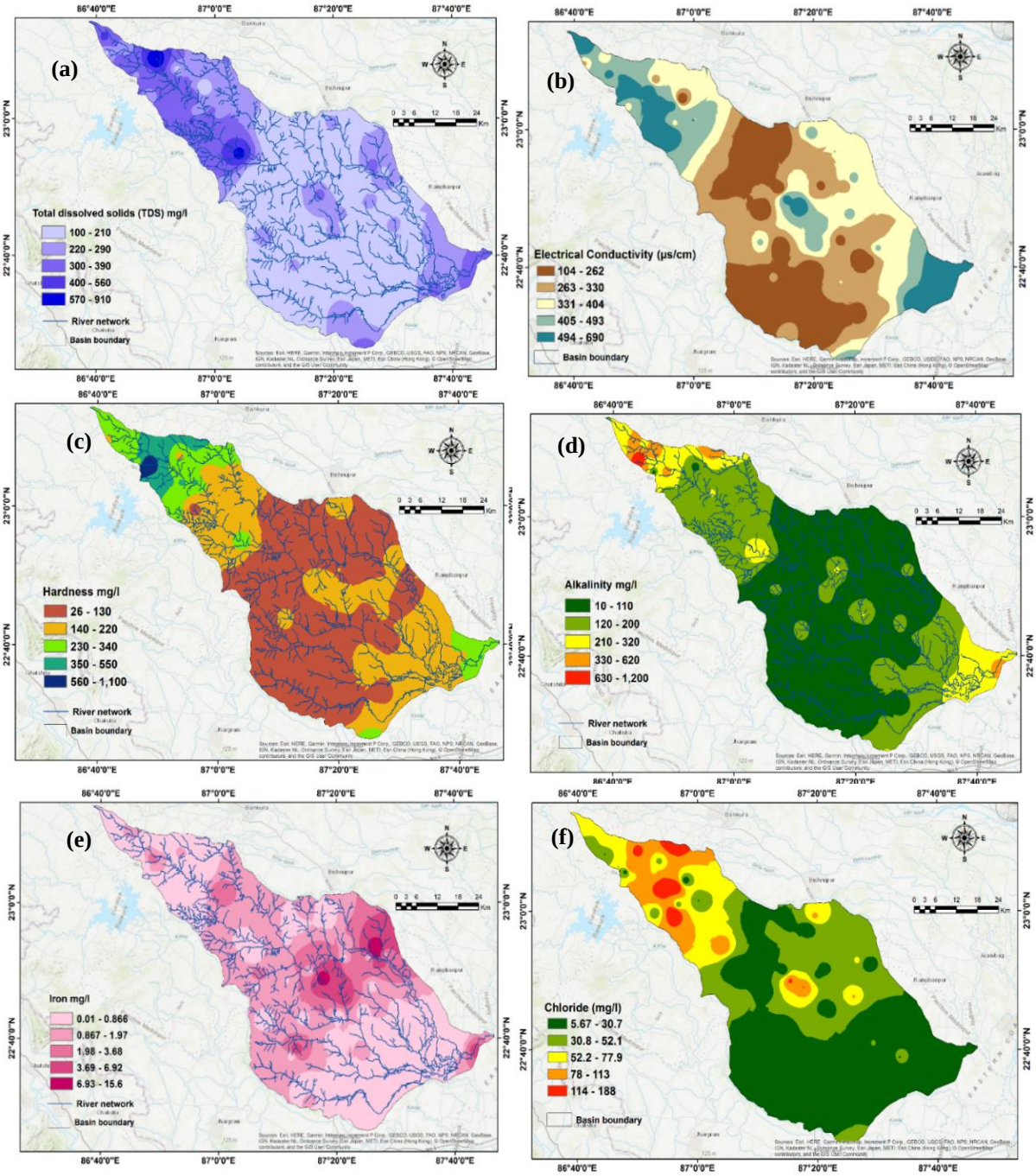

Fig. 6.7 Spatial distribution of groundwater quality parameters (a) Total dissolve solids; (b) Electrical conductivity; (c) Iron; (d) Hardness; (e) Alkalinity and (f) Chloride

Table 6.5 Water quality status of the sampling village sites

Water Quality Index	Water Quality Status	Percentage of Sampling Sites	Sampling Village Sites
0-25	Excellent	33.78	Bangla, Keshia, Sonardanga, Ranibazar, Araldili, Elora, Damodarpur, Uchachar, Nanda, Keshpur, Mandalkupi, Jadupur, Karnagarh, Satbankura, Sonajhor, Dubrajpur, Rajpur, Lalgeria, Dewanchak Garbeta, Baikunthapur, Nagri, Dhanghori, Amrakuchi, Kazirhat
26-50	Good	21.62	Mahal Danga, Jiarda, Hirabandh, Chota Tara, Kundhurka, Pingboni, Pratappur, Raskundu, Kiamacha, Pirchak, Ramgar, Dhansantra, Amanpur, Salapahari, Muragram
51-75	Poor	8.11	Piasala, Ashberia, Simlapal, Radhaballavpur, Kalapahar, Jemuasole
76-100	Very poor	9.46	Bhutsahar, Sarbot, Majura, Patharpara, Panchmura, Boga, Sholdiha
>100	Unfit for consumption	27.03	Harmasra, Dhadika, Nachankonda, Amlasuli, Tarasulipenchapara, Kandrauttarbill, Bagda, Ghatmura, Jiarpara, Benchapra, Basudevpur, Makli, Molian, Debgram, Amlagora, Ranapur, Chenchurya, Raghunathpur, Piyardanga, Amkopa, Baramura

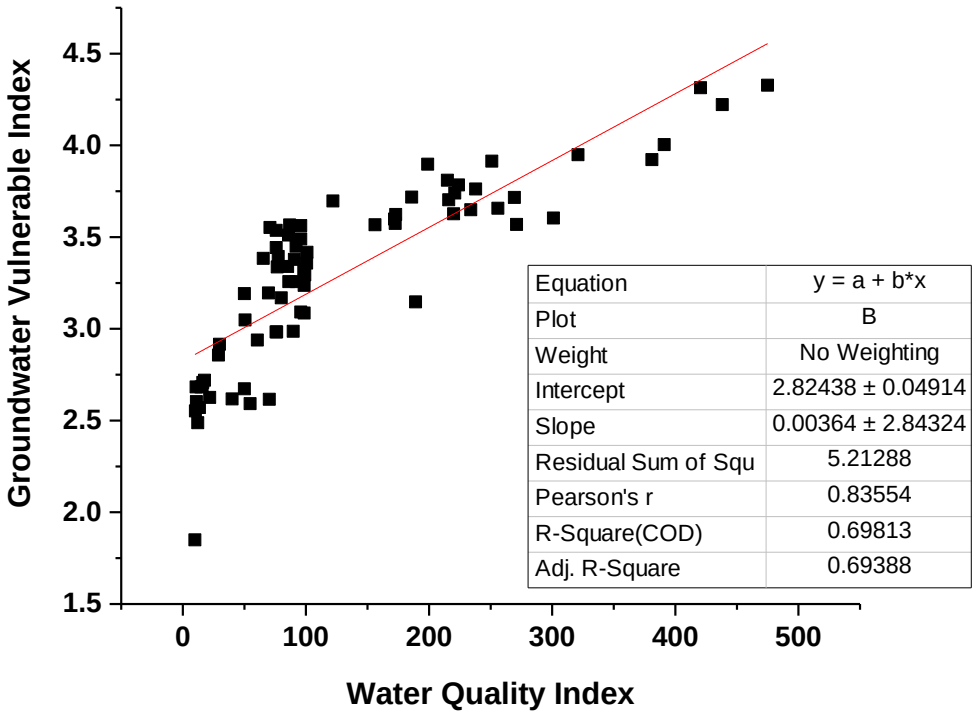

Fig. 6.8 Correlation between WQI and Groundwater Vulnerable Index

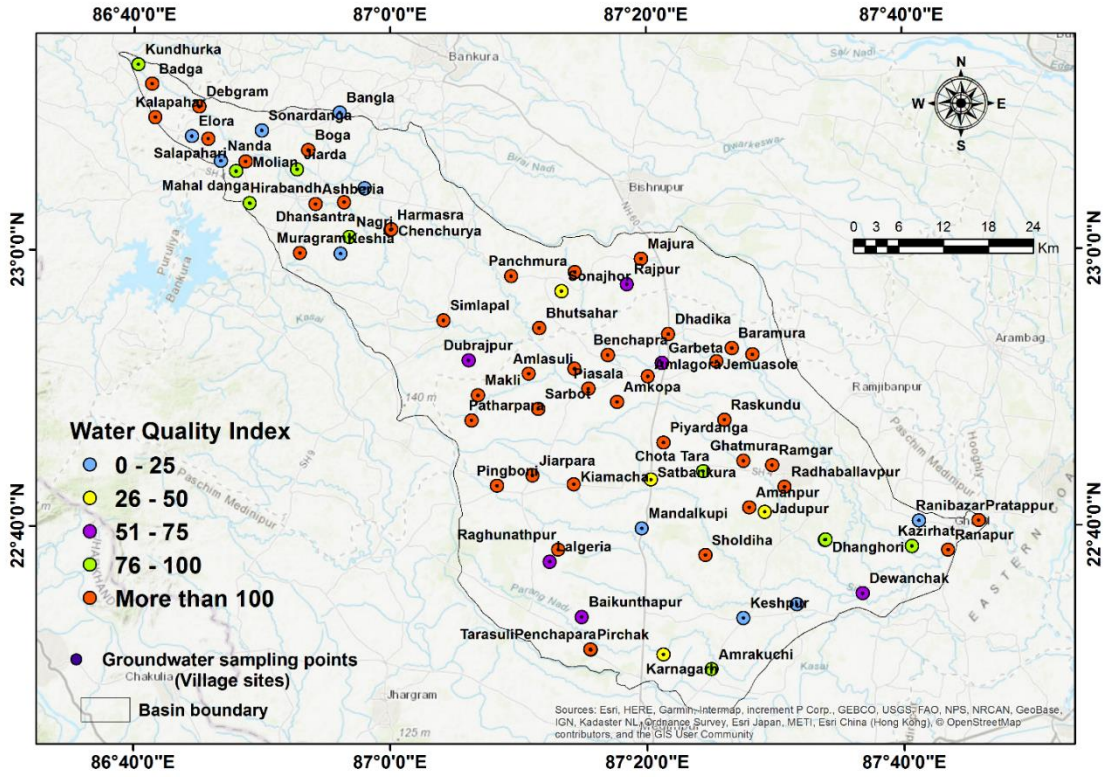

Fig. 6.9 Water Quality Index of different sites

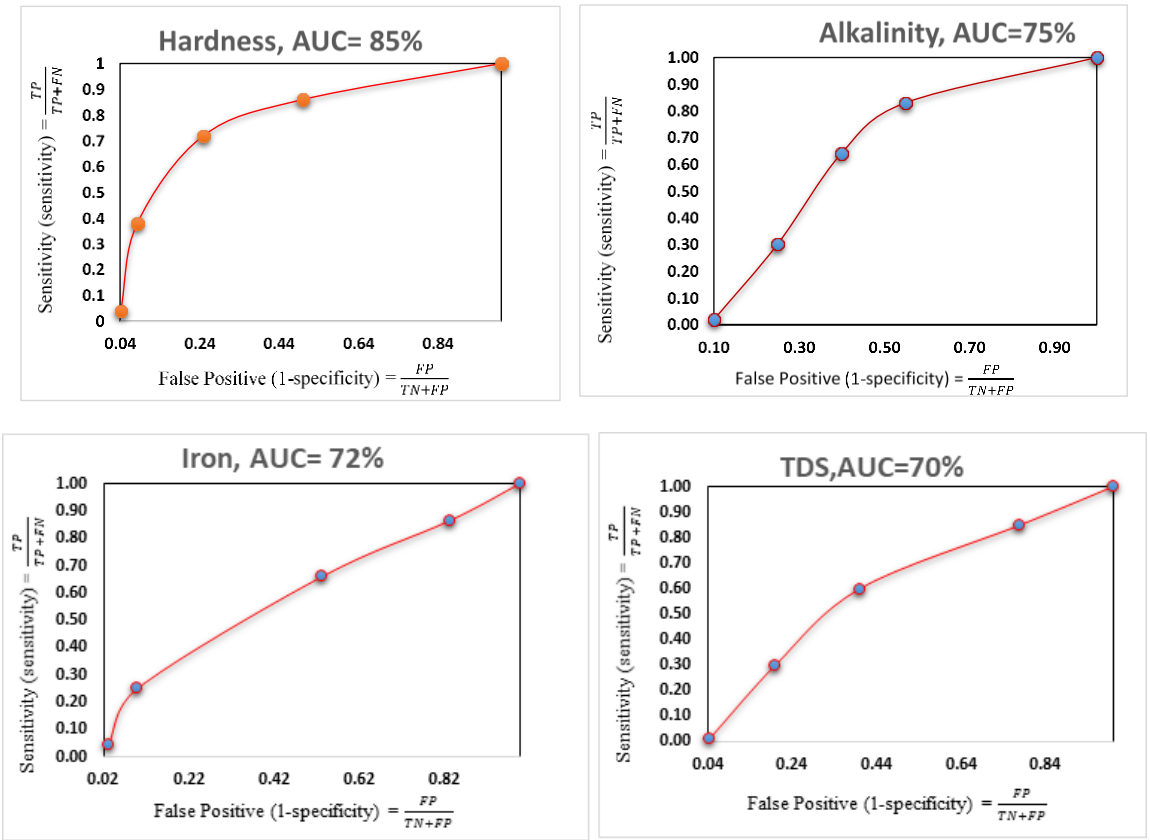

Fig. 6.10 Validation of Groundwater vulnerable index using ROC curve showing area under the curve for hardness, alkalinity, iron and TDS

A few parts of the basin also experience moderate to high groundwater recharge, further escalating groundwater pollution. Often, the recharge from precipitation events in the downstream section causes microbial contamination of shallow aquifers (Swain et al. 2022). For mapping the vulnerable zone, 13 hydrogeological, hydrological, and anthropogenic factors such as geology, groundwater level, soil media, the impact of the vadose zone, land use, land cover, recharge, specific yield, aquifer depth, hydraulic conductivity, slope, population density, pH, and groundwater-based irrigation schemes were considered (Huan, 2012) and weights has been calculated using FSE-GVI model framework. Such work has not been conducted within the river basin and is more accurate than the techniques previously used in other basins. The model output shows that in the upper section of the basin, surface contamination is lower due to the hard rock terrain, but in the middle and downstream part of the basin, contamination is higher due to fine to coarse aquifer media (Aller et al. 1987, Bhattacharya et al. 2016). Moreover, the central and lower sections of the basin are dominated by agricultural activities, which results in greater chemical fertilizer application (Das et al. 2021; NABARD, 2016). In this river basin, numerous geo-environmental hazards and hydro-environmental hazards exist, such as drought (Raha and Gayen, 2021), flood (Kar and Das, 2020), soil erosion (Aown and Kar, 2016), and groundwater pollution (Kundu and Nag, 2018). However, few studies have examined mitigation measures or solutions. Most studies focus exclusively on lateritic evolution and its origin, flooding and drought, overlooking the miseries of groundwater and ordinary people. Unlike DRASTIC, GOD, SINTACS and other techniques, this research can be considered a novel technique for cost-effectively mapping the aquifer. According to Nadiri et al. (2017) the DRASTIC model can be considered as a heuristic approach, since it can be calibrated and validated, but the vulnerability index values cannot be controlled. According to the results, the present study rejects the hypothesis that the seven factors, rating and weighting, must be constant.

To the best of the authors' knowledge and literature reviews, this is the first application of FSE-GVI framework to aquifer vulnerability. Vulnerability modeling was formulated by other types of MCDM techniques which differs from the Fuzzy Shannon Entropy framework in regard to research design as they produce assemble index and are able to drive linguistic attribute avoiding fuzzy scale (Jesiya and Gopinath, 2019; Das et al. 2023). Few papers applied Convolutional Neural Network (CNN) (Nadiri et al. 2022), Bayesian Model Averaging (BMA) (Gharekhani et al. 2022), deep convolution neural network (Jiang et al. 2021) etc. but there are uncertainties associated with the structure of these models. Applying such techniques to a large dataset slowed the convergence significantly. Gharekhani et al. 2023, constructed Level 1, MMs (Multiple Models) which comprises ANN (Artificial Neural Network), GEP (Gene Expression Programming), and SVM (Support Vector Machines) and combining the results of level 1 designed the Level 2, BMA (Bayesian Model Averaging) techniques which require many hyper parameters that may exhibit the models time-consuming during the process of completing the modeling approach and increases complexity towards vast researchers in understanding the research design. While FSE-GVI framework is clear, comprehensible, straightforward and coherent. The FSE-GVI not only simplifies the criteria network and makes the calculation more organized, but also provides room for including different other possible criterions in groundwater studies, such as vulnerability mapping to contamination and subsidence and groundwater potential studies.

FSE- GVI model of aquifer vulnerability are also important in light of the hypothesis that physical environment may be important to shield groundwater from anthropogenic or natural influences as well as pollutants that

penetrate into the subsurface environment as such new criterions such as pH, population density, and groundwater irrigation schemes has been incorporated beside specific yield. Almost all studies have neglected such parameters (see Guo et al. 2023; Nadiri et al. 2022; Elzain et al. 2023). Like DRASTIC models, they are generally validated with nitrate contamination but did not considered any anthropogenic criterions. Further, monitoring and collecting concentration data for the pollutants of interest is crucial because the concentration changes over time as a result of hydrodynamic dispersion and groundwater water replenishment during many times of the year. Nevertheless, most studies used historical data for validation (see Taghavi et al. 2023; Lakshminarayanan et al. 2022). However, the current study has been validated using immediate water samples collected from 74 dug wells/tube wells across the river basin that have high iron levels, high fluoride (upper section), and high TDS and alkalinity levels. As a management strategy, low cost environment-friendly filtration techniques can be adopted for iron removal over the region that is geogenic and too some extent anthropogenic due to growing the iron-based industries. Besides this, enhanced cropping technique, bio fertilization, irrigation from rainwater harvesting, and proper waste disposal can prevent groundwater pollution and decrease the TDS concentration in groundwater. This model can be applied in different parts of the world, but the main limitation lies in the associated parameters which can condone the local variability of a specified area and its related weight estimation.

6.1.10 Conclusion and Recommendation

An assessment of vulnerability maps provides insight into aquifers at risk of contamination and can be used for planning practices. The study aims to develop defensible tools for possible future planning practices, which can be applied to any study area with sparse data, that are already exposed to groundwater depletion and related hazards. A judicious use of groundwater is essential to sustain long-term agriculture and socio-economic development in the Shilabati river basin area. The current research thus proposes a modified approach for predicting groundwater vulnerable sites. Considering the 13 hydrogeological, geo-environmental and anthropogenic factors fuzzy Shannon entropy model has been applied for the weight optimization. Based on the findings of this study it can be concluded that:

- To overcome the traditional methods like DRASTIC, GOD etc. and to increase the robustness and optimization, FSE-GVI integrated with GIS framework has been developed to incorporate more parameters and adjust the models' rates and weights.
- Groundwater level obtained the highest weightage in the model simulation and out generation followed by hydraulic conductivity, recharge, specific yield, impact of vadose zone, pH, Land use and land cover, aquifer depth, soil media, population density, ground water-based irrigation schemes geology and slope.
- In this study, the index value ranges from 1.79-4.93 and has been classified into five classes namely very high (10.82%), high (23.20%), moderate (29.29%), low (25.02%) and very low (11.64%). The high to very highly vulnerable zone is mainly concentrated in the basin's central part or middle section and is more susceptible to contamination. Due to the shallow groundwater level and fine to coarse-grained soil, which has higher hydraulic conductivity, surface contaminants can pass through the vadose zone and contaminate the groundwater table.
- In the FSE-GVI model integrated with GIS, the modeling strategies have deliberated learning capabilities, which are evident in the performance metrics. The model has been validated using WQI and

ROC and AUC values. Most of the water quality parameters exceeded the permissible limit except chloride. The WQI values are ranged from 9.84-475.05 where 27.03% of the villages lie under the unfit for drinking. WQI values are well correlated with the output map (r=0.83), with AUC as 85% for hardness, 75% for alkalinity, 72% for iron and 70% for TDS. The identification and selection of appropriate thematic layers and justifiable weight allocation are crucial to the success of RS and GIS applications for groundwater identification.

6.1.11 Limitation and future work

With improving parameters and incorporating qualitative and quantitative aspects related to human activities and the aquifer system, the model is highly accurate. The extensive methodology utilized here using the validated numerical approach to simulate the vulnerable zone having a stratigraphical complexity and structural variability can be applied in similar terrain conditions with different climate regimes. In addition to providing a sound basis for planning sustainable groundwater management, the present study provides a step-by-step guide. Considering the logical bases of the study and its generic nature, it is applicable to other regions of India or abroad with or without appropriate modifications. To ensure a proper protection and management plan, it is recommended that aquifer water quality should be investigated and monitored more regularly, particularly in vulnerable areas. The absence of detailed hydrogeological investigations, pumping test and real-time monitoring and estimation of aquifer parameters at different locations has been a major limitation of this study. However, if the country prioritizes data collection, national research that is pivotal for sustainable development will be boosted and amplified. The current research will also be a call to all the water suppliers, public health authorities and government/non-government water resources management sectors, to collaborate and to assist in the data mining and to address the system's limitations for causing major health issues and must safe guard our drinking water sources. For the safety of the citizens, further research of the groundwater vulnerability dynamics within the district and the country will be the next plan of action.

6.2 Application of Fuzzy C means clustering and Fuzzy EDAS to assess groundwater irrigation suitability and prioritization for agricultural development

6.2.1 Introduction

Continuous use of such unsafe groundwater for irrigation may lead to the transport of detrimental contaminants into the soil, which, over time, may alter the soil's physio-chemical properties and affect the soil's fertility (Batabyal and Gupta, 2017). The dependence on groundwater in rural areas is greater than in urban areas in India. Approximately 90% and 70% of groundwater in rural regions in India is used for drinking and irrigation (Adimalla and Qian, 2022). Water contaminants such as Arsenic, fluoride, iron and nitrate are frequently found in rural areas. Additionally, these ions create carcinogenic and non-carcinogenic health risks (NCHRs) for human health. Research has shown that high concentrations of fluoride and nitrate in drinking water contribute to elevate NCHR and other diseases like blue baby .3syndrome, birth consequences, and fluorosis (Haghnazar et al. 2021). In rural areas of India, sources of groundwater pollution include animal wastes, agricultural wastes, septic tanks, and unplanned drainage patterns, as well as unnecessary use of nitrate and phosphate fertilizers for high agricultural yield (Anand and Karunanidhi, 2020). Beside this, in arid and semi-arid parts of India, salt content accumulates in the root zone of crops due to insufficient precipitation where salinity, sodicity and ion toxicity are most prevalent issues (Merouche et al. 2020). Sodic soil occurs when the proportion of Na^+ becomes high in respect to $Mg^{2+}$and Ca^{2+}. A readily permeable structure results when the majority of $Mg^{2+}$and Ca^{2+} adsorbed on the surface of soil exchange complexes. It may affect the physical structure of soils if such water is used in irrigation fields for a long time, causing adsorption of Na^+ on soil colloids. Dry soil becomes rigid and dense from dispersion and swelling, and wet soil gradually becomes impervious to irrigation water and recharge from precipitation (Mukherjee et al. 2019). To maintain a sustainable environment, it is crucial to monitor and evaluate groundwater quality on a regular basis. Moreover, of the 17 Sustainable Development Goals (SDGs) designed by the United Nations in 2015, SDG 6 of "Clean water and sanitation" aims to provide safe and affordable drinking water to the community (Swain et al. 2022). The program also emphasizes minimizing pollution and managing contaminants efficiently (UNDESA, 2016).

Maps and irrigation suitability analysis of groundwater movement and their quality are two of the major GIS applications in groundwater studies. Globally, GIS and multivariate statistical analyses have been used to examine the factors controlling groundwater quality and its suitability for drinking and irrigation (Megahed, 2020). An essential tool for groundwater resource management can be groundwater mapping that reflect the resilience of the system to long-term or short-term effects, such as droughts and floods due to resultant climate change, (NGWA, 2016). In recent years, GIS has emerged as a powerful tool for resource management research. It is thus able to address multidimensional resource management challenges, such as water management, through its accuracy, visualization, and model building capabilities (Singh et al. 2022). A groundwater map can be used to evaluate water quality problems, assess pollution vulnerability, locate diseases and vulnerable populations and facilitate targeted interventions for management of resources (Zeilhofer et al, 2007). With the spatial distribution of irrigation suitability parameters (Cordier et al. 2021), it will be possible to determine groundwater quality, areas

that can be irrigated directly without water treatment, and areas that need sustainable remediation. Such techniques have been effectively used in coastal groundwater management (Sabino et al. 2020), in hard rock terrain (Adimalla and Taloor, 2019), in karstified aquifers (Paternoster et al. 2021), in unconsolidated sedimentary zones of the quaternary layers (Mohamed et al. 2018) etc. Recent years have also witnessed fuzzy set theories extensively used to solve environmental problems (Oladipo et al. 2020). Natural phenomena can be rationally described and evaluated using fuzzy logic in conjunction with GIS. Fuzzy logic helps mitigate errors in groundwater quality assessment due to its ability to deal with ambiguity and inaccuracy (Suhas and Chaudhary, 2020). A few studies have used fuzzy logic to evaluate groundwater irrigation suitability using geochemical parameters and GIS (Kisi, 2010; Kisi et al. 2008, Ki and Ray, 2014; Suhas and Chaudhary, 2020). A review of these studies led to the formulation of the current study in a modified way, which evaluates irrigation water quality regardless of geomorphology, topography, lithology, and meteorology using Fuzzy C means clustering (soft computing technique) and Fuzzy EDAS for the foremost time. Both the techniques are new in the field of water quality research. Most of the other fuzzy system cannot be executed so easily to a problem when there is no if-then rule associated with it (Pezeshki and Mazinani, 2019). Like in case of neuro fuzzy systems, Fuzzy Synthetic Evaluation (Cheng et al. 2001), Cascaded Fuzzy Inference System (Mahapatra et al. 2011) learning phases can be computationally intensive and time consuming when there are many parameters, rules, antecedents and model delays (Nauck and Nurnberger, 2013). But these two approaches (fuzzy c-means clustering and fuzzy EDAS) used in the current research plays an important role in dealing with uneven distribution of parameters and nodes related with application of cluster centroids and membership degrees (Wang et al. 2018).

6.2.2 Research Gap and Novelty of work

A predominantly agrarian country, West Bengal has a net cropped area of 52.05 lakh ha, making up 68% of its geographical area, and 92% of its arable land is irrigated by groundwater rather than rivers, lakes, abandoned channels, or ponds (Sarkar and Islam, 2021). Groundwater in the studied river basin of the present work comprising the blocks of Puruliya, Bankura and West Medinapore district of West Bengal is affected by humans, natural phenomena, and climate change that release certain elements into water, the excess of which is detrimental (Nag 2014; Nag and Ghosh, 2013). A variety of studies have been conducted from various regions for this study area, including microbiological studies (Roy et al. 2021), studies investigating the quality of groundwater for drinking and irrigation in Puruliya (Chowdhury et al.2022), Bankura (Nag and Das, 2017), and delineation of groundwater potential zones (Bhunia et al.2021). It has been observed from previous studies, however, that spatio-temporal changes in groundwater quality are not monitored, particularly with irrigation use. The present study also addresses this gap with the objective of combining the key groundwater quality indices considered for irrigation purposes with a fuzzy clustering plot for effective decision making. For the first time this soft computing technique has been applied in this current geochemical research. Furthermore, the study explores the spatiotemporal variation of irrigation water quality and prioritize the river basin for effective management using Fuzzy EDAS and GIS techniques. The purpose of this paper is thus to present a hybrid approach to understand irrigation quality degradation and management practices in a complex terrain condition.

6.2.3 Objective of the Research Work

The main objectives of the study include the following (a) statistical hydrogeochemical analysis of the groundwater of the river basin and its spatial distribution; (b) understanding hydrogeochemical facies and its geochemical evolution; (c) application of fuzzy c means clustering for grouping the sampling points based on irrigational suitability and (d) lastly application of the fuzzy EDAS to prioritize the river basin for effective water resources management in a sustainable way.

6.2.4 Area of Investigation

Stratigraphic succession in the upper section of the Shilabati basin typically begins with a thick bed of mostly Achaean granite gneiss, slightly consolidated Quaternary sediments, Permo Carboniferous sandstones, massive granites, quartzite, and recent alluvium sediments. The dominant rocks in Puruliya and Bankura districts are granite, granitic gneiss, and phylite & mica schist. A majority of these rocks consist of muscovite, biotite, feldspar, albite, quartz and clay minerals and has an influence on the groundwater composition of the basin (Dolui et al. 2016). Hydro-geologically, the lower basin can be divided into young and older alluvium, soils overlaid by secondary laterites, sediments overlaid by primary laterite (in situ), basement crystalline complex (metamorphites) and platform margin conglomerates (Bhunia et al. 2012). In shallow, moderately weathered zones of the older alluvium, groundwater occurs in unconfined to semi- confined condition within joints, fissures, and fractures. Therefore, secondary porosity (the weathered zone and fluvio-deltaic sediments) is the primary source of groundwater occurrence, movement, and transmission within the basin. The geological aspects of the different sampling sites have been given in the Table 6. The lower section of the basin practices triple cropping, while the upper section of the basin, crops one season and uncrops the other seasons (Halder et al. 2022). Groundwater sampling has been done from 74 sites from four different sources (Fig. 6.11). According to the field survey, paddy is the most common crop, followed by potatoes, groundnuts, bringel, cabbage, sesame, mustard, and other seasonal vegetables. As reported by the farmers, potash, urea, NPK 10-26-26, diammonium phosphate, and other fertilizers are used to cultivate these crops.

6.2.5 Research Design and Methodology

6.2.5.1 Sample collection and preparation

A number of factors has been considered when selecting sampling sites, including lithology, geology, wells availability, river influence, agricultural and urban activities. From November, 2021 to mid-February, 2022, groundwater samples have been collected from 74 locations including dug wells (25-115 feet), submersible pumps (80-400 feet), tube wells (35-300 feet) and tube well mark II (60-180ft) (Fig.6.11). Following continuous purging for 20 minutes to avoid stagnant water in the pipe lines, samples has been collected and stored in pre-washed polyethylene containers using 5 % of HNO_3 solution. The in-situ measurements of temperature, pH, TDS and EC are performed by Hach Series of Portable Meters and electrodes. According to the American Public Health Association (APHA, 2005), collected samples has been analyzed using standard procedures. Complexometric titration method is used to determine bicarbonate (HCO_3^-), chloride (Cl^-), hardness and alkalinity of the samples. Anions like calcium (Ca^{2+}), magnesium (Mg^{2+}), sodium (Na^+), and potassium (K) are determined by Inductively

Coupled Plasma Atomic Emission Spectroscopy. Sulphate (SO_4^{2-}) and nitrate (NO_3^-) and phosphate (PO_4^{-3}) were determined using spectrophotometer (model- DR 2800, and iron (Fe) by UV/VIS Spectrophotometer Pharo 300. Using a potentiometric ion selective electrode, fluoride (F^-) has been determined. The levels of arsenic in this study area are below detection limits, so they are not used. Also, Ionic Balance Error (IBE) has been carried out for all groundwater samples to ensure a high level of standardization and minimize manual error. The IBE did not exceed the permissible limit of ± 5%. To display their spatial distributions, data from the measured ions and elements has been interpolated using the Inverse Distance Weighting (IDW) interpolation methods in ArcGIS 10.4 and ArcGIS Pro (Joodavi et al. 2021). Statistical analyses, correlation analyses, and graphical representations has been used to evaluate the hydrogeochemical reactions and basic hydrogeochemical processes utilizing Origin 2022b and R software. The flowchart of the research methodology has been shown in Fig. 6.12.

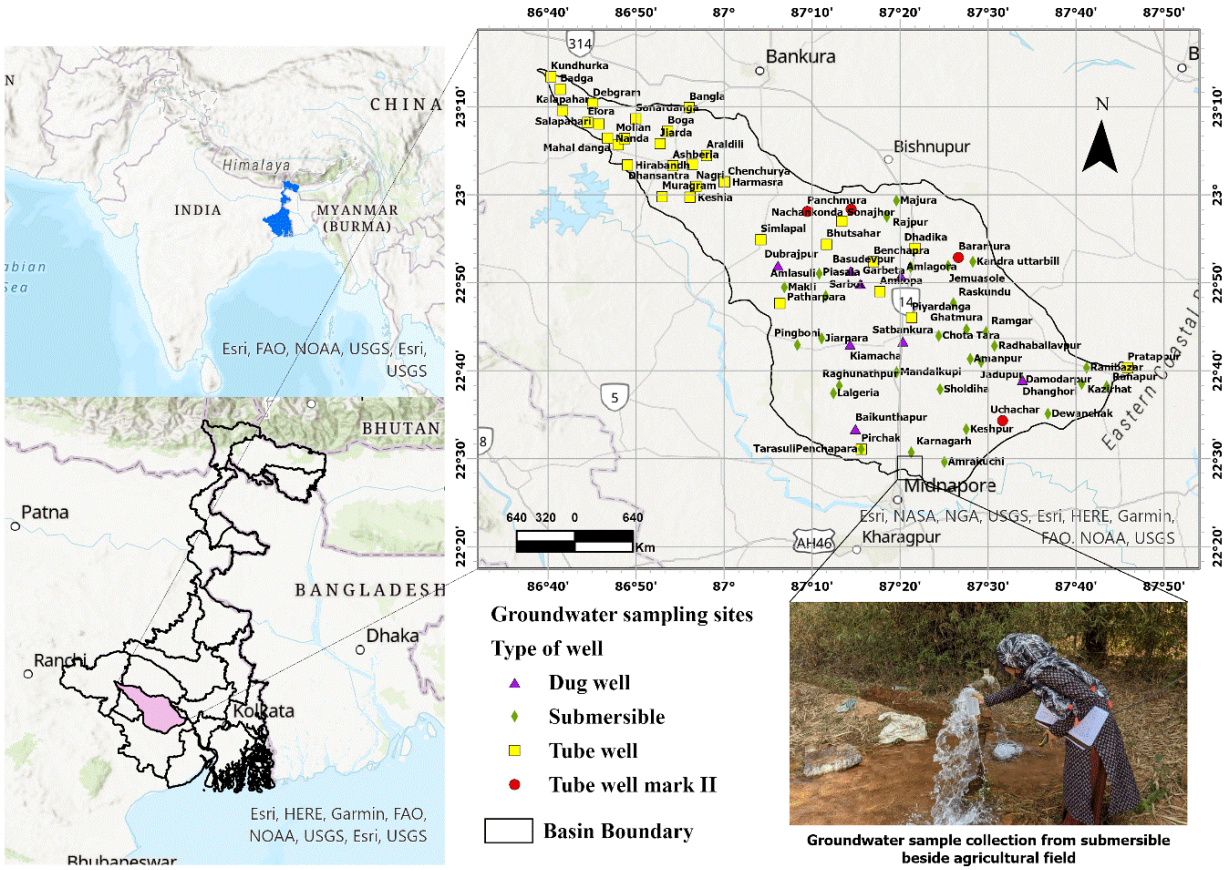

Fig. 6.11 Location of the study area and sampling sites

Table 6.6 Geological scenarios of sampling sites

Sampling sites	Geology	Age
Badga, Bangla, Debgram, Kalapahar	Granite gneiss and migmatite	Proterozoic and Pleistocene – Holocene
Sholdiha	Metamorphosed basic rocks	Paleoproterozoic
Hirabandh, Keshia, Mahaldanga, Muragram, Nanda	Mica schist, occasionally garnetiferrous	Proterozoic and Pleistocene – Holocene
Araldili, Ashberia, Boga, Chenchurya, Dhansantra, Elora, Harmasra, Jiarda Molian, Nagri, Salapahari, Sonardanga	Pink granite/biotite-granite gneiss	Proterozoic
Bhutsahar, Dubrajpur, Majura, Nachankonda, Panchmura, Rajpur, Simlapal, Sonajhor	Sand, silt and clay	Pleistocene – Holocene, Pleistocene and Meghalayan
Amanpur, Amkopa, Amlagora, Amlasuli, Baikunthapur, Baramura, Basudevpur, Benchapra, Chota Tara, Dhadika, Garbeta, Ghatmura, Jemuasole, Kandra uttarbill, Kiamacha, Makli, Mandalkupi, Patharpara, Piasala, Pingboni, Pirchak, Piyardanga Raskundu, Sarbot, Satbankura, Tarasuli Penchapara	Sands and silts in alternate clay	Pleistocene – Holocene, Pleistocene and Holocene
Amrakuchi, Damodarpur, Jadupur, Jiarpara Karnagarh, Kazirhat, Keshpur, Lalgeria Radhaballavpur, Raghunathpur, Ramgar, Ranibazar, Uchachar	Sands with silts, clay impregnated with caliche nodules	Pleistocene – Holocene, Pleistocene and Holocene
Dewanchak, Dhanghori, Pratappur, Ranapur	Sands with silts, clays associated with Fe-nodules	Pleistocene – Holocene, Pleistocene and Meghalayan

6.2.5.2 Geostatistical modeling and clustering techniques

6.2.5.2.1 Fuzzy C-means clustering of geochemical data

Fuzzy C-means (FCMs) are known for their partitioning-based algorithms (Bezdek, 1981). It assigns fuzzy membership degrees to data points according to their distance from cluster centers. The membership of the data point in a cluster center will be higher than that of the other clusters if it is closer to the cluster center (Wang et al. 2014). The fuzzy c-means clustering algorithm (FCM) is a soft clustering method. Among the hard-clustering algorithms are K-means clustering algorithm (K-means), hierarchical clustering (HCA), and other algorithms, they are subordinate to 0 or 1. The FCM, on the other hand, is a soft clustering technique, which is subordinate to the interval algorithm [0, 1] when clustering. (Yao et al. 2022). Unlike hard clustering (Mosavi et al. 2021), fuzzy c-means (FCM) techniques reduce uncertainty in identifying the members of a group by assigning a degree of membership to each member. With its fuzzy C-partition concept, FCM clustering algorithms have been successfully applied in a wide range of applications, including thermal system monitoring, data mining (Motaki et al. 2021), image segmentation (Christ and Parvathi, 2011). The FCM has been calculated using the following steps (Wang et al. 2014; Shen et al. 2021).

Step 1: FCM clustering algorithm divides a sample set ($X= \{x_1, x_2, x_3, x_4 \ldots x_n\}$) into a number of clusters/groups and identifies cluster centers by minimizing the following algorithm (Sahu et al. 2012) (Eq. 6.16).

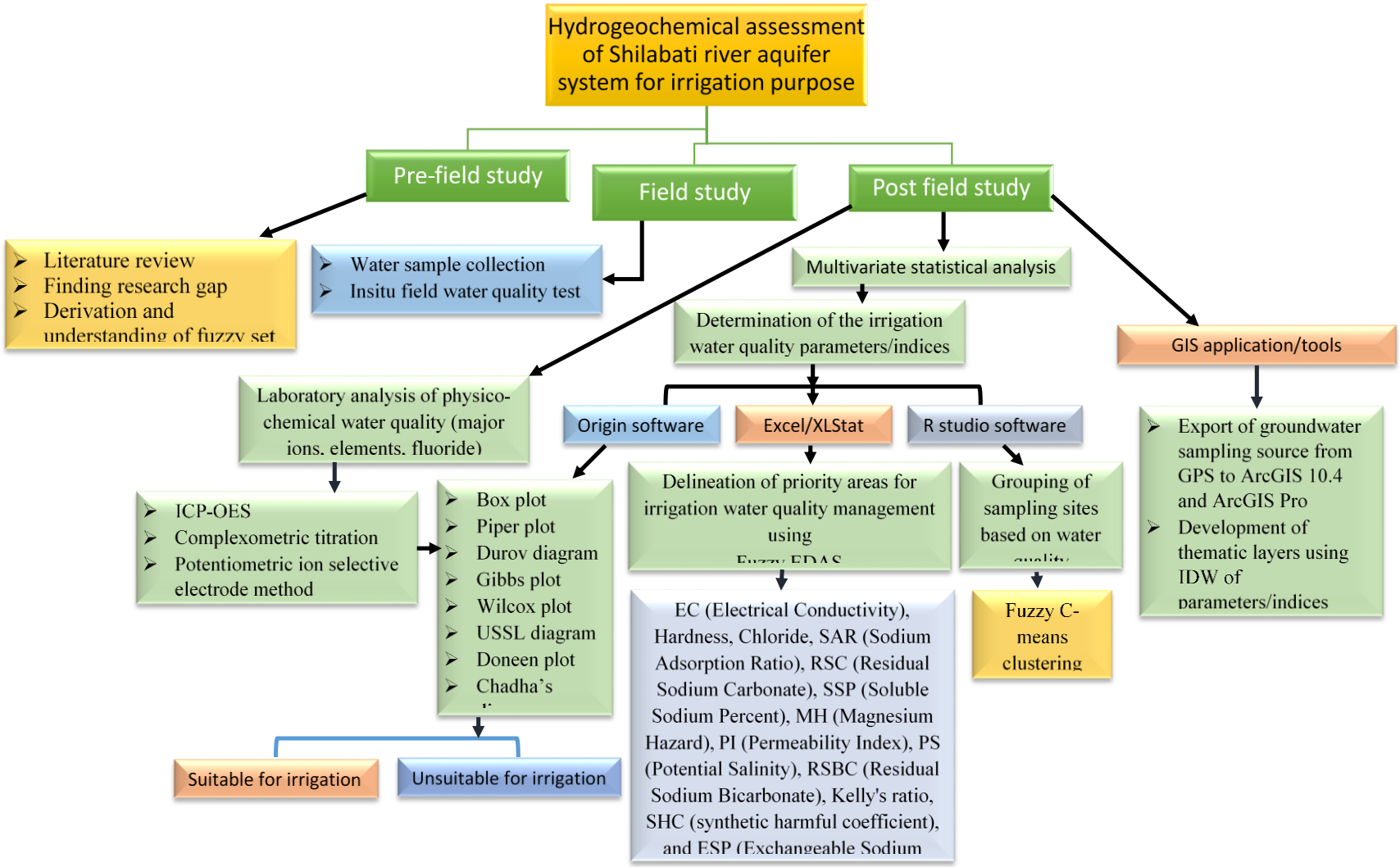

Fig. 6.12 Flowchart of the research methodology

$$_{min}Jm\ (U,V) = \sum_{i=1}^{c}\sum_{k=1}^{m} u_{ik}^{m}\, d_{ik}^{2} \quad (6.16)$$

Step 2: In this case, m is the fuzzy weighting parameter that varies over the range (1,∞). Cluster results become fuzzier as the value of m increases. The fuzzy partition matrix is designed by U, a cluster center matrix by V, n and c are the number of samples and cluster centers. u_{ik} is the fuzzy membership degree of the kth sample in the ith cluster which should meet the following three constraints (Pal and Bezdek, 1995) (Eq. 6.17)

$$u_{ik} \in (0,1),\ 1 \le i < c,\ 1 \le k \le n,$$

$$\sum_{i=1}^{c} u_{ik} = 1,\ 1 \le k \le n, \quad (6.17)$$

$$\sum_{k=1}^{n} u_{ik} = 1,\ 1 \le k \le c,$$

Step 3: From the distance d_{ik} between kth sample x_k and the centre of ith cluster Vi has been calculated by using Euclidean distance applying the following algorithm (Eq. 6.18)

$$d_{ik} = \|x_k - V_i\| = \sqrt{\sum_{j=1}^{m}(x_{kj} - V_{ij})^2},\ 1 \le i < c,\ 1 \le k \le n \quad (6.18)$$

V_{ij} has been calculated by utilizing the following algorithms (Eq. 6.19)

$$V_{ij} = \frac{\sum_{k=1}^{n} u_{ik}^{m} x_{kj}}{\sum_{k=1}^{n} u_{ik}^{m}} 1 \le i < c,\ 1 \le j \le m \quad (6.19)$$

A fuzzy cluster is constructed using an incremental optimization process that updates the fuzzy membership degree in each iteration (Sahu et al. 2012) Eq. 6.20.

$$u_{ik}^{s+1} = \frac{1}{\sum_{j=1}^{c}(d_{ik}^{s}/d_{jk}^{s})^{2/(m-1)}} \quad 1 \le i < c,\ 1 \le j \le n, \quad (6.20)$$

Where, s, is the iterative step

The cluster result can be obtained and further iteration can be stopped when the below requirement is met (Eq. 6.21)

$$\left\| U^{(s+1)} - U^{(s)} \right\| \le \epsilon, \quad (6.21)$$

The whole process has been executed in R platform and the obtained clusters has been validated using the following algorithms (Eq. 6.22-6.25)

I. Fuzzy silhouette (FS) (Campello and Hruschka, 2006) = $\frac{\sum_{j=1}^{N}(\mu_{pj}-\mu_{qj})^{\alpha} s_j}{\sum_{j=1}^{N}(\mu_{pj}-\mu_{qj})^{\alpha}}$ (6.22)

II. Partition Entropy (PS) (Bezdek, 1974) = $I_{PE}(U) = \frac{1}{n}\left(\sum_{i=1}^{c}\sum_{k=1}^{n} u_{ik}\, Log_a\,(u_{ik})\right)$ (6.23)

III. Partition Coefficient (PC) (Bezdek, 1974) = $I_{PC}(U) = \frac{1}{n}\left(\sum_{i=1}^{c}\sum_{k=1}^{n} u_{ik}^{m}\right.$ (6.24)

IV. Modified Partition Coefficient (Dave, 1996) = $I_{MPC}(U) = 1-\frac{1}{c-1}(1-I_{Pc}(U))$ (6.25)

6.2.5.2.2 Fuzzy EDAS for suitable irrigation zone prioritization

Ghorabaee et al. (2015) developed the EDAS methodology, which ranks material based on the average solution. In addition to being additive multi-criteria methods, EDAS has no interdependencies between the criteria. In contrast to TOPSIS and VIKOR, EDAS uses the average value as its reference point. EDAS is faster than TOPSIS and VIKOR because it eliminates non-prospective criteria (Ilieva et al. 2018). Its application is numerous and demonstrates its ability to tackle a wide range of problems, such as hospital site section and management, environmental management (Zavadskas et al. 2017), solid waste disposal management (Kahraman et al. 2017), and supplier selection (Keshavarz et al. 2016). In this study, EDAS modified with Fuzzy Logic has been used to capture uncertainty and vagueness in the complex systems. The fuzzy-EDAS methodology ranks alternatives according to the decreasing value of the defuzzified appraisal score (Zindani et al. 2019). The following are the steps of Fuzzy EDAS methodology (Zindani et al. 2019; IIieva et al. 2018).

Step 1: Construction of fuzzy decision matrix of Irrigational Parameters (IP) using TFN (Table 6.7) (Eq. 6.26)

$$A = [IP_{ij}]_{n\times m} = \begin{matrix} \widetilde{IP_{11}} & \widetilde{IP_{12}} & \cdots & \widetilde{IP_{1m}} \\ \widetilde{IP_{21}} & \widetilde{IP_{22}} & \cdots & \widetilde{IP_{2m}} \\ \vdots & \vdots & \ddots & \vdots \\ \widetilde{IP_{n1}} & \widetilde{IP_{n2}} & \cdots & \widetilde{IP_{mn}} \end{matrix} \quad (6.26) \qquad i = 1,2\ldots,n\ ;\ j = 1,2\ldots..m \text{ where, } IP_{ij} = (IP_{ij1}\ IP_{ij2}\ IP_{ij3}\ IP_{ij4})$$

are the trapezoidal fuzzy numbers.

Table 6.7 Linguistic fuzzy scale

Linguistic variable for fuzzy EDAS	Triangular fuzzy numbers					
Equal importance	1.000	1.000	1.000	1.000	1.000	1.000
Moderate	1.000	3.000	5.000	0.200	0.333	1.000
Strong importance	3.000	5.000	7.000	0.143	0.200	0.333
Very strong	5.000	7.000	9.000	0.111	0.143	0.200
Demonstrated	7.000	9.000	11.000	0.091	0.111	0.143

Step 2: $\widetilde{W}$ is the matrix of criteria weights, $\widetilde{W} = (\widetilde{w_{1,}} \ldots.\widetilde{w_{j,}}\ldots\ldots\widetilde{w_{m,}})$, where $\widetilde{w_j}$ is the weight of the criteria j (Eq. 6.27)

$$\widetilde{w_j} = (\widetilde{w_{j1}}\ ,\widetilde{w_{j2}}\ ,\widetilde{w_{j3}}\ ,\widetilde{w_{j4}}) \quad (6.27)$$

Step 3: The following algorithms are used to calculate the ideal solution (Eq. 6.28) (average value of fuzzy numbers for each criterion) $\widetilde{AV_j} = \frac{\sum_{i=1}^{n} IP_{ij}}{n}$ (6.28)

Step 4: By eliminating non-prospective assessments, we have calculated the positive and negative fuzzy L_{11} distances (Eq. 6.29)

$\widetilde{PDA} = [\widetilde{pda_{ij}}]_{n\times m}$ and $\widetilde{NDA} = [\widetilde{nda_{ij}}]_{n\times m}$, where,

$\widetilde{pda_{ij}} = \psi\ (L_{Il}\ (IP_{ij,}\ \widetilde{aV_j})$ and, $\widetilde{nda_{ij}} = \psi\ (L_{Il}\ (\widetilde{aV_{j,}}\ IPij)$ (6.29)

Step 5: The obtained matrix is the multiplied by the fuzzy criteria weights (Eq. 6.30)

$$\widetilde{spi} = \oplus_{j=1}^{m} (\widetilde{w_j} \otimes \widetilde{pda_{ij}} \text{ and, } \widetilde{sni} = \oplus_{j=1}^{m} (\widetilde{w_j} \otimes \widetilde{nda_{ij}} \quad (6.30)$$

Step 6: Normalization of the fuzzy distance matrix using the following algorithms (Eq. 6.31)

$$\widetilde{nspi} = \frac{\widetilde{spi}}{max_i\ (k(\widetilde{spi}))} \text{ and, } \widetilde{nsni} = \frac{\widetilde{sni}}{max_i\ (k(\widetilde{sni}))} \quad (6.31)$$

Step 7: According to the following algorithms, the average distances to the ideal fuzzy solution were obtained (Eq. 6.32)

$$\widetilde{asi} = \frac{k(\widetilde{nspi}) + k(\widetilde{nsni})}{2} \quad \text{(Eq. 6.32)}$$

6.2.6 Results and Discussion

6.2.6.1 Groundwater hydrogeochemical statistics

A summary of the statistical characteristics of all groundwater samples has been shown in Table 6.8 and the spatio-temporal variation has been presented in Fig. 6.13-6.15. According to the geological aspect of the basin, Fig. 6.16 and 6.17 shows the box plots of groundwater samples under four types of wells/groundwater sources. All the samples have been collected from the 8 types of geological section namely granite gneiss and migmatite, metamorphosed basic rocks, mica schist, occasionally garnetiferrous, pink granite/biotite-granite gneiss, sand, silt and clay, sands and silts in alternate clay, sands with silts, clay impregnated with caliche nodules and sands with silts, clays associated with Fe-nodules (Table 6. 6). As the pH ranged from 4.08 to 8.88, most of the samples are acidic, with an average of 6.34. The value varied with respect to location. In the middle section of the basin, the pH is acidic, possibly due to the presence of red-laterite with sand and silt within the alterative clay zone (Saha et al. 2021). The water temperatures of the groundwater samples range from 24.70 degrees in the upstream section to 33.35 degrees in the downstream section of the basin. An average EC of 373.19 µS/cm has been observed with values ranging from 104 to 690 µS/cm. It has been observed that the EC is higher in the upstream (rock-water interaction) and downstream section (sedimentation and confluence with the Rupnarayan river), indicating that groundwater contains more dissolved ions and its variation is much greater in the dug wells and tube wells. The concentration of EC in groundwater is highest and is mainly concentrated in the structures composed of Sands with silts, clay impregnated with caliche nodules as the areas that have a higher content of smaller soil particles (higher content of clay) conduct more electrical current (USDA, 2014). TDS in the study area vary from 102 to 914 mg/l. The groundwater in the study area falls under the fresh (TDS < 1000 mg/l) group (Freeze and Cherry 1997). The TDS in this basin may originate from natural sources and sewage discharges (Nag and Das, 2017). TDS level is higher in the upstream section which should be less than 500 mg/L (WHO, 2011) has much variation in tube wells of sand, silt and clay origin. A general acceptance level of hardness is 300 mg/L (IS 10500, 2012), whereas WHO (2011) sets a limit of 600 mg/L as an allowable limit for hardness. Total Hardness of the basin ranges from 24 to 1124 mg/l with an average value of 186 mg/l where weathering of primary minerals such as mica, feldspar, hornblende, dolomite and calcite are considered to be sources (Nag and Suchetana, 2016). According to the integrated groundwater water quality categories based on TDS and TH scatter plot (Fig. 6.18), the groundwater in this river basin is predominantly soft to very hard and falls under the freshwater

category. Groundwater in tube wells within the basin is generally hard in nature, primarily due to hydrological, geographic, geomorphic conditions and varying human activities. It can be estimated that only 30% of samples are suitable for drinking and irrigation based on both TDS and TH. Alkalinity values for all of the examined samples are significantly higher in the upstream section than the standard limit. Alkalinity in the groundwater samples varies from 10 mg/l (middle section) to 1220 mg/l (upstream). It varies more in the tube wells of granite gneiss migmatite structures as the granitic rocks are characterized by high mineralization, with alkali feldspar, amphiboles, quartz, mica, and other minerals (Akurugu et al. 2023). Concentration of manganese (Mn) ranges from 0.006 mg/l to 1.80 mg/l within the basin. When recharge events occur, reductive dissolution is caused by the presence of iron (Fe) bearing minerals in the shallow sediments of the Shilabati Basin. As high as 42.92 mg/l of iron (Fe) are present in this basin, where people reported kidney problems, gastrointestinal problems, as well as bad utensil quality leaving stains behind (Chowdhury et al. 2022). The manganese and iron concentration is higher within submersible wells of sand with silt and clay containing fe-nodules structures and areas with sands and silts in alternate clay. Due to the lack of oxygen and the long underground residence time, ferrous iron and Mn are prevalent in these structures. Magnetite, epidote, garnet, titanite, amphibole, and pyroxene in the silt fraction of the sandstones might have contributed to the high manganese and Fe content of the groundwater within the river basin (Beqiraj and Beqiraj, 2011). $Na^+$and K concentrations in groundwater range from 2.60 to 197.98 mg/l and 0.43 to 97.77 mg/l, respectively, in the study area. The high concentrations of Na^+in groundwater are likely the result of the exchange of ions among minerals. In the basin, feldspars, sodalites, and evaporites are among the minerals containing sodium and potassium. The return flow of irrigation water may also lead to an increase in potassium concentrations. Almost all compounds have a high-water soluble content. Those suffering from hypertension, heart disease, or kidney disease are adversely affected by consuming both the contaminants in water (Saha et al. 2019). Calcium (Ca^{2+}) concentrations in the upstream section range from 2.82 to 293.56 mg/l, derived from calcium-rich minerals like dolomite, gypsum and calcite. The tube wells of granitic structures show a high variation in calcium (Chakraborty et al., 2022). In the upstream part of the basin, Mg^{2+} is primarily derived from ion exchange between minerals in rocks and soils. In the groundwater samples, concentrations of Mg^{2+}+ range from 0.05 to 91.28 mg/l. As a result of weathering of carbonate and dissolution of carbonic acid in aquifers, HCO_3^-), concentrations in groundwater becomes high (Mandal et al. 2016). HCO_3^- in the study area ranges from 32 to 488 mg/l and is highest in the upstream section of the basin. Cl^- concentrations range from 5.67 mg/l to 187.94 mg/l and increase from upstream to downstream. The concentration of SO_4^{2-} ranges from 0 to 111 mg/l. The NO_3^- concentrations in samples varied between 0.10 and 11.05 mg/l in the study area. The PO_4^{-3} concentration in this basin ranges between 0.01 mg/l and 1.03 mg/l. Most of the hydrochemical variation can be seen within the groundwater samples collected from the tube wells covering 4 geological structures including Sands and silts in alternate clay, Granite gneiss, migmatite, pink granite/biotite-granite gneiss and Sand, silt and clay (Fig.6.16 and 6.17). Permeability, water table condition, and presence of organic matter control the sorption and the leaching potential of the soil. These areas are enriched with high mineralization, higher content of organic matter and clay leading to high leaching potential and more sensitivity towards groundwater (Huddleston, 1996)

Table 6.8 Descriptive statistics of the groundwater quality parameters

Groundwater quality parameters	Acceptable limit	Range	Minimum	Maximum	Sum	Mean	Median	Std. Deviation	Variance	Skewness	Kurtosis
Temperature °C	-	8.65	24.70	33.35	2151.65	29.07	29.30	1.75	3.06	-0.18	-0.16
pH	6.5-8.5˜	4.08	4.80	8.88	472.10	6.34	6.54	0.81	0.65	0.06	-0.07
EC (µS/cm)	300*	586	104	690	27616	373.19	353.5	158.49	25121.33	0.44	-.890
TDS (mg/l)	500˜	812	102	914	17618	238.08	211.0	126.83	16084.73	2.62	10.91
Hardness (mg/l)	200˜	1100	24	1124	13752	185.84	153.0	157.32	24750.03	3.34	16.91
Alkalinity (mg/l)	200˜	1210	10	1220	11286	152.51	120.0	164.51	27064.77	4.07	23.97
Iron (mg/l)	0.3˜	42.8	.03	42.92	156.14	2.11	0.43	6.16	37.93	5.20	29.60
Manganese (mg/l)	0.1˜	1.79	.006	1.80	15.64	.213	0.06	0.32	0.103	2.59	8.03
Sodium (mg/l)	200*	195.38	2.60	197.98	2156.85	29.15	20.54	33.97	1153.77	2.87	10.15
Potassium (mg/l)	12*	97.35	.43	97.77	432.38	5.84	2.63	14.66	214.89	5.53	31.28
Calcium (mg/l)	75˜	290.74	2.82	293.56	4304.29	58.16	45.00	48.48	2350.45	2.39	7.48
Magnesium (mg/l)	30˜	91.23	0.05	91.28	1007.05	13.61	8.0	16.61	276.00	3.11	11.74
Sulphate (mg/l)	200˜	111.00	0.00	111.00	1127.00	15.23	4.50	23.42	548.37	2.40	5.49
Chloride (mg/l)	250˜	182.27	5.67	187.94	3344.26	45.19	29.00	42.80	1832.69	1.79	2.81
Bicarbonate (mg/l)	150*	456	32	488	13981	188.93	168.0	82.03	6728.87	1.29	2.54
Nitrate (mg/l)	45˜	10.95	0.10	11.05	155.76	2.10	1.20	2.52	6.34	2.05	4.08
Fluoride (mg/l)	1˜	1.75	0.02	1.77	40.12	0.54	0.26	0.56	0.32	0.78	-0.98
Phosphate (mg/l)	0.1*	1.02	0.01	1.03	6.76	0.09	0.03	0.18	0.03	3.79	15.49

Note: *Acceptable limit based on WHO; ˜Acceptable limit based on BIS

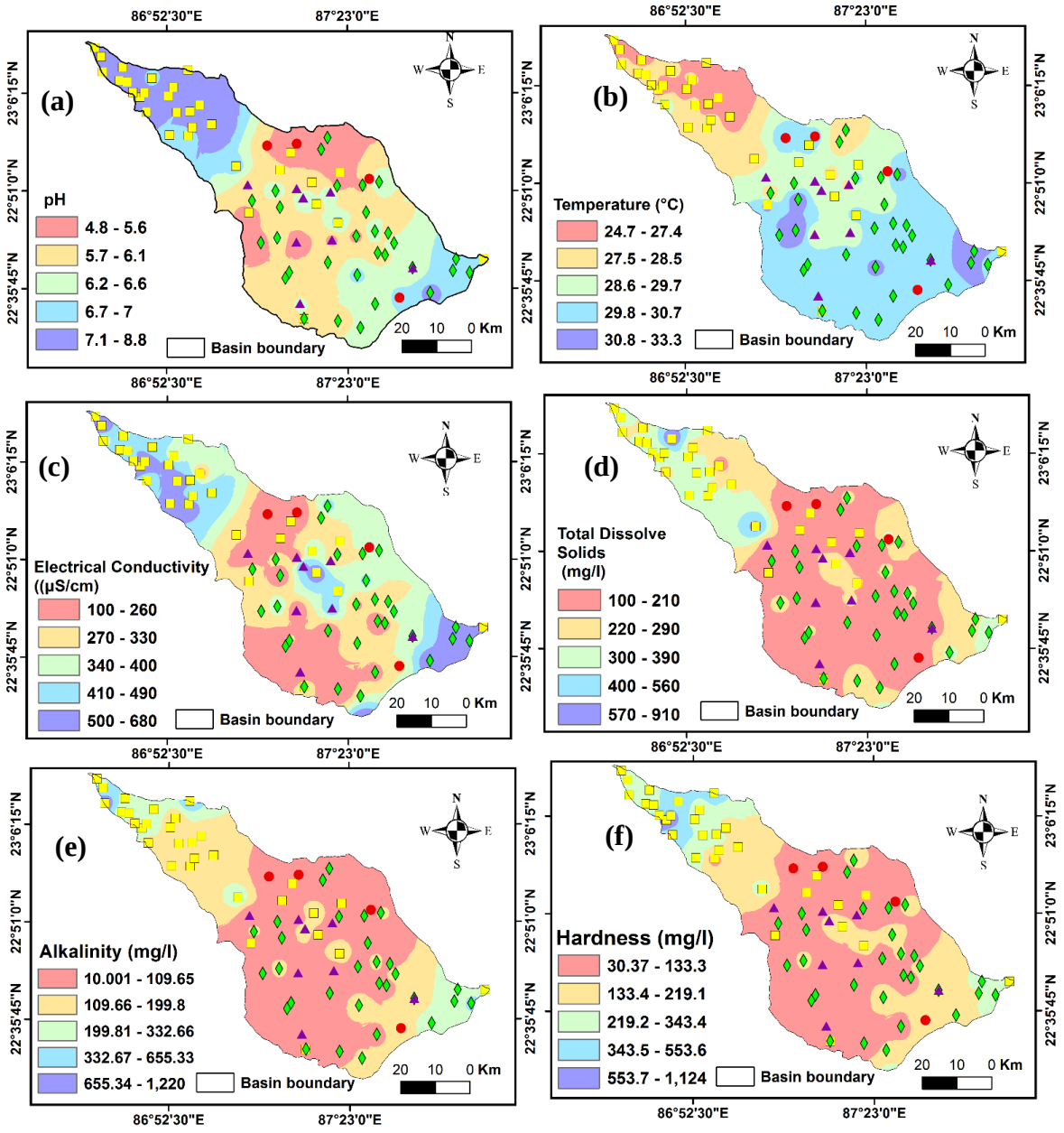

Fig. 6.13 Spatial distribution of groundwater quality parameters (a) pH; (b) Temperature; (c) Electrical Conductivity; (d) Total Dissolve Solids; (e) Alkalinity and (f) Hardness

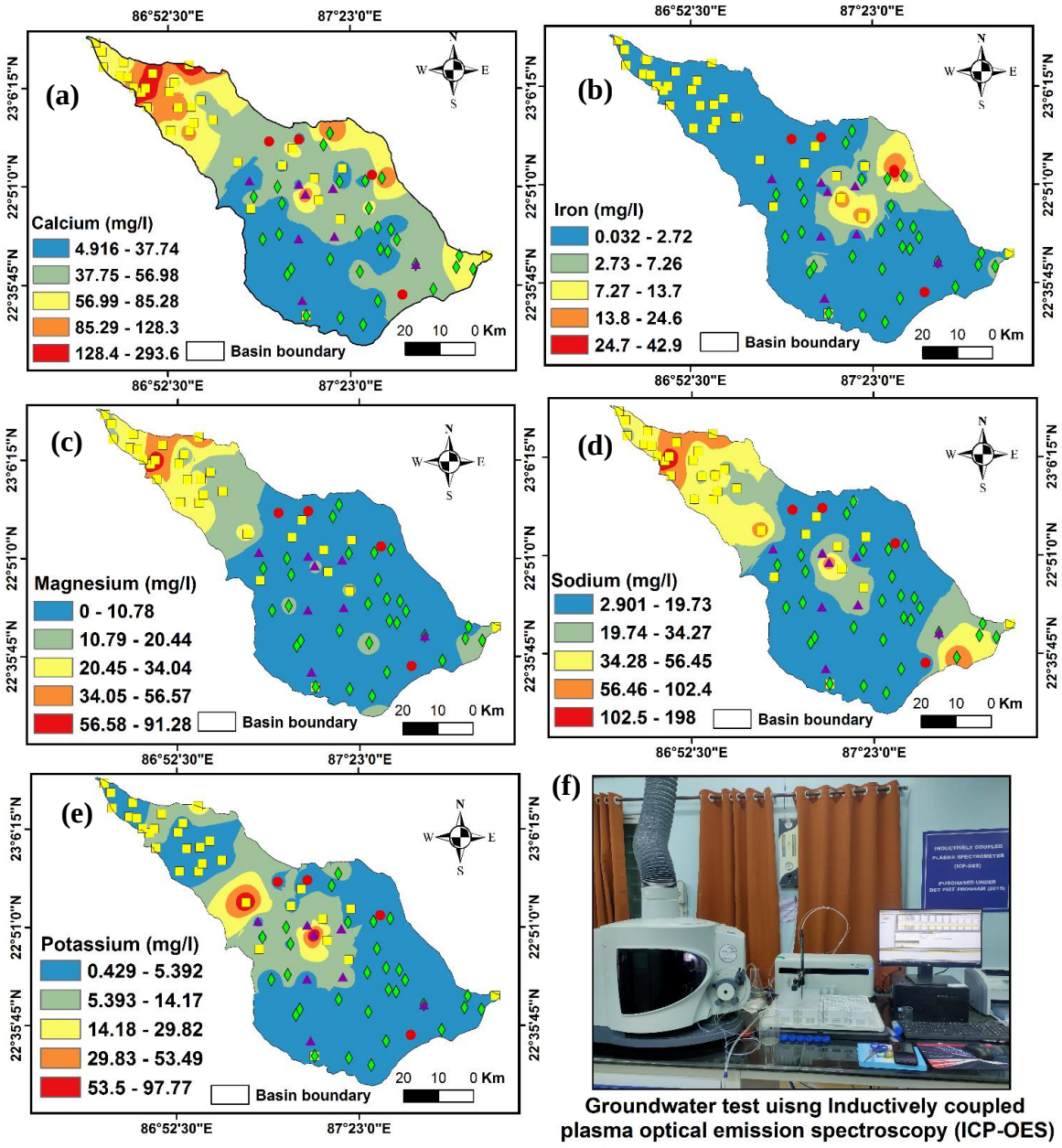

Fig. 6.14 Spatial distribution of groundwater quality parameters (a) Calcium; (b) Iron; (c) Magnesium; (d) Sodium; (e) Potassium and (f) ICP-OES

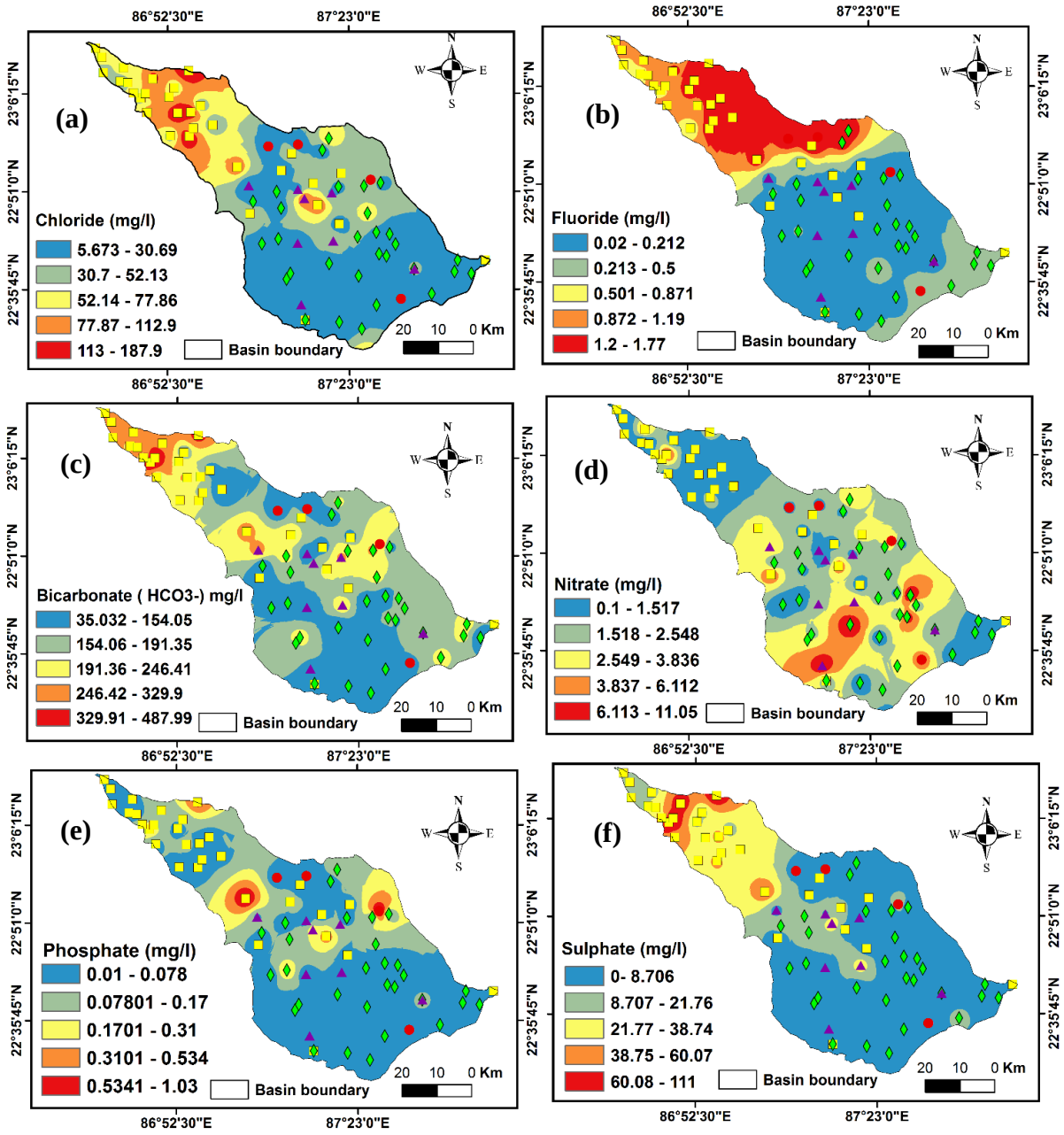

Fig. 6.15 Spatial distribution of groundwater quality parameters (a) Chloride; (b) Fluoride; (c) Bicarbonate; (d) Nitrate; (e) Phosphate and (f) Sulphate

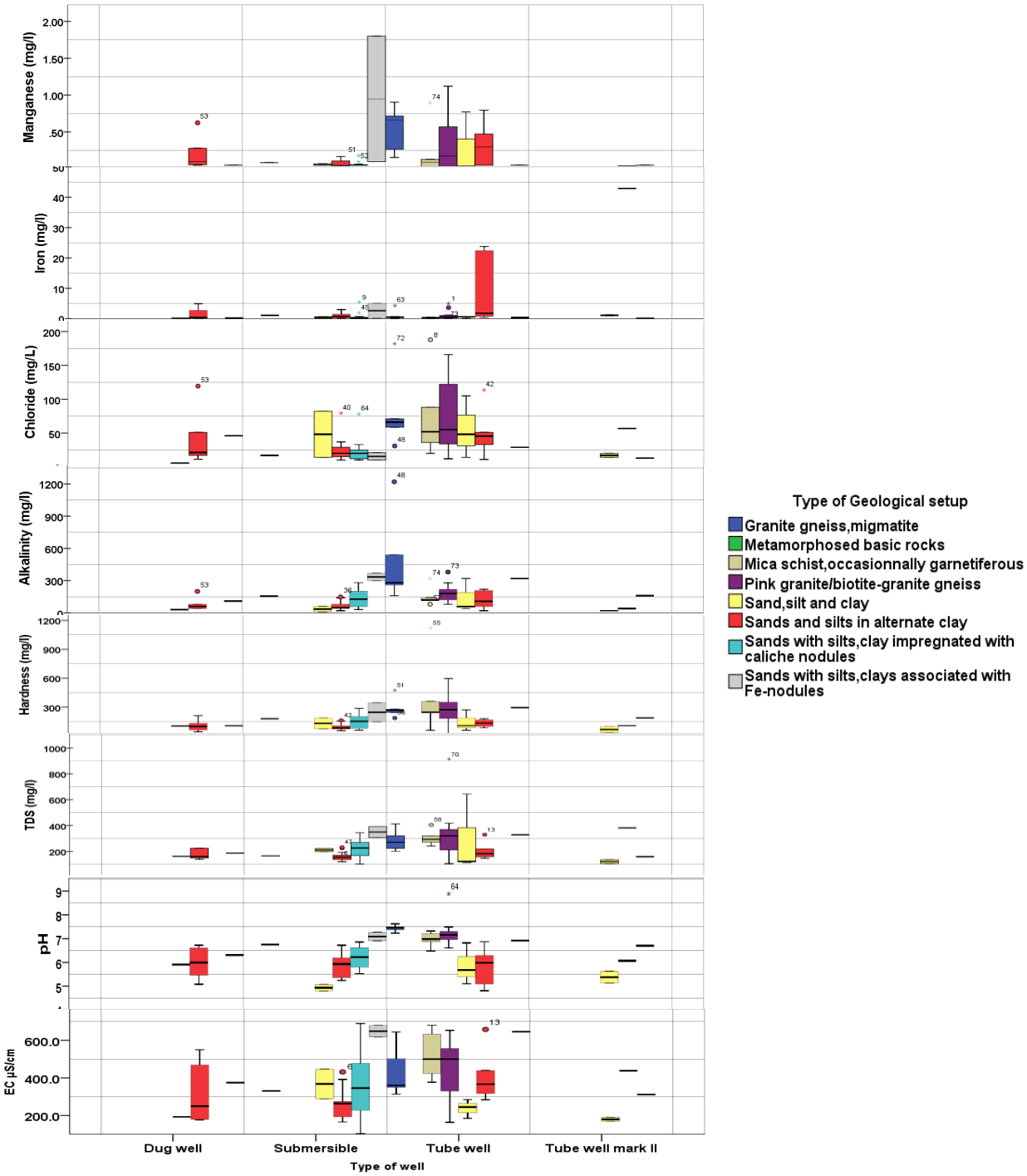

Fig. 6.16 Box and Whisker plot for physicochemical parameters

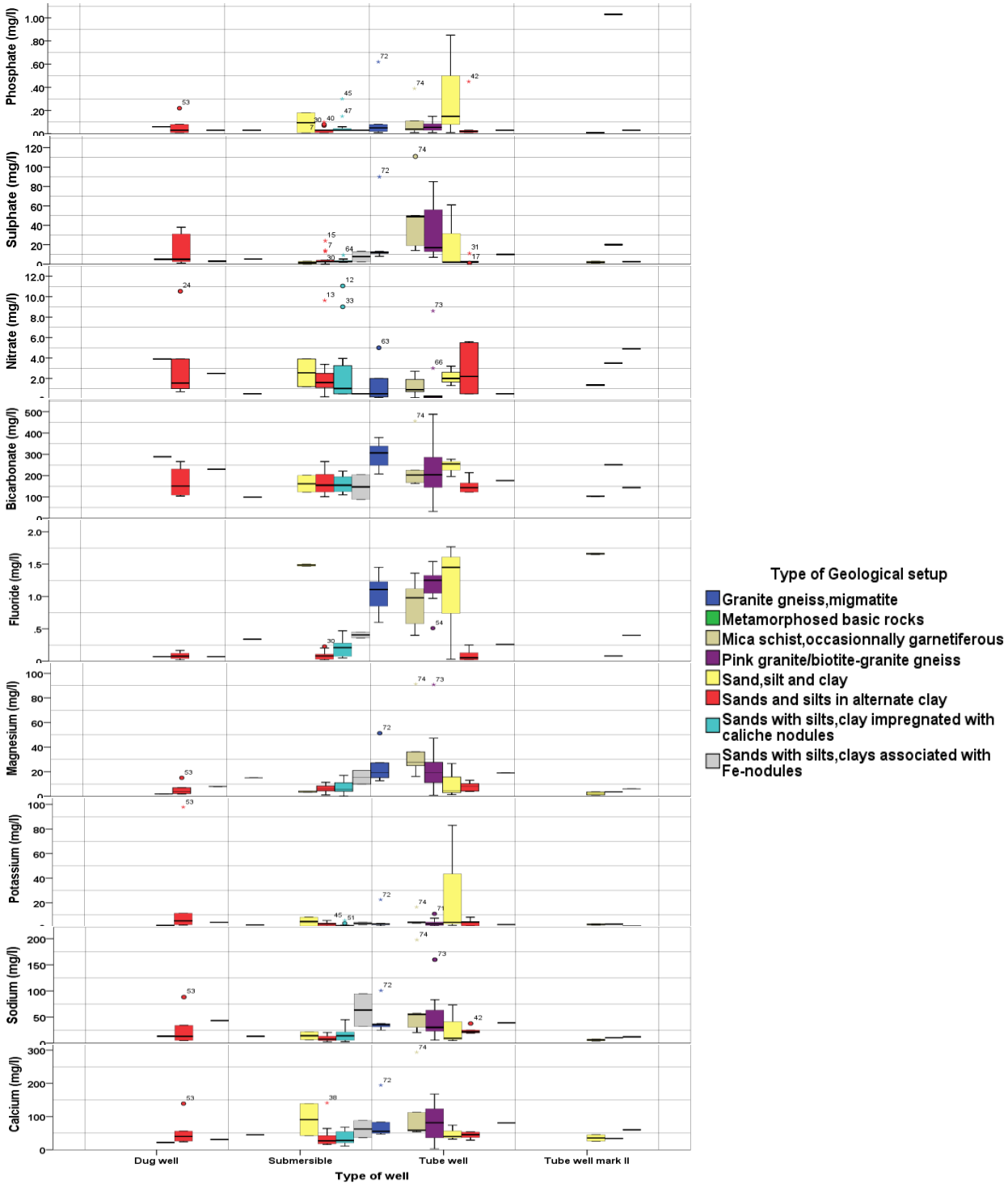

Fig. 6.17 Box and Whisker plot for physicochemical parameters

In this basin, agriculture, septic tanks, and animal wastes are the primary sources of phosphate in the ground water. The groundwater in the area is subjected to considerable contamination and hygiene problems because there is no systematic sewage collection or waste collection in core village areas. The key characteristic of land use and land cover of Shilabati basin is its vast cropland and intensive agricultural activities. Animal husbandry is another major activity among people, and these practices contribute significantly to the phosphate content of water samples. The mean F^- of samples is 0.54 mg/l with values ranging from 0.02 to 1.77 mg/l. Fluoride (F^-) is mainly concentrated in the upstream section of the basin and is mainly found in the tube wells of depth 35-300 feet. Many studies reported up to 12 mg/l of fluoride in tube wells, but the government has abandoned those (De et al. 2021). Besides consuming fluoride-contaminated groundwater, local inhabitant intake significant amounts of fluoride from crops and vegetables growing in fluoride-contaminated soils (Bhattacharya et al. 2017). According to the table from the average concentration, the abundance of the major ions in the Shilabati river basin is as follows $Ca^{2+}>Na^{+}>Mg^{2+}>K>Fe$ for cation and $HCO_3^->Cl^->SO_4^{2-}>NO_3^->PO_4^{-3}>F^-$ for anions.

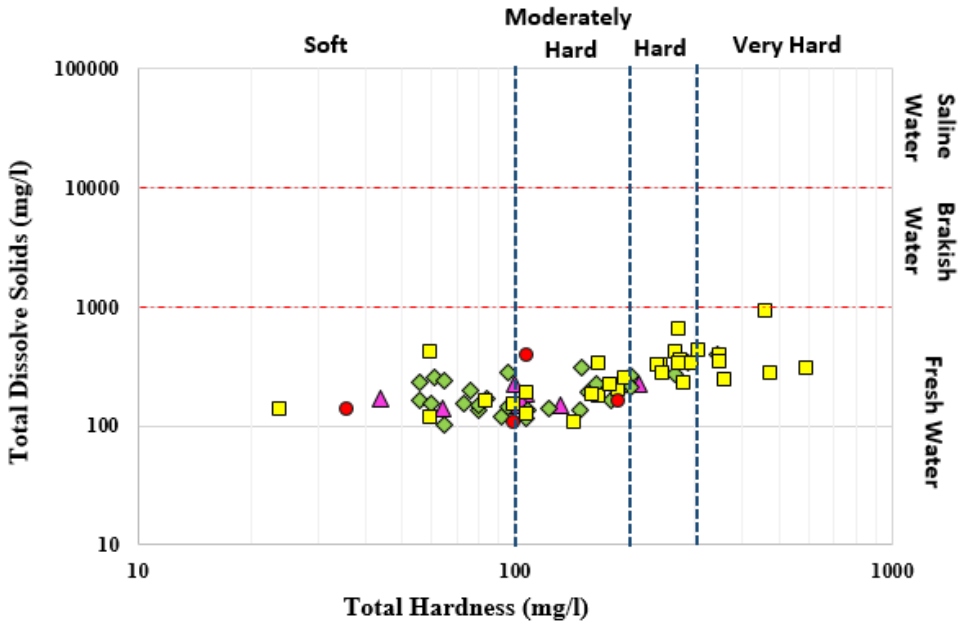

Fig. 6.18 Scatter plot between Total Hardness (TH) versus Total Dissolve Solids (TDS)

6.2.6.2 Hydrogeochemical facies and geochemical evolution process

Grapher Software (Grapher 18.4.420 (graphersupport@goldensoftware.com) has been used in this study to plot a trilinear Piper diagram (Piper, 1944) to determine the hydrochemical facies of groundwater. It is evident from the trilinear piper diagram (Fig. 6.19) that the groundwater samples exhibit chemical associations. Additionally, it can be used as a determinant of the groundwater flow pattern and the geochemical evolution of the groundwater (Sunkari et al. 2022; Ram et al. 2021). The studied groundwater samples largely originated from Ca^{2+}-HCO_3^- and mixed Ca^{2+}-Mg^{2+}-Cl^- type. It is evident from the aquifer's natural geology that these water types reflect the prevalence of ion exchange reactions, frequent rock-water interactions, and silicate and carbonate weathering. In the upstream section of the basin presence of the granitic genies, Mica schist, metamorphosed basic rocks can be the persistent source of such groundwater type. Samples of Mg^{2+}–Na^{+}–HCO_3^- and Ca^{2+}–Na^{+}–Mg^{2+}–HCO_3^- represent aquifer recharge water. During the percolation of water through the vadose zone, these samples show

much higher hardness with abundant Ca^{2+}, Mg^{2+} and HCO_3^- as derived from the lithological units. The dominant hydrochemical facies of the Shilabati basin groundwater system is $HCO_3^- – Ca^{2+}$ type. In Fig.9 , the alkaline earth metals (Ca^{2+}+ Mg^{2+}) win out over alkali cations (Na^+ + *K)* and 85% of the samples are weak acids (HCO_3^- + CO_3^{2-}) over strong acids (Cl^-+ SO_4^{2-}).In light of the distribution of cations and anion groups, it can be concluded that the predominant type of water is 85% Ca^{2+}-HCO_3^-; 14% mixed Ca^{2+}- Mg^{2+}-Cl^-; and 1% Ca^{2+}- Cl^-;. In the Shilabati basin, high EC and TDS also contribute to greater rock water interaction over a longer period of residence time (Edmunds and Smedley, 2013). For instance, it has been observed that fluoride concentrations in groundwater increase as it reaches a deeper depth within the study area (Brindha et al. 2016). Hydrogeochemical data can also be represented using the Durov diagram (Gaur et al.2022). Based on the plot of samples in fig 6.20, the dominant ions in the groundwater are Na^+ + *K* and Ca^{2+}. In contrast, there is was a noticeable difference between the anions in the groundwater. Several samples are of the bicarbonate type, suggesting that HCO_3^- is the dominant anion. The figure 6.20 also indicates two dominant groups: Mixing and reverse exchange cation exchange waters of Cl^-- Ca^{2+} type and mixing and reverse exchange cation exchange water. Almost all of the samples are mixed water types, suggesting the combined effects of water-rock contact, evaporation and human activity. The rock-water interaction in this area has also been validated using Gibb's diagram (Fig 6.21), in which three zones are represented: rock weathering dominance, precipitation, and evaporation. In hard rock aquifers, the weathering processes alter lithologies containing silicates and carbonates. According to the plots, silicate mineral weathering and carbonate dissolution mainly contributed to groundwater chemistry. Carbonate weathering is mainly responsible for controlling the concentration of dissolved solutes (Zeng et al. 2019). When a rock mineral weathers in a soil zone, CO_2 is primarily converted into HCO_3^-. Due to organic matter decomposition and root respiration, the soil zone in the subsurface environment produces high CO_2 pressures, which react with rainfall (H_2O). In the figure 6.22, the majority of the samples are in the middle sections, suggesting silicate weathering played a dominant role in the formation of groundwater chemistry. There is also a higher concentration of phyllosilicate clay minerals within this region, which most commonly found in weathered rock and residual soil than in unweathered bedrock, while muscovite, K-feldspar and biotite are observed to decline in between unweathered fresh bedrock and overlying residual soil samples (Dolui et al. 2016).

For further confirmation of this process, a diagram introduced by Chadha (1999) has also been evaluated to determine the different hydro-geochemical and ion exchange processes. On the X-axis, the difference between weaker acidic anions (HCO_3^-) and stronger acidic anions (Cl^-+ SO_4^{2-}) has been represented as a percentage equivalent (meq%), and on the Y-axis, it is shown as the difference between weaker acidic anions (HCO_3^-) and strong acidic anions (Cl^-+ SO_4^{2-}) (Fig. 6.23). The majority of samples (95%) fall into the recharge type of water, which indicates that dissolved HCO_3^- and hydro-geochemically transportable Ca^{2+} are transferred into the aquifer from the surface irrigation or precipitation. Only 5% of the samples undergo base-exchange and reverse ion exchange. The infiltration and recharge of meteoric water, which is dissolving carbonate dust in the air and in the soil zone, can therefore contribute to a higher level of calcium in groundwater within the basin (Capuano and Jones, 2020). Na^+/Cl^- ratio ranges from 0 to 16 depending on the concentration of Cl^-, as depicted by the plot of Na^+/Cl^- ratios against Cl^- concentrations (Fig. 6.24). In 99 % of samples, sodium (Na^+) has a molar ratio of ≥ 0-4, which may reflect ion exchange and/or silicate weathering. It is also evident that samples with high EC values have a molar ratio near to one, which shows evaporite minerals are dissolving in to the groundwater aquifer system (Taherian and Joodavi, 2021).

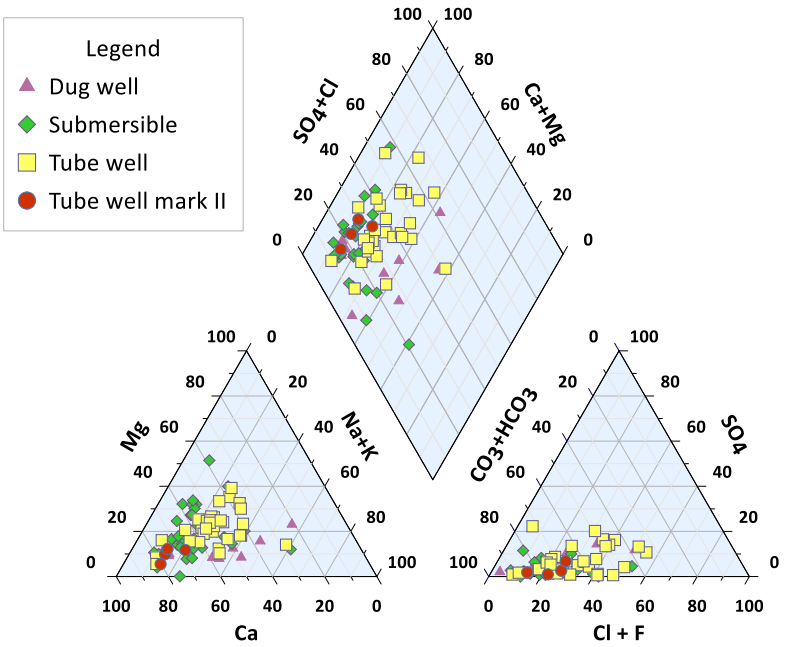

Fig. 6.19 Piper diagram demonstrating the hydrochemical compositions of water

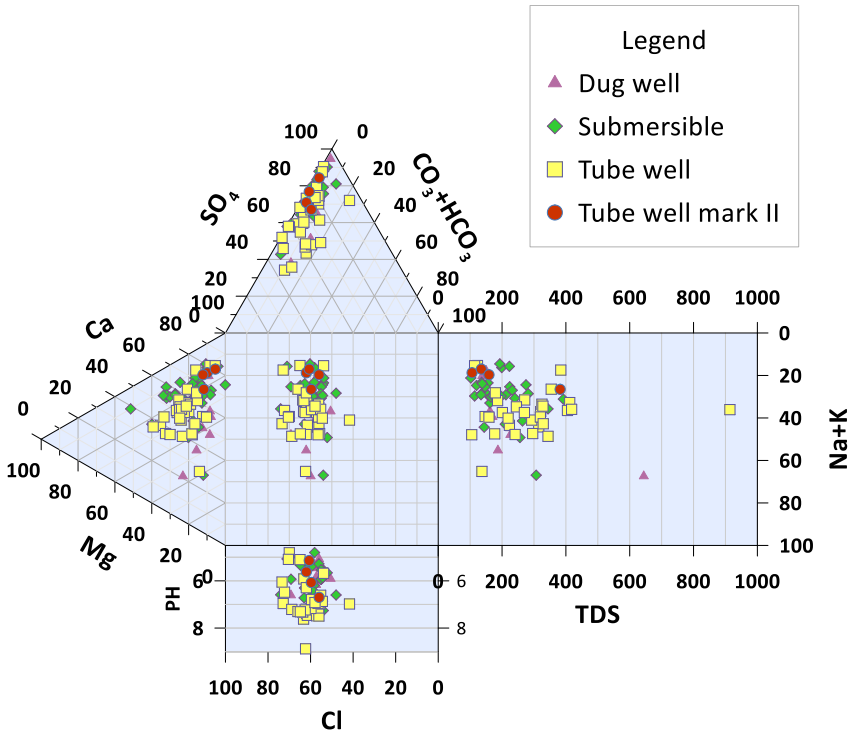

Fig. 6.20 Durov plot of the groundwater samples

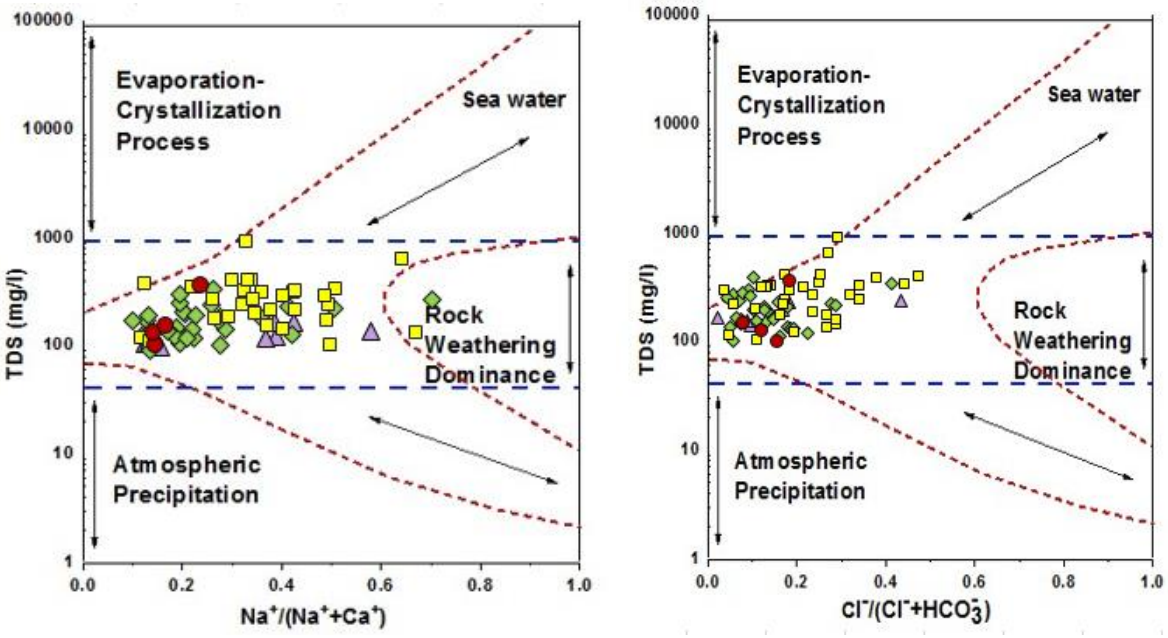

Fig. 6.21 Gibbs diagram showing the natural mechanism of groundwater chemistry

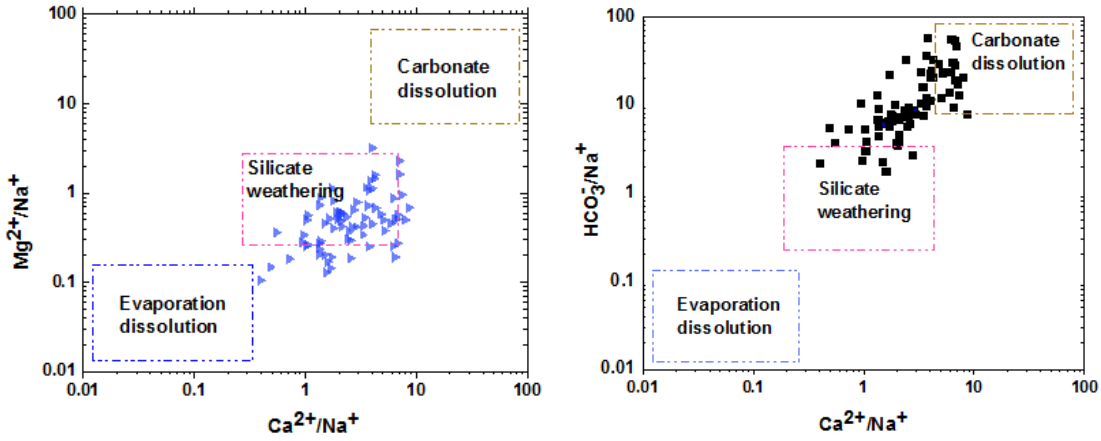

Fig. 6.22 Gibbs diagram showing the natural mechanism of groundwater chemistry

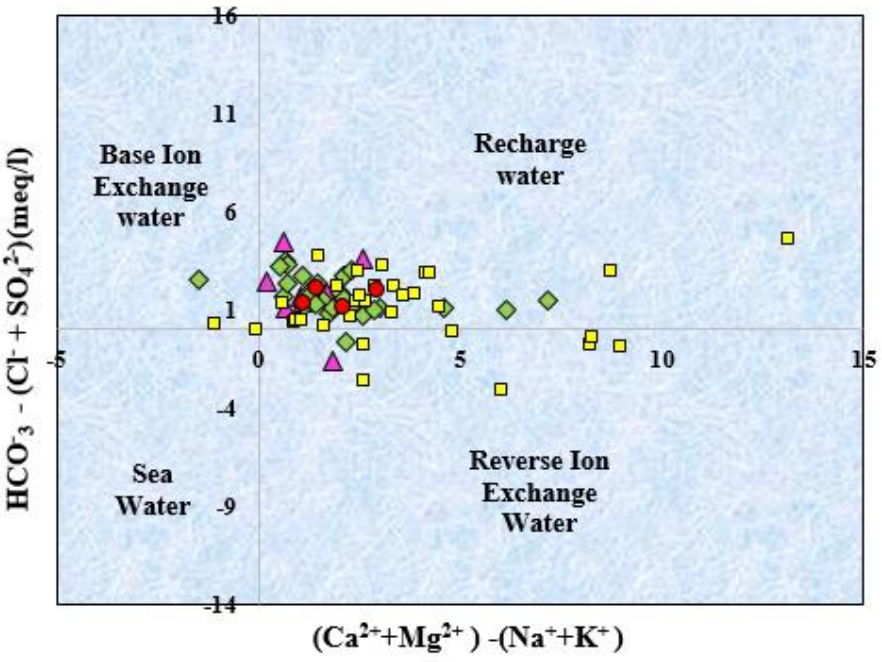

Fig. 6.23 Chadha's diagram showing the water types for groundwater quality

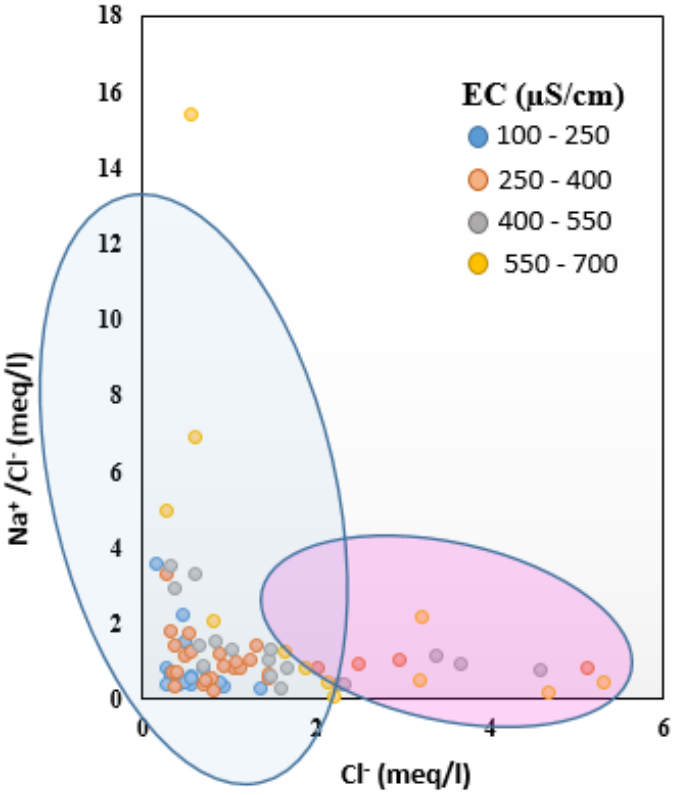

Fig. 6.24 Ionic ratio of Cl^- versus Na^+/Cl^- concentration in groundwater samples

6.2.6.3 Correlation analysis

Pearson correlation coefficient has been used to illustrate and measure associations between a number of ionic parameters in R studio version 4.2.0 (Fig.6.25 & 6.26). The correlation coefficient greater than 0.7 means a strong correlation between two parameters, while 0.5 to 0.7 indicates moderate correlation (Benesty et al. 2009). In this section, the most prominent correlation coefficient has been discussed. Upstream of the study area is exposed to Chhotanagpur plateau having extensive exposures of granite gneisses with various varieties of granite gneisses, such as quartz-biotite granite gneiss and porphyroblastic granite gneiss (Acharya and Nag, 2013). In this case, the correlations between $Na^{+}+K/SO_4^{2-}$ (0.85), Ca^{2+}/Mg^{2+} (0.80), $Ca^{2+}+Mg^{2+}/HCO_3^{-}$ (0.67), Ca^{2+}/HCO_3^{-} (0.98), Ca^{2+}/Na^{+} (0.79) and $Ca^{2+}+$ Total cation (0.80) are very strong to strong, reflecting the influence of such underlying geology. Under low pH conditions in the middle section of the basin, insoluble carbonates dissolve in the soil and in limestone formations to become soluble bicarbonates. When carbonates are dissolved in limestone, impurities like sulfates and chlorides become exposed, allowing them to pass into the groundwater flow system (Nag and Das, 2017). The very strong to moderate correlation between the $Ca^{2+}+Mg^{2+}/HCO_3^{-}+SO_4^{2-}$ (0.77), $Ca^{2+}+Mg^{2+}/Ca^{2+}$ (0.77), $Ca^{2+}+Mg^{2+}/Mg^{2+}$ (0.91), $Ca^{2+}+Mg^{2+}/Cl^{-}$ (0.55), $HCO_3^{-}+SO_4^{2-}/Ca^{2+}$ (1), $HCO_3^{-}+SO_4^{2-}/Mg^{2+}$ (0.80) are the reflectance of such chemical reactions. A positive correlation between $Na^{+}+K$ and Total cations (0.91) indicates that chemical weathering of silicate minerals in rocks and sediments has occurred throughout the basin, with less influence from carbonate dissolution. A very strong correlation between $Ca^{2+}+Mg^{2+}$ and Na^{+} (0.85) and $Ca^{2+}+Mg^{2+}$ verses Total cations (0.98) at favorable exchange sites confirmed the reverse ion exchange process within the basin. A major reason for Ca and Mg ion dominance over Na ion in this study region is the evidence of such phenomenon in the areas of loosely consolidated sand, silts, and clays. The poor correlation between Cl^{-}/Na^{+} (0.48) shows the less or no influence of salinization within the basin.

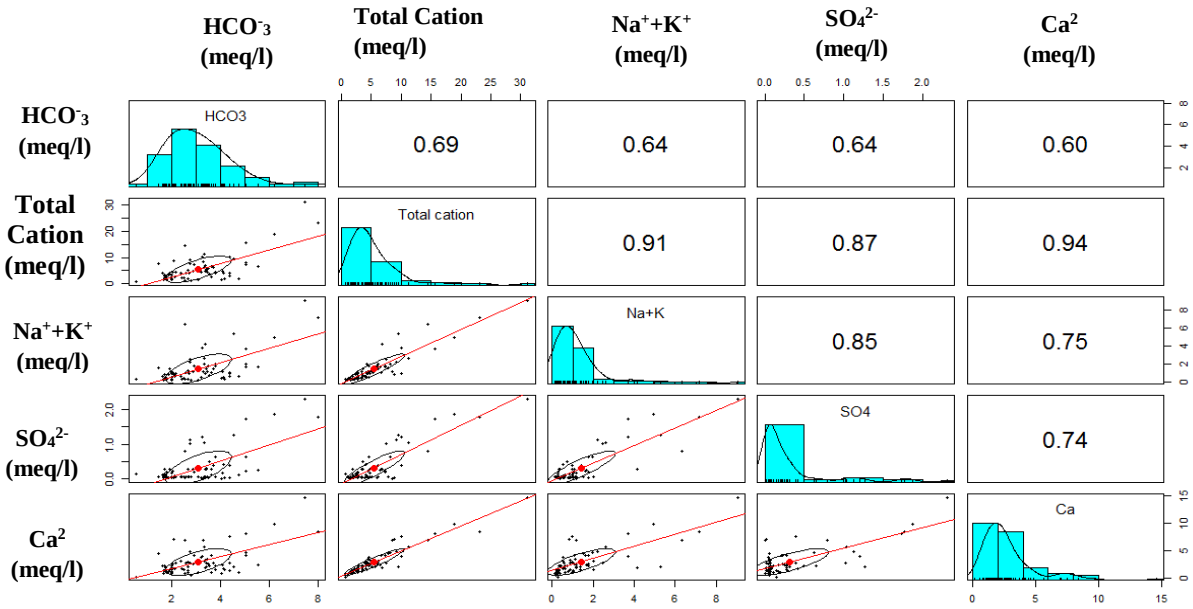

Fig. 6.25 Correlation plot between the different hydrogeochemical parameters

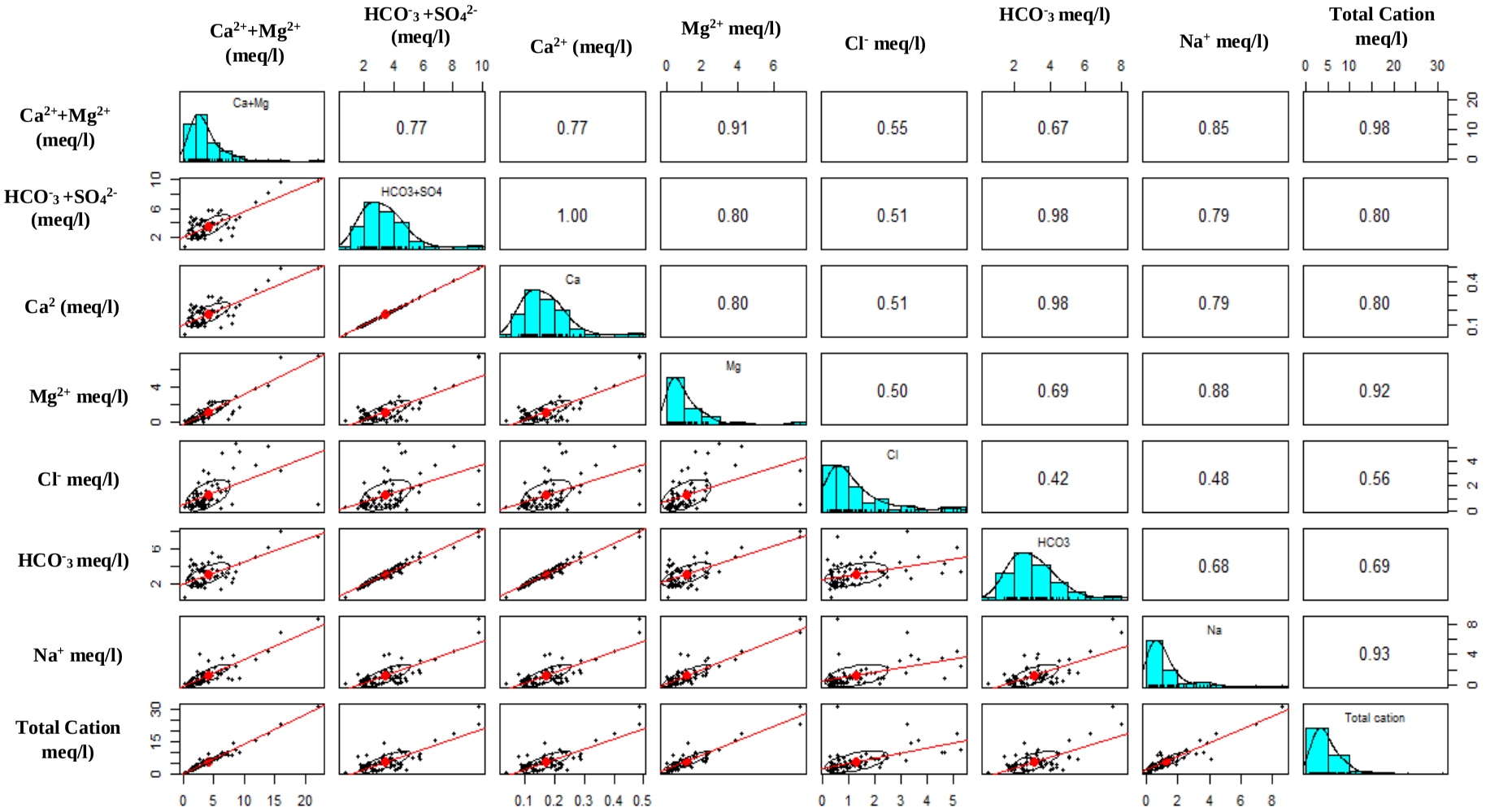

Fig. 6.26 Correlation plot between different hydrogeochemical parameters

6.2.6.4 Derivation of irrigation water quality indices and its spatial distribution

According to the table 6.9, the irrigation water quality indices has been determined using the different algorithms. A variety of water quality indices, including SAR, RSC, SSP, MH, PI, PS, RSBC, Kelly's ratio, SHC, and ESP, (Fig.6.27) has been used to assess the suitability of groundwater for irrigation in the Shilabati river basin based on the aforementioned quality parameters (Eaton, 1950). An extensive study of this type has not been conducted in the study area, where agriculture dominates the economy. Throughout the year due to the sporadic rainfall, the local farmers are dependent on groundwater as they grow rice, wheat, potato, rape, mustard, sesamum and other vegetables (Das, 2016).

In agricultural applications, the SAR value reflects the combined impact of sodium hazards, calcium and magnesium ions. There is evidence that high sodium ions in soil can negatively affect soil properties, including the texture, voids size in the soil skeleton, permeability and porosity (Sattari et al. 2018). The SAR value of the basin ranges from 0.136 to 3.551 and is classified excellent for agricultural use. In the US salinity diagram (Richards 1968), which takes EC as salinity hazard, and SAR as alkalinity hazard, shows that all groundwater samples fall into the low salinity-low sodium category (C1/S1-low to C2/S2-middle) (Fig. 6.28a). Carbonates on the soil and a high RSC reduce soil permeability and lower leaching rates, disrupting plant growth (Singh et al. 2013). Within the basin it ranges from 0.238 to 3.776. In the middle section of the stream, values greater than 2.5 are unsuitable for cultivation. When the SSP value is over 80%, the water is not suitable for irrigation as Soils with high sodium levels become salinized and alkaline as sodium combines with chloride and carbonates effecting plant growth. Plant growth and crop productivity are also adversely affected by excessive soil salinity and alkalinity. In the study area, SSP values ranged from 9.22 % to 60.92 % and in respect to EC it also falls under the excellent to good condition (Fig. 6.28b).

When magnesium hazard exceeds 50%, soil becomes alkaline, and crop yields decrease. In the present study, MH values ranged from 0.12 to 52.17, and 2% of the samples has MH values above 50. In the upstream section of the basin, magnesium ions are primarily influenced by weathering of parent rock and dissolution of calcite and dolomite. According to the PI classification (Fig. 6.28c), classes I and II are suitable for irrigation, while class III is not (Doneen, 1964). In the basin, the PI value ranges from 0.74 to 2.28. All samples fall within 75% of the maximum permeability, making them suitable for irrigation (Kundu and Nag, 2015; Majumdar et al. 2020). RSBC is also under limits and in satisfactory condition ranging from 0.009 to 7.17. As reported by Dhirendra et al. (2009), the presence of Mg^{2+} in soil enhances soil alkalinity and increases Kelly's ratio, thereby reducing crop yield. Kelly's ratio of the basin ranges from 0.081 to 1.54 and is doubtful for irrigating the agricultural fields in the upstream section. As the study area does not fall under the saline zone SHC is low which reflect the salt and alkali hazards. It ranges from 1.44 to 12.73. Soil aggregates separate into individual soil particles when concentrations of exchangeable sodium ion are high (Sarani et al. 2016). ESP can increase soil density and restrict root growth by reducing permeability and porosity. In the study area, ESP varied from 0 to 3.83 with an average of 0.03. Therefore, all the sample locations are marginal to satisfactory for irrigation purposes. To categorize the sampling sites into clusters with respect to their similarity, fuzzy C-means clustering has been used and Fuzzy EDAS for prioritization based on the need of management.

T**able 6.9** Descriptive statistics of the irrigation suitability parameters

Irrigation suitability parameters	Algorithm	Range	Class of water	Minimum	Maximum	Mean	Std. Deviation	Variance	Skewness	Kurtosis
SAR	$Na^+/\sqrt{Ca^{2+}+Mg^{2+}/2}$	<10 10-18 18-26 >26	Excellent Good Doubtful Unsuitable	0.136	3.551	0.074	0.641	0.412	1.781	4.170
RSC	$(CO_3+HCO_3^-)-(Ca^{2+}+Mg^{2+})$	<1.25 1.25-2.5 >2.5	Satisfactory Marginal Suitable	0.238	3.776	0.089	0.766	0.588	1.737	2.980
SSP	$Na^+ \times 100/(Ca^{2+}+Mg^{2+}+Na^+)$	<20 20-40 40-60 60-80 $>Na^{2+}$ 80	Excellent Good Permissible Doubtful Unsuitable	9.215	60.919	1.339	11.519	132.704	1.157	1.400
MH	$Mg^{2+} \times 100\ (Ca^{2+}+Mg^{2+})$	<50 >50	Suitable Unsuitable	0.121	57.172	1.459	12.555	157.649	0.386	-0.287
PI	$[\{Na^+ + \sqrt{(HCO_3^-)}\}/(Ca^{2+}+Mg^{2+}+Na^+)] \times 100$	>75 75-25 <25	Class I Class II Class III	0.735	2.281	0.036	0.316	0.100	0.615	0.183
PS	$Cl^- + 0.5 \times SO_4^{2-}$	<5 5-10 >10	Satisfactory Marginal Unsatisfactory	0.212	6.068	0.159	1.369	1.876	1.809	2.839
RSBC	$HCO_3^- - Ca^{2+}$	<5 5-10 <5	Satisfactory Marginal Unsatisfactory	0.009	7.176	0.156	1.345	1.811	1.694	3.785
KR	$Na^+/_{Ca^{2+}+Mg^{2+}}$	<1 1-2 >2	Good Doubtful Unsuitable	0.081	1.537	0.028	0.244	0.060	2.559	9.256
SHC	12.4 M+SAR	<25 25-36 36-44 >44	Excellent Good Injurious Suitable	1.449	12.728	0.224	1.932	3.734	1.961	6.198
ESP	(0.0126+0.01475×SAR)/(1+(-0.0126+0.01475×SAR)) ×100	<15 >15	Sodic Non-Sodic	0.000	3.825	0.072	0.626	0.393	2.364	8.604

6.2.6.5 Fuzzy C-means clustering

In this study, fuzzy c-means, fclust (An R Package for Fuzzy Clustering) library of R-Studio software, has been used to carry out the clustering of groundwater sampling sites. After a number of iterations, clusters of varying sizes (2, 3, 4 and 5) has been obtained. As a result of different configurations, such as distance measure and parameters, the clustering algorithm produced different partitions. The preferred cluster scenario is when the pairwise distances structure the points into an acceptable grouping and an algorithm successfully produces a clustering that dispose with that principal structure (Rawashdeh, 2012). The clustering of the sampling sites has been done based on the similarity of irrigation suitability indices, including SAR, RSC, SSP, MH, PI, PS, RSBC, Kelly's ratio, SHC, and ESP. A cluster's validity with respect to its underlying structure can be checked by use of cluster validity indices, such as the fuzzy silhouette index, the partition coefficient, the partial entropy, and the modified partition coefficient. The validity score for two clustering group ranges from 0.85 to 0.52, where a high value indicates that the object is harmonizing to its own cluster, and a low value indicates poor matching between neighboring clusters (Table 6.10). For clustering group of 3-5, this value is less that's why two (FCM-I & II) clustering groups of groundwater sampling sites have been chosen for the study (Fig 6.29). The degree of membership for the two-cluster group - FCM-I and FCM-II ranges from 0.05-0.98 and 0.02-0.95, based on which the closest hard clustering partition has been done. The basin has been classified into three type of agricultural field based on the source of irrigation namely canal dominated irrigated area (1046.2 km^2), groundwater dominant irrigated area (1112.4 km^2) and rain dependent irrigated area (1722.4 km^2). Cluster I (FCM-I) consist of 46 sampling sites (Amanpur, Amlagora, Amlasuli, Baramura, Chotatara etc.) located in the middle section of the basin having the similarity in terms of the local geological effect on their water quality. Groundwater from these sites are mostly suitable for agricultural production. Since this part of the basin, particularly the Bankura district, is drought-prone and agriculture is heavily dependent on groundwater (Das et al, 2021). The average rice yield per block within the basin is about 84 qu/hec (Sutradhar et al. 2019). Cluster II (FCM-II) consist of 28 sampling sites (Amkopa, Badga, Amrakuchi, Ashberia, Bangla, Elora etc.) mainly located in the upstream and few in downstream section. Upstream sampling sites show similar groundwater quality results, influenced by their local geology, where the water is in a satisfactory to marginal condition. Average rice production within this region is 1383 kg/ha from 2004-2018 and it decreased from the previous years (Roy and Jana, 2020). A high concentration of fluoride ions has also been found in groundwater in the upper part of the basin (Puruliya and Bankura district) where people with skeletal fluorosis have been reported during the field survey. In general, it can be concluded that, in the definite condition, prioritization of sampling sites is required for sustainable management to avoid human risks and to increase the agricultural production.

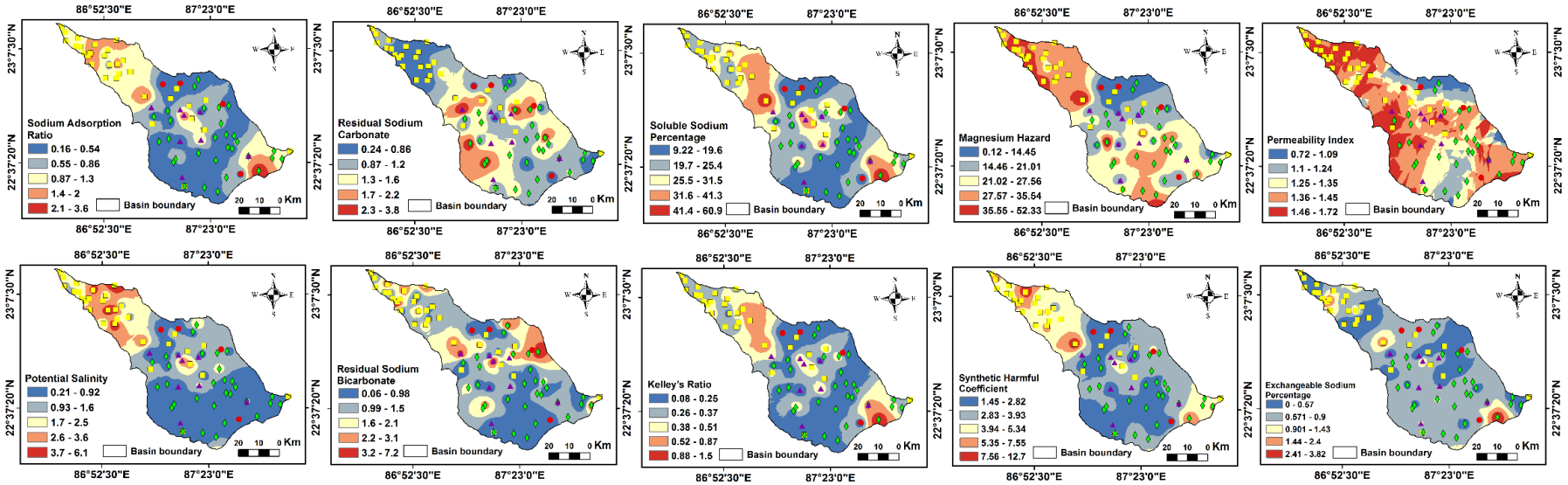

Fig. 6.27 Spatial distribution of irrigation suitability parameters over the basin.

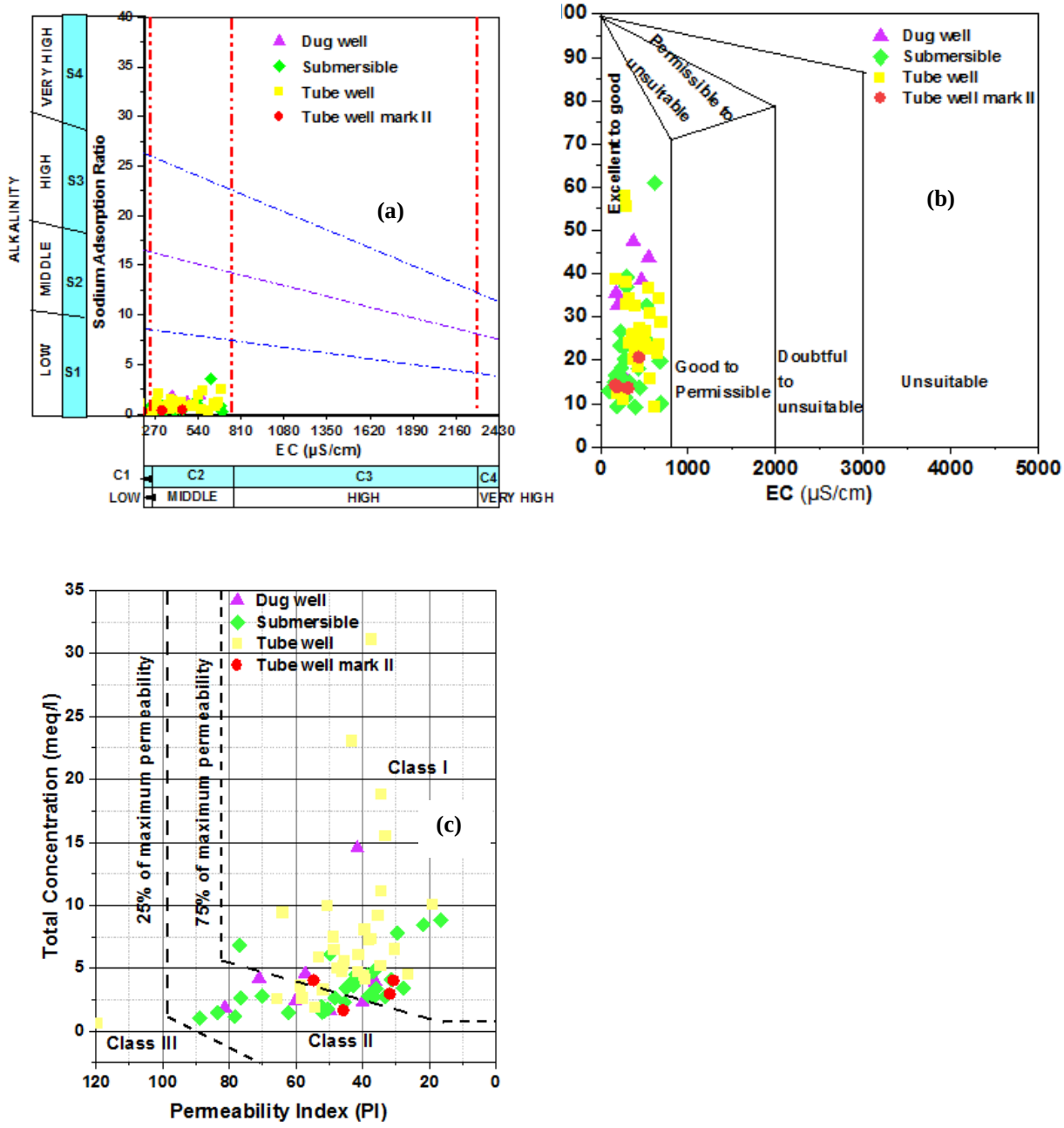

Fig. 6.28 (a) USSL classification of the groundwater samples; (b) Wilcox classification of the groundwater samples; (c) Doneen's permeability index of the groundwater samples

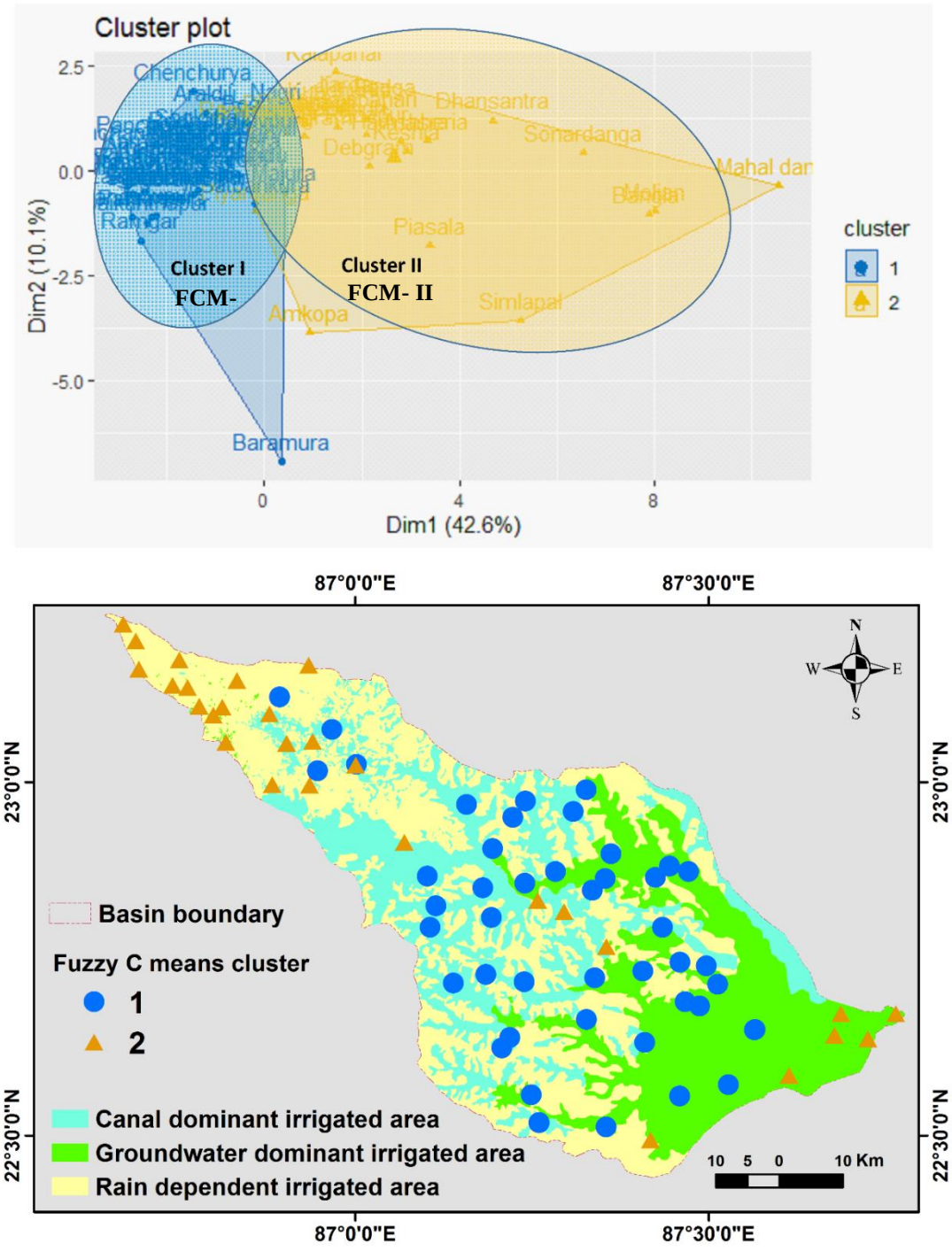

Fig. 6.29 Fuzzy c-means clustering of the groundwater sampling sites

Table 6.10 Validity scores of the Fuzzy C-means clustering technique

Fuzzy clusters	Fuzzy silhouette (FS)	Partition Entropy (PS)	Partition Coefficient (PC)	Modified Partition Coefficient (MPC)
Cluster 2	0.85	0.76	0.68	0.52
Cluster 3	0.60	0.67	0.62	0.42
Cluster 4	0.57	0.77	0.59	0.45
Cluster 5	0.51	0.64	0.52	0.42

6.2.6.6 Fuzzy EDAS basin prioritization based on irrigational suitability indices

The prioritization exercise has been completed by computing FASI values from Fuzzy EDAS techniques based on EC, Hardness, Chloride, SAR, RSC, SSP, MH, PI, PS, RSBC, Kelly's ratio, SHC, and ESP of the sampling sites. Parameters has been selected in relation to the prospect for irrigation using groundwater. Priority has been was accorded to regions with the highest scores, while regions with lower scores are given low or negligible priority. The fuzzy EDAS priority class has been classified into five groups namely very low (0.06-0.23), low (0.24-0.39), moderate (0.40-0.55), high (0.56-0.71) and very high (0.72-0.88) (Fig. 6.30). Molian, Dewanchak, Mahaldanga of Bankura districts requires the highest priority. As these sites fall in a dominant zone of rock–water interaction, chemical weathering of rock-forming minerals is the main factor influencing groundwater quality and its contamination (Nag and Das, 2017). It is also consistent with Chakraborty et al's findings, 2022 that groundwater contamination is caused by anthropogenic sources as well as some natural factors, and the study also identified a high level of iron in drinking water as a potential health hazard. Further degradation from the present condition will also affect agricultural resources as well as threaten food security and human health. Therefore, these discoveries will improve groundwater quality management for agricultural areas and growing human populations in semi-arid hydrological areas like Shilabati.

6.2.7 Conceptual outcome of the study and recommendations

The quality of water used for irrigation is fundamentally a concern in agriculture, which is influenced by a number of parameters. By using the technique of fuzzy-C means clustering and fuzzy EDAS presented in this study, geochemical exploration can be conducted accurately in any river basin at a relatively low cost and time commitment. Thus far, no such research has been conducted within the river basin or otherwise incorporating the two computing techniques. There are only a few studies that focus on block-wise aspects (Chowdhury et al. 2022; Kundu and Nag, 2018; Chakraborty et al. 2022). On the basis of these observations, the water quality of the study area has been divided into different categories and (very poor, poor, medium, good, excellent, satisfactory, marginal etc.) based on different indices. Groundwater flow in the Shilabati basin is influenced by its topography and slope. The region adjoining the Shilabati river basin is irrigated and has been found to have geogenic contamination with samples ranging from marginal to satisfactory, making it suitable for irrigation and unsuitable for some parts. Thus, crops may yield less in those regions. Additionally, excessive groundwater drawdown within the basin will contaminate these aquifers, especially in the upstream and middle sections (Bera et al. 2021). It is the unscientific exploitation of groundwater resources within basins for industrial, agricultural, drinking, and other domestic purposes that is the primary cause of groundwater table depletion in shallow unconfined aquifers (Thakur and Thomas, 2011). Human activities also pollute the sources of water supply, including dug wells and surface water of this river basin. Among these activities are the use of pit latrines by most residents and the indiscriminate dumping of waste which contributes to water contamination (Kundu and Nag, 2018). To reduce the risks to human

health within the Shilabati basin, the authors recommend that the government agencies should reduce fluoride and iron contamination in water and soil, as well as monitor the domestic and irrigation water supply. In order to ensure proper agricultural growth and better living conditions for rural communities, the following suggestions are recommended for the sustainable development of groundwater resources.

- Rainwater recharge strategies need to be implemented throughout Shilabati basin to improve the quality of groundwater.
- Introduction of GRADE (Groundwater Risk Assessment near Drinking Water Extractions) model is required that will calculate the risk of contamination when extracting water for drinking purpose.
- To reduce groundwater pollution, drainage systems and sewage lines need to be maintained properly, as many villages within the basin lack such facilities.
- For a clear and clean rural environment, especially in areas with a high population, biological treatment plants and solid waste recycling are essential,
- To remove iron and fluoride from water within the study area, low-cost technology needs to be introduced and filtration units installed.
- To build a healthy society, it is essential to create public awareness on environmental issues.

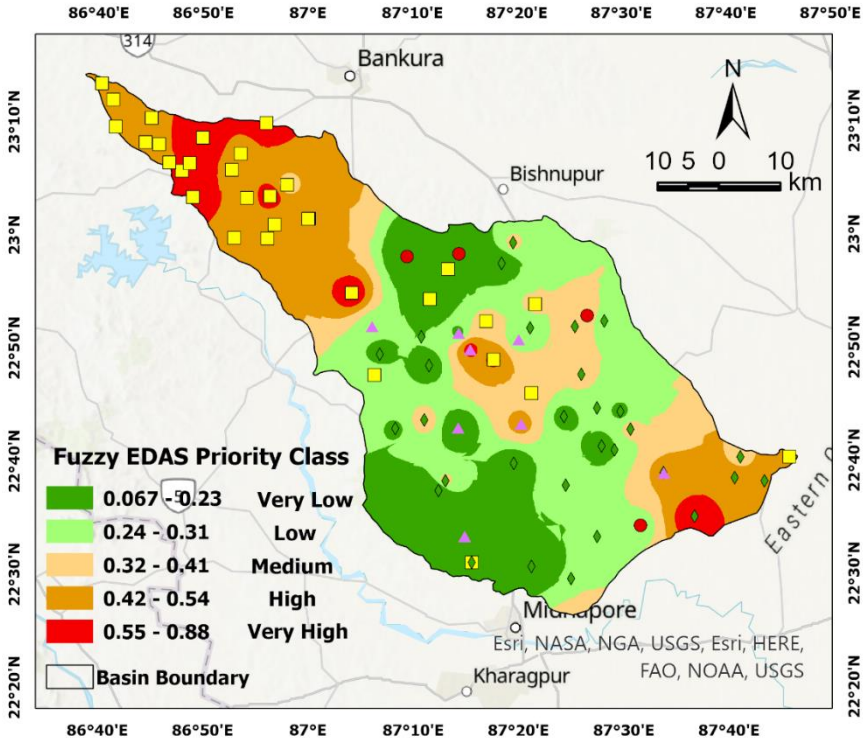

Priority class	*Class name*	*Sites*
0.06-0.23	Very Low	Nachankonda, Lalgeria, Bhutsahar, Kiamacha, Panchmura, Tarasuli Penchapara, Rajpur, Baikunthapur, Sarbot, Mandalkupi, Sonajhor, Amanpur, Makli, Karnagarh, Chotatara, Basudevpur, Ramgar, Pingboni, Jadupur, Amlasuli, Amlagora
0.24-0.39	Low	Garbeta, Keshpur, Uchachar, Ghatmura, Kandra uttarbill, Dubrajpur, Sholdiha, Chenchurya, Patharpara, Pirchak, Araldili, Benchapra, Dhadika, Majura, Damodarpur, Raghunathpur, Radhaballavpur, Jemuasole, Ranibazar, Raskundu, Baramura, Jiarpara, Piyardanga, Kalapahar
0.40-0.55	Moderate	Nagri, Nanda, Amrakuchi, Boga, Jiarda, Muragram, Ranapur,Satbankura, Elora, Ashberia, Kazirhat, Kundhurka, Debgram, Salapahari, Pratappur, Badga, Keshia, Dhanghori
0.56-0.71	High	Hirabandh, Harmasra, Amkopa, Piasala, Bangla , Simlapal, Dhansantra, Sonardanga
0.72-0.88	Very High	Molian, Dewanchak and Mahaldanga

Fig. 6.30 Fuzzy EDAS based prioritization of the basin for groundwater management and the predominant crops within the river basin

6.2.8 Conclusion and Recommendation

By using Fuzzy C-mean Clustering and Fuzzy EDAS along with some conventional methods such as SAR, RSC, SSP, MH, PI, PS, RSBC, Kelly's ratio, SHC, and ESP, this study investigated the hydrogeochemical processes that influence groundwater systems and the suitability of groundwater for irrigation. A new irrigation suitability clustering plot has been introduced, which incorporates all of the essential water quality parameters and fills the gaps of previous clustering techniques. In a GIS environment, several water quality parameters have been considered to demarcate zones of suitability and their spatial variations. Finally, by integrating all irrigation suitability parameters, fuzzy EDAS priority maps have been developed to identify areas requiring immediate sustainable management. According to the study, the following key conclusions can be drawn.

- Due to rock-water interaction, the groundwater in the upper part of the basin is primarily alkaline and moderate to very hard in nature. In the field survey, iron stains have also been observed in utensils and water supply systems (>40 mg/l) throughout the basin. The abundance of the major ions in the Shilabati river basin follows the trend of $Ca^{2+}>Na^{+}>Mg^{2+}>\ K\ >\ Fe$ for cation and $HCO_3^->Cl^->SO_4^{2-}>NO_3^-> PO_4^{-3}>F^-$ for anions. The studied groundwater samples evolved primarily from Ca^{2+}- HCO_3^- and mixed Ca^{2+}- Mg^{2+}- Cl^- types, and $HCO_3^- - Ca^{2+}$ type is the most dominant. Within the study area, ion exchange, reverse ion exchange, and silicate weathering are a few of the significant physio-chemical processes influencing the geochemical evolution.
- This study also revealed $Ca^{2+}$and Mg^{2+} ion dominance over Na ion due to the presence of loosely consolidated sand, silts, and clays. Apart from all the parameters, Kelley's ratio and RSB show that some areas are unsuitable for groundwater irrigation. Groundwater samples from the study area has been analyzed hydro chemically and showed that rock-water interactions and mixing between shallow groundwater and deep circulating groundwater played a dominant role. With few exceptions, the ion enrichment in groundwater has been attributed to anthropogenic influences through domestic discharges and agricultural activities. Moreover, hydrochemical variations in the groundwater are highest in the 4 geological structures including sands and silts in alternate clay, granite gneiss, migmatite, pink granite/biotite-granite gneiss and sand, silt and clay where the degree of chemical weathering of various rock types, quality and quantity of recharge water (high leaching potential) and inputs from sources other than rock-water interaction represent the factors that influence the groundwater chemistry during the flow path.
- Based on the irrigation suitability indices, fuzzy-C means clustering divided the sampling sites into two clustering groups which is then evaluated using fuzzy silhouette index (0.85), partition coefficient (0.76), partial entropy (0.68), and modified partition coefficient (0.52). Cluster I (FCM-I) consists of 46 sampling sites with similar geological types, while cluster II (FCM-II) consists of 28 sites. Upstream and downstream sampling sites have marginal to satisfactory groundwater quality due to rock-water interaction and anthropogenic impacts, respectively.
- The fuzzy EDAS priority class has been categorized into five classes namely very low (0.06-0.23), low (0.24-0.39), moderate (0.40-0.55), high (0.56-0.71) and very high (0.72-0.88). Molian, Dewanchak,

Mahaldanga, Hirabandh, Harmasra, Amkopa, Piasala, Bangla, Simlapal and the surrounding region should be given the highest priority for sustainable management. It has been found that groundwater in the studied region is mostly unsuitable for crops sensitive to fluoride and iron without adequate soil management.

6.2.9 Limitation and Future Work

In the current study parameter-based irrigation water quality has been applied to fuzzy GIS platforms in order to assess the overall quality of groundwater. In the field of irrigation management, determining water quality is also an important tool for policy makers and the public to understand. Additionally, the map will provide an overview of water quality for irrigation to the non-academics and end users. However, insights and lessons learned from the study may be applied universally, even if it is limited to the West Bengal river basin. Many developing countries, including other parts of India, share the same water quality issues as the current study area. Due to climate change, changes in rainfall frequency and intensive mixing of contaminants, other parts of the world may also experience water scarcity and quality issues. Several water quality issues and associated health risks can result from a combination of arid/semi-arid climate, geological risks (rock water interaction), and anthropogenic activities in those regions. To protect these water resources from further contamination and subsequent harm, administrators and decision makers should use GIS platforms and soft computing techniques to produce groundwater quality maps.

Chapter7

Novel adsorbents in remediation of hazardous environmental pollutants: In light of fluoride, iron and phosphate

7.1 Enhanced fluoride removal from groundwater using red and white kaolinite lithomarge to develop a low cost eco-friendly defluoridation unit

7.1.1 Introduction

At low levels (<1 mg/l), the Fluoride is essential for human health, particularly for the development of teeth and bone. However, fluoride concentrations above 1.5 mg/l in drinking water are not permitted by the World Health Organization (WHO), as it leads to severe dental and skeletal disorders (Khan et al. 2022). Fluoride is associated with a number of detrimental effects, including arthritis, osteoporosis, bone fragility, cancer, thyroid disease, Alzheimer's disease, and infertility in women. Increasing fluoride levels in the body can also inhibit the metabolism of lipids, carbohydrates, and vitamins (Ashoori et al. 2022). There are several ways in which fluoride enters the body, including mouthwash consumption, air, food, toothpaste, and potable water (Mesdaghinia et al. 2010). It is unfortunate that water can be polluted with fluoride simultaneously by inorganic and organic substances (Priya et al. 2022; Rezania et al. 2021). Groundwater contamination by fluoride due to natural processes or human activity has been recognized as a serious problem in many parts of the world, especially in Africa, India, the Middle East and northern China where groundwater is a vital source of drinking water (Jiang et al. 2022) .According to statistics, approximately 200 million people are affected by high concentrations of fluoride in drinking water, and approximately 70 million suffer from varying degrees of health complications (Thompson et al. 2021).

To reduce or avert the negative health impacts of high pollutant contents in drinking water, including fluoride, researchers have been developing decontamination technologies in recent decades. A comprehensive literature review of methods for eliminating fluoride from water showed that many authors have used natural and synthetic materials in their efforts. Many defluoridation techniques such as adsorption (Darwish et al. 2021), ion exchange (Rodriguez et al. 2022), electrocoagulation (Ewadh et al. 2021), reverse osmosis (Diwani et al. 2022), nano filtration (Meftaha et al. 2020), biosorption, electrodialysis (Kalsido et al. 2022) and precipitation (Wang et al. 2022a) have been considered to remove excess fluoride from water. Fluoride can be effectively removed by an ion exchange process among traditional methods, but it is limited in its effectiveness by other ions such as carbonate, sulfate, alkalinity and phosphate (Wang et al. 2022b). Additionally, this technique is expensive due to the high purchasing cost of synthetic ion exchange resins (Singh et al. 2020). Nano filtration is highly effective

at removing fluoride from water whereas membrane separation technology is capable of removing maximum ions present in water (Diawara, 2008). But some of them are vital to human health. Alum is commonly used for precipitation-coagulation defluoridation technique, which absorbs a small amount of fluoride through precipitation but leaves a large amount of aluminium fluoride soluble in the tincture (Zhong et al. 2022). It has also been claimed that the Nalgonda process eliminates fluoride most effectively (Dey et al. 2004). Nevertheless, only a small part of the fluoride was eliminated (18–33%) in the precipitates and a substantial part was converted into soluble aluminium–fluoride complex ions, which are virulent by themselves (Apparao and kartikeyan, 1986). Commercially established electrodialysis systems have been reported as an effective tool for simultaneous defluoridation and desalination (Majewska-Nowak et al. 2015). However, electrodialysis still has some disadvantages, for example, a significant stack resistance; acidic conditions in anodic compartments may corrode anodes while alkaline conditions in cathodic compartments may cause scale to form on the cathode (Al-Amshawee et al. 2020). In the absence of a suitable product recovery method, the use of these physicochemical methods is limited owing to the high cost and harmful by-products (Katiyar et al. 2020). In comparison to the above methods, adsorption is a more environmental friendly process. Aside from being economical, it also removes fluoride ions with a higher efficiency. The availability of abundant and inexpensive natural sorbents is also an advantage. Based on an exhaustive literature review, natural adsorbents were found to be little studied in regard to fluoride removal. Using natural materials (untreated charcoal), Chidambaram et al. (2013) removed fluoride from groundwater but obtained poor removal efficiency over time. In previous studies, fluoride adsorption was observed to be less effective on clay (Nabbou et al. 2019; Ayalew et al. 2023), red mud (Yi et al. 2023) and small plants (Ahmad et al. 2022). In recent years, the cost of activated carbon has increased and prompted a surge in green adsorbents, originating from agricultural waste. However due to electrostatic repulsion by the negative charge on the biochar surface, it has a low adsorption efficiency, especially for anionic contaminants in water and incur huge cost in preparation and modification (Tomczyk et al. 2020). A number of studies had demonstrated that red laterite was most effective at removing fluoride at pH 3-5 but water with such pH is unfit for drinking (Maiti et al. 2013; Sarkar et al. 2006). In addition, most studies of fluoride removal on laterite were limited to batch studies without column leaching tests or ground applications (Nabbou et al. 2019; Maiti et al. 2011; PHED, 2008). Thus, developing a cleaner and more cost-effective alternative defluoridation unit is highly demanded among the scientific communities. The current study, in light of the above research gap, used locally available natural kaolinite lithomarge-laterite soil (both white and red type), found abundantly within 50 km of the fluoride-contaminated zone, and removed fluoride without any chemical treatment (acid/base treatment). This procedure proved to be cost-effective and time-saving, with an efficient removal rate greater than 98%.

7.1.2 Research Gap and Novelty of work

In West Bengal, 12% of the population from seven out of 23 districts is affected by fluoride exposure, with fluoride concentrations exceeding 1.5 mg/l detected in groundwater in 43 blocks (PHED,2008; Chakrabarti et al. 2013). The fluoride toxicity in the western part is much higher due to its geographical location, climatic condition and rock type, covering three districts of Bankura, Purulia, and Birbhum (Samal et al. 2015; Das et al. 2016). A preliminary investigation by the authors within the Shilabati basin, covering the district of Puruliya and Bankura, witnessed various symptoms of skeletal fluorosis among people of different age groups in Lakshmisagar village, Simlapal block, Bankura (Fig.1c), which is the cause of prolonged consumption of fluoride-contaminated water.

Similarly, Das and Mondal (2016) (Das et al. 2016) found the same scenario in their study where the fluoride concentrations exceeded 1.5 mg/l within the Silai-Joypanda river basin. In previous studies in Bankura and Purulia, West Bengal, fluoride contamination of groundwater was reported and the extent of fluorosis was assessed to some extent (Bera et al. 2019; Mondal et al. 2017). No studies have been conducted in fabricating and designing defluoridation units considering other physicochemical characteristics of water and the geography of the region. Furthermore, fluoride-contaminated groundwater contributes significantly to the intake of fluoride by vegetables and crops grown within this region which needs to be managed effectively (Bhattacharya et al. 2017; Samal et al. 2020).

7.1.3 Objective of the study

Based on the above-mentioned research gap and to provide a sustainable water supply to the local people the study aims (i) to examine the suitability of using kaolinite lithomarge laterite of red and white type for fluoride removal from synthetic water and natural fluoride contaminated water from the Shilabati river basin considering pH, TDS, EC, turbidity and iron. (ii) to optimise the absorption mechanism parameters such as initial fluoride concentration, adsorbent dose, pH and ionic strength, agitation speed, time variation to conduct the column model and (iii) to examine the physico-chemical characteristics of the kaolinite lithomarge before and after fluoride adsorption using Field emission scanning electron microscopy (FESEM), Energy Dispersive X-Ray Analysis (EDX), Fourier transform infrared (FTIR) spectroscopy and x-Ray diffraction (XRD) analysis (iv) to provide a cost-benefit analysis of the defluoridation unit so that it can be easily installed in the fluoride affected villages within Shilabati river basin or any other region at a global scale.

7.1.4 Area of Investigation

Groundwater in Shilabati river basin is primarily affected by fluoride contamination which is geogenic in origin (Mondal et al. 2017). The districts of Puruliya and Bankura are the most affected within the basin, with fluoride scattered over 17 blocks in Puruliya and 10 blocks in Bankura as monitored by the Public Health Engineering Department (PHED, 2022). The presence of the gneiss, pegmatite and granite are responsible for the fluoride concentration in Puruliya and Silica and Mica in Bankura which act as a potent source of fluoride that leaches out into the groundwater system (Bera et al. 2019; Mondal et al. 2017). Several tube wells (180-80 ft.) within the river basin affected by fluoride were sealed by the government but the local population continues to use dug wells (100 ft.) for domestic purposes (Khan et al. 2022). Most affected gram Panchayat within this basin are Puncha in Puruliya, Simlapal in Simlapal, Khatra in Khatra, Hirabandh in Hirabandh and Indpur in Bankura (PHED, 2022). The predominant crop in this section of the basin is rice, followed by potato, wheat, vegetables, maize and till, which are mostly irrigated by submersible pumping wells. Besides consuming fluoride-enriched water, cultivated foods grown in this section of the basin also contribute significant amounts of fluoride to the daily dietary intake of local villagers (De et al. 2021). From a preliminary survey by the authors, skeletal fluorosis and dental fluorosis are strongly prevalent in the river basin, particularly in Lakshmisagar Gram Panchayat of Simlapal block, Bankura (Fig.7.1 a-e). In order to provide a low-cost eco-friendly defluoridation unit within the study area, water samples were collected from 11 different locations within the basin at the upstream section for the fixed bed column filter study. The natural absorbent kaolinite lithomarge laterite of both red and white type is abundantly found in Garbeta

badland popularly known as Grand Canyon of West Bengal, (Mandal et al. 2021) was collected for the fabrication of a defluoridation unit.

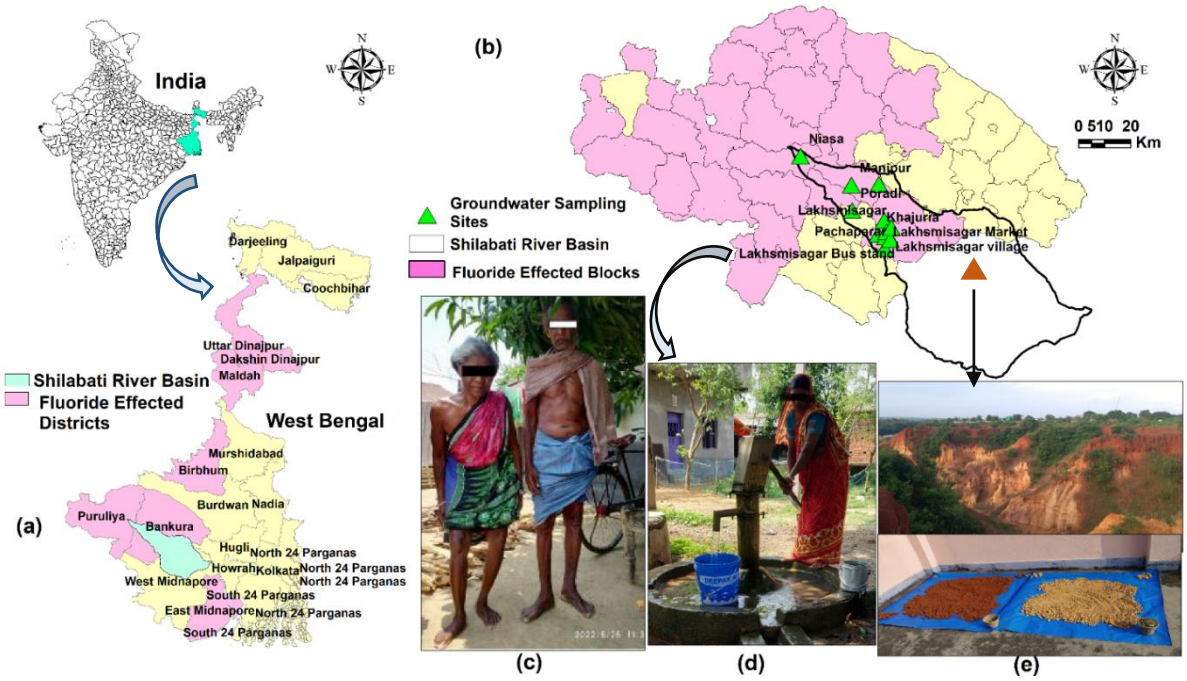

Fig. 7.1 Location of the study area (a) Shilabati river basin in West Bengal with fluoride affected districts, (b) fluoride affected blocks within the river basin and groundwater sampling sites, (c) evidences of skeletal fluorosis and bone deformation among villagers, (d) water sampling tube well and (e) collection site of natural adsorbent (Garbeta, Paschim Medinapore district).

7.1.5 Research Design and Methodology

7.1.5.1 Chemicals and consumables

All experimental mechanisms were performed using laboratory-grade chemicals. Sodium fluoride (NAF-41.98817 g/mol) (Merck-Sigma Aldrich), hydrochloric acid (HCl) (Merck-Sigma Aldrich), sodium hydroxide (NaOH) (Merck-Sigma Aldrich), ethanol (Merck-Sigma Aldrich), acetone (Merck-Sigma Aldrich), deionized water and Whatman no. 1 filter paper was used to conduct the experiment. 221.1 mg of NAF was dissolved in 1 liter of deionized water to prepare 100 mg/l of fluoride stock solution for the batch absorption test. The batch experiment was conducted by diluting the aliquot at different concentrations including 2 mg/l, 5 mg/l, 10 mg/l and 20 mg/l. For the fixed bed column leaching experiment, water samples (Fig.7.1b & 7.1d) from the fluoride contaminated zones of Shilabati river basin were collected to check the removal efficiency of the defluoridation unit. Water samples were collected from 11 locations from different groundwater sources (Table 7.1) including tube wells and dug wells where pH, Total Dissolve Solids (TDS), Electrical Conductivity (EC) and temperature were measured in-situ using Hach multi-parameter probe (HQ40d). Turbidity was measured in lab using Hach 2100Q Portable Turbidimeter. Iron was determined by inductively coupled plasma mass spectrometry (ICP-MS) and the ion-selective method was used to quantify fluoride. The column leaching test was performed with the water sample drawn from the site with the highest fluoride concentration of 2.37 mg/l (Lakshmisagar village 1).

Table 7.1 Groundwater sampling sites

Sampling sites	Latitude (N)	Longitude (E)	pH	TDS mg/l	EC µS/cm	Iron mg/l	Turbidity NTU	Fluoride mg/l	Temperature (°C)
Gharpathar	23°06'34.49"	86°59'07.32"	6.51	150	234	0.18	0.61	0.13	30.5°C
Kharjuria	22°56'09.11"	86°58'58.63"	6.59	197	308	2.00	0.72	0.30	26.0°C
Niasa	23°12'11.34"	86°41'34.60"	6.68	244	381	0.36	0.65	0.30	27.8°C
Pachaparar	22°93'05"	87°01'66"	5.65	60	93.8	0.16	0.85	0.024	27.8°C
Poradi	23°07'07.11"	86°39'52.35"	6.31	121	189	0.49	0.86	0.68	28.1°C
Manipur	23°53'05"	86°39'69"	6.50	149	233	0.35	0.52	0.19	29.1°C
Lakshmisagar (Market)	22°55' 58"	87°00' 40"	6.23	83	130	0.43	0.25	2.30	29°C
Lakshmisagar (Bus Stand)	22° 55' 38"	87°00' 39"	6.21	127	199	0.41	0.69	0.78	36°C
Lakshmisagar (Village 1)	22°55' 48"	87°00' 52"	6.40	356	574	1.22	0.56	2.37	36.2°C
Lakshmisagar (Primary Health Centre)	22°55' 07"	87°01' 42"	6.56	102	159	0.05	0.72	1.15	36.4°C
Lakshmisagar (Village 2)	22°55' 28"	87°00' 27"	6.20	351	549	0.32	0.66	0.193	37°C

7.1.5.2 Collection and synthesis of the natural adsorbent

The Neogene sedimentary sequence within the Shilabati river basin is characterized by alternate sandstone lithofacies and is abundant with kaolinite lithomarge-laterite (Ghosh et al. 2015a; Ghosh et al. 2015b). The water table fluctuation impacts lateralization processes within this region leading to high concentrations of Fe_2O_3, Al_2O_3 and SiO_2 which are beneficial for the removal of fluoride in water (Jiang et al. 2021; Keranen et al. 2014). In total, ten kilograms of kaolinite lithomarge-laterite (White and Red) were collected from the various sites (Fig. 7.1e). To remove moisture and to clean off dirt, roots, etc., the soils were dried for 20 days under normal atmospheric conditions and under direct sunlight. Subsequently, they were washed with deionized water and dried in an oven for 24 hours at 80°C. The dried soil was then stored in airtight containers for further use.

7.1.5.3 Batch experiment analysis

The fluoride adsorption efficiency of kaolinite lithomarge-laterite was determined by its structure, chemical composition, morphology, and surface properties. It is therefore trivial to investigate how the key operational factors such as pH, amount of absorbent mass, fluoride concentration at an initial state, agitation speed, particle size, contact time, temperature etc. influence fluoride uptake mechanisms. When one parameter in the batch study was optimized, the other parameters were kept constant. Plastic chemical wares were mainly used for the entire experiment. For the batch adsorption mechanism, 50 ml of spiked solution was used. The batch study was investigated with different initial concentrations of fluoride (2 mg/l, 5mg/l, 10mg/l and 20 mg/l) under varying pH conditions (4-10). The pH of all the mixtures was controlled by 0.01 (N) HCl and 0.01(N) NaOH. Kaolinite lithomarge of both types (red and white) was sieved into various particle sizes to test its highest impact on removal efficiency. Water samples were also collected and monitored at different time intervals to observe the impact of contact time. To observe the influence of acceleration speed, the samples were shaken at different revolutions per

minute (100, 200, 250) in an incubator shaker (Thermo Scientific™ MaxQ™ 6000). Lastly, the removal efficiency of this natural adsorbent was studied at various metal ion concentrations (2-20 mg/l). After the batch test fluoride, pH, TDS and EC of each sample were analysed by filtering the water through Whatman no. 1 filter paper (pore size 0.45 μm, diameter 47 mm). The ion-selective method was adopted for the quantification of fluoride in water. The Hach Intellical ISEF121 combination fluoride ISE and the HQ40d portable multimeter were used for measuring fluoride in water. As part of the fluoride detection process, Fluoride Ionic Strength Adjustor Powder Pillows (ISA) were used. The fluoride adsorption uptake, qe (mg/g) for equilibrium conditions was calculated by using the equation (Eq. 7.1) below (Keranen et al. 2014; Das et al. 2020) and the defluoridation efficiencies of kaolinite lithomarge-laterite of both types were estimated using the following algorithm (Eq.7.2) (Singh et al. 2019)

$$q_e = (C_0\text{-}C_e) * \frac{V}{W} \quad (7.1)$$

$$\% R = (C_0\text{-}C_e) * \frac{100}{C_0} \quad (7.2)$$

Fluoride concentrations at initial state (mg/l) and equilibrium condition (mg/l) were represented as C_0 and C_e. Amounts of adsorbent dose and volume of the aliquot were designated as W (gram) and V (litre) respectively.

7.1.5.4 Adsorption isotherm

The adsorption mechanism was explored with various theoretical and empirical adsorption models which attempted to predict the adsorption parameters accurately. The design of an adsorption system relies on its equilibrium relationships. To explain the defluoridation mechanism and the interaction between fluoride ions and kaolinite lithomarge within the solution at an equilibrium condition (Singh et al. 2019; Kheradmand et al. 2022; Shayesteh et al. 2021) three well-known adsorption isotherm models were used, including the Langmuir model (Eq. 7.3), Freundlich model (Eq. 7.4 and 7.5), and Temkin model (Eq. 7.6). The linear and non-linear parameters were estimated using Origin 2022b and SPSS software (IBM SPSS Statistics 23). Despite not being explicitly stated, non-linear regression provides better results than linear regression. Normally, non-linear regression can be applied to an array of models with the same set of adjusting variables, allowing the comparison of distinct model fits to be more direct. Upon analysis, Langmuir non-linear model fitted well with the data set and was therefore used. In the Langmuir adsorption model, monolayer adsorption, and energetically equivalent adsorption sites were assumed for the adsorbent to be structurally homogeneous (Langmuir, 1916). The non-linear form of the Langmuir isotherm equation was calculated using the following algorithm (Eq.7.3).

$$q_e = q_m \left(K_L \frac{C_e}{1+K_L C_e}\right) \quad (7.3)$$

Where the equilibrium adsorption capacity is represented as qe (mg/g), maximum adsorption capacity as qm and K_L is the model constant.

As the fraction of occupied sites increases, the enthalpy of adsorption decreases logarithmically according to Freundlich adsorption model, which assumes adsorption depending on a heterogeneous surface (Freundlich, 1906). The empirical form of the Freundlich isotherm model can be written as (Lagergren, 1898).

$$q_e = KC_e^{1/n} \quad (7.4)$$

K and n are the empirical constants that are the characteristics of the adsorption system, indicating the adsorption capacity and the adsorption intensity, respectively. The above equation can be linearized according to the following algorithm (Eq. 7.5).

$$\ln q_e = \ln K + \frac{1}{n} \ln C_e \quad (7.5)$$

K is the measure of adsorption capacity and 1/n is the adsorption intensity. The value of n of this model fell in the range of 1–10, indicating favourable sorption. The numerical value of 1/n < 1 indicated that adsorption capacity was slightly suppressed at lower equilibrium concentration (Anah and Astrini, 2018).

The adsorption mechanism between the kaolinite lithomarge of two types and the fluoride was also determined by Temkin isotherm. Temkin isotherm, which considers the effects of the heat of adsorption, decreases linearly with coverage of the adsorbate and adsorbent interactions (Saha et al. 2010). Temkin isotherm mechanism was calculated using the following algorithm (Eq.7.6)

$$q_e = \left(\frac{RT}{b_T}\right) \ln(K_T C_e) \quad (7.6)$$

Where b_T is the Temkin constant related to the heat of sorption (J/mol), K_T is the Temkin isotherm constant (L/g), R is the gas constant (8.314 J/mol. K) and T is the absolute temperature (K).

7.1.5.5 Adsorption kinetics

In aqueous phase adsorption, kinetic parameters play a very significant role in determining the efficiency of adsorption (Chakraborty et al. 2021). To estimate the sorption rates of fluoride-kaolinite interaction and to determine the rate expressions characteristic of possible reaction mechanisms, three common kinetic models were calculated including pseudo-first-order, pseudo-second-order, and intra-particle diffusion. An adsorbate molecule is assumed to bind to one active site of the adsorbent surface according to a pseudo-first-order model which was calculated using the following equation (Charoenchai and Tangbunsuk, 2022) (Eq.7.7 & 7.8). The equation considered for pseudo-first-order kinetics was first introduced by Lagergren (Simonin, 2016; Moussout et al. 2018).

$$\frac{d(q_t)}{d_t} = K_1 (q_e - q_t) \quad (7.7)$$

The above equation can be integrated for following boundary conditions to obtain Equation t = 0, q_t= 0, t= t, q_t = q_t

$$\ln (q_e - q_t) = \ln q_e - K_1.t \quad (7.8)$$

Where, q_e is the amount of solute on the surface of the sorbent at equilibrium, (mg/g), q_t is the amount of solute on the surface of the sorbent at time t (min), (mg/g), K_1 is the equilibrium rate constant of pseudo-first sorption, (1/min).

According to a pseudo-second-order model, an adsorbent's adsorption capacity is determined by the number of active sites on the surface and was expressed as Eq.7.9 (Charoenchai and Tangbunsuk, 2022; Ho and McKay, 1999)

$$d_{qt}/d_t = K_2(q_e - q_t)^2 \quad (7.9)$$

Where K_2 is the pseudo-second-order rate constant. After integration and applying boundary conditions, t = 0 to t = t and $q_t = 0$ to $q_t = q_t$; the integrated form of above Eq.9 becomes Eq.7.10

$$t/q_t = 1/K_2 . q_e^2 + t/q_e \quad (7.10)$$

The second-order rate constant K_2 and maximum adsorption capacity q_e was estimated by plotting the graph of t/q_t versus t for the linear pseudo-second-order model from the intercept and slope of this graph, respectively. Furthermore, the Weber-Morris intra-particle diffusion equation was used to test whether adsorbate will diffuse from the solution to the solid surface. To investigate the controlling step in the adsorption process, the intra-particle diffusion equation was used (Ma and Wang, 2015; Weber and Morris, 1964). The linearized form of the intra-particle diffusion equation was calculated using the following equation (Eq.7.11).

$$q_t = k_{id} t^{1/2} + I \quad (7.11)$$

Where, q_t is amount of solute on the surface of the sorbent at time t, (mg/gm), k_{id} is the intra-particle rate constant (mg/ (g $min^{1/2}$)), t is the time (min) and c (mg/g) is a constant that gives an idea about the thickness of the boundary layer. If the Weber–Morris plot of q_t versus $t^{1/2}$ gives a straight line, then the adsorption process is controlled by intra-particle diffusion only. In general, adsorption capacity changes with $t^{1/2}$, which do not follow a linear pattern, representing various stages in the adsorption process.

7.1.5.6 Fixed bed column studies

A de-fluoridation unit is an adsorption and filtration column (Singh et al. 2021). Before packing the natural adsorbent into the column, it was ensured that the gravel and sand were washed with water, cleaned properly, and dried. The filter was made of a transparent PVC column with a diameter of 4.5 cm and a length of 80 cm. At the bottom of the pipe, a UPVC adaptor (reducer) was attached. In the succeeding steps, the PVC column was fixed with a threaded PVC cup. For controlling the water flow, a plastic tap was connected at the bottom of the column. Three different sizes of gravel were arranged in the first 8 cm of the filter (Fig. 7.2a). The first step of the process consisted of packing gravel of size between 8 mm- 10 mm into the column up to a length of 3 cm. In the next 5 cm, gravel sized between 4.75 mm - 8 mm was packed. The next 25 cm of the column was equipped with well-graded sand with an effective size (D10) of 0.215 mm with a uniformity coefficient (D60/D10) of 2.74 (Fig. 7.2b). To avoid the absorbent from wedging inside the sand layer, a 2 cm mixed gravel layer was placed after the sand layer. In the next step, kaolinite lithomarge-laterite with a particle size of more than 1 mm to less than 2 mm (as optimized) was packed above the mixed gravel layer. 459 grams of kaolinite lithomarge were used in total in the column leaching test. A water head of 20 cm was maintained throughout to ensure uniform flow within the filter. The inlet and outlet flow rates were maintained at 4.18 ml/min (200 lit/m2/hr). The column was filled with fluoride-contaminated water (2.37 mg/l) from the Shilabati river basin using a peristaltic pump (Reviara, India). The entire experiment was carried out at a room temperature of 30 C. The column leaching test was continued until saturation was reached. Samples were collected from the outlet in a 50ml plastic beaker at every 30 min of intervals and were tested in the water quality lab for the determination of Fluoride, pH, TDS, EC, turbidity and iron.

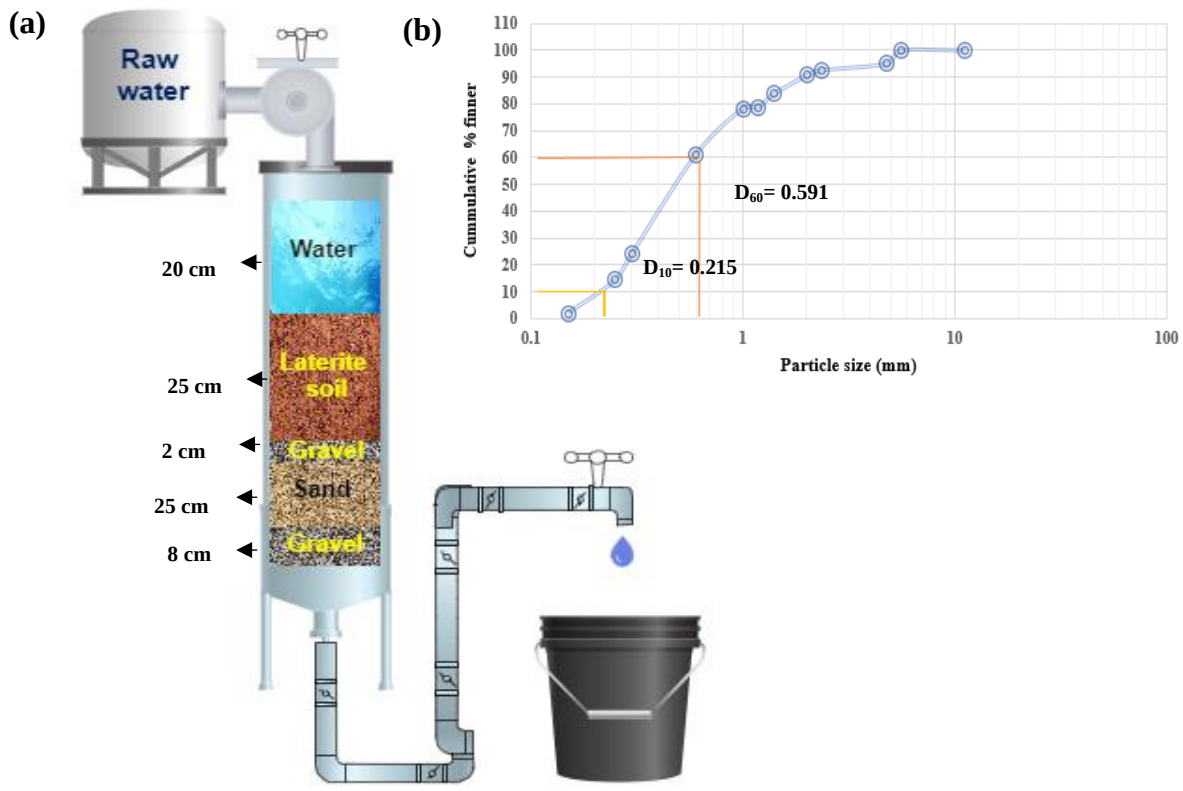

Fig. 7.2 (a) Schematic diagram of the fixed bed column used in laboratory; (b) Particle size distribution of sand for determination of effective grain size

7.1.5.7 Modeling of breakthrough curves

As adsorption dynamics were familiar and well-understood, many practical features were taken into consideration during operation of the column leaching test. Examples include sorbent capacity, operating life time, regeneration time, and ultimate regeneration time (Sarkar et al. 2006). Column studies provide detailed insights into the mechanism of the filtration process. In the current study the fixed bed column was a continuous flow model. For analyzing fluoride adsorption on the kaolinite-lithomarge-laterite (red) within the fixed bed column, the Bohart-Adams, Yoon-Nelson, and Thomas models were used (Yahya et al. 2022). It is imperative to use such models while designing fixed bed adsorption systems. The Bohart-Adams Model describes the first part of the column breakpoint curve. Bohart-Adams equation can be expressed linearly as follows (Eq.7.12) (Yahya et al. 2022, Thomson, 1944).

$$\ln {}^{C_t}/_{C_o} = k_{AB.} C_o t - k_{AB} N_o \frac{Z}{F} \qquad (7.12)$$

where: C_o is the effluent concentration, (mg/l); C_t is the effluent concentration,(mg/l); t is time, (min); k_{AB} is the kinetic constant of the Bohart-Adam model, (L/mg/min); F is the linear velocity, calculated by dividing the flow rate by the column section area,(cm/min); Z is the bed height of the column, (cm); N_0 is the saturation concentration, (mg/l).

The Yoon-Nelson Model is particularly effective for single-component systems and does not require any information about the adsorbent's type or properties. Yoon-Nelson equation was linearly expressed as Eq. 7.13 (Saha et al. 2021).

$$\frac{C_t}{C_o} = \frac{1}{1+exp^{(kYN_\tau - kYNt)}} \quad (7.13)$$

Where: C_t is the solution concentration at time t, (mg/l)); C_0 is the initial solution concentration, (mg/l); kYN is the rate constant, (min); τ is the time required for 50% adsorbate breakthrough, (min).

The Thomas model is generally used to describe the adsorption column performance and to establish breakthrough curves and is frequently used to determine the adsorption capacity of the material. The Thomas equation was linearly expressed as Eq. 7.14 (Saha et al. 2021).

$$C_t/C_o = \frac{1}{1+exp^{(mk_{Th}\, q_o) - k_{Th}\, C_0 t)}} \quad (7.14)$$

Where, C_0 is the solution concentration in the effluent, (mg/l); C_t is the solution concentration at time t in the effluent, (mg/l); k_{TH} is the Thomas rate constant, (L/min/mg); q_0 is the equilibrium compounds uptake per g, (mg/g); m is the mass of adsorbent, (g); Q is the flow rate, (ml/min).

7.1.6 Results and discussion

7.1.6.1 Point of zero charge (PZC)

An insoluble oxide/hydroxide has no charge on its surface at the point of zero charge (PZC). The PZC technique is widely used in the surface characterization of metal oxide and hydrogen oxide surfaces (Mahamood et al. 2011; Maliky et al. 2021). In the current study surface electrical properties of the natural adsorbent were determined by estimating the point of zero charge. An aliquot of 40 ml of Sodium Nitrate ($NaNO_3$ 0.1M) was used to determine the pH of the kaolinite lithomarge-laterite. The pH of the solution (2-13) was adjusted by adding 0.01 N HCl and 0.01 N NaOH to optimize different levels. The conical flasks were placed into the incubator shaker at 301K and at 150 rpm for 24 hours after adding 1 gm of kaolinite-lithomarge to each. For all the solutions, pH_0 was measured at the beginning, and pH_{24} was measured at the end of 24 hours after equilibrium stirring. Dataset from pH_0 versus pH_{24} was used to plot the final graph. The results showed no significant difference between the initial pH and the final pH at pHpzc. There was no deviation between the initial and final pH of the kaolinite lithomarge-laterite at 6.67 for red type and 6.51 for white type (Fig.7.3a and 7.3b). At pH 6.67 and 6.51 there was no drift, indicating that the adsorbent was electrically neutral, i.e., no surface charge. PZCs of kaolinite was also reported by Wieland and Stumm (1992) (Nur et al. 2017) to range between 4.0 and 7.5. According to Nur et al. (2017; Kumar et al. 2019) at pH levels lower than 6.67 and 6.51, adsorbent surfaces are positively charged, and at pH levels higher than 6.67 and 6.51, they are negatively charged. From this observation, it was evident that fluoride ions and adsorbent surfaces were electrostatically attracted and repelled.

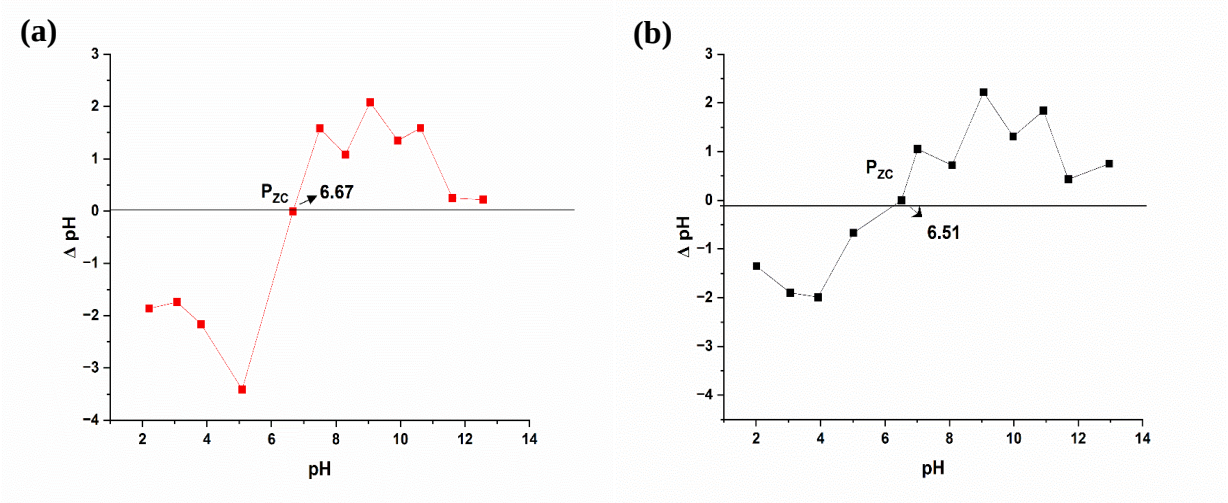

Fig. 7.3 Point of zero charge (P_{ZC}) for (a) red kaolinite lithomarge laterite soil and (b) white kaolinite lithomarge laterite soil.

7.1.6.2 Influence of particle size on fluoride adsorption

The size of particles also plays an instrumental role in the adsorption process (Kumar et al. 2019; Luo et al. 2019). Smaller particles (less than 3mm) of most adsorbents show high adsorption efficiency and could be applied in advanced treatments (Zhou et al. 2019). According to the previous studies, both the amount and kinetics of adsorption increased with decreasing particle size (Liu et al. 2017). To observe the highest removal efficiency, particle sizes between 0.15 mm to 11.2 mm were used for removal of 10 mg/l fluoride concentration and kept for 5 hours at 150 rpm with 10 gm of adsorbent dose at ph 6.5. With particle size of 2mm and smaller, the removal efficiency was 92.99% (white) and 95.49% (red) respectively (Fig.7.4a and 7.4b). Typical kaolinite lithomarge particles have more external surface area and more adsorption sites, resulting in faster adsorption kinetics. Further experimental studies were conducted using particles measuring 1-2 mm.

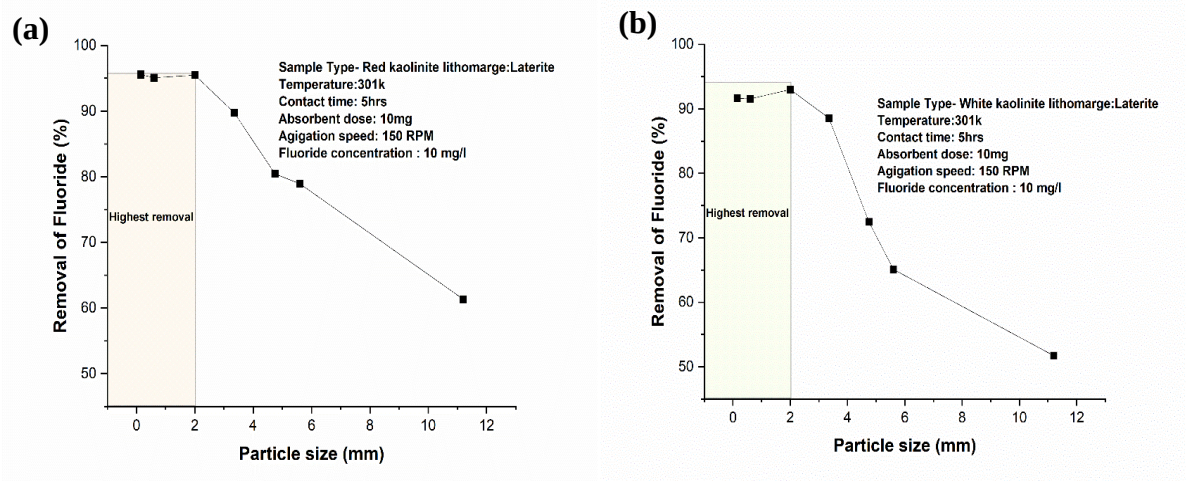

Fig. 7.4 Influence of particle size in fluoride removal efficiency for (a) red and (b) white type

7.1.6.3 Influence of stirring/agitation speed on fluoride adsorption

Figures 7.5a & 7.5b show the effect of agitation speed on fluoride removal efficiency. The experiment was conducted by adding 10 gm of kaolinite lithomarge (red and white) into the solution with fluoride concentrations of 2, 5, 10, and 20 mg/l and was kept in the incubator shaker for 5 hours at 301K under varying rpm (100, 200 and 250) at ph 6.5. In figure 7.5a and 7.5b, the adsorbent's maximum removal efficiency was at 200-250 rpm for red laterite and 100-200 rpm for white laterite. The results showed that the rate of adsorption increased with agitation speed for red laterite soil (Fig. 7.5a). It was observed that the % removal efficiency for fluoride ions was much lower at the lower stirring speed of 100 rpm. It can be argued that such variations in contaminant ion removal are due to insufficient contact between the pollutant ions and hydroxide flocs at low stirring speeds, which slows down the removal process (Das et al. 2022). As turbulence increases, the thickness of the boundary layer around the materials diminishes due to decreased surface tension. Fluoride adsorption per surface area of the white type increased weakly with increasing agitation rate (Fig.7.5b). It was found that the removal efficiency of white type adsorbent on fluoride was not that much influenced by the degree of agitation speed. As the white types are soft with plastic nature and are assumed to be the least reactive types (Ghaedi, 2021), they can be degraded by collisions resulting from high agitation speeds (Naje et al. 2017). In all the subsequent experiments, an agitation speed between 150 - 250 rpm was maintained.

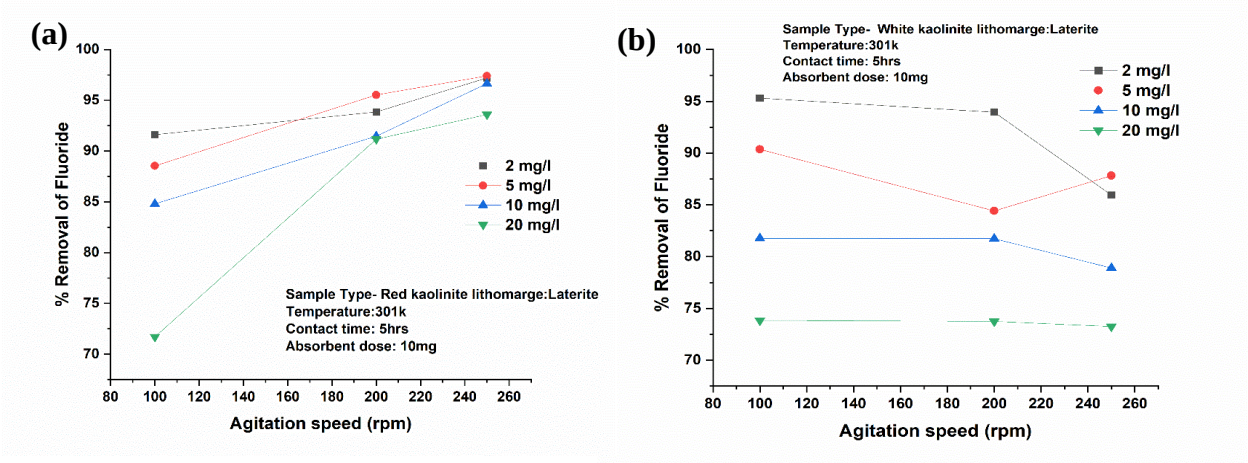

Fig. 7.5 Influence of agitation speed in fluoride removal efficiency for (a) red and (b) white type

7.1.6.4 Influence of contact time on fluoride adsorption

Fabrication of an economically viable fluoride removal system depends on the equilibrium time of the adsorption reaction. By adding the known amount of adsorbent dosage of 10 mg to each of 50 ml fluoride solution in measuring flasks containing 2 mg/l, 5 mg/l, 10 mg/l, and 20 mg/l of fluoride concentration, agitated by the incubator shaker at 200 rpm, and pH of 6.5 with varying contact time 50, 100, 150, 200, 250, 300 min and one after 24 hrs (1440 min) at 301k, the effect of contact time on the adsorption of fluoride was studied. The influence of contact time on fluoride removal efficiency was shown in Figures 7.6a and 7.6b. It was observed that with a constant dose of the Kaolinite lithomarge, the amount of fluoride adsorbed on the surface of the absorbent increased with time until the steady state was reached at 300 min which is the equilibrium time (Vinati et al. 2020; Liu et al. 2017). The maximum adsorption capacity recorded at the end of 300 minutes was found to be 97.54%

for the red type and 90.04% for the white type with a fluoride concentration of 20 mg/l. For further adsorption experiments, 300 min was considered as the optimum contact time for removing fluoride from an aqueous solution using Kaolinite lithomarge.

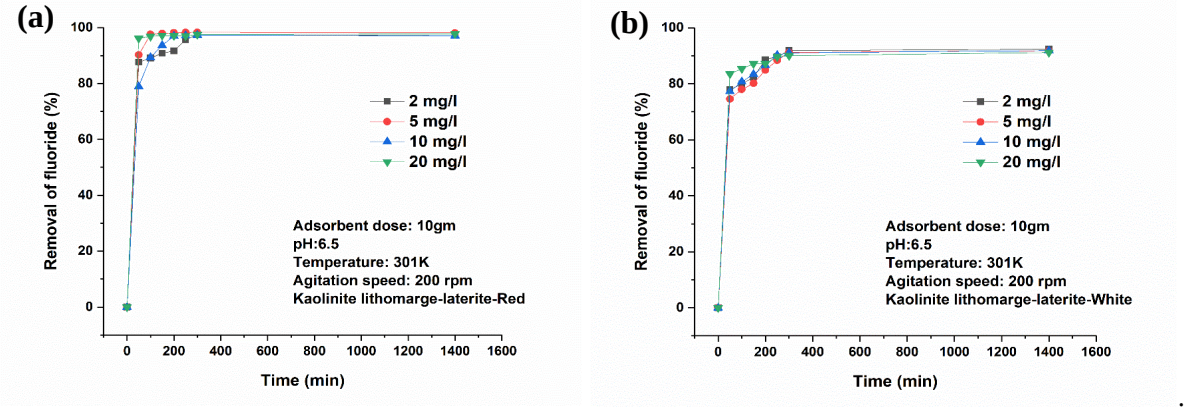

Fig. 7.6 Influence of contact time in fluoride removal efficiency for (a) red and (b) white type

7.1.6.5 Influence of pH of the solution

The pH of the material is one of the most critical factors affecting its efficiency and ionization. The pH of the adsorbent surface can influence its surface charge and acid or base ionization, resulting in a different adsorption action. Studies have shown that the greatest adsorption occurs at the isoelectric point (when the compound has zero charge) (Vinati et al. 2020). The presence of a positive charge on the surface of the synthesized adsorbent will favor the electrostatic attraction of fluoride ions under acidic conditions. Therefore, most materials cannot remove fluoride without prior acidification of the solution or treatment. Batch experiments were conducted at pH values of 4, 5, 6, 7, 8, 9 and 10 at 301k, 200 rpm and with 10gm of kaolinite lithomarge-laterite (red and white) and kept for 5 hrs. As shown in the figures (Fig. 7.7a & 7.7b), greater than 85-90% removal efficiency was obtained at pH 6.5-7 for white laterite and pH 6-6.5 for red laterite, after which it began to decline. Previous studies also showed such tendencies to be related to the fact that fluoride negative ions are attracted to surfaces charged with positive ions (Tomar et al. 2020; Srivastav et al. 2023). When the pH of the solution increased, fewer sites of positive charge were formed, resulting in a decrease in fluoride uptake. Since OH- and fluoride ions compete for binding sites in basic solutions, the higher concentration of OH- anions in the solution further reduced the adsorption capacity.

7.1.6.6 Influence of absorbent dose on fluoride adsorption

The amount of adsorbent used also influences the time-dependent adsorption process. With a fixed fluoride concentration of 2, 5 and 10 mg/L, the effect of variable dosage on removal efficiency was investigated. The experiment on the influence of adsorbent dosage (Kaolinite lithomarge-laterite-red and white) was conducted with varying dosages (4-20gm) at 301K, 150 rpm, at pH 6.50, shaken for 5 hrs. Adsorption efficiency was observed to vary greatly between the two types of adsorbent at varying dosages. Fluoride removal capacity increased with increasing dosage from 4gm to 20gm (Fig. 7.7c and 7.7d). Increasing adsorbent dosage increased the fluoride removal rates since more adsorption sites became available. Thus, a high adsorbent dose allowed fluoride ions to

access more adsorption sites, resulting in a higher removal percentage (Sartape et al. 2017; Das et al. 2020). The removal efficacy of the white type was approximately 62.45 % (2mg/l), 58.49% (5mg/l), and 51.3% (10mg/l) with 4gm of adsorbent, but with 20gm it went up to 91.89 % (2mg/l), 91.11 (5mg/l), and 90.01% (10mg/l). In contrast, red laterite showed effective removal of 91.91% (2mg/l), 89.51% (5mg/l), and 91.96% (10mg/l) fluoride with 4gm of adsorbent only. Red laterite soils are sometimes classified as mesoporous material with characteristics such as plasticity, dry cohesion, and intense capillarity thus having high adsorption capacity (Antunes et al. 2012).

7.1.6.7 Influence of temperature on fluoride adsorption

The temperature dependence of fluoride adsorption by kaolinite lithomarge was intentioned with the range of 294K -305K at pH 6.5, fluoride concentration 2 mg/L, 5mg/l, 10mg/l and 20mg/l, adsorbent dose 10 g, for 5 hrs at 200 rpm stirring speed. To explore the influence of temperature on the defluoridation of kaolinite lithomarge, the thermodynamic parameters were also estimated to study the defluoridation process (Fig.7.7e and 7.7f, and table 7.A1). Estimation of thermodynamic parameters, i.e., free energy change (ΔG°), enthalpy change (ΔH°), and entropy change (ΔS°), the equations represented below were employed (Gharbani et al. 2022).

$$\Delta G^{\circ} = -R \bullet T \bullet \ln(K_c) \tag{7.15}$$

$$\ln(K_c) = \frac{\Delta S^{\circ}}{R} - \frac{\Delta H^{\circ}}{R} \tag{7.16}$$

where K_c is representative of the adsorption equilibrium constant; R indicates the gas constant (8.314462618 J/mol/K), and T was indicative of the absolute temperature (K). The estimation of ΔH° and ΔS° was achieved by using the slope and the intercept of the Eq. (7.15& 7.16), which are obtained by plotting ln (K_c) versus 1/T in OriginPro. The positive ΔS° of the system also implies an increase in entropy at the interface between the solid-solution adsorption processes. Although the positive values of free energy change (ΔG°) favoring non-spontaneous or slow reactions at higher temperature but the calculated ΔH° (kJ/mol) and ΔS° (J/mol/K) indicate that the fluoride removal onto both the natural adsorbent (red and white) exhibited an endothermic nature, revealing that the increase of temperature promoted the capture of fluoride (Vinati et al. 2020). It was also consistent with the findings of the isotherm Temkin model (Table 7.2).

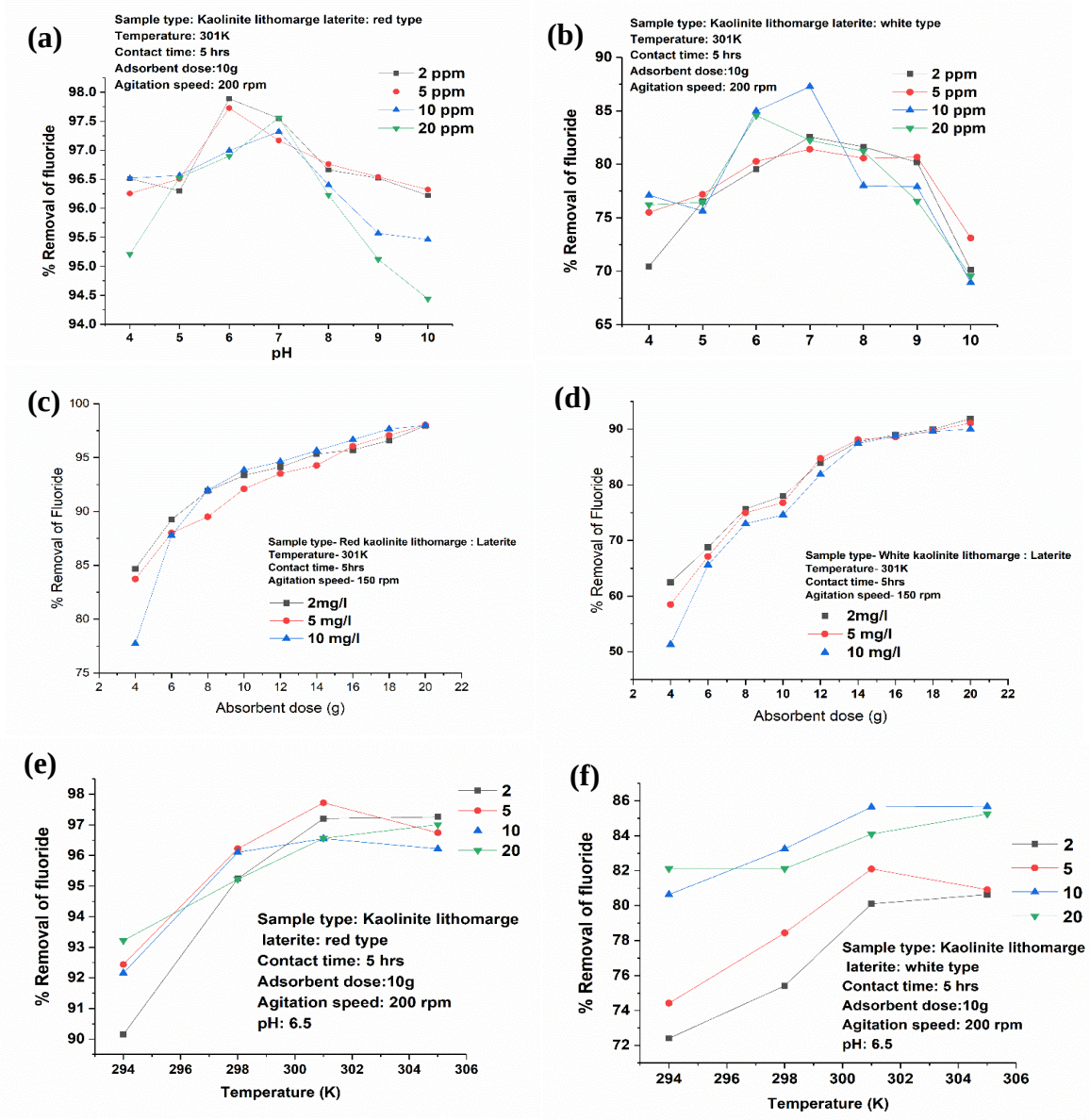

Fig. 7.7 Influence of ph of the solution (a) red and (b) white type; influence of adsorbent dose: (c) red and (d) white type and influence of temperature on fluoride adsorption: (e) red and (f) white type

Table 7.2 Thermodynamic parameters for the adsorption of Fluoride on Kaolinite lithomarge

Type of natural adsorbent	T (K)	2 mg/l			5 mg/l			10 mg/l			20mg/l		
		ΔG0 (kJ/mol)	ΔH0 (kJ/mol)	ΔS0 (kJ/mol K)	ΔG0 (kJ/mol)	ΔH0 (kJ/mol)	ΔS0 (kJ/mol K)	ΔG0 (kJ/mol)	ΔH0 (kJ/mol)	ΔS0 (kJ/mol K)	ΔG0 (kJ/mol)	ΔH0 (kJ/mol)	ΔS0 (kJ/mol K)
Kaolinite lithomarge laterite (Red)	294	7.54	95.38	300.08	6.83	65.47	201.39	6.95	51.89	154.7	6.54	60.17	182.72
	298	5.70			5.11			5.19			5.71		
	301	4.38			3.85			4.92			4.91		
	305	4.38			4.84			5.23			4.61		
Kaolinite lithomarge laterite (White)	294	10.59	32.91	76.04	10.34	27.91	60.24	9.50	27.04	59.96	9.23	16.93	25.94
	298	10.35			9.93			9.15			9.35		
	301	9.77			9.45			8.79			9.09		
	305	9.85			9.77			8.90			8.99		

7.1.6.8 Influence of initial fluoride concentration

As shown in Fig.7.8, the amount of fluoride adsorption decreases with an increase in the concentration of fluoride. It was observed that with an increase in the initial fluoride concentration from 2 mg/L to 20 mg/L, there was a decrease in the fluoride removal efficiency from 98.05% to 94.65% in the red type and 93.15% to 81.39% in the white type (Fig.7.8). Fluoride binding capacity of Kaolinite lithomarge was completely exhausted at higher fluoride concentrations. A low fluoride concentration can, however, result in a high ratio of surface active sites to total fluoride. As a result, the interactions between fluoride ions and the active sites on the adsorbent surface were sufficient for efficient fluoride removal. Kaolinite lithomarge red laterite collected from the above-mentioned region is a reddish-brown colored product of intense tropical weathering containing high quantities of iron oxides, oxyhydroxides and hydroxides, along with kaolinite and quartz, which attract more negative fluoride ions than white type (Ghosh and Guchhait,2015). It was also consistent with the findings of the EDX (Energy Dispersive X-ray Spectroscopy) study (table 7.5). A similar effect was observed during the uptake of fluoride on red mud and white mud, where a higher initial fluoride concentration decreased fluoride removal efficiency due to competition for the active adsorption sites (Vinati et al. 2020; Akafu et al.2019).

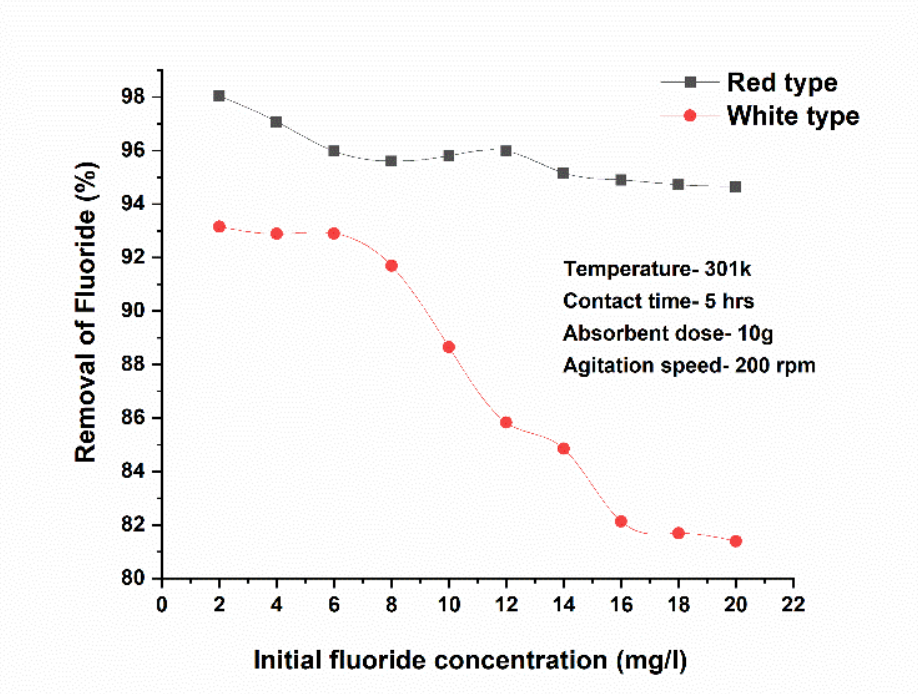

Fig. 7.8 Influence of initial concentration in fluoride removal efficiency for red and white type

7.1.6.9 Adsorption kinetics of fluoride

The nonlinear relationships between the adsorption capacities of Kaolinite lithomarge (red and white type) for fluoride removal and the contact time were plotted in Figure 7.9a-7.9f respectively. The experiment was conducted with fluoride concentrations of 2mg/l, 5mg/l, 10mg/l and 20mg/l, adsorbent dose 10g, at pH 6.5 with a stirring speed of 200 rpm for 5hrs. Single pollutant adsorption onto Kaolinite lithomarge rapidly increased within the first 50 min. After 300 min, the rates gradually became constant, and later reached equilibrium as a result of the limited surface sites of the adsorbent. To further investigate the adsorption capacity of the adsorbent, pseudo-first-order

(PFO) and pseudo-second-order (PSO) kinetic models were applied to describe the kinetic characteristics of fluoride adsorbed by Kaolinite lithomarge (red and white type). The kinetic parameters and correlation coefficients were presented in Table 7.3. For the adsorption experiments of single solutions, the experimental data were better fitted with the PSO kinetic model than the PFO kinetic model, and higher R2 values (0.99) were found in PSO for both the adsorbent and the calculated values of adsorption capacity by PSO were closer to the experimental values (Table 7.3). A strong chemical bond was established between fluoride ions and the active surface functional group of laterite soil (Ho et al. 1999). This result was also consistent with Rathore et al. 2016, which demonstrated that sorption obeys the PSO model when the initial concentration of the solute is not too high.

Furthermore, the intraparticle diffusion model (Tolkou et al. 2023) was evaluated by following the Eq. 7.11 to investigate the influence of diffusive processes (Fig.7.9e and 7.9f). As shown in Table 3, the parameters were adjusted to account for intraparticle diffusion in both soil types at different fluoride concentrations (2, 5, 10, 20 mg/l). Fluoride adsorption onto kaolinite lithomarge occurred in three stages according to the intra-particle diffusion plot in Figure 7.9e-7.9f. During the first stage, fluoride ions were attracted to the surface of the adsorbent due to adsorption on the boundary layer, and during the second stage, fluoride ions diffused into the pores (mesopores and microspores) of the adsorbent as a result of intraparticle diffusion. In the third stage, fluoride interacts chemically with the atoms within the particles, resulting in equilibrium adsorption. Experimental results showed that the correlation coefficient for red laterite was higher than that for white laterite. This indicates a greater amount of surface adsorption for red type and a slower diffusion rate of fluoride ions between the external and internal surfaces of the adsorbent.

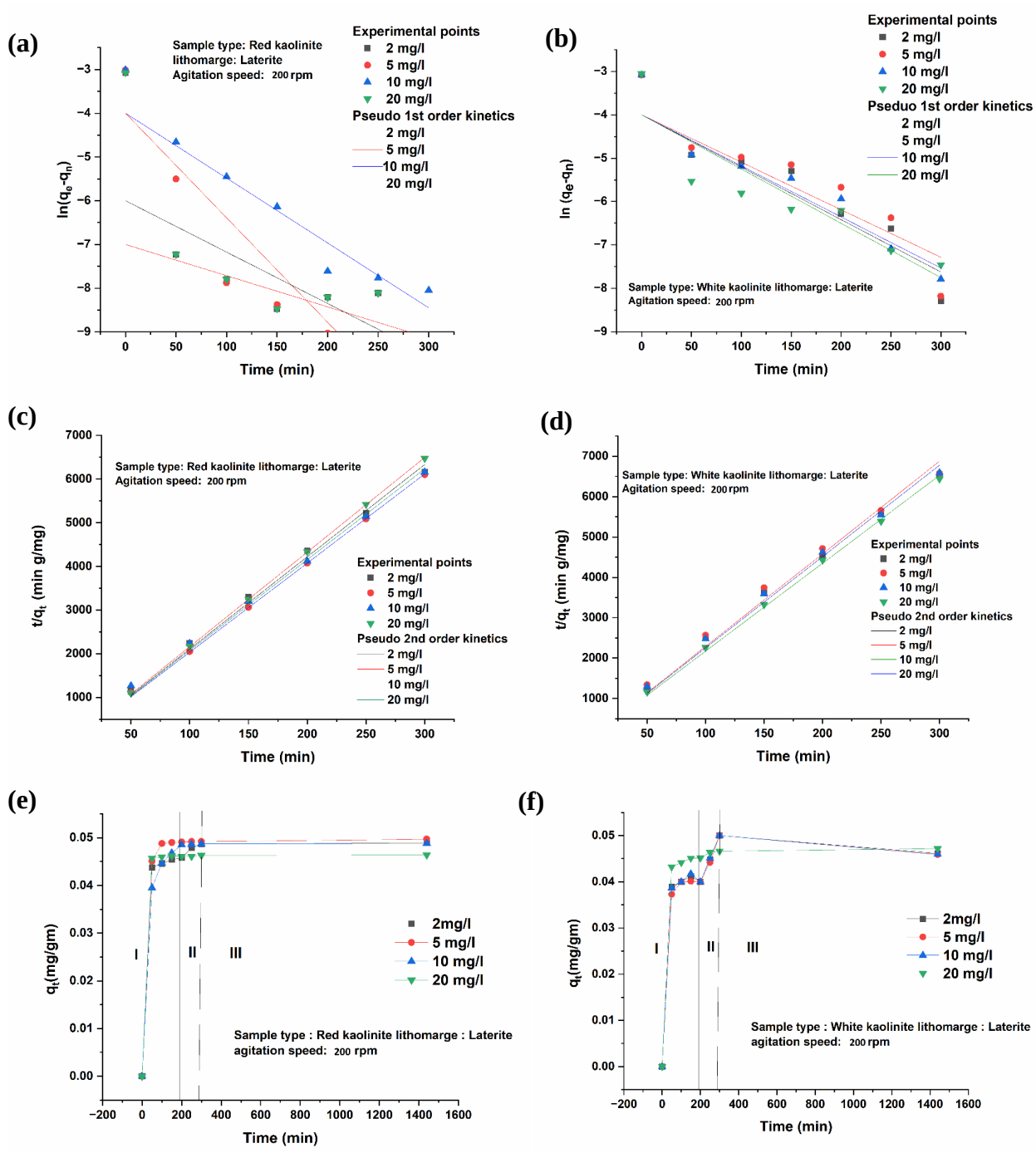

Fig. 7.9 Pseudo-first-order model for fluoride absorption onto (a) red and (b) white kaolinite lithomarge laterite soil; Pseudo-second-order model for fluoride absorption onto (c) red and (d) white kaolinite lithomarge laterite soil and Intra-particle diffusion model for fluoride absorption onto (e) red and (f) white kaolinite lithomarge laterite soil

Table 7.3 Results of rate kinetics model fit and correlation coefficients for fluoride adsorption

Kinetic equations Used for kaolinite lithomarge laterite red type	Parameters	Initial F^- concentrations (mg/l)			
		2	5	10	20
Pseudo-First Order	K_1 (sec)	-9.2×10^{-7}	-1.2×10^{-7}	-8.7×10^{-7}	-8.2×10^{-7}
	q_e,calculated (mg/gm)	0.031	0.0131	0.0057	0.0047
	q_e,experimental (mg/gm)	0.049	0.0492	0.049	0.0464
	R^2	0.6072	0.6072	0.6072	0.6072
Pseudo-Second Order	K_2 (sec)	0.0290	0.0949	0.0229	0.4237
	q_e,calculated (mg/gm)	0.0499	0.0499	0.0513	0.0464
	q_e,experimental (mg/gm)	0.0488	0.0492	0.0490	0.0464
	R^2	0.99997	0.99997	0.99997	0.99997
Kinetic equations	k_{id} (gm/ mg min $^{0.5}$)	4.78×10-4	3.30×10-4	8.81×10-4	5.24×10-5
	C (mg/gm)	0.03993	0.04417	0.03488	0.0454
	R^2	0.89079	0.51874	0.83535	0.73681
Kinetic equations used for kaolinite lithomarge laterite white type	Parameters	Initial F- concentrations (mg/l)			
		2	5	10	20
Pseudo-First Order	K_1 (sec)	-8.0×10-7	-7.6×10-7	-7.6×10-7	-6.7×10-7
	q_e,calculated (mg/gm)	0.03066	0.03352	0.02789	0.01642
	q_e,experimental (mg/gm)	0.04618	0.04589	0.04595	0.04718
	R^2	0.90287	0.87342	0.92091	0.77943
Pseudo-Second Order	K_2 (sec)	0.01913	0.01586	0.02088	0.05104
	q_e,calculated (mg/gm)	0.04817	0.04803	0.04770	0.04744
	q_e,experimental (mg/gm)	0.04618	0.04589	0.04595	0.04718
	R^2	0.99683	0.99504	0.99785	0.99945
Intra-Particle diffusion	k_{id} (gm/ mg min $^{0.5}$)	7.37×10-4	8.28×10-4	7.08×10-4	3.32×10^{-4}
	C (mg/gm)	0.03312	0.03087	0.03341	0.04086
	R^2	0.95982	0.96485	0.95982	0.95982

7.1.6.10 Adsorption isotherm

To determine the relationship between fluoride concentration and the adsorption capacity of the kaolinite lithomarge-laterite, adsorption isotherms models were used. In particular, three isotherm models were applied namely, Langmuir, Freundlich and Temkin model. Figure 7.10a- 7.10f display the fitting curves for Langmuir, Freundlich model and Temkin models. The calculated parameters of the adsorption isotherms were summarized in Table 7.4. It can be seen from the Table 7.4 that the model of Freundlich fitted the experimental results better than the Langmuir model with the higher coefficient of determination for red type (0.990) showing that the fluoride removal experiment was a multilayer adsorption on the surface of a heterogeneous adsorbent. The value

of **n** (red-1.44 and 1.685- white) according to Freundlich lying in the range 1–10 both confirmed the high bond strength between the adsorbate and the adsorbent, and it also confirmed the adsorbent surface was heterogeneous (Srivastav et al. 2013; Tolkou et al.2023).The R^2 value also indicates that Langmuir model was better suited to describe the adsorption behavior on kaolinite lithomarge-laterite of white type (R^2-0.974), suggesting a monolayer adsorption too (Sarkar et al. 2006). In contrast, the Temkin model had an R^2 value of 0.968 for white type, indicating that adsorption heat energy decreases linearly with surface coverage instead of logarithmically.

Table 7.4 Applications of the adsorption isotherms in the adsorption of fluoride

Isotherm Models	Isotherm Constants	Kaolinite lithomarge red laterite	Kaolinite lithomarge white laterite
Langmuir non-linear model	K_L (L/mg)	3.257	0.706
	q_m (mg/gm)	0.084	0.104
	R^2	0.966	0.974
Freundlich	K (gm)	0.087	0.039
	n	1.441	1.685
	R^2	0.990	0.961
Temkin	b_T (J/mol)	0.026	0.021
	K_T (L/mg)	20.964	9.133
	R^2	0.856	0.968

7.1.6.11 Continuous column experiment: Experimental setup and kinetic modeling of fixed-bed column leaching test

To improve community health and to prevent fluorosis in Shilabati River Basin, a simple water filter column with kaolinite-lithomarge laterite, sand and gravel media was fabricated to treat the groundwater with an influent fluoride concentration of 2.37 mg/l. For this experiment, 50 liters of fluoride-contaminated water (2.37 mg/l) was collected from a tube well (120 ft) located within the river basin and kaolinite lithomarge- laterite (red type) was collected from Garbeta badland of Paschim Medinapore district, West Bengal (50 km from the fluoride contaminated zone). Firstly, water samples were collected from 11 village sites of fluoride-affected zones within the basin (Table 7.1). The ph of the water ranges from 5.65 to 6.68, TDS ranges from 86-610 ppm, fluoride concentration from 0.02 to 2.37 mg/l and iron from 0.05 to 5 mg/l. The site (Lakshmisagar Village 1-22°55' 48" N , 87°00' 52"E) having the fluoride concentration of 2.37 mg/l was considered in the column leaching test having the pH of 6.40, TDS-356 mg/l, EC-574 µS/cm, iron-1.22 mg/l, Turbidity- 0.56 NTU, temperature- 36.2°C, alkalinity -320 mg/l, sodium-73.04 mg/l, potassium -82.92 mg/l, calcium -40 mg/l, Sulphate -1 mg/l, phosphate-0.85 mg/l, magnesium -150 mg/l and chloride -104.93 mg/l. Most of the water quality parameters were within the acceptable limit as per WHO, 2011 and BIS, 2017 (Table. 7. A1). It was noted by the authors during the field survey that the water source is being used for domestic purposes by locals, who suffer from skeletal fluorosis and bone deformation (Fig.7.1c).

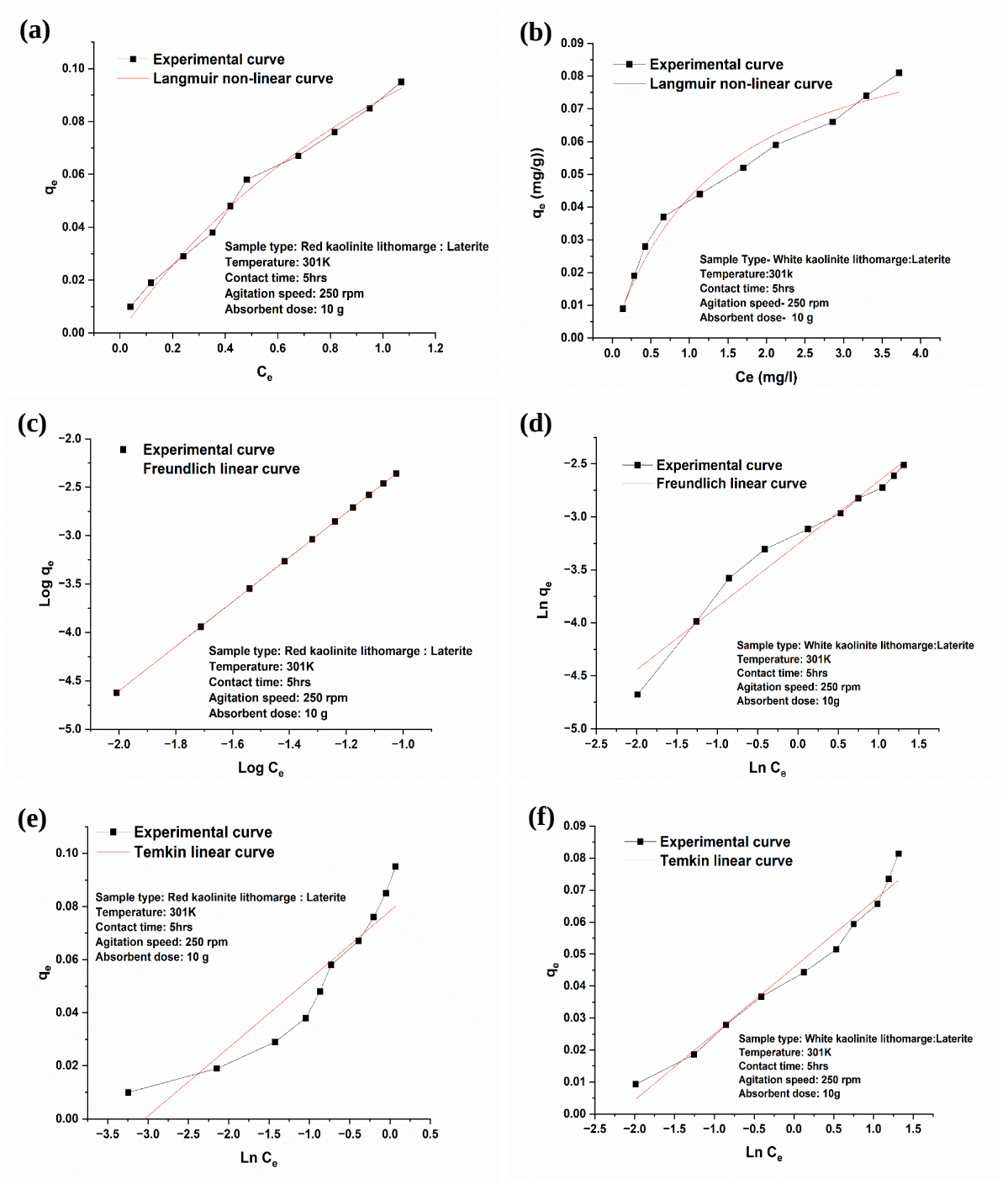

Fig. 7.10 Langmuir model for fluoride absorption onto (a) red and (b) white kaolinite lithomarge laterite soil; Freundlich model for fluoride absorption onto (c) red and (d) white kaolinite lithomarge laterite soil and Temkin model for fluoride absorption onto (e) red and (f)white kaolinite lithomarge laterite soil

A comprehensive general drinking water physicochemical analysis (pH, TDS, iron, turbidity, and EC) was conducted before and after the column leaching test at all the sampling intervals to assess the groundwater properties and suitability for consumption (Fig. 7. A1a-7. A2e). By plotting the acquired data, the breakthrough curve was used to estimate the column's performance. Column efficiency was studied in relation to metal ion concentration. Once the final concentration reached the acceptable limit (1mg/l as per BIS standard), the column

was stopped immediately after 73 hours. Observations showed that the breakthrough point was reached rapidly. The breakthrough point was observed after 3.5 hours or 210 minutes with a fluoride ion concentration of 2.37 mg/l. It was observed that the binding sites were occupied more rapidly with metal ions due to the competitive adsorption between the adsorbent and the adsorbate. To investigate the effect of interfering ions on fluoride removal, the experiment was carried out in the presence of fluoride ions and other coexisting ions mentioned above. Water quality analysis of all parameters was conducted with one sample taken after 60 minutes of outflow. It was found (Table 7.A1) that the percentage of fluoride removal was almost unchanged in the presence of the coexisting ion. Additionally, the concentration of a few parameters decreased after the filtration mechanism with a slight increase in pH (7.38). As a result of abundant mesopores and macropores coexisting within the hierarchical porous microspheres of the adsorbent, there is less competition between the ions (Wang et al. 2020). The favorable adsorption performance of Kaolinite lithomarge in the presence of competing anions makes it a suitable adsorbent for water treatment applications. Furthermore, the lower concentrations of coexisting anions occupying the active sites result in less powerful competitive adsorption and higher fluoride adsorption. The column was exhausted after 73 hours of continuous operation, demonstrating its effectiveness and sustainability in removing fluoride on a macro and micro scale. Initially, 97.13 percent of contaminants were removed within 30 minutes, which became 42.51% by 4380 minutes. At each sampling point pH, TDS, turbidity, and iron in the filtered water were analysed and found to be within acceptable limits for human consumption, however, EC slightly increased and turbidity was more than 1 NTU at the exhausting phase (Fig 7.11a- 7.11e). Approximately 26.28 liters of water passed through the adsorbent (459g). The maximum fluoride adsorption capacity (mg of the fluoride adsorbed) of the column at a given condition was calculated as 51.33 mg/g.

The breakthrough curves and the corresponding parameters of Bohart–Adams Model, Thomas model graphs and Yoon-Nelson model were plotted in fig. 7.A2a- 7.A2d and were summarized in table 7.5. The theoretical maximum dynamic adsorption capacities fitted by the Bohart–Adams Model and Thomas model graphs were 91.77 mg/g and 180.31 mg/g. Thomas model graphs and Yoon-Nelson model (R^2=0.87) had the highest coefficients of determination (R^2). Additionally, the results showed that the sorption capacities of the columns were higher than their respective batch capacities for the initial fluoride concentration (2 mg/l) as the amount of adsorbent was more (Tor et al. 2009). Therefore, kaolinite lithomarge laterite exhibited excellent dynamic adsorption of Fluoride, providing opportunities for Fluoride removal from groundwater and wastewater with high efficiency, convenience, and environmental friendliness. The adsorbent collection site in West Bengal is also one of the largest reserves of kaolinite lithomarge laterite, which needs to be conserved from external pollutants.

Table 7.5 Results of fixed bed column leaching test

Models for fixed bed column filter	Rate constants	Value
Bohart–Adams	k_{AB} (L/mg/min)	0.000189
	N_0 (mg/g)	91.773
	R^2	0.854
Yoon–Nelson	kYN (min)	0.00052
	τ (min)	5795.8
	R^2	0.868
Thomas	k_{TH} (L/ mg/min)	0.0002
	q_0 (mg/g)	180.313
	R^2	0.868

7.1.6.12 Characterization of the kaolinite lithomarge laterite: Before and after adsorption

The kaolinite-lithomarge-laterite soil is commonly found in humid tropical regions, and is primarily composed of hematite, goethite, quartz, and kaolin. On the top, it has hollow, vesicular, and botryoidal structures, which are reddish, whitish-brown, and chocolate in color. FESEM was used to demonstrate the changes in the surface morphology of the absorbent caused by the diffusion of fluoride onto both red and white types. The surface morphology of the kaolinite-lithomarge-laterite-red type of soil is illustrated in Fig.7.11a and 7.11b. This figure clearly shows that pseudo hexagonal crystal flakes dominate the white vein, which matches the morphology of red type kaolinite laterite soil. The edges of kaolinite flakes are usually ragged, but some have rounded edges. Based on the red matrix, the sample mainly contains kaolinite and tubular halloysite structures. The presence of large packets of porous soil particles was also evident in the samples (Latifi et al. 2016). The white kaolinite-lithomarge (Fig.7.11c and 7.11d) consists of a large amount of fragmented kaolinite that has irregular edges. Several halloysite morphologies exhibit clear curling directions, which might indicate a close association with platy kaolinite (Mitra et al. 2015). In laterite soil, microspores and mesopores also serve as active adsorption sites. As shown in Fig.7.11b and 7.11d the flaky form of soil particles has changed into a flocculating structure. Furthermore, the morphology changes at the edges of soil particles, and sufficient white compounds were caused by fluoride diffusion and are attached to soil particles together, making the voids in the soil less obvious. Additionally, white lumps were observed on the surfaces of soil particles. Figure 7. A3a-7. A3b shows the FESEM of fluoride mixed laterite sludge taken from the column bed filter system. The morphology and surface heterogeneity of the material changed significantly after fluoride loading. As a result of fluoride loading into the soil, crystal formation was evident in the images. Fig.7.12a- 7.12d and the table 6 depict the EDX mapping of different element analysis and confirm the presence of silicon, iron Aluminium etc. in the Kaolinite lithomarge-laterite (red and white). Further, the energy peaks on EDX spectra (Fig.7.12b-7.12d & Fig. 7. A4) in comparison to the native EDX spectra of Kaolinite lithomarge-laterite (red and white) confirm the successful adsorption of fluoride onto the adsorbent.

Table 7.6 EDX elemental analysis of red and white kaolinite lithomarge laterite soil

Element	Compound	Kaolinite lithomarge red laterite		Kaolinite lithomarge white laterite		Kaolinite lithomarge red type from fixed bed column (Weight %)
		Before adsorption Weight %	After adsorption Weight %	Before adsorption Weight %	After adsorption Weight %	
Silicon	SiO_2	66.22	92.09	49.03	65.14	69.24
Aluminium	Al_2O_3	20.17	4.22	37.30	25.80	13.77
Iron	FeO	10.05	3.04	3.00	4.61	13.76
Titanium	K_2O	2.32	0.31	9.14	4.01	2.04
Potassium	TiO_2	1.24	0.32	1.53	0.42	1.19
Fluorine	F	-	0.03	-	0.02	0.26

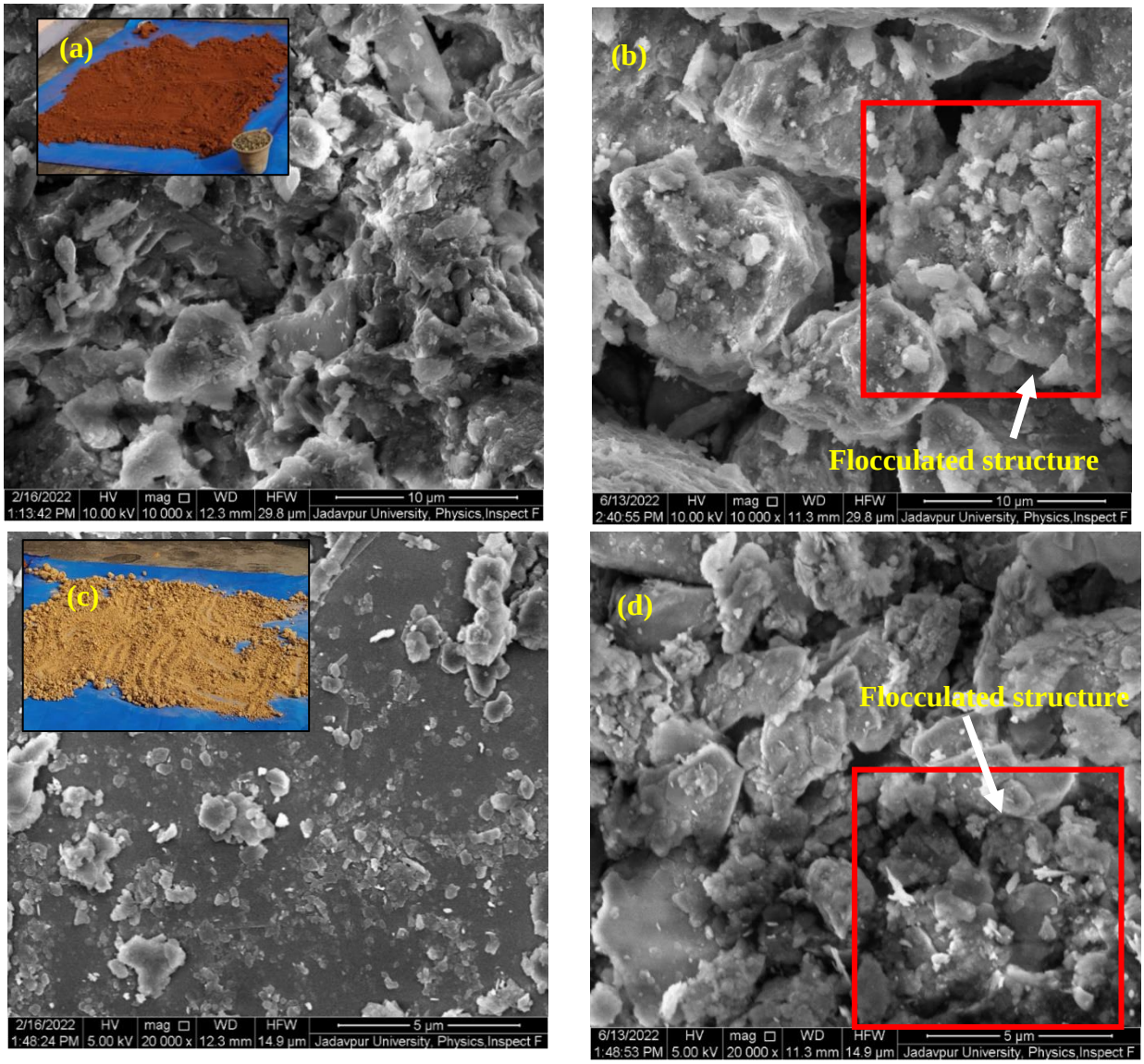

Fig. 7.11 FESEM characterizations of red and white type, (a) Red kaolinite lithomarge laterite-before adsorption; (b) Red kaolinite lithomarge -after adsorption; c) White kaolinite lithomarge –before adsorption and d) White kaolinite lithomarge – after adsorption

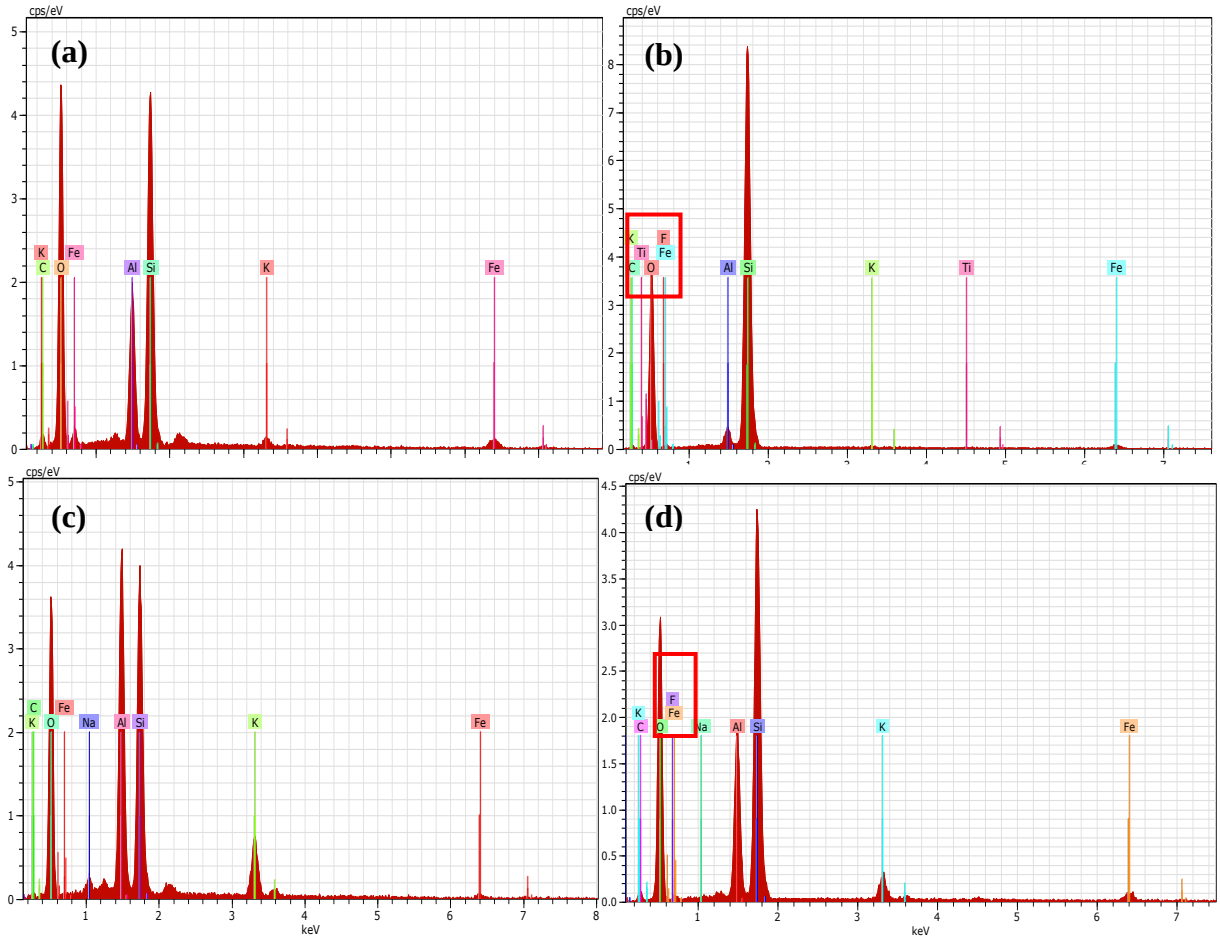

Fig. 7.12 EDX spectra of red and white laterite soil adsorbent, (a) Red laterite-before adsorption; (b) Red laterite-after adsorption (c); White laterite –before adsorption (d) and White laterite- after adsorption

Fourier Transformation Infrared (FTIR) spectral data is a simple way to gain an understanding of the octahedral, tetrahedral, and hydroxyl structural units of minerals and clays. It involves the identification of functional groups in clay minerals and compounds based on their Infrared (IR) spectra characterization and whose features could easily identify the structural groups within the clay and minerals. Figure.7.13a-7.13d and Figure 7. A5 show the FTIR spectra of the adsorbent before and after fluoride adsorption. From the FTIR analysis, the peak at 3695.6 cm-1 and 3622.39 (red) and 3695.6 and 3620.39 (white) signifies the AI-O-H stretching. The OH group of AI, Fe, and Si comes within the range of these values (Pepper et al. 2017). Such ranges signify condensation of OH stretching vibration, and stretching vibration of Si-O and have a wide peak. The peak value at 1872.88 for both types shows the C=O stretch of anhydride group. The peak at 1612.49 (red) and 1610.56 (white) for both types can be due to the presence of inner layers of H2O molecules and is associated with H-O-H bending of water. The peak for the range 1000-600 specifies the presence of Si-O-Fe, AI-OH, and Fe-OH band stretching. The peak at 538. 14 (red) and 536.14 (white) signify the presence of Fe-O band stretching. The FTIR peaks of the three laterite samples (red, white, and fixed bed column) after absorption were shifted indicating that hydroxyl and carbonyl participated in the experimental process as the removal of fluoride directly depends on the persistence of these sites on the laterite (Liang et al. 2014; Saeed et al. 2015). Besides the shift of peaks, the occurrence of new peaks was observed indicating the interaction between the fluoride and metal ions in the absorption process. The carboxyl, OH, and the electrostatic properties of kaolinite lithomarge-laterite encourage faster adsorption. The

adsorptive performance of fluoride was also significantly affected by the crystalline form of Alpha SiO_2 of trigonal structure and Alpha Al_2O_3 of hexagonal structure according to the X-Ray Diffraction (XRD)(Fig.7.14a and 7.14b) .The broadness of the peaks in the XRD pattern aligns with the following remarks from Liang et al. 2017, that approximately 80% (by weight) of adsorbent are crystalline, while the remaining 20% are amorphous materials. The possible absorption mechanism (Fig.7.14c) can be written as follows (Equation 7.7-7.21) (Jiang et al. 2021).

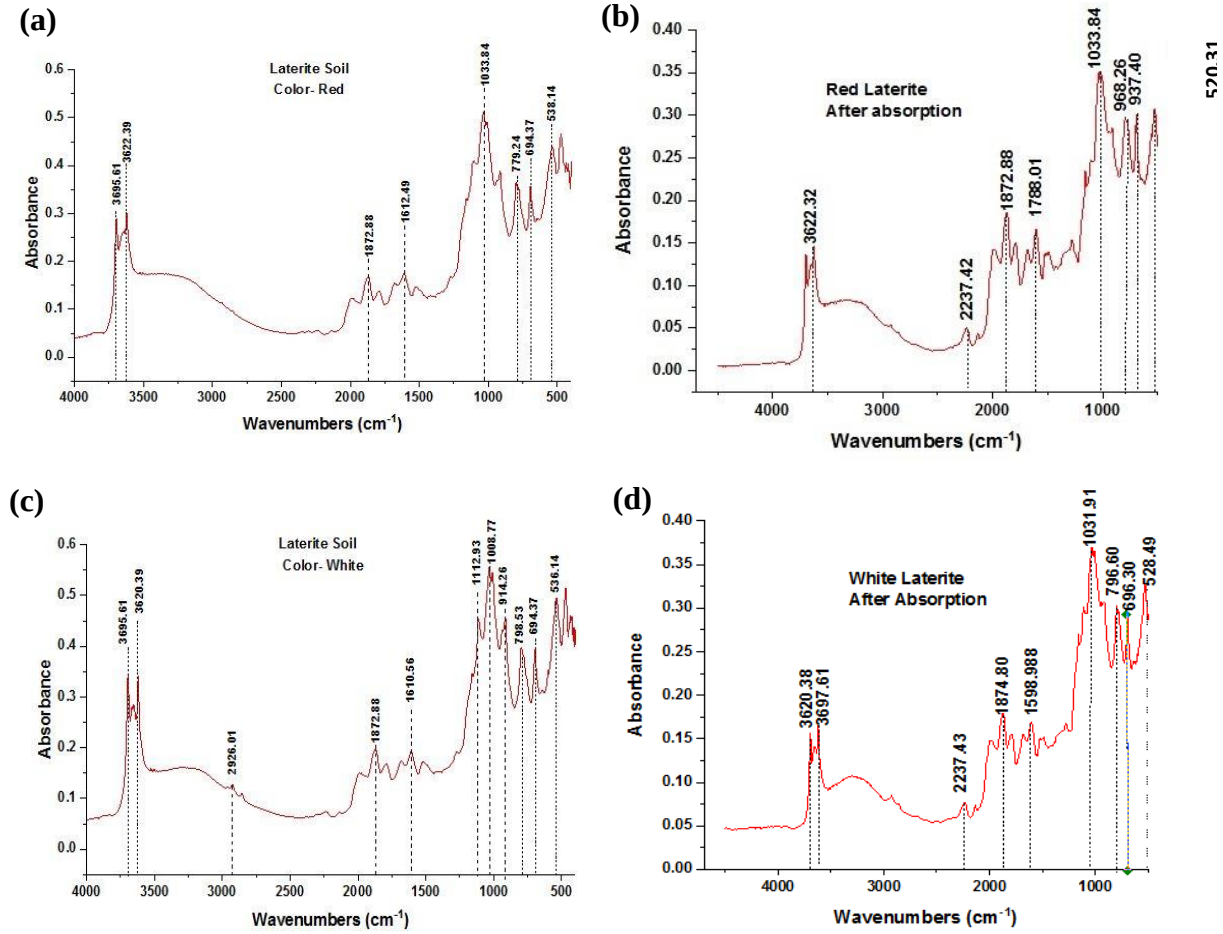

Fig. 7.13 Fourier Transformation Infrared (FTIR) spectral data of (a) before and (b) after application of red kaolinite lithomarge laterite soil and (c) before and (d) after application of white kaolinite lithomarge laterite soil

$$SiO_2 + F^- \leftrightarrow SiF + O_2 \quad (7.17)$$

$$Al_2O_3 + H^+ \leftrightarrow Al_2O_2 - OH^+ \quad (7.18)$$

$$Al_2O_3 - OH^+ + F^- \leftrightarrow Al_2O_2 - OH^+F^- \quad (7.19)$$

$$Al_2O_2 - OH^+ + H^+ \leftrightarrow Al_2O_2 - OH^+_2 \quad (7.20)$$

$$Al_2O_2 - OH^+ + F^- \leftrightarrow A_2O_2 \leftrightarrow OH^+_2F^- \quad (7.21)$$

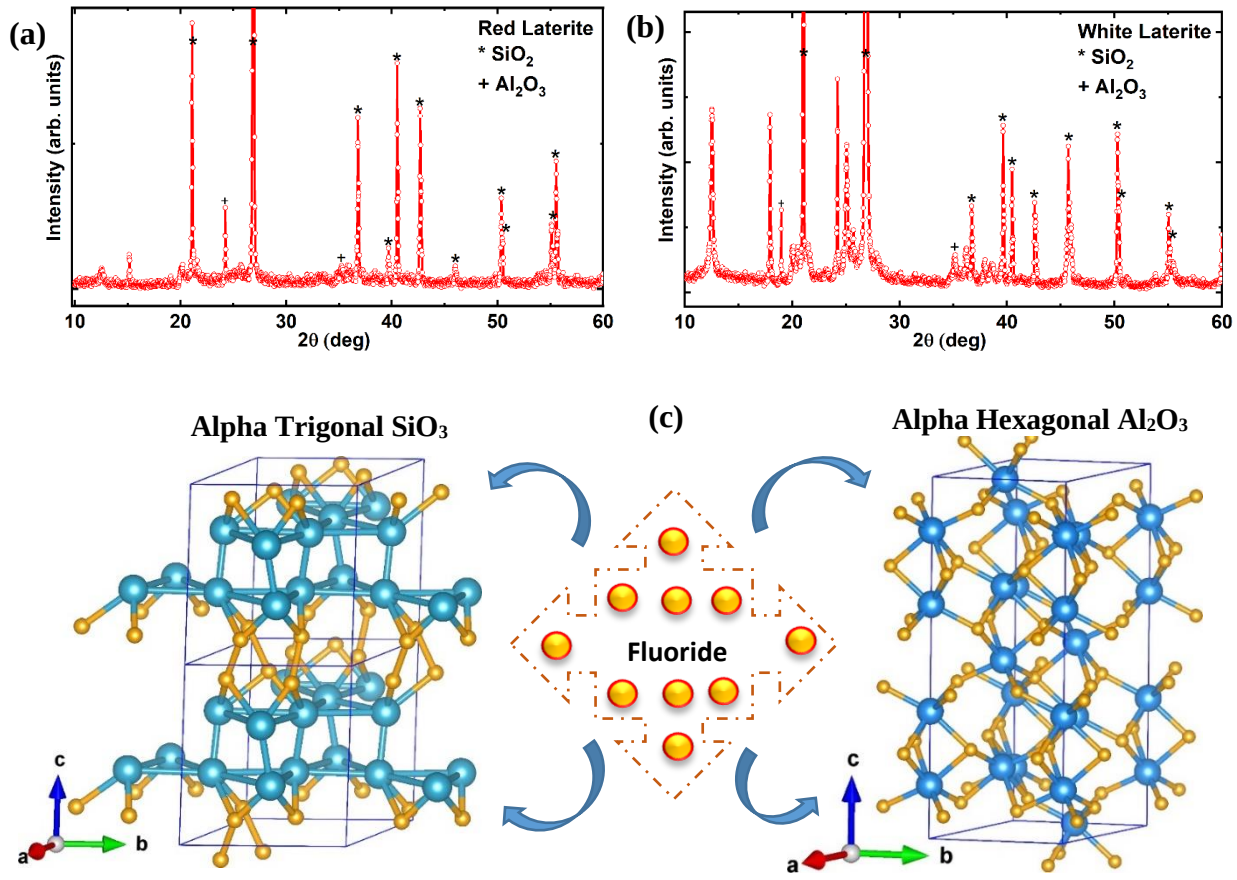

Fig. 7.14 X-ray diffraction pattern of kaolinite lithomarge of (a) red and (b) white type and (c) possible mechanism of fluoride adsorption on Alpha Trigonal SiO_3 and Alpha Hexagonal Al_2O_3 pattern revealed from XRD data.

7.1.6.13 Regeneration studies on the used natural adsorbent

Regenerative capability of the adsorbent is an essential characteristic of a successful economic adsorption operation. Regeneration experiments were conducted by initially washing the adsorbent with mild base solution 0.01 N NaOH and acid solution 0.01 HCl. At four consecutive cycles, the absorbent was successful in removing fluoride ions from synthetic contaminated water. Fig.7.15 presents the contaminant removal potential of the kaolinite lithomarge (Red and white type) in a series of regeneration (adsorption-desorption) cycles. In the fourth stage, the fluoride removal efficiency reached 82.30 % for red types and 72.1% for white types (Fig.7.15). It was also verified by EDX that a negligible concentration of fluoride was found in the sludge and residue of the first cycle which confirmed the recyclability of this natural adsorbent and its effectiveness for fluoride removal on a local and industrial scale. However, the decrease in fluoride removal efficiency by the natural adsorbent after every regeneration cycle could be caused by the chemisorption of previously adsorbed fluoride that wasn't completely removed from the adsorbent during wash. The chemisorption process involved a strong chemical bond between the kaolinite lithomarge and the fluoride, which made regeneration difficult and decreased the adsorbent's reusability (Vardhan et al. 2016).

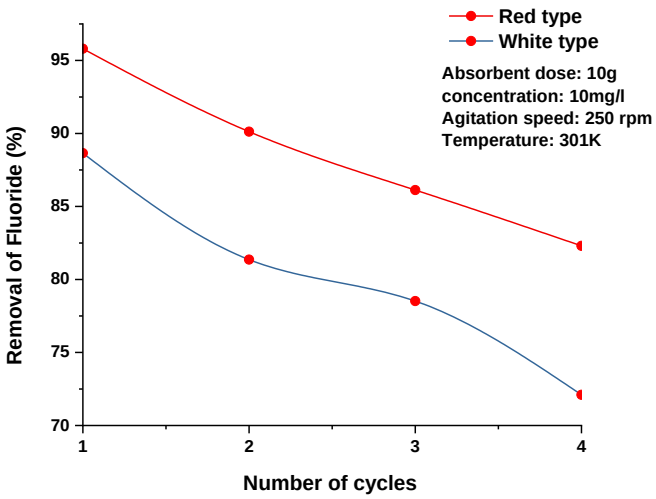

Fig. 7.15 Reusability study of red and white kaolinite lithomarge-laterite

7.1.6.14 Performance comparison of the natural adsorbent with others

From the comparison of adsorption capacities of various adsorbents in the literature listed in Table 7.7, it could be concluded that kaolinite lithomarge (red and white type) has performed comparatively well in defluoridation. In contrast to most of the adsorbents reported in the literature, kaolinite lithomarge-laterite (red and white type) exhibited a higher adsorption capacity for fluoride which is purely natural and did not need any modification prior to the filtration. The drawbacks of most of these methods include relatively low removal efficiency, high operation and maintenance costs, secondary pollution (production of toxic sludge, etc.) and complicated treatment procedures. Few studies have investigated the simultaneous adsorption of fluoride on natural adsorbents. As a result of the natural incorporation of multivalent ions in the form of their oxides (silica-alumina) in kaolinite lithomarge, enhanced adsorption capacities towards fluor ide was obtained. According to the experimental observations, the chosen low-cost natural adsorbents will be effective in removing hazardous fluoride ions from water at a large scale in a sustainable way.

Table 7.7 Comparison of various adsorbents and their potency for fluoride removal

Absorbent type	Natural adsorbent/adsorbent collected from environment	Synthetic adsorbent/Anthropogenically prepared	Chemical treatment required	Removal efficiency (%)	Experiment conducted with real groundwater	Testing of general water quality parameter after filtration	Reference
Euphorbia mayurnathanil stem	√	×	√ (Modified with $FeCl_3$)	98.62%	×	×	(Giri and Mishra, 2023)
Biochar of Moringa oleifera	×	√	×	85%	√	×	(Gourai et al. 2023)
Clinoptilolite zeolite	√	√	√ (Modified with cationic surfactant Hexadecy Trimethyl Ammonium Bromine.)	89.7%	√	×	(Ebsa,2023)
Rice husk-biochar	×	√	√ (Modified with $ZnCl_2$/$FeCl_3$)	Zn/Fe-BC: 99.01% and Zn-BC 91.90%	×	×	(Kumar et al. 2023)
Corbula trigona shell powder	√	√	√ (Modified with H_3Po^4)	89.0%	√	×	(Aw et al. 2022)
Coal fly ash	×	√	√ (modified using NaOH and $FeCl_3$)	92.0%	×	×	(Ranasinghe et al. 2022)
Black mustard husk ash	×	√	×	87.0%	×	×	(Jadhav and Jadhav, 2022)
Graphene oxide-ceria nanohybrid	×	√	×	85.0%	×	×	(Rashid et al. 2021)

Thermally Egg shells	×	√	×	70.0%	×	×	(Lee et al. 2021)
Kaolin-bentonite and magnetite nanoparticles composites	×	√	×	91.0%	×	×	(Annan et al.2021)
Ca-doped ferrihydrite	×	√	×	97.5%	×	×	(Ahmad et al. 2022)
Zirconium-based metal organic framework	×	√	×	79.0%	×	×	(Tan et al. 2020)
Porous MgO nanostructure	×	√	×	90.0%	×	×	(Borgohain et al. 2020)
Diatomaceous earth (diatomite)	√	√	√ (Modified with aluminium hydroxide solution)	89.4%	×	×	(Akafu et al. 2016)
NiAl-layered metal oxide film electrode	×	√	×	94.4%	×	×	(Bai et al. 2019)
Chitosan	×	√	×	87.0%	×	×	(Akbari et al. 2018)
Kaolinite lithomarge red and white laterite	√	×	×	Red type -98% White type- 90.01%	√	pH, TDS, EC, Iron, Turbidity	Current study

*** √= Yes; ×= No**

7.1.7 Future plan and development of community-based filtration system

In accordance with the World Health Organization (WHO), access to safe drinking water is vital for the protection of health and sustainability of life, as it is essential for drinking, cooking, and maintaining personal hygiene (Rivera et al. 2020). In light of global economic and ecological concerns, the current research is focused on using natural eco-friendly materials to remove fluoride contamination from groundwater in West Bengal. Kaolinite lithomarge laterite can be easily found as natural soil and does not require any typical modification or activation. In the current study, kaolinite-lithomarge-laterite was used as an absorbent for fluoride removal which is abundantly found within a distance of 50 km from the fluoride-affected zone of Puruliya and Bankura district, West Bengal, India. Laboratory experiments conducted with real water with fluoride concentration demonstrated the potential of this device to produce consistently fluoride-free water irrespective of fluoride concentration and speciation. Operational and maintenance costs of this defluoridation unit are very low as no chemicals and energy supply are required. In the laboratory-developed filter, the column pipe and valves are made up of one component and the cost is Rs. 400 or 4.83 USD. As the kaolinite lithomarge-laterite is abundantly found in the Garbeta Badland, of West Bengal, India, its valuation is zero. The market price of sand and gravel is Rs. 150 per 50 kg (Rs.3 or 0.036 USD per kg). The sand and gravel can also be used from the Shilabati river basin. In the current study, 501g of sand and 300g of gravel were used to filter 26.28 liters of water. Thereby the cost of sand and gravel to filter that much amount of fluoride-contaminated water can be calculated as (Eq.7.22)

$$\frac{(501+300)}{1000}(\text{kg}) \times 3(\text{Rs. per kg}) \approx \text{Rs. } 2.40 \text{ or } 0.029 \text{ USD} \qquad (7.22)$$

Hence the cost of sand and gravel media per liter of filtered water is 2.40/26.28 = Rs. 0.091 or 0.011 USD. According to the Accelerated Rural Water Supply Programme report, 2000 (ARWSP), Government of India, water demand for drinking and cooking in Indian rural areas is 3 LPCD (Litres per Capita per Day) and 5 LPCD i.e., 8 LPCD in total. Considering a family of 4 members, annual drinking and cooking water demand can be calculated as 8*4*365= 11680 liters. Therefore, the total cost of filtration using a such system in one year can be calculated as, cost of pipes, valves etc. + cost of filter media = 400 + 11680*0.091= Rs. 1462.88 or 17.98 USD. Total cost per litre of filtered water is therefore 1462.88/11680 = 0.125 Rs/liter or 0.0015 USD/liter. A defluoridation unit comprising 200 liters to 500 liters plastic drums (market price of 200 liters drum-7.84 USD and 500 liters drums-10.27 USD) with a taping system can be fabricated using the same filtration mechanism, the schematic design of which was shown in Fig.7.16. Whereas the local household can opt for a bucket instead using drums or barrels to get fluoride free water with only 30 minutes of resting time. The fluoride exposure was estimated to be 11, 5 and 3 times higher than the ATSDR's (Agency for Toxic Substances and Disease Registry (ATSDR) MRL value for infant, children and adults where they are taking 0.18-0.11, 0.08-0.04 and 0.05-0.3 mg/kg/day fluoride within the river basin [40] where drinking water is the prime source. Thus, the present study addressed such a global issue and designed a cost-effective filtration unit that will also benefit the water resources planners to execute them effectively. Long-term field-testing of household-level fluoride removal systems will however be required to assess their effectiveness and sustainability. It is expected that fluoride removal community filter could provide a significant contribution to short-term/long term elevation of fluoride problem in rural areas of developing countries around the world.

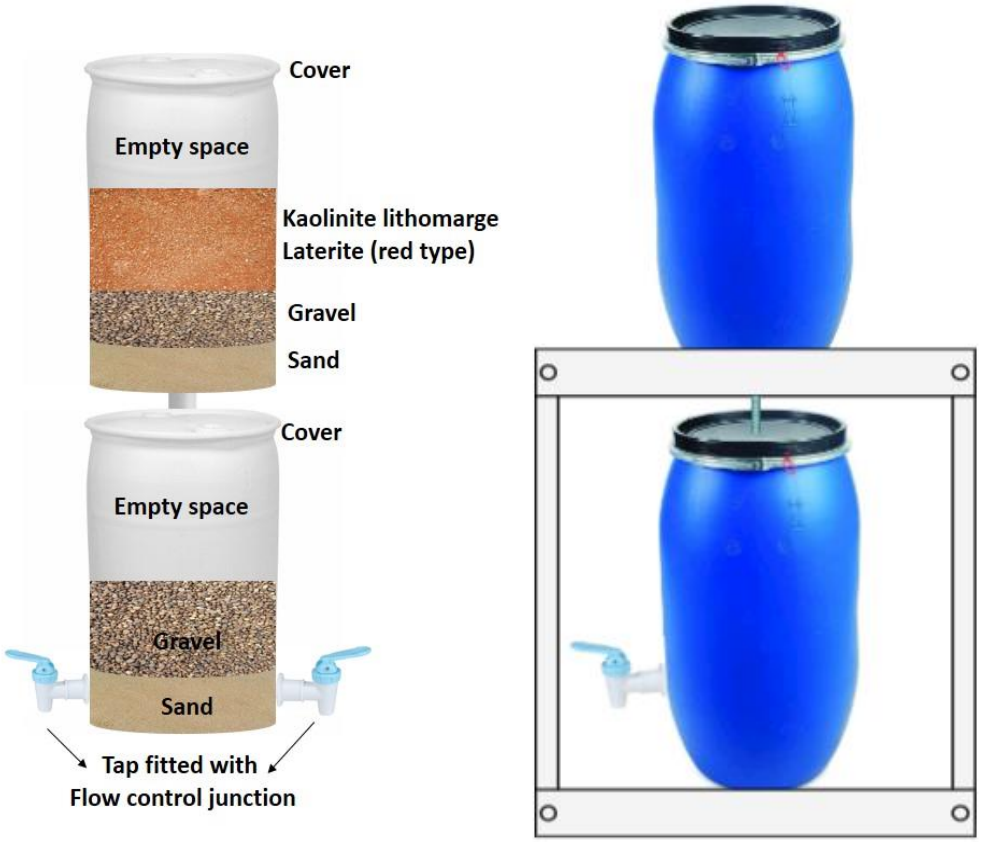

Fig. 7.16 Schematic diagram of the low-cost rural household filter for fluoride removal

7.1.8 Conclusion and Recommendation

As a novel type of natural adsorption material, kaolinite lithomarge showed significant potential in the elimination of fluoride by adsorption. Substantial work was done using synthetic water and real water to provide a low-cost defluoridation unit for the Shilabati river basin in West Bengal, which can be replicated worldwide. Kaolinite lithomarge has the advantages of high porosity, large specific surface area, abundant availability, and excellent removal efficiency of fluoride. The major findings of the study are as follows:

- The high removal efficiency of 98.05 % (red type) and 93.15% (white type) in synthetic fluoride solutions was achieved at optimum variable settings of 2.0 mg/L, 10g, 6.5, and 300 min for primary fluoride concentration, dosage, pH, and interaction time respectively.
- Langmuir isotherm model (R^2=0.97) and pseudo-second-order kinetic model (R^2=0.99) for white type and Freundlich isotherm (R^2=0.990) model and pseudo-second-order kinetic model (R^2=0.99) for the red type were fitted well with the experimental data suggesting chemisorption governed adsorption and indicated a monolayer (white) and multi-layer (red) adsorption mechanism. The adsorption process was also endothermic for fluoride removal.
- The kaolinite lithomarge could be potentially used in practical drinking water treatment, and the composite can be reused for four regeneration cycles with a removal efficiency of 82.30 % for red types

and 72.1% for white types. Dual-functional Kaolinite lithomarge can be designed. Kaolinite lithomarge is expected to be used in multifunctional platforms because it possibly can remove other negative ions effectively.

- Fluoride absorption into kaolinite lithomarge was also confirmed by FESEM, EDX, FTIR, and XRD analysis. EDX and XRD peaks confirmed the presence of SiO_2 and Al_2O_3 in significant amounts, which was the driving force for the high removal capacity.
- Using a single-column setup with sample water passing through Kaolinite lithomarge red type can effectively remove fluoride from groundwater, providing fluoride-free water at 0.0015 USD/liter. The models developed were also found to be reliable in the prediction of fluoride removal efficiency and adsorption capacity.

7.1.9 Limitation and Future Work

Based on the results of this study, a low-cost and easy-to-use community filtration system was fabricated to reduce the hardships of the local inhabitants in the Shilabati River Basin. The future work of the current study will rely on field demonstration and its suitability analysis. The biosafety of sludge to animals, plants, and mankind, will also be studied in depth. More attention will be paid to the large-scale synthesis of Kaolinite lithomarge. At present, the cost of Kaolinite lithomarge remains lower than any of the adsorbents as it is easily available in nature. The areas where this type of adsorbent is abundantly found (West Bengal) should also be protected from external contaminants (illegal dumping and littering). A study of this kind will encourage policymakers and water resources planners to successfully install the defluoridation unit within all fluoride-contaminated zones across countries with similar physiochemical conditions or necessary modifications.

7.2 Probing adsorption efficiency of low surface area hardwood biochar and its modification for an enhanced cationic (Fe+) and anionic (PO_4^{3-}) nutrient removal from aqueous solution

7.2.1 Introduction

Our water resources are becoming scarcer and degraded due to the increase in toxic and resistant synthetic organic and inorganic contaminants (Teixido et al. 2022). Inorganic contaminants like iron, arsenic, manganese, and chromium and organic contaminants like pesticides, herbicides, and animal and plant tissues from industrial production and agricultural processes can threaten ecosystems and human health (Devi et al. 2020). Iron and phosphate have been frequently detected in aqueous environments as a result of extensive groundwater exploitation (Katsoyiannis Zouboulis, 2006), with iron being used in automotive, infrastructure, iron and steel industries, machinery, and phosphorus in food, beverage, dye and fertilizer industries. Inappropriate discharge of these wastes can lead to cancerous growth and other health problems. Hemochromatosis occurs when a person absorbs too much iron from the food and water they consume (Ghosh et al. 2020). Furthermore, excess phosphorus causes the human body to shed calcium, causing our bones to become weak (Alenezi et al. 2020). Moreover, excessive phosphorus levels and calcium deposits can harm the heart, blood vessels, lungs, and eyes. Eventually, this has been linked to a higher risk of heart attack, stroke, or even death (Molenaar et al. 2014). Therefore, efficient iron and phosphate removal methods from natural and wastewater is needed urgently. Water treatment for ground and surface and waste water should adhere to the global consensus on decreasing carbon emissions and utilizing resources efficiently (Kamali et al. 2021). Biosorption, or adsorption by biomass, is an efficient, economical, and eco-friendly method for treating wastewater (Chan et al. 2020). Plant-based product/by-product (biomass) is ideal for biosorption of pollutants such as toxic heavy metals, organic compounds, detergents, pesticides, and other organic and inorganic pollutants since minimal processing is required. Therefore, they have the potential to be used in biofiltration systems (Teixido et al. 2022). There has been an increasing number of literatures on the use of biochar in water treatment. In particular, the use of biochar for the removal of persistent inorganic and organic pollutants from aqueous systems has been documented. There have been reports of organic contaminants sorbing and binding more strongly to biochar than to activated carbon commercially available (Geca et al. 2022). According to most studies aiming at achieving high removal efficiencies, feedstocks with higher surface area are preferred (Akhil et al. 2021). There is a strong correlation between temperature, time, and feedstock in determining the surface area. In addition to increasing hydrophobicity and surface area, increasing pyrolysis temperature (>600 °C) can increase the pH of biochar due to the enrichment of ash content and eventually can result in a pH increase in water, making it unsuitable for drinking (Gul et al. 2015; Enaime et al. 2020). Increasing pyrolysis temperature does increase the surface area of biochar and enhance its graphitization degree, but it primarily increases the number of micropores, which hinders rapid mass transfer. Many studies have shown that porosity increases to a certain extent, but adsorption capacity does not continue to improve, thus wasting energy and time (Shi et al. 2022).However, at lower pyrolysis temperature (<600°C), a biochar with smaller pores, smaller surface area, greater water-holding capacity, lower pH, and more oxygen-containing functional groups can be prepared which can make the biochar more effective in removing harmful pollutants in addition to being more energy and cost-efficient (Cox et al. 2012).Yet, most novel attempts have only investigated

the sorption or degradation of contaminants by high surface area engineered biochars in aqueous media. For the first time, the current study will apply a low cost low surface area pristine hardwood biochar over the most applied high surface area biochars (Table 7.8) for probing the removal capacity of selected organic and inorganic contaminants. Due to the lower surface area, simpler preparation method, and higher product yield, the torrefaction-char as an oxygen-rich-feedstock could be considered as a promising adsorbent. Many contaminants, such as phosphorus, magnesium, iron, etc., require surface functionalization rather than surface activation of the feedstock for efficient removal (Akhil et al. 2021). In order to achieve the desired outcome, metals or others can be used for functionalization rather than activation depending on the need for removal. Thus, in the current study the surface properties of hardwood biochar have been tailored using appropriate functionalization techniques to enhance adsorption efficiency for target contaminants and therefore to maximize environmental and economic benefits.

Table 7.8 Surface area of different biochars

Methodological reference	Type of biochar	Surface area (m2/g)
Estimated using Brunauer-Emmett-Teller (BET) test in the current study	Hardwood 500	6.87
	Corn straw 300	10.25
	Corn straw 500	15.18
	Wheat straw 400	17.99
	Wheat straw 500	64.97
Shen et al. 2019	Rice straw 500	22.83
Wang et al. 2018	Banana peel	98
Sigmund et al. 2017	Softwood biochar 500	30.81
Usman et al.2016	Conocarpus green waste	334.6
Wu et al. 2019	Bran, corn cob, rice straw mix	47.07

7.2.2 Research Gap and Novelty of Work

This study focuses on providing biofilters for iron and phosphate contaminated groundwater areas in India. Most areas of Eastern and Northeastern India suffer from elevated level of iron in drinking water (Gupta and Singh, 2019). In India, Northeastern states along with West Bengal, Bihar, Jharkhand, Assam, Uttar Pradesh, Madhya Pradesh, etc. are adversely affected by groundwater contaminated with iron (Chowdhury et al. 2022). Leaching from iron-bearing rocks and minerals is one of the main causes of iron in groundwater in these regions. It has been reported that iron concentrations in surface and ground water of India vary from 3 to 4 mg/L to 15 mg/L (Podgorski et al. 2022). The concentration of iron in the groundwater of West Bengal, India ranged from 2–10 mg/L (Sengupta et al. 2001). The Ganga River in Moradabad district, Uttar Pradesh, has been found to have iron concentrations up to 6 mg/L (Shah, 2022). A study conducted in Jhamarkotra, Udaipur, and Udaisagar lakes in Rajasthan found phosphate levels of more than 250 ug/l in surface and subsurface waters (Papineau et al. 2013; Das, 1999). However, the permissible limit of iron and phosphate for drinking water is 0.3 mg/L and 0.1 mg/l respectively (Khatri et al. 2017; WHO, 1997). The phosphate level in West Bengal was much higher (> 0.1 mg/l), causing eutrophication and the death of aquatic macro-invertebrates in the presence of low dissolved oxygen (Chakraborty, 2014). It is therefore important to treat water effectively in order to remove iron and phosphate and

produce safe and clean drinking water. Iron and phosphate removal methods such as supercritical fluid extraction (Anderson and Bruno, 2003), ion exchange (Khadse et al. 2015), aeration (Hashim et al. 2017), wetland treatment (Ma et al. 2020), and sequestration were widely used but are less effective in the removal of the contaminants from aqueous solution. The iron removal efficiency of these systems ranged from 40 to 80% (Khatri et al. 2017). Iron removal using Vyredox technology exhibited the lowest removal efficiency of 3.12% (Ouraddi, 2021). Due to the high capital investment in Vyredox technology and costs associated with supercritical fluid-based iron removal, these techniques have not been extensively used for iron remediation (Ahmad, 2012). In addition, the cost associated with methods based on membrane technology for phosphate and iron is very high (Paltrinieri et al. 2017; Abdullah, 2019). Recently bio-filtration systems for removing iron and phosphate are widely used in Europe, and there are a few water treatment plants in the United States and Canada, but they are almost unknown or very rare in Asian countries. However, phosphate removal using bio-adsorbent are common using rice husk (Ramola et al. 2021), wheat straw (Huang et al. 2022), corn straw (Li et al. 2022) etc. but they are costly and chances of phosphate leaching in to the solution is high. Herein, hardwood as new low surface area adsorbent for iron and phosphate removal has been introduced. To increase the surface functionalization of the feedstock as required by phosphate, Magnesium oxide (MgO) was used. Among the alkaline earth metal oxides, MgO is one of the most inexpensive and non-toxic. It has a strong affinity for phosphate, which is why it is widely used as a key component of phosphorus adsorbents (Liu et al. 2021). The novelty of the research is thus reflected by discovering and probing a new type of low surface area/ low cost adsorbent derived from hardwood waste to remove a positive (iron) and negative ion (phosphate) from aqueous solution so that it can be effectively utilized in future with suitable modifications.

7.2.3 Objective of the study

The objectives of this study were to (1) examine the adsorption properties of hardwood biochar and modified hardwood biochar for iron and phosphorus in water respectively, (2) find out the efficiency of the best modification way and the best preparation conditions for phosphate removal, (3) determine removal mechanisms and kinetics and (4) cost benefit analysis.

7.2.3.1 Research Design and Methodology

7.2.3.1.1 Materials used

The hardwood feedstock was used to cover a wide range of pore characterization, anatomical ultrastructure, and necessary modifications. In the current research low surface area hardwood biochar was used for iron removal and with modification it was used for phosphate removal from synthetic aliquot. The hardwood 500 (HW) biochar was purchased from the Oxford Charcoal Company as a very low-cost materials for remediating iron and phosphate contamination (Jiang et al. 2017). At the prior level it was washed to remove dirt, air dried for five days and then oven dried at a temperature of 100 °C for 24 hrs and was directly used for iron removal. The biochar was produced by using a traditional open fire stove method rather than a fixed temperature method, as a by-product of the charcoal burning on an open fire. The pristine biochar sample was manufactured through a slow-pyrolysis process of biomass at 500°C. All the chemical reagents like Ammonium iron (II) sulfate (Mohr's salt) $(NH_4)_2$ Fe $(SO_4)_2 \cdot 6H_2O$, Potassium dihydrogen phosphate anhydrous (KH_2PO_4), Magnesium chloride hexahydrate ($MgCl_2 \cdot 6H_2O$), Sodium chloride (NaCl) and Hydrochloric acid (HCL) was purchased from Sigma-Aldrich. In

addition, deionized water was obtained via Milli-Q gradient ultrapure water system installed at Williamson Research Centre, University of Manchester. Whatman Membrane Filter ME25 0.45µm 47mm, Fisherbrand polypropylene centrifuge 50 ml tubes and 2ml HPLC Vials - Lab Auto sampler Vials, screw cap red PTFE and white Silicone Septa and Fisherbrand Conical Polypropylene Centrifuge Tubes (15ml) were used in the study for batch adsorption test and contaminant quantification.

7.2.3.2 Synthesis of magnesium oxide loaded-hardwood biochar

Based on literature reviews (Ou et al. 2023; Oginni et al. 2020) and a few modifications and alterations, magnesium oxide-loaded hardwood biochar (MgO-Hardwood) was synthesized for phosphate removal to increase the surface area fo the feedstock. 50 g of pristine hardwood biochar of 500 µm -1.15 mm particle size was soaked in 1000 mL $MgCl_2$ solution containing 203.3 g of 1M $MgCl_2$ • 6H2O in a conical flask under mechanical stir. Latterly, the mixture was agitated at a room temperature (25°C) at 120 rpm for 12 hr following the suspension transfer in two 500 mL beakers. An aluminum wrap was used to seal the mouth of the beaker, and the mixture was allowed to stand for 24 hours. The excess water was filtered and the moisture was initially heated up at 100 ℃ (for the evaporation of moisture from biochar) for 8 hr. The pretreated biochar was put in a crucible and pyrolyzed in a laboratory chamber furnaces (Lenton ECF 12/4) with a preprogrammed heat rate of 10 ℃/min up to 500 ℃ for 1 hr. The treated biochar sample was naturally cooled overnight at a room temperature, stored in sealed bags and labelled as MgO-HW after being rinsed repeatedly with deionized water and dried overnight at 80 °C.

7.2.3.3 Microstructural, textural and elemental analysis: Characterization and analytical method

The bulk elemental compositions (Carbon, Hydrogen, Nitrogen, and Sulfur) of the HW and MgO-HW biochar samples were determined using CHN analysis, Thermo Flash Smart and Sulphur analysis by Thermo Flash 2000. The morphological structure of the HW and MgO-HW before and after adsorption were characterized by Scanning electron microscopy (TESCAN MIRA3 FEG-SEM) and the elemental content of both the samples were analyzed by energy dispersive spectrometer (Oxford Instrument Energy Dispersive X-ray detector (EDX) and analysed using AZtec and AZtecCrystal software. X-ray powder diffractometer (XRD) analysis was performed to quantify the degree of amorphous content and Crystallinity within the 2θ range of 5°– 80° using Benchtop XRD (multi sample holder) Bruker D2 Phaser and the crystalline phases were identified by DIFFRAC.EVA software. The total surface area (m^2/g), total pore volume (cm^3/g), micro pore area (m^2/g), external surface area (m^2/g), and micro-pore volume (cm^3/g) were estimated with the Brunauer-Emmett-Teller (BET) model using BET surface area analyser Micromeritics Gemini VII 2390a.The organic functional groups on the HW and MgO-HW surfaces were determined with a Fourier to transform infrared spectrometer with Diamond ATR (Bruker Invenio-S) and plotted in OriginPro.

7.2.3.4 Batch adsorption experiments

The benefits of hardwood biochar screening experiments were performed using synthetic iron and phosphate adsorption experiments at the Geotechnical Engineering laboratory in the Department of Mechanical, Aerospace and Civil Engineering, University of Manchester. 0.702 mg of Ammonium iron (II) sulfate was dissolved in 1

litre of deionized water to prepare 100 mg/l of iron stock solution and 0.143 mg of Potassium dihydrogen phosphate anhydrous was dissolved in 1 litre of deionized water to prepare 100 mg/l of phosphate solution for the batch absorption tests. Comparative experiments of iron adsorption were conducted by mixing different HW doses (0.01, 0.02, 0.05, 0.08, 0.1, 0.3, 0.5, 0.8 and 1g) with 2-30 mg/L iron solution, the mixed solution was agitated on an orbital rotational shaker at 250 rpm at 25 °C for 7 hr. The batch experiments of phosphate were performed by mixing MgO-HW feedstock (0.01, 0.03, 0.05, 0.08, .1, 0.5, 1 and 2g) with 50 mL working solution containing 2-30mg/l and agitated at 250 rpm for 15 hr at 25 °C. The adsorption kinetics of iron and phosphate were studied using various sampling time intervals (0, 50, 100, 150, 200, 250, and 300 min). The supernatant water was then collected and filtered using Whatman Membrane Filter (ME25 0.45µm 47mm) and the final concentrations of the solution were measured in order to determine the amount of iron and phosphate adsorbed by the HW and MgO-HW biochar using Inductively coupled plasma atomic emission spectroscopy (ICP-AES) and Ion Chromatography (IC) analytical at Manchester Analytical Geochemistry Unit. In order to visualize the after-adsorption effect, all solid samples were cleaned three times using ultrapure water and then oven dried at 100°C for 24 hours. For greater accuracy, all adsorption experiments were performed in triplicate. The iron and phosphate removal rate and adsorption capacity of HW and MgO-HW biochar at equilibrium condition was calculated by following the below algorithms (Zhang et al. 2023; Ou et al. 2023).

$$n = \left(\frac{C_0 - C_e}{C_0}\right) * 100 \qquad (7.23)$$

$$q_e = \frac{(C_0 - C_e) * V}{m} \qquad (7.24)$$

Where, n = contaminant removal efficiency by biochar feedstocks (%); C_0= initial contaminant concentration in the stock solution (mg/l); C_e = concentration of residual iron and phosphate at adsorption equilibrium (mg/l); qe = Adsorption capacity of equilibrium reaction, mg/g; V= volume of the stock solution (V= 0.05l) and m = mass of the feedstock (g).

7.2.3.5 Point of zero charge (pHpzc) analysis

NaCl solutions of 0.01 M were prepared at different pH levels (2-12). 0.5 g of absorbents (Hardwood and MgO-Hardwood) were added to the prepared solutions. The suspensions were incubated at 25°C and was shaken for 24 hours. Initial pH and the difference change in the pH was plotted to determine the point of zero charge (PZC). The PZC of hardwood and MgO-Hardwood was presented in figure 7.17a and 7.17b. A key reason for the alkaline nature of hardwood biochar is the presence of alkali and alkaline metals in feedstock that are not volatile during pyrolysis. Because Hardwood has a point of zero charge (PZC) of 8.44, a solution pH greater than 8.44 will result in the attraction of positively charged iron particles. The electrostatic attraction of iron and negatively charged functional groups on biochar strengthens the capacity of hardwood biochar to absorb iron (Qiu et al. 2021). In addition, MgO-HW has a point of zero charge (PZC) of 9.52, which implies that its surface will be positively charged in most natural aqueous conditions. A negatively charged phosphate can electrostatically bind to the surface of hydroxylated MgO when the solution pH is lower than MgO-HW's PZC (9.52) (Wu et al. 2019).

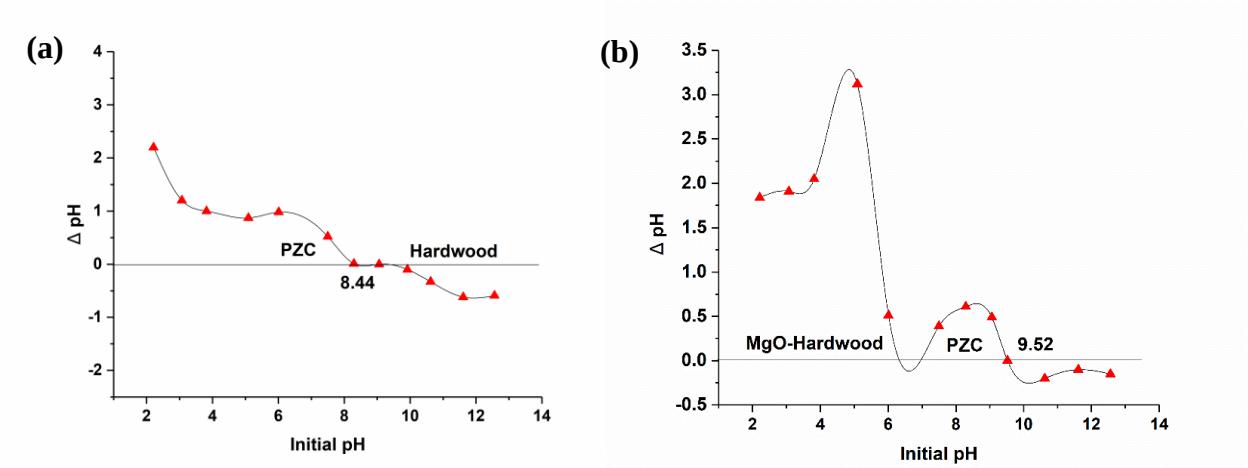

Fig. 7.17 Point of zero charge (PCZ) of hardwood and (b) point of zero charge of MgO-Hardwood

7.2.3.6 Adsorption isotherm dynamics

The isotherm study of the adsorption process will reveal how iron and phosphate interact with the solid adsorbent's surface (HW and MgO-HW) and will explain how the particle interact with the adsorbate molecules and reaches the equilibrium condition (Rajabi et al. 2022).To investigate the iron and phosphate adsorption behavior of HW and MgO-HW, the data of the isothermal adsorption experiments were fitted against five isotherm models including Dubinin–Radushkevich model, Langmuir, Freundlich, Temkin and Elovich model. Dubinin–Radushkevich (D–R), in 1946, proposed a theory of micro pore volume filling as opposed to layer-by-layer adsorption on the pore wall (Xiong et al. 2018) which describes the porosity of the adsorbents, and it is a temperature-dependent isotherm was used in this study to check the efficiency of HW and MgO-HW biochar. The Langmuir isotherm is a general isotherm model that is widely used in equilibrium studies. The monolayer adsorption on homogeneous solid surfaces was first described by Langmuir in 1918 (Chauhan et al. 2022). In addition to chemisorption, this theory can also be applied to physisorption (with a few restrictions). In the current study it was expressed in both the nonlinear and linear equations. The Freundlich isotherm model used in this study assumes that adsorption is heterogeneous and the sorption heat is not distributed uniformly on the adsorbent surface (Elmorsi et al. 2022). A Temkin isotherm model assumes that the adsorption heat (including all molecules in a layer) decreases linearly as the surface coverage of adsorbents increases without recognizing the effect of low and high concentrations was also used in the study to visualize the adsorption dynamics (Oumabady et al. 2022). Similarly, the Elovich model isotherm (Elovich and Larinov, 1962) was used in the present study, which assumes exponential growth in adsorption sites with increasing loading specifying a multi-layer adsorption mechanism (Shikuku et al. 2021). Mathematical expression and all the model parameters are summarized in table 7.9.

Table 7.9 Equilibrium isotherm models used for the iron and phosphate uptake onto hardwood and MgO hardwood

Two parameter isotherm model	Equation	Plots	Slope and intercept	Isotherm model constants	References
Langmuir isotherm	$\frac{C_e}{q_e} = \frac{1}{K_L q_{max}} + \frac{C_e}{q_{max}}$, $R_L = \frac{1}{1+K_L C_o}$	q_e vs C_e	Slope= $1/q_{max}$, intercept = $\frac{1}{K_L q_{max}}$	K_L(L/mg), q_m (mg/g)	Mabuza et al. 2022
Freundlich isotherm	$\log q_e = \log K_F + \frac{1}{n}\log C_e$	$\frac{1}{K_L q_{max}}$	Slope =1/n , intercept = $\log K_F$	K (g), n	Mabuza et al. 2022
Temkin isotherm	$q_e = \left(\frac{RT}{b_T}\right)\ln(K_T C_e)$	q_e vs $\ln C_e$	Slope = b_T, intercept= $b_T \ln K_T$	b_T (J/mol), K_T (L/mg)	Mabuza et al. 2022
Elovich isotherm	$\ln\left(\frac{q_e}{C_e}\right) = \ln K_e q_m - \frac{q_e}{q_m}$	q_e vs $\ln q_e / C_e$	Slope =	q_m (mg/g), K_e (L/mg)	Khamwichit et al. 2022
Dubinin-Radushkevich isotherm	$\ln q_e = \ln q_m - K\varepsilon^2$, $\varepsilon = RT\ln(1+\frac{1}{C_e})$, $E=\frac{1}{(2B)^{1/2}}$	ln q_e vs ε^2	Slope =	K (mol^2/kj^2), q_m (mg/g)	Ragadhita et al. 2022

7.2.3.7 Adsorption kinetic study

Adsorption kinetic models were applied to the experiment data to examine the rate of adsorption and the probable mechanism of adsorption on HW and MgO-HW feedstock (Potgieter et al. 2020). The adsorption kinetics of HW and MgO-HW was done by dispersing the chosen amount of adsorbent dose in 50 mL for iron (2, 15, 30 mg/l) and phosphate solution (2, 15, 30 mg/l). The mixture was mechanically shaken at a speed of 250 rpm and temperature of 25 °C. At predetermined intervals (0, 50, 100, 150, 200, 250, 300 minutes), the suspension was filtered through 0.45 µm membrane filters to analyze residual concentrations. Experimental results of adsorption kinetics were analyzed by using pseudo-first-order model, pseudo-second-order model, Elovich non-linear kinetic model and non-linear intraparticle diffusion model. Pseudo-first-order kinetic models were used to measure adsorption up takes with respect to time by calculating the difference between saturation concentration and adsorption amount (Ou et al. 2023). To understand biochar time step interactions with contaminants in the current study, a pseudo-second-order kinetic model assumption based on chemical sorption as a rate-limiting step was also used (Dada et al. 2021). Recently, the Elovich equation was applied to describe gas adsorption on solids as well as the adsorption of contaminants from aqueous solutions, and it was expressed in a nonlinear form (Benjelloun et al. 2021). To gain a better understanding of the adsorption mechanism and rate controlling steps affecting HW and MgO-HW adsorption kinetics, the Weber Morris non-linear intra-particle diffusion model was also tested (Lian et al. 2020). Table 7.10 summarizes the model parameters and mathematical expressions used in the kinetic study.

Table 7.10 Equilibrium kinetic models used for the iron and phosphate uptake onto hardwood and MgO hardwood

Kinetics models	Equations	plots	Kinetic model constants	References
Pseudo first order kinetics	$\ln(q_e - q_t) = lnq_e - (\frac{k_1}{2.303})t$	$\ln(q_e - q_t)\ vs\ t$	q_e (mg/g), K_1	Simonin et al. 2016
Pseudo second order kinetics	$\frac{t}{Q_t} = \frac{1}{K_2 Q_e^2} + \frac{t}{Q_e}$	t/Q_t vs t	q_e (mg/g), K_2	Simonin et al. 2016
Elovich kinetic non-linear model	$q_t = \beta \ln(t) + \beta\ln(\alpha)$	q_t vs t	α,β	Tabi et al. 2022
Intraparticle diffusion	$q_t = k_{id}t^{1/2} + k_0$	q_t vs t	k_{id} (gm/mg min $^{0.5}$),	Can, 2015

7.2.3.8 Error analysis

Nonlinear regression was used to estimate the fit of the adsorption isotherm and its related parameters (Kim and Kim, 2016). To measure the difference between experimental data and model predictions, Root-Mean-Square Error and Chi-square analysis were the two statistical methods applied in the current study. Generally, the better the predictive model performs, the lower its error value (Karunasingha, 2022). A minimization of the error function using OriginPro software were also used to determine the adsorption isotherm parameters. The two error functions were estimated based on the following algorithms (Table 7.11).

Table 7.11 Different error functions used for equilibrium isotherm/kinetics analyses

Error functions	Equation	References
The coefficient of determination (R^2)	$\frac{\sum_{i=1}^{n}(q_{e,exp} - \overline{q_{e,calc}})2}{\sum_{i=1}^{n}(q_{e,exp} - \overline{q_{e,calc}})\,2 + \sum_{i=1}^{n}(q_{e,exp} - q_{e,calc})2}$	Sampaio and Silva, 2005
Chi-square test	$\chi^2 = \sum_{i=1}^{n} \frac{(q_{e,exp} - q_{e,calc})2}{q_{e,exp}}$	Tallarida et al. 1987
Residual root mean square error (RMSE)	$\sqrt{\frac{1}{n-2}\sum_{i=1}^{n}(q_{e,exp} - q_{e,calc})\,2}$	Seo et al. 2015

$q_{e,exp}$(mg/g): Value obtained from the batch experiment, calc (mg/g): Calculated value from the isotherm for corresponding

7.2.4 Results and Discussion

7.2.4.1 Biochar screening for iron and phosphate adsorption

It is necessary to screen feedstocks prior to investigating the adsorption mechanism of iron and phosphate on low surface area biochar. Based on the availability of biochar, 5 types of low surface area (Table 7.8) feedstocks were used for the initial check and to carry forward the experimental process. As the phosphate and iron removal

efficiency of biochar may vary depending on the raw materials and modification methods used, this study compared the iron and phosphate removal efficiency of 5 types of biochar available in the laboratory including Hardwood 500 (HW 500), corn straw 300 (CSB 300), corn straw 500 (CSB 500), wheat straw 400 (WSB 400) and wheat straw 500 (WSB 500). A batch of 0.05 mg adsorbents (feedstock types) were individually added to 50 ml of 15 mg/l of iron and phosphate solution and the mixtures were shaken for 24 hrs at 250 rpm at a temperature of 25°C. The results (Fig 7.18a) have shown that for iron removal of 15 mg/l, the final concentration after 24 hrs was lowest for Hardwood 500 (0.12 mg/l) than the other feedstocks whereas highest for CSB 300 (8.1 mg/l). Consequently, hardwood 500 was used for iron removal in the subsequent experimental process, which represents a novel approach that has not been explored before. Application of hardwood biochar for iron removal will be more cost effective, effortless, less time consuming and free from energy consumption than techniques including electrocoagulation, zeolite softening/Ion exchange, filter media separation, vyredox technology, aeration etc. (Khatri et al. 2017). The results of the phosphate removal experiment have shown that phosphate concentration in the water increased dramatically in spite of adsorption by CSB 300, CSB 500, WSB 400, and WSB 500 (Fig. 7.18b). Research on adsorption materials prepared from agricultural residues has been reported in previous work (Li et al. 2022b; Ma et al.2019; Wang et al. 2018; Xinggang et al. 2016) but no studies confirmed that desorption of the excess phosphate in the contaminated solution (Ma et al. 2011). Phosphorus (P) has played a major role in the massive increase in world agricultural production in recent decades, and excessive amounts can have implications beyond the farmers' fields and can also be present in biochar (Ryan et al. 2012). Increase of phosphate in the solution may be reason for phosphors leaching from the feedstocks. Buss et al. 2018 evaluated the time-dependent release of P from the rice husk feedstock where the material was reduced to a smaller size (0.5–1 mm) using a sieve and extracted phosphate using deionized water which obtained significant results. To confirm the currents results, an EDX characterization study was conducted to check the elemental composition of the biochars. Furthermore, the hardwood feedstock successfully removed phosphate, but the removal was poor due to the low surface area (Fig. 7.18b). As hardwood biochar is not a result of agricultural output and are made from low-ash feedstocks having no or low level of P and K, and has the potential to enhance soil fertility and to enhance adsorption capabilities (Zilberman, et al. 2022). Therefore, before large-scale applications of biochar in environmental and water studies, the removal efficiency as well as the risk of P release from biochar must be evaluated simultaneously.

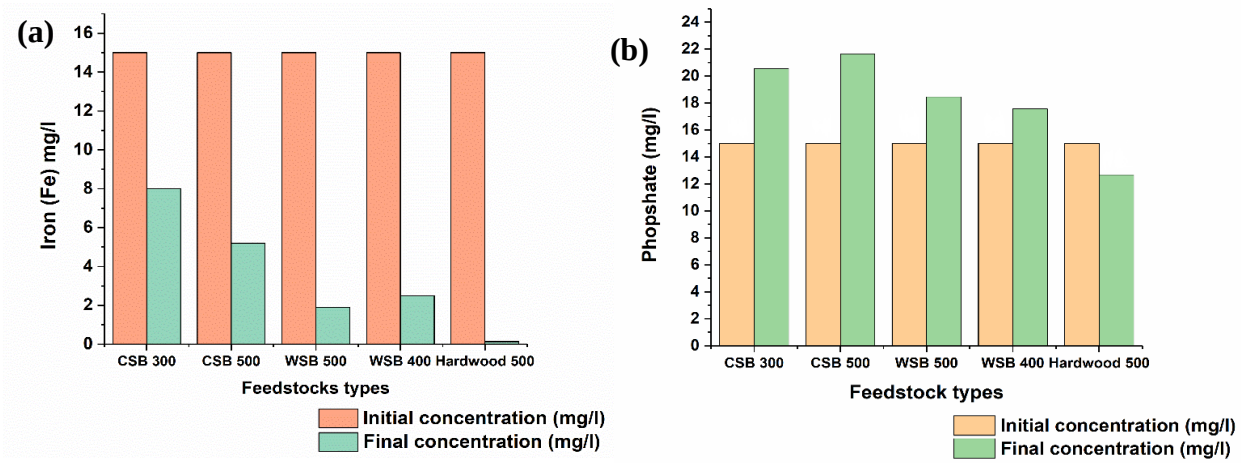

Fig. 7.18 Biochar screening for selection of biochar for (a) iron and (b) phosphate removal

7.2.4.2 Micro-structural and physico-chemical characterizations of biochars

Iron and phosphate are accessible to adsorption sites through the porosity and specific surface area of HW 500 and MgO-HW biochar, the characterization of which becomes significant to determine its ability towards adsorption capacity. The surface area and porosity of the HW 500 and MgO-HW were calculated using the Brunauer-Emmett-Teller (BET) equation as shown in table. The pristine HW 500 biochar was used for the iron removal study following the biochar screening. BET analysis showed that HW 500 biochar systems have a low surface area of 6.868 m^2/g with total pore volume of 0.009 cm^3/g, micro pore area of 2.781 m^2/g, external surface area of 4.087 and micro pore volume of 0.001 cm^3/g. A low surface area, small pore volume, smooth surface with metal ions close to zero may be responsible for the high iron adsorption capacity of unmodified HW 500 biochar. Additionally, biochars produced at low temperatures possess such characteristics with higher oxygen-containing functional groups and are better suited for removing inorganic contaminants (Enaime et al. 2020). Biochar that has been further pyrolyzed at high temperatures (500) tends to more functionalized, making it more suitable for organic contaminants like phosphate to be a sorbent. Thus, to enhance the surface properties and functionality of HW 500 it was impregnated with $MgCl_2$ 6(H_2O) at the rate of 10C up to 500 C (Arni, 2018). The BET results of the MgO shows that the surface area increased as much a 111.28 m^2/g with total pore volume of 0.074 cm3/g, micro pore area of 66.35 m^2/g, external surface area of 44.88 and micro pore volume of 0.031 cm^3/g (Table 7.12). With pyrolysis temperature of 500 °C, the pore volume of biochars also increased due to the release of generated volatile matter. Therefore, both porosity and active sites will contribute to phosphate adsorption using MgO-HW biochar (Qi et al. 2022). Zeta potential results showed that the pure HW 500 biochar nanocomposites had the highest concentration of bioactive ingredients at -20.71 mV, which is shown in Figure 7.19. Adsorption of positively charged iron molecules will be facilitated by the observed high negative electrostatic potential. Added MgO to biochar composites resulted in a zeta potential of -1.996 mV, indicating that the nanoparticles on hardwood biochar surfaces had been activated successfully. Zeta potential analysis revealed a fundamental basis for the increase in surface charge, facilitating high phosphate adsorption capacities (Venkatesh et al. 2022).

Table 7.12 BET Surface Area Analysis of Hardwood and MgO-Hardwood

Parameters	Hardwood	MgO- Hardwood (500 C - 10C/min)
Surface area (m^2/g)	6.868	111.228
Total pore volume (cm^3/g)	0.009	0.074
Micropore Area (m^2/g)	2.781	66.350
external surface area (m^2/g)	4.087	44.878
micropore volume (cm^3/g)	0.001	0.031

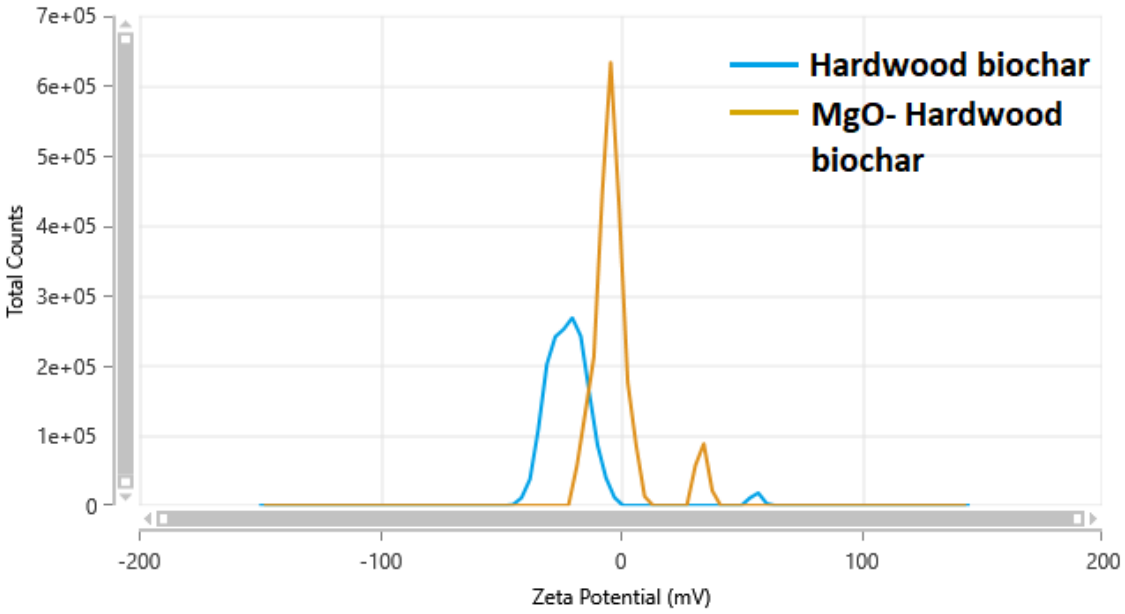

Fig. 7.19 Zeta potential distribution of hardwood and MgO-hardwood biochar

To study the surface morphology of HW 500 biochar and to investigate the effect of MgO modification on the microstructure of MgO-HW, SEM images were taken for the feedstocks. Fig.7.20a and 7.20b shows the surface characteristic structure of HW 500 and MgO-HW biochar. A few large pores were observed on the surface of HW500, which appeared to have a microporous structural network (Dutta et al. 2015). The HW 500 is designed to have tracheid, open pits, macropores and mesopores within the walls that provide a hierarchical network of porous surfaces and should improve ionic conductivity within the electrolyte (Yang et al. 2022). After the modification a few irregular crystals and nanoflake-like substances appeared on the MgO-HW surface, in contrast to the relatively smooth and clean surface of the HW 500. During the modification process, HW 500 blocks were crushed into small pieces due to vigorous stirring (Zhang et al. 2022). A layer of crystals appeared on MgO-HW, indicating that magnesium was successfully incorporated into the biochar. Additionally, MgO flakes were embedded in the surface of the HW 500 biochar during secondary carbonization. It is worth noting that MgO-HW had regular nano-MgO structures and flake particles with excellent micropore features, which could provide better phosphate adsorption performance. (Li et al. 2022). The rough surface and enlarged porosity of MgO/biochar are caused by magnesium ions impregnating the material, and a multitude of small and irregular particles are produced. Due to the emergence of pores in MgO biochar, there are more adsorption sites, which provide a channel for phosphate to diffuse into the material (Chen et al. 2022b). The results of the elemental compositions of the feedstocks from the EDX spectrum has been summarized in the table 6. Energy-disperse X-ray (EDX) results (Fig. 7.20c and 7.20d) revealed that HW 500 mainly contained C, N, O, Na, Si, S and K with high concentration of carbon (C) having 60%. In water treatment, carbon is increasingly used as a filter medium due to its capacity to remove iron and therefore hardwood can serve this purpose (Thinojah and Ketheesan, 2022). According to EDX analysis, magnesium (4.22%) and oxygen (39.54%) made up the flower-shaped nano-flakes of MgO-HW, which agrees with the chemical composition of MgO-HW feedstock (Table 7.13).

Further characterization of the HW 500 and MgO-HW with the XRD showed a change (Fig. 7.20e and 7.20f) and strong signals of Mg on the surface of modified biochar and the increase in the degree of Crystallinity (22.20%). In order to further probe the surface functional groups of the adsorbents mentioned above, ATR-FTIR conducted

at wavelengths from 500 to 4000 cm−1 were shown in Fig 7.21. From the FTIR spectra, significant differences could be observed between the HW 500 and MgO-HW feedstocks. The peaks at 2360 cm−1 indicated a carbon dioxide O=C=O stretching and a characteristic O-H bond of carboxylic group appeared at 1418 cm−1 and a weak band at 874 cm−1 indicated the –CH2 and C–H bond stretching vibrations for the HW 500 biochar. The band at 2360 cm−1 assigned as O=C=O bond stretching, which is derived from newly aromatized aromatic rings and carbonized groups for carbohydrate ring dehydration and cyclisation during pyrolysis (Chen et al. 2022b). Biochar-based nanocomposites containing MgO and Mg(OH)2 have also been confirmed by FTTR spectra of MgO-HW feedstock. A wide peak at 3363 cm−1 corresponded to asymmetric stretching vibrations of O-H groups while the decrease in the absorption band at 874 cm−1 can be the bending vibration of MgO (Jiang et al. 2022). The peak at 1615 cm−1 was also linked with the stretching vibration of N-O groups of cellulose chains (Lu et al. 2012).

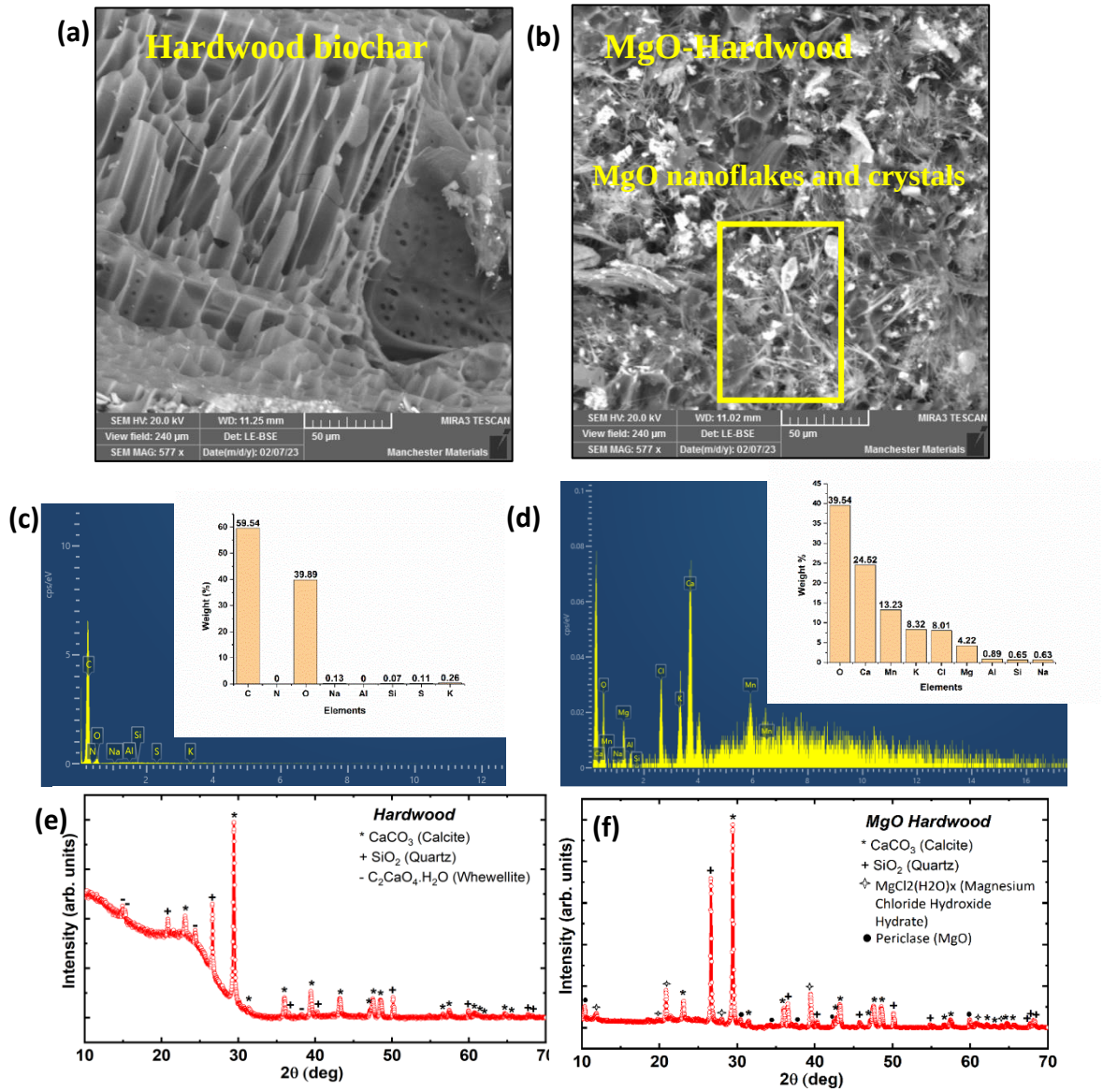

Fig. 7.20 (a) FESEM micrographs of hardwood; (b) FESEM micrographs of MgO-hardwood; (c) EDS spectrum of Hardwood; (d) EDS spectrum of MgO-Hardwood; (e) XRD Spectra of Hardwood and (d) XRD spectra of MgO-Hardwood biochar

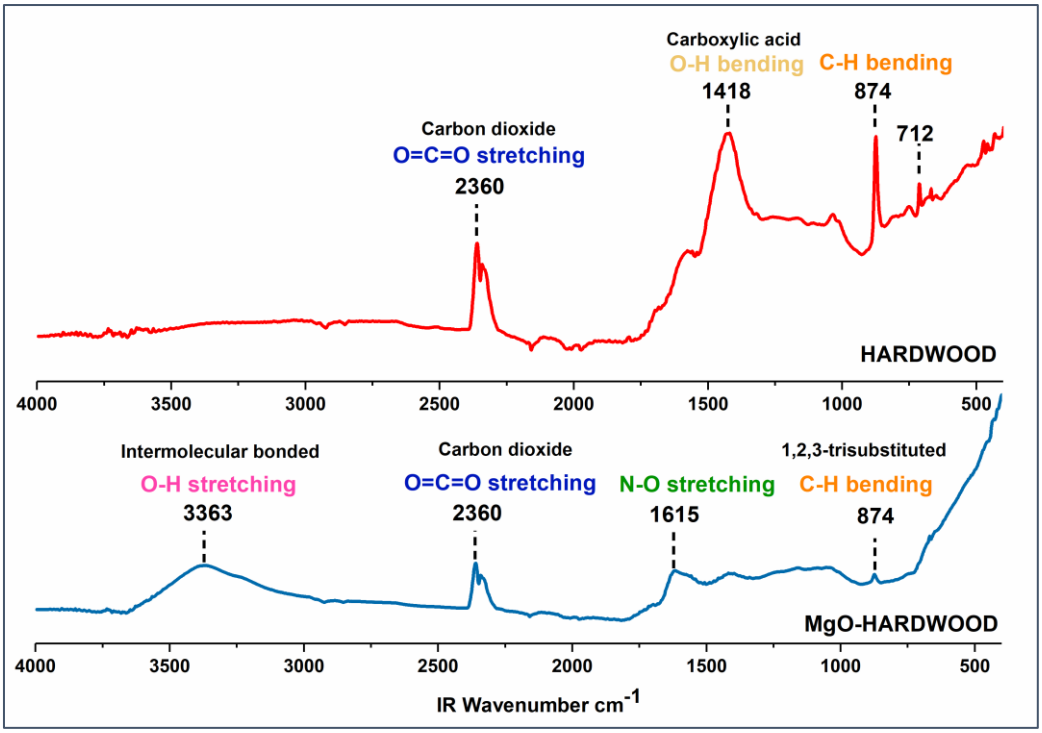

Fig. 7.21 FTIR spectra of hardwood and MgO-Hardwood feedstock

Table 7.13 Elemental composition as revealed by EDX

Hardwood		MgO-Hardwood	
Elements	Weight %	Elements	Weight %
C	59.54	O	39.54
N	0	Ca	24.52
O	39.89	Mn	13.23
Na	0.13	K	8.32
Al	0	Cl	8.01
Si	0.07	Mg	4.22
S	0.11	Al	0.89
K	0.26	Si	0.65
		Na	0.63

7.2.4.3 Effect of pH on iron and phosphate removal

It is vitally important to note that pH is one of the fundamental parameters in the adsorption process that influences the surface charge and the dissociation of functional groups on the adsorbent. Furthermore, pH plays a role in determining the degree of ionization and speciation of metals and non-metals. As a result, it is essential to determine what pH is optimum for iron adsorption on Hardwood and phosphate adsorption on MgO-Hardwood. The results depicted in Fig. 7.22a and 7.22b. clearly show that both iron and phosphate removal was apparently pH-dependent, and the removal percentage of iron was increased with increasing pH from 2.0 to 10.0 whereas the removal percentage of phosphate was decreased with increasing pH from 2.0 to 14. At pH 10, the removal

percentage of iron reached a peak (98.25 %) whereas at pH 6 the removal percentage of phosphate reached a peak of 96.22 %.

The hardwood surface was protonated and positively charged under strongly acidic conditions caused by the presence of a high concentration of H^+; as a result of electrostatic repulsion, metal ions (iron) cannot move toward a positively conductive surface of hardwood, and thus a lower removal rate was observed at low pH values (Reddy and Lee, 2014). In response to increases in pH, the adsorption sites on the hardwood became negatively charged, allowing more iron to be removed. Upon reaching pH 6, MgO-Biochar increased phosphate adsorption, but it decreased as pH became alkaline. A high pH solution is therefore detrimental to phosphate adsorption on modified biochar. Therefore, pH 6 was chosen as the optimal pH for phosphate removal in this study. This result was consistent with the results reported by Li et al. (2017c) where sugarcane crop harvest residue loaded with MgO was used for phosphate removal.

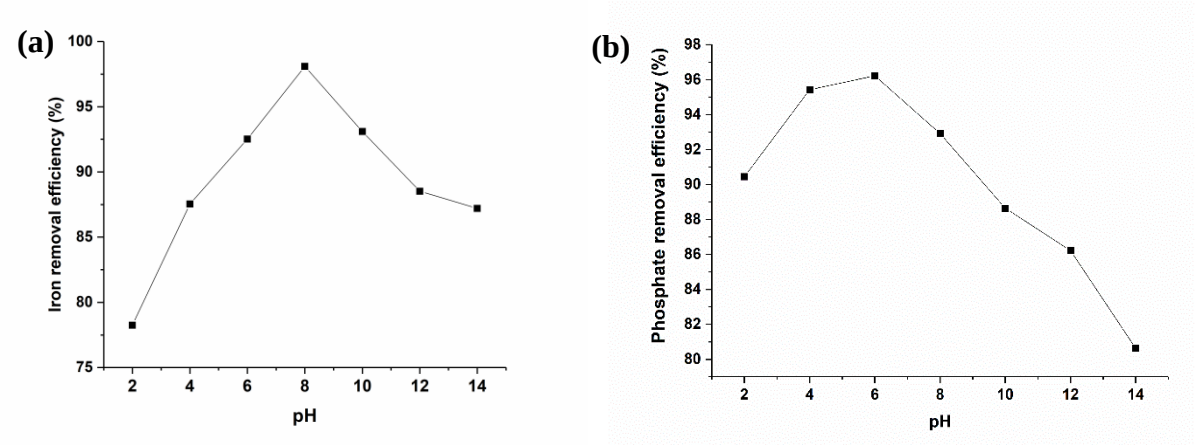

Fig. 7.22 Effect of initial solution pH on (a) iron adsorption and (b) phosphate adsorption

7.2.4.4 Effect of adsorbent dose on iron and phosphate removal

The effect of the dosage of unmodified hardwood and modified hardwood biochar (MgO-HW) on the adsorption of iron and phosphate from an aqueous solution was presented in fig. 7.23a and 7.23b. The experiments were carried out in a suspension containing different doses (0.01g-1g) of HW biochar and MgO-HW biochar and 50 mL of iron and phosphate solution of different concentrations (5mg/l, 15mg/l, and 30mg/l). After being shaken at 250 rpm at 25 °C for 7 hr for iron and 15hr for phosphate, the supernatant water was filtered to analyze the residual iron and phosphate concentration using IC and ICP-OES respectively.

The adsorption capacity of iron using HW biochar gradually increased as the dose was increased, and the removal rates initially increased and then flattened as the dosage increased, especially when the dosage was increased from 0.01-0.05g.With the increase in dosage, the adsorption active sites on the surface of biochar gradually increased and within 0.1 the removal capacity increased to 98.20% for 5 mg/l, 99.47% for 15mg/l, and 99.6% for 30mg/l. A high percentage of carbon or a large volume of adsorbing porosity in hardwood biochar could be the reason for its excellent removal capacity without any coating or modification (Bin Jusoh et al. 2005). It may be related to adsorbate' electronegativity, ionic radius, and the number of functional groups on the HW biochar surface that attracted iron molecules (Gao et al. 2022). Thus, the application of the hardwood biochar will be cost-effective

and an economically potential alternative to manganese greensand, potassium permanganate, chlorine, hydrogen peroxide, sulfo-carbon, zeolites, granular activated carbon etc.

As shown in the figure, the phosphate removal efficiency increased as the adsorbent dosage (MgO-HW) increased from 0.1 and 1g. MgO-HW biochar was found to have a relatively high efficiency of 99.52% (30 mg/l), 98.42 % (15 mg/l), and 98.70% (5 mg/l) when the adsorbent dosage was 1g. This modification of HW biochar, therefore, offers a pretty good adsorption performance of phosphate. The results were attributed to (i) the existence of significant available active sorption sites for electrostatic interaction, as well as, (ii) a high magnesium content (4.22%) and calcium content (24.52%), both of which could precipitate magnesium and calcium phosphate compounds with phosphorus anions. Compared to rice husk biochar (Ramola et al. 2021), dolomite-modified biochar (Liu et al. 2019), crab shells (Cao et al. 2022), and so on, modified biochar can be considered an effective adsorbent.

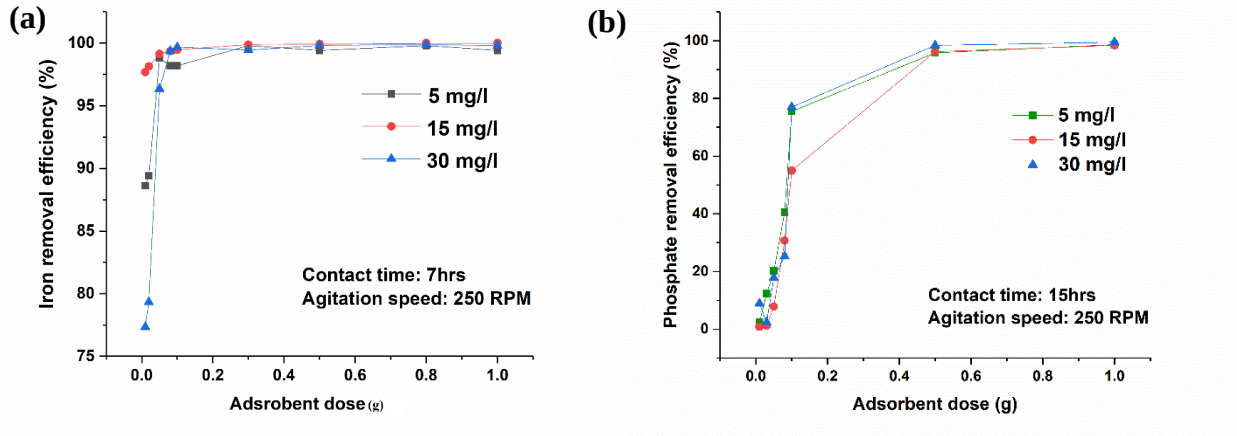

Fig. 7.23 Effect of adsorbent dose on (a) iron and (b) phosphate removal

7.2.4.5 Adsorption performance of HW and MgO-HW for iron and phosphate removal

7.2.4.5.1 Effect of initial concentration and adsorption isotherm studies

HW Biochar and MgO-HW biochar (0.5 g of solid in 50 mL of solution) were mixed with the iron and phosphate solution respectively at 2, 5, 10, 15, 20, 25 and 30mg/l at pH. All the vials were sealed and shaken at 250 rpm on an orbital shaker for 7hrs (iron) and 15hrs (phosphate) until apparent equilibrium was reached. At equilibrium, the samples were filtered, and the residual iron and phosphate concentrations were determined to observe the effect of initial concentration on pollutant removal (Fig.7.24a and 7.24b). Freundlich, Langmuir, Temkin, Elovich and Dubinin-Radushkevich isotherm (D-R) adsorption isotherms were used to investigate the adsorption performance of iron and phosphate on HW and MgO-HW biochar. The adsorption isotherm parameters, correlation coefficients, RMSE and Chi-Square results obtained by fitting five kinds of adsorption isotherm models are shown in Table 7.14.

The adsorption of iron is increased with an increase in iron concentration and remains constant. Afterwards, it dropped at 30mg/l. The removal capacity improved from 98.50% to 99.60% as the concentration was increased from 2 to 30 mg/L. According to the figure 8a, adsorption begins rapidly and then decreases gradually as

adsorption progresses. It may be due to the monolayer coverage of iron on the hardwood surface (Vasudevan et al. 2009). The results were also evident in the isotherm models (Fig. 7.25a-7.25e). With a higher R^2 value (0.98), the Langmuir model was more consistent with the isotherm. It occurred as a monolayer on HW biochar with uniformly distributed binding sites (Zareh et al. 2022). The degree of heterogeneity denoted by n is calculated to be 2.103 in the Freundlich model, which represents the chemical interaction between hardwood and iron. Temkin, Elovich, and Dubinin Radushkevich (D-R) isotherm models were also fitted to experimental data to explain the adsorption mechanism more clearly. In the Temkin model, the heat of adsorption is inversely related to the surface coverage of the adsorbent. The equilibrium binding constant KT is calculated to be 36.38 L/mg. It is evident that both physical and chemical processes are involved in the adsorption process since the heat of sorption B is 22.45 J/mol. The Elovich isotherm with R^2 value 0.90 also suggests chemisorption. Based on D-R (R^2=0.92), pore filling is the mechanism that leads to adsorption. According to this theory, adsorption occurs in multilayers involving vanderwaal's force of interaction and is applicable to the physical adsorption process. According to the D-R isotherm, the maximum adsorption was 289.82 mg/g, which is the highest among the previously conducted studies (Table 7. A1)

When the initial P concentration was changed from 2 mg/L to 30 mg/L, the adsorption rate dramatically increased. However, the adsorption amount increased gradually from 98.44% to 99.64% in the initial concentration range of 2–10 mg/L before finally becoming stable. This trend could be caused by the gradual occupation of adsorption sites during the adsorption process (Fig.7.26a-7.26e). With an R^2 of 0.99, the Temkin isotherm provided the best explanation for P sorption data on MgO-HW, which indicated a multilayer adsorption process (Table 7.14). P adsorption on MgO-HW could be explained by chemical adsorption based on strong electrostatic interactions according to the Temkin model, which was consistent with the findings of modified magnesium-impregnated corn straw biochar (Li et al. 2022d) and bamboo-activated carbon (Shao et al. 2022). It was observed that the correlation coefficient R^2 for the Langmuir equation model was also greater than for Freundlich, Elovich, and Dubinin-Radushkevich isotherms (D-R), suggesting that the Langmuir equation model can also be used to simulate homogenous adsorption, in which all sites possess the same affinity for the adsorbate. The maximum adsorption capacity of MgO-HW was 828.82 mg/g according to D-R model which is higher than Mg-modified Eucalypt stem biochar (463.5 mg/l) **(**Arbelaez et al. 2021) and others including in the table S2.

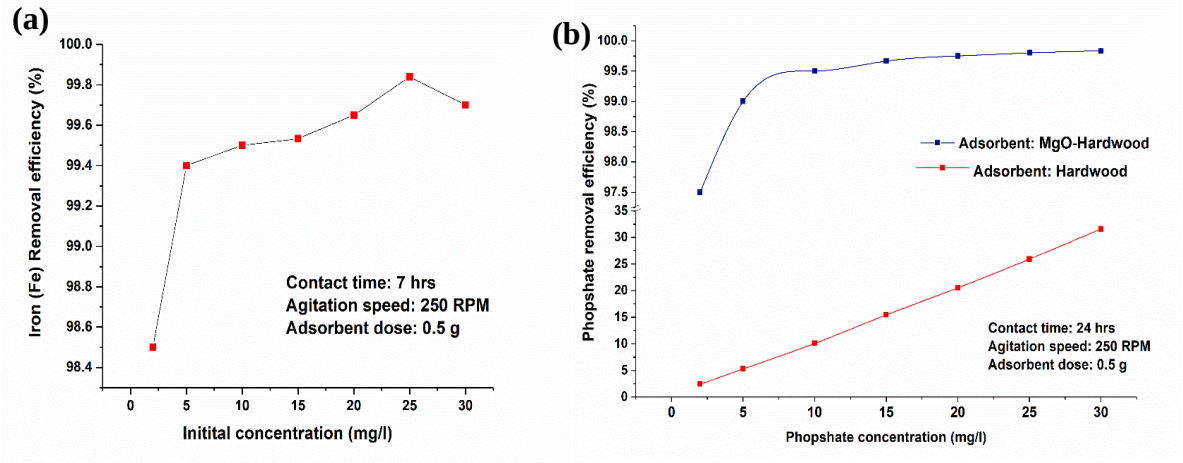

Fig. 7.24 Effect of initial concentration on (a) iron and (b) phosphate removal

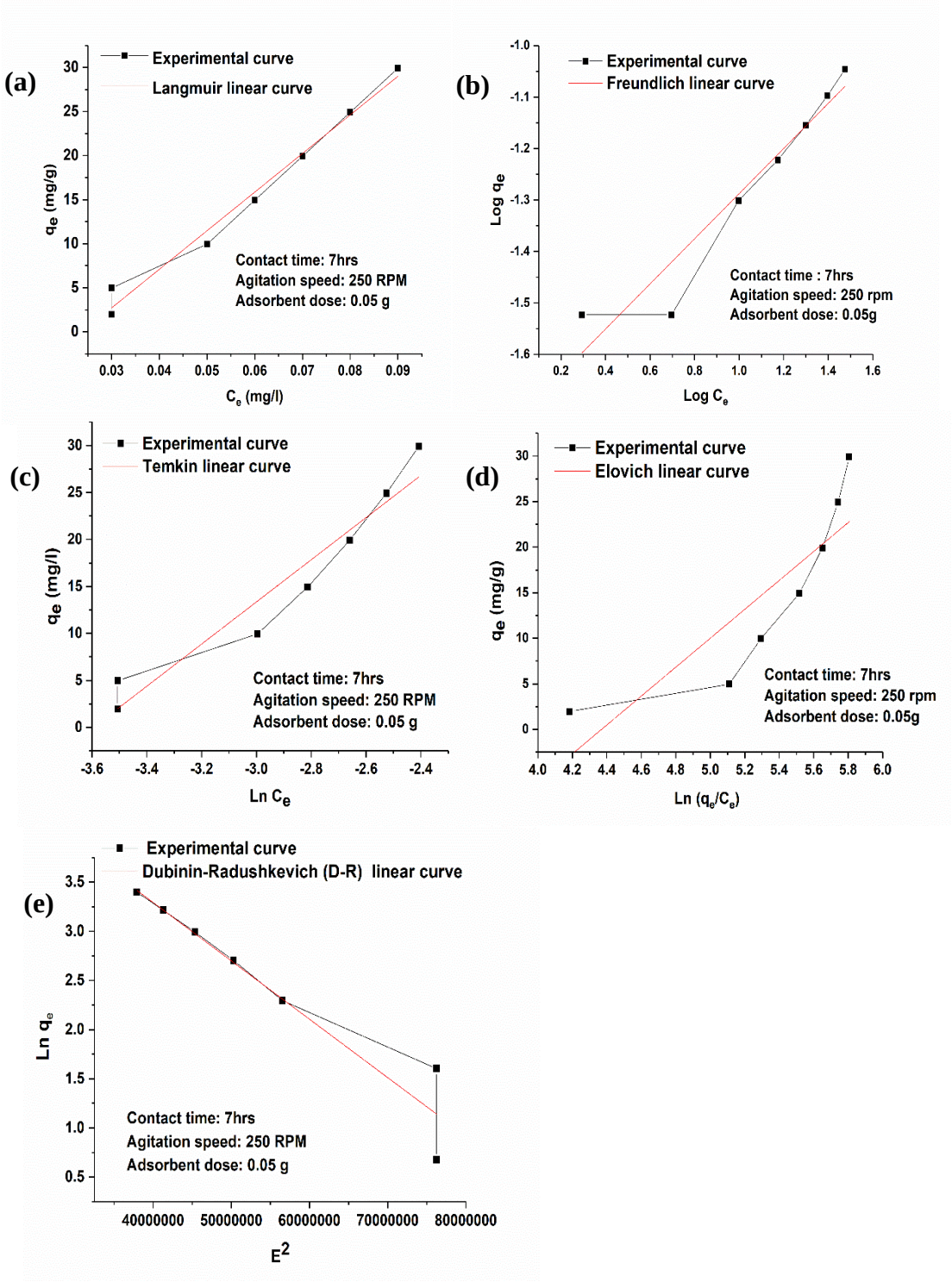

Fig. 7.25 Adsorption isotherm of iron uptake by hardwood (a) Langmuir; (b)Freundlich (c)Temkin; (d) Elovich and (e) Dubinin-Radushkevich (D-R)

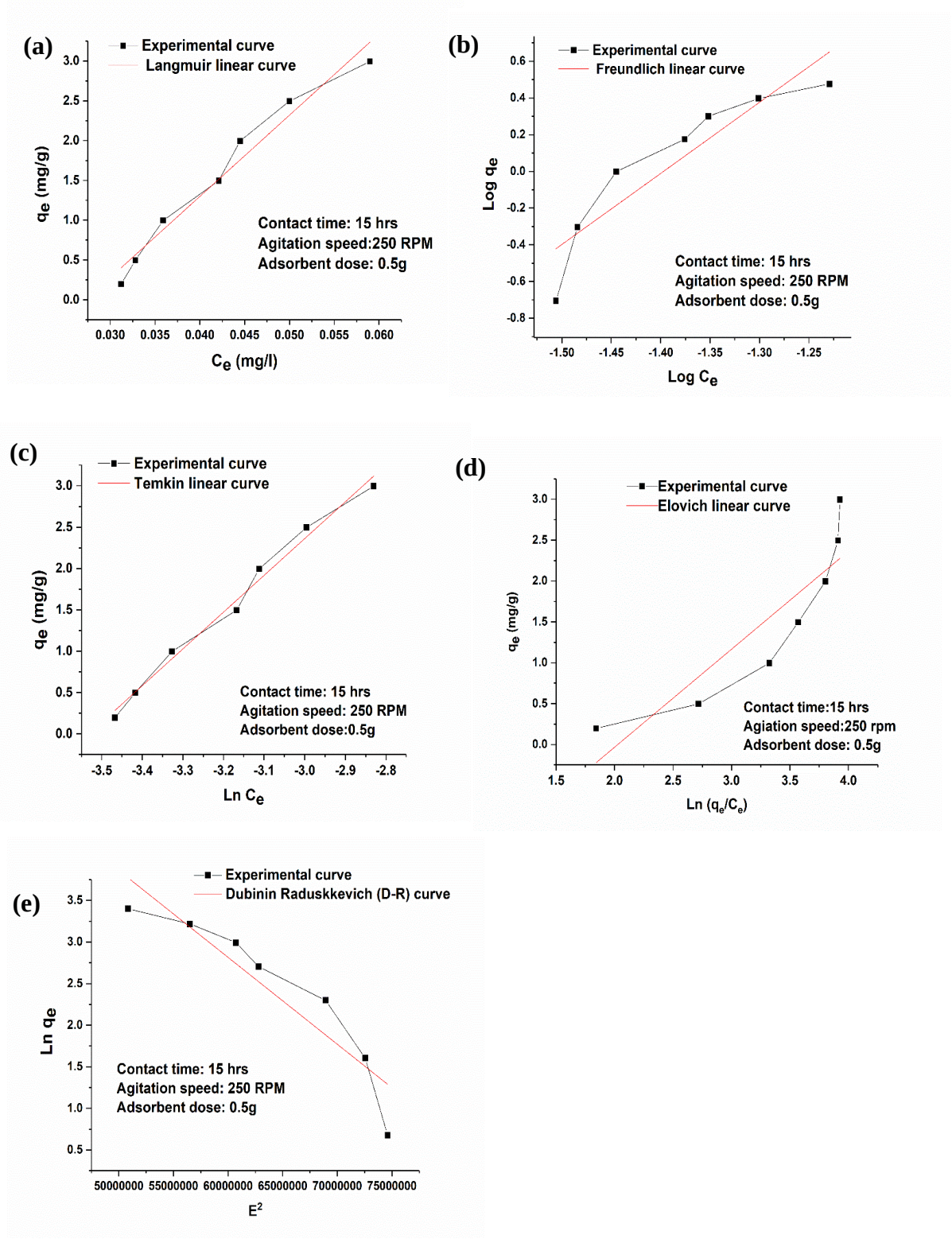

Fig. 7.26 Adsorption isotherm of phosphate uptake by MgO-hardwood (a) Langmuir; (b)Freundlich (c)Temkin; (d) Elovich and (e) Dubinin-Radushkevich (D-R)

Table 7.14 Adsorption isotherm parameters for the adsorption of iron and phosphate onto Hardwood and MgO-Hardwood

Isotherm models	Iron adsorption onto Hardwood				Phosphate adsorption onto MgO-Hardwood			
	Isotherm Constants	Values	RMSE	Chi-square test	Isotherm Constants	Values	RMSE	Chi-square test
Langmuir isotherm	q_m (mg/g)	0.002	1.401	1.9	q_m (mg/g)	0.010	0.200	0.0413
	K_L(L/mg)	-0.024			K_L(L/mg)	-0.027		
	R^2 (linear)	0.98			R^2 (linear)	0.960		
	R^2 (Non-linear)	-			R^2 (Non-linear)	0.500		
Freundlich	K (g)	5140.44	0.129	0.017	K (g)	257632.120	0.180	0.034
	n	2.103			n	3.870		
	R^2 (linear)	0.91			R^2 (linear)	0.810		
Temkin	B (J/mol)	22.45	2.85	8.12	B (J/mol)	4.450	0.123	0.015
	K_T (L/mg)	36.38			K_T (L/mg)	33.980		
	R^2 (linear)	0.94			R^2 (linear)	0.990		
Elovich	q_m (mg/g)	0.063	5.72	32.7	q_m (mg/g)	0.840	0.511	0.26
	K_e (L/mg)	0			K_e (L/mg)	0.06		
	R^2 (linear)	0.9			R^2 (linear)	0.76		
Dubinin-Radushkevich isotherm (D-R)	B(mol^2/kj^2)	5.937	0.293	0.085	B(mol^2/kj^2)	1.045	0.400	0.160
	q_m (mg/g)	289.45			q_m (mg/g)	828.82		
	R^2 (linear)	0.92			R^2 (linear)	0.833		

7.2.4.5.2 Effect of contact time and kinetics study

Using the feedstock, a batch of adsorption experiments with different reaction times (0-300 min) were performed to investigate iron and phosphate uptake rates. About 0.05 g of HW biochar was added into 50 mL of 2, 15, 30 mg/l initial iron solution and 1g of MgO-HW biochar was added into 50ml of 2, 5, 30 mg/l initial phosphate solution with neutral pH at room temperature with the stirring speed of 250 rpm. In order to better understand adsorption rates, kinetic parameters were investigated based on the pseudo-first-order, pseudo-second-order, and Elovich kinetic models as well as the Weber-Morris intraparticle diffusion model. The fitted curves and the calculated parameters of the respective models are shown in Fig. 7.27a-7.27e and 7.28a-7.28e and Table 8 respectively.

As shown in Fig.7.27a, the percentage of iron removed was calculated by dividing the difference between the measured final and initial solution concentrations by the initial metal concentration, and the percentage of iron removed was plotted against time. During the first 50 minutes, iron adsorption was quite fast, reaching 99.99% removal with HW-biochar at an initial concentration of 2mg/l, indicating an excellent candidate for iron adsorption. The mass transfer became constant after 50 minutes, and there was no significant change afterward. With a minimal dosage (0.05g), the Fe removal percentage at 15mg/l and 30mg/l was > 94%. A higher dosage will eventually result in higher Fe removal percentage. The majority of available surface sites were instantaneously occupied by external surface adsorption through diffusion in the initial adsorption stage. Once Fe accumulated on the surface of HW-biochar, it transferred to the interior where it attached to inner sites. The results were consistent with those of Sun et al. 2016 and Zareh et al. 2022 for metal adsorption with bio-adsorbents. The PSO kinetics and Elovich model were observed to govern Fe adsorption by HW-biochar (Fig 7.27b-7.27e). Based

on the results shown in Table 7.15, the PSO kinetic model and the Elovich model were the two most effective fits for HW-biochar, with the highest R^2 (0.99), lowest root means square error (RSME, 0.04-0.36), and lowest chi-square value (0.002-0.180). It was concluded from these results that adsorption was a chemical process involving Fe chelating with the active points of HW-biochar. Moreover, the fitting lines with deviations from the origin indicated that the intraparticle diffusion process (R^2=0.53-0.61) was associated with Fe uptake by HW-biochar, but it was not the only rate-manipulating process (Zhang et al. 2022b).

Fig.7.28a shows the effect of contact time on the adsorption of phosphate ions. It was observed that the removal efficiency increased in correlation with contact time. With the increase of the initial phosphate concentration (30mg/l), a higher adsorption percentage (93%) was observed. Considering the slow kinetics, precipitation appears not to be a significant factor in the MgO-HW biochar adsorption of phosphate (Tran et al. 2022). A further fitting of the experimental data revealed a slightly higher coefficient of determination (R^2) for the pseudo-first-order kinetic model (R^2=0.99) than for the pseudo-second-order kinetic model (R^2=0.91) (Table 7.15), with a lower RMSE (0.076) and chi-square value (0.006) at an initial concentration of 30 mg/l. MgO-HW biochar adsorbs phosphate ions predominantly via physical adsorption, thereby demonstrating electrostatic attraction as the main mechanism of phosphate ion adsorption (Fang et al. 2022). Furthermore, this scenario was based on the number of active sites available on MgO-Hardwood, which determined the diffusion rate. To further elaborate the function of the porous structure of MgO-HW, the experimental data were also simulated using the intraparticle diffusion model (R^2=0.99) (Fig.7.28b-7.28e). Analysis of the phosphate adsorption data of MgO-Hardwood with the intra-particle diffusion model revealed multi-linearity, suggesting that more than one step was involved in the process. Firstly, on the surface of MgO/biochar, there are adequate adsorption active sites for phosphate ions, which are easily accessible to the phosphate ions; Secondly, the limited diffusion rate of phosphate within the pore microstructure results in a decrease in adsorption rates; and finally, in the last stage, the phosphate uptake process reaches equilibrium and remains stable (Chen et al. 2022b).

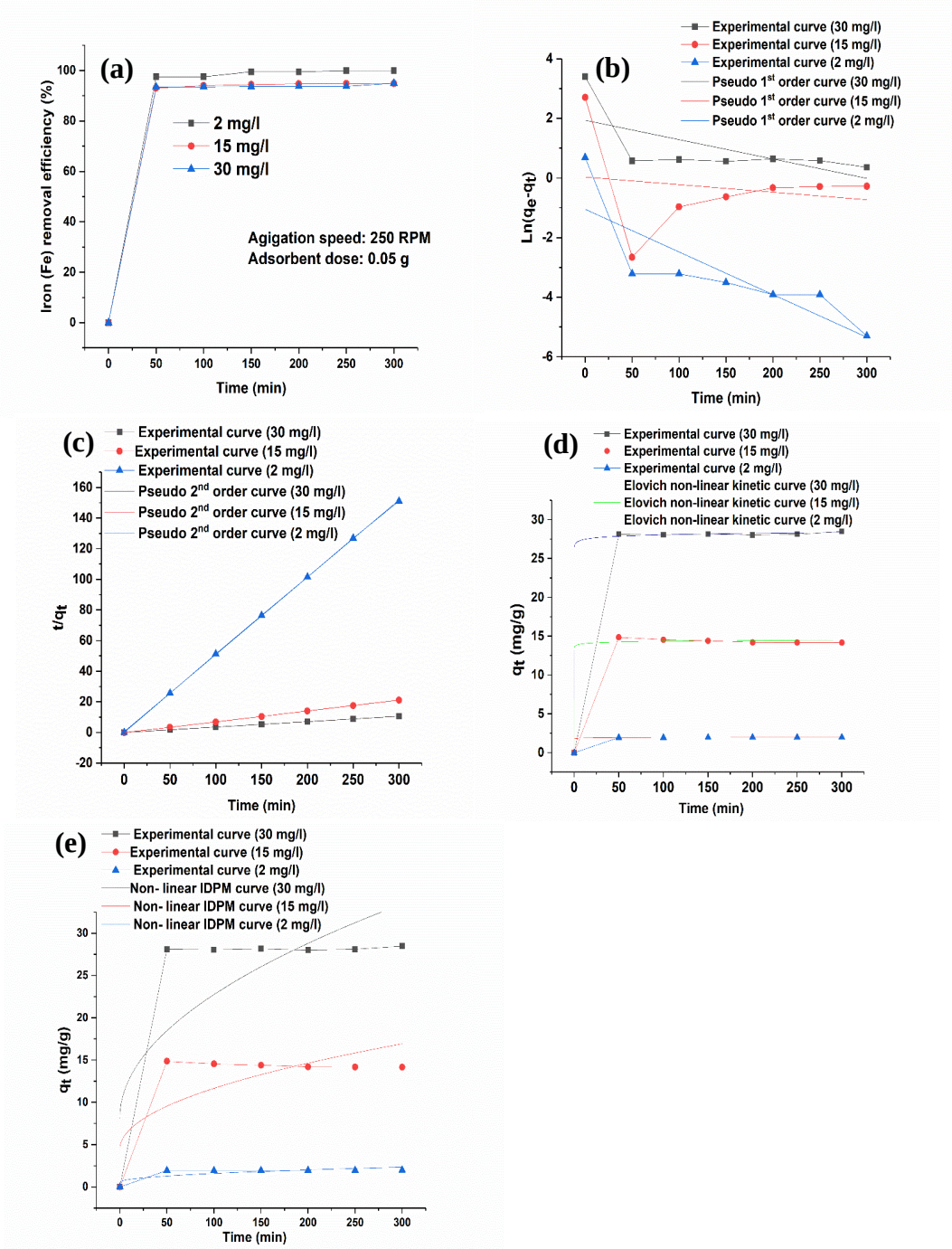

Fig. 7.27 Adsorption kinetics of iron uptake by Hardwood (a) effect of time on adsorption; (b) Pseudo 1st order (c) Pseudo 2nd order; (d) Non-linear Elovich kinetic and (e) Non-linear IDPM

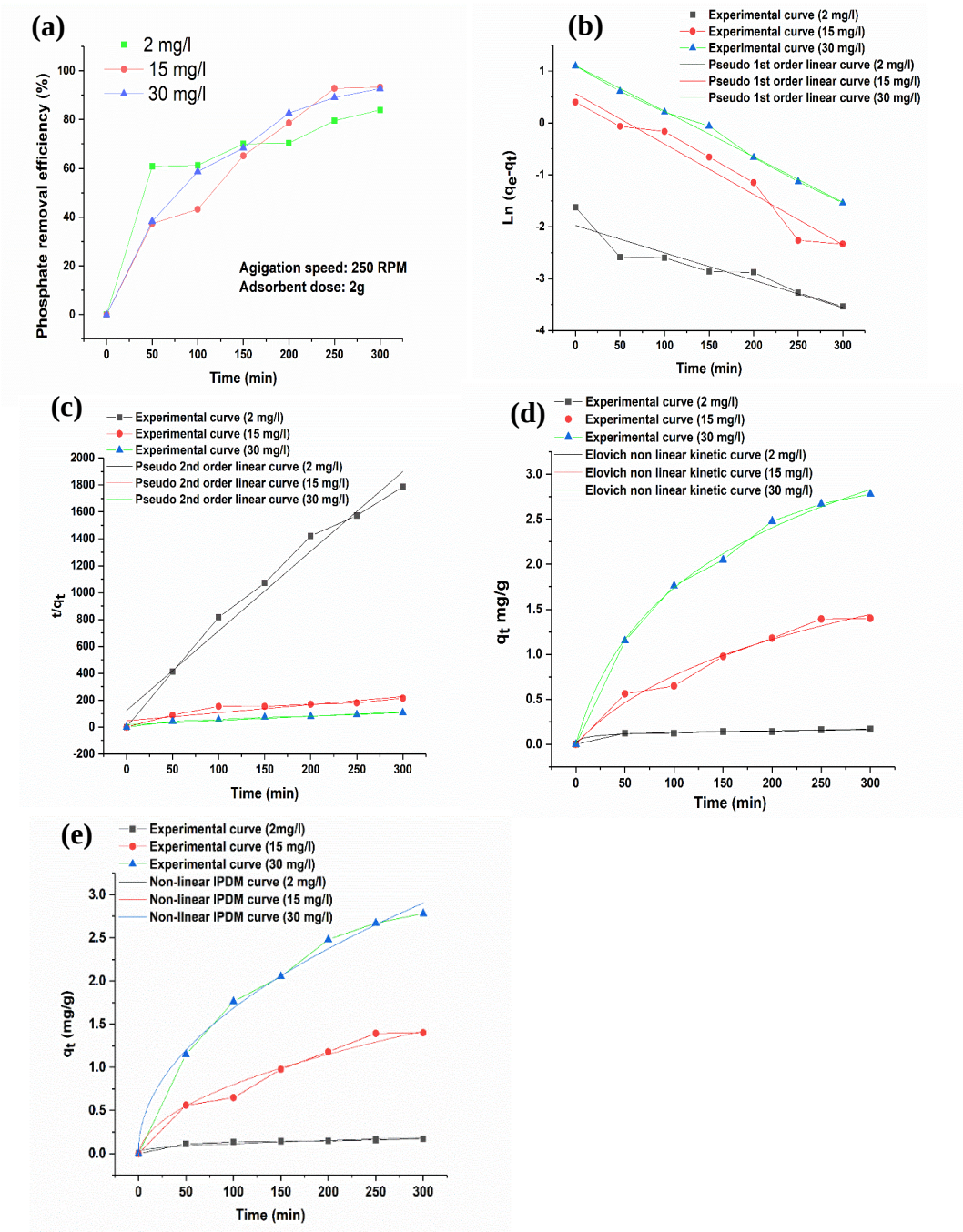

Fig. 7.28 Adsorption kinetics of phosphate uptake by MgO-Hardwood (a) effect of time on adsorption; (b) Pseudo 1st order (c) Pseudo 2nd order; (d) Elovich kinetic and (e) Non-linear IDPM

Table 7.15 Parameters for various kinetic models for iron and phosphate removal

Kinetic models		Iron adsorption onto Hardwood			Phosphate adsorption onto MgO-Hardwood		
	Parameters	2 mg/l	15 mg/l	30 mg/l	2 mg/l	15 mg/l	30 mg/l
Pseudo 1st order kinetic	q_e (mg/g)	0.350	1.031	6.93	0.139	1.759	2.829
	K_1	-4.76667×10^{-5}	-8.46	2.16667×10^{-5}	-1.666	-3.233	-2.666
	R^2	0.634	-0.14	0.308	0.846	0.935	0.99
	RMSE	1.121	1.713	0.897	0.239	0.273	0.076
	Chi-square test	1.257	2.94	0.804	0.057	0.074	0.006
Pseudo 2nd order kinetic	q_e (mg/g)	3.931	14.11	28.34	0.169	1.669	9.766
	K_2	8.121	-1542.55	31002.51	0.0002	0.059	0.571
	R^2	0.99	0.99	0.99	0.973	0.789	0.910
	RMSE	1.092	0.0377	0.0488	105.5	32.678	10.20
	Chi-square test	0.218	0.007	0.002	11130.63	1067.91	112.74
Elovich non-linear kinetic model	α	1.033×10^{2}	8.41×10^{4}	3.47×10^{-4}	0.04045	0.01212	0.03979
	β	33.66	7.35	3.70	38.42473	1.13115	0.85268
	R^2	0.99	0.99	0.99	0.98	0.97615	0.99753
	RMSE	0.18	0.36	0.18	0.00005	0.0062	0.00291
	Chi-square test	0.033	0.13	0.033	0.00777	0.07876	0.05399
Intraparticle diffusion model non-linear	k_{id} (gm/mg min $^{0.5}$)	0.103	0.102	1.461	0.009	0.085	0.167
	C (mg/g)	0.561	4.465	8.146	0.023	-0.048	0.022
	R^2	0.608	0.539	0.59	0.89	0.97	0.990
	RMSE	0.464	3.694	6.74	0.019	0.085	0.083
	Chi-square test	0.215	13.65	45.43	0.0004	0.007	0.007

7.2.4.6 Plausible mechanism and after adsorption feedstock characterization

An analysis of the FESEM, EDS images, and XRD patterns of HW and MgO-HW biochar after iron and phosphate adsorption was conducted to understand the adsorption mechanisms of iron and phosphate onto the feedstock respectively. Hardwood is capable of removing iron by four main physicochemical mechanisms, including chemisorption, redox interactions, physical adsorption, and co-precipitation as illustrated in Fig.7.29. The presence of nano-sized substances on the surface of the biochar confirms the adsorption of iron as illustrated by the FESEM results (Fig. S2a). The XRD plot before adsorption showed HW biochar consists of $CaCo_3$ (Fig. S2c). Thus Iron can get adsorbed or precipitated on the surface of calcite, thereby forming calcium siderite, $CaFe(CO_3)_2$. Calcium carbonate-based materials have been found to be effective in removing metals from industrial waste waters (Chaturvedi and Dave, 2012). The mechanism of iron removal by hardwood biochar can also occur as a result of electrostatic attraction between two oppositely charged ions (Khatri et al. 2017) (Fig. 29a). As a result of the solid sorption separation process, iron can also accumulate on the adsorbent surface as a molecular or atomic film. Additionally, the elemental mapping of hardwood biochar after loading the adsorbate confirms a high Fe content (52.14%) (Fig. S3a). The presence of carboxylic groups on HW surfaces, as seen from FTIR, can increase cation exchange capabilities and can also induce iron adsorption (Hodaifa et al., 2013). Plausible mechanisms of iron removal can be written as follows (Eq. 7.25-7.29)

$$2Fe^{3+} + 2H_2O = Fe_2(OH)_2^{4+} + 2H^+ \quad (7.25)$$

$$3Fe + 4H_2O = Fe_3O_4 + 4H_2 \quad (7.26)$$

$$2Fe + 3CaCO_3 \rightarrow 3Ca + Fe_2(CO_3)_3 \quad (7.27)$$

$$2Fe + Cl = 2FeCl_3 \quad (7.28)$$

$$Fe_2^{+3}\ \mathbf{O}^{-2}_{+3} = Fe_2O_3 \quad (7.29)$$

As shown in Fig.S2b lots of white substances appeared and attached to the surface of MgO-HW biochar after phosphate adsorption. The EDS elemental map confirmed that these substances mainly consisted of O (54.09%), Ca (19.1%), Mg (12.84%) and P (8.43%) elements (Fig S3b), demonstrating that phosphate was successfully adsorbed on the surface of MgO-HW biochar. MgO-HW biochar showed a series of strong signals after phosphate adsorption compared to the XRD pattern of MgO-HW before phosphate adsorption (Fig.S2d). These crystals existed in the forms of $Mg_3(PO4)_2$ and $Mg(OH)_2$ confirming the formation of precipitations between MgO and phosphate. $Mg_3(PO_4)_2$ and Mg(OH)2 also confirm a ligand exchange between phosphate and hydroxyl ions. Moreover, the presence of calcium in biochar can also result in the co-precipitation of calcium phosphate in different concentrations of OH. (Feng et al. 2021). Based on the above evidence, the main removal mechanisms of phosphate were physical adsorption (pore filling), co-precipitation, electrostatic attraction, and ligand exchange (Liu et al. 2019; Jiao et al. 2021). The mechanism of phosphate removal by MgO-HW was illustrated in Fig.7.29b. Plausible mechanisms of phosphate removal can be written as follows (Eq. 7.30-7.35).

$$MgCl_2.6H_2O \longrightarrow MgCl_2.2H_2O + 4H_2O\uparrow \quad (7.30)$$

$$(MgOH)Cl \longrightarrow MgO + HCl\uparrow \quad (7.31)$$

$$MgCl_2.2H_2O \longrightarrow (MgOH)Cl + H_2O + HCl\uparrow \quad (7.32)$$

$$3Ca^{2+} + 2PO_4^{3-} \longrightarrow Ca_3(PO_4)_2 \quad (7.33)$$

$$Mg_3(PO_4)_2 \longrightarrow Mg_3 + 2PO_4 \quad (7.34)$$

$$MgO+H_2O=Mg(OH)_2 \quad (7.35)$$

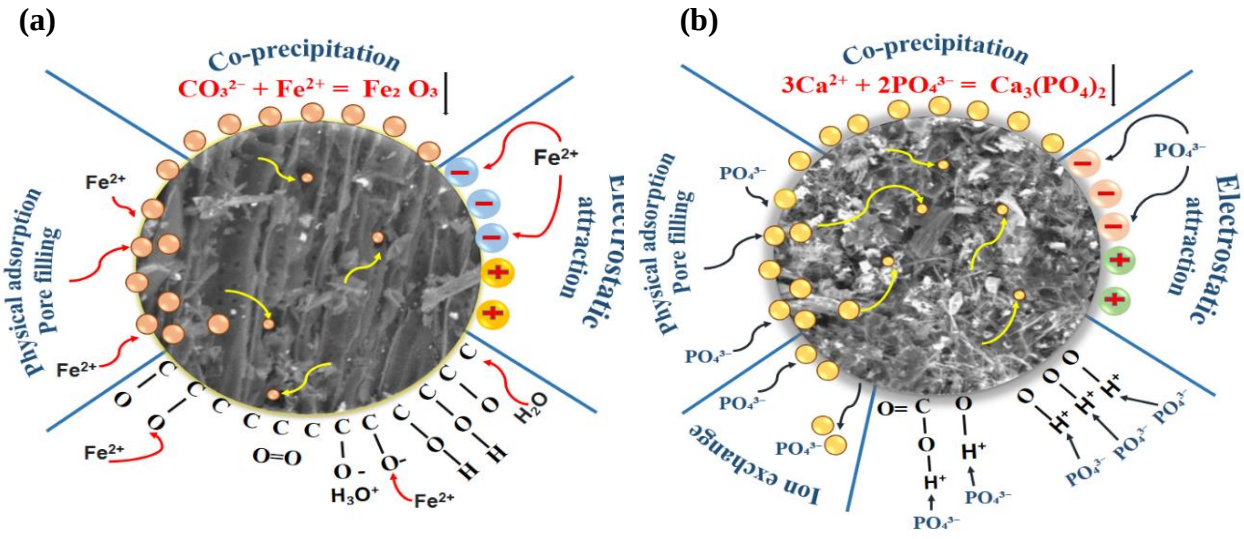

Fig. 7.29 Plausible Mechanism of (a) iron and (b) phosphate removal

7.2.5 Economic analysis and future work

As a result of their toxic, cumulative and non-biodegradable nature, heavy metal ions like Fe, as well as non-metalloids like phosphate, nitrate, ammonium etc. in the ecosystem can have a serious impact on all living organisms if exposed to a long period of time (Dey et al. 2022). Due to their better activity, economical nature, and the huge amount of availability, biological residues, mainly agricultural waste, plant/tree waste biosorbents, etc., are typically considered for toxic pollutant removal and recovery. Our results suggest that raw hardwood biochar produced from hardwood waste does not remove sufficient quantities of phosphate from the solution, in an unmodified state, but is efficient for iron removal. Therefore, without modification using magnesium oxides, it is currently not beneficial for treating water with high phosphate concentration. The present investigation, however, demonstrates the potential application of unmodified biosorbents (HW biochar) for the removal of iron from water solutions with a removal efficiency greater than 99%. Among the main items that are considered in market price by different companies are equipment costs, raw material costs (precursor), transportation costs, chemicals, water, gases, power consumption, salaries and allowances for employees, maintenance costs, and environmental impact assessments (EIAs) (Zhang et al. 2021). In comparison to other bio adsorbents, hardwood is much cheaper ($4.46/kg-Oxford Charcoal Company UK) (Table 7.16). According to the present study, the iron removal efficiency was approximately 97% when HW biochar dosage was 0.01g. Under this condition, the total cost of iron removal by the HW biochar was calculated to be $0.000044. This shows that the biochar is significantly cheaper than the most commonly used iron removal adsorbents like activated carbon (up to $45.71/kg, Henan Huasheng Charcoal Industry Ltd., http://hnhsty.com/), potassium permanganate ($69.43 /kg), ion exchange resin (up to $150/kg; Ahmed et al., 2015), Sodium hypochlorite solution ($87.29/kg) (Mamadou et al. 2021) etc. However, considering the production cost of MgO-HW, total price was about $12.8/kg consisting of biochar ($4.46/kg) and Magnesium Chloride reagent (cheapest-$ 8.34/ kg). Based on these results, MgO-biochar was significantly cheaper than rice straw ($36.6/kg), Chitosan ($15.4 /kg), Graphene ($50-$200/kg) etc. Thus, when the MgO-HW biochar dosage was 1g, the phosphate removal efficiency was observed to be approximately 99.52%. Under this condition, the total cost of phosphate removal by the MgO-HW biochar was calculated to be $0.0128. As can be seen from the table, the market price of HW biochar has been compared with other traditional and current adsorbents for iron and phosphate removal respectively. Based on the literature review, it seems that very few studies have been conducted to assess the logistical and economic feasibility of iron and phosphate removal using biochar, so a comprehensive comparative analysis of cost of a vast range of materials is not possible (Vikrant et al. 2018). Even though hardwood-derived biochar with low surface area proved to be techno-economically feasible, practical application to large-scale wastewater treatment requires consideration of the following factors including application using real water, effect of competitive adsorption (of heavy metals, organic matter, and other ions), stability of biochar, regeneration of biochar, the release of heavy metals, and sludge management etc. There can be a promising utility of the phosphate-laden MgO-HW solid obtained through remediation as a phosphate release organic fertilizer in enhancing the growth of plants and crops. Additionally, iron with HW biochar can adsorb many metal oxyanions as well as non-complexed metals, and some metal-ligand complexes, and can be used in wastewater treatment operations.

Table 7.16 Comparative analysis of adsorbent cost

Adsorbent used for iron/phosphate removal	US $ /kg	Reference
Hardwood biochar 500	4.46	https://www.oxfordcharcoal.co.uk/product/ethically-sourced-hardwood-blend-charcoal-5kg
Wheat straw 500/400	36.6	Nanjing Zhironglian Technology co., LTD
Corn straw 500/400/300	33.9	Nanjing Zhironglian Technology co., LTD
Rice straw 300	36.6	Nanjing Zhironglian Technology co., LTD
Tree branch biochar	11	Alhashimi and Aktas, 2017
Acid treated rice bran	20.45	Suzuki et al., 2007
Commercial activated carbon	45.71	Henan Huasheng Charcoal Industry Ltd., http://hnhsty.com
Chitosan	15.4	Babel and Kurniawan,2004
Filtrasorb-400AC	$20.0−22.0	Babel and Kurniawan,2005
Granular activated carbon	6.9	Alhashimi and Aktas, 2017
Fe3O4−MnO2MBC	10	Maneechakr and Mongkollertlop, 2020
Virgin wood feedstock	17.8	Alhashimi and Aktas, 2017
Potassium permanganate	69.43	https://apcpure.com/
Sodium hypochlorite solution	87.29	https://www.sigmaaldrich.com/IN/en
Graphene oxide	$50-$200	https://www.graphene-info.com/

7.2.6 Conclusion and Recommendation

In this paper, a novel green synthesis approach was employed to investigate the efficacy of hardwood biochar and MgO-HW biochar composite materials for the removal of iron and phosphate respectively from aquatic environments. Both adsorbents (Hardwood and MgO-Hardwood) were analytically characterized. The results from hardwood biochar confirmed the presence of adequate amount of carbon (59.54 %) and oxygen (39.89 %). Dissociative adsorption of oxygen is presumed to occur on the hardwood surface as a result of the oxidation process. An electron was donated by Fe ions to adsorbed oxygen, which was then reacted with a hydronium ion to form a surface hydroxyl and released water from the surface. As an added benefit, hardwood biochar immobilized iron in a short time period (Within 50 minutes, 99.99 percent of iron was removed), while its pore filling, electrostatic repulsion, co-precipitation, etc, promoted the transformation of iron to a sturdier form. Thus, to remediate iron and related heavy metals from aqueous environments, hardwood biochar may be a more effective strategy than activated carbon and membrane filters due to its low cost, easy preparation, and green appearance. Based on the results of the MgO-HW characterization, it was confirmed that MgO and MgO nanocomposites are present in good proportions. The presence of MgO nanoparticles altered the surface functional properties of biochar (surface areas, surface charges and chemical properties), which influenced phosphate adsorption. The phosphate adsorption process can be best described by the Temkin and pseudo-first-order kinetic model with the adsorption capacity of 828.82 mg/g where chemisorption based on strong electrostatic interaction played an important role.

7.2.7 Limitation and Future Work

By using a low surface area biochar in the process of removing cationic and anionic nutrients by traditional electrochemical deposition and adsorption, the current study provided an innovative solution to the problems of

high materials costs and tiresome manufacturing processes. The study also demonstrated the high value and resourcefulness of waste hardwood and the possibility of treating wastewater in a clean, efficient manner. The experimental concept requires further studies to overcome the limitations of the laboratory scale and the use of natural groundwater from field. It is recommended that future work should focus on iron and phosphorus recovery from the eluates as well as the reuse of byproducts as bio-fertilizers. Additionally, a filtering system based on the used materials needs to be developed and tested in the field.

Chapter8

Overall Conclusion and Recommendations

In order to evaluate the risks associated with groundwater and surface interaction in the Shilabati River basin of West Bengal, India, this thesis undertook a comprehensive investigation consisting of distinct yet interconnected research activities. **The focal point of the evaluation process revolved around addressing the following four key issues:**

a. The anticipation of a substantial decline in groundwater levels arises from both climate change impacts and unsustainable extraction practices in support of expanding agricultural fields.

b. Groundwater and meteorological drought coexist simultaneously within the river basin, disrupting the hydrological equilibrium.

c. The exploration of groundwater potential zones is closely linked to identifying suitable locations for Managed Aquifer Recharge, emphasizing the establishment of recommended safe groundwater yield levels.

d. The focus lies on comprehending the sources of groundwater contamination, encompassing both geogenic and anthropogenic factors. Special attention is given to eco-friendly remediation methods for three prominent pollutants in the Shilabati river basin of West Bengal: fluoride, iron, and phosphate.

e. The overall assessment highlights the alarming state of groundwater quality and severe water scarcity in the river basin. The goal is to propose a sustainable water security plan that will bring about positive changes and improve the lives of the underprivileged society.

The research activities presented in this thesis hold significant importance as they mark the pioneering investigation conducted in the Shilabati river basin, encompassing the western parts of West Bengal. **Drawing upon the key findings of the study, several noteworthy conclusions can be derived as follows:**

I. The river basin's prioritization involved the utilization of three MCDM techniques: TOPSIS, VIKOR, and COPRAS. After applying the SCCT technique, TOPSIS was determined as the most effective model. According to this model, the sub-basin Donai emerged as the most influential in terms of promoting adequate infiltration and recharging of its underground layers, resulting in groundwater yields ranging from 200-400 LPM.

II. The current study employs the fuzzy DAMETAL approach to integrate earth observation data and ancillary data in order to predict drought risk zones. The fuzzy DAMETAL model utilizes long-term trends of VCI, TCI, VHI, NDWI, SPI, SMI, and SAVI, specifically focusing on three years of rainfall deficit from the normal. Notably, there has been a notable increase in negative SPI values in recent years, serving as a primary indicator of drought. The upstream and middle sections of the basin face a severe risk of drought, with March and April being the most critical months. In April 2000, SPI recorded a

significant value of -1.60, signifying a drought condition. Throughout the basin, there are widespread instances of low/negative values and drought conditions, resulting in the depletion of surface water bodies and observed groundwater drought. The Mann Kendall test statistics have also been employed to analyze the trend in groundwater levels. The results indicate that 25% of the wells exhibit a declining trend during the monsoon period, while 45% show a declining trend in the pre-monsoon period. Additionally, 60% of the wells experience a declining trend during the post-monsoon period. This decline in groundwater levels can be primarily attributed to extensive pumping of sub-surface water and the consequent drying of river beds.

III. A novel FSI-GVI model was employed to conduct a groundwater vulnerability assessment. The analysis revealed that the central part or middle section of the basin predominantly consists of high to very high vulnerability zones, making it more prone to contamination. This susceptibility is primarily attributed to the combination of shallow groundwater levels and the presence of fine to coarse-grained soil with higher hydraulic conductivity. These factors allow surface contaminants to penetrate the vadose zone and potentially contaminate the groundwater table.

IV. The hydrochemical analysis of groundwater samples from the study area revealed significant rock-water interactions and mixing between shallow groundwater and deep circulating groundwater. These processes were found to play a dominant role in shaping the groundwater composition. While there were a few exceptions, the enrichment of ions in groundwater was primarily attributed to anthropogenic influences, including domestic discharges and agricultural activities. Furthermore, it was observed that the hydrochemical variations in groundwater were most pronounced in four geological structures: sands and silts intercalated with clay, granite gneiss, migmatite, and pink granite/biotite-granite gneiss, as well as sand, silt, and clay deposits. The degree of chemical weathering of different rock types, the quality and quantity of recharge water (with a high leaching potential), and inputs from sources other than rock-water interaction were identified as factors influencing the groundwater chemistry along its flow path. Fluoride, iron and phosphate are one of the three predominant groundwater contaminants within the river basin.

V. A design proposal has been put forward for a radial collector well and infiltration gallery at the selected site within the river basin, taking into consideration the MIKE FEFLOW model, pumping test results and drawdown estimation. The design aims to achieve a maximum safe yield of 12.096 MLD (Million Liters per Day).

VI. By employing an environmentally friendly single-column setup, wherein sample water passes through Kaolinite lithomarge red type, effective removal of fluoride from groundwater has been achieved. This process enables the production of fluoride-free water at a cost of 0.0015 USD per liter. The developed models have demonstrated reliability in accurately predicting fluoride removal efficiency and adsorption capacity. In addition, a groundbreaking green synthesis approach was utilized to assess the effectiveness of hardwood biochar and MgO-HW biochar composite materials in removing iron and phosphate from aquatic environments. Remarkably, these materials achieved an impressive removal rate of 99.99% for iron and 99.64% for phosphate, highlighting their potential for efficient water treatment applications.

The research work presented in this thesis has shed light on several crucial issues concerning the interaction between ground and surface water in the Shilabati river basin of West Bengal. **Therefore, it is essential to consider the following valuable recommendations:**

- Increased investments and efforts should be directed towards the implementation of rainwater harvesting technologies, including filtration and treatment methods, storage systems, and integration with existing water supply systems within the river basin. This approach will help mitigate issues such as drought, declining groundwater levels, and drying of surface water bodies. Financial aid, grants, and low-income loans should be provided to ensure the installation of such systems, particularly in low-income households and marginalized communities.
- Addressing the prevalent issue of sand mining and excavation along the Shilabati river course is crucial to maintain the flow and prevent drying of river channels, thereby preserving the interaction between ground and surface water. Strict enforcement of regulations, including penalties and fines for illegal activities, is necessary. Comprehensive monitoring, regular inspections of extraction sites, and the use of remote sensing, GIS, and drone surveys should be employed to detect and deter illegal mining.
- Proper drainage systems must be established in villages to prevent groundwater contamination. Many tube wells and dug wells lack a suitable concrete base. Therefore, implementing wastewater treatment systems such as biofilters, septic tanks, and constructed wetlands is essential to treat and dispose of domestic and agricultural waste before it enters the groundwater system of the river basin.
- The utilization of eco-friendly materials like biochar and natural clay, as demonstrated in this thesis for contaminant removal, should be promoted in community-level water treatment systems. Recommended designs for treatment units should be implemented on a larger scale to meet the water demand of the Shilabati river basin, accounting for present and future needs. Training programs for local villagers and community members should be conducted to ensure effective operation and maintenance of these treatment units.
- **Lastly, collaboration with local, regional, national, and international government and non-governmental entities,** water management professionals, stakeholders, and relevant authorities is crucial to facilitate the successful implementation of the research findings. Adequate funding, infrastructure, and resources should be secured through these partnerships. By embracing these recommendations, we can work towards effectively addressing the identified issues and ensuring the sustainable management of the Shilabati river basin in West Bengal.

Chapter9
Appendix

Table 4. A1 Descriptive analysis of groundwater level in premonsoon season

Well Location	Mean	Standard deviation	Skewness	Kurtosis	Variance	Median	Quartile 1	Quartile	Quartile 3	Inter quartile range
Badga	5.850	1.336	0.880	0.746	1.708	5.430	4.770	5430	6.680	1.910
Chandrakona road	11.813	3.101	0.489	-0.488	9.199	11.500	9.620	11.500	13.500	3.880
Brahmajhalur	6.199	6.27	0.085	-.1.152	6.603	5.320	4.260	5.320	8.960	4.700
Dhadika	9.296	4.846	-0.473	-1.512	22.458	11.560	2.990	11.560	13.530	10.540
Salboni	6.920	2.516	1.908	7.467	6.056	6.690	5.500	6.690	7.990	2.490
Godapaisal	6.574	1.146	-1.616	2.690	1.257	6.860	6.550	6.860	7.190	0.640
Keshpur	5.265	2.198	0.284	-0.512	4.622	5.384	3.570	5.384	6.600	3.030
Neradeul	8.421	6.405	0.559	-0.757	39.243	8.420	1.867	8.420	12.540	10.673
Raskunda	6.430	4.749	1.370	10.085	21.569	4.580	3.280	4.580	6.800	3.520
Belsula	4.76	2.433	2.753	8.946	5.614	4.100	3.600	4.100	4.900	1.300
B.D. Panchal	12.737	3.760	-0.536	0.734	13.521	13.280	11.550	13.280	14.680	3.130
Pirorgairi	5.018	2.341	2.188	9.904	5.244	4.890	3.390	4.890	5.660	1.730
Prasadpur	3.555	1.163	0.440	-0.377	1.293	3.500	2.600	3.500	4.120	1.520
Simlapal	6.357	1.573	-0.470	0.961	2.366	6.440	5.410	6.440	7.300	1.890
Khirpai	6.077	3.852	1.004	2.392	14.193	6.100	2.921	6.100	7.300	4.429
Hatirampur	6.787	1.764	0.525	-1.117	2.876	6.100	5.485	6.100	8.260	7.100
Bheduasol	6.703	0.904	-2.76	0.161	0.781	6.780	6.180	6.780	7.100	0.920
Ghalkunda	5.232	3.158	0.863	0.509	9.540	4.880	2.430	4.880	6.020	3.590
Garbeta	5.544	3.496	0.644	-0.846	11.693	40.30	2.400	4.030	7.680	5.280
Ghatal	11.193	3.971	0.183	-1.944	15.081	9.087	7.375	9.087	15.292	7.917

Table 4. A2 Descriptive analysis of groundwater level in monsoon season

Well Location	Mean	Standard deviation	Skewness	Kurtosis	Variance	Median	Quartile 1	Quartile	Quartile 3	Inter quartile range
Badga	2.573	1.779	1.538	2.611	3.159	2.230	1.430	2.230	2.480	1.050
Chandrakona road	3.366	1.882	1.482	4.817	3.389	3.320	2.250	3.320	4.440	2.190
Brahmajhalur	1.791	1.143	1.434	2.616	1.251	1.560	1.110	1.560	1.890	0.780
Dhadika	5.348	3.539	0.006	-1.427	11.981	5.650	1.510	5.650	8.510	7.000
Salboni	3.889	1.348	-0.466	-0.145	1.737	4.050	3.540	4.050	4.920	1.380
Godapaisal	3.395	0.736	-0.015	-0.142	0.518	3.320	2.820	3.320	4.080	1.260
Keshpur	2.317	3.914	3.866	17.591	15.256	1.193	0.890	1.193	2.097	1.207
Neradeul	4.539	2.541	1.953	5.375	6.457	4.454	2.540	4.454	4.890	3.350
Raskunda	1.289	1.547	3.837	18.484	2.290	0.900	0.580	0.900	1.560	0.980

Belsula	2.269	6.458	2.114	3.735	11.439	0.876	0.750	0.876	1.300	0.550
B.D. Panchal	7.702	4.168	-0.106	-0.923	16.617	7.050	5.730	7.050	11.780	6.050
Pirorgairi	16.20	1.567	3.439	15.419	2.448	1.238	0.890	1.238	1.630	0.740
Prasadpur	1.095	0.425	1.043	1.517	0.173	1.000	0.712	1.00	1.310	0.598
Simlapal	2.417	1.430	1.363	1.922	1.955	2.300	1.340	2.300	2.850	1.510
Khirpai	3.967	4.012	1.117	0.569	114.981	1.850	0.801	1.850	7.560	6.759
Hatirampur	2.176	1.330	1.353	1.801	1.693	1.753	1.350	1.753	3.250	1.900
Bheduasol	4.529	2.199	-0.257	-0.065	3.970	4.750	3.260	4.750	5.160	2.350
Ghalkunda	1.749	1.021	0.785	0.780	0.997	1.620	1.010	1.620	2.380	1.370
Garbeta	2.181	1.369	1.418	0.817	1.794	1.570	1.350	1.570	2.00	0.650
Ghatal	11.323	3.677	0.146	-1.883	12.934	9.800	8.152	9.800	15.250	7.098

Table 4. A3 Descriptive analysis of groundwater level in post monsoon season

Well Location	Mean	Standard deviation	Skewness	Kurtosis	Variance	Median	Quartile 1	Quartile	Quartile 3	Inter quartile range
Badga	2.643	0.991	0.888	0.624	0.939	2.530	1.770	2.530	3.260	1.490
Chandrakona road	5.707	3.130	0.272	-0.737	9.737	6.430	2.500	6.430	7.560	5.060
Brahmajhalur	3.902	2.449	-0.009	-1.839	5.735	3.610	1.260	3.610	6.250	4.990
Dhadika	5.514	3.273	-0.048	-1.172	10.023	5.30	2.300	5.630	7.770	5.470
Salboni	4.696	2.029	1.068	2.074	3.939	4.920	3.540	4.920	5.350	1.810
Godapaisal	5.722	2.234	0.884	1.4602	4.773	5.700	4.050	5.700	6.640	5.590
Keshpur	3.803	4.481	3.372	6.558	19.209	2.110	1.570	2.110	4.080	2.510
Neradeul	6.606	5.225	0.939	-0.156	26.110	3.598	2.345	3.598	11.560	9.215
Raskunda	2.869	1.550	1.841	6.376	2.299	2.740	1.800	2.740	3.640	1.840
Belsula	1.566	1.488	1.530	1.683	2.117	0.930	0.700	0.930	1.890	1.190
B.D. Panchal	10.014	3.673	-0.165	-1.472	12.653	9.410	6.590	9.410	13.630	7.040
Pirorgairi	2.923	2.283	1.470	1.720	4.986	2.086	1.370	2.086	3.870	2.500
Prasadpur	1.929	0.883	1.195	3.510	0.746	1.960	1.440	1.960	2.420	0.980
Simlapal	4.694	1.981	0.029	-0.687	3.755	4.790	3.090	4.790	6.020	2.930
Khirpai	4.310	3.221	0.355	-1.374	3.924	4.000	1.307	4.000	8.200	6.893
Hatirampur	3.483	1.758	-0.191	-1.367	2.957	3.890	1.833	3.890	5.150	3.317
Bheduasol	5.133	1.398	1.063	1.287	1.871	4.820	4.300	4.820	5.720	1.420
Ghalkunda	2.723	1.556	0.057	-1.672	2.316	2.330	1.330	2.330	4.450	3.120
Garbeta	4.500	3.178	0.567	-0.897	9.661	4.710	1.660	4.170	7.300	5.640
Ghatal	8.580	2.294	-0.096	-0.873	5.035	8.833	6.250	8.833	10.480	4.230

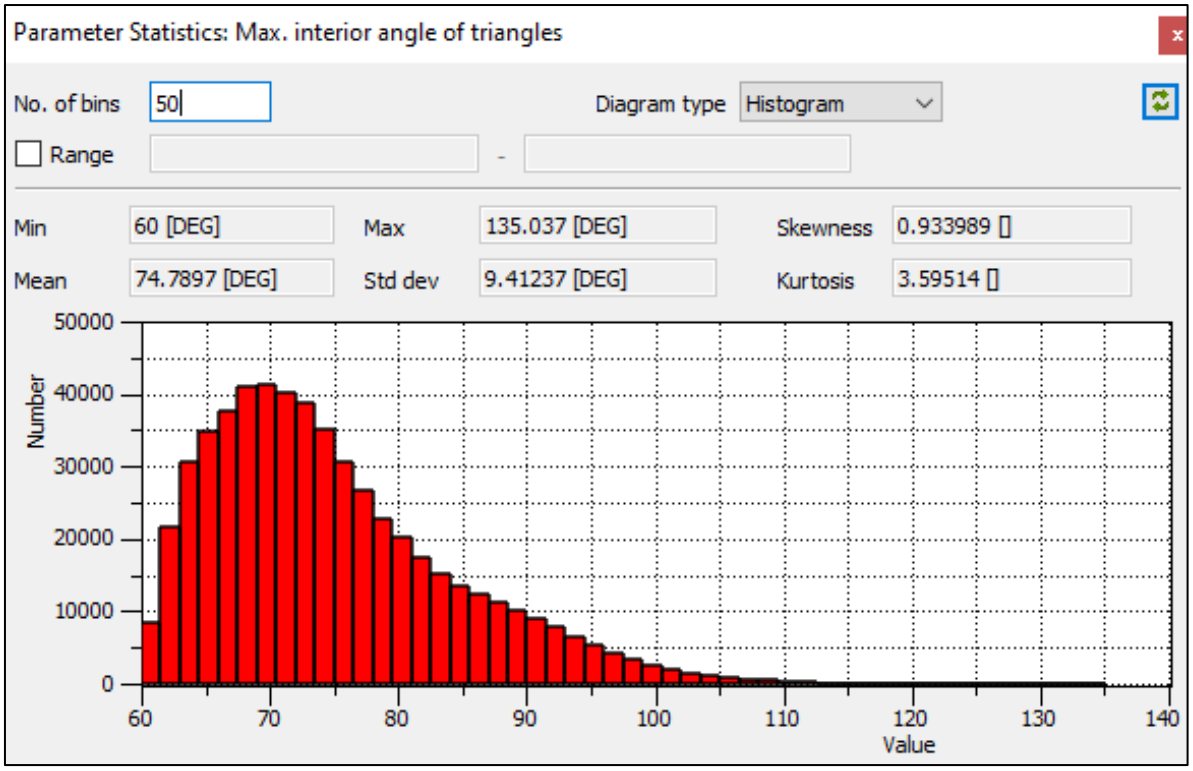

Fig. 5. A1. Parameter statistics for maximum interior angle of triangles or quadrangles after the smoothing operation.

Table 5. A1 Fuzzy AHP weights of the conditioning factors

Conditioning factors	Permeability	Anisotropy	Longitudinal conductance	Hydraulic conductivity	Longitudinal resistance	Porosity	Water holding capacity	Resistivity of formation	Bulk density	Transverse resistance	Fracture Porosity	Moisture content	Transmissivity	Fuzzy AHP weights
Permeability	(1,1,1)	(3/2,2,5/2)	(3/2,2,5/2)	(2/5,1/2,2/3)	(3/2,2,5/2)	(1/2,1,3/2)	(1,3/2,2)	(1,3/2,2)	(3/2,2,5/2)	(3/2,2,5/2)	(1/2,2/3,1)	(1,3/2,2)	(1/2,2/3,1)	0.0930
Anisotropy	(2/5,1/2,2/3)	(1,1,1)	(3/2,2,5/2)	(2/5,1/2,2/3)	(3/2,2,5/2)	(1,3/2,2)	(2/5,1/2,2/3)	(2/5,1/2,2/3)	(3/2,2,5/2)	(3/2,2,5/2)	(2/3,1,2)	(2/5,1/2,2/3)	(2/5,1/2,2/3)	0.0662
Longitudinal conductance	(2/5,1/2,2/3)	(2/5,1/2,2/3)	(1,1,1)	(2/5,1/2,2/3)	(1/2,2/3,1)	(2/5,1/2,2/3)	(2/5,1/2,2/3)	(2/5,1/2,2/3)	(3/2,2,5/2)	(3/2,2,5/2)	(2/5,1/2,2/3)	(2/5,1/2,2/3)	(2/5,1/2,2/3)	0.0490
Hydraulic conductivity	(3/2,2,5/2)	(3/2,2,5/2)	(3/2,2,5/2)	(1,1,1)	(3/2,2,5/2)	(1/2,2/3,1)	(1,3/2,2)	(3/2,2,5/2)	(2,5/2,3)	(3/2,2,5/2)	(1,3/2,2)	(3/2,2,5/2)	(3/2,2,5/2)	0.1197
Longitudinal resistance	(2/5,1/2,2/3)	(2/5,1/2,2/3)	(1,3/2,2)	(2/5,1/2,2/3)	(1,1,1)	(2/5,1/2,2/3)	(2/5,1/2,2/3)	(2/5,1/2,2/3)	(3/2,2,5/2)	(3/2,2,5/2)	(1/2,2/3,1)	(2/5,1/2,2/3)	(1/2,2/3,1)	0.0544
Porosity	(1,3/2,2)	(1/2,2/3,1)	(3/2,2,5/2)	(1,3/2,2)	(3/2,2,5/2)	(1,1,1)	(2/3,1,2)	(1,3/2,2)	(2/3,1,2)	(1/2,2/3,1)	(1/2,2/3,1)	(2/5,1/2,2/3)	(1/2,2/3,1)	0.0757
Water holding capacity	(1,3/2,2)	(3/2,2,5/2)	(3/2,2,5/2)	(1,3/2,2)	(3/2,2,5/2)	(1/2,2/3,1)	(1,1,1)	(1,3/2,2)	(3/2,2,5/2)	(1/2,2/3,1)	(1/2,2/3,1)	(1,3/2,2)	(1,3/2,2)	0.0966
Resistivity of formation	(2/5,1/2,2/3)	(3/2,2,5/2)	(3/2,2,5/2)	(2/5,1/2,2/3)	(3/2,2,5/2)	(1,3/2,2)	(1,3/2,2)	1,1,1	(3/2,2,5/2)	(2/5,1/2,2/3)	(2/5,1/2,2/3)	(2/5,1/2,2/3)	(2/5,1/2,2/3)	0.0675
Bulk density	(2/5,1/2,2/3)	(2/5,1/2,2/3)	(2/5,1/2,2/3)	(1/3,2/5,1/2)	(2/5,1/2,2/3)	(1/2,2/3,1)	(2/5,1/2,2/3)	(3/2,2,5/2	1,1,1	(2/5,1/2,2/3)	(2/5,1/2,2/3)	(2/5,1/2,2/3)	(2/5,1/2,2/3)	0.0391
Transverse resistance	(2/5,1/2,2/3)	(2/5,1/2,2/3)	(2/5,1/2,2/3)	(2/5,1/2,2/3)	(2/5,1/2,2/3)	(1,3/2,2)	(1,3/2,2)	(3/2,2,5/2)	(3/2,2,5/2)	1,1,1	(1/2,2/3,1)	(1/2,2/3,1)	(1/2,1,3/2)	0.0635
Fracture Porosity	(1,3/2,2)	(1/2,2/3,1)	(3/2,2,5/2)	(2/5,1/2,2/3)	(1,3/2,2)	(1,3/2,2)	(1,3/2,2)	(3/2,2,5/2)	(3/2,2,5/2)	(1,3/2,2)	1,1,1	(1/2,2/3,1)	(2/5,1/2,2/3)	0.0856
Moisture content	(1/2,1,3/2)	(3/2,2,5/2)	(3/2,2,5/2)	(2/5,1/2,2/3)	(3/2,2,5/2)	(3/2,2,5/2)	(1/2,2/3,1)	(3/2,2,5/2)	(3/2,2,5/2)	(1,3/2,2)	(1,3/2,2)	1,1,1	(1/2,2/3,1)	(1/2,1,3/2)
Transmissivity	(1,3/2,2)	(3/2,2,5/2)	(3/2,2,5/2)	(2/5,1/2,2/3)	(1,3/2,2)	(1,3/2,2)	(1/2,2/3,1)	(3/2,2,5/2)	(3/2,2,5/2)	(1,3/2,2)	(3/2,2,5/2)	(1,3/2,2)	1,1,1	0.0979

Table 5. A2 Fuzzy AHP weights of the sub-conditioning factors

Conditioning factors	Class	Class Range	Area in Sq. Km	Area in %	Fuzzy AHP weights	Remarks
Longitudinal conductance	1	0.048-2.122	2387.04	61.50	0.451	Very high GWP and very low PC
	2	2.123-6.271	1221.59	31.475	0.250	High GWP and Low PC
	3	6.272-13.93	165.74	4.27	0.189	Moderate GWP and moderate PC
	4	13.94-25.26	69.66	1.79	0.142	Low GWP and high PC
	5	25.27-40.74	37.04	0.95	0.105	Very low GWP and very high PC
Longitudinal Resistance	1	0.006-32.775	903.85	23.28	0.052	Very low GWP
	2	32.776-58.054	1614.44	41.59	0.048	Low GWP
	3	58.055-89.886	771.32	19.87	0.087	Moderate GWP
	4	89.887-139.51	432.19	11.13	0.125	High GWP
	5	139.52-238.75	159.27	4.10	0.189	Very high GWP
Transverse Resistance	1	48.66-57570	1771.83	45.65	0.145	Very low GWP
	2	57580-187000	1526.49	39.33	0.157	Low GWP
	3	187100-421900	312.10	8.04	0.189	Moderate GWP
	4	422000-723800	179.38	4.62	0.195	High GWP
	5	723900-1222000	91.30	2.35	0.257	Very high GWP
Coefficient of Electrical Anisotropy	1	0.592-120.786	2601.34	67.03	0.052	Very low GWP
	2	120.787-407.403	864.04	22.26	0.098	Low GWP
	3	407.404-869.688	199.82	5.15	0.105	Moderate GWP
	4	869.689-1498.4	139.25	3.59	0.115	High GWP
	5	1498.41-2358.25	76.65	1.97	0.254	Very high GWP
Formation Resistivity	1	0-105	2933.17	75.58	0.012	Very low GWP
	2	106-407	655.58	16.89	0.027	Low GWP
	3	48-1000	199.79	5.15	0.098	Moderate GWP
	4	1010-1850	59.37	1.53	0.105	High GWP
	5	1860-297	33.19	0.86	0.147	Very high GWP
Fracture porosity	1	0-0.396	2408.55	62.06	0.048	Very low GWP
	2	0.396-1.1	880.47	22.69	0.059	Low GWP
	3	1.101-2.09	335.31	8.64	0.088	Moderate GWP
	4	2.091-3.38	192.91	4.97	0.142	High GWP
	5	3.39-5.611	63.86	1.65	0.189	Very high GWP
Bulk Density	1	1.26-1.481	509.78	13.13	0.027	Very low GWP
	2	1.481-1.587	1232.30	31.75	0.035	Low GWP
	3	1.588-1.686	1618.19	41.69	0.058	Moderate GWP

	4	1.687-1.855	439.48	11.32	0.079	High GWP
	5	1.856-2.197	81.35	2.10	0.088	Very high GWP
Porosity	1	26.83-38.75	539.02	13.89	0.115	Very high GWP
	2	38.76-43.25	1285.82	33.13	0.098	High GWP
	3	43.26-48.91	1233.40	31.78	0.085	Moderate GWP
	4	48.92-59.27	772.50	19.90	0.558	Low GWP
	5	59.28-76.67	50.35	1.30	0.459	Very low GWP
Permeability	1	3.414-21.66	1873.75	48.28	0.114	Very low GWP
	2	21.67-32.89	1202.50	30.98	0.125	Low GWP
	3	32.9-48.8	543.12	13.99	0.137	Moderate GWP
	4	48.81-77.34	215.54	5.55	0.148	High GWP
	5	77.35-122.7	46.19	1.19	0.189	Very high GWP
Hydraulic Conductivity	1	1.553-44.549	2820.77	72.68	0.147	Very low GWP
	2	44.55-96.143	605.32	15.60	0.189	Low GWP
	3	96.144-168.38	271.28	6.99	0.201	Moderate GWP
	4	168.39-285.32	147.97	3.81	0.251	High GWP
	5	285.33-440.11	35.76	0.92	0.289	Very high GWP
Transmissivity	1	10.152-212.49	2245.26	57.85	0.159	Very low GWP
	2	212.5-414.82	1119.89	28.85	0.170	Low GWP
	3	414.83-784.3	396.89	10.23	0.189	Moderate GWP
	4	784.31-1400.1	79.13	2.04	0.199	High GWP
	5	1400.2-2253.4	39.93	1.03	0.205	Very high GWP
Moisture content (%)	1	0.99-7.14	1564.01	40.30	0.112	Very low GWP
	2	7.105-12.91	1311.38	33.79	0.124	Low GWP
	3	12.92-20.31	582.53	15.01	0.135	Moderate GWP
	4	20.32-32.32	367.42	9.47	0.145	High GWP
	5	32.33-51.13	55.75	1.44	0.225	Very high GWP
Water holding capacity (%)	1	17.26-37.89	1109.18	28.58	0.144	Very low GWP
	2	37.9-46.24	958.44	24.69	0.157	Low GWP
	3	46.25-54.86	1088.43	28.04	0.192	Moderate GWP
	4	54.87-64.78	583.49	15.03	0.254	High GWP
	5	64.79-83.84	141.55	3.65	0.299	Very high GWP

Table 6. A1 Weights assigned to the sub parameters

Parameter	Class	Area in sq.km	Area in %	Fuzzy weight	Rank
Slope in degrees	0-0.56	1199.53	30.91	0.348	1
	0.57-1.2	1594.96	41.10	0.230	2
	1.3-1.9	838.22	21.60	0.176	3
	2-5.5	246.22	6.35	0.130	4
	5.6-20	1.4175	0.04	0.112	5
Soil media	Fine-fine loamy	725.12	18.69	0.068	7
	Fine- very fine	11.57	0.30	0.065	8
	Fine	814.77	21.01	0.075	6
	Fine loamy	1320.96	34.05	0.103	5
	Fine loamy- coarse loamy	548.15	14.13	0.126	4
	Gravelly loam	30.89	0.80	0.216	1
	Gravelly loam-loam	83.64	2.16	0.162	3
	Fine loamy- sandy	343.78	8.86	0.169	2
pH	5.6-6.1	343.92	8.86	0.171	1
	6.2-6.4	373.23	9.62	0.120	2
	6.5-6.7	524.16	13.51	0.070	4
	6.8-6.9	1753.86	45.19	0.067	5
	7-7.4	885.73	22.82	0.072	3
Geology	Gravel, sand, silt and clay	35.94	0.93	0.103	1
	Granite gneiss	495.22	12.77	0.053	6
	Lateritic soil/ laterite	1605.08	41.38	0.046	8
	Sand, silt & gravel (present day deposit)	185.72	4.79	0.086	3
	Yellowish brown fine sand, silt, clay	294.51	7.59	0.073	4
	Gravel and conglomerate	0.56	0.01	0.070	5
	Hornblende gneiss	1.42	0.04	0.039	11
	Hornblende schist, amphibolite, meta ultrabasite	2.01	0.05	0.038	12
	Mica schist with hornblende schist	123.34	3.18	0.039	11
	Grit and clay	0.32	0.01	0.040	10
	Quartz tourmaline rock	0.42	0.01	0.040	10
	Sand, silt, clay , calcareous concretions	1127.20	29.06	0.088	2
	Hornblende schist and epidiorite	3.12	0.08	0.040	10
	Gabbro	0.62	0.02	0.048	7
	Mica schist / schist	0.03	0.00	0.040	10
	Tourmaline quartz rock	0.80	0.02	0.040	10
	Quartzite, cherty quartzite	0.63	0.02	0.040	10

	Unclassified sediment, clay&grit and conglomerate	2.04	0.05	0.041	9
	Pegmatite	0.30	0.01	0.041	9
Aquifer depth	Shallow aquifer (5-15mbgl)	919.39	23.63	0.343	1
	Semi confined (20mbgl)	1682.82	43.25	0.222	2
	Unconfined aquifer (30 mbgl)	647.61	16.64	0.164	3
	Unconfined aquifer (40-50mbgl)	576.64	14.82	0.126	4
	Unconfined to confined 45-80mbgl)	64.65	1.66	0.137	5
Specific yield	0.015 (1.5%)	1.95	0.05	0.129	5
	0.025 (2.5%)	1604.40	41.34	0.119	4
	0.03 (3%)	625.92	16.13	0.156	3
	0.06 (6%)	187.91	4.84	0.240	2
	0.1(10%)	1460.88	37.64	0.357	1
Impact of vadose zone	Sands with silts, clays associated with Fe-nodules	342.36	8.81	0.157	1
	Sands with silts, clay impregnated with caliche nodules	768.88	19.78	0.140	2
	Sands and silts in alternate layer	1352.44	34.80	0.121	3
	Sand, silt and clay	784.14	20.17	0.111	4
	Pink granite/biotite-granite gneiss	442.71	11.39	0.098	5
	Mica schist, occasionnally garnetiferrous	113.09	2.91	0.087	6
	Metamorphosed basic rocks	2.89	0.07	0.074	7
	Laterite	7.42	0.19	0.069	8
	Granite gneiss, migmatite	51.69	1.33	0.058	9
	Granite gneiss	15.91	0.41	0.047	10
	Ferruginous sediments with rock fragments	5.23	0.13	0.037	11
Hydraulic conductivity (micrometer/sec)	0.42-1.41	826.34	21.30	0.222	4
	1.41-4.23	2389.86	61.61	0.224	3
	14.11-42.34	548.15	14.13	0.256	2
	42.34-141.14	114.54	2.95	0.302	1
Groundwater level (mbgl)	1.5-5.16	1195.30	30.80	0.347	1
	5.17-7.09	1653.60	42.61	0.236	2
	7.10-9.56	549.99	14.17	0.181	3
	9.57-13.1	296.83	7.65	0.128	4
	13.2-21.2	185.44	4.78	0.108	5
Recharge (Ham)	3.3785 - 1,293.4	828.84	21.36	0.103	1
	1,293.5 - 2,583.5	1613.49	41.57	0.126	2
	2,583.6 - 3,873.5	1144	29.48	0.172	3
	3,873.6 - 5,163.6	142.16	3.66	0.259	4

	5,163.7 - 6,453.6	152.67	3.93	0.339	5
Land use and land cover	Lateritic exposure	65.78	1.69	0.150	3
	Sand bar	5.73	0.15	0.083	5
	Settlement	61.21	1.58	0.172	1
	Water body	29.27	0.75	0.081	8
	Wet fallow	985.84	25.40	0.087	5
	Open forest	72.47	1.87	0.082	7
	Dry fallow	1106.75	28.52	0.151	2
	Dense forest	229.52	5.91	0.081	8
	Agricultural Land	1324.6	34.13	0.112	4
Population density (Persons/sq.km)	153.38-386.44	1202.364	30.98	0.109	5
	386.45-571.04	1201.838	30.97	0.142	4
	571.05-809.49	933.201	24.05	0.185	3
	809.50-1155.60	448.011	11.54	0.242	2
	1157.70-2124.80	95.4909	2.46	0.323	1
Groundwater based irrigation schemes	4-251	502.508	12.95	0.106	5
	251-771	313.284	8.07	0.139	4
	771-1347	1051.28	27.09	0.190	3
	1347-2527	1186.66	30.57	0.220	2
	2527-3681	827.447	21.32	0.343	1

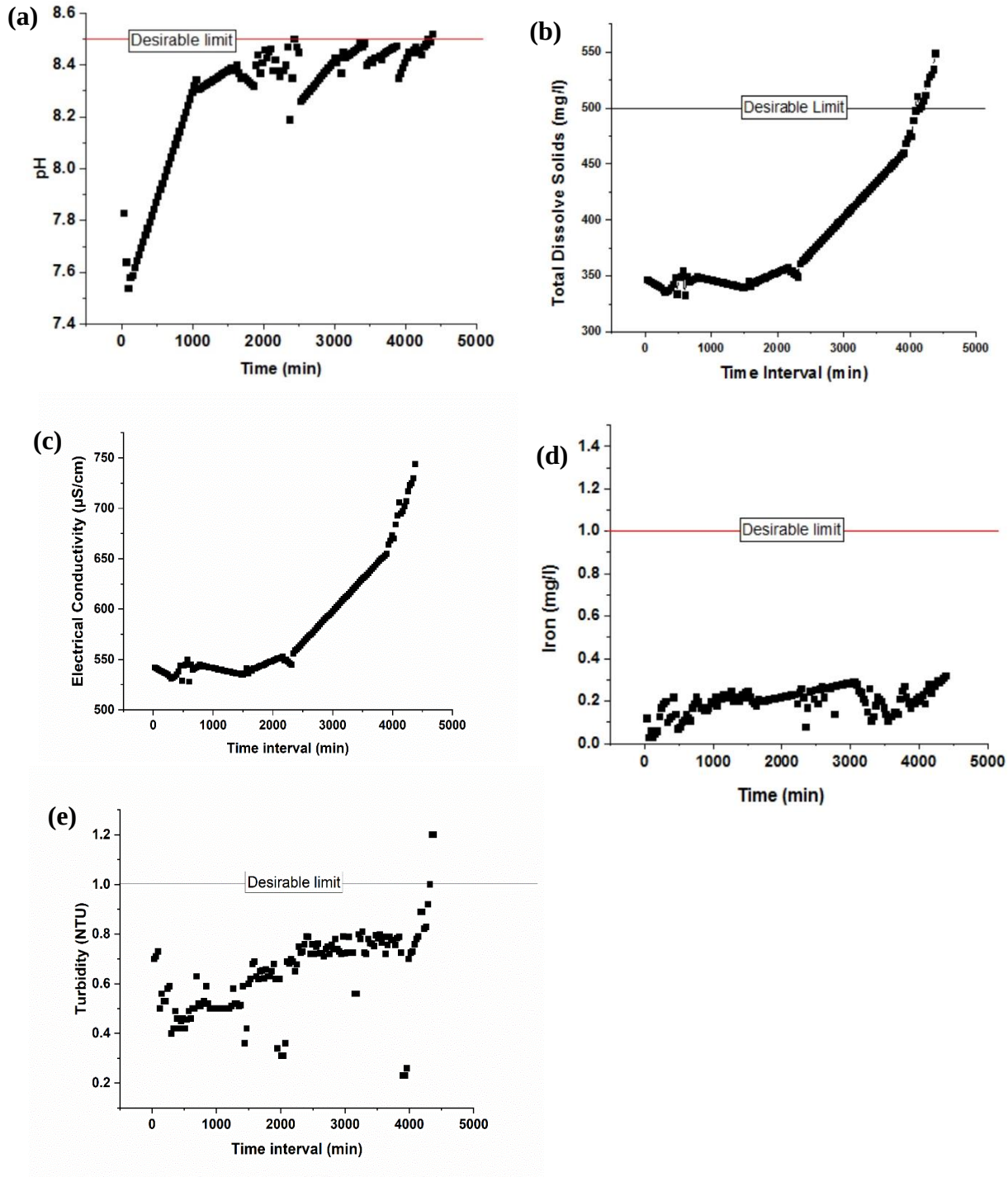

Fig. 7. A1 (a) ph; (b) TDS (mg/l); (c) EC (µS/cm); (d) Iron (mg/l) (e) Turbidity (NTU) as obtained from the fixed bed column leaching test

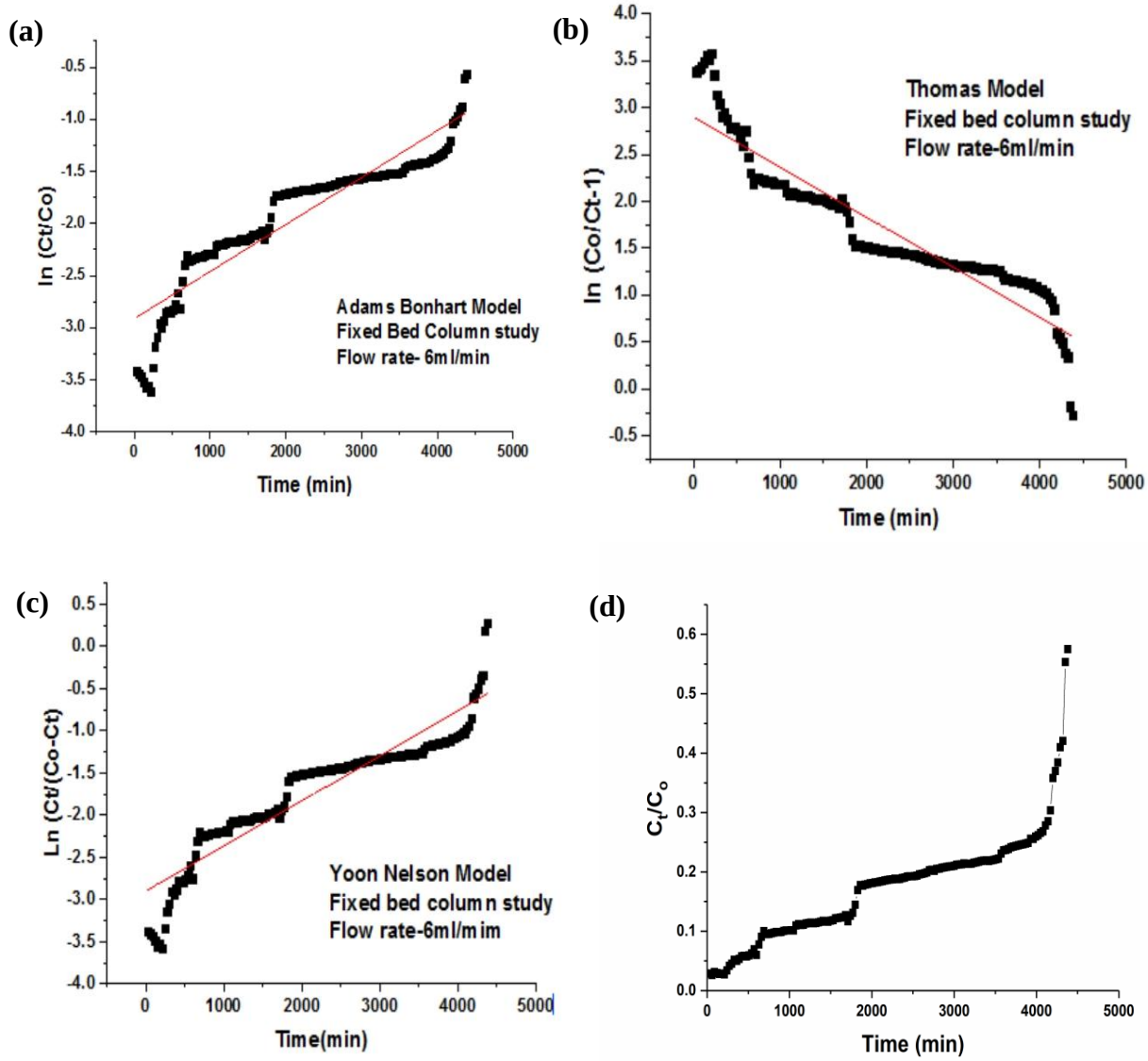

Fig. 7. A2. Linear plot of (a) Adams Bonhart Model; (b) linear plot of Thomas model and (c) linear plot of Yoon Nelson model (d) fluoride breakthrough curve

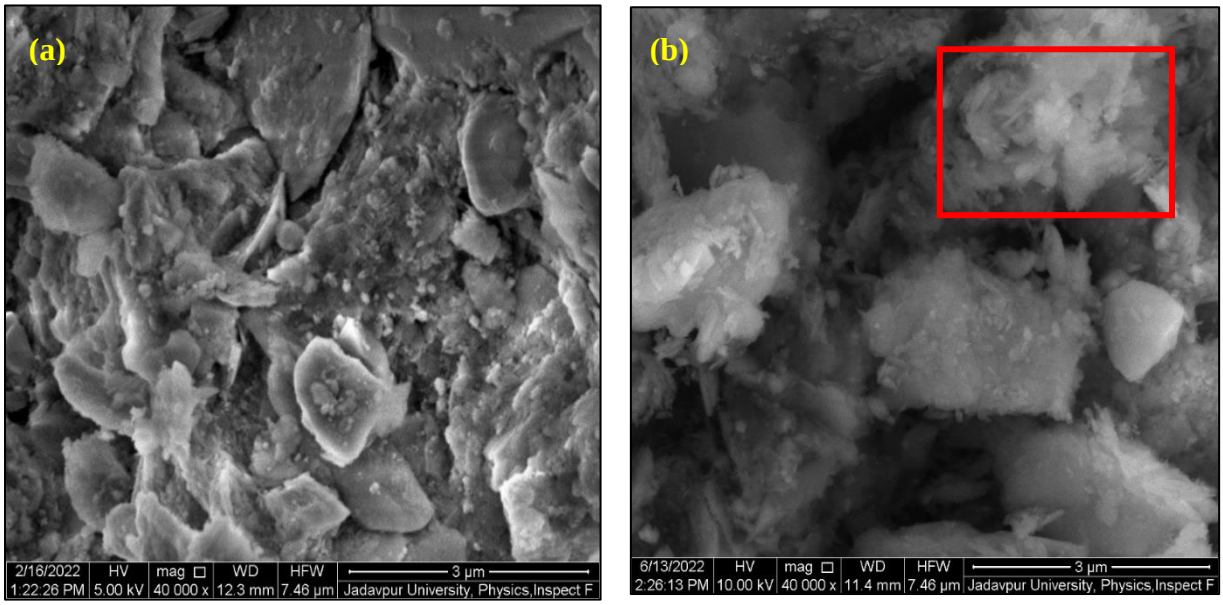

Fig. 7. A3. FESEM characterizations of red kaolinite lithomarge laterite soil at 3µm scale- (a) before and (b) after the fixed column bed filtration study

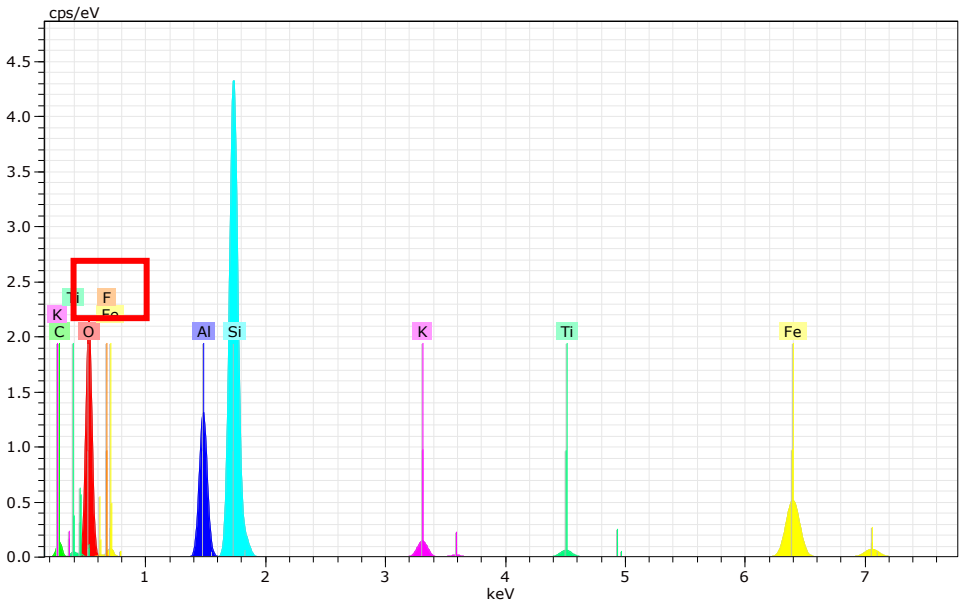

Fig. 7. A4. EDX spectra of column filter sludge

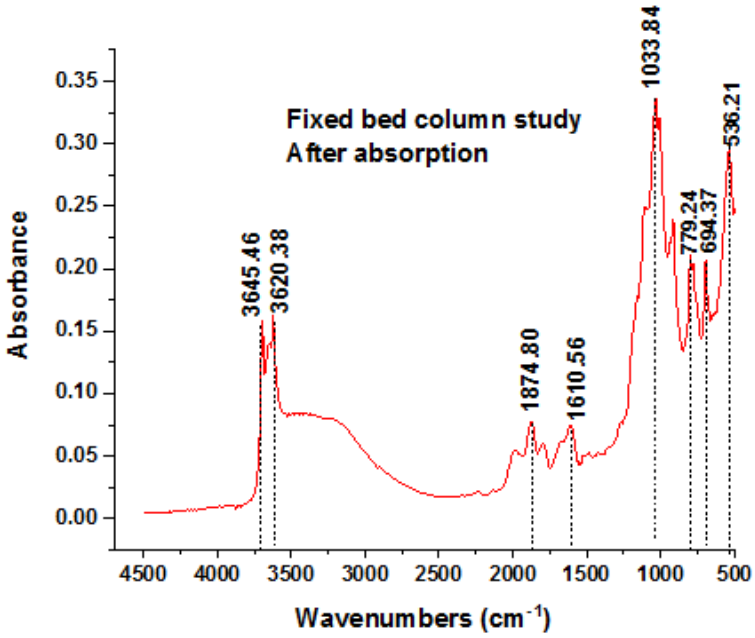

Fig. 7. A5. Fourier Transformation Infrared (FTIR) spectral data of column filter sludge

Table 7. A1. Water quality analysis of Lakshmisagar Village 1: before and after column leaching test

Parameters	WHO limit, 2011	BIS Acceptable Limit (BIS, 2012)	Water collected from field (Lakshmisagar Village 1)	After running through column leaching test (after 60 min)
pH	Not Specified	6.5–8.5	6.4	7.38
TDS	1000	500	356	347
EC (µS/cm)	300	Not Specified	574	550
Iron (mg/l)	0.3	0.3	1.22	0.12
Turbidity NTU	5	1	0.56	0.7
Fluoride (mg/l)	1.5	1	2.37	0.07
Temperature (°C)	Not Specified	Not Specified	36.2	30
Alkalinity (mg/l)	Not Specified	200	320	40
Sodium (mg/l)	200	-	73.04	7.5
Potassium (mg/l)	12	Not Specified	82.92	2.62
Calcium (mg/l)	Not Specified	75	40	18
Sulphate (mg/l)	250	200	1	0
Phosphate (mg/l)	0.1	Not Specified	0.85	0.01
Magnesium (mg/l)	100	30	150	2.302
Chloride (mg/l)	250	250	104.93	19.85

Chapter10
References

Abdullah, N., Yusof, N., Lau, W. J., Jaafar, J., & Ismail, A. F. (2019). Recent trends of heavy metal removal from water/wastewater by membrane technologies. Journal of Industrial and Engineering Chemistry, 76, 17-38.

Abdullateef, L., Tijani, M.N., Nuru, N.A., John, S., Mustapha, A., (2021). Assessment of groundwater recharge potential in a typical geological transition zone in Bauchi, NE-Nigeria using remote sensing/GIS and MCDA approaches. Heliyon. 2021;7 (4): e06762. Published 2021 Apr 30. doi:10.1016/j.heliyon.2021.e06762

Aburub, F., & Hadi, W. (2016). Predicting groundwater areas using data mining techniques: Groundwater in Jordan as case study. International Journal of Computer and Information Engineering, 10(9), 1621-1624.

Acharya T, Nag SK (2013) Study of Groundwater Prospects of the Crystalline Rocks in Purulia District, West Bengal, India Using Remote Sensing Data. Earth Resour. 2013, 1, 54–59. [CrossRef]

Acharya, G. D., Hathi, M. V., Patel, A.D., Parmar, K.C., (2008). Chemical properties of groundwater in bhiloda taluka region, north Gujarat, India. E-Journal of Chemistry. 2008;5(4):792–796. doi: 10.1155/2008/592827.

Acharya, T., Prasad, R. (2017). Litho stratigraphic contact–a significant site for hydrogeological investigation in crystalline fractured-rock terrains. J Earth Syst Sci 126(1). https://doi.org/10.1007/s12040-016-0784-9

Adebayo, O.S., and Abraham, A., (2017). Aquifer, Classification and Characterization Submitted: June 30th, 2017Reviewed: November 24th, 2017Published: August 1st, 2018, DOI: 10.5772/intechopen.72692

Adhikari, R. K., Mohanasundaram, S., & Shrestha, S. (2020). Impacts of land-use changes on the groundwater recharge in the Ho Chi Minh city, Vietnam. Environmental Research, 185, 109440.

Adimalla N, Qian H (2022). Evaluation of non-carcinogenic causing health risks (NCHR) associated with exposure of fluoride and nitrate contaminated groundwater from a semi-arid region of south India. Environ Sci Pollut Res (2022). https://doi.org/10.1007/s11356-022-21771-0

Adimalla N, Taloor AK (2019). Hydrogeochemical investigation of groundwater quality in the hard rock terrain of South India using Geographic Information System (GIS) and groundwater quality index (GWQI) techniques. Groundwater for Sustainable Development, 100288. doi:10.1016/j.gsd.2019.100288

Aeschbach-Hertig W, Gleeson T (2012). Regional strategies for the accelerating global problem of groundwater depletion. Nature Geosci 5, 853–861. https://doi-org.manchester.idm.oclc.org/10.1038/ngeo1617

Afrasiabi, A., Tavana, M., Di Caprio, D. (2022). An extended hybrid fuzzy multi-criteria decision model for sustainable and resilient supplier selection. Environ Sci Pollut Res 29, 37291–37314 (2022). https://doi.org/10.1007/s11356-021-17851-2

AghaKouchak A, Farahmand A, Melton FS, Teixeira J, Anderson M C, Wardlow B D, Hain C R (2015) Remote sensing of drought: Progress, challenges and opportunities. Reviews of Geophysics, 53(2), 452–480. doi:10.1002/2014rg000456

Aguş, O., Abalı, Y., Arslan, O., & Keskin, N. O. S. (2019). Facile and controlled production of silver borate nanoparticles. SN Applied Sciences, 1, 1-8.

Agyemang, V.O. (2022). Geophysical investigation of groundwater potential and aquifer protective capability in selected communities within Cape Coast municipality, Ghana. Appl Water Sci 12, 23 (2022). https://doi.org/10.1007/s13201-021-01558-3

Aher S, Shinde S, Guha S, Majumder. (2017). Identification of drought in Dhalai river watershed using MCDM and ANN models. J. Earth Syst. Sci. 2017, 126, 21.

Ahmad, A., Kurniawan, S. B., Abdullah, A. R. Othman, H. A. Hasan, (2022). Exploring the extraction methods for plant-based coagulants and their future approaches. Science of the Total Environment, (2022). 818, 151668.

Ahmad, M. (2012). Iron and Manganese removal from groundwater: Geochemical modeling of the Vyredox method (Master's thesis).

Ahmad, W., Iqbal, J., Nasir, M.J. et al., (2021). Impact of land use/land cover changes on water quality and human health in district Peshawar Pakistan. Sci Rep 11, 16526 2021. https://doi.org/10.1038/s41598-021-96075-3

Ahmed, M. B., Zhou, J. L., Ngo, H. H., & Guo, W. (2015). Adsorptive removal of antibiotics from water and wastewater: progress and challenges. Science of the Total Environment, 532, 112-126.

Aisuebeogun AO, Ezekwe IC (2013). Application of Basin Morphometry Laws in catchments of the south-western quadrangle of south-eastern Nigeria. Front. Earth Sci. 7: 361–374.https://doi.org/10.1007/s11707-013-0356-0

Akafu, T., Chimdi, A., & Gomoro, K. (2019). Removal of fluoride from drinking water by sorption using diatomite modified with aluminum hydroxide. Journal of analytical methods in chemistry, 2019.

Akbari, H., Jorfi, S., Mahvi, A. H., Yousefi, M., & Balarak, D. (2018). Adsorption of fluoride on chitosan in aqueous solutions: determination of adsorption kinetics. Fluoride, 51(4), 319-327.

Akhil, D., Lakshmi, D., Kartik, A. et al. (2021). Production, characterization, activation and environmental applications of engineered biochar: a review.(2021) Environ Chem Lett 19, 2261–2297 (2021). https://doi.org/10.1007/s10311-020-01167-7

Akhter, G., Ge, Y., Hasan, M., & Shang, Y. (2022). Estimation of Hydrogeological Parameters by Using Pumping, Laboratory Data, Surface Resistivity and Thiessen Technique in Lower Bari Doab (Indus Basin), Pakistan. Applied Sciences, 12(6), 3055.

Akram, W.S.K., Mondal, I., Bandyopadhyay, J., (2019). Crop suitability analysis in water resource management of Paschim Medinipur District, India: a remote sensing approach. Sustain. Water Resour. Manag. 5, 797–815, 2019. https://doi.org/10.1007/s40899-018-0262-4

Akram. M., Ramzan, N., Feng, F. (2022). Extending COPRAS Method with Linguistic Fermatean Fuzzy Sets and Hamy Mean Operators", Journal of Mathematics, vol. (2022), Article ID 8239263, 26 pages, 2022. https://doi.org/10.1155/2022/8239263

Aktar N (2015) Agricultural Productivity and Productivity Regions in West Bengal, The NEHU Journal, Vol XIII, No. 2, July-December 2015, pp-49-61

Akter, T., Jhohura, F.T., Akter, Fet. Al., (2016). Water Quality Index for measuring drinking water quality in rural Bangladesh: a cross-sectional study. J Health Popul Nutr 35, 4. https://doi.org/10.1186/s41043-016-0041-5

Akurugu B A, Obuobie E, Yidana SM, Stisen S, Seidenfaden I K, Chegbeleh LP (2022).Groundwater resources assessment in the Densu Basin: A review. Journal of Hydrology: Regional Studies, 40, 101017.

Alahacoon N, Edirisinghe M, Ranagalage M (2021).Satellite-Based Meteorological and Agricultural Drought Monitoring for Agricultural Sustainability in Sri Lanka. Sustainability, 13, 3427. https://doi.org/10.3390/su13063427

Alam, M. F., Pavelic, P., Villholt, K.G., Sikka, A., Pande, S. (2022). Impact of high-density managed aquifer recharge implementation on groundwater storage, food production and resilience: A case from Gujarat, India. Journal of Hydrology: Regional Studies, 44, [101224]. https://doi.org/10.1016/j.ejrh.2022.101224

Alamne, S.B., Assefa, T.T., Belay, S.A. et al., (2022). Mapping groundwater nitrate contaminant risk using the modified DRASTIC model: a case study in Ethiopia. Environ Syst Res 11, 8. https://doi.org/10.1186/s40068-022-00253-9

Al-Amshawee, S., Yunus, M. Y. B. M., Azoddein, A. A. M., Hassell, D. G., Dakhil, I. H., & Hasan, H. A. (2020). Electrodialysis desalination for water and wastewater: A review. Chemical Engineering Journal, 380, 122231.

Alarifi, S. S., Abdelrahman, K., & Hazaea, B. Y. (2022). Depicting of groundwater potential in hard rocks of southwestern Saudi Arabia using the vertical electrical sounding approach. Journal of King Saud University-Science, 34(7), 102221.

AL-Darwish, N., & Abu-Sharar, T. M. (2021). Kinetics of fluoride adsorption onto native and Mg (OH) 2-amended limestone. Applied Water Science, 11, 1-13.

Alfy, M.E., Lashin, A., Faraj, T. et al. (2019). Quantitative hydro-geophysical analysis of a complex structural karst aquifer in Eastern Saudi Arabia. Sci Rep 9, 2825 (2019). https://doi.org/10.1038/s41598-019-39192-4

Alhashimi, H.; Aktas, C. (2017). Life cycle environmental and economic performance of biochar compared with activated carbon: A meta-analysis. Resources, Conservation and Recycling 2017, 118, 13−26 (19) (PDF) Functional Biochar and Its Balanced Design.

Ali, S., Fakhri, Y., Golbini, M., Thakur, S. K., Alinejad, A., Parseh, I., & Bhattacharya, P. (2019). Concentration of fluoride in groundwater of India: a systematic review, meta-analysis and risk assessment. Groundwater for Sustainable Development, 9, 100224.

Ali, S., Khorrami, B., Jehanzaib, M., Tariq, A., Ajmal, M., Arshad, A., & Khan, S. N. (2023). Spatial downscaling of GRACE data based on XGBoost model for improved understanding of hydrological droughts in the indus basin irrigation system (IBIS). Remote Sensing, 15(4), 873.

Ali, W., Rasool, A., Junaid, M., & Zhang, H. (2019). A comprehensive review on current status, mechanism, and possible sources of arsenic contamination in groundwater: a global perspective with prominence of Pakistan scenario. Environmental geochemistry and health, 41, 737-760.

Alkhatib, J., Engelhardt, I., Sauter, M. (2021). Identification of suitable sites for managed aquifer recharge under semi-arid conditions employing a combination of numerical and analytical techniques. Environ Earth Sci 80, 554 (2021). https://doi.org/10.1007/s12665-021-09797-y

Aller, L., Bennet, T., Lehr, J.H., Petty, R.J. and Hacket, G., (1985). DRASTIC: A standardized system for evaluating groundwater pollution using hydrological settings. Prepared by the National water Well Association for the US EPA Office of Research and Development, Ada

Al-Maliky, E. A., Gzar, H. A., & Al-Azawy, M. G. (2021). Determination of point of zero charge (PZC) of concrete particles adsorbents. In IOP Conference Series: Materials Science and Engineering (Vol. 1184, No. 1, p. 012004). IOP Publishing.

Alsulaiman, M.A., Aboukarima, A.M. (2016). Prediction of unsaturated hydraulic conductivity of agricultural soils using artificial neural network and c#", Journal of Agriculture and Ecology Research International, v. 5, n. 4, 21622, 2016 (12)

Altaf S, Meraj G, Romshoo SA (2014). Morphometry and land cover based multi-criteria analysis for assessing the soil erosion susceptibility of the western Himalayan watershed. Environ Monit Assess 186, 8391–8412 (2014). https://doi.org/10.1007/s10661-014-4012-2

Amar, S., Sudiarso, A., Herliansyah, M.K. (2020). The Accuracy Measurement of Stock Price Numerical Prediction. Journal of Physics: Conference Series, 1569, 032027. doi:10.1088/1742-6596/1569/3/032027

Ameri A A, Pourghasemi H R, Cerda A (2018). Erodibility prioritization of sub-watersheds using morphometric parameters analysis and its mapping: A comparison among TOPSIS, VIKOR, SAW, and CF multi-

criteria decision making models. Science of the Total Environment, 613-614: 1385–1400. doi:10.1016/j.scitotenv.2017.09.210

Ameur, M., Aouiti, S., Hamzaoui-Azaza, F., Cheikha, L. B., & Gueddari, M. (2021). Vulnerability assessment, transport modeling and simulation of nitrate in groundwater using SI method and modflow-MT3DMS software: case of Sminja aquifer, Tunisia. Environmental Earth Sciences, 80, 1-16.

Amiri, V., Sohrabi, N., Li, P. et al. (2022). Estimation of hydraulic conductivity and porosity of a heterogeneous porous aquifer by combining transition probability geostatistical simulation, geophysical survey, and pumping test data. Environ Dev Sustain (2022). https://doi.org/10.1007/s10668-022-02368-6

Amparan P, Alvarez P, Quintero V, Aragón V, Ramos R, Salvador M, Guerrero V (2019). A Multivariate Geomorphometric Approach to Prioritize Erosion-Prone Watersheds. Sustainability, 11: 5140. doi:10.3390/su11185140

Anah, L., & Astrini, N. (2018). Isotherm adsorption studies of Ni (II) ion removal from aqueous solutions by modified carboxymethyl cellulose hydrogel. In IOP Conference Series: Earth and Environmental Science (Vol. 160, No. 1, p. 012017). IOP Publishing.

Anand B, Karunanidhi D (2020). Long term spatial and temporal rainfall trend analysis using GIS and statistical methods in Lower Bhavani basin, Tamil Nadu, India, Indian J Mar Science, 49 (3) (2020), pp. 419-427

Andersen, W. C., & Bruno, T. J. (2003). Application of a gas–liquid entraining rotor to supercritical fluid extraction: Removal of iron (III) from water. Analytica chimica acta, 485(1), 1-8.

Annan, E., Nyankson, E., Agyei-Tuffour, B., Armah, S. K., Nkrumah-Buandoh, G., Hodasi, J. A. M., & Oteng-Peprah, M. (2021). Synthesis and characterization of modified kaolin-bentonite composites for enhanced fluoride removal from drinking water. Advances in Materials Science and Engineering, 2021, 1-12.

Annual food report (2018). Irrigation and waterways directorate. Government of West Bengal. https://wbiwd.gov.in/uploads/anual_flood_report/ANNUAL_FLOOD_REPORT_2018.pdf

Annual Report 2018-2019, Central Water Commission, Government of India Ministry of Water Resources, River Development & Ganga Rejuvenation, http://cwc.gov.in/sites/default/files/arcwc2018-19.pdf

Antelmi, M., Alberti, L., Barbieri, S., & Panday, S. (2021). Simulation of thermal perturbation in groundwater caused by Borehole Heat Exchangers using an adapted CLN package of MODFLOW-USG. Journal of Hydrology, 596, 126106.

Antonakos, A.K., Lambrakis, N.J., (2007). Development and testing of three hybrid methods for the assessment of aquifer vulnerability to nitrates, based on the drastic model, an example from NE Korinthia, Greece. J Hydrol 333:288–304

Antunes, M. L. P., Couperthwaite, S. J., da Conceicao, F. T., Costa de Jesus, C. P., Kiyohara, P. K., Coelho, A. C. V., & Frost, R. L. (2012). Red mud from Brazil: thermal behavior and physical properties. Industrial & Engineering Chemistry Research, 51(2), 775-779.

Aown, A., Kar, N.S., (2016). Lateritic Badland of Sinhati, Bankura, West Bengal: A Geomorphic Investigation. In: Das, B., Ghosh, S., Islam, A., Ismail, M. (eds) Neo-Thinking on Ganges-Brahmaputra Basin Geomorphology. Springer Geography. Springer, Cham. https://doi.org/10.1007/978-3-319-26443-1_2

APHA (2005). Standard Methods for the Examination of Water and Wastewater. 21st Edition, American Public Health Association/American Water Works Association/Water Environment Federation, Washington DC.

Apparao, B. V., & Karthikeyan, G. (1986). Permissible limits of fluoride ion in drinking water in Indian rural environment. Indian Journal of Environmental Protection, 6, 172-175.

Arabameri A, Pradhan B, Pourghasemi HR, Rezaei K (2018) Identification of erosion-prone areas using different multi-criteria decision-making techniques and GIS. Geomatics, Natural Hazards and Risk, 9:1129–1155. doi:10.1080/19475705.2018.1513084

Arabameri, A., Pal, S. C., Rezaie, F., Nalivan, O. A., Chowdhuri, I., Saha, A., & Moayedi, H. (2021). Modeling groundwater potential using novel GIS-based machine-learning ensemble techniques. Journal of Hydrology: Regional Studies, 36, 100848.

Arabameri, A., Pourghasemi, H.R. (2019). Spatial Modeling of Gully Erosion Using Linearand Quadratic Discriminant Analyses in GIS and R. In Spatial Modeling in GIS and R for Earth and Environmental Sciences, Elsevier, 2019, pp. 299–321

Arbelaez Breton, L., Mahdi, Z., Pratt, C., & El Hanandeh, A. (2021). Modification of hardwood derived biochar to improve phosphorus adsorption. Environments, 8(5), 41.

Arefin R, Mohir M M I & Alam J (2020). Watershed prioritization for soil and water conservation aspect using GIS and remote sensing: PCA-based approach at northern elevated tract Bangladesh. Appl Water Sci, 10, 9. https://doi.org/10.1007/s13201-020-1176-5

Arekhi M, Saglam S, Ozkan UY (2020) Drought monitoring and assessment using Landsat TM/OLI data in the agricultural lands of Bandar-e-Turkmen and Gomishan cities, Iran. Environ Dev Sustain 22, 6691–6708 . https://doi.org/10.1007/s10668-019-00509-y

Arni, S.A. (2018). Comparison of slow and fast pyrolysis for converting biomass into fuel. Renew. Energy 2018, 124, 197–201

Arunbose, S., Srinivas, Y., Rajkumar, S., Nair, N. C., & Kaliraj, S. (2021). Remote sensing, GIS and AHP techniques based investigation of groundwater potential zones in the Karumeniyar river basin, Tamil Nadu, southern India. Groundwater for Sustainable Development, 14, 100586.

Arya S, Subramani T, Karunanidhi D (2020). Delineation of groundwater potential zones and recommendation of artificial recharge structures for augmentation of groundwater resources in Vattamalaikarai Basin, South India. Environ Earth Sci. 79, 102. https://doi.org/10.1007/s12665-020-8832-9 1

Asadabadi, M.R., Chang, E., Saberi, M., Zhou, Z., (Reviewing editor) (2019). Are MCDM methods useful? A critical review of Analytic Hierarchy Process (AHP) and Analytic Network Process (ANP), Cogent Engineering, 6:1, DOI: 10.1080/23311916.2019.1623153

Asfaw D, Workineh G (2019). Quantitative Analysis of Morphometry on Ribb and Gumara Watersheds: Implications for Soil and Water Conservation. International Soil and Water Conservation Research. doi:10.1016/j.iswcr.2019.02.003

Asfaw, D., Mengistu, D., (2020). Modeling megech watershed aquifer vulnerability to pollution using modified DRASTIC model for sustainable groundwater management, Northwestern Ethiopia, Groundwater for Sustainable Development, 11. 100375, ISSN 2352-801X,https://doi.org/10.1016/j.gsd.2020.100375.

Ashoori, R., Samaei, M. R., Yousefinejad, S., Azhdarpoor, A., Emadi, Z., Mohammadpour, A., ... & Khaneghah, A. M. (2022). Simultaneous removal of fluoride and nitrate from synthetic aqueous solution and groundwater by the electrochemical process using non-coated and coated anode electrodes: A human health risk study. Environmental Research, 214, 113938.

Aw, S., Briton, B. G. H., Drogui, P., Yao, K. B., & Adouby, K. (2022). Removal of fluoride in groundwater by adsorption using hydroxyapatite modified Corbula trigona shell powder. Chemical Engineering Journal Advances, 12, 100386.

Ayalew, A.A, (2023). Comparative adsorptive performance of adsorbents developed from kaolin clay and limestone for de-fluoridation of groundwater. South African Journal of Chemical Engineering, (2023). 44, 1-13

Ayogu CN, Phil-Eze PO, Ayogu N O. et al (2019). Morphometric analysis and the validity of Hortonian postulations in Anambra drainage basin, Nigeria. Spat. Inf. Res. 27: 505–520. https://doi.org/10.1007/s41324-019-00252-6

Ayrım Y, Atalay K, Can Gulin (2018). A New Stochastic MCDM Approach Based on Copras. International Journal of Information Technology & Decision Making. 17. 10.1142/S0219622018500116.

Babel, S.; Kurniawan, T. A. (2004). Cr(VI) removal from synthetic wastewater using coconut shell charcoal and commercial activated carbon modified with oxidizing agents and/or chitosan. Chemosphere2004, 54 (7), 951−967 (19) (PDF) Functional Biochar and Its Balanced Design.

Baeumler, P., Hupe, K. & Irnich, D. (2023). Proposal of a diagnostic algorithm for myofascial trigger points based on a multiple correspondence analysis of cross-sectional data. BMC Musculoskelet Disord 24, 62 (2023). https://doi.org/10.1186/s12891-023-06129-y

Bai, Z., Hu, C., Liu, H., & Qu, J. (2019). Selective adsorption of fluoride from drinking water using NiAl-layered metal oxide film electrode. Journal of Colloid and Interface Science, 539, 146-151.

Baig MRI, Shahfahad Naikoo MW et al. (2021).Spatio-temporal analysis of precipitation pattern and trend using standardized precipitation index and Mann–Kendall test in coastal Andhra Pradesh. Model. Earth Syst. Environ. (2021). https://doi.org/10.1007/s40808-021-01262-w

Bakeshlou, E.A., Khamseh, A.A., Asl, M.A.G. et al., (2010). Evaluating a green supplier selection problem using a hybrid MODM algorithm. J Intell Manuf 28, 913–927. https://doi.org/10.1007/s10845-014-1028-y

Barzegar, R., Razzagh, S., Quilty, J., Adamowski, J., Pour, H. K., & Booij, M. J. (2021). Improving GALDIT-based groundwater vulnerability predictive mapping using coupled resampling algorithms and machine learning models. Journal of hydrology, 598, 126370.

Basu, S. R., Bera, B., (2010). Jalobigyan (Text Book of Hydrology). https://www.researchgate.net/publication/327578595_Jalobigyan_Text_Book_of_Hydrology (access date (April, 2021). doi:10.1007/s11269-010-9749-y

Batabyal AK, Gupta S (2017). Fluoride-contaminated groundwater of Birbhum district, West Bengal, India: Interpretation of drinking and irrigation suitability and major geochemical processes using principal component analysis. Environ Monit Assess. 2017 Aug;189(8):369. doi: 10.1007/s10661-017-6041-0. Epub 2017 Jul 4. PMID: 28676931.

Batayneh, A. T. (2013). The estimation and significance of Dar-Zarrouk parameters in the exploration of quality affecting the Gulf of Aqaba coastal aquifer systems. Journal of Coastal Conservation, 17, 623-635.

Baxter, C., Hauer, F.R., Woessner, W.W. (2003). Measuring groundwater-stream water exchange: New techniques for installing mini piezometers and estimating hydraulic conductivity. Transactions of the American Fisheries Society, 132, no. 3: 493–502.

Bayewu, O. O., Oloruntola, M. O., Mosuro, G. O., Laniyan, T. A., Ariyo, S. O., & Fatoba, J. O. (2018). Assessment of groundwater prospect and aquifer protective capacity using resistivity method in Olabisi Onabanjo University campus, Ago-Iwoye, Southwestern Nigeria. NRIAG Journal of Astronomy and Geophysics, 7(2), 347-360.

Behera, A.K., Pradhan, R.M., Kumar, S., Chakrapani, G.J., Kumar, P. (2022). Assessment of Groundwater Flow Dynamics Using MODFLOW in Shallow Aquifer System of Mahanadi Delta (East Coast), India. Water 2022, 14, 611.https://doi.org/10.3390/w14040611

Benesty J, Chen J, Huang Y, Cohen I (2009).Pearson Correlation Coefficient. In: Noise Reduction in Speech Processing. Springer Topics in Signal Processing, vol 2. Springer, Berlin, Heidelberg. https://doi.org/10.1007/978-3-642-00296-0_5

Beqiraj A, Beqiraj E (2011). Effects of sediment mineralogy to high-iron content in the groundwater of Rrogozhina Aquifer (Western Albania). Studia UBB Geologia, 56(2), 25-30.

Bera A, Das S (2021). Water Resource Management in Semi-arid Purulia District of West Bengal, in the Context of Sustainable Development Goals. In: Shit P.K., Bhunia G.S., Adhikary P.P., Dash C.J. (eds) Groundwater and Society. Springer, Cham. https://doi.org/10.1007/978-3-030-64136-8_23

Bera B, Shit PK, Sengupta N et al (2022). Steady declining trend of groundwater table and severe water crisis in unconfined hard rock aquifers in extended part of ChotaNagpur Plateau, India. Appl Water Sci 12, 31 (2022). https://doi.org/10.1007/s13201-021-01550-x

Bera B, Shit PK, Sengupta N, Saha S, Bhattacharjee S (2021). Trends and variability of drought in the extended part of Chhota Nagpur plateau (Singbhum Protocontinent), India applying SPI and SPEI indices. Environ Challenges 5:100310. https://doi.org/10.1016/j.envc.2021.100310

Bera S, Chatterjee DN (2019). Delineation of crop combination region and changing pattern of cropping intensity: A Geographical Analysis in Ghatal sub-division, Paschim Medinipur district, West Bengal. Res. J. Humanities and Social Sciences. 2019; 10(1):127-136. doi: 10.5958/2321-5828.2019.00021.4

Bera, A., & Das, S. (2021). Water resource management in semi-arid Purulia district of West Bengal, in the context of sustainable development goals. Groundwater and society: applications of geospatial technology, 501-519.

Bera, A., Mukhopadhyay, B. P., & Barua, S. (2020). Delineation of groundwater potential zones in Karha river basin, Maharashtra, India, using AHP and geospatial techniques. Arabian Journal of Geosciences, 13, 1-21.

Bera, A., Mukhopadhyay, B. P., Chowdhury, P., Ghosh, A., Biswas, S., (2021). Groundwater vulnerability assessment using GIS-based DRASTIC model in Nangasai River Basin, India with special emphasis on agricultural contamination. Ecotoxicology and Environmental Safety, 214, 112085. doi:10.1016/j.ecoenv.2021.112085

Bera, B., & Ghosh, A. (2019). Fluoride dynamics in hydrogeological diversity and Fluoride Contamination Index mapping: a correlation study of North Singbhum Craton, India. Arabian Journal of Geosciences, 12(24), 802.

Bera, B., Bhattacharjee, S., Chamling, M., et al., (2021). Fluoride Hazard and Risk Enumeration of Hard Rock Unconfined Aquifers in the Extended Part of Chhota Nagpur Gneissic Complex. J Geol Soc India 97, 199–209 (2021). https://doi.org/10.1007/s12594-021-1651-0

Bera, B., Shit, P.K., Sengupta, N. et al. (2022). Steady declining trend of groundwater table and severe water crisis in unconfined hard rock aquifers in extended part of Chota Nagpur Plateau, India. Appl Water Sci 12, 31 (2022). https://doi.org/10.1007/s13201-021-01550-x

Bertosio, C., Provost, C., Athanase, M., Sennéchael, N., Garric, G., Lellouche, J. M., & Park, T. (2022). Changes in freshwater distribution and pathways in the Arctic Ocean since 2007 in the Mercator Ocean global operational system. Journal of Geophysical Research. Oceans, 127(6), e2021JC017701.

Beskese, A., Demir, H.H., Ozcan, H.K. et al. (2015). Landfill site selection using fuzzy AHP and fuzzy TOPSIS: a case study for Istanbul. Environ Earth Sci 73, 3513–3521 (2015). https://doi.org/10.1007/s12665-014-3635-5

Beyer, W. (1964). Zur Bestimmung der Wasserdurchlässigkeit von Kiesen und Sanden aus der Kornverteilungskurve [Determination of the hydraulic conductivity of gravels and sands from particle distribution curves]. Wasserwirtsch Wassertech 14(6):165–168

Bezdek JC (1974). Cluster validity with fuzzy sets", J of Cybernetics, vol. 3, no. 3, pp. 58-72, 1974

Bezdek JC (1981). Pattern Recognition with Fuzzy Objective Function Algorithms. New York: Plenum, 1981.

Bhanja SN, Mukherjee A, Rangarajan R, Scanlon BR, Malakar P, Verma S (2019) Long-term groundwater recharge rates across India by in situ measurements. Hydrology and Earth System Sciences, 23: 711–722. doi:10.5194/hess-23-711-2019

Bhatnagar, S., Taloor, A. K., Roy, S., & Bhattacharya, P. (2022). Delineation of aquifers favorable for groundwater development using Schlumberger configuration resistivity survey techniques in Rajouri district of Jammu and Kashmir, India. Groundwater for Sustainable Development, 17, 100764.

Bhattacharya P, Samal AC, Banerjee S, Pyne J, Santra SC (2017). Assessment of Potential Health Risk of Fluoride Consumption through rice, Pulses, and Vegetables in Addition to Consumption of Fluoride-Contaminated Drinking Water of West Bengal, India. Environ. Sci. Pollut. Res. 24 (25), 20300–20314. doi:10.1007/s11356-017-9649-2

Bhattacharya, R. K., Chatterjee, N. D., & Das, K. (2020). An integrated GIS approach to analyze the impact of land use change and land cover alteration on ground water potential level: A study in Kangsabati Basin, India. Groundwater for sustainable development, 11, 100399.

Bhattacharya, R.K., Das Chatterjee, N., Dolui, G. (2016). Grain size characterization of instream sand deposition in controlled environment in river Kangsabati, West Bengal. Model. Earth Syst. Environ. 2, 118 (2016). https://doi.org/10.1007/s40808-016-0173-z

Bhunia G, Maity P & Shit P (2021). Spatial Appraisals of Groundwater Recharge Potential Zone Identification Using Remote Sensing and GIS. Groundwater and Society (pp.407-427)10.1007/978-3-030-64136-8_19.

Bhunia G, Samanta S, Pal D, Pal B (2012). Assessment of Groundwater Potential Zone in Paschim Medinipur District, West Bengal–A Meso-scale study using GIS and Remote Sensing Approach. Journal of Environment and Earth Science. 2: 41-59.

Bhunia P, Das P, Maiti R (2020). Meteorological Drought Study Through SPI in Three Drought Prone Districts of West Bengal, India. Earth Syst Environ 4, 43–55 (2020). https://doi.org/10.1007/s41748-019-00137-6

Bhunia, G.S. (2020). An approach to demarcate groundwater recharge potential zone using geospatial technology. Appl Water Sci 10, 138 (2020). https://doi.org/10.1007/s13201-020-01231-1

Bin Jusoh, A., Cheng, W. H., Low, W. M., Nora'aini, A., & Noor, M. M. M. (2005). Study on the removal of iron and manganese in groundwater by granular activated carbon. Desalination, 182(1-3), 347-353.

BIS (Bureau of Indian Standards), Drinking Water Specification, (2017) http://cgwb.gov.in/documents/wq-standards.pdf

Biswas B (2020). Changing crop concentration and agricultural efficiency: A study in West Bengal, India. GeoJournal (2020). https://doi.org/10.1007/s10708-020-10267-4

Biswas B, Ghosh D.C., Dasgupta M.K., Trivedi N., Timsina J., Dobermann A. (2006). Integrated assessment of cropping systems in the Eastern Indo-Gangetic plain, Field Crops Research, Volume 99, Issue 1,2006, Pages 35-47, ISSN 0378-4290,https://doi.org/10.1016/j.fcr.2006.03.002.

Biswas, S., Mukhopadhyay, B.P., Bera, A., (2020). Delineating groundwater potential zones of agriculture dominated landscapes using GIS based AHP techniques: a case study from Uttar Dinajpur district, West Bengal, Environ. Earth Sci., 79 (12), 10.1007/s12665-020-09053-9

Biswas, T., Pal, S. C., Ruidas, D., Islam, A. R. M. T., Saha, A., Costache, R., & Shit, M. (2023). Modelling of groundwater potential zone in hard rock-dominated drought-prone region of eastern India using integrated geospatial approach. Environmental Earth Sciences, 82(3), 81.

Bloomfield J P, Marchant B P (2013). Analysis of Groundwater Drought using Variant of Standardised Precipitation Index. Hydrology and Earth System Sciences Discussions. 10. 7537-7574. 10.5194/hessd-10-7537-201

Bloomfield J. P., Marchant B. P., McKenzie A. A. (2018). Changes in groundwater drought associated with anthropogenic warming. Hydrology and Earth System Science. Vol 23 No.3 pp-1393-1408, 10.5194/hess-23-1393-2019

Bobrowsky, P. T., & Marker, B. (Eds.). (2018). Encyclopedia of engineering geology (pp. 506-507). Berlin: Springer.

Bordbar, M., Neshat, A., Javadi, S., (2019). Modification of the GALDIT framework using statistical and entropy models to assess coastal aquifer vulnerability. Hydrol Sci J 64(9):1117–1128

Boretti A., Rosa L. (2019) Reassessing the projections of the World Water Development Report. npj Clean Water 2, 15 (2019). https://doi.org/10.1038/s41545-019-0039-9

Borgohain, X., Boruah, A., Sarma, G. K., & Rashid, M. H. (2020). Rapid and extremely high adsorption performance of porous MgO nanostructures for fluoride removal from water. Journal of Molecular Liquids, 305, 112799.

Božović, D., Polomčić, D., Bajić, D., Ratković, J. (2019). Hydrodynamic analysis of radial collector well ageing at Belgrade well field, Journal of Hydrology, Volume 582,2020,124463,ISSN 0022-1694,https://doi.org/10.1016/j.jhydrol.2019.124463.

Brasil Neto R M, Santos CAG, Silva JFCBdC et al. (2021). Evaluation of the TRMM product for monitoring drought over Paraíba State, northeastern Brazil: a trend analysis. Sci Rep 11, 1097 (2021). https://doi.org/10.1038/s41598-020-80026-5

Bresciani, E., Cranswick, R.H., Banks, E.W., Batlle-Aguilar, J., Cook, P.G., Batelaan, O. (2018). Using hydraulic head, chloride and electrical conductivity data to distinguish between mountain-front and mountain-

block recharge to basin aquifers, Hydrol. Earth Syst. Sci., 22, 1629–1648, https://doi.org/10.5194/hess-22-1629-2018, 2018.

Bresciani, M., Giardino, C., Fabbretto, A., Pellegrino, A., Mangano, S., Free, G., Pinardi, M. (2022). Application of New Hyperspectral Sensors in the Remote Sensing of Aquatic Ecosystem Health: Exploiting PRISMA and DESIS for Four Italian Lakes. Resources, 11(2), p.8.

Brindha K, Jagadeshan G, Kalpana L, and Elango L (2016). Fluoride in weathered rock aquifers of southern India: Managed Aquifer Recharge for mitigation. Environmental Science and Pollution Research, Vol. 23, 8302-8316. 10.1007/s11356-016-6069-7

Brodie, R., Sundaram, B., Tottenham, R., Hostetler, S., Ransley, T. (2007). An overview of tools for assessing groundwater–surface water connectivity. Bureau of Rural Sciences, Canberra, Australia, 131 p.

Brown, R.M., McClellan, N.I., Deininger, R.A., Tozer, R.G., (1972). A water quality index—do we dare?–Water Sew Works117 : 339—343

Buchanan, J., Henig, E., Henig, M. (1998). Objectivity and subjectivity in thedecision making process. Annals of Operations Research 80, 333–345 (1998). https://doi.org/10.1023/A:1018980318183

Bui et al (2012) Spatio-Temporal Analysis of Recent Groundwater –Level Trends in the Red River Delta , Vietnam. Hydrogeol J (2012) 20: 1635. https://doi.org/10.1007/s10040-012-0889-4

Butler, J.J., Tsou, M.S. (2003). Pumping-induced leakage in a bounded aquifer: an example of a scale-invariant phenomenon," Water Resources Research, vol. 39, no. 12, p. 1344, 2003.

C.K. Diawara,(2008). Nanofiltration process efficiency in water desalination. Sep. Purif. Rev. 2008. 37, 303–325

Campello RJGB, Hruschka ER (2006).A fuzzy exten-sion of the silhouette width criterion for cluster analysis. Fuzzy Sets and Systems, 157(21), 2858-2875. https://doi.org/10.1016/j.fss.2006.07.006

Cao, L., Ouyang, Z., Chen, T. et al. (2022). Phosphate removal from aqueous solution using calcium-rich biochar prepared by the pyrolysis of crab shells. Environ Sci Pollut Res 29, 89570–89584 (2022). https://doi.org/10.1007/s11356-022-21628-6

Cao, Y., Zhang, W., Zhu, Y., Ji, X., Xu, Y., Wu, Y., Hoitink, A.J.F. (2020). Impact of trends in river discharge and ocean tides on water level dynamics in the Pearl River Delta, Coastal Engineering, Volume 157,2020,103634, ISSN 0378-3839,https://doi.org/10.1016/j.coastaleng.2020.103634.

Capuano RM, Jones CR (2020). Cation exchange in groundwater chemical evolution and prediction of paleo-groundwater flow: a natural system study, Water Resour. Res., 56 (2020), Article e2019WR026318

Cardenas, M.B. (2009). Stream-aquifer interactions and hyporheic exchange in gaining and losing sinuous streams, Water Resour. Res., 45, W06429, doi:10.1029/2008WR007651, 2009.

Carlowicz M (1996).Natural hazards need not lead to natural disasters. Eos, Trans. Am. Geophys. 6 Union, 77, 149

Carmona G, Varela-Ortega C, Bromley J (2013) Supporting Decsion Making Under Uncertanity: Development of Participatory integrated Model for Water Management in the Middle Guadiana River Basin. Environ Model Softw 50:144-157. https://doi.org/10.1016/j.envsoft.2013.09.007

Casanova, J., Devau, N., Pettenati, M. (2016). Managed Aquifer Recharge: An Overview of Issues and Options. In: Jakeman, A.J., Barreteau, O., Hunt, R.J., Rinaudo, JD., Ross, A. (eds) Integrated Groundwater Management. Springer, Cham. https://doi.org/10.1007/978-3-319-23576-9_16

Casanova, M., Tapia, E., Seguel, O., Salazar, O. (2016). Direct measurement and prediction of bulk density on alluvial soils ofcentral Chile. Chilean J Agric Res. 76: 105–113

Cavus Y, Aksoy H (2019) Spatial Drought Characterization for Seyhan River Basin in the Mediterranean Region of Turkey. Water, 11(7), 1331–. doi:10.3390/w11071331

Census of India 2011, West Benagl, Distrcit Statistical Handbook, Paschim Medinapore, Series 20

Central Ground Water Board (CGWB). (2022). Ground Water Year Book of West Bengal & Andaman & Nicobar Islands (2022), Ministry of Jal Shakti, Department of Water, http://cgwb.gov.in/Regions/ER/Reports/GWY%20Book%20WB%20&%20AN%20Islands_2021-22.pdf

Central Ground Water Board, Ministry of Water Resources, River Development and Ganga Rejuvenation, Government of India (2017-2018) Ground Water Year Book- India 2017-2018

Central Ground Water Board, Ministry of Water Resources, River Development and Ganga Rejuvenation, Government of India, (2015-2016) Ground Water Year Book of West Bengal & Anadaman & Nicobar Islands

CGWB, Central Groundwater Board, 2022. Aquifer Mapping and Management Plan of Purulia District West Bengal, Purulia District West Bengal. http://cgwb.gov.in/AQM/NAQUIM_REPORT/WEST

Chadha DK (1999) A proposed new diagram for geochemical classification of natural waters and interpretation of chemical data, Hydrogeol. J., 7 (5) (1999), pp. 431-439

Chakrabarti, S., & Bhattacharya, H. N. (2013). Inferring the hydro-geochemistry of fluoride contamination in Bankura district, West Bengal: a case study. Journal of the Geological Society of India, 82, 379-391.

Chakraborty Baisakhi, et al. (2022) Evaluation of groundwater quality and its impact on human health: a case study from Chotanagpur plateau fringe region in India." Applied Water Science, vol. 12, no. 3, Mar. 2022,

Chakraborty, B., Roy, S., Bera, A. et al., (2022). Groundwater vulnerability assessment using GIS-based DRASTIC model in the upper catchment of Dwarakeshwar river basin, West Bengal, India. Environ Earth Sci 81, 2. https://doi.org/10.1007/s12665-021-10002-3

Chakraborty, B., Roy, S., Bera, A., Adhikary, P. P., Bera, B., Sengupta, D., & Shit, P. K. (2022). Groundwater vulnerability assessment using GIS-based DRASTIC model in the upper catchment of Dwarakeshwar river basin, West Bengal, India. Environmental Earth Sciences, 81, 1-15.

Chakraborty, P., and Daspattyanaka, P., (2019). Assessment of Housing Condition as a Measure of Quality of Rural Life: A Comparative Study of Humgarh and Amkopa Villages of Garbeta-II Block, Paschim Medinipur District, West Bengal. Indian Journal of Spatial Science Autumn Issue, 10 (2) 2019 pp. 42 – 51

Chakravorty, P. P., Sinha, M., & Chakraborty, S. K. (2014). Impact of industrial effluent on water quality and benthic macro invertebrate diversity in fresh water ponds in Midnapore district of west Bengal, India. Journal of Entomology and zoology studies, 2(3), 93-101.

Chan, S. S., Khoo, K. S., Chew, K. W., Ling, T. C., & Show, P. L. (2022). Recent advances biodegradation and biosorption of organic compounds from wastewater: Microalgae-bacteria consortium-A review. Bio resource Technology, 344, 126159.

Chand, R. (2022). Indian Agriculture Towards 2030—Need for a Transformative Vision. In: Chand, R., Joshi, P., Khadka, S. (eds) Indian Agriculture Towards 2030. India Studies in Business and Economics. Springer, Singapore. https://doi.org/10.1007/978-981-19-0763-0_1

Chang NB, Chen HW, Ning SK (2001) Identification of river water quality using the Fuzzy Synthetic Evaluation approach. J Environ Manage 2001,63(3):293–305. 10.1006/jema.2001.0483

Chang, D. Y. (1996). Applications of the extent analysis method on fuzzy AHP. European journal of operational research, 95(3), 649-655.

Chapagain, S.K., Mohan, G., Rimba, A.B. et al., (2022). Analyzing the relationship between water pollution and economic activity for a more effective pollution control policy in Bali Province, Indonesia. Sustain Environ Res 32, 5. https://doi.org/10.1186/s42834-021-00115-6

Chapuis, R.P., Allaire V, Marcotte, D., Chouteau, M., Acevedo, N., Gagnon, F. (2005). Evaluating the hydraulic conductivity at three different scales within an unconfined sand aquifer at Lachenalia, Quebec. Canadian Geotechnical Journal 42 (4), 1212–1220

Charoenchai, M., & Tangbunsuk, S. (2022). Effect of ternary polymer composites of macroporous adsorbents on adsorption properties for heavy metal removal from aqueous solution. Environmental Science and Pollution Research, 29(55), 84006-84018.

Chatterjee P, Chakraborty S (2013) Gear Material Selection using Complex Proportional Assessment and Additive Ratio Assessment-based Approaches: A Comparative Study International Journal of Materials Science and Engineering.1:2

Chatterjee, N., Bose, G.A. (2013). COPRAS-F base multi-criteria group decision making approach for site selection of wind farm. Decision Science Letters. 2013; 2(1): 1–10.

Chatterjee, U. (2018). Water Scarcity in Semi-Arid Regions of Bankura District, West Bengal,India-Problems and Prospects. KhojAn Int Peer Rev J Geogr. 5(1):87.https://doi.org/10.5958/2455-6963.2018.00007.3

Chaturvedi, S., & Dave, P. N. (2012). Removal of iron for safe drinking water. Desalination, 303, 1-11.

Chaudhury, S. (2022). Inter-decadal Variability of Precipitation Patterns Increasing the Runoff Intensity in Lower Reach of Shilabati River Basin, West Bengal. In: Mandal, S., Maiti, R., Nones, M., Beckedahl, H.R. (eds) Applied Geomorphology and Contemporary Issues. Geography of the Physical Environment. Springer, Cham. https://doi.org/10.1007/978-3-031-04532-5_9.

Chen, C.T. (2000). Extensions of the TOPSIS for group decision-making under fuzzy environment Fuzzy Set Syst, 114 (1) (2000), pp. 1-9

Chen, D., Cen, K., Zhuang, X., Gan, Z., Zhou, J., Zhang, Y., & Zhang, H. (2022a). Insight into biomass pyrolysis mechanism based on cellulose, hemicellulose, and lignin: Evolution of volatiles and kinetics, elucidation of reaction pathways, and characterization of gas, biochar and bio-oil. Combustion and Flame, 242, 112142.

Chen, J., Yang, S. T., Li, H. W., Zhang, B., and Lv, J. R., (2013). Research on Geographical Environment Unit Division Based on the Method of Natural Breaks (Jenks), Int. Arch. Photogramm. Remote Sens. Spatial Inf. Sci., XL-4/W3, 47–50, https://doi.org/10.5194/isprsarc

Chen, T., & Guestrin, C. (2016). Xgboost: A scalable tree boosting system. In Proceedings of the 22nd acm sigkdd international conference on knowledge discovery and data mining (pp. 785-794).

Chen, W., Feng, J., Liu, S., Zhang, J., Cai, Y., Lv, Z., & Tan, X. (2022b). A green and economical MgO/biochar composite for the removal of U (VI) from aqueous solutions. Chemical Engineering Research and Design, 180, 391-401

Chen, X., Dong, W., Ou, G., Wang, Z., Liu, C. (2013). Gaining and losing stream reaches have opposite hydraulic conductivity distribution patterns. Hydrol Earth Syst Sci 17:2569–2579

Chen, X.H. (2000). Measurement of streambed hydraulic conductivity and its anisotropy. Environ Geol 39(12):1317–1324

Chen, X.H. (2004). Streambed hydraulic conductivity for rivers in southcentral Nebraska. J Am Water Resour Assoc 40(3):561–574

Cheng, C., Chen, X.H. (2007). Evaluation of methods for determination of hydraulic properties in an aquifer-aquitard system hydrologically connected to a river. Hydrogeol J 15:669–678

Chidambaram S, Prasanna MV, Venkatramanan S, Nepolian M, Pradeep K, Banajarani P, Thivya C, Thilagavathi R (2022) Groundwater quality assessment for irrigation by adopting new suitability plot and spatial analysis based on fuzzy logic technique, Environmental Research, Volume 204, Part A,2022,111729,

Chidambaram, S., Ramanathan, A. L., & Vasudevan, S. (2003). Fluoride removal studies in water using natural materials. Water Sa, 29(3), 339-344.

Chinnasamy, P., Maheshwari, B., Dillon, P., Purohit, R., Dashora, Y., Soni, P., Dashora, R., (2018). Estimation of specific yield using water table fluctuations and cropped area in a hardrock aquifer system of Rajasthan, India, Agricultural Water Management, Volume 202, 2018, Pages 146-155, ISSN 0378-3774,https://doi.org/10.1016/j.agwat.2018.02.016.

Chin-Yi C, Tung-Shen Wu, Mei-Lan Li, Ching-Tang W (2018). Integration of Importance performance Analysis And Fuzzy DEMATEL. International Journal of Computer Science & Information Technology (IJCSIT) Vol 10, No 3, June 2018

Choudhari P, P Nigam G K, Singh S K, Thakur S (2018) Morphometric based prioritization of watershed for groundwater potential of Mula river basin, Maharashtra, India. Geology, Ecology, and Landscapes, 1–12. doi:10.1080/24749508.2018.1452482

Choudhary, S., Pingale, S. M., & Khare, D. (2022). Delineation of groundwater potential zones of upper Godavari sub-basin of India using bi-variate, MCDM and advanced machine learning algorithms. Geocarto International, 1-31.

Chowdhury P, Mukhopadhyay B P, Bera A (2022) Hydrochemical assessment of groundwater suitability for irrigation in the north-eastern blocks of Purulia district, India using GIS and AHP techniques, Physics and Chemistry of the Earth, Parts A/B/C, Volume 126,2022,103108,ISSN 1474-7065,https://doi.org/10.1016/j.pce.2022.103108

Chowdhury, A., Jha, M.K. & Chowdary, V.M. (2010). Delineation of groundwater recharge zones and identification of artificial recharge sites in West Medinipur district, West Bengal, using RS, GIS and MCDM techniques. Environ Earth Sci 59, 1209–1222 (2010). https://doi.org/10.1007/s12665-009-0110-9

Chowdhury, P., Mukhopadhyay, B. P., & Bera, A. (2022). Hydrochemical assessment of groundwater suitability for irrigation in the north-eastern blocks of Purulia district, India using GIS and AHP techniques. Physics and Chemistry of the Earth, Parts A/B/C, 126, 103108.

Christ MCJ and Parvathi RMS (2011) Fuzzy c-means algorithm for medical image segmentation," 2011 3rd International Conference on Electronics Computer Technology, 2011, pp. 33-36, doi: 10.1109/ICECTECH.2011.5941851.

CIP progress report, 1997-1998. Intensification of potato production in rice based cropping system: Rapid rural appraisal of West Bengal

Collins, M., Knutti, R., Arblaster, J., Dufresne, J.L., Fichefet, T., Friedlingstein, P., Gao, X., Gutowski, W.J., Johns, T., Krinner, G., Shongwe, M., Tebaldi, C., Weaver, A.J., Wehner, M. (2013). Long-term climate change: projections, commitments and irreversibility. In: Stocker, T.F., Qin, D., Plattner, G.K., Tignor, M., Allen, S.K., Boschung, J., Nauels, A., Xia, Y., Bex, V., Midgley, P.M. (Eds.), Climate Change 2013: The Physical Science Basis. Contribution of Working Group I to the Fifth Assessment Report of the Intergovernmental Panel on Climate Change. Cambridge University Press, Cambridge, United Kingdom and New York, NY, USA, pp. 1029–1136.

Collins, S., Houben, G.J. (2020). Horizontal and radial collector wells: simple tools for a complex problem. Hydrogeol J 28, 1925–1935 (2020). https://doi.org/10.1007/s10040-020-02120-2

Cordier T, Alonso-Sáez L, Apothéloz-Perret-Gentil L, et al. (2021) Ecosystems monitoring powered by environmental genomics: a review of current strategies with an implementation roadmap. Mol Ecol. 2021;301(13):2937–58.

Corniello, A., Ducci, D., Napolitano, P., (1997). Comparison between parametric methods to evaluate aquifer pollution vulnerability using a GIS: an example in the Piana Campana. Engineering Geology and the Environment, Balkema, Rotterdam, the Netherlands. 1997 1721–1726.

Cox, J.; Downie, A.; Hickey, M.; Jenkins, A.; Lines-Kelly, R.; McClintock, A.; van Zwieten, L. Biochar in Horticulture: Prospects for the Use of Biochar in Australian Horticulture; HAL Report; NSW Trade and Investment: Sydney, Australia, 2012; ISBN 9781742563497.

Craig, I., Green, A., Scobie, M., & Schmidt, E. (2005). Controlling evaporation loss from water storages. University of Southern Queensland.

Cunillera-Montcusí, D., Beklioğlu, M., Cañedo-Argüelles, M., Jeppesen, E., Ptacnik, R., Amorim, C. A., & Matias, M. (2022). Freshwater salinisation: a research agenda for a saltier world. Trends in Ecology & Evolution.

Dalezios NR, Blanta A, Spyropoulos N (2013) Remotely sensed spatiotemporal features of agrometeorological drought, in Advances in Meteorology. Climatology and Atmospheric Physics,409-414.https://doi.org/10.1007/978-3-642-29172-2_58

Dar, T., Rai, N., & Bhat, A. (2021). Delineation of potential groundwater recharge zones using analytical hierarchy process (AHP). Geology, Ecology, and Landscapes, 5(4), 292-307.

Das A, Khan A, Daspattanayak P. et al. (2016) Regional model for agricultural imbalances in West Bengal, India. Model. Earth Syst. Environ. 2, 58 (2016). https://doi.org/10.1007/s40808-016-0107-9

Das K, Sarkar D (2016) Soil degradation: Status and management options in West Bengal. SATSA Mukhapatra-Annual Technical Issue.20

Das M, Parveen T, Ghosh D. et al. (2021) Assessing groundwater status and human perception in drought-prone areas: a case of Bankura-I and Bankura-II blocks, West Bengal (India). Environ Earth Sci 80, 636 (2021). https://doi.org/10.1007/s12665-021-09909-8

Das P, Gottsche FM, Olesen FS, Fischer H (2002) Land surface temperature and emissivity estimation from passive sensor data: theory and practice-current trends. International Journal of Remote Sensing 23: 2563– 2594.

Das VK (2020) K-Means Clustering Vs. Hierarchical Clustering. Global Tech Council. file:///E:/P.hd%202018 May/Paperpublished_unpublished/Morphometric%20analysis/Reference/New/KMeans%20Clustering%20vs%20Hierarchical%20Clustering.html

Das, B. (1999). Environmental pollution of Udaisagar Lake and impact of phosphate mine, Udaipur, Rajasthan, India. Environmental Geology 38, 244–248 (1999). https://doi.org/10.1007/s002540050421

Das, B., & Pal, S. C. (2019). Combination of GIS and fuzzy-AHP for delineating groundwater recharge potential zones in the critical Goghat-II block of West Bengal, India. HydroResearch, 2, 21-30.

Das, B., Pal, S. C., Malik, S., & Chakrabortty, R. (2019). Modeling groundwater potential zones of Puruliya district, West Bengal, India using remote sensing and GIS techniques. Geology, Ecology, and Landscapes, 3(3), 223-237.

Das, D., & Nandi, B. K. (2022). Removal of co-existing Fe (II), As (V) and fluoride ions from groundwater by electrocoagulation. Groundwater for Sustainable Development, 17, 100752.

Das, D., & Sengar, A. (2022). A fuzzy analytic hierarchy process-based analysis for prioritization of barriers to the adoption of eHealth in India. International Journal of Medical Informatics, 165, 104830.

Das, J., Rahman, A. S., Mandal, T., & Saha, P. (2020). Challenges of sustainable groundwater management for large scale irrigation under changing climate in Lower Ganga River basin in India. Groundwater for sustainable development, 11, 100449.

Das, K., & Mondal, N. K. (2016). Dental fluorosis and urinary fluoride concentration as a reflection of fluoride exposure and its impact on IQ level and BMI of children of Laxmisagar, Simlapal Block of Bankura District, WB, India. Environmental monitoring and assessment, 188, 1-14.

Das, L., Das, P., Bhowal, A., & Bhattachariee, C. (2020). Treatment of malachite green dye containing solution using bio-degradable Sodium alginate/NaOH treated activated sugarcane baggsse charcoal beads: Batch, optimization using response surface methodology and continuous fixed bed column study. Journal of Environmental Management, 276, 111272.

Das, M., Parveen, T., Ghosh, D., & Alam, J. (2021). Assessing groundwater status and human perception in drought-prone areas: a case of Bankura-I and Bankura-II blocks, West Bengal (India). Environmental Earth Sciences, 80(18), 636.

Das, M., Parveen, T., Ghosh, D., et al., (2021). Assessing groundwater status and human perception in drought-prone areas: a case of Bankura-I and Bankura-II blocks, West Bengal (India). Environ Earth Sci 80, 636 (2021). https://doi.org/10.1007/s12665-021-09909-8

Das, N., Mukhopadhyay S., (2020). Application of multi-criteria decision-making technique for the assessment of groundwater potential zones: a study on Birbhum district, West Bengal, India. Environ Dev Sustain

Das, P., Panda, S. (2022). GIS-Supported Database Towards Transforming Monocropped Areas for Yearlong Cultivation in Paschim Medinipur, West Bengal, India. In: Bhunia, G.S., Chatterjee, U., Lalmalsawmzauva, K., Shit, P.K. (eds) Anthropogeomorphology. Geography of the Physical Environment. Springer, Cham. https://doi.org/10.1007/978-3-030-77572-8_18

Das, R., Saha, S., (2022). Spatial mapping of groundwater potentiality applying ensemble of computational intelligence and machine learning approaches, Groundwater for Sustainable Development, Volume 18,2022,100778,ISSN 2352-801X,https://doi.org/10.1016/j.gsd.2022.100778.

Das, S. (2017). Delineation of groundwater potential zone in hard rock terrain in Gangajalghati block, Bankura district, India using remote sensing and GIS techniques. Model. Earth Syst. Environ. 3, 1589–1599 (2017). https://doi.org/10.1007/s40808-017-0396-7

Das, S., Mukherjee, J., Bhattacharyya, S. et al. (2022). Detection of groundwater potential zones using analytical hierarchical process (AHP) for a tropical river basin in the Western Ghats of India. Environ Earth Sci 81, 416 (2022). https://doi.org/10.1007/s12665-022-10543-1

Dastorani, M., 2022. Application of fuzzy-AHP method for desertification assessment in Sabzevar area of Iran. Nat Hazards (2022). https://doi.org/10.1007/s11069-021-05177-8

Datta P, Das S (2019) Analysis of long-term precipitation changes in West Bengal, India: AN approach to detect monotonic trends influenced by autocorrelations. Dyn Atmos Oceans. https://doi.org/10.1016/j.dynatmoce.2019.101118

Dave RN (1996) Validating fuzzy partitions obtained through c-shells clustering", Pattern Recognition Letters, vol. 17, pp. 613-623,1996.

Dayal KS, Deo RC, Apan AA (2018) Spatio-temporal drought risk mapping approach and its application in the drought-prone region of south-east Queensland, Australia. Nat Hazards 93, 823–847 (2018). https://doi.org/10.1007/s11069-018-3326-8

De A, Mridha D, Ray I, Joardar M, Das A, Chowdhury NR and Roychowdhury T (2021) Fluoride Exposure and Probabilistic Health Risk Assessment Through Different Agricultural Food Crops From Fluoride Endemic Bankura and Purulia Districts of West Bengal, India. Front. Environ. Sci. 9:713148. doi: 10.3389/fenvs.2021.713148

De, A., Mridha, D., Joardar, M., Das, A., Chowdhury, N. R., & Roychowdhury, T. (2022). Distribution, prevalence and health risk assessment of fluoride and arsenic in groundwater from lower Gangetic plain in West Bengal, India. Groundwater for Sustainable Development, 16, 100722.

De, A., Mridha, D., Ray, I., Joardar, M., Das, A., Chowdhury, N. R., & Roychowdhury, T. (2021). Fluoride exposure and probabilistic health risk assessment through different agricultural food crops from fluoride endemic Bankura and Purulia districts of West Bengal, India. Frontiers in environmental science, 282.

Debelo G, Tadele K, Koriche SA (2017) Morphometric analysis to identify erosion prone areas on the upper blue Nile using GIS (Case study of Didessa and Jema sub-basin, Ethiopia). International Research Journal of Engineering and Technology. 04:1773–1784

Dehdasht G, Ferwati M S, Zin, RM, Abidin NZ (2020) A hybrid approach using entropy and TOPSIS to select key drivers for a successful and sustainable lean construction implementation. PLOS ONE, 15(2), e0228746. doi:10.1371/journal.pone.0228746

Devineni, N., Perveen, S. & Lall, U. (2022). Solving groundwater depletion in India while achieving food security. Nat Commun 13, 3374 (2022). https://doi.org/10.1038/s41467-022-31122-9

Dey, K.K., Dwivedi V K, Mishra S (2018) Analysis of Long –Period Seasonal Variation of Temperature for the District of Bankura and Puruliya in a Time of Climate Change. International Journal of Current Research. Vol-10 Issue-11, pp-75495-75497

Dey, S., Goswami, S., & Ghosh, U. C. (2004). Hydrous ferric oxide (HFO)—a scavenger for fluoride from contaminated water. Water, Air, and Soil Pollution, 158, 311-323.

Dey, S., Kotaru, N. S. A., Veerendra, G. T. N., & Sambangi, A. (2022). The removal of iron from synthetic water by the applications of plants leaf biosorbents. Cleaner Engineering and Technology, 9, 100530.

Dhiman, H. S., & Deb, D. (2020). Fuzzy TOPSIS and fuzzy COPRAS based multi-criteria decision making for hybrid wind farms. Energy, 202, 117755.

Dhirendra MJ, Kumar A, Agrawal N (2009) Assessment of the irrigation water quality of river Ganga in Haridwar district, Rasāyan, J. Chem., 2 (2009), pp. 285-292

Dibaj, M., Javadi, A. A., Akrami, M., Ke, K. Y., Farmani, R., Tan, Y. C., & Chen, A. S. (2020). Modelling seawater intrusion in the Pingtung coastal aquifer in Taiwan, under the influence of sea-level rise and changing abstraction regime. Hydrogeology Journal, 28(6), 2085-2103.

Dibaj, M., Javadi, A. A., Akrami, M., Ke, K. Y., Farmani, R., Tan, Y. C., & Chen, A. S. (2021). Coupled three-dimensional modelling of groundwater-surface water interactions for management of seawater intrusion in Pingtung Plain, Taiwan. Journal of Hydrology: Regional Studies, 36, 100850.

Diersch HJG, Kolditz O (2002) Variable-density flow and transport in porous media: Approaches and challenges. Adv. Water Resour. 2002, 25, 899–944.

Dikpal R L, Renuka Prasad T J, Satish K (2017) Evaluation of morphometric parameters derived from Cartosat-1 DEM using remote sensing and GIS techniques for Budigere Amanikere watershed, Dakshina Pinakini Basin, Karnataka, India. Applied Water Science, 7:4399–4414. Doi:10.1007/s13201-017-0585-6

Dillon, P., & Arshad, M. (2016). Managed aquifer recharge in integrated water resource management. Integrated groundwater management: Concepts, approaches and challenges, 435-452.

Dillon, P., Fernández Escalante, E., Megdal, S. B., & Massmann, G. (2020). Managed aquifer recharge for water resilience. Water, 12(7), 1846.

Dillon, P., Stuyfzand, P., Grischek, T., Lluria, M., Pyne, R. D. G., Jain, R. C., & Sapiano, M. (2019). Sixty years of global progress in managed aquifer recharge. HYDROGEOLOGY JOURNAL.

Dingle, E. H., Kusack, K. M., & Venditti, J. G. (2021). The gravel-sand transition and grain size gap in river bed sediments. Earth-Science Reviews, 222, 103838.

Dodge, Y. (2008). Randomized Block Design In: The Concise Encyclopedia of Statistics.

Doke, A. B., Zolekar, R. B., Patel, H., & Das, S. (2021). Geospatial mapping of groundwater potential zones using multi-criteria decision-making AHP approach in a hardrock basaltic terrain in India. Ecological Indicators, 127, 107685.

Doll P (2009) Vulnerability to the Impact of Climate Change on Renewable Groundwater Resources: A Global – Scale Assessment. Environmental Research Letters. 4. 035006. 10.1088/1748-9326/4/3/035006.

Doll, P. and Florke, M (2005) Global-Scale estimation of diffuse groundwater recharge: model tuning to local data for semi-arid and arid regions and assessment of climate change impact, Frankfurt Hydrology Paper 03, Institute of Physical Geography, Frankfurt University, Frankfurt, Germany, http://www.geo.uni-frankfurtde/ipg/ag/dl/fpublikationen 2005/FHP03DoellFloerke2005.pdf (last access: May 2018),2005.

Dolui G, Chatterjee S, Das Chatterjee N (2016) Geophysical and geochemical alteration of rocks in granitic profiles during intense weathering in southern Purulia district, West Bengal, India. Model. Earth Syst. Environ. 2, 132. https://doi.org/10.1007/s40808-016-0188-5

Doneen LD (1964) Notes on Water Quality in Agriculture. Department of Water Science and Engineering, University of California, Davis.

Dong G, Zhang H, Moise A, Hanson L, Linag P, Ye H (2016) CMIP5 Model –Simulated Onset, Duration and Intensity of the Asian Summer Monsoon in Current and Future Climate. Clim Dyn 46: 355. https://doi.org/10.1007/s00382-015-2588-z

Dožić, S., & Kalić, M. (2015). Comparison of two MCDM methodologies in aircraft type selection problem. Transportation Research Procedia, 10, 910-919.

DRCSC report (2017) Enhancing Adaptive Capacity and Increasing Resilience of Small and Marginal Farmers of Purulia and Bankura Districts, West Bengal to Climate Change, School of Oceanographic Studies Jadavpur University

Du T L T, Bui D Du, Nguyen, M D, Lee H (2018) Satellite-Based, Multi-Indices for Evaluation of Agricultural Droughts in a Highly Dynamic Tropical Catchment, Central Vietnam. Water, 10(5), 659– . doi:10.3390/w10050659

Duan H, Deng Z, Deng F, Wang D (2016) Assessment of Groundwater Potential Based on Multicriteria Decision Making Model and Decision Tree Algorithms. Mathematical Problems in Engineering 1–11. doi:10.1155/2016/2064575

Duarte, L., Espinha Marques, J., Teodoro A.A., (2019). An Open Source GIS-Based Application for the Assessment of Groundwater Vulnerability to Pollution. Environments. 6(7):86. https://doi.org/10.3390/environments6070086

Durner, W., & Flühler, H. (2006). Soil hydraulic properties. Encyclopedia of hydrological sciences.

Dusabe M, Wronski T, Gomes-Silva G et al. (2019) Biological water quality assessment in the degraded Mutara rangelands, northeastern Rwanda. Environ Monit Assess 191, 139. https://doi.org/10.1007/s10661-019-7226-5

Dutta D, Kundu A, Patel NR, Saha SK, Siddiqui AR (2015) Assessment of agricultural drought in Rajasthan (India) using remote sensing derived Vegetation Condition Index (VCI) and Standardized Precipitation Index (SPI). The Egyptian Journal of Remote Sensing and Space Science, 18(1), 53–63. doi:10.1016/j.ejrs.2015.03.006

Dutta, B., Raghavan, V. G., Orsat, V., & Ngadi, M. (2015). Surface characterization and classification of microwave pyrolysed maple wood biochar. Biosystems Engineering, 131, 49-64.

Eaton FM (1950) Significance of carbonates in irrigation waters, Soil Sci., 69 (1950), pp. 123-134, 10.1097/00010694-195002000-00004

Edmunds WM, Smedley PL, (2013) Fluoride in natural waters. In: Essentials of Medical Geology. Springer, Dordrecht, pp. 311–336.

El Diwani, G., Amin, S. K., Attia, N. K., & Hawash, S. I. (2022). Fluoride pollutants removal from industrial wastewater. Bulletin of the National Research Centre, 46(1), 1-9.

El Garouani A, Aharik K & El Garouani S (2020) Water balance assessment using remote sensing, Wet-Spass model, CN-SCS, and GIS for water resources management in Saïss Plain (Morocco). Arab J Geosci 13, 738 https://doi.org/10.1007/s12517-020-05730-y

El Motaki S, Yahyaouy A, Gualous H et al. (2021) A new weighted fuzzy C-means clustering for workload monitoring in cloud datacenter platforms. Cluster Comput 24, 3367–3379 (2021). https://doi.org/10.1007/s10586-021-03331-2

El Mountassir, O., Bahir, M., Chehbouni, A., Dhiba, D., & El Jiar, H. (2022). Assessment of groundwater quality and the main controls on its hydrochemistry in a changing climate in Morocco (Essaouira Basin). Sustainability, 14(13), 8012.

El-Naqa, A., & Al-Shayeb, A. (2009). Groundwater protection and management strategy in Jordan. Water resources management, 23, 2379-2394.

Elvis, B. W. W., Arsene, M., Théophile, N. M., Bruno, K. M. E., & Olivier, O. A. (2022). Integration of shannon entropy (SE), frequency ratio (FR) and analytical hierarchy process (AHP) in GIS for suitable groundwater potential zones targeting in the Yoyo river basin, Méiganga area, Adamawa Cameroon. Journal of Hydrology: Regional Studies, 39, 100997.

Elzain, E.H., Chung, Y.S., Venkatramanan, S., Selvam, S., Ahemd, H.A., Seo, Y.K., Bhuyan, S., Yassin, M.A., (2022). Novel machine learning algorithms to predict the groundwater vulnerability index to nitrate pollution at two levels of modeling, Chemosphere, Volume 314, 137671,ISSN 0045-6535,https://doi.org/10.1016/j.chemosphere.2022.137671.

Enaime G, Baçaoui A, Yaacoubi A, Lübken M. (2020). Biochar for Wastewater Treatment—Conversion Technologies and Applications. Applied Sciences. 2020; 10(10):3492. https://doi.org/10.3390/app10103492

Engelenburg V J, Hueting R , Rijpkema S, Teuling J A , Uijlenhoet R, Ludwig F (2017). Impact of Changes in Groundwater Extractions and Climate Change on Groundwater- Dependent Ecosystem in a Complex Hydrogeological Settings. Water Resour Manage (2018) 32: 259. https://doi.org/10.1007/s11269-017-1808-1

Epting J, Michel A, Affolter A, Huggenberger P (2021). Climate change effects on groundwater recharge and temperatures in Swiss alluvial aquifers, Journal of Hydrology X, 11, 100071,ISSN 2589-9155,https://doi.org/10.1016/j.hydroa.2020.100071.

Ewadh, H. M., Al Imari, M. J., Jawad, S. F., & Mubarak, H. A. (2021). Fluoride removal using electrocoagulation technique. In IOP Conference Series: Earth and Environmental Science (Vol. 877, No. 1, p. 012047). IOP Publishing.

F. A. O. (2003). The irrigation challenge: Increasing irrigation contribution to food security through higher water productivity from canal irrigation systems. IPTRID Issue Paper 4, IPTRID Secretariat, Food and Agricultural Organization of the United Nations, Rome.

Famiglietti, J. S. (2014). The global groundwater crisis. Nature Climate Change, 4(11), 945-948.

Fang, Y., Ali, A., Gao, Y., Zhao, P., Li, R., Li, X., & Pan, J. (2022). Preparation and characterization of MgO hybrid biochar and its mechanism for high efficient recovery of phosphorus from aqueous media. Biochar, 4(1), 40.

Fannakh, A., & Farsang, A. (2022). DRASTIC, GOD, and SI approaches for assessing groundwater vulnerability to pollution: a review. Environmental Sciences Europe, 34(1), 1-16.

FAO, IFAD, UNICEF, W, and W, (2017) The State Of Food Security And Nutrition In The World. 32 Building Resilience For Peace And Food Security. Rome, http://www.fao.org/3/a-I7695e.pdf 33 (Accessed January 3, 2018).

Farhan Y, Anbar A, Al-Shaikh N, Mousa R (2017) Prioritization of Semi-Arid Agricultural Watershed Using Morphometric and Principal Component Analysis, Remote Sensing, and GIS Techniques, the Zerqa River Watershed, Northern Jordan. Agricultural Sciences. 08: 113-148. 10.4236/as.2017.81009.

Farooq, S.H., Prusty, P., Singh, R.K. et al., (2018). Fluoride contamination of groundwater and its seasonal variability in parts of Purulia district, West Bengal, India. Arab J Geosci 11, 709 (2018). https://doi.org/10.1007/s12517-018-4062-9

Fausey, N. R. (2004). Drainage, surface and subsurface. Encyclopedia of Soils in the Environment, 409-413.

Feng, Y., Zhao, D., Qiu, S., He, Q., Luo, Y., Zhang, K., & Wang, F. (2021). Adsorption of phosphate in aqueous phase by biochar prepared from sheep manure and modified by oyster shells. ACS omega, 6(48), 33046-33056.

Fenta AA, Yasuda H, Shimizu K, Haregeweyn N, Woldearegay K (2017) Quantitative analysis and implications of drainage morphometry of the Agula watershed in the semi-arid northern Ethiopia. Applied Water Science, 7: 3825–3840. doi:10.1007/s13201-017-0534-4

Ferris, J. G. (1950). A quantitative method fcr determining ground-water characteristics for drainage design. Agric. Engng., 31, 285-291.

Fischer, C., Aubron, C., Trouvé, A., Sekhar, M., & Ruiz, L. (2022). Groundwater irrigation reduces overall poverty but increases socioeconomic vulnerability in a semiarid region of southern India. Scientific Reports, 12(1), 8850.

Fishel, F.M., and Ferrell, J.A., (2019). Water pH and the Effectiveness of Pesticides. Agronomy Department, UF/IFAS Extension

Freeze RA, Cherry JA (1997) Groundwater. Prentice Hall, Englewood

Freeze, R. A., & Cherry, J. A. (1977). Groundwater. Prentice-hall.

Freundlich, H.M.F., (1906), Über die Adsorption in LösungenZ. für Phys. Chem., 57A (1906), pp. 385-470Google Scholar

Frye, A. D. (2013). The persistence of losing and gaining stream reaches.

Fuentes, I., & Vervoort, R. W. (2020). Site suitability and water availability for a managed aquifer recharge project in the Namoi basin, Australia. Journal of Hydrology: Regional Studies, 27, 100657.

Fusco, F., Allocca, V., Coda, S., Cusano, D., Tufano, R., De, V.P, (2020). Quantitative Assessment of Specific Vulnerability to Nitrate Pollution of Shallow Alluvial Aquifers by Process-Based and Empirical Approaches. Water, 12(1), 269–. doi:10.3390/w12010269

Gaikwad, S. K., Gaikwad, S. P., Wagh, V. M., Meshram, D. C., Kadam, A. K., Muley, A. A., & Sahu, U. L. (2022). Appraisal of groundwater from lithological diversity of the western coastal part, Maharashtra, India: An integrated hydrogeochemical, geospatial and statistical approaches. Marine Pollution Bulletin, 178, 113595.

Ganapathi H (2018). Assessment Of Drought Severity Using Standard Precipitation Index In Ahmednagar District, India.Assessment, International Research Journal of Engineering and Technology (IRJET) V. 5, N. 5, P. 1777-1780,

Ganapuram S , R Nagarajan , Sekhar , G C (2016) Identification of groundwater drought prone zones in Pedda vagu and Ookachetti vagu watersheds, tributaries of the Krishna River, India, Geocarto International, 31:4, 385-407, DOI: 10.1080/10106049.2015.1047472

Gang, K., Yanqun, L., Yi, P., & Yong, S. (2012). Evaluation of classification algorithms using MCDM and rank correlation. International Journal of Information Technology & Decision Making, 11(01), 197-225.

Gao Z, Liang RY, Xuan T (2019) VIKOR method for ranking concrete bridge repair projects with target-based criteria. Results in Engineering, 3, 100018. doi:10.1016/j.rineng.2019.100018

Gao, Y., Wang, Q., Ji, G., & Li, A. (2022). Degradation of antibiotic pollutants by persulfate activated with various carbon materials. Chemical Engineering Journal, 429, 132387.

García, H.L. and Martín, M.A.G., 2018. The Mathematics of the Uncertain, vol. 142, pp. 643, 2018.

Gaur N, Sarkar A, Dutta D. et al. (2022) Evaluation of water quality index and geochemical characteristics of surfacewater from Tawang India. Sci Rep 12, 11698 (2022). https://doi.org/10.1038/s41598-022-14760-3

Ge, S. (2003). Hydrology| Ground and Surface Water. Encyclopedia of Atmospheric Sciences, 973-979.

GEC (2015) MoWR RD GR, 2017 MoWR Rd Gr Report of the Ground Water Resource Estimation Committee (GEC-2015) Ministry of Water Resources, River Development & Ganga Rejuvenation Government of India (MoWR, RD&GR), Govt. of India (2017)

GEC (Groundwater Estimation Committee) (1997) Groundwater resource estimation methodology. Report of Ministry of Water Resources, New Delhi, India

Gęca, M., Wiśniewska, M., & Nowicki, P. (2022). Biochars and activated carbons as adsorbents of inorganic and organic compounds from multicomponent systems–A review. Advances in Colloid and Interface Science, 102687.

Geleta Ebsa, D., & Kebede, A. B. (2021). Defluoridation of drinking water by modified natural zeolite with Cationic surfactant, in case of Ziway town, Ethiopia. Drinking Water Engineering and Science Discussions, 1-14.

Geneva (2004).Guidelines for Drinking-Water Quality, Vol 1, Recommendation, (3rd Ed), Geneva (2004).

Ghaedi, M. (Ed.). (2021). Adsorption: Fundamental processes and applications. Academic Press.

Ghaleb F, Mario M, Sandra A, (2015) Regional Landsat-Based Drought Monitoring from 1982 to 2014. Climate, 3(3), 563–577.doi:10.3390/cli3030563

Gharbani, P., & Mehrizad, A. (2022). Preparation and characterization of graphitic carbon nitrides/polyvinylidene fluoride adsorptive membrane modified with chitosan for Rhodamine B dye removal from water: Adsorption isotherms, kinetics and thermodynamics. Carbohydrate Polymers, 277, 118860.

Gharekhani, M., Nadiri, A.A., Khatibi, R.K., Sadeghfam, S., Moghaddam, A.A., (2022). A study of uncertainties in groundwater vulnerability modelling using Bayesian model averaging (BMA),Journal of Environmental Management, Volume 303. 114168, ISSN 0301-4797,ttps://doi.org/10.1016/j.jenvman.2021.114168.

Ghassemi-Golezani, K., & Farhangi-Abriz, S. (2022). Improving plant available water holding capacity of soil by solid and chemically modified biochars. Rhizosphere, 21, 100469.

Ghodeif, K., Grischek, T., Bartak, R., Wahaab, R., & Herlitzius, J. (2016). Potential of river bank filtration (RBF) in Egypt. Environmental Earth Sciences, 75, 1-13.

Ghorabaee K M, Zavadskas EK, Olfat L, Turskis Z (2015) Multi-criteria inventory classification using a new method of evaluation based on distance from average solution (EDAS). Informatica 26(3), 435–451 (2015)

Ghorabaee M K, Zavadskas EK, Amiri M, Turskis Z (2016) Extended EDAS method for fuzzy multi-criteria decision-making: an application to supplier selection. Comput Commun Control 11(3):358–371

Ghorabaee, M. K. (2016). Developing an MCDM method for robot selection with interval type-2 fuzzy sets. Robotics and Computer-Integrated Manufacturing, 37, 221-232.

Ghorabaee, M. K., Amiri, M., & Azimi, P. (2015). Genetic algorithm for solving bi-objective redundancy allocation problem with k-out-of-n subsystems. Applied Mathematical Modelling, 39(20), 6396-6409.

Ghosh A, Mandal S (2019) Application of multivariate statistics towards the geochemical evaluation of fluoride enrichment in groundwater at Shilabati river bank, West Bengal, India. Environmental Engineering Research 2: 279-288.DOI: https://doi.org/10.4491/eer.2018.178

Ghosh K G (2018). Geo-Statistical Assessment of the Intensity, Duration, Frequency and Trend of Drought over Gangetic West Bengal, Eastern India, Topics in Hydrometerology, Theodore V Hromadka II and Prasada Rao, IntechOpen, DOI: 10.5772/intechopen.80037

Ghosh K G (2019) Spatial and temporal appraisal of drought jeopardy over the Gangetic West Bengal, eastern India. Geoenviron Disasters. 6. https://doi.org/10.1186/s40677-018-0117-1

Ghosh KG (2016) Long range climatic variability over Birbhum District, west Bengal and their impact on rainfed Aman crop in the context of climate change: adoption and mitigation. In: Chattopadhyay PK, Kushwaha DS (eds) Rural health, women empowerment and agriculture: issues and challenges, chap 21, 1st edn. New Delhi Publishers, New Delhi, pp 277–298

Ghosh S, Bhattacharya K (2012) Multivariate erosion risk assessment of lateritic badlands of Birbhum West Bengal, India: A case study. J Earth Syst Sci.121, 1441–1454. https://doi.org/10.1007/s12040-012-0243-1

Ghosh S, Guchhait S K, Hu X F (2015) Characterization and evolution of primary and secondary laterites in north western Bengal Basin, West Bengal, India. Journal of Paleogeography.4, 203-230, https://doi.org/10.3724/SP.J.1261.2015.00074.

Ghosh, A., Adhikary, P. P., Bera, B., Bhunia, G. S., & Shit, P. K. (2022). Assessment of groundwater potential zone using MCDA and AHP techniques: case study from a tropical river basin of India. Applied Water Science, 12(3), 37.

Ghosh, P. K., & Jana, N. C. (2018). Groundwater potentiality of the Kumari River Basin in drought-prone Purulia upland, Eastern India: a combined approach using quantitative geomorphology and GIS. Sustainable Water Resources Management, 4, 583-599.

Ghosh, S., & Kundu, S. (2022). Morphometric characterization and erosion assessment of gullies in the lateritic badlands of Eastern India using ALOS AW3D30 DEM and topographic indices. Geocarto International, 1-34.

Ghosh, S., Das, D., Gayen, S. K., & Bhardwaj, P. (2023). Delineation of groundwater potential zones using the AHP technique: a case study of Alipurduar district, West Bengal. Modeling Earth Systems and Environment, 1-31.

Gidey E, Dikinya O, Sebego R et al. (2018) Analysis of the long-term agricultural drought onset, cessation, duration, frequency, severity and spatial extent using Vegetation Health Index (VHI) in Raya and its environs, Northern Ethiopia. Environ Syst Res 7, 13 (2018). https://doi.org/10.1186/s40068-018-0115-z

Giri, A. K., & Mishra, P. C. (2023). Optimization of different process parameters for the removal efficiency of fluoride from aqueous medium by a novel bio-composite using Box-Behnken design. Journal of Environmental Chemical Engineering, 11(1), 109232.

Giri, S., Kang, Y., MacDonald, K., Tippett, M., Qiu, Z., Lathrop, R. G., & Obropta, C. C. (2023). Revealing the sources of arsenic in private well water using Random Forest Classification and Regression. Science of The Total Environment, 857, 159360.

Githinji, T. W., Dindi, E. W., Kuria, Z. N., & Olago, D. O. (2022). Application of analytical hierarchy process and integrated fuzzy-analytical hierarchy process for mapping potential groundwater recharge zone using GIS in the arid areas of Ewaso Ng'iro–Lagh Dera Basin, Kenya. HydroResearch, 5, 22-34.

Glass, J., Junghanns, R., Schlick, R., & Stefan, C. (2022). The INOWAS platform: A web-based numerical groundwater modelling approach for groundwater management applications. Environmental Modelling & Software, 155, 105452.

Gocic M, Trajkovic S (2013) Analysis of Changes in Meteorological Variables using Mann Kendall and Sen's Slope Estimator Statistical Test In Serbia. Global and Planetary Change. 100,172-182 https://doi.org/10.1016/j.gloplacha.2012.10.014

Godwin, I. A., Reba, M. L., Leslie, D. L., Adams, R. F., & Rigby, J. R. (2022). Feasibility of farm-scale infiltration galleries for managed aquifer recharge in an agricultural alluvial aquifer of Northeast Arkansas. Agricultural Water Management, 264, 107531.

Gorai, A.K., (2022). Sensitivity Analysis of GIS-based Fuzzy-AHP Model for Prediction of Slope Failure Susceptibility Index. J Indian Soc Remote Sens. https://doi.org/10.1007/s12524-021-01488-2

Goswami, T., & Ghosal, S. (2022). Understanding the suitability of two MCDM techniques in mapping the groundwater potential zones of semi-arid Bankura District in eastern India. Groundwater for Sustainable Development, 17, 100727.

Goswami, T., Ghosal, S. Examining the groundwater level in a semi-arid district of eastern India: spatiotemporal trends, determinants, and future prospects. Environ Dev Sustain (2022). https://doi.org/10.1007/s10668-022-02512-2

Gourai, M., Nayak, A. K., Nial, P. S., Satpathy, B., Bhuyan, R., Singh, S. K., & Subudhi, U. (2023). Thermal plasma processing of Moringa oleifera biochars: adsorbents for fluoride removal from water. RSC advances, 13(7), 4340-4350.

Gowrisankar, G., Jagadeshan, G., & Elango, L. (2017). Managed aquifer recharge by a check dam to improve the quality of fluoride-rich groundwater: a case study from southern India. Environmental monitoring and assessment, 189(4), 200.

Graham, J.P., Polizzotto, M.L., (2013). Pit latrines and their impacts on groundwater quality: a systematic review. Environ Health Perspect. 2013;121(5):521-530. doi:10.1289/ehp.1206028

Green T.R. (2016) Linking Climate Change and Groundwater. In: Jakeman A.J., Barreteau O., Hunt R.J., Rinaudo JD., Ross A. (eds) Integrated Groundwater Management. Springer, Cham

Grischek, T., Schoenheinz, D., Worch, E., & Hiscock, K. (2020). Bank filtration in Europe—An overview of aquifer conditions and hydraulic controls. Management of aquifer recharge for sustainability, 485-488.

Grochowalski, J. H., & Hendrickson, A. (2023). Detecting Group Collaboration Using Multiple Correspondence Analysis. Journal of Educational Measurement.

Groenendyk, D. G., Ferre, T. P., Thorp, K. R., & Rice, A. K. (2015). Hydrologic-process-based soil texture classifications for improved visualization of landscape function. PloS one, 10(6), e0131299.

Gul, M., Lo, H. W., & Yucesan, M. (2021). Fermatean fuzzy TOPSIS-based approach for occupational risk assessment in manufacturing. Complex & Intelligent Systems, 7, 2635-2653.

Gul, S.; Whalen, J.K.; Thomas, B.W.; Sachdeva, V.; Deng, H. (2015).Physico-chemical properties and microbial responses in biochar-amended soils: Mechanisms and future directions. Agric. Ecosyst. Environ. 2015, 206, 46–59

Gumma M K, Mohanty S, Nelson A, Arnel R, Mohammed I A, Das SR (2015) Remote sensing based change analysis of rice environments in Odisha, India. Journal of Environmental Management, 148, 31–41. https://doi.org/10.1016/j.jenvman.2013.11.039

Gun (2012) Groundwater and Global Change: Trends, Opportunities and Challenges. France. International Hydrological Programme

Guo, X., Gui, X., Xiong, H., Hu, X., Li, Y., Cui, H., & Ma, C. (2023). Critical role of climate factors for groundwater potential mapping in arid regions: insights from Random Forest, XGBoost, and LightGBM algorithms. Journal of Hydrology, 129599.

Guo, X., Yang, Z., Li, C., Xiong, H., Ma, C., (2023). Combining the classic vulnerability index and affinity propagation clustering algorithm to assess the intrinsic aquifer vulnerability of coastal aquifers on an integrated scale, Environmental Research, 217, 114877, ISSN 0013-9351,https://doi.org/10.1016/j.envres.2022.114877.

Gupta, A., & Singh, E. J. (2019). Arsenic–iron relationships in aquifers of North East India: implications for public health and the environment. Environmental management, 63, 437-443.

Gupta, D., & Patel, P. P. (2021). Mapping groundwater level fluctuation and utilisation in Puruliya District, West Bengal. Geostatistics and geospatial technologies for groundwater resources in India, 413-442.

Gust L, D'journo X B. (2015)The use of correlation functions in thoracic surgery research. Journal of thoracic disease, 7:E11–E15. https://doi.org/10.3978/j.issn.2072-1439.2015.01.54

Habuda-Stanić, M., Ergović Ravančić, M., & Flanagan, A. (2014). A review on adsorption of fluoride from aqueous solution. Materials, 7(9), 6317-6366.

Haghizadeh A, Siahkamari S, Haghiabi A H, Rahmati O (2017) Forecasting flood-prone areas using Shannon's entropy model. Journal of Earth System Science, 126(3). doi:10.1007/s12040-017-0819-x

Haghnazar H, Johannesson KH, González-Pinzón R, Pourakbar M, Aghayani E, Rajabi A, Hashemi AA (2022) Groundwater geochemistry, quality, and pollution of the largest lake basin in the Middle East: comparison of PMF and PCA-MLR receptor models and application of the source-oriented, HHRA approach. Chemosphere 288:132489. https://doi.org/10.1016/J.CHEMOSPHERE.2021.132489

Halder S, Roy M B & Roy P K (2020) Analysis of groundwater level trend and groundwater drought using Standard Groundwater Level Index: a case study of an eastern river basin of West Bengal, India. SN Appl. Sci. 2, 507. https://doi.org/10.1007/s42452-020-2302-6

Halder S, Roy M B, Roy PK (2021) Modelling soil erosion risk of a tropical plateau basin to identify priority areas for conservation. Environ Earth Sci 80, 646 (2021). https://doi.org/10.1007/s12665-021-09941-8

Halder S, Roy MB, Roy PK (2020) Fuzzy logic algorithm based analytic hierarchy process for delineation of groundwater potential zones in complex topography. Arab J Geosci 13, 574. https://doi.org/10.1007/s12517-020-05525-1

Halder S, Roy MB, Roy PK (2021) Tropical plateau basin prioritisation for sustainable groundwater management using classical algorithms. Arab J Geosci 14, 2187 (2021). https://doi.org/10.1007/s12517-021-08496-z

Halder S, Roy MB, Roy PK (2022) Modelling drought vulnerability tracts under changed climate scenario using fuzzy DEMATEL and GIS techniques. Theor Appl Climatol (2022). https://doi.org/10.1007/s00704-022-04165-7

Hamdan, I., Margane, A., Ptak, T. et al., (2016). Groundwater vulnerability assessment for the karst aquifer of Tanour and Rasoun springs catchment area (NW-Jordan) using COP and EPIK intrinsic methods. Environ Earth Sci 75, 1474 (2016). https://doi.org/10.1007/s12665-016-6281-2

Hamilton, Z. K., & van Wormer, J. (2015). Customizing offender assessment, Washington State Institute for Criminal Justice

Hamza, S.M., Ahsan, A., Imteaz, M.A, et al., (2017). GIS-based FRASTIC model for pollution vulnerability assessment of fractured-rock aquifer systems. Environ Earth Sci 76, 197 (2017). https://doi.org/10.1007/s12665-017-6520-1

Hancock, P. J. (2002). Human impacts on the stream–groundwater exchange zone. Environmental management, 29(6), 763-781.

Hao Z, Singh VP, Xia Y (2018) Seasonal drought prediction: advances, challenges, and future prospects. Rev Geophys 56(1):108–141. https://doi.org/10.1002/2016RG000549

Haq, M. A., Jilani, A. K., & Prabu, P. (2021). Deep learning based modeling of groundwater storage change. CMC-Computers, Materials & Continua, 70, 4599-4617.

Harb, O. M., Salem, M. S., Abd EL-Hay, G. H., & Makled, K. M. (2016). Fog water harvesting providing stability for small Bedwe communities lives in North cost of Egypt. Annals of Agricultural Sciences, 61(1), 105-110.

Hasan, M., Shang, Y., Jin, W., & Akhter, G. (2021). Estimation of hydraulic parameters in a hard rock aquifer using integrated surface geoelectrical method and pumping test data in southeast Guangdong, China. Geosciences Journal, 25, 223-242.

Hashim, K. S., Shaw, A., Al Khaddar, R., Pedrola, M. O., & Phipps, D. (2017). Iron removal, energy consumption and operating cost of electrocoagulation of drinking water using a new flow column reactor. Journal of environmental management, 189, 98-108.

Hazen, A. (1893) Some physical properties of sand and gravels, with special reference to their use in filtration. Twenty Fourth Annual Report, State Board of Health of Massachusetts, pp 541–556

Hembram, T.K., Paul, G.C. & Saha, S., (2019). Spatial prediction of susceptibility to gully erosion in Jainti River basin, Eastern India: a comparison of information value and logistic regression models. Model. Earth Syst. Environ. 5, 689–708 (2019). https://doi.org/10.1007/s40808-018-0560-8

Ho, Y. S., & McKay, G. (1999). Pseudo-second order model for sorption processes. Process biochemistry, 34(5), 451-465.

Hoang, N. A. T., Covatti, G., & Grischek, T. (2022). Methodology for evaluation of potential sites for large-scale riverbank filtration. Hydrogeology Journal, 30(6), 1701-1716.

Hodaifa, G., Ochando-Pulido, J. M., Alami, S. B. D., Rodriguez-Vives, S., & Martinez-Ferez, A. (2013). Kinetic and thermodynamic parameters of iron adsorption onto olive stones. Industrial crops and products, 49, 526-534.

Horton R (1945) Erosional development of streams and their drainage basins; Hydrophysical approach to quantitative morphology. Bull Geol Soc Am. 56:275–370.

Horton R E (1932) Drainage-basin characteristics. Transactions, American Geophysical Union, 13(1), 350. doi:10.1029/tr013i001p00350

https://www.nrcs.usda.gov/wps/portal/nrcs/site/soils/home/file:///E:/P.hd%202018May/My%20Ph.d%20Calculation/Aquifer%20vulnerability%20index/Saturated%20Hydraulic%20Conductivity%20_%20NRCS%20Soils.html

Hu, B., Song, X., Lu, Y., Liang, S., & Liu, G. (2022). Fluoride enrichment mechanisms and related health risks of groundwater in the transition zone of geomorphic units, northern China. Environmental Research, 212, 113588.

Hu, B., Teng, Y., Zhai, Y., Zuo, R., Li, J., & Chen, H. (2016). Riverbank filtration in China: A review and perspective. Journal of Hydrology, 541, 914-927.

Huan, H., Wang, J., Teng, Y., (2012). Assessment and validation of groundwater vulnerability to nitrate based on a modified DRASTIC model: A case study in Jilin City of northeast China. Science of The Total Environment, 440(), 14–23. doi:10.1016/j.scitotenv.2012.08.037

Huang J, Zhu W, Li Y, Huang R, Sedano F, Su W, Dong J, Tian L, Huang Y, Zhu De, Zhang X (2018) Comparison of three remotely sensed drought indices for assessing the impact of drought on winter wheat yield. International Journal of Digital Earth, 1–23. doi:10.1080/17538947.2018.1542040

Huang, C. S., Tsou, P. R., & Yeh, H. D. (2012). An analytical solution for a radial collector well near a stream with a low-permeability streambed. Journal of Hydrology, 446, 48-58.

Huang, Y., He, Y., Zhang, H., Wang, H., Li, W., Li, Y., & Hu, G. (2022). Selective adsorption behavior and mechanism of phosphate in water by different lanthanum modified biochar. Journal of Environmental Chemical Engineering, 10(3), 107476.

Hubbs, S. A. (2006). Evaluating streambed forces impacting the capacity of riverbed filtration systems. In Riverbank Filtration Hydrology: Proceedings of the NATO Advanced Research Workshop on Riverbank Filtration Hydrology Bratislava, Slovakia September 2004 (pp. 21-42). Springer Netherlands.

Huddleston JH (1996).How soil properties affect groundwater vulnerability to pesticide contamination. Oregon State University. https://wellwater.oregonstate.edu/sites/wellwater.oregonstate.edu/files/well-water/pdf/how_soil_properties_affect_groundwater_vulnerability.pdf

Huete, AR (1988). A soil-adjusted vegetation index (SAVI). Remote Sensing of Environment, 25(3), 295–309. doi:10.1016/0034-4257(88)90106-x

Huisman, L., & Huisman, L. (1972). Groundwater recovery (Vol. 336). London: Macmillan.

Humphreys, E., 2010. Halting the Groundwater Decline in North-West India—Which Crop Technologies will be Winners?, Advances in Agronomy, 109, 155–217. doi:10.1016/B978-0-12-385040-9.00005-0

Hvorslev, M. J. (1951). Time lag and soil permeability in ground-water observations, Waterways Experiment Station, Corps of Engineers. US Army, Bulletin, 36, 49.

Hwang CL, Yoon K (1981) Multiple Attribute Decision Making: Methods and Applications. Springer-Verlag, NewYork. http://dx.doi.org/10.1007/978-3-642-48318-9

ICAR-ATARI (Zone-X) (2019) Annual Report 2018-19. ICAR-Agricultural Technology Application Research Institute (ATARI), Hyderabad 160p.

Ifediegwu, S. I. (2022). Assessment of groundwater potential zones using GIS and AHP techniques: a case study of the Lafia district, Nasarawa State, Nigeria. Applied Water Science, 12(1), 10.

Ikirri, M., Boutaleb, S., Ibraheem, I. M., Abioui, M., Echogdali, F. Z., Abdelrahman, K., & Faik, F. (2023). Delineation of Groundwater Potential Area using an AHP, Remote Sensing, and GIS Techniques in the Ifni Basin, Western Anti-Atlas, Morocco. Water, 15(7), 1436.

Ilamurugan, O., Jothibasu, A. Anbazhagan, S., (2022). Geospatial technology and modified DRASTIC model to assess the groundwater pollution vulnerability along a stretch of Cauvery River, South India. Environ Earth Sci 81, 85 (2022). https://doi.org/10.1007/s12665-022-10208-z

Ilieva G, Yankova T, Klisarova-Belcheva S (2018) Decision analysis with classic and fuzzy EDAS modifications. Comp. Appl. Math. 37, 5650–5680 (2018). https://doi.org/10.1007/s40314-018-0652-0

Indelman, P., Moltyaner, G., & Dagan, G. (1999). Determining the Hydraulic Conductivity Spatial Structure at the Twin Lake Site by Grain-Size Distribution. Groundwater, 37(2), 223-227.

IPCC (2007) Climate Change 2007: Synthesis Report. Contribution of Working Groups I, II and III to the Fourth Assessment Report of the Intergovernmental Panel on Climate Change [Core Writing Team, Pachauri, R.K and Reisinger, A. (eds.)]. IPCC, Geneva, Switzerland, 104 pp

Jadhav, A. S., & Jadhav, M. V. (2022). Use of response surface methodology for optimization of fluoride removal efficiency by adsorption on black mustard husk ash. Materials Today: Proceedings, 61, 150-157.

Jain SK, Keshri R, Goswami A, Sarkar A, Chaudhry A (2009) Identification of drought-vulnerable areas using NOAA AVHRR data. International Journal of Remote Sensing, 30(10), 2653–2668. doi:10.1080/01431160802555788

Jamei, M., Karbasi, M., Malik, A., Jamei, M., Kisi, O., & Yaseen, Z. M. (2022). Long-term multi-step ahead forecasting of root zone soil moisture in different climates: Novel ensemble-based complementary data-intelligent paradigms. Agricultural Water Management, 269, 107679.

Jana SK, Roy J (2020) Biodiversity And Impacts Of Climate Change In Home Gardens: Evidence From A Study In West Bengal, India. Current State And Future Impacts Of Climate Change On Biodiversity. Igi Global

Jasechko, S., & Perrone, D. (2021). Global groundwater wells at risk of running dry. Science, 372(6540), 418-421.

Jaydhar, A. K., Pal, S. C., Saha, A., Islam, A. R. M. T., & Ruidas, D. (2022). Hydrogeochemical evaluation and corresponding health risk from elevated arsenic and fluoride contamination in recurrent coastal multi-aquifers of eastern India. Journal of Cleaner Production, 369, 133150.

Jeyaseelan AT (2003) Droughts & Floods Assessment and Monitoring Using Remote Sensing and GIS. In M. V. K Sivakumar et al. (Eds.), Satellite Remote Sensing and GIS Applications in Agricultural Meteorology (Vol. 291). Geneva, Switz: World Meteoro-logical Organisation.

Jhariya, D.C., Kumar, T., Pandey, H.K. et al., (2019). Assessment of groundwater vulnerability to pollution by modified DRASTIC model and analytic hierarchy process. Environ Earth Sci 78, 610 https://doi.org/10.1007/s12665-019-8608-2

Ji L, Peters AJ (2003) Assessing Vegetation Response to Drought in the Northern Great Plains Using Vegetation and Drought Indices. Remote Sensing of Environment, 87, 85-98. http://dx.doi.org/10.1016/S0034-4257(03)00174-3

Jiang S, Liu R, Ren L et al.(2020) Evaluation and Hydrological Application of CMADS Reanalysis Precipitation Data against Four Satellite Precipitation Products in the Upper Huaihe River Basin, China. J Meteorol Res 34, 1096–1113 (2020). https://doi.org/10.1007/s13351-020-0026-6

Jiang, G., Jin, L., Pan, Q., Peng, N., Meng, Y., Huang, L., & Wang, H. (2022). Structural modification of aluminum oxides for removing fluoride in water: crystal forms and metal ion doping. Environmental Technology, 43(21), 3248-3261.

Jiang, H., Zhang, J., Luo, K., Xing, W., Du, J., Dong, Y.,& Tang, W. (2022). Effective fluoride removal from brackish groundwaters by flow-electrode capacitive deionization (FCDI) under a continuous-flow mode. Science of The Total Environment, 804, 150166.

Jiang, M., Yang, Y., Lei, T., Ye, Z., Huang, S., Fu, X., & Li, H. (2022). Removal of phosphate by a novel activated sewage sludge biochar: Equilibrium, kinetic and mechanism studies. Applications in Energy and Combustion Science, 9, 100056.

Jiang, S., Nguyen, T.A.H., Rudolph, V. et al. (2017) Characterization of hard- and softwood biochars pyrolyzed at high temperature. Environ Geochem Health 39, 403–415 (2017). https://doi.org/10.1007/s10653-016-9873-6

Jiang, Z., Gao, H., Wu, L., Li, Y., Cui, B., (2021). A prediction model of shallow groundwater pollution based on deep convolution neural network. International Journal of Environmental Technology and Management, Inderscience Enterprises Ltd, vol. 24(3/4), pages 278-293.

Jiao, G. J., Ma, J., Li, Y., Jin, D., Guo, Y., Zhou, J., & Sun, R. (2021). Enhanced adsorption activity for phosphate removal by functional lignin-derived carbon-based adsorbent: Optimization, performance and evaluation. Science of The Total Environment, 761, 143217.

John J, Jaganathan R, Dharshan Shylesh, DS (2022) Mapping of Soil Moisture Index Using Optical and Thermal Remote Sensing. In: Marano G.C., Ray Chaudhuri S., Unni Kartha G., Kavitha P.E., Prasad R., Achison R.J. (eds) Proceedings of SECON'21. SECON 2021. Lecture Notes in Civil Engineering, vol 171. Springer, Cham. https://doi.org/10.1007/978-3-030-80312-4_65

Johnson, A. L., (1967). Specific yield: compilation of specific yields for various materials, Water Supply Paper 1662-D,

Joodavi A, Aghlmand R, Podgorski J, Dehbandi R, Abbasi A (2021) Characterization, geostatistical modeling and health risk assessment of potentially toxic elements in groundwater resources of northeastern

Iran. Journal of Hydrology: Regional Studies, 37, 1-15. [100885]. https://doi.org/10.1016/j.ejrh.2021.100885

Joseph, J., Scheidegger, J. M., Jackson, C. R., Barik, B., & Ghosh, S. (2022). Is flood to drip irrigation a solution to groundwater depletion in the Indo-Gangetic plain?. Environmental Research Letters, 17(10), 104002.

Joshi, N., Rahaman, M. M., Thakur, B., Shrestha, A., Kalra, A., & Gupta, R. (2020). Assessing the effects of climate variability on groundwater in Northern India. In World Environmental and Water Resources Congress 2020: Groundwater, Sustainability, Hydro-Climate/Climate Change, and Environmental Engineering (pp. 41-52). Reston, VA: American Society of Civil Engineers.

Jozaghi, A., Alizadeh, B., Hatami, M., Flood, I., Khorrami, M., Khodaei, N., & Ghasemi Tousi, E. (2018). A comparative study of the AHP and TOPSIS techniques for dam site selection using GIS: A case study of Sistan and Baluchestan Province, Iran. Geosciences, 8(12), 494.

Kadam, A., Umrikar, B., Bhagat, V., Wagh, V., & Sankua, R. N. (2021). Land suitability analysis for afforestation in semi-arid watershed of Western Ghat, India: A groundwater recharge perspective. Geology, Ecology, and Landscapes, 5(2), 136-148.

Kahraman, C., Keshavarz Ghorabaee, M., Zavadskas, E. K., Cevik Onar, S., Yazdani, M., & Oztaysi, B. (2017). Intuitionistic fuzzy EDAS method: an application to solid waste disposal site selection. Journal of Environmental Engineering and Landscape Management, 25(1), 1-12.

KahramanC, Ghorabaee KM, Zavadskas EK, Onar S C, MYazdani M, Oztaysi B (2017) Intuitionistic fuzzy EDAS method: an application to solid waste disposal site selection, Journal of Environmental Engineering and Landscape Management, 25:1, 1-12, DOI: 10.3846/16486897.2017.1281139

Kaiser H (1974) An index of factorial simplicity. Psychometrika, 39, 31-6.

Kalbus, E., Reinstorf, F., & Schirmer, M. (2006). Measuring methods for groundwater, surface water and their interactions: a review. Hydrology and Earth System Sciences Discussions, 3(4), 1809-1850.

Kalsido, A. W., Tekola, B., Mogessie, B., & Alemayehu, E. (2022). Excess fluoride issues and mitigation using low-cost techniques from groundwater: A review. Cost Effective Technologies for Solid Waste and Wastewater Treatment, 241-263.

Kamali, M., Appels, L., Kwon, E. E., Aminabhavi, T. M., & Dewil, R. (2021). Biochar in water and wastewater treatment-a sustainability assessment. Chemical Engineering Journal, 420, 129946.

Kamangar, M., Katorani, S., Tekyekhah, J., Sohrabnejad, C., & Haderi, F. G. (2019). A novel hybrid MCDM model to select a suitable location for implement groundwater recharge. Plant Archives, 19(2), 87-98.

Kamble MVK, Ghosh M, Rajeevan R P, Samui (2010) Drought monitoring over India through normalized difference vegetation index (NDVI). Mausam 61: 537–546.

Kansara, S., Modgil, S., & Kumar, R. (2022). Structural transformation of fuzzy analytical hierarchy process: a relevant case for Covid-19. Operations Management Research, 1-16.

Kar B, Saha J, Saha JD (2012) Analysis of meteorological drought: the scenario of West Bengal. Indian J Spat Sci 3(2):1–11

Kar N S & Das S (2020) Flood-Prone Ghatal Region, India: A Study on Post-'Phailin' Inundations of 2013. Water Management in South Asia, Springer International Publishing

Karanth, K. R. (1987). Ground water assessment, development, and management. Tata McGraw-Hill Education.

Karki, R., Srivastava, P., Kalin, L., Mitra, S., & Singh, S. (2021). Assessment of impact in groundwater levels and stream-aquifer interaction due to increased groundwater withdrawal in the lower Apalachicola-Chattahoochee-Flint (ACF) River Basin using MODFLOW. Journal of Hydrology: Regional Studies, 34, 100802.

Karnieli A, Agam N, Pinker RT, Anderson M, Imhoff ML, Gutman GG, Goldberg A (2010) Use of NDVI and land surface temperature for drought assessment: merits and limitations. J Clim 23(3):618–633

Karunasingha, D. S. K. (2022). Root mean square error or mean absolute error? Use their ratio as well. Information Sciences, 585, 609-629..

Kasenow, M. (2002). Determination of hydraulic conductivity from grain size analysis. Water Resources Publication.

Kathirvelu, K., Yesudhas, A. V. P., & Ramanathan, S. (2023). Spectral unmixing based random forest classifier for detecting surface water changes in multitemporal pansharpened Landsat image. Expert Systems with Applications, 224, 120072.

Katiyar, P., Yadu, B., Korram, J., Satnami, M. L., Kumar, M., & Keshavkant, S. (2020). Titanium nanoparticles attenuates arsenic toxicity by up-regulating expressions of defensive genes in Vigna radiata L. journal of environmental sciences, 92, 18-27.

Kaur, L., Rishi, M. S., Singh, G., & Thakur, S. N. (2020). Groundwater potential assessment of an alluvial aquifer in Yamuna sub-basin (Panipat region) using remote sensing and GIS techniques in conjunction with analytical hierarchy process (AHP) and catastrophe theory (CT). Ecological Indicators, 110, 105850.

Kazakis, N. (2018). Delineation of suitable zones for the application of managed aquifer recharge (MAR) in coastal aquifers using quantitative parameters and the analytical hierarchy process. Water, 10(6), 804.

Kazakis, N., Voudouris, K.S., (2015). Groundwater vulnerability and pollution risk assessment of porous aquifers to nitrate: modifying the DRASTIC method using quantitative parameters J. Hydrol., 525, pp. 13-25,

Keranen, A., Leiviska, T., Hormi, O., Tanskanen, J., (2014) Removal of nitrate by modified pine sawdust: Effects of temperature and co-existing anions,Journal of Environmental Management,Volume 147,2015,Pages 46-54,ISSN 0301-4797, (2014) https://doi.org/10.1016/j.jenvman.2014.09.006.

Kesuma, D.A., Purwanto, P., Putranto, T.T., Rahmani, T.P.D., (2017). Factor weighting in DRASTIC modelling for assessing the groundwater vulnerability in Salatiga groundwater basin, Central Java Province, Indonesia. IOP Conference Series: Earth and Environmental Science, 70, 012008–. doi:10.1088/1755-1315/70/1/012008

Khadse, G.K., Patni, P.M. & Labhasetwar, P.K. (2015). Removal of iron and manganese from drinking water supply. Sustain. Water Resour. Manag. 1, 157–165 (2015). https://doi.org/10.1007/s40899-015-0017-4

Khalid Awan, U., Tischbein, B., & Martius, C. (2015). Simulating Groundwater Dynamics Using Feflow-3D Groundwater Model Under Complex Irrigation and Drainage Network of Dryland Ecosystems of Central Asia. Irrigation and Drainage, 64(2), 283-296.

Khan, B. A., Ahmad, M., Iqbal, S., Bolan, N., Zubair, S., Shafique, M. A., & Shah, A. (2022). Effectiveness of the engineered pinecone-derived biochar for the removal of fluoride from water. Environmental Research, 212, 113540.

Khan, U., & Rudra, S. Hydro-Geochemistry of Fluoride Concentration in Groundwater and Potential Human Health Risks from the Parts of Bankura District, West Bengal. West Bengal.

Khatri, N., Tyagi, S., & Rawtani, D. (2017). Recent strategies for the removal of iron from water: A review. Journal of Water Process Engineering, 19, 291-304.

Khatun S (2016) Estimation of Surface Runoff and its Seasonality of Kushkarni River Basin. International Research Journal of Earth Science. 4, 1-10.

Kheradmand, A., Negarestani, M., Kazemi, S., Shayesteh, H., Javanshir, S., & Ghiasinejad, H. (2022). Adsorption behavior of rhamnolipid modified magnetic Co/Al layered double hydroxide for the removal of cationic and anionic dyes. Scientific Reports, 12(1), 14623.

Ki SJ, Ray C (2014) Using fuzzy logic analysis for siting decisions of infiltration trenches for highway runoff control, Sci. Total Environ., 493 (2014), pp. 44-53, 10.1016/j.scitotenv.2014.05.121

Kilinc, H. C., Ahmadianfar, I., Demir, V., Heddam, S., Al-Areeq, A. M., Abba, S. I., & Yaseen, Z. M. (2023). Daily Scale River Flow Forecasting Using Hybrid Gradient Boosting Model with Genetic Algorithm Optimization. Water Resources Management, 1-16.

Kim, H., Yang, S., Rao, S. R., Narayanan, S., Kapustin, E. A., Furukawa, H., & Wang, E. N. (2017). Water harvesting from air with metal-organic frameworks powered by natural sunlight. Science, 356(6336), 430-434.

Kipp Jr, Kenneth. L. (1997). Guideto the Revised Heat and Solute Transport Simulator: HST3D Version 2. Water-resources investigations report, 97, 4157.

Kisi O (2010) Discussion of "Application of neural network and adaptive neuro-fuzzy inference systems for river flow prediction". Hydrol Sci J 55(8):1453–1454. doi:10.1080/02626667.2010.527848

Kisi O, Haktanir T, Ardiclioglu M, Ozturk O, Yalcin E, Uludag S (2008) Adaptive neuro-fuzzy computing technique for suspended sediment estimation. Adv Eng Softw 40(6):438–444. doi:10.1016/j.advengsoft.2008.06.004

Kogan FN (1995) Application of vegetation index and brightness temperature for drought detection. Advances in Space Research, 15(11): 91–100. DOI: 10.1016/0273-1177(95)00079-T.

Kolios, A., Mytilinou, V., Lozano-Minguez, E., & Salonitis, K. (2016). A comparative study of multiple-criteria decision-making methods under stochastic inputs. Energies, 9(7), 566.

Konikow, L. F. (2011). Contribution of global groundwater depletion since 1900 to sea-level rise. Geophysical Research Letters, 38(17).

Koon, A.B., Anornu, G.K., Dekongmen, W.B., Sunkari, E.D., Agyare, A., Gyamfi, C., (2023).Evaluation of groundwater vulnerability using GIS-based DRASTIC model in Greater Monrovia, Montserrado County, Liberia,UrbanClimate,Volume48,2023,101427,ISSN2212-0955,https://doi.org/10.1016/j.uclim.2023.101427.

Koutalakis P, Zaimes GN (2022) River Flow Measurements Utilizing UAV-Based Surface Velocimetry and Bathymetry Coupled with Sonar. Hydrology 2022, 9, 148. https://doi.org/10.3390/hydrology9080148

Kozeny, J. (1927). Uber kapillare Leitung des Wassers im Boden-Aufstieg, Versickerung und Anwendung auf die Bewasserung, Sitzungsberichte der Akademie der Wissenschaften Wien. Mathematisch Naturwissenschaftliche Abteilung, 136, 271-306.

Krause, S., Hannah, D. M., Fleckenstein, J. H., Heppell, C. M., Kaeser, D., Pickup, R., & Wood, P. J. (2011). Inter-disciplinary perspectives on processes in the hyporheic zone. Ecohydrology, 4(4), 481-499.

Krishankumar, R., Garg, H., Arun, K., Saha, A., Ravichandran, K. S., & Kar, S. (2021). An integrated decision-making COPRAS approach to probabilistic hesitant fuzzy set information. Complex & Intelligent Systems, 7(5), 2281-2298.

Krogulec E (2018) Evaluating the risk of groundwater drought in groundwater-dependent ecosystems in the central part of the Vistula River Valley, Poland. Ecohydrology and Hydrobiology.Vol-18 Issue 1, pp-82-91, https://doi.org/10.1016/j.ecohyd.2017.11.003

Kros, J., Mol-Dijkstra, J.P., Wamelink, G.W.W. et al.(2016). Modelling impacts of acid deposition and groundwater level on habitat quality and plant species diversity. Ecol Process 5, 22 (2016). https://doi.org/10.1186/s13717-016-0066-0

Kruć, R. H., Dragon, K., Gorski, J., Nagy-Kovacs, Z., & Grischek, T. (2020). Geohydraulic conditions and post-treatment at riverbank filtration sites in Eastern Europe. Baltica, 33(1).

Kumar D, Singh AK, Taloor A K, Singh DS (2020) Recessional pattern of Thelu and Swetvarn glaciers between 1968 and 2019, Bhagirathi basin, Garhwal Himalaya, India. Quaternary International, (), S1040618220302512–. doi:10.1016/j.quaint.2020.05.017

Kumar S , Rathnam E V (2019) Analysis and Prediction of Groundwater Level Trends using Four Variations of Mann Kendall Test and ARIMA Modelling. Journal of Geological Society of India (2019) 94: 281. https://doi.org/10.1007/s12594-019-1308-4

Kumar, A., Krishna, A.P., 2018. Groundwater vulnerability and contamination risk assessment using GIS-based modified DRASTIC-LU model in hard rock aquifer system in India. Geocarto International, (), 1–66. doi:10.1080/10106049.2018.1557259

Kumar, C. P. (2019). An overview of commonly used groundwater modelling software.

Kumar, P. S., Korving, L., Keesman, K. J., van Loosdrecht, M. C., & Witkamp, G. J. (2019). Effect of pore size distribution and particle size of porous metal oxides on phosphate adsorption capacity and kinetics. Chemical Engineering Journal, 358, 160-169.

Kumar, P., Herath, S., Avtar, R. et al. Mapping of groundwater potential zones in Killinochi area, Sri Lanka, using GIS and remote sensing techniques. Sustain. Water Resour. Manag. 2, 419–430 (2016). https://doi.org/10.1007/s40899-016-0072-5

Kumar, R., Dwivedi, S. B., & Gaur, S. (2021). A comparative study of machine learning and Fuzzy-AHP technique to groundwater potential mapping in the data-scarce region. Computers & Geosciences, 155, 104855.

Kumar, R., Sharma, P., Rose, P. K., Sahoo, P. K., Bhattacharya, P., Pandey, A., & Kumar, M. (2023). Co-transport and deposition of fluoride using rice husk-derived biochar in saturated porous media: Effect of solution chemistry and surface properties. Environmental Technology & Innovation, 30, 103056.

Kumar, S., Kumar, S., & Barman, A. G. (2018). Supplier selection using fuzzy TOPSIS multi criteria model for a small scale steel manufacturing unit. Procedia computer science, 133, 905-912.

Kumar, S., Narjary, B., Vivekanand, Islam, A., Yadav, R. K., & Kamra, S. K. (2022). Modeling climate change impact on groundwater and adaptation strategies for its sustainable management in the Karnal district of Northwest India. Climatic Change, 173(1-2), 3.

Kundu A, Nag SK (2015) Delineation of Groundwater Quality for Drinking and Irrigation Purposes: A Case Study of Chhatna Block, Bankura District, West Bengal, International Bulletin of water Resources & Development, Vol-1, 1

Kundu A, Nag SK (2018) Assessment of groundwater quality in Kashipur Block, Purulia district, West Bengal. Appl Water Sci 8, 33 (2018). https://doi.org/10.1007/s13201-018-0675-0

Kundu, M., Zafor, A. & Maiti, R. (2023). Assessing the nature of potential groundwater zones through machine learning (ML) algorithm in tropical plateau region, West Bengal, India. Acta Geophys. (2023). https://doi.org/10.1007/s11600-023-01042-3

Kuo, M. C. T., Wang, W. L., Lin, D. S., Lin, C. C., & Chiang, C. J. (1994). An image-well method for predicting drawdown distribution in aquifers with irregularly shaped boundaries. Groundwater, 32(5), 794-804.

Kwon, E., Park, J., Park, W.B., Kang, B.R., Hyeon, B.S., Woo., N.C., (2022). Nitrate Vulnerability of Groundwater in Jeju Volcanic Island, Korea Sci. Total Environ., 807, p. 151399

Lachassagne, P., Dewandel, B., & Wyns, R. (2021). Hydrogeology of weathered crystalline/hard-rock aquifers—guidelines for the operational survey and management of their groundwater resources. Hydrogeology Journal, 29(8), 2561-2594.

Lagergren, S. K. (1898). About the theory of so-called adsorption of soluble substances. Sven. Vetenskapsakad. Handingarl, 24, 1-39.

Lakshminarayanan, B., Ramasamy, S., Anuthaman, S.N. et al., (2022). New DRASTIC framework for groundwater vulnerability assessment: bivariate and multi-criteria decision-making approach coupled with metaheuristic algorithm. Environ Sci Pollut Res 29, 4474–4496. https://doi.org/10.1007/s11356-021-15966-0

Lakshsmi V (2013) Remote Sensing of Soil Moisture", International Scholarly Research Notices, vol. 2013, Article ID 424178, 33 pages, 2013. https://doi.org/10.1155/2013/424178

Langmuir, I. (1916). The constitution and fundamental properties of solids and liquids. Part I. Solids. Journal of the American chemical society, 38(11), 2221-2295.

Larned, S.T., Unwin, M.J., Boustead, N .C. (2015). Ecological dynamics in the riverine aquifers of a gaining and 1089 losing river, Freshwater Science, 34, 245-262, 10.1086/678350, 2015.

Latifi, N., Marto, A., & Eisazadeh, A. (2016). Physicochemical behavior of tropical laterite soil stabilized with non-traditional additive. Acta Geotechnica, 11, 433-443.

Le TTH, Zeunert S, Lorenz M et al (2017) Multivariate statistical assessment of a polluted river under nitrification inhibition in the tropics. Environ Sci Pollut Res 24:13845–13862 (2017). https://doi.org/10.1007/s11356-017-8989-2

Lee, J. I., Hong, S. H., Lee, C. G., & Park, S. J. (2021). Fluoride removal by thermally treated egg shells with high adsorption capacity, low cost, and easy acquisition. Environmental Science and Pollution Research, 28, 35887-35901.

Leng, G., Huang, M., Tang, Q., & Leung, L. R. (2015). A modeling study of irrigation effects on global surface water and groundwater resources under a changing climate. Journal of Advances in Modeling Earth Systems, 7(3), 1285-1304.

Lge, O.O., Adunbarin, O.O. & Olaleye, I.M. (2022).Groundwater potential and aquifer characterization within Unilorin campus, Ilorin, Southwestern Nigeria, using integrated electrical parameters. Int J Energ Water Res 6, 353–370 (2022). https://doi.org/10.1007/s42108-021-00160-2

Li RJ (1999) Fuzzy Method in Group Decision Making. Comput. Math. Appl. 1999, 38, 91–101

Li X, Zhang L, Yang G et al. (2015) Impacts of human activities and climate change on the water environment of Lake Poyang Basin, China. Geoenviron Disasters 2, 22. https://doi.org/10.1186/s40677-015-0029-2

Li, A., Xie, H., Qiu, Y., Liu, L., Lu, T., Wang, W., & Qiu, G. (2022b). Resource utilization of rice husk biomass: Preparation of MgO flake-modified biochar for simultaneous removal of heavy metals from aqueous solution and polluted soil. Environmental Pollution, 310, 119869.

Li, H., Cui, S., Tan, Y., Peng, Y., Gao, X., Yang, X., & Chen, Q. (2022a). Synergistic effects of ball-milled biochar-supported exfoliated LDHs on phosphate adsorption: Insights into role of fine biochar support. Environmental Pollution, 294, 118592.

Li, J., An, X., Li, Q., Wang, C., Yu, H., Zhou, X., & Geng, Y. A. (2022). Application of XGBoost algorithm in the optimization of pollutant concentration. Atmospheric Research, 276, 106238.

Li, J., Wang, S., (2022). Seasonal variations and long-term trends of groundwater over the Canadian landmass. Hydrogeol J (2022). https://doi.org/10.1007/s10040-022-02460-1

Li, L., Chen, Q., Zhao, C., Guo, B., Xu, X., Liu, T., & Zhao, L. (2022). A novel chitosan modified magnesium impregnated corn straw biochar for ammonium and phosphate removal from simulated livestock wastewater. Environmental Technology & Innovation, 26, 102519.

Li, Mo, Xiaoxu Cao, Dong Liu, Qiang Fu, Tianxiao Li, and Ruochen Shang. (2022).Sustainable management of agricultural water and land resources under changing climate and socio-economic conditions: A multi-dimensional optimization approach. Agricultural Water Management 259 (2022): 107235.

Li, R., Wang, J. J., Zhou, B., Zhang, Z., Liu, S., Lei, S., & Xiao, R. (2017). Simultaneous capture removal of phosphate, ammonium and organic substances by MgO impregnated biochar and its potential use in swine wastewater treatment. Journal of Cleaner Production, 147, 96-107

Liang, W., Couperthwaite, S. J., Kaur, G., Yan, C., Johnstone, D. W., & Millar, G. J. (2014). Effect of strong acids on red mud structural and fluoride adsorption properties. Journal of colloid and interface science, 423, 158-165.

Lima, M.L., Zelaya, K. & Massone, H., (2011). Groundwater Vulnerability Assessment Combining the Drastic and Dyna-Clue Model in the Argentine Pampas. Environmental Management 47, 828–839. https://doi.org/10.1007/s00267-011-9652-1

Liu, B., He, Z., Liu, R., Montenegro, A. C., Ellis, M., Li, Q., & Baligar, V. C. (2021a). Comparative effectiveness of activated dolomite phosphate rock and biochar for immobilizing cadmium and lead in soils. Chemosphere, 266, 129202.

Liu, G., Wang, J., Xue, W., Zhao, J., Wang, J., & Liu, X. (2017). Effect of the size of variable charge soil particles on cadmium accumulation and adsorption. Journal of Soils and Sediments, 17, 2810-2821.

Liu, H., Colombi, T., Jäck, O., Keller, T., & Weih, M. (2022). Effects of soil compaction on grain yield of wheat depend on weather conditions. Science of the Total Environment, 807, 150763.

Liu, S., Huang, Q., Zhang, W., Ren, D., Xu, X., Xiong, Y., & Huang, G. (2023). An improved estimation of soil water and salt dynamics by considering soil bulk density changes under freeze/thaw conditions in arid areas with shallow groundwater tables. Science of the Total Environment, 859, 160342.

Liu, X., Wang, Y., Smith, R. L., Fu, J., & Qi, X. (2021b). High-capacity structured MgO-Co adsorbent for removal of phosphorus from aqueous solutions. Chemical Engineering Journal, 426, 131381.

Liu, Y. Q., & Cinquepalmi, S. (2021c). Exploration of mechanisms for calcium phosphate precipitation and accumulation in nitrifying granules by investigating the size effects of granules. Water Research, 206, 117753

Lohani, T. K., Ayana, M. T., Mohammed, A. K., Shabaz, M., Dhiman, G., & Jagota, V. (2023). A comprehensive approach of hydrological issues related to ground water using GIS in the Hindu holy city of Gaya, India. World Journal of Engineering, 20(2), 283-288.

Lu, H., Zhang, W., Yang, Y., Huang, X., Wang, S., & Qiu, R. (2012). Relative distribution of Pb2+ sorption mechanisms by sludge-derived biochar. Water research, 46(3), 854-862.

Luo, Y., Chen, J., Wu, C., Zhang, J., Tang, J., Shang, J., & Liao, Q. (2019). Effect of particle size on adsorption of norfloxacin and tetracycline onto suspended particulate matter in lake. Environmental Pollution, 244, 549-559.

Ma, J., Wu, S., Shekhar, N.V.R., Biswas, S., Sahu, A.K., (2020). Determination of Physicochemical Parameters and Levels of Heavy Metals in Food Waste Water with Environmental Effects. Bioinorg Chem Appl. 2020 Aug 20;2020:8886093. doi: 10.1155/2020/8886093. PMID: 32884567; PMCID: PMC7455830.

Ma, Q., & Wang, L. (2015). Adsorption of Reactive blue 21 onto functionalized cellulose under ultrasonic pretreatment: Kinetic and equilibrium study. Journal of the Taiwan Institute of Chemical Engineers, 50, 229-235.

Ma, Y., Dai, W., Zheng, P., Zheng, X., He, S., & Zhao, M. (2020). Iron scraps enhance simultaneous nitrogen and phosphorus removal in subsurface flow constructed wetlands. Journal of hazardous materials, 395, 122612.

Maasri, A., Jähnig, S. C., Adamescu, M. C., Adrian, R., Baigun, C., Baird, D. J., & Worischka, S. (2022). A global agenda for advancing freshwater biodiversity research. Ecology Letters, 25(2), 255-263.

Machiwal D, Jha M K, Mal B C (2010) Assessment of Groundwater Potential in a Semi-Arid Region of India Using Remote Sensing, GIS and MCDM Techniques. Water Resources Management, 25: 1359–1386. doi:10.1007/s11269-010-9749-y

Magesh N S, Chandrasekar N, Soundranayagam JP (2012) Delineation of groundwater potential zones in Theni district, Tamil Nadu, using remote sensing, GIS and MIF techniques. Geoscience Frontiers.3, 189-196. https://doi.org/10.1016/j.gsf.2011.10.007

Maghsoodi I A, Abouhamzeh G, Khalilzadeh M, Zavadskas E K (2018) Ranking and selecting the best performance appraisal method using the MULTIMOORA approach integrated Shannon's entropy. Frontiers of Business Research in China, 12(1). doi:10.1186/s11782-017-0022-6

Mahala A (2020) Land Degradation Processes of Silabati River Basin, West Bengal, India: A Physical Perspective. In: Shit P., Pourghasemi H., Bhunia G. (eds) Gully Erosion Studies from India and Surrounding Regions. Advances in Science, Technology & Innovation (IEREK Interdisciplinary Series for Sustainable Development). Springer, Cham. https://doi.org/10.1007/978-3-030-23243-6_16

Mahala, A. (2021). Delineating the status of groundwater in a plateau fringe region using multi-influencing factor (MIF) and GIS: a study of Bankura District, West Bengal, India. Geostatistics and geospatial technologies for groundwater resources in India, 215-237.

Mahapatra SS, Nanda SK, Panigrahy BK (2011) A Cascaded Fuzzy Inference System for Indian river water quality prediction. Adv Eng Softw 2011,42(10):787–796. 10.1016/j.advengsoft.2011.05.018

Mahato, M. K., & Jana, N. C. (2022). Mapping and Reclamation of Wastelands in Drought-Prone Purulia District of West Bengal, India Using Remote Sensing and GIS. In Climate, Environment and Disaster in Developing Countries (pp. 189-216). Singapore: Springer Nature Singapore.

Maheshwari, B., Varua, M., Ward, J., Packham, R., Chinnasamy, P., Dashora, Y., ... & Rao, P. (2014). The role of transdisciplinary approach and community participation in village scale groundwater management: insights from Gujarat and Rajasthan, India. Water, 6(11), 3386-3408.

Mahmood, T., Saddique, M. T., Naeem, A., Westerhoff, P., Mustafa, S., & Alum, A. (2011). Comparison of different methods for the point of zero charge determination of NiO. Industrial & Engineering Chemistry Research, 50(17), 10017-10023.

Mahmoudi P, Ghaemi A, Rigi A et al.(2021) Recommendations for modifying the Standardized Precipitation Index (SPI) for Drought Monitoring in Arid and Semi-arid Regions. Water Resour Manage 35, 3253–3275 (2021). https://doi.org/10.1007/s11269-021-02891-7

Mahmud, S., Hamza, S., Irfan, M., Huda, S. N. U., Burke, F., & Qadir, A. (2022). Investigation of groundwater resources using electrical resistivity sounding and Dar Zarrouk parameters for Uthal Balochistan, Pakistan. Groundwater for sustainable development, 17, 100738.

Maiti, A., Basu, J. K., & De, S. (2011). Chemical treated laterite as promising fluoride adsorbent for aqueous system and kinetic modeling. Desalination, 265(1-3), 28-36.

Maiti, D. K., Roy, S., A. Datta, A., Banerjee, A., (2013). Aqueous fluoride ion sensing by a new perylenediimide derivative: Interaction between the hydrated fluoride and the aromatic molecule. Chemical Physics Letters, 588, 76–81. (2013) doi:10.1016/j.cplett.2013.09.056

Maity, S. K., & Maiti, R. (2013). Hydrodynamics at the Junction of Silabati, Dwarakeswar and Rupnarayan Rivers at Bandar, Paschim Medinipur, West Bengal, India. Earth Science India, 6.

Majewska-Nowak, K., Grzegorzek, M., & Kabsch-Korbutowicz, M. A. Ł. G. O. R. Z. A. T. A. (2015). Removal of fluoride ions by batch electrodialysis. Environment Protection Engineering, 41(1).

Majumdar S, Singh S, Sahoo PR (2020) Characterization of organic matter and its implications for pyrite hosted refractory gold mineralization along the South Purulia Shear Zone, eastern India, Ore Geology Reviews, Volume 124,2020,103584, ISSN 0169-1368, https://doi.org/10.1016/j.oregeorev.2020.103584

Makhdumi W, Dwarakish G (2019) Prioritisation of watersheds using TOPSIS and VIKOR method. 6. 10.1117/12.2532024

Malakar, Pragnaditya, Abhijit Mukherjee, Soumendra N. Bhanja, Sudeshna Sarkar, Dipankar Saha, and Ranjan Kumar Ray. (2021).Deep learning-based forecasting of groundwater level trends in India: Implications for crop production and drinking water supply." ACS ES&T Engineering 1, no. 6 (2021): 965-977.

Malakiya AD, Suryanarayana TMV (2016) Assessment of Drought Using Standardized Precipitation Index (SPI) and Reconnaissance Drought Index (RDI): A Case Study of Amreli District." (2016).

Malczewski, J., & Rinner, C. (2015). Multicriteria decision analysis in geographic information science (Vol. 1, pp. 55-77). New York: Springer.

Malekian, A., & Pour Reza, M. (2018). Identifying and prioritizing of appropriate sites for artificial recharge using Hierarchical Fuzzy TOPSIS (Case study: Fatoieh Plain). Iranian journal of Ecohydrology, 5(1), 1-10.

Mallick, J., Khan, R. A., Ahmed, M., Alqadhi, S. D., Alsubih, M., Falqi, I., & Hasan, M. A. (2019). Modeling groundwater potential zone in a semi-arid region of Aseer using fuzzy-AHP and geoinformation techniques. Water, 11(12), 2656.

Mallick, J., Talukdar, S., Alsubih, M., Almesfer, M. K., Shahfahad, Hang, H. T., & Rahman, A. (2022). Integration of statistical models and ensemble machine learning algorithms (MLAs) for developing the novel hybrid groundwater potentiality models: a case study of semi-arid watershed in Saudi Arabia. Geocarto International, 37(22), 6442-6473.

Mamadou, F., Mbacké, S. F., Moussa, D. E. H., Aminata, M. F., & Guèye, D. M. C. (2021). Iron in Water: Study of Iron Removal Kinetics in Chemically Reconstituted Waters: Application to Groundwater of South Pout (PS2 Site). Open Journal of Metal, 11(1), 1-10.

Mandal, R., & Chakrabarty, P. (2021). Badlands of gangani in West Bengal, India: An assessment on account of geotourism development. International Journal of Geoheritage and Parks, 9(2), 147-156.

Maneechakr, P.; Mongkollertlop, S. Investigation on adsorption behaviors of heavy metal ions (Cd2+, Cr3+, Hg2+ andPb2+) through low-cost/active manganese dioxide-modified magnetic biochar derived from palm kernel cake residue. J. Environ. Chem. Eng.2020, 8 (6), 104467

Mann H B (1945) Non-parametric Tests against Trend, Econometrica 13:163-171

Manna M, Mondal B (2019) The Emerging issue of forestdegradation in Purulia district. in West Bengal : Geoinformatics for Sustainable Environment Management (pp.137–156). NSOU, Kolkata

Maqsoom, A., Aslam, B., Khalid, N., Ullah, F., Anysz, H., Almaliki, A. H., & Hussein, E. E. (2022). Delineating groundwater recharge potential through remote sensing and geographical information systems. Water, 14(11), 1824.

Marazuela, M. Á., García-Gil, A., Santamarta, J. C., Gasco-Cavero, S., Cruz-Pérez, N., & Hofmann, T. (2022). Stormwater management in urban areas using dry gallery infiltration systems. Science of the Total Environment, 823, 153705.

Martinez, C. J. (2010). Mini-piezometers for Measuring Groundwater to Surface Water Exchange: AE454/AE454, 12/2009. EDIS, 2010(2).

Mas, J., (2018). Receiver Operating Characteristic (ROC) Analysis. In: Camacho Olmedo, M., Paegelow, M., Mas, JF., Escobar, F. (eds) Geomatic Approaches for Modeling Land Change Scenarios. Lecture Notes in Geoinformation and Cartography. Springer, Cham. https://doi.org/10.1007/978-3-319-60801-3_30

Masdari, M., & Khezri, H. (2021). Service selection using fuzzy multi-criteria decision making: a comprehensive review. Journal of Ambient Intelligence and Humanized Computing, 12(2), 2803-2834.

Masitoh F, Rusydi A N (2019) Vegetation Health Index (VHI) analysis during drought season in Brantas Watershed. IOP Conference Series: Earth and Environmental Science, 389, 012033–. doi:10.1088/1755-1315/389/1/012033

Masood M, Yeh P J F, Hanasaki N, Takeuchi K (2015) Model study of the impacts of future climate change on the hydrology of Ganges–Brahmaputra–Meghna basin. Hydrology and Earth System Sciences, 19: 747–770. doi:10.5194/hess-19-747-2015

Masroor, M., Sajjad, H., Kumar, P., Saha, T. K., Rahaman, M. H., Choudhari, P., & Saito, O. (2023). Novel Ensemble Machine Learning Modeling Approach for Groundwater Potential Mapping in Parbhani District of Maharashtra, India. Water, 15(3), 419.

Mathias, S. A., Sorensen, J. P., & Butler, A. P. (2017). Soil moisture data as a constraint for groundwater recharge estimation. Journal of Hydrology, 552, 258-266.

Mavromatis T (2010). Use of drought indices in climate change impact assessment studies: an application to Greece. International Journal of Climatology 30(9), doi:10.1002/joc.1976

McFEETERS S K (1996). The use of the Normalized Difference Water Index (NDWI) in the delineation of open water features. International Journal of Remote Sensing, 17(7), 1425–1432. doi:10.1080/01431169608948714

Meerkhan, H., Freitas, L., Pereira, A.J.S.C. et al., (2022). Delineating springs safeguard zones with DISCO-URBAN index: a valuable tool for groundwater vulnerability mapping in local-scale urban areas. Discov Water 2, 2 (2022). https://doi.org/10.1007/s43832-022-00011-z

Meftaha, N., Mejdib, A., Ezzeddinea, A., Bedouib, A., & Hannachia, A. (2020). Nanofiltration polishing membrane process for fluoride removal. In practice, 2, 2.

Megahed, H.A. (2020) GIS-based assessment of groundwater quality and suitability for drinking and irrigation purposes in the outlet and central parts of Wadi El-Assiuti, Assiut Governorate, Egypt. Bull Natl Res Cent 44, 187 (2020). https://doi.org/10.1186/s42269-020-00428-3

Meng, C., Yang, W., Wang, D., Hao, Z., & Li, M. (2023). Development and testing of vehicle-mounted soil bulk density detection system. Measurement, 211, 112604.

Mengistu, T. D., Chang, S. W., Kim, I. H., Kim, M. G., & Chung, I. M. (2022). Determination of potential aquifer recharge zones using geospatial techniques for proxy data of Gilgel Gibe Catchment, Ethiopia. Water, 14(9), 1362.

Mengistu, T. D., Chang, S. W., Kim, I. H., Kim, M. G., & Chung, I. M. (2022). Determination of potential aquifer recharge zones using geospatial techniques for proxy data of Gilgel Gibe Catchment, Ethiopia. Water, 14(9), 1362.

Merouche A, Selvam S, Imessaoudene Y. et al. (2020) Assessment of dam water quality for irrigation in the northeast of catchment Cheliff-Zahrez, Central Algeria. Environ Dev Sustain 22, 5709–5730 (2020). https://doi.org/10.1007/s10668-019-00447-9

Mesa, L. M. (2006) Morphometric analysis of a subtropical Andean basin (Tucumán, Argentina). Environmental Geology, 50: 1235–1242. doi:10.1007/s00254-006-0297-y

Mesdaghinia, A., Vaghefi, K. A., Montazeri, A., Mohebbi, M. R., & Saeedi, R. (2010). Monitoring of fluoride in groundwater resources of Iran. Bulletin of environmental contamination and toxicology, 84, 432-437.

Meshram SG, Sharma SK (2017) Prioritization of watershed through morphometric parameters: a PCA-based approach. Appl Water Sci. 7:1505–1519.

Meshram, SG, Alvandi E, Meshram C et al. (2020) Application of SAW and TOPSIS in Prioritizing Watersheds. Water Resour Manage 34, 715–732 (2020). https://doi.org/10.1007/s11269-019-02470-x

Metwaly, M. M., AbdelRahman, M. A., & Abdellatif, B. (2022). Heavy metals and micronutrients assessment in soil and groundwater using geospatial analyses under agricultural exploitation in dry areas. Acta Geophysica, 1-29.

Mezni, I., Chihi, H., Hammami, M. A., Gabtni, H., & Baba Sy, M. (2022). Regionalization of natural recharge zones using analytical hierarchy process in an arid hydrologic basin: A contribution for managed aquifer recharge. Natural Resources Research, 31(2), 867-895.

Milan, V., & Andjelko, S. (1992). Determination of hydraulic conductivity of porous media from grain-size composition (No. 551.49 V 986).

Milledge, D.G., Gurjar, S.K., Bunce, J.T.,Tare, V., Sinha,R., Carbonneau, P.E., (2018). Population density controls on microbial pollution across the Ganga catchment, Water Research, 128, 82-91,ISSN 0043-1354,https://doi.org/10.1016/j.watres.2017.10.033

Miller V (1953) A quantitative geomorphic study of drainage basin characteristics in the clinch mountain area, Virginia and Tennessee. Project NR 389–402. Technical Report 3. Columbia University. Department of Geology ONR: New York.

Miraki, S., Zanganeh, S. H., Chapi, K., Singh, V. P., Shirzadi, A., Shahabi, H., & Pham, B. T. (2019). Mapping groundwater potential using a novel hybrid intelligence approach. Water resources management, 33, 281-302.

Mishra A K, Singh V P (2009) Analysis of drought severity-area-frequency curves using a general circulation model and scenario uncertainty. Journal of Geophysical Research, 114(D6), D06120–. doi:10.1029/2008jd010986

Mitra, S., Thakur, L. S., Rathore, V. K., & Mondal, P. (2016). Removal of Pb (II) and Cr (VI) by laterite soil from synthetic waste water: single and bi-component adsorption approach. Desalination and Water Treatment, 57(39), 18406-18416.

Moghbeli A, Delbari M, Amiri M (2020) Application of a standardized precipitation index for mapping drought severity in an arid climate region, southeastern Iran. Arab J Geosci 13, 221 (2020). https://doi.org/10.1007/s12517-020-5201-7

Mohamed N H, Lamsali H, Sathyamoorthy D (2015). Multi-Criteria Decision Making (MCDM) For Technical Evaluation of Tenderers: A Review of Methods Employed. Defence S T Tech Bull 8(1), 90–102

Mohamed, A.K., Liu, D., Mohamed, M.A.A. et al. (2018). Groundwater quality assessment of the quaternary unconsolidated sedimentary basin near the Pi river using fuzzy evaluation technique. Appl Water Sci 8, 65 (2018). https://doi.org/10.1007/s13201-018-0711-0

Mohammad S M, Shukla JP, Mishra SN (2019). Relationship of LST, NDBI and NDVI using landsat-8 data in Kandaihimmat watershed, Hoshangabad, India, Indian Journal of Geo Marine Sciences, Vol. 48 (01), January, 25-31

Mohapatra, M., Anand, S., Mishra, B. K., Giles, D. E., & Singh, P. (2009). Review of fluoride removal from drinking water. Journal of environmental management, 91(1), 67-77.

Momin, B. G., Ray, R., & Patra, S. K. (2018). Determining saturated hydraulic conductivity of medium land soils under different cropping systems in semi-arid red and lateritic region.

Mondal G C, Singh A K, Singh TB (2016) Major Ion Chemistry and Groundwater Quality Assessment in Purulia District. Indian Journal of Environmental Protection, 36 (1). pp. 1-16. ISSN 0253-7141

Mondal, S., & Kumar, S. (2017). Investigation of fluoride contamination and its mobility in groundwater of Simlapal block of Bankura district, West Bengal, India. Environmental Earth Sciences, 76, 1-9.

Moratiel, R., Snyder, R. L., Durán, J. M., & Tarquis, A. M. (2011). Trends in climatic variables and future reference evapotranspiration in Duero Valley (Spain). Natural Hazards and Earth System Sciences, 11(6), 1795-1805.

Mosavi A, Golshan M, Choubin B. et al. (2021). Fuzzy clustering and distributed model for streamflow estimation in ungauged watersheds. Sci Rep 11, 8243 (2021). https://doi.org/10.1038/s41598-021-87691-0.

Mosavi, A., Sajedi Hosseini, F., Choubin, B. et al. (2021). Ensemble Boosting and Bagging Based Machine Learning Models for Groundwater Potential Prediction. Water Resour Manage 35, 23–37 (2021). https://doi.org/10.1007/s11269-020-02704-3

Moussout, H., Ahlafi, H., Aazza, M., & Maghat, H. (2018). Critical of linear and nonlinear equations of pseudo-first order and pseudo-second order kinetic models. Karbala International Journal of Modern Science, 4(2), 244-254.

Muhammad MN, Cavus N (2017) Fuzzy DEMATEL method for identifying LMS evaluation criteria. Procedia Computer Science, 120(), 742–749. doi:10.1016/j.procs.2017.11.304

Muhammad, A.M., Zhonghua, T., Dawood, A.S., Earl, B., (2015). Evaluation of local groundwater vulnerability based on DRASTIC index method in Lahore, Pakistan. Geofísica Internacional, 54(1), 67–81. doi:10.1016/j.gi.2015.04.003

Mukherjee I, Singh UK, Patra PK (2019). Exploring a multi-exposure-pathway approach to assess human health risk associated with groundwater fluoride exposure in the semi-arid region of east India. Chemosphere 233, 164–173. https://doi.org/ 10.1016/j.chemosphere.2019.05.278.

Mukherjee I, Singh UK, Singh RP (2021). An overview on heavy metal contamination of water system and sustainable approach for remediation. In: Singh, A., Agrawal, M., Agrawal, S.B. (Eds.), Water Pollution and Management Practices. Springer Singapore, Singapore, pp. 255–277. https://doi.org/10.1007/978-981-15- 8358-2_11.

Mukherjee, A., Bhanja, S. N., & Wada, Y. (2018). Groundwater depletion causing reduction of baseflow triggering Ganges river summer drying. Scientific reports, 8(1), 12049.

Mukherjee, D. M. (2016). A study on groundwater in West Bengal with reference to other states in India. Int J Sci Eng Res, 7(1), 646.

Mukherji, A. (2022). Sustainable groundwater management in India needs a water-energy-food nexus approach. Applied Economic Perspectives and Policy, 44(1), 394-410.

Mulubrhan, F., Mokhtar, A. A., & Muhammad, M. (2014). Comparative analysis between fuzzy and traditional analytical hierarchy process. In MATEC web of conferences (Vol. 13, p. 01006). EDP Sciences.

Murad H, Islam S AKM (2011). Drought Assessment Using Remote Sensing And Gis In North-West Region Of Bangladesh. International Conference On Water & Flood Management (ICWFM-2011)

Murthy CS, Laxman B, Sesha Sai MV R (2015). Geospatial analysis of agricultural drought vulnerability using a composite index based on exposure, sensitivity and adaptive capacity. Int J Disaster Risk Reduction, 12: 163–171

NABARD District Profile: North 24 Parganas (2016), https://www.nabard.org/demo/auth/writereaddata/tender/2510160002WB_NORTHPARGANAS.pdf

Nabbou, N., Belhachemi, M., Boumelik, M., Merzougui, T., Lahcene, D., Harek, Y., ... & Jeguirim, M. (2019). Removal of fluoride from groundwater using natural clay (kaolinite): Optimization of adsorption conditions. Comptes Rendus Chimie, 22(2-3), 105-112.

Nadiri, A.A., Gharekhani, M., Khatibi, R., Moghaddam, A.A., (2017). Assessment of groundwater vulnerability using supervised committee to combine fuzzy logic models. Environ.Sci. Pollut. Res. 24, 8562–8577.

Nadiri, A.A., Moazamnia, M., Sadeghfam, S., Gnanachandrasamy, G., Venkatramanan, S., 2022. Formulating Convolutional Neural Network for mapping total aquifer vulnerability to pollution, Environmental Pollution, 304,2022,119208,ISSN 0269-7491,https://doi.org/10.1016/j.envpol.2022.119208.

Nadiri, A.A., Sedghi, Z., Khatibi,R., Sadeghfam, S., (2018). Mapping specific vulnerability of multiple confined and unconfined aquifers by using artificial intelligence to learn from multiple DRASTIC frameworks, Journal of Environmental Management, 227, 415-428, ISSN 0301-4797,https://doi.org/10.1016/j.jenvman.2018.08.019.

Nag SK (2014) Evaluation of hydrochemical parameters and quality assessment of the groundwater in Gangajalghati Block, Bankura District, West Bengal, India. Arab J Sci Eng 39:5715–5727

Nag SK, Das S (2017) Assessment of groundwater quality from Bankura I and II Blocks, Bankura District, West Bengal, India. Appl Water Sci 7, 2787–2802 (2017). https://doi.org/10.1007/s13201-017-0530-8

Nag SK, Ghosh P (2013) Variation in groundwater levels and water quality in Chhatna Block, Bankura District, West Bengal, A GIS approach. J Geol Soc India 81(2):261–280

Nag SK, Suchetana B (2016) Groundwater quality and its suitability for irrigation and domestic purposes: a study in rajnagar block, Birbhum district, West Bengal India. J Earth Sci Clim Change 7:337. https://doi.org/10.4172/2157-7617.1000337

Nag, S.K., Chowdhury, P., Das, S. et al., (2021). Deciphering prospective groundwater zones in Bankura district, West Bengal: a study using GIS platform and MIF techniques. Int J Energ Water Res 5, 323–341 (2021). https://doi-org.manchester.idm.oclc.org/10.1007/s42108-020-00110-4

Nag, S.K., Das, S., (2017). Assessment of groundwater quality from Bankura I and II Blocks, Bankura District, West Bengal, India. Appl Water Sci 7, 2787–2802. https://doi.org/10.1007/s13201-017-0530-8

Naidu, S., Gupta, G., Shailaja, G. et al. (2021). Spatial behavior of the Dar-Zarrouk parameters for exploration and differentiation of water bodies aquifers in parts of Konkan coast of Maharashtra, India. J Coast Conserv 25, 11 (2021). https://doi.org/10.1007/s11852-021-00807-6

Nair, A. M., Prasad, K. R., & Srinivas, R. (2022). Groundwater vulnerability assessment of an urban coastal phreatic aquifer in India using GIS-based DRASTIC model. Groundwater for Sustainable Development, 19, 100810.

Naje, A. S., Chelliapan, S., Zakaria, Z., Ajeel, M. A., & Alaba, P. A. (2017). A review of electrocoagulation technology for the treatment of textile wastewater. Reviews in Chemical Engineering, 33(3), 263-292.

Namous M, Hssaisoune M, Pradhan B, Lee C-W, Alamri A, Elaloui A, Edahbi M, Krimissa S, Eloudi H, Ouayah M, Elhimer H, Tagma T (2021) Spatial Prediction of Groundwater Potentiality in Large Semi-Arid and Karstic Mountainous Region Using Machine Learning Models. Water. 2021; 13(16):2273. https://doi.org/10.3390/w13162273

Narsimha A, Sudarshan V (2016) Assessment of fluoride contamination in groundwater from basara, adilabad district, telangana state, India, Applied Water Science, 7 (2016), pp. 2717-2725,

Naseef, A.U.T., Reeba, T., 2016. Identification of Suitable Sites for Water Harvesting Structures in Kecheri River Basin. Procedia Technology, 24(), 7–14. doi:10.1016/j.protcy.2016.05.003

Nauck DD, Nürnberger A (2013) Neuro-fuzzy Systems: a short historical review. In: Moewes C, Nürnberger A (eds) Computational intelligence in intelligent data analysis. Studies in computational intelligence, vol 445. Springer, Berlin

Neuman, S. P. (1972). Theory of flow in unconfined aquifers considering delayed response of the water table. Water Resources Research, 8(4), 1031-1045.

NGWA (2016) Consensus Definitions of Groundwater Sustainability and Resilience National Groundwater Association (2016)

Nikam SP, Purohit RC, Shinde MG, Singh PK, Jain HK, Dahiphle P (2014) Principal component analysis for morphometric modelling for small watersheds of Tapi basin in India. International Journal of agricultural Engineering 7: 186-189

NOAA (2023) Extremes. https://www.ncdc.noaa.gov/extremes/. Accessed 21 Jan 2023

Noaa, N. (2019). State of the climate: Global climate report for annual 2018. URL www. ncdc. noaa. gov/sotc/global/201813.

Noiva K, Fernández J E, Wescoat J L (2016) Cluster analysis of urban water supply and demand: Toward large-scale comparative sustainability planning. Sustainable Cities and Society, 27: 484–496. doi:10.1016/j.scs.2016.06.003

Novinpour, E.A., Moghimi, H,., & Kaki, M., (2022). Aquifer vulnerability based on classical methods and GIS-based fuzzy optimization method (case study: Chahardoli plain in Kurdistan province, Iran). Arab J Geosci 15, 360 (2022). https://doi.org/10.1007/s12517-022-09549-7

NRSA (National Remote Sensing Agency) (2008) Groundwater Prospects Mapping Using Remote Sensing and Geographic Information System. Rajiv Gandhi National Drinking Water Mission Project, Manual, 256

Nugraha, G.U., Nur, A.A., Pranantya, P.A. et al. (2023). Analysis of groundwater potential zones using Dar-Zarrouk parameters in Pangkalpinang city, Indonesia. Environ Dev Sustain 25, 1876–1898 (2023). https://doi.org/10.1007/s10668-021-02103-7

Nugraha, G.U., Ridwansyah, I., Marganingrum, D., Hartanto, P.R.F., Lubis, R. F., Bakti, H., (2021). Transport Modelling In Jakarta Groundwater Basin using QSWATMOD . IOP Conference Series: Earth and Environmental Science, . doi:10.1088/1755-1315/789/1/012045

Nur, T., Loganathan, P., Kandasamy, J., & Vigneswaran, S. (2017). Removal of strontium from aqueous solutions and synthetic seawater using resorcinol formaldehyde polycondensate resin. Desalination, 420, 283-291.

Nwachukwu, S., Bello, R. & Balogun, A.O. (2019). Evaluation of groundwater potentials of Orogun, South–South part of Nigeria using electrical resistivity method. Appl Water Sci 9, 184 (2019). https://doi.org/10.1007/s13201-019-1072-z

Oginni, O., Yakaboylu, G. A., Singh, K., Sabolsky, E. M., Unal-Tosun, G., Jaisi, D., & Shah, A. (2020). Phosphorus adsorption behaviors of MgO modified biochars derived from waste woody biomass resources. Journal of Environmental Chemical Engineering, 8(2), 103723.

Oke, S.A., Fourie, F., (2017). Guidelines to groundwater vulnerability mapping for Sub-Saharan Africa. Groundwater for Sustainable Development, 5, 168–177. doi:10.1016/j.gsd.2017.06.007

Oladipo J O, Aboyeji OS, Akinwumiju AS, Adelodun AA (2020) Fuzzy logic Interference for characterization of surface water potability in ikare rural community, Nigeria Journal of Geovisualization and Spatial Analysis, 4 (2020), 10.1007/s41651-019-0044-z

Oli, I. C., Opara, A. I., Okeke, O. C., Akaolisa, C. Z., Akakuru, O. C., Osi-Okeke, I., & Udeh, H. M. (2022). Evaluation of aquifer hydraulic conductivity and transmissivity of Ezza/Ikwo area, Southeastern Nigeria, using pumping test and surficial resistivity techniques. Environmental Monitoring and Assessment, 194(10), 719.

Olsen J, Anderson N, Knudsen Mads (2012).Variability of the North Atlantic Oscillation over the past 5,200 years. Nature Geoscience. 5. 808-812. 10.1038/ngeo1589.

Omeje, E.T., Obiora, D.N., Okeke, F.N. et al., (2023). Investigation of aquifer vulnerability and sensitivity analysis of modified drastic and sintacs models: a case study of Ovogovo Area, Eastern Nigeria. Acta Geophys. https://doi.org/10.1007/s11600-022-00992-4

Onu, U P, Xi Q, Xu L (2017). A Fuzzy TOPSIS model Framework for Ranking Sustainable Water Supply Alternatives. Water Resources Management, 31:2579–2593. doi:10.1007/s11269-017-1636-3

Opricovic S, Tzeng GH (2003) Defuzzification within a multicriteria decision model, International Journal of Uncertainty, Fuzziness and Knowlege-Based Systems, vol. 11, no. 5, pp. 635–652, 2003.

Ortiz-López, C.S., Veses, V., Garcia-Bautista, J.A. et al., 2018. Risk factors for the presence of dental black plaque. Sci Rep 8, 16752 (2018). https://doi.org/10.1038/s41598-018-35240-7

Osinubi, K. J., & Amadi, A. A. (2009). Hydraulic performance of compacted lateritic soil-bentonite mixtures permeated with municipal solid waste landfill leachate (No. 09-0620).

Osman, A. I. A., Ahmed, A. N., Chow, M. F., Huang, Y. F., & El-Shafie, A. (2021). Extreme gradient boosting (Xgboost) model to predict the groundwater levels in Selangor Malaysia. Ain Shams Engineering Journal, 12(2), 1545-1556.

Ou, W., Lan, X., Guo, J., Cai, A., Liu, P., Liu, N., & Lei, Y. (2023). Preparation of iron/calcium-modified biochar for phosphate removal from industrial wastewater. Journal of Cleaner Production, 383, 135468.

Ouatiki, H., Boudhar, A., Leblanc, M., Fakir, Y., & Chehbouni, A. (2022). When climate variability partly compensates for groundwater depletion: An analysis of the GRACE signal in Morocco. Journal of Hydrology: Regional Studies, 42, 101177.

Ouedraogo, M., Pessel, M., Durand, V., Saintenoy, A., Kamagate, B., & Savane, I. (2022). Multifrequency electromagnetic method for the hydrogeophysical characterization of hard-rock aquifers: the case of the upstream watershed of White Bandama (northern Ivory Coast). BSGF-Earth Sciences Bulletin, 193(1), 11.

Ouhamdouch, S., Bahir, M., Ouazar, D., & Zouari, K. (2022). Isotopic signature of groundwater and climate change within a semi-arid environment. Groundwater for Sustainable Development, 17, 100729.

Ourradi, Y. (2021). In-situ removal of iron and manganese from groundwater (Master's thesis).

Padhi, S., & Tokunaga, T. (2018). Surface Complexation Modeling of Fluoride Adsorption by Soil and the Role of Dissolved Aluminum on Adsorption. Vadose Zone Journal, 17(1), 1-14.

Pal NR and Bezdek JC (1995) On cluster validity for the fuzzy c-means model," IEEE Transactions on Fuzzy Systems, vol. 3, no. 3, pp. 370–379, 1995

Pal, S. C., Ghosh, C., & Chowdhuri, I. (2020). Assessment of groundwater potentiality using geospatial techniques in Purba Bardhaman district, West Bengal. Applied Water Science, 10, 1-13.

Pal, S.K. (2016). A geomorphological study on regular flood of lower Shilabati river basin and its impact on the arable land. International journal of interdisciplinary and multidisciplinary research (2456–4567), Volume I Number I June 2016

Palchaudhuri, M., & Biswas, S. (2016). Application of AHP with GIS in drought risk assessment for Puruliya district, India. Natural Hazards, 84, 1905-1920.

Palmajumder, M., Chaudhuri, S., Das, V.K. et al., 2021. An appraisal of geohydrological status and assessment of groundwater quality of Indpur Block, Bankura District, West Bengal, India. Appl Water Sci 11, 59 (2021). https://doi.org/10.1007/s13201-021-01389-2

Paltrinieri, L., Wang, M., Sachdeva, S., Besseling, N. A., Sudhölter, E. J., & De Smet, L. C. (2017). Fe 3 O 4 nanoparticles coated with a guanidinium-functionalized polyelectrolyte extend the pH range for phosphate binding. Journal of Materials Chemistry A, 5(35), 18476-18485.

Pan Y, Gong H, Zhou D, Li X, Nakagoshi N (2011) Impact of land use on Groundwater Recharge in Guishui River Baisn, China. Geogr. Sci. (2011) 21: 734. https://doi.org/10.1007/s11769-011-0508-7

Panada A, Sahu N (2019) Trend analysis of seasonal rainfall and temperature pattern in Kalahandi, Bolangir and Koraput districts of Odisha, India. Atmospheric Science Letters. https://doi.org/10.1002/asl.932

Pande, C. B., Moharir, K. N., Singh, S. K., & Varade, A. M. (2020). An integrated approach to delineate the groundwater potential zones in Devdari watershed area of Akola district, Maharashtra, Central India. Environment, Development and Sustainability, 22, 4867-4887.

Pande, C. B., Moharir, K. N., Singh, S. K., Elbeltagi, A., Pham, Q. B., Panneerselvam, B., ... & Kouadri, S. (2022). Groundwater flow modeling in the basaltic hard rock area of Maharashtra, India. Applied Water Science, 12, 1-14.

Pani, S., Chakrabarty, A., & Bhadur, S. (2016). Groundwater potential zone Identification by analytical hierarchy process (AHP) weighted overlay in GIS Environment—a case study of Jhargram Block, Paschim Medinipur. Int J Remote Sens Geosci (IJRSG), 5(3), 1-10.

Panneerselvam, B., Muniraj, K., Pande, C., Ravichandran, N., Thomas, M., & Karuppannan, S. (2022). Geochemical evaluation and human health risk assessment of nitrate-contaminated groundwater in an industrial area of South India. Environmental Science and Pollution Research, 29(57), 86202-86219.

Panthi J, Aryal S, Dahal P, Bhandari P, Krakauer NY, Pandey VP (2016) Livelihood vulnerability approach to assessing climate change impacts on mixed agro-livestock smallholders around the Gandaki River Basin in Nepal. Regional Environmental Change 16(4): 1121–1132.

Papineau, D., Purohit, R., Fogel, M. L., & Shields-Zhou, G. A. (2013). High phosphate availability as a possible cause for massive cyanobacterial production of oxygen in the Paleoproterozoic atmosphere. Earth and Planetary Science Letters, 362, 225-236.

Paradowski, B., & Szyjewski, Z. (2022). Comparative analyses of multi-criteria methods in supplier selection problem. Procedia Computer Science, 207, 4593-4602.

Pareta K, Pareta U (2012) Quantitative geomorphological analysis of a watershed of Ravi River Basin, H.P. India," International Journal of Remote Sensing and GIS 1: 41–56

Parihari, S., Chatterjee, N. D., Das, K., & Bhattacharya, R. K. (2023). Role of groundwater potentiality and soil nutrient status on agricultural productivity: A case study in Paschim Medinipur District, West Bengal. In Case Studies in Geospatial Applications to Groundwater Resources (pp. 39-66). Elsevier.

Parkhurst, D. L., Kipp, K. L., Engesgaard, P., & Charlton, S. R. (2004). PHAST—A program for simulating ground-water flow, solute transport, and multicomponent geochemical reactions. US Geological survey techniques and methods, 6, A8.

Patel, M. P., Gami, B., Patel, A., Patel, P., & Patel, B. (2020). Climatic and anthropogenic impact on groundwater quality of agriculture dominated areas of southern and central Gujarat, India. Groundwater for sustainable development, 10, 100306.

Patel, P., Mehta, D., & Sharma, N. (2022). A review on the application of the DRASTIC method in the assessment of groundwater vulnerability. Water Supply, 22(5), 5190-5205.

Paternoster M, Buccione R, Canora F, Buttitta D, Panebianco S, Rizzo G, Sinisi R, Summa V, Mongelli G (2021) Hydrogeochemistry and Groundwater Quality Assessment in the High Agri Valley (Southern Italy), Geofluids, vol. 2021, Article, ID 6664164, 15 pages, 2021. https://doi.org/10.1155/2021/6664164

Pathak A A, Dodamani B M (2019) Trend Analysis of Groundwater Levels and Assessment of Regional Groundwater Drought: Ghataprabha River Basin, India Natural Resources Research (2019) 28: 631. https://doi.org/10.1007/s11053-018-9417-0

Patra S, Sahoo S, Pulak M, Mahapatra S C (2018) Impacts of Urbanization on Land use /cover Changes and its Probable implications on local climate and groundwater level. Journal of Urban Management Volume 7, Issue 2, September 2018, Pages 70-84

Patra, P. (2020). Comparative analysis of multi-temporal drought indices using monthly precipitation data: a study in the southwestern part of West Bengal, India. Geoecology of landscape dynamics, 149-165.

Paul, A., Mallik, I., Sardar, J., & Bandyopadhyay, J. (2022). Soil loss risk assessment of lateritic badland surface of Garhbeta Block-I, West Bengal, India using an integrated approach of Revised Universal Soil Loss Equation (RUSLE) algorithm and geospatial techniques. Safety in Extreme Environments, 4(2), 149-170.

Paul, S., Guha, T., Dey, S., Paul, S., Kundu, R., 2022. Amelioration of cadmium toxicity by enhancing nitrogen assimilation and photosynthetic activity by two different nitrogen supplements in rice (Oryza sativa L.) cv. Lalat, Plant Stress, 4,100082, ISSN 2667-064X,https://doi.org/10.1016/j.stress.2022.100082.

Pepper, R. A., Couperthwaite, S. J., & Millar, G. J. (2017). Value adding red mud waste: High performance iron oxide adsorbent for removal of fluoride. Journal of environmental chemical engineering, 5(3), 2200-2206.

Pezeshki Z, Mazinani SM (2019) Comparison of artificial neural networks, fuzzy logic and neuro fuzzy for predicting optimization of building thermal consumption: a survey. Artif Intell Rev 52, 495–525 (2019). https://doi.org/10.1007/s10462-018-9630-6

Pham, B. T., Jaafari, A., Van Phong, T., Mafi-Gholami, D., Amiri, M., Van Tao, N., ... & Prakash, I. (2021). Naïve Bayes ensemble models for groundwater potential mapping. Ecological Informatics, 64, 101389.

PHED, Public Health Engineering Department. Government of West Bengal. A Note on Fluoride Contamination of Ground Water in West Bengal, 2008 (http://www.wbphed.gov.in).

PHED, Water quality dashboard. (2022) https://www.wbphed.gov.in/en/home

Piao, S., Friedlingstein, P., Ciais, P., de Noblet-Ducoudré, N., Labat, D., & Zaehle, S. (2007). Changes in climate and land use have a larger direct impact than rising CO2 on global river runoff trends. Proceedings of the National academy of Sciences, 104(39), 15242-15247.

Pike RJ, Wilson SE (1971) Elevation-relief ratio, hypsometric integral, and geomorphic area-altitude analysis. Geol Soc America Bull 82:1079–1084. https://doi.org/10.1130/0016-7606(1971)82[1079:ERHIAG]2.0.CO;2

Piper AM (1944) A graphic procedure in the geochemical interpretation of water analysis. Am Geoph Union Trans 25:914–923

Pliakas, F., & Petalas, C. (2011). Determination of hydraulic conductivity of unconsolidated river alluvium from permeameter tests, empirical formulas and statistical parameters effect analysis. Water Resources Management, 25, 2877-2899.

Podgorski, J., Araya, D., & Berg, M. (2022). Geogenic manganese and iron in groundwater of Southeast Asia and Bangladesh–Machine learning spatial prediction modeling and comparison with arsenic. Science of the Total Environment, 833, 155131.

Poff, N. L., & Olden, J. D. (2017). Can dams be designed for sustainability?. Science, 358(6368), 1252-1253.

Ponnusamy, D., & Elumalai, V. (2022). Determination of potential recharge zones and its validation against groundwater quality parameters through the application of GIS and remote sensing techniques in uMhlathuze catchment, KwaZulu-Natal, South Africa. Chemosphere, 307, 136121.

Portmann F T, Doll P, Eisner S, Florke M (2013) Impact of Climate Change on Renewable Groundwater Resources : Assessing the Benifts of Avoided Greenhouse Gas Emissions using Selected CMIP5 Climate Projections. Environmental Research Letters. 8. 024023. 10.1088/1748-9326/8/2/024023.

Potgieter, J.H., Pardesi, C. & Pearson, S. A kinetic and thermodynamic investigation into the removal of methyl orange from wastewater utilizing fly ash in different process configurations. Environ Geochem Health 43, 2539–2550 (2021). https://doi.org/10.1007/s10653-020-00567-6

Pourkhosravani, M., Jamshidi, F., Sayari, N., 2021. Evaluation of groundwater vulnerability to pollution using DRASTIC, composite DRASTIC, and nitrate vulnerability models. Environ. Health Eng. Manag. 2021; 8 (2) :129-140, URL: http://ehemj.com/article-1-745-en.html

Prabhakaran A, Jawahar Raj N (2018) Drainage morphometric analysis for assessing form and processes of the watersheds of Pachamalai hills and its adjoinings, Central Tamil Nadu, India. Applied Water Science, 8. doi:10.1007/s13201-018-0646-5

Priya, A., Anusha, G., Thanigaivel, S., Karthick, A., Mohanavel, V., Velmurugan, P., ... & Chelliapan, S. (2023). Removing microplastics from wastewater using leading-edge treatment technologies: a solution to microplastic pollution—a review. Bioprocess and Biosystems Engineering, 46(3), 309-321.

Public Health Engineering Department, (PHED) Govt. of West Bengal Report, http://www (2009) wbphed.gov.in/Static_pages/fluoride.html

Qi, X., Yin, H., Zhu, M., Yu, X., Shao, P., & Dang, Z. (2022). MgO-loaded nitrogen and phosphorus self-doped biochar: High-efficient adsorption of aquatic Cu2+, Cd2+, and Pb2+ and its remediation efficiency on heavy metal contaminated soil. Chemosphere, 294, 133733.

Qin, Z., Wang, G., Zhang, Y., Wang, C., Wu, J., Su, K., ... & Hu, X. (2023). A novel evaluation scheme of resistivity anisotropy in near-tight sandstones using conventional geophysical logs: A case study of the Triassic Chang 8 oil layer, Zhenjing area, Ordos Basin. Journal of Applied Geophysics, 213, 105017.

Qiu, B., Tao, X., Wang, H., Li, W., Ding, X., & Chu, H. (2021). Biochar as a low-cost adsorbent for aqueous heavy metal removal: A review. Journal of Analytical and Applied Pyrolysis, 155, 105081.

Qiu, W., Ma, T., Wang, Y., Cheng, J., Su, C., & Li, J. (2022). Review on status of groundwater database and application prospect in deep-time digital earth plan. Geoscience Frontiers, 13(4), 101383.

Raghunath HM (1987) Groundwater. Wiley Eastern Ltd., Delhi, 563.

Raha S, Gayen SK (2020) Simulation of meteorological drought using exponential smoothing models: a study on Bankura District, West Bengal, India. SN Appl. Sci. 2, 909 (2020). https://doi.org/10.1007/s42452-020-2730-3

Raha, S., Gayen, S.K., 2021. Drought-Induced Human Mobility in Purulia District of West Bengal. In: Rukhsana, Haldar, A., Alam, A., Satpati, L. (eds) Habitat, Ecology and Ekistics. Advances in Asian Human-Environmental Research. Springer, Cham. https://doi.org/10.1007/978-3-030-49115-4_15

Rahaman S A, Ajeez S A, Aruchamy S, Jegankumar R (2015) Prioritization of Sub Watershed Based on Morphometric Characteristics Using Fuzzy Analytical Hierarchy Process and Geographical Information System – A Study of Kallar Watershed, Tamil Nadu. Aquatic Procedia, 4:1322–1330.

Rahman, M. M., AlThobiani, F., Shahid, S., Virdis, S. G. P., Kamruzzaman, M., Rahaman, H., ... & Ghandourah, E. I. (2022). GIS and remote sensing-based multi-criteria analysis for delineation of groundwater potential zones: a case study for industrial zones in Bangladesh. Sustainability, 14(11), 6667.

Rahmati, O., Nazari Samani, A., Mahdavi, M., Pourghasemi, H. R., & Zeinivand, H. (2015). Groundwater potential mapping at Kurdistan region of Iran using analytic hierarchy process and GIS. Arabian Journal of Geosciences, 8, 7059-7071.

Raj, S., Rawat, K. S., Singh, S. K., & Mishra, A. K. (2022). Groundwater potential zones identification and validation in Peninsular India. Geology, Ecology, and Landscapes, 1-15.

Rajput, H., Goyal, R. & Brighu, U., 2020. Modification and optimization of DRASTIC model for groundwater vulnerability and contamination risk assessment for Bhiwadi region of Rajasthan, India. Environ Earth Sci 79, 136. https://doi.org/10.1007/s12665-020-8874

Raju S K, Kumar N D (2011) Classification of microwatersheds based on morphological characteristics. Journal of Hydro-Environment Research, 5:101–109. doi:10.1016/j.jher.2010.09.002

Rajwade YA, Swain DK, Tiwari KN. et al. (2015) Evaluation of Field Level Adaptation Measures Under the Climate Change Scenarios in Rice Based Cropping System in India. Environ. Process. 2, 669–687 (2015). https://doi.org/10.1007/s40710-015-0115-1

Ram, A. et al. (2021) Groundwater quality assessment using water quality index (WQI) under GIS framework. Appl. Water Sci. 11(2), 1–20 (2021).

Ramola, S., Belwal, T., Li, C. J., Liu, Y. X., Wang, Y. Y., Yang, S. M., & Zhou, C. H. (2021). Preparation and application of novel rice husk biochar–calcite composites for phosphate removal from aqueous medium. Journal of Cleaner Production, 299, 126802.

Ran, J., Xiang, R., Li, J., Xiao, K., & Zheng, B. (2022). Spatiotemporal Variations in the Water Quality of Qionghai Lake, Yunnan–Guizhou Plateau, China. Water, 14(15), 2451.

Rana R, Ganguly R, Gupta A K (2018) Indexing method for assessment of pollution potential of leachate from non-engineered landfill sites and its effect on ground water quality. Environ Monit Assess 190, 46. https://doi.org/10.1007/s10661-017-6417-1

Ranasinghe, R. A. J. C., Hansima, M. A. C. K., & Nanayakkara, K. G. N. (2022). Adsorptive removal of fluoride from water by chemically modified coal fly ash: Synthesis, characterization, kinetics, and mechanisms. Groundwater for Sustainable Development, 16, 100699.

Rani, P., Mishra, A. R., Mardani, A., Cavallaro, F., Alrasheedi, M., & Alrashidi, A. (2020). A novel approach to extended fuzzy TOPSIS based on new divergence measures for renewable energy sources selection. Journal of Cleaner Production, 257, 120352.

Rao, N. S., Dinakar, A., & Sun, L. (2022). Estimation of groundwater pollution levels and specific ionic sources in the groundwater, using a comprehensive approach of geochemical ratios, pollution index of groundwater, unmix model and land use/land cover–A case study. Journal of Contaminant Hydrology, 248, 103990.

Rashid, U. S., Das, T. K., Sakthivel, T. S., Seal, S., & Bezbaruah, A. N. (2021). GO-CeO_2 nanohybrid for ultra-rapid fluoride removal from drinking water. Science of the Total Environment, 793, 148547.

Rasool, U., Yin, X., Xu, Z., Rasool, M. A., Senapathi, V., Hussain, M., ... & Trabucco, J. C. (2022). Mapping of groundwater productivity potential with machine learning algorithms: A case study in the provincial capital of Baluchistan, Pakistan. Chemosphere, 303, 135265.

Rathore, V. K., Dohare, D. K., & Mondal, P. (2016). Competitive adsorption between arsenic and fluoride from binary mixture on chemically treated laterite. Journal of Environmental Chemical Engineering, 4(2), 2417-2430.

Ravindra, B., Subba Rao, N., & Dhanamjaya Rao, E. N. (2022). Groundwater quality monitoring for assessment of pollution levels and potability using WPI and WQI methods from a part of Guntur district, Andhra Pradesh, India. Environment, Development and Sustainability, 1-31.

Rawashdeh M, Ralescu AL (2012) Fuzzy Cluster Validity with Generalized Silhouettes. MAICS.

Reddy, D. H. K., & Lee, S. M. (2014). Magnetic biochar composite: facile synthesis, characterization, and application for heavy metal removal. Colloids and Surfaces A: Physicochemical and Engineering Aspects, 454, 96-103.

Rezania, S., Kamyab, H., Rupani, P. F., Park, J., Nawrot, N., Wojciechowska, E., ... & Cabral-Pinto, M. M. (2021). Recent advances on the removal of phosphorus in aquatic plant-based systems. Environmental Technology & Innovation, 24, 101933.

Richard-Ferroudji, A., Raghunath, T. P., & Venkatasubramanian, G. (2018). Managed aquifer recharge in India: Consensual policy but controversial implementation. Water Alternatives, 11(3), 749-769.Fouladgar MM, Yazdani-Chamzini A, Zavadskas EK, Haji Moini SH (2012) A new hybrid model for evaluating the working strategies: case study of Construction Company. Technological and Economic Development of Economy. 2012; 18(1): 164–188.

Richards LA (1968) Diagnosis and Improvement of Saline and Alkali Soils, US Dept Agriculture Handbook, 60, Washington DC, USA

Riegler, A. (2012). Influence of groundwater levels on zero river flow: North Branch, Ashburton River, New Zealand. na.

Ringleb, J., Sallwey, J., & Stefan, C. (2016). Assessment of managed aquifer recharge through modeling—A review. Water, 8(12), 579.

Rinne, J. K., Miri, S., Oksala, N., Vehkaoja, A., & Kössi, J. (2023). Evaluation of a wrist-worn photoplethysmography monitor for heart rate variability estimation in patients recovering from laparoscopic colon resection. Journal of Clinical Monitoring and Computing, 37(1), 45-53.

Rivera-Sánchez, S. P., Ocampo-Ibáñez, I. D., Silva-Leal, J. A., Flórez-Elvira, L. J., Castaño-Hincapié, A. V., Dávila-Estupiñan, A., ... & Pérez-Vidal, A. (2020). A novel filtration system based on ceramic silver-impregnated pot filter combined with adsorption processes to remove waterborne bacteria. Scientific Reports, 10(1), 1-7.

Rivett, M. O., Ellis, P. A., Greswell, R. B., Ward, R. S., Roche, R. S., Cleverly, M. G., ... & Dowle, J. (2008). Cost-effective mini drive-point piezometers and multilevel samplers for monitoring the hyporheic zone. Quarterly Journal of Engineering Geology and Hydrogeology, 41(1), 49-60.

Robert, M., Bergez, J. E., & Thomas, A. (2018). A stochastic dynamic programming approach to analyze adaptation to climate change–Application to groundwater irrigation in India. European journal of operational research, 265(3), 1033-1045.

Robins, N.S., 1998. Recharge: the key to groundwater pollution and aquifer vulnerability. In: ROBINS, N. S. (ed.) Groundwater Pollution, Aquifer Recharge and Vulnerability. Geological Society, London, Special Publications,130,

Rodríguez-Iglesias, J., Alcalá, L., Megido, L., & Castrillón, L. (2022). Removal of fluoride from coke wastewater by aluminum doped chelating ion-exchange resins: a tertiary treatment. Environmental Science and Pollution Research, 1-11.

Rohde, L. E., Clausell, N., Ribeiro, J. P., Goldraich, L., Netto, R., Dec, G. W., ... & Polanczyk, C. A. (2005). Health outcomes in decompensated congestive heart failure: a comparison of tertiary hospitals in Brazil and United States. International journal of cardiology, 102(1), 71-77.

Rojas O, Vrieling A, Rembold F (2011) Assessing drought probability for agricultural areas in Africa with coarse resolution remote sensing imagery. Remote Sensing of Environment .115(2), 343–352. doi:10.1016/j.rse.2010.09.006

Rong, L., Duan, X., Feng, D., & Zhang, G. (2017). Soil moisture variation in a farmed dry-hot valley catchment evaluated by a redundancy analysis approach. Water, 9(2), 92.

Ronghang, M., Gupta, A., Mehrotra, I., Kumar, P., Patwal, P., Kumar, S., ... & Sandhu, C. (2019). Riverbank filtration: A case study of four sites in the hilly regions of Uttarakhand, India. Sustainable water resources management, 5, 831-845.

Roodposhti, M.S., Aryal, J., Shahabi, H., Safarrad, T., 2016 Fuzzy shannon entropy: a hybrid gis-based landslide susceptibility mapping method. Entropy 18:343

Rosmadi, A. F., Shaharudin, S. M., Rajoo, M., Tarmizi, R. A., & Saiful, M. (2023). Mapping of Students' Academic Performance in Online Learning Environment during Pandemic Using Multiple Correspondence Analysis. International Journal of Information and Education Technology, 13(1).

Roy M, Shamim F, Chatterjee S (2021) Evaluation of Physicochemical and Biological Parameters on the Water Quality of Shilabati River, West Bengal, India, Water Science, 35:1, 71-81, DOI: 10.1080/23570008.2021.1928902

Roy SS, jana NC (2019) Agricultural Productivity and Efficiency in Purulia District, West Bengal, Int. J. Rev. and Res. Social Sci. 2019; 7(2):283-292.DOI: 10.5958/2454-2687.2019.00016.9

Roy, M., Shamim, F., Chatterjee, S., 2021. Evaluation of Physicochemical and Biological Parameters on the Water Quality of Shilabati River, West Bengal, India . Water Science, doi:10.1080/23570008.2021.1928902

Roy, P., Pal, S. C., Chakrabortty, R., Chowdhuri, I., Saha, A., & Shit, M. (2022). Climate change and groundwater overdraft impacts on agricultural drought in India: Vulnerability assessment, food security measures and policy recommendation. Science of The Total Environment, 849, 157850.

Ruidas, D., Pal, S. C., Towfiqul Islam, A. R. M., & Saha, A. (2023). Hydrogeochemical evaluation of groundwater aquifers and associated health hazard risk mapping using ensemble data driven model in a water scares plateau region of eastern India. Exposure and Health, 15(1), 113-131.

Russo R C, Rashleigh B, Ambrose RB (2008) Watershed Management in the United States. In: Gönenç İ.E., Vadineanu A., Wolflin J.P., Russo R.C. (eds) Sustainable Use and Development of Watersheds. NATO Science for Peace and Security Series (Series C: Environmental Security). Springer, Dordrecht. https://doi.org/10.1007/978-1-4020-8558-1_11

Sabino H, Menezes J, L.A.D. LimaIndexing LAD (2020) The Groundwater Quality Index for human consumption (GWQIHC) for urban coastal aquifer assessment, Environmental Earth Sciences, 79 (2020), 10.1007/s12665-020-8882-z

Sadhasivam N, Bhardwaj A, Pourghasemi HR et al (2020) Morphometric attributes-based soil erosion susceptibility mapping in Dnyanganga watershed of India using individual and ensemble models. Environ Earth Sci 79, 360 (2020). https://doi.org/10.1007/s12665-020-09102-3

Saeed, K. A., Kassim, K. A., Nur, H., & Yunus, N. Z. M. (2015). Strength of lime-cement stabilized tropical lateritic clay contaminated by heavy metals. KSCE Journal of Civil Engineering, 19, 887-892.

Saha A, Patil M, Goyal V C, Rathore D S (2018) Assessment and Impact of Soil Moisture Index in Agricultural Drought Estimation Using Remote Sensing and GIS Techniques. Proceedings, 7(1), 2–. doi:10.3390/ECWS-3-05802

Saha S, Pal SK(2021) Threshold phosphorus level of acidic soils of eastern India. Environ Monit Assess 193, 803 (2021). https://doi.org/10.1007/s10661-021-09608-8

Saha S, Reza AHMS, Roy MK(2019) Hydrochemical evaluation of groundwater quality of the Tista floodplain, Rangpur, Bangladesh. Appl Water Sci 9, 198 (2019). https://doi.org/10.1007/s13201-019-1085-7

Saha, J., Patra, U.K., Paul, S., 2017. Assessment of Fluoride Contamination Scenario of Groundwater: A Study on Purulia-I and Purulia-II Block, Purulia District, West Bengal. International Journal of Current Research 9(6):53386-53393

Saha, N., Das, L., Das, P., Bhowal, A., & Bhattacharjee, C. (2021). Comparative experimental and mathematical analysis on removal of dye using raw rice husk, rice husk charcoal and activated rice husk charcoal: batch, fixed-bed column, and mathematical modeling. Biomass Conversion and Biorefinery, 1-18.

Saha, P., Chowdhury, S., Gupta, S., Kumar, I., 2010. Insight into adsorption equilibrium, kinetics and thermodynamics of Malachite Green onto clayey soil of Indian origin. Chem Eng J 165:874–882. https://doi.org/10.1016/j.cej.2010.10.048

Saha, R., Wankhede, T., Das, I. C., Kumaranchat, V. K., & Reddy, K. S. (2023). Geospatial Data Analysis Using Fuzzy Analytical Hierarchy Process to Delineate Groundwater Potential Zone in a Semi-arid Hard Rock Terrain. Journal of the Geological Society of India, 99(1), 129-138.

Saharwardi MS, Kumar P, Sachan D (2021) Evaluation and projection of drought over India using high-resolution regional coupled model ROM. Clim Dyn (2021). https://doi.org/10.1007/s00382-021-05919-1

Sahoo, S., Chakraborty, S., Pham, Q. B., Sharifi, E., Sammen, S. S., Vojtek, M., & Linh, N. T. T. (2021). Recognition of district-wise groundwater stress zones using the GLDAS-2 catchment land surface model during lean season in the Indian state of West Bengal. Acta Geophysica, 69, 175-198.Senapati, U., & Das, T. K. (2021). Assessment of basin-scale groundwater potentiality mapping in drought-prone upper Dwarakeshwar River basin, West Bengal, India, using GIS-based AHP techniques. Arabian Journal of Geosciences, 14(11), 960.

Sahu H B, Mahapatra SS, and Panigrahi DC (2012) Fuzzy c-means clustering approach for classification of Indian coal seams with respect to their spontaneous combustion susceptibility," Fuel Processing Technology, vol. 104, pp. 115–120, 2012.

Salah Md E, Turki A M, Al-Othman E M (2012) Assessment of Water Quality of Euphrates River Using Cluster Analysis. Journal of Environmental Protection, Vol. 3 No. 12, 2012, pp. 1629-1633. doi: 10.4236/jep.2012.312180.

Saleh, H., Fenner, R.A., Kapetas, L. (2019). Managing aquifer recharge using stormwater as a drought mitigation strategy in London, in: Proceedings of the 38th IAHR World Congress. IAHR, Panama

Salem, G S A, Kazama S, Shahid S, Dey N C (2018) Impacts of climate change on groundwater level and irrigation cost in a groundwater dependent irrigated region. Agricultural Water Management.Volume 208, 30 September 2018, Pages 33-42

Samal, A. C., Bhattacharya, P., Mallick, A., Ali, M. M., Pyne, J., & Santra, S. C. (2015). A study to investigate fluoride contamination and fluoride exposure dose assessment in lateritic zones of West Bengal, India. Environmental Science and Pollution Research, 22, 6220-6229.

Samal, A. K., Mishra, P. K., & Biswas, A. (2020). Assessment of origin and distribution of fluoride contamination in groundwater using an isotopic signature from a part of the Indo-Gangetic Plain (IGP), India. HydroResearch, 3, 75-84.

Samal, A.K., Mishra, P.K., Biswas, A., 2020. Assessment of origin and distribution of fluoride contamination in groundwater using an isotopic signature from a part of the Indo-Gangetic Plain (IGP), India. HydroResearch, 3(), 75–84. doi:10.1016/j.hydres.2020.05.001

Sampaio, E. V., & Silva, G. C. (2005). Biomass equations for Brazilian semiarid caating a plants. Acta Botanica Brasilica, 19, 935-943.

Sanchez-Vila, X., Guadagnini, A., & Carrera, J. (2006). Representative hydraulic conductivities in saturated groundwater flow. Reviews of Geophysics, 44(3).

Sandeep P, Obi Reddy, GP, Jegankumar R, Arun Kumar K C (2021) Monitoring of agricultural drought in semi-arid ecosystem of Peninsular India through indices derived from time-series CHIRPS and MODIS datasets. Ecological Indicators, 121, 107033. doi:10.1016/j.ecolind.2020.107033

Sandhu, C. S. S. (2015). A concept for the investigation of riverbank filtration sites for potable water supply in India.

Sandhu, C., Grischek, T., Kumar, P., & Ray, C. (2011). Potential for riverbank filtration in India. Clean Technologies and Environmental Policy, 13, 295-316.

Sankar, K., Karunanidhi, D., Kalaivanan, K., Subramani, T., Shanthi, D., & Balamurugan, P. (2023). Integrated hydrogeophysical and GIS based demarcation of groundwater potential and vulnerability zones in a hard rock and sedimentary terrain of Southern India. Chemosphere, 316, 137305.

Santra A, Santra Mitra S (2020) Space-Time Drought Dynamics and Soil Erosion in Puruliya District of West Bengal, India: A Conceptual Design. J Indian Soc Remote Sens 48, 1191–1205 (2020). https://doi.org/10.1007/s12524-020-01147-y

Sarani F, Ahangar AG, Shabani A (2016) Predicting ESP and SAR by artificial neural network and regression models using soil pH and EC data (Miankangi Region, Sistan and Baluchestan Province, Iran). Arch. Agron Soil Sci. 62 (1), 127–138.

Saranya, T., & Saravanan, S. (2020). Groundwater potential zone mapping using analytical hierarchy process (AHP) and GIS for Kancheepuram District, Tamilnadu, India. Modeling Earth Systems and Environment, 6(2), 1105-1122.

Saravanan, S., Pitchaikani, S., Thambiraja, M. et al., 2023. Comparative assessment of groundwater vulnerability using GIS-based DRASTIC and DRASTIC-AHP for Thoothukudi District, Tamil Nadu India. Environ Monit Assess 195, 57. https://doi.org/10.1007/s10661-022-10601-y

Saravanan, S., Pitchaikani, S., Venkatesan, G., 2020. Assessment and evaluation of groundwater vulnerability index maps of Upper Palar River Basin, Tamilnadu, India. J Earth Syst Sci 129, 162 (2020). https://doi.org/10.1007/s12040-020-01425-w

Sarkar B, Islam A (2021) Assessing the suitability of groundwater for irrigation in the light of natural forcing and anthropogenic influx: a study in the Gangetic West Bengal, India. Environ Earth Sci 80, 807 (2021). https://doi.org/10.1007/s12665-021-10087-w

Sarkar T, Mishra M (2018) Soil Erosion Susceptibility Mapping with the Application of Logistic Regression and Artificial Neural Network. J geovis spat anal. 2, 8. https://doi.org/10.1007/s41651-018-0015-9

Sarkar, A., Paul, B., & Darbha, G. K. (2022). The groundwater arsenic contamination in the Bengal Basin-A review in brief. Chemosphere, 134369.

Sarkar, M., Pal, S. C., & Islam, A. R. M. T. (2022). Groundwater quality assessment for safe drinking water and irrigation purposes in Malda district, Eastern India. Environmental Earth Sciences, 81(2), 52.

Sarkar, T., Kannaujiya, S., Taloor, A. K., Ray, P. K. C., & Chauhan, P. (2020). Integrated study of GRACE data derived interannual groundwater storage variability over water stressed Indian regions. Groundwater for sustainable development, 10, 100376.

Sartape, A. S., Mandhare, A. M., Jadhav, V. V., Raut, P. D., Anuse, M. A., & Kolekar, S. S. (2017). Removal of malachite green dye from aqueous solution with adsorption technique using Limonia acidissima (wood apple) shell as low cost adsorbent. Arabian Journal of Chemistry, 10, S3229-S3238.Abdeta GC, Tesemma AB, Tura AL et al. (2020) Morphometric analysis for prioritizing sub-watersheds and management planning and practices in Gidabo Basin, Southern Rift Valley of Ethiopia. Appl Water Sci 10, 158. https://doi.org/10.1007/s13201-020-01239-7

Sathyan R, Parthiban P, Dhanalakshmi R et al (2021) A combined big data analytics and Fuzzy DEMATEL technique to improve the responsiveness of automotive supply chains. J Ambient Intell Human Comput 12, 7949–7963 (2021). https://doi.org/10.1007/s12652-020-02524-8

Sattari MT, Farkhondeh A, Patrick Abraham J (2018) Estimation of sodium adsorption ratio indicator using data mining methods: a case study in Urmia Lake basin, Iran. Environ Sci Pollut Res 25, 4776–4786 (2018). https://doi.org/10.1007/s11356-017-0844-y

Schilling J, Hertig E, Tramblay Y. et al (2020) Climate change vulnerability, water resources and social implications in North Africa. Reg Environ Change 20, 15 (2020). https://doi.org/10.1007/s10113-020-01597-7

Schmidt, C., Conant Jr, B., Bayer-Raich, M., & Schirmer, M. (2007). Evaluation and field-scale application of an analytical method to quantify groundwater discharge using mapped streambed temperatures. Journal of Hydrology, 347(3-4), 292-307.

Schumm S A (1956) Evolution of drainage systems and slopes in badlands at Perth Amboy, New Jersey. Bulletin of Geological Society of America: 67:597–646

Schwartz, F. W., & Zhang, H. (2002). Fundamentals of ground water. John Wiley & Sons.

Seker S, Zavadskas E (2017) Application of Fuzzy DEMATEL Method for Analyzing Occupational Risks on Construction Sites. Sustainability, 9(11), 2083–. doi:10.3390/su9112083

Sen P K (1968) Estimates of Regression Coefficient based on Kendall's tau. Journal of the American Statistical Association 63,1379-1389

Senapati U, Das TK (2021) Geospatial Assessment of Agricultural Drought Vulnerability Using Integrated Three-Dimensional Model In The Upper Dwarakeshwar River Basin In West Bengal, India, Theoretical and Applied Climatology. 10.21203/rs.3.rs-684936/v1

Şener, E. Appraisal of groundwater pollution risk by combining the fuzzy AHP and DRASTIC method in the Burdur Saline Lake Basin, SW Turkey. Environ Sci Pollut Res 30, 21945–21969 (2023). https://doi.org/10.1007/s11356-022-23651-z

Sengupta, A. K., Gupta, A., & Deb, A. K. (2001). Arsenic crisis in Indian subcontinent: a local solution to a global problem. Water 21, 3436.

Seo, Y., Kim, S., & Singh, V. P. (2015). Estimating spatial precipitation using regression kriging and artificial neural network residual kriging (RKNNRK) hybrid approach. Water Resources Management, 29, 2189-2204.

Sequeira, M., Adlemo, A., & Hilletofth, P. (2022). A hybrid fuzzy-AHP-TOPSIS model for evaluation of manufacturing relocation decisions. Operations Management Research, 1-28.

Shah, B. A. (2022, January). Groundwater arsenic and iron contamination in the Gangetic Plains of India: safe drinking water option on quaternary stratigraphy. In New Prospects in Environmental Geosciences and Hydrogeosciences: Proceedings of the 2nd Springer Conference of the Arabian Journal of Geosciences (CAJG-2), Tunisia 2019 (pp. 561-564). Cham: Springer International Publishing.

Shah, T. (2009). Climate change and groundwater: India's opportunities for mitigation and adaptation. Environmental Research Letters, 4(3), 035005.

Shaji, E., Santosh, M., Sarath, K. V., Prakash, P., Deepchand, V., & Divya, B. V. (2021). Arsenic contamination of groundwater: A global synopsis with focus on the Indian Peninsula. Geoscience frontiers, 12(3), 101079.

Shamsuddin, A.S., Ismail, S.N.S, Abidin, E.Z. et al., 2021. Application of GIS-based DRASTIC model approaches in assessing groundwater vulnerability for shallow alluvial aquifer deposited. Arab J Geosci 14, 2693 (2021). https://doi-org.manchester.idm.oclc.org/10.1007/s12517-021-08865-8

Shamsuddin, M. K. N., Sulaiman, W. N. A., Ramli, M. F., & Kusin, F. M. (2019). Vertical hydraulic conductivity of riverbank and hyporheic zone sediment at Muda River riverbank filtration site, Malaysia. Applied Water Science, 9, 1-22.

Shamsudduha, M., Zahid, A., Burgess, W.G., 2019. Security of deep groundwater against arsenic contamination in the Bengal Aquifer System: a numerical modeling study in southeast Bangladesh. Sustain. Water Resour. Manag. 5, 1073–1087 (2019). https://doi.org/10.1007/s40899-018-0275-z

Shannon C E (1948) A mathematical theory of communication. The Bell System Technical Journal 379–423, https://doi.org/10.1145/584091.584093.

Shao, Y., Li, J., Fang, X., Yang, Z., Qu, Y., Yang, M., & Wang, H. (2022). Chemical modification of bamboo activated carbon surface and its adsorption property of simultaneous removal of phosphate and nitrate. Chemosphere, 287, 132118.

Shao, Z., Huq, Md. E., Cai, B., Altan, O., Li, Y., 2020. Integrated remote sensing and GIS approach using Fuzzy-AHP to delineate and identify groundwater potential zones in semi-arid Shanxi Province, China, Environmental Modelling & Software, Volume 134,2020,https://doi.org/10.1016/j.envsoft.2020.104868.

Sharadqah, S., 2017. Contamination risk evaluation of groundwater in the canton of Portoviejo-Ecuador, using susceptibility index and two intrinsic vulnerability models. Am J Environ Sci 13(1):65–76

Sharma A, Ganguly R, Gupta AK (2020) Impact assessment of leachate pollution potential on groundwater: an Indexing method. J Environ Eng 146(3):05019007. https://doi.org/10.1061/(ASCE) EE.1943-7870.0001647

Sharma R (2009) Craton and fold belts of India, lecture notes in earth sciences, vol 127. Springer, New York. doi:10.1007/978-3-642-01459-8_2

Sharma SK, Gajbhiye S, Tignath S (2015) Application of principal component analysis in grouping geomorphic parameters of a watershed for hydrological modeling. Appl Water Sci 5, 89–96 (2015). https://doi.org/10.1007/s13201-014-0170-1

Sharma, S., Bhattacharya, A., 2017. Drinking water contamination and treatment techniques. Appl Water Sci 7, 1043–1067 (2017). https://doi.org/10.1007/s13201-016-0455-7

Shayesteh, H., Raji, F., & Kelishami, A. R. (2021). Influence of the alkyl chain length of surfactant on adsorption process: a case study. Surfaces and Interfaces, 22, 100806.

Shekhar S, Kumar S, Densmore A L et al. (2020) Modelling water levels of northwestern India in response to improved irrigation use efficiency. Sci Rep 10, 13452 (2020). https://doi.org/10.1038/s41598-020-70416-0

Shen YEH, Chen T, Xiao Z, Liu B, Chen Y (2021) High-dimensional Data Clustering with Fuzzy C-Means: Problem, Reason, and Solution. In I. Rojas, G. Joya, & A. Català (Eds.), Advances in Computational

Intelligence: 16th International Work-Conference on Artificial Neural Networks, IWANN 2021, Virtual Event, June 16–18, 2021, Proceedings, Part I (1st ed., Vol. LNCS/LNTCS 12861, pp. 89-100). (Lecture Notes in Computer Science; Vol. LNCS/LNTCS 12861). Springer Nature Switzerland AG. https://doi.org/10.1007/978-3-030-85030-2_8

Shen, Z., Hou, D., Jin, F., Shi, J., Fan, X., Tsang, D. C., & Alessi, D. S. (2019). Effect of production temperature on lead removal mechanisms by rice straw biochars. Science of the Total Environment, 655, 751-758.

Shi, W., Wang, H., Yan, J., Shan, L., Quan, G., Pan, X., & Cui, L. (2022). Wheat straw derived biochar with hierarchically porous structure for bisphenol A removal: Preparation, characterization, and adsorption properties. Separation and Purification Technology, 289, 120796.

Shirmard, H., Farahbakhsh, E., Müller, R. D., & Chandra, R. (2022). A review of machine learning in processing remote sensing data for mineral exploration. Remote Sensing of Environment, 268, 112750.

Shit K P, Nandi A S, Bhunia G S (2015) Soil Erosion Risk Mapping using RUSLE model on Jhargram Sub-Division at West Bengal in India. Modeling Earth Systems and Environment, 1, 1-12.

Shit M, Mondal P (2019) Spatio-temporal Changes of Land use and land cover in Bankura-I and Bankura-II C.D. Block, Bankura District, West Bengal. International Journal of Scientific Research and Reviews. 8, 3209-3216.

Shit P K, Bhunia G, Maiti R (2013) Assessment of Factors Affecting Ephemeral Gully Development in Badland Topography: a Case Study at Garbheta Badland (Pashchim Medinipur). Int J Geosci. 4,461–470. doi: https://doi.org/10.4236/ijg.2013.42043

Shit P K, Maiti R (2012) Mechanism of Gully-Head Retreat-A Study at Ganganir Danga, Paschim Medinipur, West Bengal. Ethiopian Journal of Environmental Studies and Management 5:332–34. DOI: 10.4314/ejesm.v5i4.2

Shit P K, Paira R, Bhunia G, Maiti R (2015) Modeling of potential gully erosion hazard using geo-spatial technology at Garbheta block, West Bengal in India. Model. Earth Syst. Environ. 1, 2. https://doi.org/10.1007/s40808-015-0001-x

Shu, Y., Li, H., & Lei, Y. (2018). Modelling groundwater flow with MIKE SHE using conventional climate data and satellite data as model forcing in Haihe Plain, China. Water, 10(10), 1295.

Sigmund, G., Hüffer, T., Hofmann, T., & Kah, M. (2017). Biochar total surface area and total pore volume determined by N2 and CO2 physisorption are strongly influenced by degassing temperature. Science of the Total Environment, 580, 770-775.

Silvestri S, Bryan E, Ringler C, Herrero M, Okoba B (2012) Climate change perception and 2 adaptation of agro-pastoral communities in Kenya. Regional Environmental Change, 12(4), 3 791–802. https://doi.org/10.1007/s10113-012-0293-6

Simonds, F. W., & Sinclair, K. A. (2002). Surface water-ground water interactions along the Lower Dungeness River and vertical hydraulic conductivity of streambed sediments, Clallam County, Washington, September 1999-July 2001. Water-Resources Investigations Report, 2, 4161.

Simonin, J. P. (2016). On the comparison of pseudo-first order and pseudo-second order rate laws in the modeling of adsorption kinetics. Chemical Engineering Journal, 300, 254-263.

Singh AK, Bharati RC, Pedpati A (2013) An assessment of faba bean (Vicia faba L.) current status and future prospect. African J Agric Res 8:6634–6641. https://doi.org/10.5897/AJAR2013.7335

Singh R, Upreti P, Allemailem KS, Almatroudi A, Rahmani AH, Albalawi GM (2022) Geospatial Assessment of Ground Water Quality and Associated Health Problems in the Western Region of India. Water 2022, 14, 296. https:// doi.org/10.3390/w14030296

Singh TP, Nandimath P, Kumbhar V. et al (2021) Drought risk assessment and prediction using artificial intelligence over the southern Maharashtra state of India. Model. Earth Syst. Environ. 7, 2005–2013 (2021). https://doi.org/10.1007/s40808-020-00947-y

Singh, N., Kumari, S., & Khan, S. (2021). Improved fluoride removal efficiency using novel defluoridation pencil. Materials Today Communications, 28, 102521.

Singh, O., Kasana, A., Singh, K. P., & Sarangi, A. (2020). Analysis of drivers of trends in groundwater levels under rice–wheat ecosystem in Haryana, India. Natural Resources Research, 29, 1101-1126.

Singh, S., German, M., Chaudhari, S., & Sengupta, A. K. (2020). Fluoride removal from groundwater using zirconium impregnated anion exchange resin. Journal of environmental management, 263, 110415.

Singha, S., Pasupuleti, S., Singha, S. S., Singh, R., & Kumar, S. (2021). Prediction of groundwater quality using efficient machine learning technique. Chemosphere, 276, 130265.

Sishodia R P, Skhula S , Graham W D, Wani S P , Garg K K (2016) Bi-decadal Groundwater Level Trends in a Semi-arid South Indian Region: Declines, causes and management. Journal of Hydrology: Regional Studies, Volume 8, December 2016, Pages 43-58

Sishodia, R. P., Shukla, S., Wani, S. P., Graham, W. D., & Jones, J. W. (2018). Future irrigation expansion outweigh groundwater recharge gains from climate change in semi-arid India. Science of the Total Environment, 635, 725-740.

Sithara, S., Pramada, S. K., & Thampi, S. G. (2020). Impact of projected climate change on seawater intrusion on a regional coastal aquifer. Journal of Earth System Science, 129, 1-15.

Siva Prasad, Y., Venkateswara Rao, B., 2018.Groundwater recharge estimation studies in a khondalitic terrain of India. Appl Water Sci 8, 102 (2018). https://doi.org/10.1007/s13201-018-0738-2

Slichter, C. S. (1899). Theoretical investigation of the motion of ground waters. The 19th Ann. Rep. US Geophys Survey., 304-319.

Somers L D, McKenzie J M (2020) A review of groundwater in high mountain environments. WIREs Water. doi:10.1002/wat2.1475

Sophocleous, M. (2002). Interactions between groundwater and surface water : the state of the science, Hydrogeol. J., 10 (2002), pp. 52-67, 10.1007/s10040-001-0170-8

Spiridonoff, S. V. (1964). Design and use of radial collector wells. Journal-American Water Works Association, 56(6), 689-698.

Sprenger, C., Hartog, N., Hernández, M., Vilanova, E., Grützmacher, G., Scheibler, F., & Hannappel, S. (2017). Inventaire des sites de gestion des aquifères par recharge en Europe: développement historique, situation actuelle et perspectives. Hydrogeology Journal, 25(6), 1909-1922.

Sresto, M. A., Siddika, S., Haque, M. N., & Saroar, M. (2022). Groundwater vulnerability assessment in Khulna district of Bangladesh by integrating fuzzy algorithm and DRASTIC (DRASTIC-L) model. Modeling Earth Systems and Environment, 8(3), 3143-3157.

Sridhar, N., Ezhisaivallabi, K., Poongothai, S., & Palanisamy, M. (2018). Groundwater flow modelling using visual MODFLOW—A case study of lower Ponnaiyar sub-watershed, Tamilnadu, India. International Journal of Engineering Research in Mechanical and Civil Engineering, 3(2), 109-114.

Srivastav, A. L., Singh, P. K., Srivastava, V., & Sharma, Y. C. (2013). Application of a new adsorbent for fluoride removal from aqueous solutions. Journal of Hazardous materials, 263, 342-352.

Sruthi S, Aslam M M (2015) Agricultural Drought Analysis Using the NDVI and Land Surface Temperature Data; a Case Study of Raichur District. Aquatic Procedia, 4, 1258–1264. https://doi.org/10.1016/j.aqpro.2015.02.164

Stafford, M. J., Holländer, H. M., & Dow, K. (2022). Estimating groundwater recharge in the assiniboine delta aquifer using HYDRUS-1D. Agricultural Water Management, 267, 107514.

Standen, K., Costa, L. R., & Monteiro, J. P. (2020). In-channel managed aquifer recharge: a review of current development worldwide and future potential in Europe. Water, 12(11), 3099.

State of Environment Report–West Bengal (2016), https://www.wbpcb.gov.in/writereaddata/files/SOE_Report_2016_1.pdf

Strahler A (1952) Dynamic Basis of Geomorphology. Geological Society of America Bulletin, 63, 923-938.

Strahler A (1967) Introduction to Physical Geography. New York (605 Third Avenue), 10016: John Wiley & Sons, Inc., 1965. 455 P. Science Education, 51: 416–416. doi:10.1002/sce.3730510498

Suhas S, J Chaudhary J K (2020) A Comparative Study of Fuzzy Logic and WQI for Groundwater Quality Assessment, Procedia Computer Science, Volume 171, 2020, Pages 1194-1203, ISSN 1877-0509, https://doi.org/10.1016/j.procs.2020.04.128.

Sulaiman N H , Kamarudin, M K A , Dasuki A , Amran M , Azaman F, Abidin I Z, Hairoma N (2015). Trend Analysis of Pahang River using Non-parametric Analysis: Mann Kendall's Trend Test. Malaysian Journal of Analytical Sciences, Vol 19 No 6 (2015): 1327 – 1334

Sun, Y., Li, J., Huang, T., & Guan, X. (2016). The influences of iron characteristics, operating conditions and solution chemistry on contaminants removal by zero-valent iron: A review. Water Research, 100, 277-295.

Sunkari E D, Seidu J, Ewusi A (2022) Hydrogeochemical evolution and assessment of groundwater quality in the Togo and Dahomeyan aquifers, Greater Accra Region, Ghana, Environmental Research, Volume 208, 2022,112679, ISSN 0013-9351,https://doi.org/10.1016/j.envres.2022.112679.

Sutradhar A, Chakrabortty D, Chattaraj M (2019) Identification of agricultural productivity regions and its major determinants: a case study from Bankura district, West Bengal. Int J Res Soc Sci 9(5):661–678

Suzuki, R. M., Andrade, A. D., Sousa, J. C., & Rollemberg, M. C. (2007). Preparation and characterization of activated carbon from rice bran. Bioresource technology, 98(10), 1985-1991.

Swain S, Sahoo S & Taloor AK (2022) Groundwater quality assessment using geospatial and statistical approaches over Faridabad and Gurgaon districts of National Capital Region, India. Appl Water Sci 12, 75 (2022). https://doi.org/10.1007/s13201-022-01604-8

Swain, S., Taloor, A. K., Dhal, L., Sahoo, S., & Al-Ansari, N. (2022). Impact of climate change on groundwater hydrology: a comprehensive review and current status of the Indian hydrogeology. Applied Water Science, 12(6), 120.

Taghavi, N., Niven, R.K., Kramer, M., Paull, D.J., 2023. Comparison of DRASTIC and DRASTICL groundwater vulnerability assessments of the Burdekin Basin, Queensland, Australia, Science of The Total Environment, Volume858, Part 3, ,159945, ISSN 0048-9697, https://doi.org/10.1016/j.scitotenv.2022.159945.

Tahama, K., Baride, A., Gupta, G., Erram, V. C., & Baride, M. V. (2022). Spatial variation of sub-surface heterogenieties within the dyke swarm of Nandurbar region, Maharashtra, India, for groundwater exploration using Inverse Distance Weighted technique. HydroResearch, 5, 1-12.

Taherian P, Joodavi A (2021) Hydrogeochemical characteristics and source identification of salinity in groundwater resources in an arid plain, northeast of Iran: implication for drinking and irrigation purposes. Acque Sotterranee - Italian J. Groundwater 10 (2), 21–31. https://doi.org/10.7343/as-2021-502

Takmil, F., Esmaeili, H., Mousavi, S. M., & Hashemi, S. A. (2020). Nano-magnetically modified activated carbon prepared by oak shell for treatment of wastewater containing fluoride ion. Advanced Powder Technology, 31(8), 3236-3245.

Tallarida, R. J., Murray, R. B., Tallarida, R. J., & Murray, R. B. (1987). Chi-square test. Manual of pharmacologic calculations: with computer programs, 140-142.

Tan et al (2020) Drought Disaster Risks under CMIP5 RCP Scenarios in Ningxia Hui Autonomous Regions, China. Nat Hazards. https://doi.org/10.1007/s11069-019-038110

Tan, T. L., Nakajima, H., & Rashid, S. A. (2020). Adsorptive, kinetics and regeneration studies of fluoride removal from water using zirconium-based metal organic frameworks. RSC advances, 10(32), 18740-18752.

Tang, Y., Huo, J., Zhu, D., & Yuan, Z. (2022). Simulation of the Water Storage Capacity of Siling Co Lake on the Tibetan Plateau and Its Hydrological Response to Climate Change. Water, 14(19), 3175.

Taşan, M., Taşan, S., & Demir, Y. (2023). Estimation and uncertainty analysis of groundwater quality parameters in a coastal aquifer under seawater intrusion: a comparative study of deep learning and classic machine learning methods. Environmental Science and Pollution Research, 30(2), 2866-2890.

Tavana, M., Shaabani, A., Di Caprio, D., & Amiri, M. (2021). An integrated and comprehensive fuzzy multicriteria model for supplier selection in digital supply chains. Sustainable Operations and Computers, 2, 149-169.

Taylor, R. G., Todd, M. C., Kongola, L., Maurice, L., Nahozya, E., Sanga, H., & MacDonald, A. M. (2013). Evidence of the dependence of groundwater resources on extreme rainfall in East Africa. Nature Climate Change, 3(4), 374-378.

Teixidó, M., Charbonnet, J. A., LeFevre, G. H., Luthy, R. G., & Sedlak, D. L. (2022). Use of pilot-scale geomedia-amended biofiltration system for removal of polar trace organic and inorganic contaminants from stormwater runoff. Water research, 226, 119246.

Thakur GS, Thomas T (2011) Analysis of groundwater levels for detection of trend in Sagar District, Madhya Pradesh. J Geol Soci India 77:303–308. https://doi.org/10.1007/s12594-011-0038-z

Thakurdesai S C, Pise S K (2016) A Study of relief and slope of upper Kundalika River basin, Raigad, Maharashtra. International Journal of Interdisciplinary Research in Science Society and Culture.2, 2455-2909.

Thao NTT, Khoi DN, Xuan TT et al. (2019) Assessment of Livelihood Vulnerability to Drought: A Case Study in Dak Nong Province, Vietnam. Int J Disaster Risk Sci 10, 604–615 (2019). https://doi.org/10.1007/s13753-019-00230-4

Thapa, B.R., Ishidaira, H., Gusyev, M., Pandey, V .P., Udmale, P., Hayashi, M., Shakya, N.M., 2019. Implications of the Melamchi water supply project for the Kathmandu Valley groundwater system. Water Policy, 21(S1), 120–137.

Thinojah, T., & Ketheesan, B. (2022). Iron removal from groundwater using granular activated carbon filters by oxidation coupled with the adsorption process. Journal of Water and Climate Change, 13(5), 1985-1994.

Thirumalaivasan, D., Karmegam. M., Venugopal. K., 2003. AHP-DRASTIC: software for specific aquifer vulnerability assessment using DRASTIC model and GIS, Environmental Modelling & Software, Volume 18, Issue 7,2003,Pages 645-656,https://doi.org/10.1016/S1364-8152(03)00051-3.

Thomas, H. C. (1944). Heterogeneous ion exchange in a flowing system. Journal of the American chemical society, 66(10), 1664-1666.

Thompson, M. O., & Kearns, J. P. (2021). Modeling and experimental approaches for determining fluoride diffusion kinetics in bone char sorbent and prediction of packed-bed groundwater defluoridator performance. Water Research X, 12, 100108.

Tian W, Cao Y, Ismael A, Stone D, Liang J (2014) Roles of regulated internalization in the polarization of cell surface receptors. **Conf Proc IEEE Eng Med Biol Soc** 2014:1166-9 Water , 8(1), 11; https://doi.org/10.3390/w8010011

Tiwari A, Ahuja A, Vishwakarma B D, Jain K (2019) Groundwater Potential Zone (GWPZ) for Urban Development Site Suitability Analysis in Bhopal, India. J Indian Soc Remote Sens .47, 1793–1815. https://doi.org/10.1007/s12524-019-01027-0

Tiwari V, Qamer FM, Matin MA, Ellenburg WL, Yousafi W, Kamal M (2021) In-Season Crop-Area Mapping for Wheat and Rice in Afghanistan and Bangladesh. In: Bajracharya B., Thapa R.B., Matin M.A. (eds) Earth Observation Science and Applications for Risk Reduction and Enhanced Resilience in Hindu Kush Himalaya Region. Springer, Cham. https://doi.org/10.1007/978-3-030-73569-2_5

Tiwari V, Wahr J , Swenson S, Singh B (2011) Land water storage variation over Southern India from space gravimetry. Current Science, 101(4), 536-540.

Todd K (1980). Groundwater Hydrology. Published by John Wiley & Sons, New York Chichester, - 2nd Edition.

Todd, D. K., & Mays, L. W. (2004). Groundwater hydrology. John Wiley & Sons.

Tolkou, A. K., Trikalioti, S., Makrogianni, O., Trikkaliotis, D. G., Deliyanni, E. A., Kyzas, G. Z., & Katsoyiannis, I. A. (2023). Magnesium modified activated carbons derived from coconut shells for the removal of fluoride from water. Sustainable Chemistry and Pharmacy, 31, 100898.

Tomar, V., Prasad, S., & Kumar, D. (2014). Adsorptive removal of fluoride from aqueous media using Citrus limonum (lemon) leaf. Microchemical Journal, 112, 97-103.

Tomczyk, A., Sokołowska, Z., & Boguta, P. (2020). Biochar physicochemical properties: pyrolysis temperature and feedstock kind effects. Reviews in Environmental Science and Bio/Technology, 19, 191-215.

Tomer, T., Katyal, D., Joshi, V., 2019. Sensitivity analysis of groundwater vulnerability using DRASTIC method: A case study of National Capital Territory, Delhi, India. Groundwater for Sustainable Development, 9(), 100271. doi:10.1016/j.gsd.2019.100271

Tor, A., Danaoglu, N., Arslan, G., & Cengeloglu, Y. (2009). Removal of fluoride from water by using granular red mud: batch and column studies. Journal of hazardous materials, 164(1), 271-278.

Tran, D. T., Pham, T. D., Dang, V. C., Pham, T. D., Nguyen, M. V., Dang, N. M., & Nghiem, L. D. (2022). A facile technique to prepare MgO-biochar nanocomposites for cationic and anionic nutrient removal. Journal of Water Process Engineering, 47, 102702.

Trefry, M. G., & Muffels, C. (2007). FEFLOW: A finite-element ground water flow and transport modeling tool. Groundwater, 45(5), 525-528.

Tsai Sang-Bing, Chien Min-Fang, Xue Youzhi, Li Lei, Jiang Xiaodong, Chen Quan, Zhou Jie, Wang Lei, Deng, Yong (2015) Using the Fuzzy DEMATEL to Determine Environmental Performance: A Case of Printed Circuit Board Industry in Taiwan. PLOS ONE, 10(6), e0129153–. doi:10.1371/journal.pone.0129153

Tyagi, S., Singh, P., Sharma, B., Singh , R., 2014. Assessment of water quality for drinking purpose in District Pauri of Uttarkhand India. Appl Ecol Environ Sci. 2014;2(4):94–9

Tyralis, H., Papacharalampous, G., & Langousis, A. (2019). A brief review of random forests for water scientists and practitioners and their recent history in water resources. Water, 11(5), 910.

UNDESA (2016) The sustainable development goals report 2016. United Nations Department of Economic and Social Affairs. https://doi.org/10.18356/3405d09f-en

USBR (1990) Earth Manual-Part 2. US Department of the Interior Bureau of Reclamation, Denver

USDA, 2014. https://cropwatch.unl.edu/documents/USDA_NRCS_EC_guide.pdf

USGS (1998) Spatial Variation in Saturated Hydraulic Conductivity of Sediments at a Crude-Oil Spill Site Near Bemidji, Minnesota, Water-Resources Investigations Report 98-4053

Usman, A.R.A., Ahmad, M., El-Mahrouky, M. et al. chemically modified biochar produced from conocarpus waste increases NO3 removal from aqueous solutions. Environ Geochem Health 38, 511–521 (2016). https://doi.org/10.1007/s10653-015-9736-6

Van De Griend A, Owe M (1993) On the Relationship between Thermal Emissivity and the Normalized Difference Vegetation Index for Nature Surfaces International. Journal of Remote Sensing, 14, 1119-1131. https://doi.org/10.1080/01431169308904400

Vardhan, V., & Srimurali, M. (2016). Removal of fluoride from water using a novel sorbent lanthanum-impregnated bauxite. SpringerPlus, 5(1), 1-18.

Varma, A. (2017). Groundwater resource and governance in Kerala: Status, issues and prospects. Forum for Policy Dialogue on Water Conflicts in India.

Vasudevan, S., Jayaraj, J., Lakshmi, J., & Sozhan, G. (2009). Removal of iron from drinking water by electrocoagulation: adsorption and kinetics studies. Korean journal of chemical engineering, 26, 1058-1064

Velasquez M, Hester P T (2013) An Analysis of Multi-Criteria Decision Making Methods. International Journal of Operations Research Vol. 10, No. 2, 56-66

Venkatesh, R., Karthi, N., Kawin, N., Prakash, T., Kannan, C. R., Karthigairajan, M., & Bobe, K. (2022). Synthesis and Adsorbent Performance of Modified Biochar with Ag/MgO Nanocomposites for Heat Storage Application. Adsorption Science & Technology, 2022.

Vienken, T., & Dietrich, P. (2011). Field evaluation of methods for determining hydraulic conductivity from grain size data. Journal of hydrology, 400(1-2), 58-71.

Vig, N., Ravindra, K., & Mor, S. (2022). Heavy metal pollution assessment of groundwater and associated health risks around coal thermal power plant, Punjab, India. International Journal of Environmental Science and Technology, 1-16.

Vikrant, K., Kim, K. H., Ok, Y. S., Tsang, D. C., Tsang, Y. F., Giri, B. S., & Singh, R. S. (2018). Engineered/designer biochar for the removal of phosphate in water and wastewater. Science of the Total Environment, 616, 1242-1260.

Vinati, A., Rene, E. R., Pakshirajan, K., & Behera, S. K. (2020). Activated red mud as a permeable reactive barrier material for fluoride removal from groundwater: parameter optimisation and physico-chemical characterisation. Environmental technology, 41(25), 3375-3386.

Vincent, C. N. (2005). Hydrogeology of the Upper Selwyn Catchment.

Vishwajith K P, Sahu P K , Noman Md, Dhekale B S, Narasimhaiah L (2015) Clustering of the Districts of West Bengal Based on Spatial and Temporal Distribution of Grundwater Table Depth Towards Effective Monitoring and Management of the Valuable Water Resources. Nature Environment and Pollution Technology, Vol 14 No. 3 pp-501-508

Vousoughi F D, Dinpashoh Y, Aalami M T , JhaJharia D (2013) Trend Analysis of Groundwater using Non-Parametric Methods (Case Study: Ardabil Plain). Stoch Environ Res Risk Assess 27: 547. https://doi.org/10.1007/s00477-012-0599-4

Vrouhakis, I., Tziritis, E., Stamatis, G., Panagopoulos, A., 2022. Groundwater Vulnerability Analysis of Tirnavos Basin, Central Greece: An Application of RIVA Method. Water. 2022; 14(4):534. https://doi.org/10.3390/w14040534

Wada Y, van Beek L P, van Kempen C M, Reckman J W, Vasak S, Bierken M F (2010) Global depletion of groundwater resources, Geophys. Res. Lett., 37, L20402, https://doi.org/10.1029/2010GL044571

Wada, Y., Van Beek, L. P., Sperna Weiland, F. C., Chao, B. F., Wu, Y. H., & Bierkens, M. F. (2012). Past and future contribution of global groundwater depletion to sea-level rise. Geophysical Research Letters, 39(9).

Wadi, D., Wu, W., Malik, I., Fuad, A., & Thaw, M. M. (2022). Assessment and feasibility of the potential artificial groundwater recharge in semi-arid crystalline rocks context, Biteira district, Sudan. Scientific African, 17, e01298.

Wang G (2005) Agricultural drought in a future climate: Results from 15 global climate models 6 participating in the IPCC 4th assessment. Clim. Dyn., 25, 739–753, doi:10.1007/s00382-005- 7 0057-9

Wang G, Mang S, Cai H. et al. (2016) Integrated watershed management: evolution, development and emerging trends. J. For. Res. 27, 967–994. https://doi.org/10.1007/s11676-016-0293-3

Wang Jl, Yu Yh (2021) Comprehensive drought monitoring in Yunnan Province, China using multisource remote sensing data. J. Mt. Sci. 18, 1537–1549 (2021).

Wang Q, Guo S, Hu J. et al. (2018) Spectral partitioning and fuzzy C-means based clustering algorithm for big data wireless sensor networks. J Wireless Com Network 2018, 54 (2018). https://doi.org/10.1186/s13638-018-1067-8

Wang Y, Zhang Q,Yao Yb (2020) Drought vulnerability assessment for maize in the semiarid region of northwestern China. Theor Appl Climatol 140, 1207–1220 (2020). https://doi.org/10.1007/s00704-020-03138-y

Wang Z, Zhao N, Wang W, Tang R, Li S (2015) A Fault Diagnosis Approach for Gas Turbine Exhaust Gas Temperature Based on Fuzzy C-Means Clustering and Support Vector Machine", Mathematical Problems in Engineering, vol. 2015, Article ID 240267, 11 pages, 2015. https://doi.org/10.1155/2015/240267

Wang, J., Sun, P., Xue, H., Chen, J., Zhang, H., & Zhu, W. (2020). Red mud derived facile hydrothermal synthesis of hierarchical porous α-Fe2O3 microspheres as efficient adsorbents for removal of Congo red. Journal of Physics and Chemistry of Solids, 140, 109379.

Wang, L., Xu, Z., Fu, Y., Chen, Y., Pan, Z., Wang, R., & Tan, Z. (2018). Comparative analysis on adsorption properties and mechanisms of nitrate and phosphate by modified corn stalks. RSC advances, 8(64), 36468-36476.

Wang, Z., Su, J., Ali, A., Zhang, R., Yang, W., Xu, L., ... & Gao, Z. (2022). Synergistic removal of fluoride from groundwater by seed crystals and bacteria based on microbially induced calcium precipitation. Science of The Total Environment, 806, 150341.

Wang, Z., Zhao, Y., Wen, T., Zhang, T., Chen, L., Zhang, Q., & Song, S. (2022). Enhanced removal of fluoride from water through precise regulation of active aluminum phase using CaCO3. Environmental Science and Pollution Research, 29(45), 68555-68563.

WBPCB (2009), West Bengal Pollution Control Board. 2009. A state of environment report: water resource and its quality in West Bengal, Kolkata, 352.

Weber Jr, Walter J., and J. Carrell Morris. "Equilibria and capacities for adsorption on carbon." Journal of the Sanitary Engineering Division 90.3 (1964): 79-108.Wada Y et al (2010) Past and future contribution of global groundwater depletion to sea-level rise. Geophys Res Lett 39(9), L09402. doi: 10.1029/2012gl051230

Wekesa, G. (2018). Characterization of the aquifer suite within Nairobi County and its environs with respect to the chemical composition and depth (Doctoral dissertation, University of Nairobi).

White, P. A., Kovacova, E., Zemansky, G., Jebbour, N., & Moreau-Fournier, M. (2012). Groundwater-surface water interaction in the Waimakariri River, New Zealand, and groundwater outflow from the river bed. Journal of Hydrology (New Zealand), 1-23.

WHO (1997) Guidelines for drinking-water quality, 2nd ed. Vol. 3. Surveillance and control of community supplies. Geneva, World Health Organization (http://www.who.int/water_ sanitation health/dwq/gdwq2v1/en/index2.html).

WHO (World Health Organization), Publication Data Guidelines for drinking-water quality - 4th ed., (2011)https://apps.who.int/iris/bitstream/handle/10665/44584/9789241548151_eng.pdf

Wieland, E., & Stumm, W. (1992). Dissolution kinetics of kaolinite in acidic aqueous solutions at 25 C. Geochimica et Cosmochimica Acta, 56(9), 3339-3355.

Winter, T. C., LaBaugh, J. W., & Rosenberry, D. O. (1988). The design and use of a hydraulic potentiomanometer for direct measurement of differences in hydraulic head between groundwater and surface water. Limnology and Oceanography, 33(5), 1209-1214.

Woessner, W. W. (2000). Stream and fluvial plain ground water interactions: rescaling hydrogeologic thought. Groundwater, 38(3), 423-429.

Woessner, W. W. (2017). Hyporheic zones. In Methods in Stream Ecology, Volume 1 (pp. 129-157). Academic Press.

Wolny, F., Marciniak, M., & Kaczmarek, M. (2018). A method for the estimation of dual transmissivities from slug tests. Hydrogeology journal, 26(2).

World Health Organization, WHO. Drinking-water fact sheet. Geneva: WHO; 2017.

Wu, Q., Xian, Y., He, Z., Zhang, Q., Wu, J., Yang, G., & Long, L. (2019). Adsorption characteristics of Pb (II) using biochar derived from spent mushroom substrate. Scientific Reports, 9(1), 1-11.

Wu, R., Podgorski, J., Berg, M., & Polya, D. A. (2021). Geostatistical model of the spatial distribution of arsenic in groundwaters in Gujarat State, India. Environmental geochemistry and health, 43, 2649-2664.

Wu, X., Li, B. & Ma, C., 2018. Assessment of groundwater vulnerability by applying the modified DRASTIC model in Beihai City, China. Environ Sci Pollut Res 25, 12713–12727. https://doi.org/10.1007/s11356-018-1449-9

Xiang, Z., Bailey, R. T., Nozari, S., Husain, Z., Kisekka, I., Sharda, V., & Gowda, P. (2020). DSSAT-MODFLOW: A new modeling framework for exploring groundwater conservation strategies in irrigated areas. Agricultural Water Management, 232, 106033.

Ximenes, M., Duffy, B., Faria, M.J. et al., 2018. Initial observations of water quality indicators in the unconfined shallow aquifer in Dili City, Timor-Leste: suggestions for its management. Environ Earth Sci 77, 711 (2018). https://doi.org/10.1007/s12665-018-7902-8

Xiong, H., Wang, Y., Guo, X., Han, J., Ma, C., & Zhang, X. (2022). Current status and future challenges of groundwater vulnerability assessment: A bibliometric analysis. Journal of Hydrology, 128694.

Xu, P., Feng, W., Qian, H., Zhang, Q., 2019. Hydrogeochemical characterization and irrigation quality assessment of shallow groundwater in the Central-Western Guanzhong Basin, China. Int. J. Environ. Res. Public Health 16, 1492 (2019).

Yadav, L. S., Mishra, B. K., & Kumar, A. (2019). Adsorption of phenol from aqueous solutions by bael furit shell activated carbon: Kinetic, equilibrium, and mass transfer studies. Theoretical Foundations of Chemical Engineering, 53, 122-131.

Yadav, M. K., Saidulu, D., Gupta, A. K., Ghosal, P. S., & Mukherjee, A. (2021). Status and management of arsenic pollution in groundwater: A comprehensive appraisal of recent global scenario, human health

impacts, sustainable field-scale treatment technologies. Journal of Environmental Chemical Engineering, 9(3), 105203.

Yahya, M. D., Aliyu, A. S., Obayomi, K. S., Olugbenga, A. G., & Abdullahi, U. B. (2020). Column adsorption study for the removal of chromium and manganese ions from electroplating wastewater using cashew nutshell adsorbent. Cogent Engineering, 7(1), 1748470.

Yahya, M. D., Obayomi, K. S., Orekoya, B. A., Olugbenga, A. G., & Akoh, B. (2021). Process evaluation study on the removal of Ni (II) and Cu (II) ions from an industrial paint effluent using kola nut pod as an adsorbent. Journal of Dispersion Science and Technology, 43(1), 105-113.

Yang, L., Takkallapally, C., Gabhi, R. S., Jiang, W., Kirk, D. W., & Jia, C. Q. (2022). Wood biochar monolith-based approach to increasing the volumetric energy density of super capacitor. Industrial & Engineering Chemistry Research, 61(23), 7891-7901

Yao R, Yan Y, Wei C, Luo M, Xiao Y and Zhang Y (2022) Hydrochemical Characteristics and Groundwater Quality Assessment Using an Integrated Approach of the PCA, SOM, and Fuzzy c-Means Clustering: A Case Study in the Northern Sichuan Basin. Front. Environ. Sci. 10:907872. doi: 10.3389/fenvs.2022.907872

Yazdani, M., Alidoosti, A., & Zavadskas, E. K. (2011). Risk analysis of critical infrastructures using fuzzy COPRAS. Economic research-Ekonomska istraživanja, 24(4), 27-40.

Yesilnacar, E., and Topal, T., 2005. Landslide susceptibility mapping: a comparison of logistic regression and neural networks methods in a medium scale study, Hendek region (Turkey)Eng. Geol., 2005 (79) (2005), pp. 251-266

Yi, M., Wang, K., Wei, H., Wei, D., Wei, X., Wei, B., ... & Cui, X. (2023). Efficient preparation of red mud-based geopolymer microspheres (RM@ GMs) and adsorption of fluoride ions in wastewater. Journal of Hazardous Materials, 442, 130027.

Yin L, Hu G, Huang, J. et al. (2011) Groundwater-recharge estimation in the Ordos Plateau, China: comparison of methods. Hydrogeol J 19, 1563–1575. https://doi.org/10.1007/s10040-011-0777-3

Yu, H., Wu, Q., Zeng, Y., Zheng, L., Xu, L., Liu, S., Wang, D., 2022. Integrated variable weight model and improved DRASTIC model for groundwater vulnerability assessment in a shallow porous aquifer,Journal of Hydrology, Volume 608,2022,127538,ISSN 0022-1694,https://doi.org/10.1016/j.jhydrol.2022.127538

Yu, L., Porwal, A., Holden, E. J., & Dentith, M. C. (2012). Towards automatic lithological classification from remote sensing data using support vector machines. Computers & Geosciences, 45, 229-239.

Yu, OY., Raichle, B. & Sink, S. Impact of biochar on the water holding capacity of loamy sand soil. Int J Energy Environ Eng 4, 44 (2013). https://doi.org/10.1186/2251-6832-4-44

Yu. H., Wu, Q., Zeng, Y., Zheng, L., Xu, L., Liu, S., Wang, D., 2022. Integrated variable weight model and improved DRASTIC model for groundwater vulnerability assessment in a shallow porous

aquifer,Journal of Hydrology, Volume 608,2022,127538,ISSN 0022-1694,https://doi.org/10.1016/j.jhydrol.2022.127538.

Yuan, X., Zheng, C., 2022. Improved Intuitionistic Fuzzy Entropy and Its Application in the Evaluation of Regional Collaborative Innovation Capability. Sustainability 2022, 14, 3129. https://doi.org/ 10.3390/su14053129

Zare, M., Nikoo, M.R., Nematollahi, B. et al., 2022. Progressive improvement of DRASTICA and SI models for groundwater vulnerability assessment based on evolutionary algorithms. Environ Sci Pollut Res (2022). https://doi.org/10.1007/s11356-022-19620-1

Zareh, M.M., El-Sayed, A.S. & El-Hady, D.M. Biosorption removal of iron from water by Aspergillus niger. npj Clean Water 5, 58 (2022). https://doi.org/10.1038/s41545-022-00201-1

Zavadskas EK, Kaklauskas A (1996) Multiple criteria evaluation of buildings. Vilnius: Technika.

Zavadskas EK, Cavallaro F, Podvezko V, Ubarte I, Kaklauskas A (2017) MCDM assessment of a healthy and safe built environment according to sustainable development principles: a practical neighborhood approach in Vilnius. Sustainability 9(5):702

Zaveri, E., Grogan, D. S., Fisher-Vanden, K., Frolking, S., Lammers, R. B., Wrenn, D. H., ... & Nicholas, R. E. (2016). Invisible water, visible impact: groundwater use and Indian agriculture under climate change. Environmental Research Letters, 11(8), 084005.

Zeilhofer P, Zeilhofer LVAC, Hardoim EL, De Lima ZM, Oliveira CS (2007) GIS Applications for Mapping and Spatial Modeling of Urban-Use Water Quality: A Case Study in District of Cuiabá, Mato Grosso, Brazil. Cad. Saúde Pública 2007, 23, 875–884.

Zektser I S, Everett L G (2004) Groundwater Resources of The World and Their Use UNESCO : Series on Groundwater n.6.

Zeng S, Liu Z, Kaufmann G (2019) Sensitivity of the global carbonate weathering carbon-sink flux to climate and land-use changes. Nat Commun 10, 5749 (2019). https://doi.org/10.1038/s41467-019-13772-4

Zhang X (2015) Conjunctive surface water and groundwater management under climate change. Frontiers in Environmental Science, 3. doi:10.3389/fenvs.2015.00059

Zhang, G., Hu, W., Cao, D., Zhang, Z., Huang, Q., Chen, Z., & Blaabjerg, F. (2022). A multi-agent deep reinforcement learning approach enabled distributed energy management schedule for the coordinate control of multi-energy hub with gas, electricity, and freshwater. Energy Conversion and Management, 255, 115340.

Zhang, H., Li, R., & Zhang, Z. (2022b). A versatile EDTA and chitosan bi-functionalized magnetic bamboo biochar for simultaneous removal of methyl orange and heavy metals from complex wastewater. Environmental Pollution, 293, 118517.

Zhang, M., Lin, K., Li, X., Wu, L., Yu, J., Cao, S., & Ok, Y. S. (2022a). Removal of phosphate from water by paper mill sludge biochar. Environmental Pollution, 293, 118521.

Zhang, P., Duan, W., Peng, H., Pan, B., & Xing, B. (2021). Functional biochar and its balanced design. ACS Environmental Au, 2(2), 115-127.

Zhang, Y., Liu, S., Cheng, F., Shen, Z., 2018a. WetSpass-Based Study of the Effects of Urbanization on the Water Balance Components at Regional and Quadrat Scales in Beijing, China. Water. 2018; 10(1):5. https://doi.org/10.3390/w10010005

Zhang, Y., Wu, J., Xu, B.2018b. Human health risk assessment of groundwater nitrogen pollution in Jinghui canal irrigation area of the loess region, northwest China. Environ. Earth Sci. 77, 1–12 (2018).

Zhang, Z., Huang, G., Zhang, P., Shen, J., Wang, S., & Li, Y. (2023). Development of iron-based biochar for enhancing nitrate adsorption: Effects of specific surface area, electrostatic force, and functional groups. Science of The Total Environment, 856, 159037.

Zhang, Z., Li, M., Si, B., & Feng, H. (2018). Deep rooted apple trees decrease groundwater recharge in the highland region of the Loess Plateau, China. Science of the Total Environment, 622, 584-593.

Zhong, X., Chen, C., Yan, K., Zhong, S., Wang, R., & Xu, Z. (2022). Efficient coagulation removal of fluoride using lanthanum salts: distribution and chemical behavior of fluorine. Frontiers in Chemistry, 10, 859969.

Zhou, K., Diehl, E., Tang, J., 2022. Deep convolutional generative adversarial network with semi-supervised learning enabled physics elucidation for extended gear fault diagnosis under data limitations, Mechanical Systems and Signal Processing, 185, 109772,ISSN 0888-3270,https://doi.org/10.1016/j.ymssp.2022.109772.

Zhou, Q., Wang, W., Shuang, C., Wang, M., Ma, Y., & Li, A. (2014). Reusable magnetic microspheres for efficient removal of atrazine in aqueous media. Chemical Engineering Journal, 253, 190-197.

Zhuo, L., Pute, W., Hao, F., et al. (2009). Simulation experiment on the effect of bulk density on soil water infiltration capacity. Journal of Agricultural Engineering, 2009, 25(6):40-45. DOI:10.3969/j.issn.1002 -6819.2009.06.007.

Zongji, Y., Jianping, Q., Xiaogang, Z., 2010. Regional landslide zonation based on entropy method in Three Gorgesarea, China. In Proceedings of the Fuzzy Systems and Knowledge Discovery (FSKD), Yantai, China,10–12 August 2010; pp. 1336–1339

Zubair M, Asif Iqbal M, Shil A, Haque E, Moshiul Hoque M, Sarker I H (2021) An Efficient K-Means Clustering Algorithm for Analysing COVID-19. In: Abraham A., Hanne T., Castillo O., Gandhi N., Nogueira Rios T., Hong TP. (eds) Hybrid Intelligent Systems. HIS 2020. Advances in Intelligent Systems and Computing, vol 1375. Springer, Cham. https://doi.org/10.1007/978-3-030-73050-5_43

ANNEXURE

Commonwealth Scholarship Commission in the UK

Woburn House
20-24 Tavistock Square
London WC1H 9HF
United Kingdom

T +44 (0) 207 380 6700
F +44 (0) 207 387 2655

cscuk.fcdo.gov.uk

17 April 2023
Our Reference: INCN-2021-67

To Whom It May Concern

Confirmation of Commonwealth Scholarship

According to our records Sudipa Halder held a Commonwealth Split-site Scholarship to complete a PhD at the University of Manchester from March 2022 to March 2023. During the period of the award, a monthly stipend was paid to Scholars at the rate of £ £1,133. The Commission also paid part of the tuition fees to the University of Manchester at the overseas rate for her one year of study.

The UK Commonwealth Scholarship Commission manages the UK's contribution to the Commonwealth Scholarship and Fellowship Plan (CSFP) which is an international programme under which member governments offer scholarships and fellowships to citizens of other Commonwealth countries. The CSFP is one of the largest and most prestigious scholarships schemes for international study in the world. Since it was established in 1959, over 30,000 individuals have benefited. The UK Commonwealth Scholarship Commission awards over 800 scholarships and fellowships for postgraduate study and professional development to Commonwealth citizens each year.

The UK Commonwealth Scholarship Commission aims to contribute to the UK's international development aims and wider overseas interests, support excellence in UK higher education, and sustain the principles of the Commonwealth. We select candidates on the basis of merit and their potential to contribute to the development needs of their home countries. Candidates complete a rigorous and highly competitive selection process. UK Commonwealth Scholarships are funded by the Foreign, Commonwealth & Development Office (FCDO) in conjunction with UK Universities.

I hope this letter provides you with the information you need but please contact the Commission if you have any further questions.

Yours sincerely

K S Scott

Kirsty Scott, Alumni Relations Manager

Environmental Science and Pollution Research
https://doi.org/10.1007/s11356-023-28885-z

RESEARCH ARTICLE

Understanding the exchange process between ground and surface water using mini drive point piezometer and mathematical models to identify suitable managed aquifer recharge sites

Sudipa Halder[1,2] · Malabika Biswas Roy[3] · Pankaj Kumar Roy[1]

Received: 11 April 2023 / Accepted: 16 July 2023
© The Author(s), under exclusive licence to Springer-Verlag GmbH Germany, part of Springer Nature 2023

Abstract
In the current study, subsurface characteristics within the complex formation of the Shilabati basin system of West Bengal, India, extending over an area of 3888 km^2, have been estimated using a cost-effective piezometer and MIKE FEFLOW package based on a steady-state numerical model. Pore size and fine particle content of streambeds are affected by two opposing flow contraptions. Such opposite flow conditions are likely to affect the hydraulic conductivity of the streambed. However, analogies of the hydraulic conductivity (K_h) of streambeds for losing and gaining streams have not been well documented in the recent past. The K_h value from the piezometer has been highest at the Dakshin Pairachali site (6.765 m/day), with the stream gaining water from the discharge of the local aquifer. Analysis of the stream-aquifer interaction using the FEFLOW model has allowed us to understand the groundwater water head of the basin ranging from 160.33 to 0.32 m.a.s.l (meters above sea level). The present study also constitutes the first attempt for the identification of suitable sites for the implementation of managed aquifer recharge (MAR) technology in West Bengal, India, to manage extreme drought events. The suitable sites have been identified by means of three fuzzy multi-criteria decision analysis based on nine criteria: river discharge, moisture content, porosity, drainage type, rainfall, land use type, geology, aquifer material, and hydraulic conductivity. To design a radial collector well and infiltration gallery for the selected site in an anisotropic, homogeneous, unconfined, and semi-infinite aquifer near a fully penetrating stream, a pumping test has been conducted to optimize a safe yield of 12.096 MLD (megaliters per day).

Keywords Hydraulic conductivity · Mini drive point piezometer · MIKE FEFLOW · Fuzzy TOPSIS · Fuzzy COPRAS

Introduction

Groundwater is the main source of fresh water in arid and semi-arid areas due to a lack of surface water resources (Swain et al. 2022). Climate change will intensify the existing variability in surface water resources in sub-tropical and humid regions, resulting in increased groundwater use as communities try to meet growing freshwater demands. Thus, aquifers across the globe are being overexploited due to increasing water demand with an imbalance between the extraction and the replenishment of the groundwater. In arid and semi-arid regions, precipitation is highly variable and erratic, which leads to low groundwater recharge rates and high surface runoff. If sufficient water storage systems are not installed, excess water will flow through the atmosphere as evapotranspiration and as surface runoff (Alkhatib et al. 2021; Collins et al. 2013). Over the last century, land use changes and riverbed disturbance caused by sand mining have increased global runoff by 0.08 mm/year^2 and accounted for 50% of the upward trend (Piao et al. 2007). Water resources may also be under great pressure due to an increase in evaporation caused by increased temperature (Moratiel et al. 2011). Over land and ocean, the surface temperature of 2021 has been 1.51 °F (0.84 °C)

Responsible Editor: Marcus Schulz

✉ Pankaj Kumar Roy
pankaj.kroy@jadavpuruniversity.in

[1] School of Water Resources Engineering, Jadavpur University, Kolkata, West Bengal, India

[2] Department of Mechanical, Aerospace and Civil Engineering, University of Manchester, Manchester, United Kingdom

[3] Department of Geography, Women's College, Kolkata, West Bengal, India

Published online: 26 July 2023

Catena 229 (2023) 107206

Contents lists available at ScienceDirect

Catena

journal homepage: www.elsevier.com/locate/catena

Groundwater vulnerability assessment for drinking water suitability using Fuzzy Shannon Entropy model in a semi-arid river basin

Sudipa Halder [a,b], Malabika Biswas Roy [c], Pankaj Kumar Roy [a,*], Majid Sedighi [b]

[a] School of Water Resources Engineering, Jadavpur University, Kolkata, West Bengal, India
[b] Department of Mechanical, Aerospace and Civil Engineering, University of Manchester, Manchester, United Kingdom
[c] Department of Geography, Women's College, Calcutta, Kolkata, West Bengal, India

ARTICLE INFO

Keywords:
Groundwater
Fuzzy Logic
Water Quality Index
Hydraulic Conductivity
Specific yield
MCDM

ABSTRACT

Groundwater protection against geogenic and anthropogenic diffuse pollutants are of preeminent importance for convoying groundwater-dependent hydro-aquatic ecosystems and safeguarding human health by securing a safe and sustainable water security plan. Mapping groundwater vulnerability to pollution represents a topical area of research where traditional models suffer from inherent prejudices. A novel approach to identify groundwater vulnerable zones is thus presented in this study by combining Fuzzy Shannon Entropy (FSE) with a decision support algorithm to replace DRASTIC, GOD and other related methods. We proposed a contemporary "FSE-GVI" framework for assessing aquifer vulnerability, which for the first time expands and redesigns the seven original geological and hydrogeological parameters with geochemical and anthropogenic factors. Applying such technique weights of 13 geo-environmental and hydrogeological factors (slope, soil, pH, recharge), and anthropogenic factors (land use land cover, population density, groundwater based schemes for irrigation) has been optimized. The computed map has been categorized into very high (10.82%), high (23.20%), moderate (29.29%), low (25.02%) and very low (11.64%).The groundwater of the river basin is rated on a scale of excellent, good, poor, very poor and unfit for consumption. The model is compared to 74 groundwater quality data, and the findings demonstrate an excellent correlation between water quality index ($r = 0.84$), Total dissolve solids (70%), iron (72%), hardness (85%) and alkalinity levels (75%).The findings of the research reveals 27.3 % of the sampling sites (villages) under poor water quality and 23.21% of very high vulnerable zone which requires competent planning, development, managerial technique to safeguard groundwater resources.

1. Introduction

The concept of groundwater management refers to a broad range of activities that include the prevention of contamination of groundwater (Li & Wang, 2022; Pandey et al. 2020). To develop useful strategies to protect groundwater contamination, vulnerability identification is the first important step. Idea of groundwater vulnerability has been dealt with by many authors (Aller et al. 1985; Oroji, 2019; Novinpour et al. 2022) across the different climatic regions of the world namely humid tropical regions (Nugraha et al. 2021; Saravanan et al. 2020), sub-tropical region (Tomer et al. 2019), arid and semi-arid region (Pourkhosravani et al. 2021) Mediterranean region (Vrouhakis et al. 2022) and in the temperate region (Oke and Fourie, 2017). Scientists and managers have implemented such techniques in different hydro-geocritical zones, including coastal tracts (Bordbar et al., 2019b), alluvial zones (Fusco et al. 2020), hard rock terrains (Kumar and Krishna, 2018), and karstic aquifers (Hamdan et al. 2016). The factors that determine the vertical and horizontal transport of contaminants, such as the area of recharge, slope, soil texture, soil structure, soil depth, geology, flow rate, hydraulic conductivity, unscientific pumping from shallow aquifers, and poor land-use practices, which need to be assessed in order to prevent further degradation of water quality. A variety of natural pollutants can be transported through sedimentary soil and rock, including fluoride, arsenate, nitrate, iron, etc. The effects depend on their concentration and human interference (Sharma and Bhattacharya, 2017). Thereby it is necessary to differentiate protection zones from vulnerability using different colors so that they can be easily categorized and interpreted (Meerkhan et al. 2022). As a result of various scale

* Corresponding author.
E-mail addresses: shalder.swre.rs@jadavpuruniversity.in (S. Halder), malabikabiswasroy@gmail.com (M.B. Roy), pankaj.kroy@jadavpuruniversity.in (P.K. Roy), majid.sedighi@manchester.ac.uk (M. Sedighi).

https://doi.org/10.1016/j.catena.2023.107206
Received 27 October 2022; Received in revised form 15 February 2023; Accepted 3 May 2023
Available online 16 May 2023
0341-8162/© 2023 Elsevier B.V. All rights reserved.

Environmental Science and Pollution Research (2023) 30:57529–57557
https://doi.org/10.1007/s11356-023-26394-7

RESEARCH ARTICLE

Application of fuzzy C-means clustering and fuzzy EDAS to assess groundwater irrigation suitability and prioritization for agricultural development in a complex hydrogeological basin

Sudipa Halder[1,2] · Shuvoshri Bhattacharya[3] · Malabika Biswas Roy[4] · Pankaj Kumar Roy[1]

Received: 4 October 2022 / Accepted: 7 March 2023 / Published online: 25 March 2023
© The Author(s), under exclusive licence to Springer-Verlag GmbH Germany, part of Springer Nature 2023

Abstract

The current research is focused on detecting a river basin suitable for agriculture and priority for management using a new clustering tool of groundwater quality with fuzzy logic technique in R and Geographical Information System. A new fuzzy clustering-soft computing technique has been executed to determine the different hydrochemical zones considering 13 essential parameters such as electrical conductivity, hardness, chloride, sodium adsorption ratio, residual sodium carbonate, soluble sodium percent, magnesium hazard, permeability index, potential salinity, residual sodium bicarbonate, Kelly's ratio, synthetic harmful coefficient, and exchangeable sodium percentage. The derived fuzzy C-mean clustering (FCM) outperformed other available hard computing techniques like hierarchical clustering, K-means clustering, and agglomerative clustering. It divided the sampling sites into 2 clustering groups (FCM I and FCM II) which has been validated using fuzzy silhouette index (0.85), the partition coefficient (0.76), the partial entropy (0.68), and the modified partition coefficient (0.52). The hydrogeochemical analysis confirmed that the rock-water interaction, chemical weathering, and ion exchange process are predominant in the aquifer system of the study area. According to the correlation plots, the studied groundwater samples largely evolved from $Ca^{2+} - HCO_3^-$, mixed $Ca^{2+} - Mg^{2+} - Cl^-$ types, and $HCO_3^- - Ca^{2+}$ types. The spatial distribution map and the hydrochemical analysis also gives a clear depiction of the fluoride (> 1.0 mg/l) and high iron (> 0.3 mg/l) contamination in groundwater quality, making it unsuitable for both drinking and irrigation. A fuzzy EDAS priority map has been prepared based on all the irrigation suitability parameters which concludes that the groundwater at the upstream and downstream section of the basin requires the most attention. Based on the highest priority for management, five zones have been delineated: very high (5.98%), high (22.31%), medium (16.39%), low (32.30%), and very low (23.02). The findings of this study will be beneficial to planners and policymakers as they can develop schemes to solve similar problems across the country.

Keywords Hydro-geochemical analysis · Fuzzy C-means clustering · Fuzzy EDAS · Geographical information system (GIS) · Piper diagram · Shilabati river basin

Responsible Editor: Xianliang Yi

✉ Pankaj Kumar Roy
Pankaj.kroy@jadavpuruniversity.in

Sudipa Halder
sudipa.halder92@gmail.com

Shuvoshri Bhattacharya
shuvoshri.bhattacharya@gmail.com

Malabika Biswas Roy
malabikabiswasroy@gmail.com

[1] School of Water Resources Engineering, Jadavpur University, Kolkata, West Bengal, India

[2] Department of Mechanical, Aerospace and Civil Engineering, University of Manchester, Manchester, UK

[3] ISGP Program II, Panchayat and Rural Development Department, Government of West Bengal, Kolkata, India

[4] Department of Geography, Women's College, Calcutta, Kolkata, West Bengal, India

Journal of Water Process Engineering 53 (2023) 103698

Contents lists available at ScienceDirect

Journal of Water Process Engineering

journal homepage: www.elsevier.com/locate/jwpe

Enhanced fluoride removal from groundwater using red and white kaolinite lithomarge to develop a low cost eco-friendly defluoridation unit in rural areas of Shilabati river basin, West Bengal

Sudipa Halder [a,b], Pratik Maiti [a], Sayak Karmakar [a], Malabika Biswas Roy [c], Pankaj Kumar Roy [a,*]

[a] School of Water Resources Engineering, Jadavpur University, Kolkata, India
[b] Department of Mechanical, Aerospace and Civil Engineering, University of Manchester, United Kingdom of Great Britain and Northern Ireland
[c] Department of Geography, Women's College, Calcutta, Kolkata, India

ARTICLE INFO

Keywords:
Fixed bed column
Kaolinite lithomarge
Alpha hexagonal Al_2O_3
Alpha trigonal SiO_2
Natural adsorbent

ABSTRACT

Fluoride is an anionic pollutant found in high concentrations (>2 mg/l) in the Shilabati river basin of West Bengal, India, which has reported numerous serious cases of skeletal fluorosis and bone deformation in recent years. This study investigated fluoride adsorption on kaolinite lithomarge (red and white laterite) from Paschim Medinapore (West Bengal, India), exploring both kinetic and equilibrium facets with a series of batch tests and a fixed bed column study using natural water. Based on the X-ray Powder Diffraction analysis, Alpha SiO_2 with trigonal structure and Alpha Al_2O_3 with hexagonal structure of this natural adsorbent played a critical role in fluoride absorption mechanism. Experimental results showed that based on pH values relevant to the fluoride enriched groundwater, kaolinite lithomarge of red type was the most efficient having an effective removal efficiency (98.32 %) at pH 6.58 whereas the white type demonstrated the highest removal efficacy of 95.31 % at pH 6.51. The modelled breakthrough curves were obtained, and they were in good accordance with the corresponding experimental data. Finally, water samples were collected from 11 sites from the fluoride contaminated zone within the river basin and natural groundwater was filtered using kaolinite lithomarge of red type obtaining a removal capacity of 97.13 % within 30 min, for the initial concentration of 2.37 mg/l. The prototype tested in the laboratory showed promising contaminant removal as a low-cost, time saving, natural filtration option supplying a liter of fluoride free water for 0.0015 USD.

1. Introduction

The quest for clean water continues to grow substantially as a result of an increasing population combined with urbanization and industrialization. Besides arsenic, nitrate, and phosphate, fluoride is another toxic chemical linked to large-scale health issues through widespread drinking and irrigation water revelations [1]. The element fluorine makes up approximately 0.3 g per kilogram of the Earth's crust and can be found as fluoride in a number of rocks and minerals [2]. The key minerals, e.g. topaz, luorite, cryolite, sellaite, amphiboles, apatite, villiaumite, mica, and few clays, and their analogous host rocks such as granite, shale and syenite, can emancipate fluoride into groundwater [3]. The fluoride mostly occurs as fluorspar (CaF_2), sellaite (MgF_2), fluorapatite [$3Ca_3$ $(PO_4)_2$ Ca (F, Cl_2)] and cryolite (Na_3AlF_6) [4,5] Fluorspar and cryolite, which are both insoluble in water, are found in sedimentary and igneous rocks respectively [6]. At low levels (<1 mg/l), the Fluoride is essential for human health, particularly for the development of teeth and bone. However, fluoride concentrations above 1.5 mg/l in drinking water are not permitted by the World Health Organization (WHO), as it leads to severe dental and skeletal disorders [7]. Fluoride is associated with a number of detrimental effects, including arthritis, osteoporosis, bone fragility, cancer, thyroid disease, Alzheimer's disease, and infertility in women. Increasing fluoride levels in the body can also inhibit the metabolism of lipids, carbohydrates, and vitamins [8]. There are several ways in which fluoride enters the body, including mouthwash consumption, air, food, toothpaste, and potable water [9]. It is unfortunate that water can be polluted with fluoride simultaneously by inorganic and organic substances [10,11]. Groundwater contamination by fluoride due to natural processes or human activity has been recognized as a serious problem in many parts of the

* Corresponding author.
E-mail addresses: sudipa.halder@postgrad.manchester.ac.uk (S. Halder), pankaj.kroy@jadavpuruniversity.in (P.K. Roy).

https://doi.org/10.1016/j.jwpe.2023.103698
Received 23 December 2022; Received in revised form 21 March 2023; Accepted 28 March 2023
Available online 14 April 2023
2214-7144/© 2023 Elsevier Ltd. All rights reserved.

Bulletin of the National Research Centre

REVIEW

Open Access

Assessment of wetland potential and bibliometric review: a critical analysis of the Ramsar sites of India

Malabika Biswas Roy[1*], Swetasree Nag[2], Sudipa Halder[2] and Pankaj Kumar Roy[2]

Abstract

Background: This study focussed on effective bibliometric analysis of research on Ramsar sites in India within the last 30 years using VOS viewer software. The study focused on the estimation of the current areal extent and meteorological impact on wetland together with bibliometric analysis. The online data source of Web of Science has been used to extract all the relevant documents on Indian Ramsar sites published within a period of 1989 to 2020.

Main body: The main objective is to analyze the trend of research on the Indian Ramsar site both qualitatively and quantitatively. The peak of research growth has been lifted after the twentieth century as most of the Indian water bodies have been designated or put into the land from this period. A geographical location-based mapping was prepared based on the number of publications during the study period to observe the growing research interest in wetland studies in India. The highest publications have been documented on East Calcutta Wetland located in West Bengal followed by Loktak Lake in Manipur, Deepor Beel in Assam and others. The most frequently used keywords were "Ramsar site", "India", "wetland", "wetlands", "remote sensing" etc. India published most of the documents on wetland studies in the Indian context. England, Australia, Canada also had various international collaborative works with Indian researchers.

Conclusions: The research output shows an upward research trend on Indian Ramsar sites both quantitative and qualitatively. Such kind of research can provide a panoramic view towards the worldwide research trend and help to generate further effective approaches for the betterment of our environment.

Keywords: Ramsar sites, Bibliometric analysis, Web of Science, VOSviewer, Research trend

Background

Wetlands are considered as a unique ecological unit, which contributes enormous goods and services to human society (Prasad et al. 2002). It also consists of rich biodiversity and states, as the most valuable natural resource on the earth (Whitehouse et al. 2008). They are the invaluable resources of the environment, resource potential ecology and biodiversity in India (Biswas Roy et al. 2016). Globally the areal extent of wetlands accounts for about 12.1 million km^2 showing diverse characteristics in its geographical locations, dominant species, soil–water chemistry etc. Such productive natural resources can also be well utilised by several landless people of rural India, where pisciculture activity is very dominant (Biswas Roy et al. 2016). Not only that, several other environmental benefits like flood management, groundwater recharge, water supply, irrigational activities are also well practiced in wetland areas. In this regard to gain international importance Ramsar Convention on wetlands has been signed in the year of 1971 to conserve and augment the ecological functions of wetlands. In India, only 37 wetlands are designated as Ramsar sites (MoEFCC 2020). Environmental education and awareness is required to

*Correspondence: malabikabiswasroy@gmail.com
[1] Department of Geography, Women's College, Calcutta, Kolkata, West Bengal, India
Full list of author information is available at the end of the article

© The Author(s) 2022. **Open Access** This article is licensed under a Creative Commons Attribution 4.0 International License, which permits use, sharing, adaptation, distribution and reproduction in any medium or format, as long as you give appropriate credit to the original author(s) and the source, provide a link to the Creative Commons licence, and indicate if changes were made. The images or other third party material in this article are included in the article's Creative Commons licence, unless indicated otherwise in a credit line to the material. If material is not included in the article's Creative Commons licence and your intended use is not permitted by statutory regulation or exceeds the permitted use, you will need to obtain permission directly from the copyright holder. To view a copy of this licence, visit http://creativecommons.org/licenses/by/4.0/.

Modeling Earth Systems and Environment (2022) 8:5565–5584
https://doi.org/10.1007/s40808-022-01392-9

ORIGINAL ARTICLE

Modelling groundwater potential zone using fuzzy logic and geospatial technology of an deltaic island

Pankaj Kumar Roy[1] · Saurabh Kumar Basak[1] · Sk Mohinuddin[1] · Malabika Biswas Roy[2] · Sudipa Halder[1] · Tuhin Ghosh[3]

Received: 1 January 2022 / Accepted: 1 April 2022 / Published online: 23 April 2022
© The Author(s), under exclusive licence to Springer Nature Switzerland AG 2022

Abstract

Increasing urbanization and growth of population have increased the demand for various water resources especially the groundwater resources in Sagar Island, South 24 Parganas, West Bengal, India. Thus Groundwater resources should be managed properly with the application of various scientific propositions and modern techniques. In this research, identification of groundwater potential zonation (GWPZ) has been done using remote sensing–geographic information system (RS–GIS) technology and Fuzzy-AHP approach on a single platform. The main objective of the research is to use the Fuzzy-AHP approach to demarcate GWPZs utilizing 10 geo-environmental parameters. The study successfully identifies the GWPZs within the area of interest and categorizes GWPZs has been classified into five different classes following the groundwater availability that is very high potential 6.84%), high (36.23%), medium (27.68%), low (17.53%) and very low (11.72%). The originated GWPZ map has been verified using geophysical data collected from the field survey to test the model's performance. The validation results demonstrated that the applied technique yields considerably reliable findings that can aid in long-term planning and management for sustainable use of groundwater resources in different coastal tracts.

Keywords Groundwater potential zone · Fuzzy-analytical hierarchy process · Remote sensing · Geographic information system

Introduction

In India Groundwater is a vital resource that provides water to communities and industries. It is used for the preservation of the environment and human well-being (IPCC 2001; Arefin 2020). The steady growth in groundwater consumption has little or no regard for the environment's balance (Zhang et al. 2019; Nhamo et al. 2020). Around 44% of the world's groundwater is used for domestic and agricultural applications, and 27% for industrial use. In India, it is used for irrigation and drinking water (Patra et al. 2018a, b). It is also used for drinking water and irrigation. Around 90% of the groundwater in India is used for agricultural irrigation, including Sagar Island (Schneider 2018). Furthermore, groundwater use in this deltaic island gets incremented in recent years as a result of expanding socioeconomic change. Unfortunately, a lack of groundwater has posed a threat to the residents of this region (Gayen and Zaman 2013). As a result, identifying and assessing critical parameters is essential for determining groundwater potential (Patra et al. 2018a, b). Furthermore, as a result of industrial expansion

✉ Pankaj Kumar Roy
pk1roy2014@gmail.com

Saurabh Kumar Basak
skbasak200@gmail.com

Sk Mohinuddin
mohinuddintom@gmail.com

Malabika Biswas Roy
malabikabiswasroy@gmail.com

Sudipa Halder
sudipa.halder92@gmail.com

Tuhin Ghosh
tuhin.ghosh@jadavpuruniversity.in

1 School of Water Resources Engineering, Jadavpur University, Kolkata 700 032, India

2 Women's College, Calcutta, Kolkata 700 003, India

3 School of Oceanographic Studies, Jadavpur University, Kolkata 700 032, India

Theoretical and Applied Climatology (2022) 150:425–452
https://doi.org/10.1007/s00704-022-04165-7

ORIGINAL PAPER

Modelling drought vulnerability tracts under changed climate scenario using fuzzy DEMATEL and GIS techniques

Sudipa Halder[1,2] · Malabika Biswas Roy[3] · Pankaj Kumar Roy[1]

Received: 5 February 2022 / Accepted: 30 July 2022 / Published online: 11 August 2022
© The Author(s), under exclusive licence to Springer-Verlag GmbH Austria, part of Springer Nature 2022

Abstract

The present study identifies drought risk zones in a river basin by analysing Landsat images from three selected precipitation deficit years (2000, 2009 & 2018). A set of seven parameters including standard precipitation index (SPI), long-term temperature condition index (TCI), long-term vegetation condition index (VCI), vegetation health index (VHI), long-term soil moisture index (SMI), long-term soil adjusted vegetation index (SAVI) and long-term normalised difference water index (NDWI) has been assessed, and drought risk zones have been identified using the fuzzy DEMATEL model to classify the causative and effective groups better represented through the causal diagram. A summary of the results shows that VHI, SPI, and TCI are the three most influential indicators of drought. A yield anomaly index (YAI) has been calculated for validation and the cropping pattern has been mapped.

1 Introduction

One of the predominant global crisis in due respect to climate change consequences is drought. It poses serious challenges to our water and food security, as well as the financial and economic setup of the developing world. Drought can be classified into four categories as recommended by America Meteorological Society which includes meteorological drought, agricultural drought, socio-economic drought, and hydrological drought (Huang et al. 2020) which has an adverse effect on socio-economic spheres (Singh et al. 2021). Drought is the inevitable consequence of climate change inclusive of precipitation and temperature variability at an extreme stage. Dearth of precipitation events over a long period is the foremost cause of occurrence of the drought (Dalezios et al. 2013).

✉ Malabika Biswas Roy
malabikabiswasroy@gmail.com

Sudipa Halder
sudipa.halder92@gmail.com

Pankaj Kumar Roy
pankaj.kroy@jadavpuruniversity.in

[1] School of Water Resources Engineering, Jadavpur University, Kolkata-32, India

[2] Department of Mechanical, Aerospace and Civil Engineering, University of Manchester, Manchester, England

[3] Department of Geography, Women's College, Calcutta, Kolkata 700003, India

There is a direct connection between meteorological drought, hydrological drought, and agricultural drought; imbalances in one have an impact on the other. Consequences of drought are diverse in nature and damage cost is hard to estimate (Jovanovic et al. 2013). Due to poor rainfall over a period, agricultural regions in arid or semi-arid regions are mainly affected by the vicious cycle of drought, which reduces soil moisture conditions. Drought modulates the soil moisture condition as soil wetness controls the lateral and sensible heat flux on the earth surface leading to the initiation and maintenance of convection (Dr T. Mavromatis 2010). Incapability of land discourages cultivation and creates serve and hostile environmental situation towards plants, animals, livestock potential, and biomass potential which ultimately dismantle the economic, financial, and food security of human being (Silvestri et al. 2012). At a global scale, one-fifth of the damages caused by natural events is mainly drought which estimates an expense of around USD 80 billion per year (White 2003; Carlowicz 1996). According to IPCC report of 2007, an increase of temperature by 2 to 3 °C will disrupt the crop and livestock productivity in the tropical areas as consequences of desertification and affected area will be Asia, Sub-Saharan Africa, and Latin American countries (FAO 2017). Climate change together with ongoing unrestrainable anthropogenic activities has been ruling out the drought like condition particularly in the south western and southern parts of Asia. It was estimated that 42% of the land area under the Indian continent has suffered severe drought in the year 2019 and was

COMPREHENSIVE ASSESSMENT OF META-ANALYSIS AND CONTINGENT VALUATION TECHNIQUE FOR SUSTAINABLE MANAGEMENT OF WETLAND OF MIDDLE GANGA PLAIN

Malabika Biswas Roy [1], Abhishek Kumar [2], Debanjana Chatterjee [3], Sudipa Halder [4]

[1] Department of Geography, Women's College, Kolkata, India
[2] Ballia Water Research and Social Welfare Trust, Ballia, Uttar Pradesh, India
[3] School of Water Resources Engineering, Jadavpur University, Kolkata, India
[4] Badamtala High School, Budge Budge, Kolkata, India

Manuscript received: August 19, 2021
Revised version: January 17, 2022

Biswas Roy M., Kumar A., Chatterjee D., Halder S., 2022. Comprehensive assessment of meta-analysis and contingent valuation technique for sustainable management of wetland of Middle Ganga Plain. *Quaestiones Geographicae* 41(2), Bogucki Wydawnictwo Naukowe, Poznań, pp. 153–165. 3 figs, 11 tables.

Abstract: In this study, the functions and threats of Suraha Tal Wetland are identified by the stated preference method and weightage is given according to their rank. The objective of the study is to determine the total economic value of Suraha Tal Wetland. The direct value can be drawn from the market price and from a survey of the stakeholders. Suraha Tal Wetland is also famous for the presence of the Jai Prakash Narayan Birds Sanctuary, which makes it a biodiversity-enriched area. The indirect value has been drawn from a review of the literature on Suraha Tal Wetland and the relevance of this literature is justified through the comprehensive meta-analysis (CMA) software. The total valuation of the wetland has been calculated. The paper concludes with suggestions for a few management strategies for better wetland management.

Keywords: Suraha Tal Wetland, comprehensive meta-analysis, total economic valuation, wetland valuation

Corresponding author: Malabika Biswas Roy, Department of Geography, Women's College, Calcutta, P-29, Khirode Vidyavinode Ave, Baghbazar, Kolkata, West Bengal 700003, India; e-mail: malabikabiswasroy@gmail.com

Introduction

Wetlands occupy 6% of the world's surface area. They provide numerous services and goods not only to the local people but also to those who live in far-off areas (Costanza et al. 1997). To the general public, however, the term 'value' is often associated with principles and ethics. Valuation is the process of determining the current worth of things, objects or assets (Report on Wetland Valuation, 2003). Wetlands can be evaluated in different ways such as the valuation of ecosystem services, recreational value, values of wetland function, economic value and biological value (Biswas et al. 2021).

In environmental economics, the 'total economic valuation' (TEV) is a way to estimate the economic value of the environment. TEV comprises use and non-use values. A use value is further classified as (i) a direct use value and (ii) indirect use value. The non-use value includes (i) an option value, (ii) quasi-option value and (iii) existence value (Freeman 1993; Vao et al. 2012; Biswas et al. 2015; Venkatachalam, Jayanthi 2016).

© 2022 Author(s)
This is an open access article distributed under the Creative Commons Attribution license

sciendo
https://doi.org/10.2478/quageo-2022-0015

Arabian Journal of Geosciences (2021) 14: 2187
https://doi.org/10.1007/s12517-021-08496-z

ORIGINAL PAPER

Tropical plateau basin prioritisation for sustainable groundwater management using classical algorithms

Sudipa Halder[1] · **Malabika Biswas Roy**[2] · **Pankaj Kumar Roy**[1]

Received: 22 December 2020 / Accepted: 20 September 2021 / Published online: 21 October 2021
© Saudi Society for Geosciences 2021

Abstract

Groundwater crisis is playing a serious concern in the Shilabati river basin located in a tropical plateau fringe region of the south eastern part of West Bengal, India. The river rises from the geological structure of Chotonagpur gneissic complex where groundwater recharge is very poor and is affected by yearly drought scenarios with a prolonged shortage of water supply. The present research is to address this issue through a number of statistical techniques and multicriteria decision-making approaches (MCDM). To accomplish the research objectives, morphometric attributes of 9 sub-watersheds of Shilabati river basin having a total area of 3881 km^2 have been estimated. Principle component analysis (PCA) has been used to group these attributes into three components and K-means clustering categorised the sub-watershed into 3 cluster based on morphometric asymmetry. Basin prioritisation based on recharge and infiltration capacity using three MCDM techniques like Technique for Order of Preference by Similarity to Ideal Solution (TOPSIS), Complex Proportional Assessment (COPRAS) and VlseKriterijumska Optimizacija I Kompromisno Resenje (VIKOR) ranked the sub-watersheds where TOPSIS has been selected as the best model using spearman rank correlation coefficient test. According to the TOPSIS model, Donai sub-watershed ranked 1st and proved greater amplitude in recharging its aquifer where the yield capacity of wells ranges from 200 to 400 LPM (litre per minute). The sub-watersheds like Betal and Joypanda need sustainable management at the prior level as validated by groundwater yield data where the yield capacity of wells ranges from 10 to 100 LPM. The methodology is proficient enough for the decision-makers to execute groundwater management and planning strategies substantially.

Keywords Principle component analysis · TOPSIS · K-means clustering · Infiltration capacity · Groundwater yield

Introduction

Water scarcity is now one of the major issues at a global level largely driven by the enormous growth of the human population and exaggerated by impact of climate change through precipitation and temperature alterations. Drying of the river and water bodies is due to the increase in the magnitude and intensity of temperature anomalies which has become quite evident. The global temperature rose by 0.85 °C from 1800 to 2012 which may further trend to increase accelerating the current situation (Li et al. 2015). Besides the climatic impacts, geology, relief, geomorphic attributes, structural symmetry, etc. are the foremost dominant factors controlling the water ecosystem at a basin scale (Mesa 2006). To address numerous hydrological, hydrogeological and hydro-morphological scenarios acting within a basin requires a watershed management plan and strategies. Watershed is also a biophysical response unit as well as holistic ecosystem that highlights the material, information and energy flow through it (Wang et al. 2016). A watershed is a topographically demarcated area drained by a network of streams namely a river system. It is mainly the total area scaling from the originating point of a stream up to its mouth or draining point. Watersheds are the main source of navigation, drinking water supply,

Responsible Editor: Broder J. Merkel

✉ Malabika Biswas Roy
malabikabiswasroy@gmail.com

Sudipa Halder
sudipa.halder92@gmail.com

Pankaj Kumar Roy
pk1roy2014@gmail.com

[1] School of Water Resources Engineering, Jadavpur University, Kolkata-32, India

[2] Department of Geography, Women's College, Calcutta, Kolkata 700003, India

Environmental Earth Sciences (2021) 80:646
https://doi.org/10.1007/s12665-021-09941-8

ORIGINAL ARTICLE

Modelling soil erosion risk of a tropical plateau basin to identify priority areas for conservation

Sudipa Halder[1] · Malabika Biswas Roy[2] · Pankaj Kumar Roy[1]

Received: 5 November 2020 / Accepted: 1 September 2021 / Published online: 17 September 2021
© The Author(s), under exclusive licence to Springer-Verlag GmbH Germany, part of Springer Nature 2021

Abstract

Soil erosion induced by physical and anthropogenic activities needs serious concern to deal with. In recent days, watersheds have been facing acute soil loss because of deforestation, poor land use management and unscientific agricultural practices. The present paper highlights the goal to decipher soil erosion-susceptible zones in a rain-fed river basin of India having a complex topography comprising the extension of Chotonagpur plateau and parts of Bengal basin. Fuzzy logic algorithm-based analytical hierarchy process (FAHP) with remote sensing and geographical information system (GIS) were used to execute the objective. The soil erosion-susceptible zone (SESZ) was identified assimilating the 14 geo-environmental, hydro-meteorological and anthropogenic conditioning factors such as slope, drainage density, relative relief, stream power index, topographic wetness index, runoff, soil texture, land use and land cover, rainfall erosivity factor, distance from road, distance from settlement, distance from river, geomorphology and soil bareness index based on which sub-basin prioritization for sustainable soil conservation was made. The soil erosion-susceptible zone was classified into five classes, namely very low soil erosion zone (13.20%), low soil erosion zone (25.75%), moderate soil erosion zone (27.62%), high soil erosion zone (21.90%) and very high soil erosion zone (11.53%). Receiver operating characteristics (ROC) curve was generated where area under the curve (AUC) came as 0.82 and a correspondence analysis between the SESZ and the first three ranked factors was also made which together proves the accuracy of the model.

Keywords Fuzzy AHP · Soil erosion-susceptible zone (SESZ) · Receiver operating characteristics curve (ROC) · Area under the curve (AUC)

Introduction

Soil is an important natural resource that provides valuable ecosystem services by supplying 98.8% of the food to meet the human need, helps carbon storage, accelerates the flow and movement of groundwater, helps in greenhouse gas regulation, flood mitigation, etc. (Kopittke el al. 2019). The topsoil lies closest to the surface of the Earth and is enriched with essential nutrients that are highly exposed to water and wind erosion. Degradation of the global soils is more common due to the emerging effect of economic development, population explosion and climate change (Montanarella et al. 2016). Soil erosion is now one of the global environmental threats to agricultural productivity, which in the long run will affect the food security of a nation. Soil erosion is the combined effect of physical and anthropogenic factors, which include unscientific alteration of land use and land cover by the growing human settlement. According to Borrelli et al. (2017), human-induced land use and land cover change is the prime reason which led to the 2.5% increase in the soil erosion from the year 2001 to 2012. Water-induced soil erosion in agricultural areas ranges from 23.7 to 120 Pg year $^{-1}$, whereas rill and gully erosion estimates are 17 Pg year $^{-1}$ (Doetterl et al. 2012; Borrelli et al. 2017). According to an FAO report (2015), 0.3% of the reduction in the crop yield is caused by soil erosion and if this rate of loss continues it will lead to 10% reduction in crop yield by 2025.

✉ Malabika Biswas Roy
malabikabiswasroy@gmail.com

Sudipa Halder
sudipa.halder92@gmail.com

Pankaj Kumar Roy
pk1roy2014@gmail.com

[1] School of Water Resources Engineering, Jadavpur University, Kolkata 32, India

[2] Department of Geography, Women's College, Kolkata 700003, India

Arabian Journal of Geosciences (2020) 13: 574
https://doi.org/10.1007/s12517-020-05525-1

ORIGINAL PAPER

Fuzzy logic algorithm based analytic hierarchy process for delineation of groundwater potential zones in complex topography

Sudipa Halder[1] · Malabika Biswas Roy[2] · Pankaj Kumar Roy[1]

Received: 5 March 2019 / Accepted: 3 June 2020 / Published online: 1 July 2020
© Saudi Society for Geosciences 2020

Abstract

Groundwater crisis under the changed climate scenario has now become a global concern. Land use and land cover change and rapid urbanization are some of the prime causes of it. Aquifers are in a vulnerable condition due to the extensive abstraction and over exploitation as the groundwater draft exceeds the groundwater recharge. It is in this context, the present study has been carried out to identify groundwater potential zones of Garbeta block of Paschim Medinapore district of West Bengal, India, which is located in a critical terrain condition and faces extreme water scarcity in terms of both surface and groundwater availability. The region experiences an average annual groundwater level fluctuation between 9 and 11 m. Demarcation of the groundwater potential zones has been made using Fuzzy Analytical Hierarchy Process (Fuzzy AHP) integrated with geospatial techniques. Fuzzy weights have been entrusted to eleven physical parameters namely land use and land cover, soil, geology geomorphology, lineament density, drainage density, relative relief, distance from river, slope, groundwater level fluctuation and normalised difference water index (NDWI), and the final map has been prepared within geospatial environment. The groundwater potential zones have been classified into five classes: very low potential (18.30%), low potential (26.42%), moderate potential (25.99%), high potential (19.55%) and very high potential (9.75%). The calculated results have been validated through field based groundwater level survey. Such studies will provide new vision and incur valuable information to the stakeholders for sustainable water resources management and effective identification of suitable locations for groundwater extraction.

Keywords Fuzzy AHP · Groundwater potential index · Groundwater level fluctuation · Geospatial techniques

Introduction

Water is an important source to sustain life on earth, but with the growing population density, these valuable natural resources have been under stress both in its qualitative and quantitative aspects. Further due to the increase in the variability of surface water resources, the groundwater demand will far exceed the groundwater storage and recharge under changed climate (Kundzewicz and Doll 2009). Drying up of the most river basins, irregularity in the canal water supply system, increase in the precipitation and temperature variability, and decline in groundwater level are giving a treat to global food security. Such uncontrolled consequences of human dependence on groundwater have led the rapid degradation of the world's major aquifer system (Turner et al. 2019). Again with the agrarian development, electrification and modernisation of pumping system, the global groundwater abstraction has been increased from 312 km^3/year in the 1960s to about 743 km^3/year in 2000 (Wada et al. 2010). Therefore, development of groundwater resource and its management for beneficial use is needed which involves planning in terms of the entire groundwater basin (Todd 2009). Before managing it substantially, delineation of groundwater potential zone acts as a prerequisite work. This underground storage is highly influenced by surface and sub-surface hydrological and hydraulic characteristics like slope of land, geology, topography,

Responsible Editor: Biswajeet Pradhan

✉ Malabika Biswas Roy
malabikabiswasroy@gmail.com

[1] School of Water Resources Engineering, Jadavpur University, Kolkata, India

[2] Department of Geography, Women's College, Calcutta, Kolkata, India

Research Article

Analysis of groundwater level trend and groundwater drought using Standard Groundwater Level Index: a case study of an eastern river basin of West Bengal, India

Sudipa Halder[1] · Malabika Biswas Roy[2] · Pankaj Kumar Roy[1]

Received: 3 December 2019 / Accepted: 18 February 2020 / Published online: 28 February 2020
© Springer Nature Switzerland AG 2020

Abstract
Global water demand has far exceeded the total available water resources which in turn have put a serious concern on food security. Changes in the land use and land cover scenario and rapid population growth are putting unavoidable stress over the water resources of the nation. The Indian aquifer system is facing an acute crisis due to the unscientific abstraction of groundwater for agricultural, industrial and domestic sector by the 1.3 billion growing population. To investigate the groundwater degradation, 20 wells from a river basin of West Bengal have been selected to study their seasonal groundwater level trend using Mann–Kendall test statistics from 1996 to 2018 where 60% of the wells are showing a decline in water level particularly in post-monsoon season. These wells are mainly located near the agricultural land where extraction of groundwater from submersible pumping wells is extensive as observed from socio-economic survey. Agglomerated hierarchical cluster analysis has been executed to classify the wells based on their magnitude of fluctuation. The wells have been classified in four clusters where cluster I consists most of the wells about 15 numbers whose fluctuation ranged between 1.8 and 4.33 m below groundwater level (mbgl). Finally, Standard Groundwater Level Index has been applied to understand the groundwater drought years. Well locations like Simlapal, Bheduasol and Neradeul have a higher frequency of drought years. The recharge potential of the wells is now decreasing day by day. Such kind of studies is required and will help the stakeholders to focus on sustainable management of this valuable water resource.

Keywords Mann–Kendall · Hierarchical clustering · Groundwater level · Groundwater drought

1 Introduction

Groundwater is an important source of freshwater reserve where billions of habitants solely depend for their diverse utilisation. Groundwater crisis in the recent years has become a global concern as its vulnerability increased with greater frequency and magnitude. One of the prime causes of the shortage of groundwater storage and a decline in water level is climate change together with extensive extraction of groundwater from the shallow aquifer for agriculture, industry and other domestic purpose. Drying up of the river bed leads to poor discharge or infiltration into the sub-surface layer therefore sustaining the river stage, and health is in current need. In recent years, global warming together with climate change has led to the deficit of precipitation and an increase in evapotranspiration through a temperature rise directly influencing the recharge of a region. Variability of precipitation, temperature and evapotranspiration as predicted from

Electronic supplementary material The online version of this article (https://doi.org/10.1007/s42452-020-2302-6) contains supplementary material, which is available to authorized users.

✉ Pankaj Kumar Roy, pk1roy2014@gmail.com; pk1roy@yahoo.co.in; Sudipa Halder, sudipa.halder92@gmail.com; Malabika Biswas Roy, malabikabiswasroy@gmail.com | [1]School of Water Resources Engineering, Jadavpur University, Kolkata 700032, India. [2]Women's College, Calcutta, Kolkata 700003, India.

IJEP 38 (8) : 659-670 (2018)

Study of Ganga River Health Condition Based on Water Quality Indicators with Environmental Aspects and Adaptation Strategies Thereof

Pankaj Kumar Roy[1], Sudipa Halder[1], Swetasree Nag[1], Malabika Biswas Roy[2] and Arunabha Majumder[1]

1. Jadavpur University, School of Water Resources Engineering, Kolkata-700 032

2. Women's College, Calcutta, Kshirode Vidyavinode Avenue, Kolkata-700 003

The challenge on environmental sustainability before India is taking a frightful shape when it comes to the pollution of water. The long stretch of Ganga which is regarded as the holy flow is being messed up by the different anthropogenic activities. Ganga has now become contaminated in its many arms giving rise to a question to our water availability. There has been a long tradition of idol immersion and is too popular in the Ghats of Kolkata whose harmful effects are creating alteration on various components of a river of which water and soil are the most prominent. In this study in order to curb such situation and to establish a rapid assessment the physico-chemical parameters of water samples were collected from different hotspot areas at before and after idol immersion activity and were analyzed as prescribed by APHA guideline. Soil samples were also collected from the same position and tested accordingly in the laboratory of School of Water Resources Engineering, Jadavpur University. Water quality index (WQI) was calculated using the result indicated an increase in pollution load after immersion and quality deterioration characteristics change as well. The water quality index values reflected that an overall water quality is getting deteriorated at a greater extent immediately when the idol immersion process is going on. The results also highlighted that higher amount of lead was used as a raw material received in the river Ganga which may come from idol immersion. Thus it can be concluded that the overall health condition of river Ganga is getting hampered which may reduce the saturation value of dissolved oxygen and disturb the ecological flow at higher rate near by the bank.

KEYWORDS

Water quality index (WQI), Ganga river, Idol immersion, Rapid assessment.

INTRODUCTION

Besides being effected from the various sources of disposal from the inhabiting bank of Ganges, idol immersion is a major seasonal anthropogenic activity which years after years hampering the normal ecological flow of the channels leading to the degradation of water quality and loss of aquatic species. In India, mainly the Hindu religious group celebrate Durga Puja during September to October in every year. Idol immersion is a part of that festival. The materials which are being used to prepare such idols are changing from day to day with the growing economic price. The old clay models are now replaced with plaster of Paris, harmful paints, iron rods, plastics, decorative, etc. The plaster of Paris doesn't dissolve quickly into the water which consist of gypsum, sulphur, magnesium, etc., reduces the dissolved oxygen level in the water and kills fish and other organisms and increases the eutrophication and concentration of pollutant in both water and the soil. Moreover, the chemical paints used to polish these idols contain various heavy metals which are potent carcinogenic and highly toxic are responsible for adding further pollution load

© 2018 - Kalpana Corporation

CHAPTER

25

Land reclamation and reuse of waste water on the backdrop of urban sprawl of Kolkata metropolitan: a case study of East Kolkata, Wetland, India

Pankaj Kumar Roy[1,*], Malabika Biswas Roy[2], Sritama Chatterjee[1], Sudipa Halder[1], Swetasree Nag[1], Arunabha Majumder[1]

[1]*School of Water Resources Engineering, Jadavpur University, Kolkata, West Bengal, India;* [2]*Department of Geography, Women's College, Kolkata, West Bengal, India*

[*]*Corresponding author: pk1roy2014@gmail.com*

Chapter outline head

25.1 Introduction **557**
25.2 Land reclamation **560**
25.3 Importance of study area—EKW **561**
25.4 Land use pattern due to urban planning **565**
25.5 Materials and methods **569**
25.6 Results and discussions **569**
25.6.1 Land use and land cover change detection 569
25.6.2 Wastewater reuse efficiency 572
25.6.3 Impact of change in land use and land cover pattern on groundwater quality 572
25.7 Discussion **573**
25.8 Conclusion **578**
References **578**
Further reading **579**

25.1 Introduction

The land reclamation has an age-old history all over the world. Land reclamation of study area which dates back to the era of British Rule in India when this area was known to be Salt Water Lakes brings forth contemporary development of planned sewerage and drainage system of the Calcutta city passing

Land Reclamation and Restoration Strategies for Sustainable Development. https://doi.org/10.1016/B978-0-12-823895-0.00027-0
Copyright © 2021 Elsevier Inc. All rights reserved.

Chapter 3
Trend Analysis of Highly Cited Papers on Sustainable Watershed Management: A Bibliometric Review

Malabika Biswas Roy, Sudipa Halder, Arnab Ghosh, Snehamanju Basu, and Pankaj Kumar Roy

Introduction

Sustainable watershed management is an important concern under changed climate scenario. The main theme of the sustainable watershed management is to conserve the present environmental stability for meeting future needs. Sustainable management in water resources is at urgent need. Loss of storage due to siltation, fall of groundwater table, recession of glaciers, incidence of drought and floods, quality degradation, salinity ingress, recycling and reuse and drying of rivers makes it important to analyse and conserve a watershed in a sustainable way. Reddy et al. [1] found watershed management will carter to the soil moisture enhancement which is deteriorating at an alarming rate. In 2017, Zhou et al. [2] examined surface water resources by using Soil Accounting Matrix (SAM) in Gaotoi country of China. Zhang et al. [3] made a study on green space water use for the purpose of maintaining and enhancement of water security of China. Integrated water management scheme is needed for the improvement of irrigational efficiency and increase of infiltration rate of rainfall. Lang et al. [4] advocated that water yield in a basin can

M. B. Roy (✉)
Department of Geography, Women's College, Calcutta, Kolkata 700003, India
e-mail: malabikabiswasroy@gmail.com

S. Halder · A. Ghosh · P. K. Roy
School of Water Resources Engineering, Jadavpur University, Kolkata 700032, India
e-mail: sudipa.halder92@gmail.com

A. Ghosh
e-mail: arnabghosh996@gmail.com

P. K. Roy
e-mail: pk1roy2014@gmail.com

S. Basu
Jadavpur University, Kolkata, West Bengal, India
e-mail: drsnehamanju@gmail.com

© The Author(s), under exclusive license to Springer Nature Singapore Pte Ltd. 2021

P. K. Roy et al. (eds.), *Advances in Water Resources Management for Sustainable Use*,
Lecture Notes in Civil Engineering 131,
https://doi.org/10.1007/978-981-33-6412-7_3

Chapter 18
Assessment of Drought Using Multi-parameter Indices

Shuvoshri Bhattacharya, Sudipa Halder, Swetasree Nag, Pankaj Kumar Roy, and Malabika Biswas Roy

Introduction

Drought is one of the slow calamities that can put danger to the environment, hydrology, agriculture, economy and society worldwide. The basic concept of drought in our community is shortage of rainfall, lack of surface water, scarcity of water in society [1]. Drought is a complicated phenomenon and is difficult to study. It is often tough to find out the exact initiation of drought. Drought is roughly classified into four segments, i.e. Meteorological drought (deficit of precipitation), Hydrological Drought (shortage of total water), Agriculture Drought (scarcity of soil moisture and production decrease due to water) and Socio-economic Drought (inadequate water supply and demand) [2]. The reason for drought can be occurred by natural or anthropogenic activities. It is a clumping physical process and its effects vary spatially so it can be called a 'crawling disaster' [3]. Generally, meteorological drought rises when an area receives less than 75% rainfall over a season. But a rapid cutting of forests, global warming is also the cause of drought in recent days.

S. Bhattacharya (✉) · S. Halder · S. Nag
School of Water Resources Engineering, Jadavpur University, Kolkata 700032, India
e-mail: shuvoshri.bhattacharya@gmail.com

S. Halder
e-mail: sudipa.halder92@gmail.com

S. Nag
e-mail: nag.swetasree@gmail.com

P. K. Roy
Jadavpur University, Kolkata 700032, India
e-mail: pk1roy2014@gmail.com

M. B. Roy
Women's College, Calcutta, Kolkata 7000003, India
e-mail: malabikabiswasroy@gmail.com

© The Author(s), under exclusive license to Springer Nature Singapore Pte Ltd. 2021

P. K. Roy et al. (eds.), *Advances in Water Resources Management for Sustainable Use*,
Lecture Notes in Civil Engineering 131,
https://doi.org/10.1007/978-981-33-6412-7_18

Chapter 31
Soil Loss Estimation for Sustainable Watershed Conservation in Semi-arid Bengal Basin

Sudipa Halder, Malabika Biswas Roy, Shuvoshri Bhattacharya, Souvik Mondal, and Pankaj Kumar Roy

Introduction

Soil loss is one of the most important natural and human-induced menace to a watershed. Rapid urbanization, deforestation and unscientific agricultural practices are the prime reason. Geomorphic events like weathering, mass wasting and landslide are the physical mechanics to induce soil erosion. Soil erosion in an agricultural dominated watershed is a loss to economy and trade [1]. Soil loss results in the reduction of infiltration storage, degradation of soil structure, fertility loss and effectiveness of the plant root zone that results in the loss of soil productivity [2]. Global soil loss is about 75 billion tonnes from the agricultural field due to the poor implementation of the cropping practices [3]. Flora and fauna of the environment are also effected by soil loss. Eroded sediment from agricultural fields carry a huge amount of nutrients and when deposited in the nearby lakes and ponds increases the eutrophication process [4]. Soil erosion impedes the development of plant and vegetation succession from seedling to whole plant growth period affecting germination, reproduction and pollination [5]. Management of soil con-

S. Halder · S. Bhattacharya · S. Mondal · P. K. Roy
School of Water Resources Engineering, Jadavpur University, Kolkata 700032, India
e-mail: sudipa.halder92@gmail.com

S. Bhattacharya
e-mail: shuvoshri.bhattacharya@gmail.com

S. Mondal
e-mail: souvik134@gmail.com

P. K. Roy
e-mail: pk1roy2014@gmail.com

M. B. Roy (✉)
Department of Geography, Women's College, Calcutta, Kolkata 700003, India
e-mail: malabikabiswasroy@gmail.com

© The Author(s), under exclusive license to Springer Nature Singapore Pte Ltd. 2021

P. K. Roy et al. (eds.), *Advances in Water Resources Management for Sustainable Use*,
Lecture Notes in Civil Engineering 131,
https://doi.org/10.1007/978-981-33-6412-7_31

Chapter 9
Assessment of Stream Flow Impact on Physicochemical Properties of Water and Soil in Forest Hydrology Through Statistical Approach

Malabika Biswas Roy, Pankaj Kumar Roy, Sudipa Halder, Gourab Banerjee, and Asis Mazumdar

Abstract Forests affect the hydrology of watersheds in various ways with different hydrological parameters such as evapotranspiration, infiltration, intercepting cloud moisture, surface runoff, and groundwater. Sikkim, a part of northeastern India, a hilly area, is basically a critical terrain condition, and collection of secondary and primary data might be a challenging task to assess overall impacts, particularly on hydrological services. Three micro-watersheds, categorized as undisturbed, semidisturbed, and disturbed catchments covering a distance of 12 km at Geyzing, located in West Sikkim, were selected for this research work. Hydro-meteorological instruments were installed and recorded data for 4 years in three micro-watersheds to monitor the impact of forest cover on stream discharge and water quality. A composite rectangular weir was installed at field level to accommodate measuring stream discharge during the monsoon period as well as the pre-monsoon period. Water and soil quality parameters were analyzed during the monsoon as well as the pre-monsoon period. The overall impact of forests on the hydrological regime of a watershed is twofold. First, comparatively less discharge from a forest watershed during the rainy months shows that the forest controls excess runoff downstream. Second, forests induce infiltration, which leads to more uniform flow all year from the dense forest watershed stream. Conversions to forestland would have the potential to reduce erosion and subsequent sedimentation, as well as reduce levels of nutrients and pesticides in surface runoff and groundwater. These improvements in water quality can be a function of lower amounts of runoff and leaching as well as lower concentrations of potential pollutants.

M. B. Roy
Women's College, Kolkata, India

P. K. Roy (✉)
FISLM, School of Water Resources Engineering, Jadavpur University, Kolkata, India

S. Halder · G. Banerjee · A. Mazumdar
School of Water Resources Engineering, Jadavpur University, Kolkata, India

© The Author(s), under exclusive license to Springer Nature Switzerland AG 2021

M. N. Islam, A. van Amstel (eds.), *India: Climate Change Impacts, Mitigation and Adaptation in Developing Countries*, Springer Climate,
https://doi.org/10.1007/978-3-030-67865-4_9